



**Università
degli Studi
di Ferrara**

**DOTTORATO DI RICERCA IN
TERAPIE AVANZATE E FARMACOLOGIA SPERIMENTALE**

**CICLO
XXXVI**

COORDINATRICE Prof.ssa VARANI KATIA

***SARS-CoV-2 INFECTION: EFFECT ON HOST
IMMUNE SYSTEM AND ATYPICAL COVID-19
ASSOCIATED-DISEASES***

Settore Scientifico Disciplinare MED/07

Dottoranda

Dott.ssa Rizzo Sabrina

Tutore

Prof.ssa Rizzo Roberta

Co-tutore

Dott.ssa Bortolotti Daria

Anni 2020/2023

Preface

This work is the result of my three years of PhD studies at the Department of Chemical, Pharmaceutical and Agricultural Sciences – Section of Microbiology (University of Ferrara).

Firstly, I really want to thank Professor Rizzo Roberta for give me the opportunity to became a member of her research group, in which I learn so much about the microbiology world. I was lucky to meet a mentor that helped me find my way.

It was a pleasure to meet during my PhD course Professor Di Luca Dario, that transmitted knowledge and wisdom as figure of excellence in microbiology field.

I want to thank warmly Dr. Bortolotti Daria for all theoretical and practical teachings she gave me from the beginning, I'll always carry them with me. Also, thanks to Dr. Gentili Valentina for helped me with my doubts with her precious suggestions.

Then, I have to thank my labmate, Giovanna and Silvia for making the work days lighter and for sharing with me these three special years, not only as colleagues but also as friends. They were also important as support with my personal questions.

I also like to say thanks to Elia, my reference and support person for many years, without which I wouldn't have reached this important milestone. And also thank to my lifelong friends, especially Giulia and Simone, for having always been present in my life and for having shared so much with me.

Last, but not least, I thank with all my heart my Mum and Dad, for have believed in me and in this experience. I hope that they will be proud of me.

Thank you all from my heart.

Sincerely,

Sabrina

The present thesis is based on the following publications:

- I. Bortolotti D, Gentili V, **Rizzo S**, Rotola A, Rizzo R: SARS-CoV-2 Spike 1 protein control Natural killer cells activation via HLA-E/NKG2A pathway. *Cells* (2020). 9 (9), 1975.
- II. Bortolotti D, Gentili V, **Rizzo S**, Schiuma G, Beltrami S, Strazzabosco G, Fernandez M, Caccuri F, Caruso A, Rizzo R: TLR3 and TLR7 RNA Sensor Activation during SARS-COV-2 Infection. *Microorganisms* (2021). 9 (9), 1820.
- III. Bortolotti D, Gentili V, **Rizzo S**, Schiuma G, Beltrami S, Spadaro S, Campo G, D. Carosella E, Papi A, Rizzo R, Contoli M: Increased sHLA-G is associated with improved COVID-19 outcome and reduced neutrophil adhesion. *Viruses* (2021). 13 (9), 1855.
- IV. Bortolotti D, Simioni C, Neri L. M, Rizzo R, Semprini C. M, Occhionorelli S, Laface I, Sanz J. M, Schiuma G, **Rizzo S**, Varano G, Beltrami S, Gafà R, Passaro A: Relevance of VEGF and CD147 in different SARS-CoV-2 positive digestive tracts characterized by thrombotic damage. *FASEB Journal* (2021). 35 (12), e21969.
- V. Gentili V, Pazzi D, **Rizzo S**, Schiuma G, Marchini E, Papadia S, Sartorel A, Di Luca D, Caccuri F, Bignozzi C. A, Rizzo R: Transparent Polymeric Formulations Effective against SARS-CoV-2 Infection. *ACS Appl. Mater. Interfaces* (2021). 13, 46, 54648-54655.
- VI. Rizzo R, Bortolotti D, Morandi L, **Rizzo S**, Schiuma G, Beltrami S, Papi A, Contoli M: Humoral and adaptive immune responses to the SARS-CoV-2 vaccine. *International Journal of Infectious Diseases* (2022). 122, 412-414.
- VII. Schiuma G, Beltrami S, Santi E, Scutiero G, Sanz J M, Semprini C M, **Rizzo S**, Fernandez M, Zidi I, Gafà R, Greco P, Passaro A, Bortolotti D, Rizzo R: Effect of SARS-CoV-2 infection in pregnancy on CD147, ACE2 and HLA-G expression. *Placenta* (2023). 132 (2023) 38-43.
- VIII. Beltrami S, **Rizzo S**, Caccuri F, Rizzo R, Schiuma G, Bortolotti D: SARS-CoV-2 Systemic Effects New Clues. *Microorganisms* (2023). 11(5):1209.
- IX. Beltrami S, **Rizzo S**, Schiuma G, Speltri G, Di Luca D, Rizzo R, Bortolotti D: Gestational Viral Infections: Role of Host Immune System. *Microorganisms* (2023). 11(7), 1637.
- X. Gentili V, Bortolotti D, Morandi L, **Rizzo S**, Schiuma G, Beltrami S, Casciano F, Papi A, Contoli M, Zauli G, Rizzo R: Natural Killer Cells in SARS-CoV-2-Vaccinated Subjects with Increased Effector Cytotoxic CD56dim Cells and Memory-Like CD57+NKG2C+CD56dim Cells. *Front. Biosci. (Landmark Ed)* (2023). 28(7), 156.
- XI. Gentili V, Strazzabosco G, Salgari N, Mancini A, **Rizzo S**, Beltrami S, Schiuma G, Casciano F, Alogna A, Passarella D, Davinelli S, Scampagnini G, Medoro A, Rizzo R: Ozonated Oil in Liposome Eyedrops Reduces the Formation of Biofilm, Selection of Antibiotic-Resistant Bacteria, and Adhesion of Bacteria to Human Corneal Cells. *Int. J. Mol. Sci.* (2023). 24, 14078.

SARS-CoV-2 infection: effect on host immune system and atypical COVID-19 associated-diseases

Contents	Pages
Introduction.....	5
1. SARS-CoV-2.....	5
1.1. Origin and classification.....	5
1.2. SARS-CoV-2 structure.....	7
1.3. Viral genome	9
1.4. Spike protein and Nucleoprotein.....	13
2. SARS-CoV-2 pathogenetic mechanism	16
2.1. SARS-CoV-2 tropism: ACE2 and CD147 receptors	16
2.2. Replication and transmission of SARS-CoV-2.....	24
3. SARS-CoV-2 associated diseases.....	28
3.1. COVID-19.....	29
3.2. Atypical COVID-19	32
3.3 COVID-19 diagnosis and risk factors	41
4. Pharmacological treatments and vaccination.....	43
5. Methods and results.....	49
5.1. Evaluation of SARS-CoV-2 infection effect on host immune system.....	49
5.1.1 SARS-CoV-2 vaccination effect on host immune system	134
5.2. SARS-CoV-2 atypical infections	148
5.2.1. SARS-CoV-2 and pregnancy	148
5.2.2. SARS-CoV-2 and bowel diseases	192
6. SARS-CoV-2 treatment.....	205
7. Novelty of the thesis.....	214
8. Conclusions and perspective.....	215
9. Other works.....	238
10. References.....	312

SARS-CoV-2 infection: effect on host immune system and atypical COVID-19 associated-diseases

Abstract

Severe Acute Respiratory Syndrome CoronaVirus-2 (SARS-CoV-2) is a *Betacoronavirus* and the etiological agent of CoronaVirus Disease-19 (COVID-19), which is also correlated to the global pandemic in 2020.

Comparing to MERS and SARS-CoV, SARS-CoV-2 has major impact in terms of pathogenesis, due to both high transmission rate and its wide tissue tropism. In fact, SARS-CoV-2 ability to infect several tissues is due to the large distribution of Angiotensin-converting enzyme 2 (ACE2) and Cluster of Differentiation 147 (CD147), two of the main receptors used during viral entry phase through interaction with the viral Spike protein (SP). SARS-CoV-2 transmissibility is also increased by recombinant events that occur in the viral ssRNA+ genome, mainly on the SP gene, generating Variants of Concern (VOCs) with improved ability of transmission.

Since SARS-CoV-2 primary transmission route is represented by respiratory spread of the virus through infected droplets, the typical pathogenesis associated to the virus consists in the onset of a severe pulmonary disease, called COVID-19 (CoronaVirus Disease 2019), characterized by cytokine storm and acute respiratory distress syndrome (ARDS). Thanks to the wide expression of SARS-CoV-2 cellular receptors, its infection might also develop extrapulmonary diseases and long-COVID-19 condition, impairing gastrointestinal, hepatic, renal, cardiac, placental and neurological systems.

During my PhD course, I investigated the mechanisms at the base of typical and atypical SARS-CoV-2 infection, focusing on its modulation of host immune system.

In the defense against viral infection, several innate immune effectors are recruited to drive a local immune response and inflammation. This process is mainly triggered by the recognition of “non self” pathogen components, defined as PAMPs (Pathogen Associated Molecular Patterns) by Pattern Recognition Receptors (PRRs). In particular, during SARS-CoV-2 infection, its RNA genome is recognized by intracellular RNA sensors, which include endosomal Toll-like Receptors (TRLs). In particular, I reported the main role of TLR3 and TLR7 receptors in innate anti-SARS-CoV-2 response, which lead to a peculiar interferon and cytokine production.

Another key actor in the recognition of viral infection is represented by Human Leukocyte Antigen class (HLA) molecules, involved in the antigen presentation process and in host

immune activation. View the crucial role of HLA molecules, their expression is often modulated by viruses as an immune escape mechanism. Specifically, I reported that SARS-CoV-2 exploits the expression of non-classical immunomodulatory HLA class I molecules, HLA-G and HLA-E, to avoid host immune system recognition.

I investigated the association between HLA-G expression and immune dysfunctions observed in COVID-19 patients, focusing on neutrophils recruitment, confirming HLA-G alteration induced by the virus as the main cause of neutrophils infiltration and inflammation which characterizes the disease.

Again, I reported that Natural Killer (NK) cell exhaustion described in COVID-19 patients seems to involve SP loading on HLA-E on infected cells and its interaction with the inhibitory NKG2A/CD94 receptor expressed on NK cells, driving the suppression of their cytotoxic functions.

Another interesting aspect, concerning SARS-CoV-2 interaction with host immune system, is referred on SARS-CoV-2 vaccination.

I confirmed the efficacy of vaccination (BNT162b2 Comirnaty) in inducing both humoral and cell-mediated immunity against SARS-CoV-2, sustaining the protection by vaccination. In addition, in this thesis I analyzed the potential effect of anti-SARS-CoV-2 vaccination in restoring NK cell functions, revealing that one month following the booster dose there was an enrichment in NK activated cells, with presented memory-like features.

Host immune system impairment is also crucial in the onset of COVID-19 extra-pulmonary pathologies. Among these, SARS-CoV-2 gut infections are the most frequent. Gastrointestinal-COVID-19 is characterized by altered gut functions and the analysis of COVID-19 patients bowel biopsies showed a detrimental vascular effect, sustained by elevated Vascular Endothelial Growth Factor (VEGF) expression levels. This condition seems to involve the engagement of CD147 receptor and HLA-G expression as immune-escape strategies, possibly impact not only bowel function, but also pregnancy outcome. We assess viral infection at placental level, by analyzing the expression of HLA-G and other markers (ACE2, CD147, CD56), demonstrating their alteration in presence of SARS-CoV-2 infection.

The occurrence of atypical COVID-19, as in gut and placenta, required the administration of therapies even more efficient and specific. Thus, I also evaluated the potential employment of synthetic polymeric formulations in counteract SARS-CoV-2 infection.

In addition, during my PhD course I also participated to other studies concerning the impact of herpetic infections in human diseases. In particular, I investigated the role of Human Herpesvirus-6 (HHV-6) in neurodegenerative processes (Alzheimer Disease and Multiple

Sclerosis) and pregnancy (primary idiopathic infertility, IUGR), and in collaboration with the Chemistry group of Professor Trapella of the University of Ferrara, I evaluated the possible use of rhodanine-based molecule as an alternative antiviral therapy. Again, in collaboration with the Dermatology Group of Professor Borghi of the University of Ferrara, I also analyzed the involvement of Human Herpesvirus-8 (HHV-8) in oncogenesis (Kaposi Sarcoma). Always concerning the dermatology field, during my PhD I also spent 3 months abroad at the University of Zurich, where I investigated the regenerative and anti-inflammatory properties of snail mucus, acquiring skills in immunohistochemistry that I exploited also in all the studies described above.

Finally, I also performed some studies on emergent resistances to common antibiotics, evaluating the antimicrobial effect of new formulation for the treatment of ocular infections. All the data herein described are already published in peer-reviewed international journals.

SARS-CoV-2 infection: effect on host immune system and atypical COVID-19 associated-diseases

Introduction

1. SARS-CoV-2

1.1. Origin and classification

In late December 2019, several healthcare facilities reported clusters of patients with unknown pneumonia in Wuhan, Hubei Province, China [1]. In the bronchoalveolar-lavage fluid of these patients was observed the presence of a novel coronavirus, named “Severe Acute Respiratory Syndrome CoronaVirus-2” (SARS-CoV-2) [2]. On March 11th, 2020, World Health Organization (WHO) declared the pandemic status, due to the worldwide spread of SARS-CoV-2 infection [3]. The detrimental impact of infection-associated diseases across the globe was established among the most notorious pandemics that have ever been observed in human history, currently reporting nearly 658 millions of confirmed cases, and over 6.68 million fatalities as of early March 2021 [1].

The rapid diffusion of SARS-CoV-2 is often compared to the previous CoronaViruses (CoVs) pandemic, even if the first report of a coronavirus infection in animals occurred in the late 1920, when an acute respiratory infection of domesticated chickens emerged in North America [4]. After SARS-CoV in 2003, another episode of coronavirus pandemic appeared, originating the Middle East respiratory syndrome CoronaVirus (MERS-CoV) in 2012 [5]. Compared to SARS-CoV and MERS-CoV, SARS-CoV-2 is less pathogenic but more transmissible, thanks to the presence of asymptomatic infected subjects which contributed to its rapid spread [6].

Coronaviruses (CoVs) are a group of positive-stranded RNA viruses, included in *Orthocoronaviridae* subfamily, *Coronaviridae* family, order *Nidoviridae* [7]. The genetic characterization leads to classify CoVs into four distinctive genera [8] (Figure 1):

- *Alphacoronavirus* (alpha-CoVs),
- *Betacoronavirus* (beta-CoVs),
- *Gammacoronavirus* (gamma-CoVs),
- *Deltacoronavirus* (delta-CoVs).

The alpha-CoVs and beta-CoVs are found mostly in mammals, but also in humans. The alpha-CoVs infecting humans include Human CoronaVirus-229E (HCoV-229E) and Human CoronaVirus-NL63 (HCoV-NL63), while in the group of beta-CoVs infecting humans we can find Human CoronaVirus-HKU1 (HCoV-HKU1), Human CoronaVirus-OC43 (HCoV-OC43), MERS-CoV, SARS-CoV and SARS-CoV-2 [9], which belongs in particular to the *Sarbecovirus* subgroup. On the contrary, gamma-CoVs and delta-CoVs were found primarily in birds (Figure 1) [10].

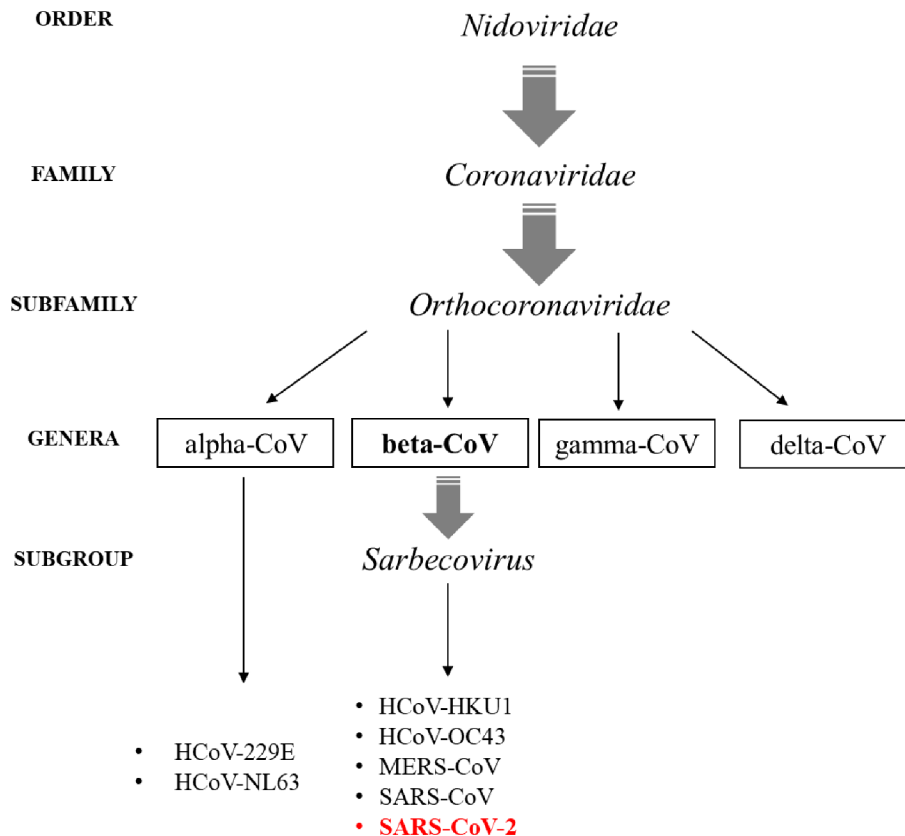


Figure 1. Taxonomy classification of coronaviruses and SARS-CoV-2.

Despite coronaviruses present typically a zoonotic source, they can acquire the ability to infect humans by crossing animal barriers through the so called “spillover” process. Members of the SARS-related viral species, included SARS-CoV-2, infect different mammalian hosts, as bats, carnivores, pangolins and primates [11]. Despite the different studies on SARS-CoV-2 zoonosis, its real origin remains undefined. The most accredited hypothesis supports the bats-pangolin-human transmission, that might have been occurred at the Huanan Seafood Wholesale Market of Wuhan and Huanan (China) [3, 12]. In fact, both SARS-CoV and SARS-CoV-2 events were associated with markets selling of live animals, particularly civets and raccoon dogs [13], known to be susceptible to SARS-CoV-

2 infection [14], as confirmed by the detection of the virus in the section that traded wildlife and domestic animal products, following the closure of these markets [15]. Several phylogenetic analyses support the origin of SARS-CoV-2 from horseshoe bat species (*Rhinolophus affinis*) [16]. This is supported by the evidence of a 96,2% nucleotide homology between SARS-CoV-2 and CoV-RaTG13 found in these bats. Furthermore, recent studies suggested that a group of endangered small mammals, known as pangolins (*Manis javanica*), could also convey ancestral beta-CoVs related to SARS-CoV-2, with an 85-92% nucleotide sequence homology [17].

Again, SARS-CoV-2 genome presents an high homology rate with SARS-CoV and MERS-CoV sequences (79% and 50%, respectively), that can explain their common pathogenesis and symptomatology, primarily correlated to acute respiratory syndrome, which begins as flu-like illness, associated to headache, diarrhea, shivering, fever, malaise and myalgia, that progresses to pneumonia, respiratory system failure and death in a few cases [18]. Consequently, SARS-CoV-2 has been included in the same respiratory coronavirus family of SARS-CoV and MERS-CoV and identified as a new emergent virus.

1.2. SARS-CoV-2 structure

SARS-CoV-2 is a single-stranded-positive RNA (ssRNA+) coronavirus, presenting spherical and oval shape [19], with a diameter ranges between 60 nm and 120 nm [20]. In the external part, viral particles included a spherical envelope, deriving from host cell membrane during the final phase of infection. SARS-CoV-2 envelope expressed spike-like projections on surface, giving it a crown-like structures, hence the nomenclature coronavirus [21].

The virion composition includes four structural proteins, which from inside to outside are (Figure 2) [22]:

- nucleocapsid or N protein,
- membrane or M protein,
- envelope or E protein,
- spike or S Protein (SP).

The N protein has a size from 43 to 50 kD and possesses three highly conserved domains. N protein composes the SARS-CoV-2 nucleocapsid, with the function to protect viral genome. Depending of its position in the virion, the N protein has two different shapes, helical or

spherical [1] and its main function consists in trigger the packaging of viral RNA into helical ribonucleocapsid [23].

Concerning the S protein, it is in the external part of viral particle, where it is assembled as a homotrimer and inserted in multiple copies into the envelope in a crown-like shape (Figure 2). The S protein is one of the most studied molecular components of SARS-CoV-2, due to its role in mediating firstly the binding with the host receptor (mainly ACE2), followed by fusion and entry phases of virus into the target cells [24].

Due to the crucial role of N and S protein in SARS-CoV-2 tropism and pathogenesis, and their involvement in COVID-19 therapy design, the molecular structure and the specific functions of these proteins will be further discussed below.

Also, M protein represents another important SARS-CoV-2 protein. It is the most abundant structural protein of virus, consisting in a type-III glycoprotein, characterized by three transmembrane domains (Figure 2) [25]. M protein plays a crucial role in the assembly of viral particle, molding the characteristic shape of viral envelope through the interaction with S and E proteins and providing the matrix to which nucleocapsid can attach for viral synthesis [26, 27]. Furthermore, it is hypothesized that M protein might be involved in the regulation of SARS-CoV-2 replication and in the packing of RNA genome into matured viral particles [28], playing a role in both viral assembly and homeostasis.

M protein is also able to affect host immune response. Even if some studies reported its function as an immune-activator of humoral and cellular immunity [25, 29], others reported a possible effect of this protein as a negative regulator of the innate immune system [30].

Finally, E protein is the smallest of structural molecules localized in SARS-CoV-2 envelope (Figure 2). It is a short polypeptide constituted by 76-109 amino acids, with two distinct domains: a single α -helical transmembrane domain at N-terminal and a charged cytoplasmatic tail at the C-terminus [31]. The E protein performs its function interacting with other structural proteins, especially with M protein, to maintain the shape of viral particle, promoting its release by infected cells.

During SARS-CoV-2 replication, E proteins is abundantly expressed, and it is primarily located in the Endoplasmic Reticulum-Golgi Intermediate Compartment (ERGIC), where it participates in increasing the viral protein folding load on Golgi [32]. This mechanism results in aberrant cellular protein folding, leading to a condition known as “unfolded-protein response”, that may lead to cell apoptosis. After the translocation of E protein in Golgi, it might self-assembles into an oligomer that mimic ion channels [33, 34] and, after interaction with endoplasmic reticulum, generate specialized structure in the ERGIC to facilitate the release of matured virus [32].

Interestingly, E protein appears to be highly conserved among the CoVs and, due to the fundamental role of E protein in SARS-CoV-2 pathogenesis, live attenuated vaccines based on the deletion of this molecule have been developed [35].

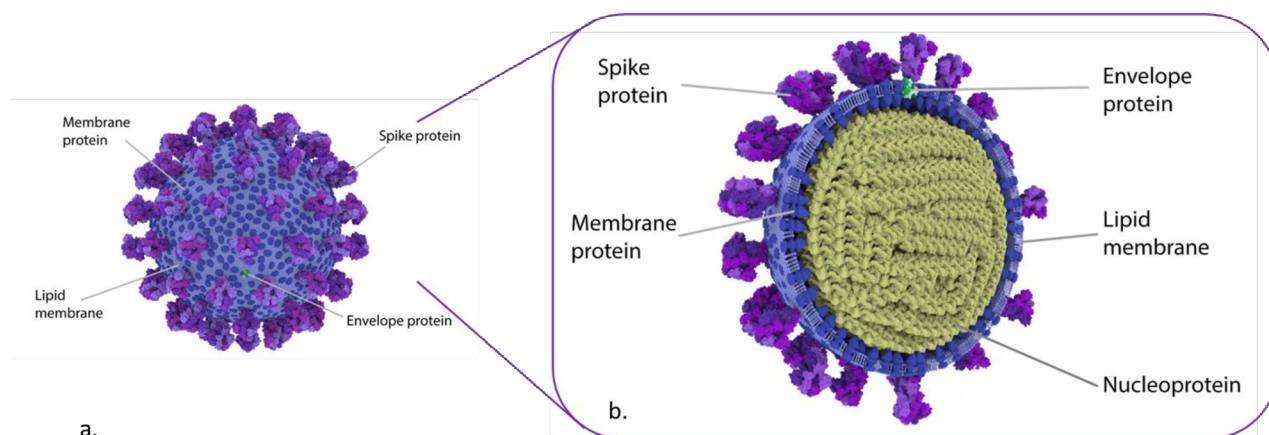


Figure 2. External (a) and internal (b) representation of SARS-CoV-2 structure with the main structural proteins: spike (S), membrane (M), envelope (E) and nucleocapsid (N).

1.3. Viral genome

SARS-CoV-2 genome presents the typical *Betacoronaviruses* structure. Its genome consists in a ssRNA, with a size of approximately 29.9 kilobases (kb), recently sequenced [36].

SARS-CoV-2 RNA is one of the larger genomes among RNA viruses and includes 5'-cap, 3'-poly-A tail structure and the two main Open Reading Frames (ORFs), 1a (ORF1a) and 1b (ORF1b) (Figure 3). This part is followed by a shorter sequence, which encodes the structural proteins spike (S sequence), membrane (M sequence), envelope (E sequence) and nucleocapsid (N sequence). Finally, in the terminal part of 3' tail, other accessory proteins are present [25] (Figure 3).

ORF1a is the longest ORF of SARS-CoV-2 genome and occupies almost two-third portion of the whole genome, while ORF1b overlaps with ORF1a and encode for sixteen nonstructural proteins (nsps), with multiple enzymatic functions (Figure 3), including the formation of transcription/replication complexes and the modulation of viral RNA replication and transcription [21].

For instance, nsp1 can specifically bind to 40S ribosomal subunit of host cells to accelerate the degradation of messenger RNA (mRNA) in infected cells [37]. Crystal structure of SARS-CoV-2 nsp1 suggests that its 180aa monomer may obstruct the entry of mRNA in ribosomal subunit of infected cells, causing a reduction in cellular protein synthesis and an increase of virus survival [38]. Furthermore, nsp1 interferes with innate immune response involved in the clearance of viral infection [38]. Therefore, nsp1 may be a potential antiviral

target, due to its participation in multiple stages of the viral life cycle. Interestingly, SARS-CoV-2 shares with SARS-CoV 84% of the nsp1 amino acid sequence, which indicates common functions carried out by this nsp in both viruses [25].

While nsp1 functions have been deeply investigated, the role of nsp2 is not completely clear. Nsp2 is the most variable nonstructural protein among the CoVs [36] and seems to be able to interact with several signals involved in host cell cycle and its role in viral replication process is confirmed by evidences that the deletion of its coding sequence attenuates viral growth and RNA synthesis [39]. Recently, it was reported that nsp2 sequence could present mutation due to positive selective pressure, conferring more contagiousness to SARS-CoV-2 than SARS-CoV [40].

In fact, as mentioned above, SARS-CoV and SARS-CoV-2 share high sequence similarity, also concerning nsp3 too, which presents a homology of 75% in those viruses [41]. Nsp3 is the largest nonstructural protein (213 kilodalton, kD) encoded by SARS-CoV-2 genome and plays a crucial role in the manifestation of cytokine storm during viral infection. This occurs because the protein acts as a scaffold, binding host proteins to promote viral replication and survival [42].

Nsp3 contains at least seven subdomains, a N-terminal acidic domain (called nsp2a), a X-domain (called nsp3b) and a papain-like proteinase PL^{pro} (or nsp3d). PL^{pro} is a cysteine protease that participates in the maintenance of SARS-CoV-2 infection through the translation of ORF1a and ORF1b sequences into polyproteins 1a (pp1a) and 1b (pp1b). In particular, PL^{pro} of nsp3 realized its proteolytic cleavage on pp1a [43] for the formation of nsp1, nsp2 and nsp3.

More specifically, PL^{pro} recognizes a specific tetrapeptide motif between nsp1 and nsp2 (glycine-180/alanine-181), nsp2 and nsp3 (glycine-818/alanine-819) and nsp3 and nsp4 (glycine-2740/lysine-2741). The hydrolysis of one of these amino acid sequence leads to the release of the three nonstructural proteins, which are essential for SARS-CoV-2 replication and viral RNA synthesis [43]. View the importance of PL^{pro} in the success of viral infection, it is an attractive antiviral drug target [44].

Similarly, also nsp5 is involved in the ORF1a/b proteolytic cleavage, that occurs to product other functional viral proteins forming a complex responsible of virus genome replication. Nsp5 is a 33 kD cysteine protease, also known as the main protease M^{pro} or 3CL^{pro}, that has a function in the modulation of SARS-CoV-2 replication cycle [45]. For this, several studies report the effectiveness of some inhibitors against SARS-CoV-2, targeting the nsp5 [46].

All the other nonstructural proteins not mentioned yet, are summarized below [19, 25]:

- **nsp4**: its transmembrane regions mediate the interaction between viral replication complex and cellular membranes;
- **nsp6**: leads to changes in host antiviral defenses, such as in the autophagic lysosomal machinery;
- **nsp7**: attends in replication/transcription complex;
- **nsp8**: catalyzes the synthesis of RNA primers;
- **nsp9**: is a single-stranded RNA-binding protein implicated in the virulence of virus;
- **nsp12**: is a key component of the SARS-CoV-2 RNA-dependent RNA polymerase (RdRp);
- **nsp13**: is a helicase (Hel) that function during synthesis of SARS-CoV-2 RNA and contributes in 5'-RNA capping. It unwinds double-stranded RNA in 5'→3' direction and presents single-stranded template to polymerase for further elongation.

Several studies report that interactions among the different nsps are needed to efficiently carry out key viral molecular mechanisms. As an example, it is known that nsp12 can synthesize RNA independently, but its binding to nsp7 and nsp8 increases its polymerase efficiency, while the binding of nsp12 to nsp13 increases its helicase activity [47]. The importance of this improvement of nsps effect SARS-CoV-2 infection is supported by the evidence that PL^{pro}, M^{pro}, nsp12, nsp7 and nsp8 interaction is crucial to form a functional replication-transcription complex, which contributed to viral genome synthesis and mRNA capping [48].

Despite the data available on nsps collaborations in the pathogenesis of SARS-CoV-2, the role of accessory proteins has not been fully understood. The ORFs genes encoding for accessory proteins are dominantly clustered at 3' end of viral genome and codify for the accessory proteins 3a, 3b, 3c, 3d, 6, 7a, 7b, 8, 9b, 9c and 10 (Figure 3) [49]. It has been supposed that accessory proteins might be essential in virus life cycle, as demonstrated by the role of 3a and 7a proteins in ion-channel activity, upregulation of host inflammation regulators (as NF-κB) and induction of host cell apoptosis [50].

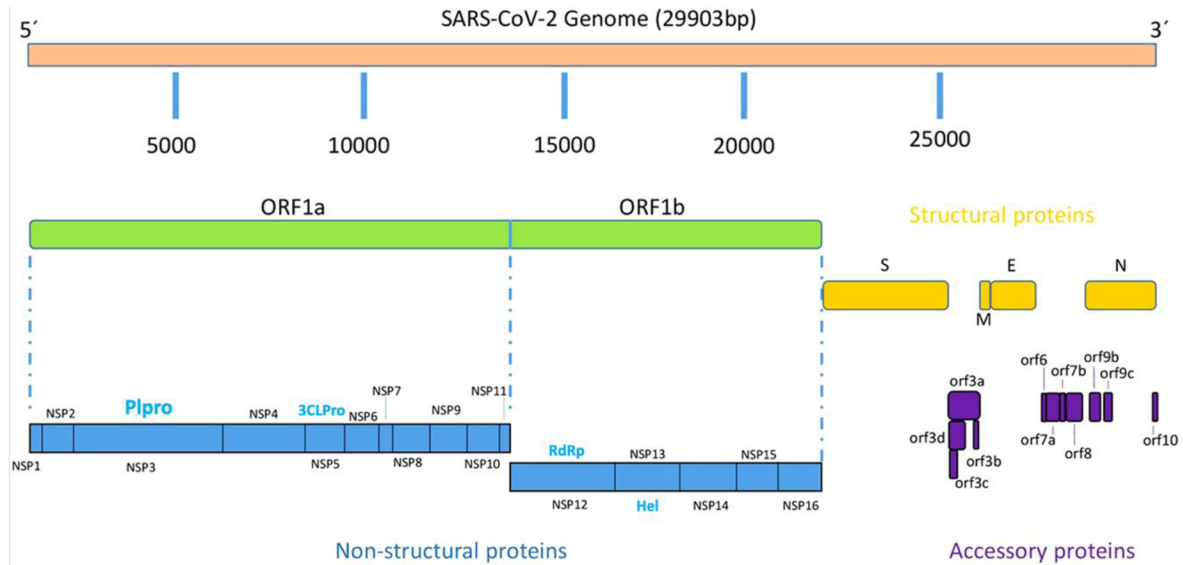


Figure 3. Genomic organization of SARS-CoV-2.

After the spread of pandemic, SARS-CoV-2 genome characterization represented a hot topic of investigation, with the purpose to identify its origin and evolution. Through high throughput sequencing, the genome of SARS-CoV-2 was analyzed and compared to the main CoVs, mostly SARS-CoV and MERS-CoV. As previously mentioned, SARS-CoV-2 showed a genetic similarity of 79% and 50% with SARS-CoV and MERS-CoV, respectively [1]. However, the coding regions of SARS-CoV-2 shows a similar genomic organization compared to bat coronaviruses and SARS-CoV, the only significant difference was the major length of SARS-CoV-2 S protein [51].

The similar organization among the CoVs genome is due to the presence of the same protein-coding sequence, which on the other hand might be subject to a positive selection during evolution of viruses [52]. This evidence is supported by the analysis of nucleotide nonsynonymous and/or synonymous substitutions, as recombination event in viral genomic sequence: the genome of SARS-CoV-2 can be considered an ensemble of several recombinant regions, which had undergone to amino acid changes. These types of recombination led to positive selection in viral genome, particularly in SARS-CoV-2 ORFs [52]. In fact, recombination events were found with highest frequency in ORF1a, that codify the N-terminus of S protein [1].

As a result of events of recombination from the original Alpha B.1.1.7 virus of Wuhan, several variants called “Variants Of Concern” (VOCs) have been generated. VOCs present mutations in their spike domain, which substantially increase the binding affinity in protein-receptor complex [53]. Among the main variants, Beta (B.1.351), Gamma (B.1.1.28), Delta

(B.1.617.2) and Omicron (B.1.1.529) are the most studied [54]. Delta and Omicron VOCs are identified as the major cause of transmissibility increase, severe disease onset and reduced effectiveness of treatments [55, 56]. Omicron is the most heavily mutated variant among all the SARS-CoV-2 VOCs, that, because of its essential mutation on viral S protein, unlocks the way for a partial resistance to immunity induced by COVID-19 vaccines, together with enhanced viral transmissibility [57].

Since SARS-CoV-2 VOCs have been linked to a rapid spread in human populations and to vaccine resistance, they were deeply studied to evaluate alternative pharmacological treatments and vaccines for COVID-19 disease.

1.4. Spike protein and Nucleoprotein

Among the SARS-CoV-2 molecules, S and N protein represent the principal topic of studies, due to their role in host cells entry and in the nucleocapsid composition, respectively.

Focusing on Spike protein, its structural biology has been identified very rapidly since the initial outbreak of pandemic. In particular, S protein monomer is a type-I membrane protein, belonging to the class I of viral fusion proteins, presenting 66 N-linked glycans, that forms homotrimers [58] protruding from the viral surface [22]. In particular, the homotrimer protein is composed by two functional subunits: S1 and S2. The S1 encoding sequences includes N-terminal domain (NTD), receptor binding domain (RBD) and C-terminal domain, while S2 subunit contains fusion peptide (FP) sequence, fusion-peptide proximal region (FPPR), heptad repeat 1 (HR1), central helix (CH), connector domain (CD), heptad repeat 2 (HR2), transmembrane domain (TM), and cytoplasmic tail (CT) [59] (Figure 4a). In particular, the presence of RBD in S1 subunit forms the apex of S protein and makes this portion capable to bind angiotensin-converting enzyme 2 (ACE2) target receptor, to enter into cells, while the function of S2 subunit involves its fusion with the viral membranes on host cells [22]. Moreover, S1 subunit exists in two different states, closed and open, and its conformational changes between the two states is essential in the initial step of SARS-CoV-2 infection [59]. In fact, in the closed or “down” conformation, RBD recognition motifs does not protrude from viral interface, while on the contrary, in the open or “up” state it is capable to fuse the viral membrane with cell surface [60] (Figure 4b). The entry of SARS-CoV-2 into the cells can be also expressed as a mechanism of accessibility or inaccessibility of RBD domain to ACE2 receptor: in the S1 down conformation RBD is inaccessible to receptor, while when S1 switch to the up conformation exposes RBD and its recognition motif to ACE2, allowing virus adhesion and entry in the cell [22].

The S1 changes from “down” to “up” conformation is started by host proteases cleavage of the two major sites of S protein [61], the S1/S2 site, that separates S1 from the S2 subunit, and the S2’ site, within the S2 subunit [62] (Figure 4a). In particular, S1/S2 site of S protein is cleaved by furin [60], while transmembrane protease serine 2 (TMPRSS2) is responsible for S2’ cleavage [63].

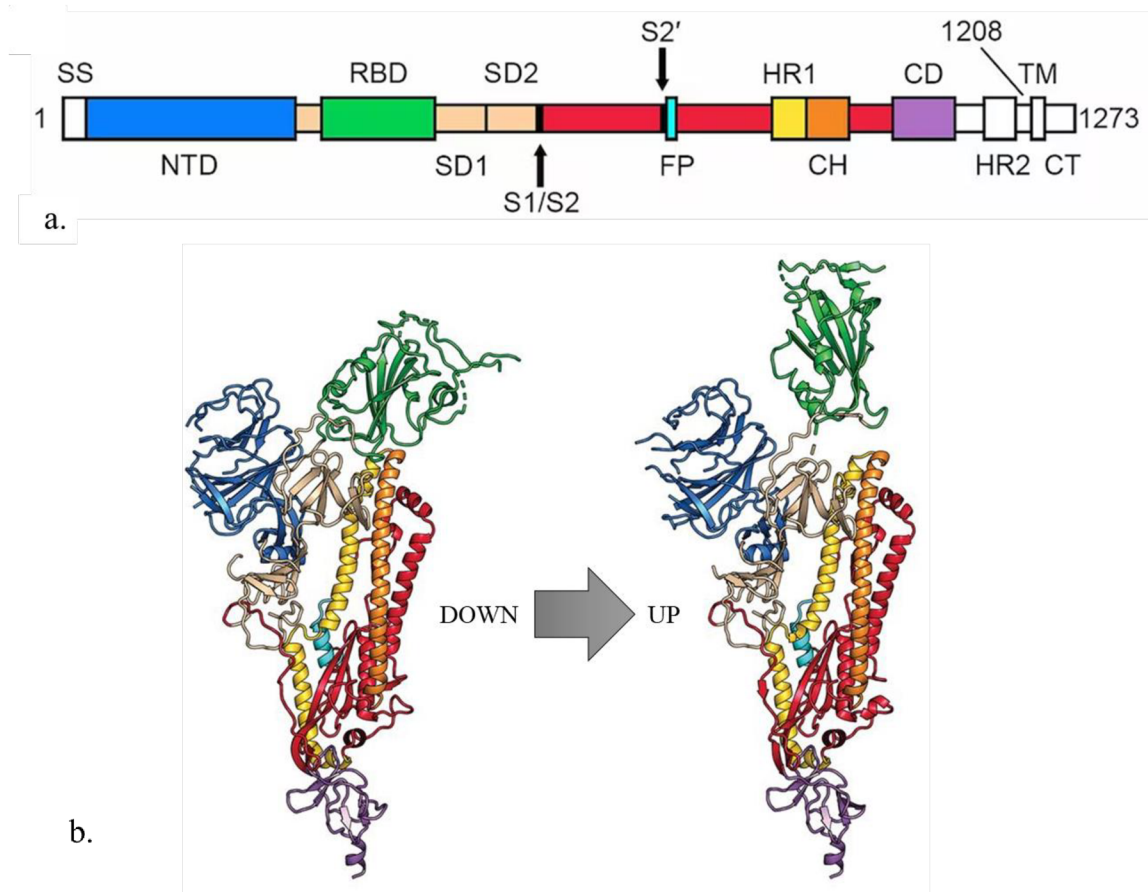


Figure 4. Schematic structure of Spike protein (SP) domains: N-terminal domain (NTD); receptor binding domain (RBD); fusion peptide (FP), heptad repeat 1 (HR1), central helix (CH), connector domain (CD), heptad repeat 2 (HR2), transmembrane domain (TM); cytoplasmic tail (CT) (a). 3D SP structure in up and down conformation (b).

Different studies reported that the presence of a fusion peptide at the amino terminus of S2 subunit might be critical for membrane fusion, since only S2’ cleavage, but not S1/S2, is essential for membrane fusion activity. Concerning furin-mediated S1/S2 cleavage, it destabilizes the S protein, promoting its binding to ACE2 [64] thanks to a further cleavage at the S2’ site by cellular TMPRSS2. In fact, this protease triggers an extensive and irreversible conformational change to induce membrane fusion, through the creation of pores into cell membrane, allowing the viral genome release inside cell cytoplasm [65]. In effect, the timing of the S protein conformational change is highly regulated, because this alteration

during fusion process is irreversible. Thus, once the S protein undergoes to the final conformational change, it completely loses its membrane fusion functions [1].

Concerning S protein structure, RBD represents the part of major interest, because of its implication in ACE2 binding. ACE2 recognition by RBD is possible through a specific portion, named receptor-binding motif (RBM), containing the major binding sites in its bottom part [66] which leads to the formation of RBD-ACE2 complexes, similarly to what is observed during SARS-CoV infection [60]. However, SARS-CoV and SARS-CoV-2 RBDs binding to ACE2 showed a different strength, with SARS-CoV-2 RBD binding 3-4-fold higher than SARS-CoV [59]. This evidence may explain the higher infectivity and transmissibility of SARS-CoV-2, compared with SARS-CoV.

Unfortunately, SARS-CoV-2 S protein undergoes to frequent sequence changes, including deletions, mutations, and recombination events. Currently, the S protein is the principal target for vaccine development, but the several mutations in its antigenic epitopes made difficult the development of new pharmacological treatments, included vaccines [67].

Also, N protein has been considered as a target for vaccines design [68]. In the N protein structure three highly conserved domains could be found: N-terminal domain (NTD), RNA-binding domain or a linker region (N-arm), C-tail and C-terminal domain (CTD) [9] (Figure 5). Although the NTD of CoVs shows highly similar structure, the SARS-CoV-2 NTD possesses different surface charge distributions, probably adapted for more efficient binding to RNA genome [69]. Among these, NTD and CTD are the most important structural and functional domains [25]:

1. NTD binds RNA; this is possible since its major portion is occupied by positively charged amino acids that are able to bind viral genome;
2. CTD mediates dimerization of N protein by self-association and contains nuclear localization signal. Also, it has a role in nucleocapsid protein oligomerization and in N-M protein-protein interactions.

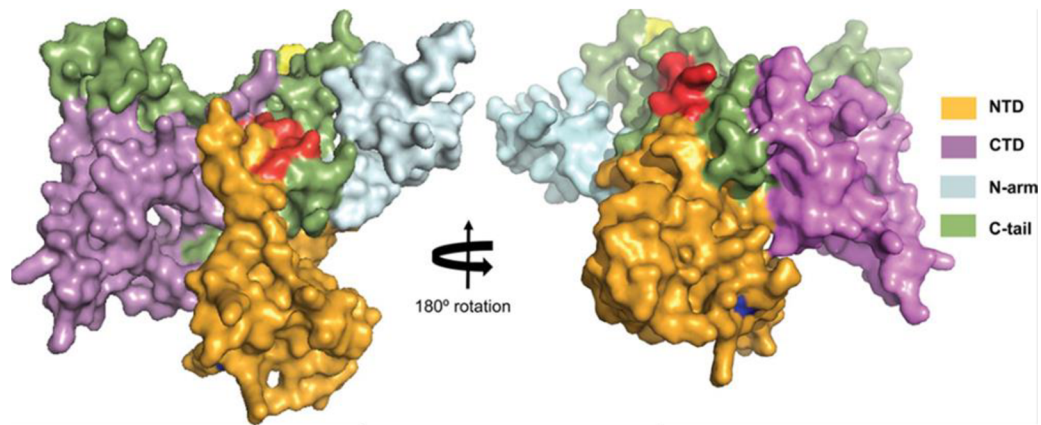


Figure 5. Crystal structure of nucleoprotein of SARS-CoV-2: N-terminal domain (NTD), C-terminal domain (CTD), N-terminal RNA binding domain (N-arm) and C-tail (C-tail).

The collaboration of the three N protein domains and their phosphorylation allows the structural dynamism that facilitate their binding to viral RNA [70]. In fact, even if the N protein is the exclusive structural molecule that organize SARS-CoV-2 nucleocapsid, it plays also key functions in RNA replication and transcription by preserving the ribonucleoprotein (RNP) complex [71], which is important to protect viral genome and to maintains reliable viral replication [72]. In addition, N protein interacts with E and M proteins to facilitate virion envelope formation, particle assembly and it is involved in host-virus interaction too [73]. Concerning this, N protein regulates host cell cycle, including apoptosis, to facilitate virus multiplication and spread [74]. Due to this role, the presence of N protein in SARS-CoV-2 infected cells is often used as diagnostic marker [75].

2. SARS-CoV-2 pathogenetic mechanism

2.1. SARS-CoV-2 tropism: ACE2 and CD147 receptors

SARS-CoV-2 interacts with several receptors on host cells. The most studied SARS-CoV-2 cellular receptor is ACE2, initially identified as a homolog of ACE receptor [76].

ACE2 consists of 805 amino acids, it presents only a single extracellular N-terminal domain containing the active catalytic site, a C-terminal membrane anchor, and a conserved zinc-binding domain [77]. The C-terminus of ACE2 is a carboxypeptidase, that removes single amino acids from its substrates [78]. The sequence encoding ACE2 receptor is located on the Xp22 chromosome, it is formed by 18 exons and 20 introns with a total size of 40 kb, generating six variants through alternative splicing [79].

ACE2 could exist in two forms: membrane-bound (mACE2) or soluble (sACE2). mACE2 is a full-length receptor, consisting in a transmembrane part and an extracellular domain, involved in SARS-CoV-2 S protein binding and virus cell entry, while sACE2 lacks the transmembrane domain and once secreted diffuses in circulation at low concentrations [80]. Similarly, ACE2 receptor plays a crucial role in the Renin-Angiotensin-Aldosterone System (RAAS), involved in the regulation of blood pressure and electrolyte homeostasis [81]. In physiological condition, angiotensinogen produced by the liver is cleaved by renin enzyme, resulting in the formation of angiotensin I (Ang I). Then, ACE catalyzes the conversion of Ang I into angiotensin II (Ang II) [82], which binds angiotensin II type-I receptor (AT1R), inducing vasoconstriction, blood pressure elevation, renal sodium reabsorption, potassium excretion, aldosterone synthesis, induction of inflammation and activation of pro-fibrotic pathways [83]. In this RAAS phase, ACE2 cleaves Ang II to angiotensin (1–7), which binds Mas receptor (MasR) (a G protein-coupled receptor (GPCR)) inducing vasodilation, anti-inflammatory and anti-fibrotic effects [84]. Furthermore, ACE2 cleaves Ang I into angiotensin (1–9), which is in turn converted into angiotensin (1–7) by ACE (Figure 6). Thus, tissue ACE/ACE2 balance is crucial to determine the availability of the different angiotensin peptides to regulate the inflammatory and fibrotic mechanisms [81]. ACE2 receptor does not act only in RAAS, but also in the gastrointestinal (GI) setting, in which it has been described as a key regulator of intestinal amino acid homeostasis, expression of antimicrobial peptides, local innate immunity and gut microbial ecology [85]. In addition, recently it was confirmed the role of ACE2 in Kinin-Kallikrein System (KKS) involved in the regulation of several physiological processes, such as coagulation, inflammation and pain [86]. This system exerts its function through the production of active peptides, most of all bradykinin (BK), a potent vasodilator that counterbalanced the vasoconstriction promote by RAAS [87]. Moreover, BK positively regulates tissue plasminogen secretion and thrombus formation [88].

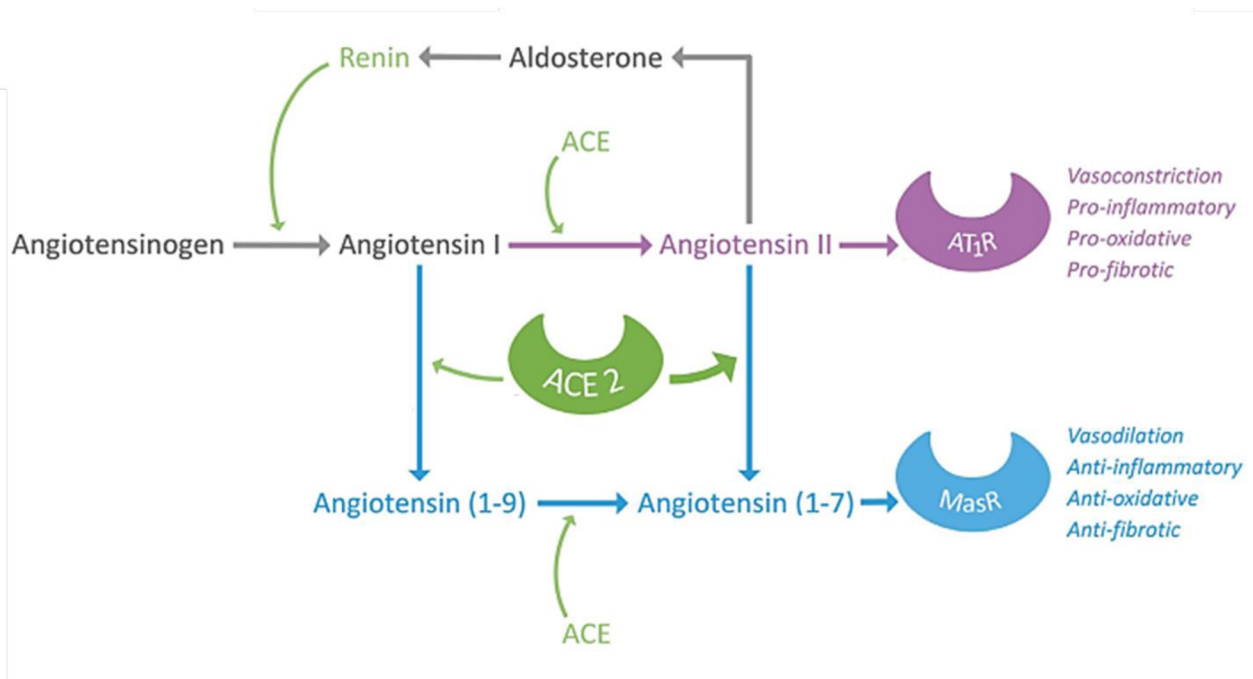


Figure 6. Role of ACE2 in the renin-angiotensin-aldosterone system (RAAS) during physiological conditions.

When viral infection is established, RAAS pathways and homeostasis are deregulated. In fact, ACE2 might be negatively regulated by SARS-CoV-2 via internalization and/or downregulation [89], causing an accumulation of Ang II that leads to vasoconstriction, oxidative stress, inflammation, atrophy and fibrosis, due to the activation of Ang II/AT₁R pathway [90]. As a matter of fact, several studies report that AT₁R can induce apoptosis in human lung alveolar epithelial cells, in response to Ang II [91]. Ang II, besides being a potent vasoconstrictor, promotes endothelial dysfunction through cyclooxygenase-2 (COX-2) activation, producing vasoactive prostaglandins and reactive oxygen species (ROS) [92]. The high levels of Ang II consequent to viral infection causes in turn the activation of host immune response, resulting in the hyperinflammatory state observed in patients during the late phase of infection [80], characterized by NF- κ B activation and proinflammatory cytokine release, as IL-6, IL-1 β and Tumor Necrosis Factor α (TNF α) [93].

Moreover, ACE2 internalization and downregulation observed during SARS-CoV-2 infection affect also the KKS, creating an imbalance and contributing to lungs hyperinflammation and local vascular leakage, which leads to angioedema [94].

Interestingly, when ACE2 downregulation by SARS-CoV-2 is correlated to a worsening of tissue damage (particularly at pulmonary and vascular level), it also may result in a decreased viral cell entry and viral spread. Thus, according to the evidence that SARS-CoV-2 infects ACE2-expressing cells with greater efficiency than SARS-CoV, the hypothesis that the virus could exploit other cellular factors for viral attachment and entry has been explored. The

ability of SARS-CoV-2 to interact with other cellular receptors than ACE2 will be further discussed later in this thesis.

SARS-CoV-2 shows tropism for several human tissues and for this reason its infection is associated to a wide spectrum of symptoms in affected patients. The ubiquitous distribution of ACE2 among tissues, together with the use of other receptor for cell entry, can explain the multi-organ dysfunction linked to SARS-CoV-2 pathology, which is mainly respiratory, and it is defined CORonaVIRus Disease-19 (COVID-19) [95]. In fact, besides respiratory system, ACE2 expression was also reported in male and female reproductive apparatus, vascular and cardiac cells, and nervous system. On the contrary, no ACE2 expression was observed in blood cells [96], lymphoid tissues and hepatobiliary structures [97].

During SARS-CoV-2 pandemic, patients presented respiratory-like illnesses that progressed to Acute Respiratory Distress Syndrome (ARDS), suggesting the lungs, and in particular lung parenchyma, as the primary site for viral infection [98, 99]. Once virus enters into the respiratory tract, the first kind of cells targeted by the virus are nasopharynx or trachea multiciliate cells, or sustentacular cells in the nasal olfactory mucosa [100], followed by vascular endothelial cells and alveolar macrophages [101] (Figure 7). In case SARS-CoV-2 infection is not cleared, it can spread from the upper respiratory tract to the lower, or by gradual dissemination along the tracheobronchial tree. Alternatively, the initial site of infection can be the lower respiratory tract too, leading to alveoli infection, inflammation and limited gas exchange [102]. In this site, SARS-CoV-2 uses alveolar type 2 (AT2) cells as target, which are responsible for pulmonary surfactants secretion [103] (Figure 7).

The establishment of SARS-CoV-2 infection in these cells type is mainly due to their ACE2 positivity, but their permissiveness to viral entry depends also on additional cellular intrinsic factors, such as TMPRSS2 expression [104] and ACE2 transcriptional regulation. In particular, ACE2 gene expression in human airway epithelial cells has been reported to be upregulated by type I and II interferons (IFN-I and INF-II), which are highly produced during viral infection [105].

As mentioned before, the wide distribution of ACE2 receptor among human organs, together with the ability of SARS-CoV-2 to bind also other cellular receptors, is essential for viral spread to other sites than lungs. Notably, SARS-CoV-2 genome was reported also outside respiratory tract, mostly at gastrointestinal (GI) and kidney level [106, 107].

In fact, SARS-CoV-2 infection and COVID-19 are often been associated to complications of GI, because of its abundant ACE2 and TMPRSS2 expression, specifically in the brush border of enterocytes [108] (Figure 7). Zang et al. observed that the expression of ACE2 is significantly higher in small intestines than in all other organs, including lungs [109].

However, ACE2 marker was rarely seen in the esophageal epithelium, because it is mainly composed of squamous epithelial cells, that express less ACE2 than glandular epithelial cells [110]. The absence of ACE2 expression in esophageal mucosa is in accordance with the absence of viral nucleocapsid protein staining in tissue biopsies [110].

The high presence of ACE2 receptor in GI system is correlated to gut illness frequently reported in patients with COVID-19. As a proof of concept, at least 20% of those presented a detectable SARS-CoV-2 RNA in feces, gastric, duodenal and rectal glandular epithelial cells, even after respiratory symptoms [111]. The significant intestinal symptomatology induced by SARS-CoV-2 and the presence of viral genome in GI system, leads to speculate a possible fecal-oral transmission, which has never been confirmed [112].

Concerning renal system, ACE2 expression is highly in brush border of proximal tubular cells and in glomerulus, moderately in parietal epithelial cells, while glomerular endothelial cells and mesangial cells are negative [81] (Figure 7). In these cell types the expression of ACE2 is 100-fold higher than in lung tissue [113]. In addition to ACE2, cells of proximal renal tubules expressed TMPRSS, which increases their susceptibility to SARS-CoV-2 infection [114]. Renal injury is commonly described in COVID-19 cases with viral RNA positivity in kidney specimens, in association with increased morbidity and mortality [115, 116]. Renal clinical disease observed in COVID-19 patients might be correlated to SARS-CoV-2 infection by both indirect factors, as cytokine production, and direct viral replication in kidney epithelial cells [113]. The deregulation of renal physiological mechanisms is due to ACE2 downmodulation by SARS-CoV-2, leading to an increase of Ang II activity that may contribute in the initiation of kidney injury [117].

Also, the investigation of the effect of SARS-CoV-2 infection at reproductive level has gain attention. ACE2 is abundantly expressed in the epithelial cells, ovary, particularly in oocytes, and its mRNA has been identified in human uterus [118] (Figure 7). The presence of ACE2 in these tissues is important for the modulation of multiple reproductive processes, such as steroid secretion [119], follicle development [120] and oocyte maturation, influencing the ovulation, corpus luteum progression [121] and regulating endometrium regeneration [122]. Moreover, ACE2 is widely expressed in human placenta, mainly at level of syncytiotrophoblast, cytotrophoblast, decidual cells, endothelium and vascular smooth muscle of villi (Figure 7). During pregnancy, ACE2 regulates Ang II and Ang (1-7) to control blood pressure and fetus development, contributing to the normal uterine physiology [123]. These functions are guaranteed by a specific expression level of ACE2 receptor during pregnancy, which is higher in early gestation, while less abundant in the late phase [124].

An aberrant expression of Ang II and Ang (1-7), that might be also induced by SARS-CoV-2 via modulation of ACE2, could lead to hypertension, pre-eclampsia and eclampsia [125]. According to the evidence of ACE2 high placental expression, a potential vertical transmission of the virus was suggested. For instance, recently SARS-CoV-2 presence was reported in infants' nasopharyngeal and anal swabs [126] and a neonate born by a COVID-19-positive mother was found with elevated anti-SARS-CoV-2 IgM [127]. The assumption of breastfeeding transmission was evaluated too, reporting a correlation between mother positivity and child-transmission during [128]. Although these studies were not be able to definitely confirm SARS-CoV-2 vertical transmission, the infection in both pregnant women and fetuses has been associated to several complications, including premature birth, fetal distress, premature and cesarean section [129].

Even if female reproductive tract has been deeply investigated being directly involved in gestational development, also SARS-CoV-2 infection at male reproductive system has been considered. The presence of ACE2 mRNA was described in different testicular cell types, including Leydig cells, Sertoli cells, the seminiferous duct and spermatogonia cells [130, 131] (Figure 7), supporting a possible SARS-CoV-2-mediated impairment of male gonadal functions [132]. Again, the susceptibility of testis and male reproductive cells to SARS-CoV-2 infection have suggested their function as reservoir of infection, potentially linked to male infertility [133, 134]. This hypothesis was supported by the evidence that the rate of positive ACE2 testis in infertile men was higher than in healthy men, indicating that SARS-CoV-2 could increase the incidence of reproductive disorders, through the abnormal activation of ACE2 pathway [135]. Furthermore, it has been shown that testicular expression of ACE2 is age related [136] and young male patients are more likely to be targeted by SARS-CoV-2 testicular infection than older patients due to higher ACE2 expression, showing an increased risk of developing infertility.

Moreover, SARS-CoV-2 infection and COVID-19 are associated to other types of extrapulmonary symptoms, as thrombotic events in several positive subjects. To support the role of viral infection in this type of disease, studies reported that ACE2 was identified in endothelial cells of human blood vessels and microvasculature (Figure 7), as well as TMPRSS2 in human vascular endothelium [137]. Although the expression of ACE2 in cardiovascular tissues is not elucidated, the effect of its modulation during viral infections has been already described. As previously mentioned, the SARS-CoV-2/ACE2 binding induces the downregulation of the receptor, creating ACE/ACE2 imbalance that promotes tissue injury by potentially promoting prothrombotic cascades in the vessels [138]. In fact, the presence of a low ACE/ACE2 ratio in the vascular endothelium prevents prothrombotic

cascade from activation, by catalyzing degradation of Ang II in Ang (1–7), which induces antithrombotic effects [82].

ACE2 has also a role in nervous system. The enzymatic activity of ACE2 has already been detected in human brain tissues and cerebrospinal fluid [139], indicating its significant expression within the human central nervous system. This is supported by the evidence of a huge ACE2 presence in cells body of neurons, with less expression in axons and dendrites [140]. In these cell types, ACE2 exerts its beneficial effects in ischemic brain injury, by shifting the balance between Ang II and Ang (1–7), in favor of the latter [70]. Due to the ACE2 positivity of neurons, these cells might be a possible target for SARS-CoV-2 infection, according to the neurotropism already described for several CoVs [140].

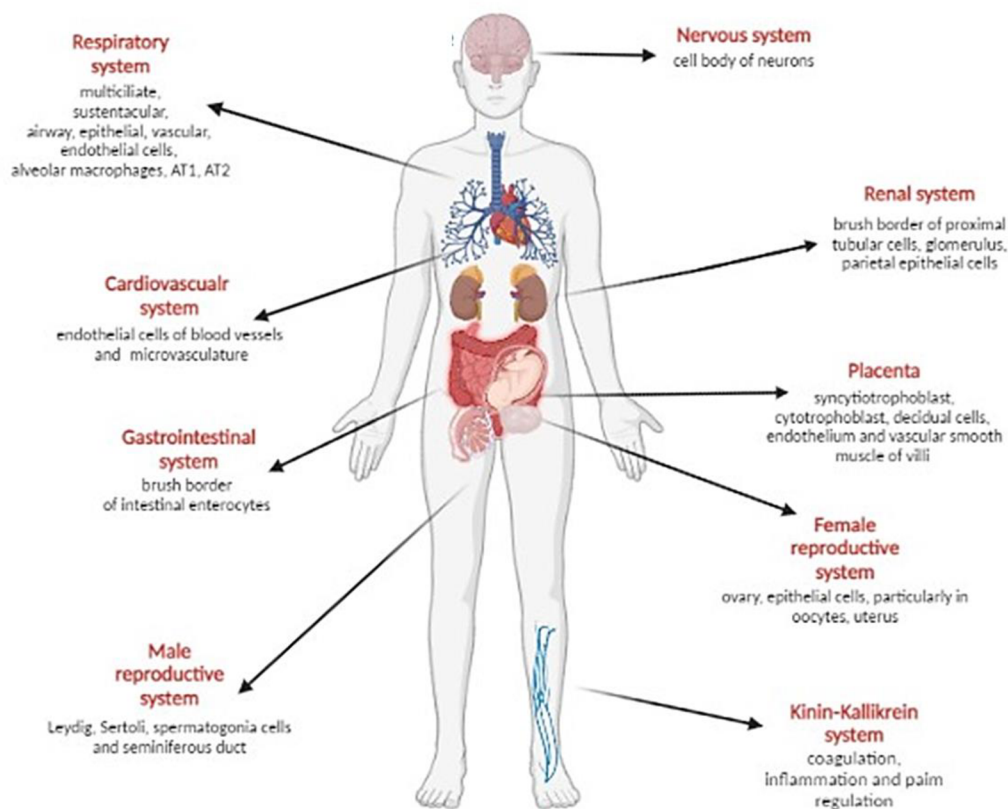


Figure 7. ACE2 expression in respiratory, cardiovascular, gastrointestinal, nervous, renal, kinnin-kallikrein, placenta, male and female reproductive human systems.

After the discovery of ACE2 as the primary receptor responsible of SARS-CoV-2 entry, also other alternative routes of infection have been investigated. Several studies demonstrated that SARS-CoV-2 Spike is also able to interact with the host cell receptor Cluster of differentiation 147 (CD147). CD147 is a type 1 transmembrane glycoprotein, included in

the immunoglobulin superfamily (IgSF) [141], and also known as extracellular matrix metalloproteinase inducer (EMMPRIN) [142] or basigin, since it is coded by BSG gene, located on human chromosome 19 [143]. The splicing process and variation in transcription initiation sites induce the synthesis of four CD147 isoforms, named basigin 1, 2, 3 and 4 [144], expressed in [145]:

- basigin 1 in retina;
- basigin 2 is ubiquitous, mainly found in heart, kidney, skeletal muscles and testis;
- basigin 3 in bone marrow, fetal liver, lung, testis and thymus;
- basigin 4 is similar to basigin 3 expression, in normal tissues.

The transmembrane domains structure of CD147 contains 21 residues crucial in anchoring receptor to cell membrane [146]. Particularly, the hydrophobic region of transmembrane domain contains a conserved glutamic acid residue, and leucine zipper like sequence [147]: these interact with membrane components, providing support in the binding between CD147 and cell membrane [148]. CD147 structure includes also an extracellular portion, fundamental in cell-cell communication, through cytokine synthesis and cytoplasmatic region too [149].

CD147 has been described to have a role in both viral infection [150, 151] and tumor development [152-155] (Figure 8), where the molecules is involved in angiogenesis through Vascular Endothelial Growth Factor (VEGF) expression (Figure 8). In addition, the tissue invasion by cancer cells is supported CD147 interaction with integrin $\alpha 6\beta$ and $\alpha 3\beta$ [156, 157].

Besides the CD147 involvement in pathological condition, it also acts as a signaling receptor for cyclophilins, which are responsible for chemotaxis in cell-mediated immunity and inflammation in presence of pathogens [158].

Different tissues express CD147, including lungs, brain, heart, liver, kidney, immune and blood cells [159] and might appear upregulated during pathological conditions [160], such as cardiovascular diseases, where the receptor is expressed by vascular endothelium in the absence of ACE2 [161], underlying its potential implication in vascular damages associated to SARS-CoV-2 infection [162]. Furthermore, CD147 is also involved in kidney acute ischemic and chronic fibrotic injuries [163], in pulmonary hypertension [164] and its peculiar expression was also reported on immune cells [165], suggesting a pivotal role in inflammation [166].

View CD147 implication in different alteration of tissue homeostasis and inflammatory processes, CD147 represents an interesting candidate in SARS-CoV-2 tropism, and infection investigations.

Wang et al. described CD147 as an additional entry receptor for SARS-CoV-2, demonstrating for the first time the interaction between SARS-CoV-2 Spike protein and CD147 on host cells. In particular, the implication of CD147 SARS-CoV-2 entry phase was confirmed by the fact that the modulation of receptor levels affected the ability by virus to infect target cells [167]. Moreover, this study showed that CD147 was involved in viral infection of ACE2-negative immune cells where CD147 overexpression facilitates the infection [167]. Interestingly, in lung tissues of COVID-19 patients, CD147 does not co-localize with ACE2, suggesting that CD147 and ACE2 expression are exclusively independent in single lung cells, indicating that these two receptors may be complementary factors in mediating virus infection [167]. As previously mentioned, referred on ACE2, the presence of viral infection reduces also CD147 expression on target cells. Interestingly, CD147 silencing decreases ACE2 expression, suggesting a possible direct and indirect effect of CD147 on viral entry via ACE2 modulation [162].

2.2. Replication and transmission of SARS-CoV-2

SARS-CoV-2 infection in host cells is characterized by specific replication phases, described below.

1) Viral entry

The main protein involved in SARS-CoV-2 entry phase is the S protein, that to become functional needs to undergo energetic changes to acquire a stable state [22]. In fact, as described for SARS-CoV and other CoVs, a conformational change provides to S protein sufficient energy to overcome the binding between virus and, typically, ACE2 expressed on cellular membranes [168]. Following ACE2 engagement, S protein activation can be induced with two proteolytic cleavages: the first interests the S1-S2 boundary, while the second occurs into the S2' site [22], as previously described.

The ACE2-S protein binding is necessary to exposes spike RBD site to host peptidase and proteases, to trigger membrane fusion.

- Interaction of S protein with ACE2 receptor

The first step of SARS-CoV-2 infection interest the interface between RBD of viral S protein and ACE2 (Figure 9). In particular, this binding employes almost twenty amino acidic

residues of both ACE2 and RBD, forming the hydrophilic concave chain that allows the interaction [22]. As previously mentioned, studies about the soluble structures of Spike trimer in complex with monomeric ACE2, confirm that receptor interacts with RBD in its up conformation [80]. In prefusion state, the structure of S2 presents a strong binding between the fusion-peptide region and connector domain of RBD, maintaining the down conformation of this one [169]. Then, ACE2 engagement induces a conversion of S protein to post fusion conformation, in which S1 dissociates as a monomer, while S2 adopts a rigid shape [24].

The ACE2 binding is possible due to several molecular changes in S1 subunit [170], while on the contrary, S2 subunit remains largely unchanged upon ACE2 binding [22]. The result of ACE2 recruitment by SARS-CoV-2 consists in the exposition of S1 and S2 sites of S protein which became accessible to be cleaved and activated by host cell proteases (Figure 9).

- *Cleavage of S1-S2 boundary by furin*

One of the main factors of the huge SARS-CoV-2 infectivity consists in the presence of a furin site at the S1/S2 boundary. In fact, the cleavage of S1/S2 and S2' are typically necessary for SARS-CoV-2 entry process. The first activation of S protein is performed by furin on a multibasic site located at the S1-S2 junction, during virus maturation into infected cell. The processing of S protein by furin at S1/S2 cleavage site occurs following viral replication in the ERGIC [171] and it is fundamental to activate membrane fusion by the second cleavage event.

After ACE2 binding, the cleavage of the S1/S2 boundary by furin divides S1 by S2 subunits. This is a prerequisite for the cleavage of S2' site by other proteases [172] and is essential to initiate the membrane fusion process. The exposed S2' is a target site for the cleavage by host TMPRSS2 protease at the membrane surface [84, 173] or by cathepsin L [174] in the endosomal compartment, following ACE2-mediated endocytosis [175] (Figure 9). Thus, viral entry is dependent by the cellular proteases, and TMPRSS2 and cathepsin L are the two majors involved in Spike protein activation.

- *TMPRSS2 role in viral entry*

After S1/S2 cleavage, S2' site must be cut by TMPRSS2 on cell surface to properly initiate viral fusion, or alternatively, by cathepsins L, after virus transfer into endosomes (Figure 9).

- *Cathepsin role in viral entry*

Even though SARS-CoV-2 prefers activation by TMPRSS2, it is possible that target cells express low levels of this protease, or that ACE2-S protein complex does not assemble with TMPRSS2. Furthermore, another 120 amino acids cleavage portion was found upstream to S2' site cleaved by TMPRSS2 [176], suggesting the potential presence of different protease that may cleave at S2' [177]. In fact, the S2' portion, once exposed by furin, can be internalized via clathrin-mediated endocytosis into the late endolysosome, where the acid environment activates clathrin proteolytic functions [175] (Figure 9). This mechanism is mediated by cathepsins, a non-specific protease with endopeptidase and exopeptidase activities, which participate in proteolysis in the late endosomes and lysosomes [178]. These proteases are divided into three classes: aspartic (D and E), serine (G) and cysteine (B, C, K, L, S and V) cathepsins. Among these, cysteine proteases (cathepsins B, L and S) mostly contribute to viral entry [22], and particularly cathepsin L has been to participate in the cleavage of S2' site of SARS-CoV-2 S protein.

2) *Membrane fusion*

After the activation of viral S protein subunits via TMPRSS2 or clathrine enzymes, the S2' site is cleaved, exposing the fusion peptide (FP) [176]. Moreover, the dissociation of S1 from S2 subunit initiated by furin, induces a dramatic conformational change in S2 that shifts near the fusion peptide, inducing its proteolytic cleavage [22] and prompting the fusion with cell membrane (Figure 9).

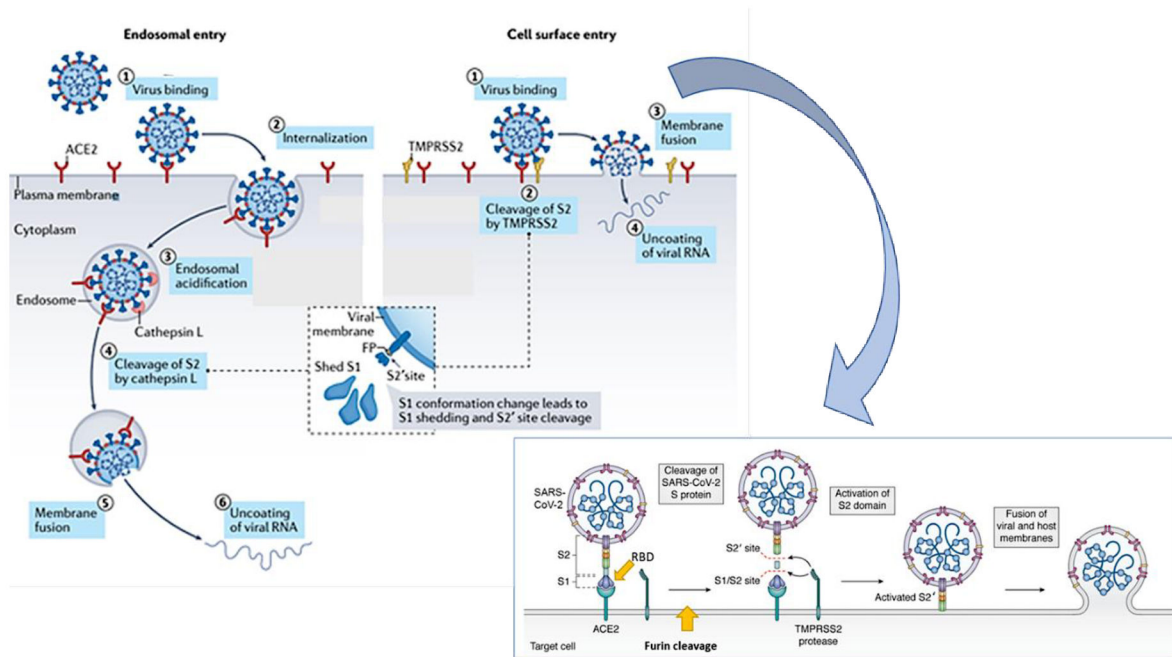


Figure 9. Mechanisms of SARS-CoV-2 entry into host cells: on left side the endosomal entry via cathepsin L-dependent ways, on right side the TMPRSS2 entry mechanism. On bottom part, representation of SP cleavage by the host proteases furin and TMPRSS2 [22].

3) RNA release, transcription, replication, and protein translation

Following membrane fusion, SARS-CoV-2 genomic positive RNAs (+gRNAs) is uncoated and released into cellular cytosol (Figure 10). Replication, transcription, and translation processes of viral genome are common to all of RNA viruses. Replication of SARS-CoV-2 consists in the synthesis of a complementary full-length negative-strand RNA (-RNA) from +gRNA, which will be used as a template to produce +gRNA genomes. After their synthesis, +gRNAs are packaged into new virions [168] (Figure 10).

The expression of SARS-CoV-2 proteins in infected cells depends primarily on the translation of gRNA, and subgenomic RNAs (sg-mRNAs) [179, 180]. First, SARS-CoV-2 +gRNAs recruit the host ribosomes, serving as mRNA for the translation of ORF1a and ORF1b replicases [181]. ORF1a and ORF1b are translated in the specific non-structural proteins pp1a and pp1ab, respectively, which are precursors of non-structural proteins [19] (Figure 10). The premature production of these proteins is due to their direct implication in nucleic acid metabolism, promotion of non-structural proteins catalytic activity and stimulation of RNA synthesis and processing. Most importantly, the gRNA sequence might be also translated into additional viral polymerases, specifically nsp7, nsp8 and nsp12, that will lead to viral RdRp polymerase formation. RdRp is a specific machinery, implicated in SARS-CoV-2 genome replication and responsible of viral gRNA synthesis [182].

Subsequently, RdRp use +gRNA template to synthesize complementary full-length negative strands and a set of negative sg-RNAs [182] (Figure 10). These will be use as template for +gRNA and +sg-RNA. In the next phase, the new +gRNA and +sg-RNA will be used in two different ways: the genomic +RNA will function as transcripts to replicate further viral genomes, while +sg-RNAs will be the template for the translation of E, M, N and S SARS-CoV-2 structural proteins [183] (Figure 10).

It is note that, in the production of new gRNA or sgRNA, several mRNA intermediates are also involved. Newsworthy, the 5' capping of mRNA, occurring in the nucleus, is important for viral mRNA stability, translation initiation and escape from the immune response [184], while the 3' tail polyadenylation of mRNAs is essential for negative-strand synthesis [185]. Importantly, SARS-CoV-2 also developed several mechanisms of proofreading, to avoid the wrong adding or lacking nucleotides during the synthesis and translation of new viral genomes [186].

4) Virion assembly and release

New gRNAs are synthesized into cytoplasm and then coated with N protein to generate the nucleocapsid structure of SARS-CoV-2 [168] (Figure 10).

On the contrary, other viral structural proteins (M, E and S proteins) are transcribed and then translated in ER, to be incorporated into envelope at the ERGIC by budding process (Figure 10). At the end of replication, the enveloped and mature virion is exported out the cell by exocytosis [182] (Figure 10).

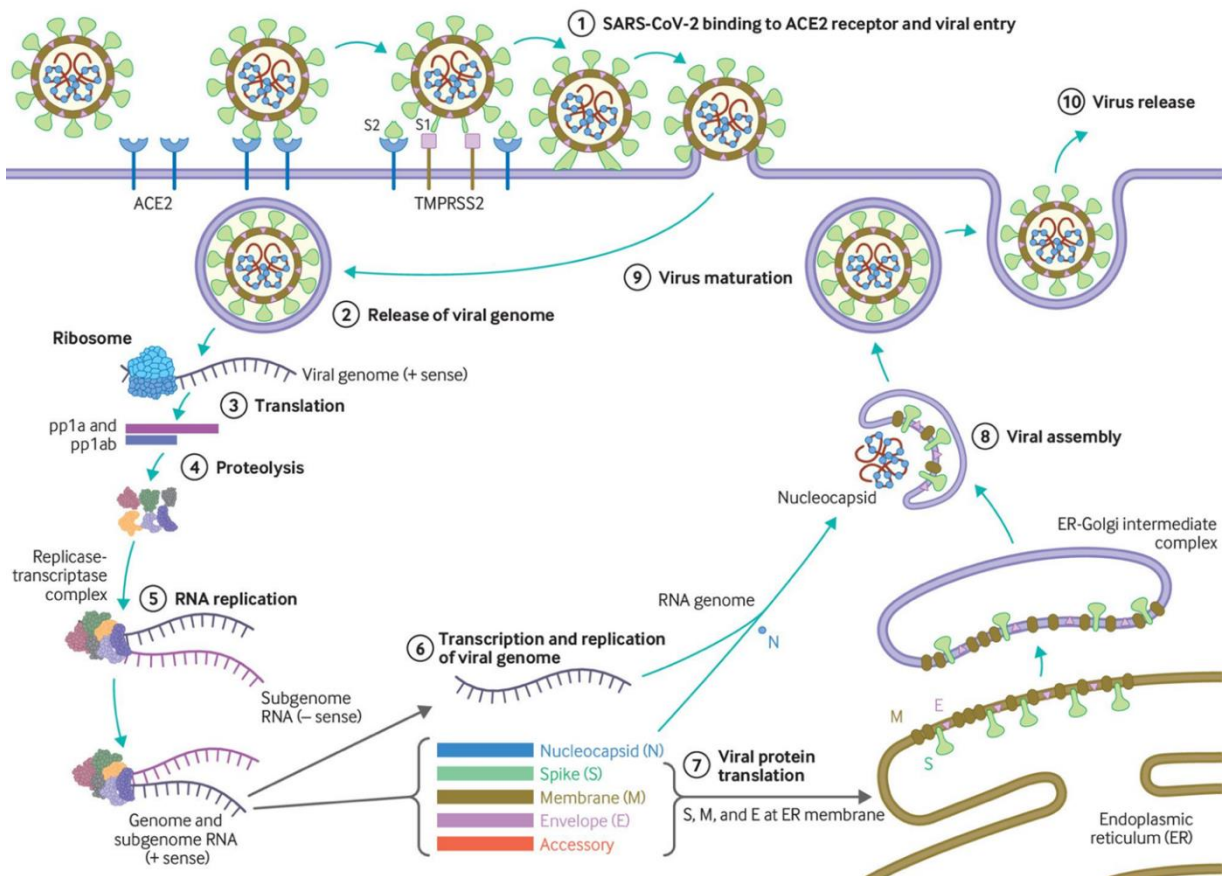


Figure 10. Schematic representation of SARS-CoV-2 genome replication and synthesis of viral proteins. After the binding of viral SP to ACE2 receptor and membrane fusion, the viral genome is release into host cytoplasm. Then, viral RNA and proteins are synthesized for viral assembly, maturation, and virion release.

3. SARS-CoV-2 associated diseases

Human coronaviruses commonly use as primary transmission way the respiratory route. Early reports of patients, with lung ground glass opacities, cough, and other pulmonary symptoms, suggested that also SARS-CoV-2 is transmitted in this manner [187]. The airborne transmission involves aerosol droplets, which are diffused in the environment with

sneezing, coughing or close conversation with infected subject. The droplets size plays an important role in viral transmission, in particular the particles smaller than 5 μm might be diffuse for more than one meter, thus persisting in the air for long periods [188]. Furthermore, the direct transmission of respiratory droplets is reinforced by productive SARS-CoV-2 replication in both upper and lower respiratory tract.

Human-to-human transmission has also been associated to direct contacts, between infected and uninfected subjects. In addition, during pandemic was observed a spread of SARS-CoV-2 infections from nonsymptomatic or presymptomatic individuals to other subjects, which contrasts with the previous dynamics of transmission observed for SARS-CoV. The presence of asymptomatic subjects and their identification was one of the main concerns in the resolution of COVID-19 pandemic.

In addition to direct respiratory transmission, another possible way for SARS-CoV-2 indirect transmission have been explored. In fact, once released, the infected droplets can also contaminate objects, such as door handles or desks, persisting on several materials (as ceramic, glass or steel) for hours and days [187, 189], increasing the risk to spread the virus through contact with these infected surfaces.

Moreover, due to the intestinal tropism of SARS-CoV-2, a possible fecal-oral transmission of the virus was also hypothesized [190]. As previously mentioned, infected patients developed gastrointestinal symptoms, thus a possible transmission through the infected feces was investigated, confirming the presence of SARS-CoV-2 RNA or still active viral particles in feces samples for up to 4 days [191]. In addition, the sexual way can be a possible route of transmission, as supported by the vulnerability of human testis to viral infection [192], together with SARS-CoV-2 mother-fetus vertical transmission [191, 193].

Thus, the further investigation of the possible SARS-CoV-2 transmission routes is fundamental to limit viral spread, avoiding unsafe behaviors and reducing possible infective sources.

3.1. COVID-19

COVID-19 is the pathology associated to SARS-CoV-2 infection. During COVID-19, a heterogenous involvement of organs and systems is observed, causing various tissue damages that arise both during and post infection.

The incubation period of COVID-19 is very short: the median range is 4-5 days before symptom onset, respect to 2-11 days in SARS-CoV infection [188]. Generally, around 98% of patients develop symptoms within 12 days by viral exposure [194] that can persist until

14 days [195], even if the illness can become severe earlier, approximately 1 week after symptoms onset [102].

Despite the development of typical symptoms, it is known that SARS-CoV-2 infection can also induce to an asymptomatic disease. This clinical condition made difficult the identification of infective sources and constituted a problem in the vigilance of SARS-CoV-2 spread. In fact, asymptomatic COVID-19 cases, although positive for SARS-CoV-2 infection, do not develop symptoms after infection, while presymptomatic subjects develop symptoms later in the course of infection, both acting as potential drivers of viral transmission. Asymptomatic/paucisymptomatic positive patients usually present mild respiratory disease, including common symptoms in the upper respiratory apparatus during primary infection, and other aspecific signs as fever, headache, chest pain, myalgia, diarrhea and vomiting [188, 196] (Table 1), in line with the wide tropism of the virus [197, 198].

Positivity for SARS-CoV-2 infection can be mostly identified in the presence of cough (60-86%) and shortness of breath (53-80%), due to the contagion of mucous membranes in the upper respiratory tract [199, 200]. Also, SARS-CoV-2 can infect nasal and pharyngeal epithelia, site of the olfactory mucosa, causing changing in taste, smell sense and anosmia (64–80%) (Table 1) [201, 202].

Once reached the upper ways, the virus directly accesses the lower respiratory tract and infects bronchial and alveolar epithelial cells [203]. From mild symptomatology, the infection might evolve into moderate and severe COVID-19, in which the most common symptom are dyspnea (shortness of breath) and hypoxemia, resulting in respiratory failure [204] (Table 1). In particular, patients could incur into Acute Respiratory Distress Syndrome (ARDS) in the case of serious hypoxemia, characterized by hyperinflammation, pulmonary damage and loss of lung tissue functions, in the presence of bilateral radiographic opacities [102] (Table 1).

The hyperactivation of immune response reported in COVID-19 patients, confirms the involvement of SARS-CoV-2 in the modulation of both innate and adaptive immunity. During infection, innate immunity is associated to lung injury, caused by an important release of pro-inflammatory cytokines (such as IL-1 α , IL-1 β , IL-4 and IL-6), that trigger the cytokine storm state [205] (Table 1).

Furthermore, most of SARS-CoV-2 positive patients were found with an important lymphopenia, similarly to SARS and MERS [206]. In particular, in a recent study it was shown that about 85% of patients with severe COVID-19 suffered of this condition [196, 207] (Table 1), which interest particularly Natural Killer (NK) and cytotoxic T cells (CTLs), which are critical in performing the antiviral activity towards the virus. Interesting, although

T cells could be increased at the onset of COVID-19, these patients tended to have low total CD8+ and CD4+ T cell counts [208]. In fact, lymphocytosis is another important feature of COVID-19 condition, especially found in patients who required Intensive Care Unit (ICU) and in those who were older than 60 years [209], where both high serum levels of pro-inflammatory cytokines and lymphocytes' count are used during hospitalization as predictors of patient survival in concomitance to ARDS condition [210, 211].

The histological analysis of lung biopsies collected from patients with ARDS revealed an extended tissue injury, also known as diffuse alveolar damage (DAD). DAD is typically characterized by an initial exudative phase with oedema, dying cells and inflammation [212] (Table 1), followed by hyperplasia, as an attempt to regenerate the alveoli, and alveolar oedema with microvascular thrombosis [213]. This condition limited oxygen exchange, since fibrin-rich exudates and fluid accumulation closed the alveoli [102] (Table 1).

The common symptoms occurring during SARS-COV-2 infection are indicated as “acute COVID-19”. A study from England identified three clusters of symptoms during acute illness [214] (Table 1):

1. **respiratory symptom cluster**, with cough, shortness of breath and fever;
2. **musculoskeletal symptom cluster**, with myalgia, headache and fatigue;
3. **enteric symptom cluster**, with abdominal pain, vomiting and diarrhea.

Nevertheless, a report conducted in Italy found that 87% of people discharged from hospitals presented persistence of at least one symptom, even at 60 days [215]. In absence of fever or features of acute illness, the commonly reported problems were fatigue (53,1%), dyspnea (43,4%), joint pain, (27,3%) and chest pain (21,7%) and other symptoms such as cough, skin rashes, palpitations, headache, and diarrhea. Patients also reported inability to do routine daily activities, in addition to mental health issues, such as anxiety, depression and post-traumatic stress disorders [216]. Another study confirmed a frequency of breathlessness and excessive fatigue, even at 3 months from hospitalization [217]. The persistence of one or more symptoms of acute COVID-19, or also appearance of new symptoms for weeks or months after the initial SARS-CoV-2 infection is called “long-COVID” or “post-COVID syndrome” [218].

The symptomatology reported during both acute and long-COVID-19 supported the hypothesis that the initial SARS-CoV-2 infection at lung level can lead to various extra-pulmonary complications [219], evolving in an atypical syndrome.

3.2. Atypical COVID-19

SARS-CoV-2 lung infection, typically associated to COVID-19 onset, has as major manifestation cytokine storm and ARDS [1], but could possibly induce extrapulmonary diseases, targeting gastrointestinal, hepatic, renal, cardiac, placental and neurological systems [219, 220]. The reflection of SARS-CoV-2 impairment in various human systems is correlated to new clues in COVID-19 patients ([221], paper attached).

ACE2 expression in enterocytes is a contributor factor to develop gastrointestinal COVID-19. Commonly, SARS-CoV-2 positive patients presented prevalence of gastrointestinal symptoms, among these anorexia, diarrhea, vomiting, abdominal pain, bleeding and diminished appetite [110] (Table 1). Moreover, SARS-CoV-2 infection in gut epithelial cells could induce dysbiosis, associated to intestinal inflammation [222] (Table 1). The gastrointestinal implication correlated to COVID-19 symptomatology can be caused by an overproduction of IL-17A during the cytokine storm. IL-17A increases neutrophil recruitment [110], causing gut damage due to this immune response ([221], paper attached). Again, also liver manifestations, particularly hepatocellular injuries, have been reported in COVID-19 patients [223] (Table 1). The alteration in hepatic functions associated to SARS-Cov-2 infection is distinguished by precisely biochemical signs, including elevated liver transaminases, high C-reactive protein (CRP), hypo-albuminemia and hyper-ferritinaemia, that reflect the acute-state of inflammation [224] (Table 1).

SARS-CoV-2 infection has been reported to cause also renal complications. Acute kidney injury (AKI) and nephropathies were associated with systemic infection, resulting in ischemia-reperfusion injury, rhabdomyolysis-associated tubular toxicity, cardiorenal syndrome (such as renal hypoperfusion, hypotension, and venous congestion) and nephrotoxic drug interactions [225] (Table 1). Further, angiopathy and disseminated intravascular coagulation induced by viral proteins lead to endothelial dysfunction and thrombosis, contributing to the pathogenesis of AKI [113, 226] (Table 1).

The manifestation of SARS-CoV-2 infection is frequently correlated to acute myocardial injury [221], with worsened outcome and increased mortality rates of COVID-19 patients [81] (Table 1). In this contest, several mechanisms have been proposed, including viral-induced myocarditis, cytokine-mediated injury, microvascular injury or myocardial infarction [227].

Moreover, microvascular endothelial cells (mECs) dysfunction reflects serious ARDS, involving changes in vascular permeability, activation of procoagulant pathways and the consequently disruption of the alveolar-capillary barrier, as previously mentioned [228]. When the endothelium is disrupted, vascular coagulative proteins interact with tissue factors,

triggering the extrinsic coagulation pathway and the cleavage of fibrinogen into fibrin [229]. The formation of fibrin thrombi is counteracted by the fibrinolysis pathway, which is inhibited by plasminogen activator inhibitor 1 (PAI1) to induced coagulation. During SARS-CoV-2 infection, the coagulation pathway is altered, inducing an increase of PAI1 expression that leads to a worse respiratory status [230]. Thus, the alveolar epithelial damage, together with an imbalance in coagulation and fibrinolysis, are specific signs of COVID-19 pathology ([221], paper attached). Caccuri et al. confirmed that SARS-CoV-2 infection in human lung microvascular ECs sustains inflammatory and vascular dysfunctions, leading to vascular detriment and leakage [231]. The same fibrotic process is responsible for the formation of fibrin thrombi, which are found in the small arterial vessels of severe COVID-19 cases [232, 233] (Table 1). Responsible of this process are the recruited neutrophils, which release neutrophil extracellular traps (NETs) to activate factor XII of coagulation cascade, producing in severe COVID-19 patients deposit of fibrin [234, 235]. SARS-CoV-2 infection can interest placenta annexes, which are characterized by a lower TMPRSS2 expression respect to other tissues (as lungs) ([221], paper attached). In fact, the co-expression of both ACE2 and TMPRSS2, needed to increase viral entry efficacy, was reported only in few placental cells and chorioamniotic membranes throughout gestation [236, 237], suggesting its possible effect on placental and transplacental sites [238] (Table 1). As a matter of fact, SARS-CoV-2 can infect the placenta, as documented by a congenital infection during the first trimester of pregnancy in fetal organs, for instance lungs and kidney [238] (Table 1), which possibly involve the expression other receptors for the virus, such as CD147 [239].

Furthermore, during pregnancy may occur a dysregulated inflammatory response to pathogens, probably due to a defective interferon response, known to have a pivotal immunomodulatory role on normal pregnancy [240]. In fact, a significant lower IFN- γ amount in the peripheral and cord blood of pregnant COVID-19-women was observed [241]. The modulation of IFN- γ levels by SARS-CoV-2 can subvert IFN- γ antiviral effect, impairing the fetal microenvironment and increasing viral susceptibility of newborns [242] (Table 1).

Moreover, during COVID-19 some patients presented symptoms that could be attributed to neurological involvement, among these headaches, confusion, and anosmia with dysgeusia [243] (Table 1). Despite the evidence that SARS-CoV-2 can alter the neurophysiological processes, are still unknown the precisely pathological mechanisms.

System / organ		Symptoms
PULMONARY		Fever, chest pain, myalgia, cough, shortness of breath, changing taste and smell (anosmia), dyspnea, hypoxemia, ARDS, release of pro-inflammatory cytokines, DAD, oedema, dying cells, hyaline membranes, inflammation, fluid accumulation
EXTRAPULMONARY (ATYPICAL COVID-19)	IMMUNE	Lymphopenia
	GASTROINTESTINAL	Anorexia, diarrhea, vomiting, abdominal pain, dysbiosis, intestinal inflammation Hepatocellular injury, elevated liver transaminases, CRP, hypo-albuminemia, hyper-ferritinaemia
	RENAL	AKI, ischemia-reperfusion injury, rhabdomyolysis-associated tubular toxicity, cardiorenal syndrome (e.g. renal hypoperfusion, hypotension and venous congestion), nephrotoxic drug interactions
	CIRCULATORY	Fibrin thrombi, microvascular endothelial cell damage
	CARDIAC	Acute myocardial injury
	PLACENTA	Placental, transplacental and congenital infection, impairing fetal microenvironment, increasing viral susceptibility of newborns
	NEUROLOGICAL	Headache, confusion, anosmia, dysgeusia

Table 1. Overview of COVID-19-associated symptoms and diseases in the pulmonary and extrapulmonary systems.



Editorial

SARS-CoV-2 Systemic Effects: New Clues

Silvia Beltrami ^{1,†}, Sabrina Rizzo ^{1,†}, Francesca Caccuri ², Roberta Rizzo ¹, Daria Bortolotti ^{1,*} and Giovanna Schiuma ^{1,‡}

¹ Department of Chemical, Pharmaceutical and Agricultural Science, University of Ferrara, 44121 Ferrara, Italy

² Department of Microbiology and Virology, “Spedali Civili”, 25126 Brescia, Italy

* Correspondence: brtdra@unife.it; Tel.: +39-0532-455398

† These authors equally contributed to this work.

‡ These authors equally contributed to this work.

To date, much discussion has been had on severe acute respiratory syndrome coronavirus 2 (SARS-CoV-2) lung infection associated with COVID-19 onset, of which the major manifestation is characterized by a “cytokine storm” [1] and acute respiratory distress syndrome (ARDS) in severely affected patients (Figure 1).

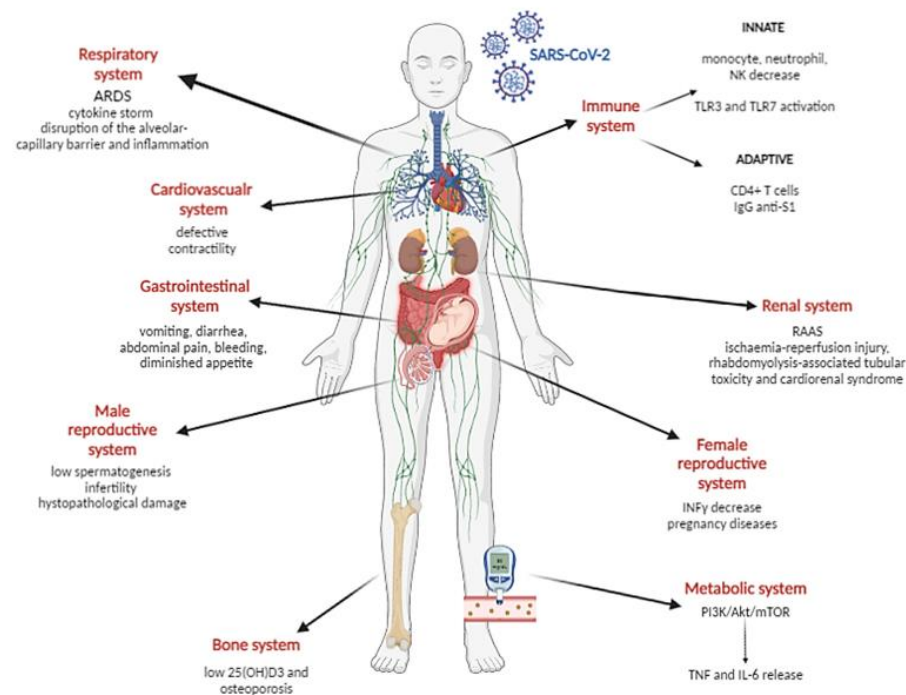


Figure 1. Schematic representation of SARS-CoV-2 infection effects on the immune (innate and adaptive), renal, metabolic, bone, gastrointestinal, cardiovascular, respiratory, bone, female and male reproductive systems.

ARDS reflects dramatic microvascular endothelial cell (mEC) dysfunction, which encompasses changes in vascular permeability, inflammation, activation of procoagulant pathways and disruption of the alveolar–capillary barrier [2,3] (Figure 1). The study conducted by Caccuri et al. confirms that the SARS-CoV-2 infection of human lung microvascular ECs (HL-mECs) sustains inflammatory and vascular dysfunction, leading to vascular detriment and leakage [4]. Having uncovered the intracellular expression of viral RNA and proteins in the absence of cytopathic effects and infectious viral progeny release,



Citation: Beltrami, S.; Rizzo, S.; Caccuri, F.; Rizzo, R.; Bortolotti, D.; Schiuma, G. SARS-CoV-2 Systemic Effects: New Clues. *Microorganisms* **2023**, *11*, 1209. <https://doi.org/10.3390/microorganisms11051209>

Received: 27 February 2023

Accepted: 7 April 2023

Published: 5 May 2023



Copyright: © 2023 by the authors. Licensee MDPI, Basel, Switzerland. This article is an open access article distributed under the terms and conditions of the Creative Commons Attribution (CC BY) license (<https://creativecommons.org/licenses/by/4.0/>).

researchers have been able to demonstrate that HL-mECs support an abortive SARS-CoV-2 replication. This occurs without the presence of ACE2 expression, which is necessary for the active replication of SARS-CoV-2 in ECs [5].

This observation is implicit of the ability of SARS-CoV-2 to employ an alternative receptor to infect HL-mECs, even though a low-level expression of ACE2 cannot be completely disregarded. Many viruses have an arginine-glycine-aspartic acid (RGD) motif on the viral envelope, recognized by integrins, that is critical in the mechanisms behind virus infection and cell internalization [6,7]. In particular, it was reported that the conserved RGD motif may be a mechanism by which SARS-CoV-2 interacts with integrins. Microarray analysis revealed that following infection, HL-mECs release many pro-inflammatory and pro-angiogenic molecules, which induces the development of an angiogenic phenotype in HL-mECs. The modification of SARS-CoV-2-infected HL-mECs to inflammatory and angiogenic responses was validated by proteome analysis, which also unveiled the expression of antiviral molecules, among which are annexin A6 and MX1.

Considering that ARDS represents one of the major causes of mortality for severe COVID-19 subjects, a therapy based on pulmonary rehabilitation (PR), known to be effective against multiple pulmonary diseases [8,9], has been exploited for COVID-19 treatments [10]. The primary benefits of PR involve the improvement of physical performance, quantified as the functional independence measurement (FIM) and 6 min walking distance (6-MWD), and the wellbeing of patients, described using the feeling thermometer (FT) parameter. However, since not all patients benefit from the PR treatment to the same extent, such as some post-COVID-19 patients, further studies are necessary to identify the reasons for this difference in response to therapy in order to develop optimized concepts within PR [11].

Although the respiratory tract represents the main site of entry for the virus, the spectrum of the clinical manifestation of SARS-CoV-2 is wide, since the primary infection could lead to important systemic effects [7].

Theoretically, SARS-CoV-2 can directly invade any organ system that expresses the ACE2 receptor, resulting in symptoms that are vague or unusual [12]. In fact, as the pandemic spread and new SARS-CoV-2 variants arose, more COVID-19 patients experienced several nonspecific or unusual extra-pulmonary symptoms involving different body systems, including systemic inflammation, hypercoagulability and renin-angiotensin-aldosterone system dysregulation (RAAS) [13]. In particular, SARS-CoV-2 infection has been described in association to renal complication, including nephropathies associated with systemic SARS-CoV-2 infection, rhabdomyolysis-associated tubular toxicity and cardiorenal syndrome (such as renal hypoperfusion, hypotension, nephrotoxic drug interactions and venous congestion) [14,15] (Figure 1). In fact, SARS-CoV-2 is able to modulate ACE2 expression in several cells of the cardiovascular system, such as cardiomyocytes, fibroblast and pericytes, triggering the neurohumoral system and resulting in defective contractibility, among other significant cardiac morbidities [16–18] (Figure 1).

In addition, another major site of extrapulmonary infection of SARS-CoV-2 is represented by the gastrointestinal tract, due to the high expression of ACE2 in enterocytes. The incipient manifestations of COVID-induced gastrointestinal (GI) problems include vomiting, diarrhea, abdominal pain, bleeding, diminished appetite or a combination of the former [19].

Another important aspect of the core of SARS-CoV-2 gastrointestinal infection is the presence of several comorbidities in patients. Diabetes mellitus is among the most frequently occurring of the major COVID-19 comorbidities [20–23], often associated to a high risk of severe prognosis [24–26]. In fact, the excessive amounts of insulin produced by diabetic patients seem to induce the PI3K/Akt/mTOR pathway, already active in COVID-19, which promotes the release of tumor necrosis factor (TNF) and interleukin-6 (IL-6) [27–29], consequently aggravating the inflammatory status already altered in COVID-19 patients [30]. Similarly to observations in pulmonary pathology, some therapeutic strategies could exploit the treatment of certain comorbidities to improve the conditions

therapies, metformin is one of the most used, consisting of an oral hypoglycemic agent inhibiting the PI3K/Akt/mTOR pathway [31–33] that causes inflammation in both diabetes mellitus and COVID-19. For this reason, the use of metformin can be considered a potential anti-inflammatory treatment to improve the prognosis of patients with both COVID-19 and diabetes [34,35].

Nevertheless, besides the several therapeutic approaches, it has been demonstrated that prevention is critical in decreasing infection rates and sequelae. Although vitamin D3 supplementation is still controversial in the prevention of infection [36,37], a meta-analysis asserted that a low serum 25-hydroxyvitamin D3 [25(OH)D3] level was associated with a higher risk of SARS-CoV-2 infection [38]. Similarly, Romero-Ibarguengoitia et al. [39] showed that individuals with 25(OH)D3 levels between 20 and 100 ng/mL and vitamin D3 supplementation have a lower rate of SARS-CoV-2 infection, reinforcing the importance of supplementation in the prevention of COVID-19.

The importance of therapies and prevention appears to be crucial in view of the ability of SARS-CoV-2 to infect a wide range of tissues and organs. Recently, even more interest has been paid to SARS-CoV-2 infection at the reproductive tract level. In particular, the male reproductive system could present peculiar clinical manifestations in response to SARS-CoV-2 infection, possibly leading to exacerbated conditions due to a stronger type I immune response, characterized by a lower CD4/CD8 T cell ratio [40]. The increased ACE2 expression, and the levels of transmembrane protease serine 2 (TMPRSS2) and cathepsins [41,42] within the testes, and the deleterious role of testosterone in the interim of infection, could impede spermatogenesis and cause male infertility [43] (Figure 1). Despite SARS-CoV-2 infection potentially resulting in testicular damage and testosterone level impairment, whether these consequences of certain severe COVID-19 cases is caused by direct SARS-CoV-2 infection, indirect inflammatory and oxidative stress, or a combination of these mechanisms, is not completely clear. The study conducted by Campos et al. suggested that testicular damage observed in severe COVID-19 cases could be partly due to a direct SARS-CoV-2 infection of testicular cells. In fact, in a study conducted in an animal model, SARS-CoV-2 RNA was detected in the testes of golden Syrian hamsters infected intranasally, which also showed signs of mild disease. Most of the viral RNA was found during the first week following infection, without any significant histopathological damage. Moreover, the hamster testes exposed to SARS-CoV-2 *ex vivo* were susceptible to infection, as demonstrated by increasing virus titers in the medium and the presence of viral RNA in the seminiferous tubules and the interstitium. In contrast, SARS-CoV-2 titers remained stable in hpSertoli cells, suggesting that these cells might support low levels of SARS-CoV-2 infection [44].

Despite the female reproductive tract expressing low ACE2 levels than testes, SARS-CoV-2 infection seriously considered within fertility clinics, as the infection has the potential to be implicated in placental annexes. Because of the peculiar tolerogenic environment needed to protect the semi-allogenic fetus from the maternal immune system attack during pregnancy, a dysregulated inflammatory response to viruses may occur, probably due to a defective interferon response known to be crucial in antiviral responses [45]. In fact, in normal pregnancy and immunocompetent physiological conditions, IFN- γ plays a pivotal immunomodulatory role [46], thus it might be supposed that SARS-CoV-2 infection could affect the pregnancy course by specifically modulating IFN- γ levels. This hypothesis is supported by Cennamo et al., who observed significantly lower IFN- γ amounts in the peripheral and cord blood of pregnant COVID-19-infected women (Figure 1), suggesting that this alteration, possibly due to SARS-CoV-2 infection as an attempt to subvert the IFN- γ antiviral effect, could affect the fetal microenvironment, increasing the viral susceptibility of newborns [47].

This evidence confirmed the importance of a correct activation of innate immune response to efficiently counteract SARS-CoV-2 and infection susceptibility. Nevertheless, the cytokine storm condition and/or immunosuppression becomes even more complicated in COVID-19 patients with a peculiar immunological status, such as pregnancy.

In fact, even if SARS-CoV-2 infection interferes with all tissues and cells previously mentioned, the immune system is perhaps one of the most involved. In particular, it has been reported that SARS-CoV-2 infection innate immune response modulation could result in both immune hyperactivation or weakening [48].

As described by several studies, many cases of COVID-19 are characterized by a decreased innate immune response, with low monocyte levels [49], high neutrophil count [50] and natural killer (NK) cell anergic status [51]. In particular, one of the first-line defenses during viral infection is represented by innate antiviral systems, such as RNA-sensors activation, which include different pattern recognition receptors (PRRs), such as RG-I and Toll-like receptors (TLRs). Rizzo et al. demonstrated that specific intracellular TLRs, TLR3 and TLR7, constitute important mediators of anti-viral response during SARS-CoV-2 infection, through the recognition of viral RNA genome. The authors used a Calu-3/MRC-5 3D in vitro lung model, and reported that, after SARS-CoV-2 infection, viral RNA genome recognition by TLR3 and TLR7 led to peculiar responses in terms of production of pro-inflammatory interleukins (ILs) and interferons (IFNs). Precisely, TLR3 engagement was involved in IFN- α and IFN- β production and the secretion of pro-inflammatory cytokines (IL-1 α , IL-1 β , IL-4, IL-6), while TLR7 activation regulates type-1 IFN, IFN γ and IFN- λ 3 expression [52] (Figure 1). This study supported the role of these pathways in COVID-19 symptomatology and suggested TLRs as a potential target for new therapies.

Moreover, besides the activation of innate antiviral systems, such as RNA sensing, the adaptive immune system also plays a central role during SARS-CoV-2 infection. Both humoral and cellular-mediated responses are active mostly against the S1 domain of the SARS-CoV-2 spike protein, with a major activation of CD4+ T cells that support antibody generation too. Antibody responses to SARS-CoV-2, specifically immunoglobulin G (IgG), are fundamental in providing protection against viral infection (Figure 1). Furthermore, the induction of virus-specific neutralizing antibodies within the airways is considered the main immune defense, following natural SARS-CoV-2 infection or vaccination [53].

As a matter of fact, a recent study indicates a direct correlation between SARS-CoV-2 neutralizing antibody titer, IgG amount and clinical COVID-19 outcomes. In particular, the study showed that in some subjects, despite having high levels of anti-S1 IgG antibodies, a re-infection may occur. This result indicates that the presence of adequate anti-S1 IgG titers, but not of relevant neutralizing antibodies, represents a possible risk factor for SARS-CoV-2 re-infection [54], supporting the importance of an adequate humoral immune response in SARS-CoV-2 infection resolution.

Conclusions

Since the occurrence of the new SARS-CoV-2 infection pandemic, more evidence reported that the virus can infect several tissues and organs due to the diffuse expression of SARS-CoV-2 receptors and new entry mechanisms exploited by new SARS-CoV-2 variants.

Nevertheless, even if the respiratory tract remains the main site of SARS-CoV-2 infection, the spectrum of SARS-CoV-2 clinical manifestation is wide [43], and COVID-19 patients experience several complications and adverse manifestation aggravated by the presence of comorbidities, such as diabetes mellitus [23].

In this view, the use of both existing therapies and prevention is crucial in decreasing infection rates.

This is also true concerning the reproductive system and particularly pregnancy, where SARS-CoV-2 can take advantage of the peculiar maternal immune system asset, affecting pregnancy outcomes and the fetal microenvironment [47]. In fact, an efficient immune activation is essential to counteract SARS-CoV-2 infection, at both innate and acquired levels. Hence, the continuous monitoring of new variants of SARS-CoV-2 and the increased knowledge of the mechanisms underlying both viral spread strategies and immune response efficiency toward the infection, are fundamental in identifying potential risk factors and developing more efficient strategies for prevention and treatment therapies.

Author Contributions: Conceptualization, D.B. and F.C.; methodology, R.R. and D.B.; writing—original draft preparation, S.B., S.R. and G.S.; writing—review and editing, R.R., D.B. and G.S.; supervision, R.R. and D.B. All authors have read and agreed to the published version of the manuscript.

Funding: This research received no external funding. It is part of a Special Issue, titled “SARS-CoV-2 Systemic Effects: New Clues” of the journal *Microorganisms*, and is led by Daria Bortolotti and Francesca Caccuri as the Guest Editors.

Institutional Review Board Statement: Not applicable.

Informed Consent Statement: Not applicable.

Acknowledgments: We are deeply thankful to all authors and reviewers who provided their contribution to this Special Issue.

Conflicts of Interest: The authors declare no conflict of interest.

References

- Kalinina, O.; Golovkin, A.; Zaikova, E.; Aquino, A.; Bezrukikh, V.; Melnik, O.; Vasilieva, E.; Karonova, T.; Kudryavtsev, I.; Shlyakhto, E. Cytokine Storm Signature in Patients with Moderate and Severe COVID-19. *Int. J. Mol. Sci.* **2022**, *23*, 8879. [[CrossRef](#)]
- Guan, W.J.; Ni, Z.Y.; Hu, Y.; Liang, W.H.; Ou, C.Q.; He, J.X.; Liu, L.; Shan, H.; Lei, C.L.; Hui, D.S.C.; et al. Clinical Characteristics of Coronavirus Disease 2019 in China. *N. Engl. J. Med.* **2020**, *382*, 1708–1720. [[CrossRef](#)] [[PubMed](#)]
- Matthay, M.A.; Zemans, R.L.; Zimmerman, G.A.; Arabi, Y.M.; Beitler, J.R.; Mercat, A.; Herridge, M.; Randolph, A.G.; Calfee, C.S. Acute respiratory distress syndrome. *Nat. Rev. Dis. Prim.* **2019**, *5*, 18. [[CrossRef](#)] [[PubMed](#)]
- Caccuri, F.; Bugatti, A.; Zani, A.; De Palma, A.; Di Silvestre, D.; Manocha, E.; Filippini, F.; Messali, S.; Chioldelli, P.; Campisi, G.; et al. SARS-CoV-2 Infection Remodels the Phenotype and Promotes Angiogenesis of Primary Human Lung Endothelial Cells. *Microorganisms* **2021**, *9*, 1438. [[CrossRef](#)]
- Nascimento Conde, J.; Schutt, W.R.; Gorbunova, E.E.; Mackow, E.R. Recombinant ACE2 Expression Is Required for SARS-CoV-2 To Infect Primary Human Endothelial Cells and Induce Inflammatory and Procoagulative Responses. *mBio* **2020**, *11*, e03185-20. [[CrossRef](#)]
- Sigrist, C.J.; Bridge, A.; Le Mercier, P. A potential role for integrins in host cell entry by SARS-CoV-2. *Antivir. Res.* **2020**, *177*, 104759. [[CrossRef](#)]
- Cao, M.; Zhang, D.; Wang, Y.; Lu, Y.; Zhu, X.; Li, Y.; Xue, H.; Lin, Y.; Zhang, M.; Sun, Y.; et al. Clinical Features of Patients Infected with the 2019 Novel Coronavirus (COVID-19) in Shanghai, China. *medRxiv* **2020**. [[CrossRef](#)]
- Spruit, M.A.; Singh, S.J.; Garvey, C.; ZuWallack, R.; Nici, L.; Rochester, C.; Hill, K.; Holland, A.E.; Lareau, S.C.; Man, W.D.; et al. An official American Thoracic Society/European Respiratory Society statement: Key concepts and advances in pulmonary rehabilitation. *Am. J. Respir. Crit. Care Med.* **2013**, *188*, e13–e64. [[CrossRef](#)]
- McCarthy, B.; Casey, D.; Devane, D.; Murphy, K.; Murphy, E.; Lacasse, Y. Pulmonary rehabilitation for chronic obstructive pulmonary disease. *Cochrane Database Syst. Rev.* **2015**, *2015*, CD003793. [[CrossRef](#)]
- Bertolucci, F.; Saggiocco, L.; Tolaini, M.; Posteraro, F. Comprehensive rehabilitation treatment for sub-acute COVID-19 patients: An observational study. *Eur. J. Phys. Rehabil. Med.* **2021**, *57*, 208–215. [[CrossRef](#)]
- Spielmanns, M.; Buelow, M.M.; Pekacka-Egli, A.M.; Cecon, M.; Spielmanns, S.; Windisch, W.; Hermann, M. Clinical and Functional Predictors of Response to a Comprehensive Pulmonary Rehabilitation in Severe Post-COVID-19 Patients. *Microorganisms* **2021**, *9*, 2452. [[CrossRef](#)] [[PubMed](#)]
- Albini, A.; Di Guardo, G.; Noonan, D.M.; Lombardo, M. The SARS-CoV-2 receptor, ACE-2, is expressed on many different cell types: Implications for ACE-inhibitor- and angiotensin II receptor blocker-based cardiovascular therapies. *Intern. Emerg. Med.* **2020**, *15*, 759–766. [[CrossRef](#)]
- Gupta, A.; Madhavan, M.V.; Sehgal, K.; Nair, N.; Mahajan, S.; Sehrawat, T.S.; Bikdeli, B.; Ahluwalia, N.; Ausiello, J.C.; Wan, E.Y.; et al. Extrapulmonary manifestations of COVID-19. *Nat. Med.* **2020**, *26*, 1017–1032. [[CrossRef](#)]
- Leshner, A.M.; Song, W.C. Review: Complement and its regulatory proteins in kidney diseases. *Nephrology* **2010**, *15*, 663–675. [[CrossRef](#)]
- Izzedine, H.; Jhaveri, K.D. Acute kidney injury in patients with COVID-19: An update on the pathophysiology. *Nephrol. Dial. Transplant.* **2021**, *36*, 224–226. [[CrossRef](#)] [[PubMed](#)]
- Nishiga, M.; Wang, D.W.; Han, Y.; Lewis, D.B.; Wu, J.C. COVID-19 and cardiovascular disease: From basic mechanisms to clinical perspectives. *Nat. Rev. Cardiol.* **2020**, *17*, 543–558. [[CrossRef](#)] [[PubMed](#)]
- Azevedo, R.B.; Botelho, B.G.; Hollanda, J.V.G.; Ferreira, L.V.L.; Junqueira de Andrade, L.Z.; Oei, S.; Mello, T.S.; Muxfeldt, E.S. COVID-19 and the cardiovascular system: A comprehensive review. *J. Hum. Hypertens.* **2021**, *35*, 4–11. [[CrossRef](#)]
- Soumya, R.S.; Unni, T.G.; Raghu, K.G. Impact of COVID-19 on the Cardiovascular System: A Review of Available Reports. *Cardiovasc. Drugs Ther.* **2021**, *35*, 411–425. [[CrossRef](#)]
- Ma, C.; Cong, Y.; Zhang, H. COVID-19 and the Digestive System. *Am. J. Gastroenterol.* **2020**, *115*, 1003–1006. [[CrossRef](#)]

20. Singh, A.K.; Gupta, R.; Ghosh, A.; Misra, A. Diabetes in COVID-19: Prevalence, pathophysiology, prognosis and practical considerations. *Diabetes Metab. Syndr.* **2020**, *14*, 303–310. [[CrossRef](#)]
21. Di Castelnuovo, A.; Bonaccio, M.; Costanzo, S.; Gialluisi, A.; Antinori, A.; Berselli, N.; Blandi, L.; Bruno, R.; Cauda, R.; Guaraldi, G.; et al. Common cardiovascular risk factors and in-hospital mortality in 3,894 patients with COVID-19: Survival analysis and machine learning-based findings from the multicentre Italian CORIST Study. *Nutr. Metab. Cardiovasc. Dis.* **2020**, *30*, 1899–1913. [[CrossRef](#)]
22. Mancusi, C.; Grassi, G.; Borghi, C.; Ferri, C.; Muiesan, M.L.; Volpe, M.; Iaccarino, G.; Group, S.-R.I. Clinical Characteristics and Outcomes of Patients with COVID-19 Infection: The Results of the SARS-RAS Study of the Italian Society of Hypertension. *High Blood Press. Cardiovasc. Prev.* **2021**, *28*, 5–11. [[CrossRef](#)]
23. Pinchera, B.; Schiano Moriello, N.; Buonomo, A.R.; Di Filippo, I.; Tanzillo, A.; Buzzo, G.; Villari, R.; Gentile, I.; Federico Li Covid, T. Diabetes and SARS-CoV-2 Infection: The Potential Role of Antidiabetic Therapy in the Evolution of COVID-19. *Microorganisms* **2023**, *11*, 145. [[CrossRef](#)]
24. Cariou, B.; Hadjadj, S.; Wargny, M.; Pichelin, M.; Al-Salameh, A.; Allix, I.; Amadou, C.; Arnault, G.; Baudoux, F.; Bauduceau, B.; et al. Phenotypic characteristics and prognosis of inpatients with COVID-19 and diabetes: The CORON-ADO study. *Diabetologia* **2020**, *63*, 1500–1515. [[CrossRef](#)]
25. Shi, Q.; Zhang, X.; Jiang, F.; Zhang, X.; Hu, N.; Bimu, C.; Feng, J.; Yan, S.; Guan, Y.; Xu, D.; et al. Clinical Characteristics and Risk Factors for Mortality of COVID-19 Patients With Diabetes in Wuhan, China: A Two-Center, Retrospective Study. *Diabetes Care* **2020**, *43*, 1382–1391. [[CrossRef](#)]
26. Singh, A.K.; Gillies, C.L.; Singh, R.; Singh, A.; Chudasama, Y.; Coles, B.; Seidu, S.; Zaccardi, F.; Davies, M.J.; Khunti, K. Prevalence of co-morbidities and their association with mortality in patients with COVID-19: A systematic review and meta-analysis. *Diabetes Obes. Metab.* **2020**, *22*, 1915–1924. [[CrossRef](#)]
27. Radtke, F.; MacDonald, H.R.; Tacchini-Cottier, F. Regulation of innate and adaptive immunity by Notch. *Nat. Rev. Immunol.* **2013**, *13*, 427–437. [[CrossRef](#)]
28. Cho, S.H.; Raybuck, A.L.; Blagih, J.; Kemboi, E.; Haase, V.H.; Jones, R.G.; Boothby, M.R. Hypoxia-inducible factors in CD4(+) T cells promote metabolism, switch cytokine secretion, and T cell help in humoral immunity. *Proc. Natl. Acad. Sci. USA* **2019**, *116*, 8975–8984. [[CrossRef](#)]
29. Pinchera, B.; Scotto, R.; Buonomo, A.R.; Zappulo, E.; Stagnaro, F.; Gallicchio, A.; Viceconte, G.; Sardanelli, A.; Mercinelli, S.; Villari, R.; et al. Diabetes and COVID-19: The potential role of mTOR. *Diabetes Res. Clin. Pract.* **2022**, *186*, 109813. [[CrossRef](#)] [[PubMed](#)]
30. Walrand, S.; Guillet, C.; Boirie, Y.; Vasson, M.P. Insulin differentially regulates monocyte and polymorphonuclear neutrophil functions in healthy young and elderly humans. *J. Clin. Endocrinol. Metab.* **2006**, *91*, 2738–2748. [[CrossRef](#)] [[PubMed](#)]
31. Pinchera, B.; Spirito, L.; Buonomo, A.R.; Foggia, M.; Carrano, R.; Salemi, F.; Schettino, E.; Papa, F.; La Rocca, R.; Crocetto, F.; et al. mTOR Inhibitor Use Is Associated With a Favorable Outcome of COVID-19 in Patients of Kidney Transplant: Results of a Retrospective Study. *Front. Med.* **2022**, *9*, 852973. [[CrossRef](#)] [[PubMed](#)]
32. Inoki, K.; Zhu, T.; Guan, K.L. TSC2 mediates cellular energy response to control cell growth and survival. *Cell* **2003**, *115*, 577–590. [[CrossRef](#)] [[PubMed](#)]
33. Musi, N.; Hirshman, M.F.; Nygren, J.; Svanfeldt, M.; Bavenholm, P.; Rooyackers, O.; Zhou, G.; Williamson, J.M.; Ljunqvist, O.; Efendic, S.; et al. Metformin increases AMP-activated protein kinase activity in skeletal muscle of subjects with type 2 diabetes. *Diabetes* **2002**, *51*, 2074–2081. [[CrossRef](#)]
34. Hariyanto, T.I.; Kurniawan, A. Metformin use is associated with reduced mortality rate from coronavirus disease 2019 (COVID-19) infection. *Obes. Med.* **2020**, *19*, 100290. [[CrossRef](#)]
35. Isoda, K.; Young, J.L.; Zirluk, A.; MacFarlane, L.A.; Tsuboi, N.; Gerdes, N.; Schonbeck, U.; Libby, P. Metformin inhibits proinflammatory responses and nuclear factor-kappaB in human vascular wall cells. *Arterioscler. Thromb. Vasc. Biol.* **2006**, *26*, 611–617. [[CrossRef](#)]
36. Griffin, G.; Hewison, M.; Hopkin, J.; Kenny, R.A.; Quinton, R.; Rhodes, J.; Subramanian, S.; Thickett, D. Perspective: Vitamin D supplementation prevents rickets and acute respiratory infections when given as daily maintenance but not as intermittent bolus: Implications for COVID-19. *Clin. Med.* **2021**, *21*, e144–e149. [[CrossRef](#)]
37. Bassatne, A.; Basbous, M.; Chakhtoura, M.; El Zein, O.; Rahme, M.; El-Hajj Fuleihan, G. The link between COVID-19 and Vitamin D (VIVID): A systematic review and meta-analysis. *Metabolism* **2021**, *119*, 154753. [[CrossRef](#)]
38. Teshome, A.; Adane, A.; Girma, B.; Mekonnen, Z.A. The Impact of Vitamin D Level on COVID-19 Infection: Systematic Review and Meta-Analysis. *Front. Public Health* **2021**, *9*, 624559. [[CrossRef](#)]
39. Romero-Ibarguengoitia, M.E.; Gutiérrez-González, D.; Cantú-López, C.; Sanz-Sánchez, M.Á.; González-Cantú, A. Effect of Vitamin D3 Supplementation vs. Dietary-Hygienic Measures on SARS-CoV-2 Infection Rates in Hospital Workers with 25-Hydroxyvitamin D3 [25(OH)D3] Levels ≥ 20 ng/mL. *Microorganisms* **2023**, *11*, 282. [[CrossRef](#)]
40. Al-Kuraishy, H.M.; Al-Gareeb, A.I.; Faidah, H.; Al-Maiah, T.J.; Cruz-Martins, N.; Batiha, G.E. The Looming Effects of Estrogen in COVID-19: A Rocky Rollout. *Front. Nutr.* **2021**, *8*, 649128. [[CrossRef](#)] [[PubMed](#)]
41. Qi, J.; Zhou, Y.; Hua, J.; Zhang, L.; Bian, J.; Liu, B.; Zhao, Z.; Jin, S. The scRNA-seq Expression Profiling of the Receptor ACE2 and the Cellular Protease TMPRSS2 Reveals Human Organs Susceptible to SARS-CoV-2 Infection. *Int. J. Environ. Res. Public Health* **2021**, *18*, 284. [[CrossRef](#)] [[PubMed](#)]

42. Gye, M.C.; Kim, S.T. Expression of cathepsin L in human testis under diverse infertility conditions. *Arch. Androl.* **2004**, *50*, 187–191. [[CrossRef](#)]
43. Louis, T.J.; Qasem, A.; Abdelli, L.S.; Naser, S.A. Extra-Pulmonary Complications in SARS-CoV-2 Infection: A Comprehensive Multi Organ-System Review. *Microorganisms* **2022**, *10*, 153. [[CrossRef](#)] [[PubMed](#)]
44. Campos, R.K.; Camargos, V.N.; Azar, S.R.; Haines, C.A.; Eyzaguirre, E.J.; Rossi, S.L. SARS-CoV-2 Infects Hamster Testes. *Microorganisms* **2021**, *9*, 1318. [[CrossRef](#)] [[PubMed](#)]
45. Hadjadj, J.; Yatim, N.; Barnabei, L.; Corneau, A.; Boussier, J.; Smith, N.; Pere, H.; Charbit, B.; Bondet, V.; Chenevier-Gobeaux, C.; et al. Impaired type I interferon activity and inflammatory responses in severe COVID-19 patients. *Science* **2020**, *369*, 718–724. [[CrossRef](#)] [[PubMed](#)]
46. Murphy, S.P.; Tayade, C.; Ashkar, A.A.; Hatta, K.; Zhang, J.; Croy, B.A. Interferon gamma in successful pregnancies. *Biol. Reprod.* **2009**, *80*, 848–859. [[CrossRef](#)]
47. Cennamo, M.; La Civita, E.; Sarno, L.; Carbone, G.; Di Somma, S.; Cabaro, S.; Troisi, J.; Sirico, A.; Improda, F.P.; Guida, M.; et al. Low Interferon-gamma Levels in Cord and Peripheral Blood of Pregnant Women Infected with SARS-CoV-2. *Microorganisms* **2023**, *11*, 223. [[CrossRef](#)]
48. Schiuma, G.; Beltrami, S.; Bortolotti, D.; Rizzo, S.; Rizzo, R. Innate Immune Response in SARS-CoV-2 Infection. *Microorganisms* **2022**, *10*, 501. [[CrossRef](#)]
49. Rajamanickam, A.; Kumar, N.P.; Pandiarajan, A.N.; Selvaraj, N.; Munisankar, S.; Renji, R.M.; Venkatramani, V.; Murhekar, M.; Thangaraj, J.W.V.; Kumar, M.S.; et al. Dynamic alterations in monocyte numbers, subset frequencies and activation markers in acute and convalescent COVID-19 individuals. *Sci. Rep.* **2021**, *11*, 20254. [[CrossRef](#)]
50. Meizlish, M.L.; Pine, A.B.; Bishai, J.D.; Goshua, G.; Nadelmann, E.R.; Simonov, M.; Chang, C.H.; Zhang, H.; Shallow, M.; Bahel, P.; et al. A neutrophil activation signature predicts critical illness and mortality in COVID-19. *Blood Adv.* **2021**, *5*, 1164–1177. [[CrossRef](#)]
51. Bortolotti, D.; Gentili, V.; Rizzo, S.; Rotola, A.; Rizzo, R. SARS-CoV-2 Spike 1 Protein Controls Natural Killer Cell Activation via the HLA-E/NKG2A Pathway. *Cells* **2020**, *9*, 1975. [[CrossRef](#)] [[PubMed](#)]
52. Bortolotti, D.; Gentili, V.; Rizzo, S.; Schiuma, G.; Beltrami, S.; Strazzabosco, G.; Fernandez, M.; Caccuri, F.; Caruso, A.; Rizzo, R. TLR3 and TLR7 RNA Sensor Activation during SARS-CoV-2 Infection. *Microorganisms* **2021**, *9*, 1820. [[CrossRef](#)] [[PubMed](#)]
53. Moss, P. The T cell immune response against SARS-CoV-2. *Nat. Immunol.* **2022**, *23*, 186–193. [[CrossRef](#)] [[PubMed](#)]
54. Hocher, B.; Schonbrunn, A.; Chen, X.; Kramer, B.K.; von Baehr, V. Outliers Matter—Correlation between S1 IgG SARS-CoV-2 Antibodies and Neutralizing SARS-CoV-2 Antibodies. *Microorganisms* **2022**, *10*, 2067. [[CrossRef](#)]

Disclaimer/Publisher’s Note: The statements, opinions and data contained in all publications are solely those of the individual author(s) and contributor(s) and not of MDPI and/or the editor(s). MDPI and/or the editor(s) disclaim responsibility for any injury to people or property resulting from any ideas, methods, instructions or products referred to in the content.

3.3 COVID-19 diagnosis and risk factors

The presence of any of the symptoms mentioned before is functional in the diagnosis of SARS-CoV-2 infection. Molecular detection of viral nucleic acid represents the diagnostic gold standard, based on the use of commercially available detection kits targeting ORF1b, N, E or S viral proteins [244]. The presence of SARS-CoV-2 is evaluated in a variety of respiratory samples, including throat swabs, posterior oropharyngeal saliva, nasopharyngeal swabs, sputum and bronchial fluid [198]. Viral nucleic acid can be also found in specimens from the intestinal tract or blood, even when respiratory samples were negative. There are also several serological tests available, able to detect antibodies to N or S protein [245], mainly used to confirm a contact with the virus and to assess the response to the therapy.

During the spread of SARS-CoV-2 pandemic, a different predisposition to infection and to the develop of severe COVID-19 among the patients was observed. To explain this

condition, different studies have evaluated the possible risk factors associated to increased infection susceptibility, including increased age, gender, genetic predispositions and comorbidity are the mains, which are discussed below.

Age

The population appears to be susceptible to SARS-CoV-2 infection at any age, with a median age of infection of about 50 years [188, 196]. Clinical signs, however, change with age: generally, men over 60 years with co-morbidities are more likely to develop serious respiratory illness and to need hospitalization, while most young adults and children have only mild diseases, or are asymptomatic [246].

Gender

Referring to gender, males appeared to be more frequent among deceased patients [247]. Possible reason of male predominance among COVID-19 patients may be due to the exposure, lifestyle factors (as smoking) [248], immune system regulation drive by sexual hormones, or gender differences in Renin-Angiotensin-Aldosterone System regulation [249, 250]. Also, they might be different in ACE2 expression within chromosomal and in testicular tissues [50, 251].

Instead, female present more susceptibility to SARS-CoV-2 infection during pregnancy, with higher risk to develop severe illness when contract virus [81].

Comorbidities

Comorbidities as hypertension, cardiovascular diseases (heart failure or cardiac arrhythmia), diabetes, kidney failure, chronic pulmonary disease and cancer emerged as the most common among SARS-CoV-2-positive patients [252]. In subjects with COVID-19, one of the most frequent comorbidity is represented by diabetes mellitus [253], which is often associated to a high risk of severe prognosis [254]. In fact, the PI3K/Akt/mTOR pathway, which is already active in COVID-19, appears to be induced by the excessive levels of insulin, produced by diabetic individuals. This condition encourages the production of TNF, and IL-6 [255].

In addition, obesity predisposes to the development of chronic diseases, also constituting an independent risk factor. In fact, the body mass index (BMI) is significantly higher among severe COVID-19 patients [256]. Thus, the role of these comorbidities in viral susceptibility is characterized by their increased or decreased in ACE2 expression, as well as a shift in ACE/ACE2 balance, or in cytokine overstimulation [257].

Genetics

Genetic predispositions might be a factor to develop severe COVID-19. Many studies have hypothesized whether ACE2 expression and polymorphism, and serum ACE2 levels, could explain why some people are more inclined to a severe phenotype, while others remain asymptomatic [258]. The different residues in the ACE2 protein can affect how it binds to the SARS-CoV-2 Spike protein, which could explain the different symptoms during COVID-19 [80]. This is confirmed by the presence of specific variants among the populations, that could affect SARS-CoV-2 binding [259, 260].

Concerning the predisposition of population to infection, ACE2 expression in the lungs have been suggested to increase with age [81], providing an explanation for the higher disease severity observed in critically older COVID-19 patients (especially males) [261]. In fact, several clinical reports suggested that male sex, combined with increasing age, pre-existing comorbidities and no healthy lifestyle represent risk factors for a difficult infection outcome [262]. Also, it has been reported that COVID-19 is highly frequent in subjects affected by AKI, which are major in western population, due to a higher expression of ACE2 in podocytes, compared to the Asian population [113].

Furthermore, polymorphism and genetic variants also interest TMPRSS2, that might influence the severity of COVID-19 [263]. Identification of a genomic variability in TMPRSS2, that in turn affects its expression, suggests that European and American populations could be more susceptible to SARS-CoV-2 infection, due to their higher expression of the protease [264].

4. Pharmacological treatments and vaccination

The spread of SARS-CoV-2 pandemic all over the world induced the need of the discovery and development of specific COVID-19 treatments, based on the evaluation of the different pathological stages of the disease. In particular, during the early stages of SARS-CoV-2 infection antiviral agents could be used to prevent its progression, but in case of late COVID-19, the therapy is mainly based on immunomodulatory drugs [265]. These types of pharmacological therapies have the common aim to block the development of infection into critical forms, avoiding the ICU with invasive procedures (such as intubation).

Among the category of therapies proposed for COVID-19 treatment, most are represented by drugs that interfere with the entry phase of the virus into host cells, inhibiting the first phase of its replication. To this class belong Chloroquine and Hydroxychloroquine, identified immediately as a potential drugs able to interfere with the entry of SARS-CoV-2

[206] (Figure 11). They were used to prevent and cure autoimmune diseases, as rheumatoid arthritis and systemic lupus erythematosus, as well as malaria [266]. The role of these molecules in counteract viral entry was first observed *in-vitro*, showing an inhibitory effect on SARS-CoV-2 mRNA production [267]. Among the viral-entry inhibitory drugs there is also Umifenovir, which targets the interaction between the S protein and ACE2 receptor, to inhibit membrane fusion (Figure 11). Furthermore, Camostat mesylate was evaluated as pharmacological treatment that can prevent SARS-CoV-2 from entering lung cells, by blocking TMPRSS2 [268] (Figure 11).

Beside the use of drugs against viral entry, another strategy employs molecules able to inhibit SARS-CoV-2 replication. In particular, replication inhibitors include Lopinavir, Ritonavir and Remdesivir [206]. Lopinavir, as well as Ritonavir, is commonly used as inhibitor for Human Immunodeficiency Virus-type 1 (HIV-1) protease, altering the maturation of HIV-1 and its infectivity [269]. Thus, Lopinavir and Ritonavir are usually administered in combination to enhance the bioavailability of the first, inhibiting its metabolic inactivation [270], increasing their antiviral effect [271]. Lopinavir and Ritonavir have been already reported to show *in-vitro* inhibitory activity against SARS-CoV and MERS-CoV [272], due to their role in reducing 3CL^{pro} activity [273] (Figure 11) and these suggests their use in case of COVID-19 patients with less severe symptoms, in the early stages of disease, resulting in a lower rate of ARDS or mortality [270, 274].

Otherwise, Ribavirin is a guanosine analog that acts as a chain terminator, inhibiting RNA polymerase, already used to treat patients with chronic hepatitis C, in combination with interferons [275] (Figure 11). The use of Ribavirin, with the addition of corticosteroids, was observed to resolute the main symptoms within few weeks by infection, in patients with SARS-CoV-2 pneumonia [276].

Another drug belonging to the class of nucleotide analogues that interferes with viral replication is Remdesivir, an adenosine analog previously used during the Ebola epidemic in Africa [265] that targets the viral RdRp complex, interfering with the synthesis of new RNAs (Figure 11), resulted to be effective in the treatment of moderate and severe COVID-19 [206]. A study conducted by Beigel et al. suggest that early treatment with Remdesivir could prevent lung disease progression and mechanical ventilation needing [277].

The treatment of COVID-19 pathogenesis exploits the fact that SARS-CoV-2 triggers a strong immune response, which is the cause of cytokine storm. An altered inflammatory response and, in some individuals, an aberrant release of pro-inflammatory cytokines, including IL-6, INF- γ and TNF- α , are associated to a significant damage induced by the virus [278]. Hence, immunomodulatory drugs, which are mostly used in rheumatology to decrease

the pathology-associated inflammatory response, may be a supplemental suitable treatment for COVID-19. In fact, the use of corticosteroid, particularly dexamethasone, was often observed in the case of serious SARS-CoV-2 infection, to inhibit the secretion of inflammatory cytokines [279] (Figure 11).

The modulation of immune hyperactivation due to COVID-19 condition also exploits the administration of monoclonal antibodies, such as Tocilizumab and Anakinra, which are the most used [280]. The first is a monoclonal antibody that binds IL-6 receptor in a specific manner, previously used to prevent and treat various types of arthritis and correlated cytokine release [281] (Figure 11). Due to its effect in attenuating cytokine production, it was showed to be effective in the treatment of severe COVID-19. In a study conducted in Bologna and Reggio Emilia, between February and March 2020, was observed that both intravenous and subcutaneous administration of Tocilizumab reduced the risk of invasive mechanical ventilation or death, in severe patients [282]. In the resolution of ARDS condition, it can be also used Anakinra, a monoclonal antibody able to inhibit the effect of proinflammatory IL-1 α and IL-1 β , acting as their receptor antagonist [280] (Figure 11). Alternatively, other potential treatment approaches consist in the use of soluble recombinant human ACE2 and monoclonal antibodies or fusion inhibitors that target Spike protein [283, 284].

The potential effectiveness of type-I IFNs in the early treatment of COVID-19 was supported by *in vitro* data, that showed how SARS-CoV-2 is sensitive to the molecule. The inhalation of IFN- α vapor is already used in China, as COVID-19 treatment guideline [91].

Moreover, the immune response against SARS-CoV-2 might be mitigate by immunotherapies based on inflammatory cytokine neutralization, reducing inflammation associated to lung damage.

Convalescent plasma treatment is proper in this contest. It consist in a biological preparation containing polyclonal antibodies collected from recovered COVID-19 patients [285], used to induce a passive immunization in non-responder severe patients. Again, also intravenous immunoglobulin (IVIG) is used. IVIG is a liquid composition that can rapidly increase immunoglobulin G (IgGs) levels in the blood, directly neutralizing exogenous antigens [286]. It is preferable extract IgGs by patients from the same city or area because lifestyle, diet and the environment are implicated in the development of specific antibodies. A study supports the effect of immunoglobulin therapy, demonstrating that the early application of high-dose IVIG can improve the prognosis of severe COVID-19 patients [287].

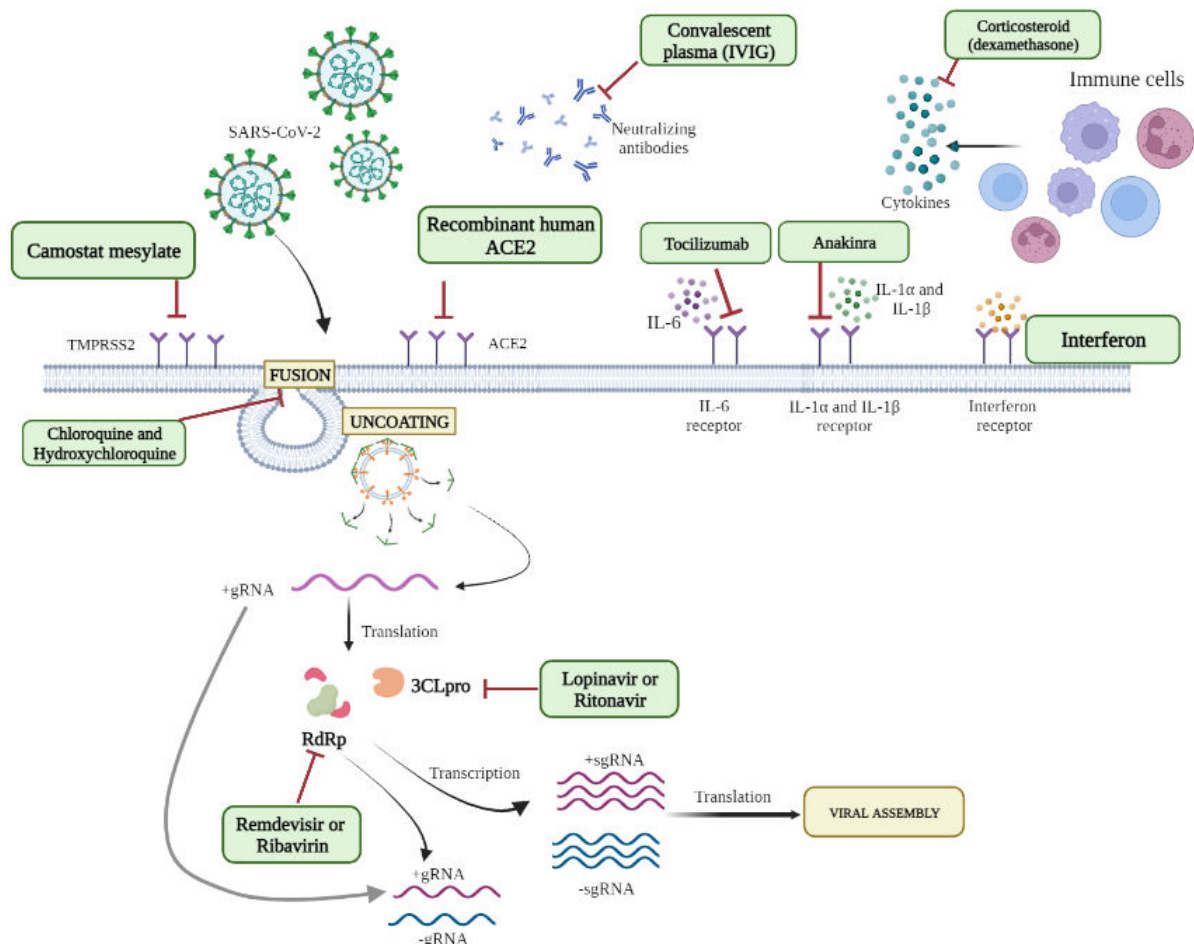


Figure 11. SARS-CoV-2 therapeutic targets in severe COVID-19 therapy. On left side drugs that interfere with viral entry and replication, on the right-side immunomodulatory therapies with monoclonal antibodies and corticosteroids.

In addition to the necessity of reducing SARS-CoV-2 transmission and pathogenesis by pharmacological and non-pharmacological measures, including the use of masks and social isolation, a variety of vaccinations have been developed [288]. The initial success of COVID-19 vaccination lowered the probability of SARS-CoV-2 infection, as well as the severity of symptoms, due to the increase of the adaptive immunity activation. Currently, S protein is the major target for vaccine development, but RBD is also the primary target of the neutralizing antibodies, elicited by natural infection or vaccination [289].

The available vaccines are included in several classes, based on their production and mechanism of action, and can be summarized in [290]:

- non-replicating viral vector vaccine;
- DNA vaccine;
- mRNA vaccine;
- protein-subunit based vaccine.

The non-replicating viral vector vaccines induce a strong immune response enhancing both humoral and cellular immunity, and previously had been used against Spike proteins of MERS-CoV [291]. Non-replicating viral vectored vaccines candidates against SARS-CoV-2 are based on adenoviruses, which contain the codifying-sequence of S protein. This comports a specific limitation, due to the easily exposition of subjects to the vector virus and the development of adenoviral immunity, which quickly immunized them after the first dose of vaccine. Zhu et al. demonstrated that the candidate non-replicating adenovirus type-5 (Ad5)-vectored COVID-19 vaccine is effective and safe [292]. Among the non-replicating SARS-CoV-2 vaccines, AstraZeneca, Johnson&Johnson and Sputnik V were being mass-produced by relevant companies, and they are currently used in the vaccination campaign in many countries [290].

DNA-based COVID-19 vaccine consists in insert genes into DNA plasmids as a vector inject through electroporation into host cells, to encode a specific viral antigen [293]. Then, the expressed antigen is presented by antigen-presenting cells (APCs), as lymphocytes B, macrophages, and dendritic cells, to be recognized by adaptive immune system. The advantages of these vaccines are the non-infectiveness, the easy production in a short time, and the cost-effectiveness and stability [290]. In addition, one of the benefits of DNA vaccines is the greater thermal stability, compared to mRNA vaccines. An example of SARS-CoV-2 DNA-based vaccine is INO-4800, which consists of a plasmid containing a N-terminal IgE leader sequence and the sequence of SARS-CoV-2 S protein, produced in guinea pigs [294].

mRNA-based vaccines were the mostly used during vaccination campaign. They contain mRNA molecules that, after their injection will be translated into the target protein into the host cell cytoplasm [290]. As described for DNA-based vaccines, also RNA-based vaccines have the aim to encode for viral antigens that will be presented to adaptive immune cells.

Unfortunately, mRNA vaccines are instable and one way to overcome this problem is to place mRNA inside lipid nanoparticles, which act in the same time as delivery carrier and adjuvants [295]. Thus, SARS-CoV-2 S protein mRNA is included in a lipid nanoparticle and injected intramuscularly, to allow the mRNA content to reach the cell cytoplasm, where the viral protein is synthetized in the ribosomes [290]. Then, the S protein achieves the cellular membrane, loaded on the Major Histocompatibility Complex (MHC)-I and -II, [296] to activate immune cells, especially T-helper (Th) cells. The induction of Th cells is fundamental to synthetized cytokines, such as IL-2, IL-4 and IL-5 and to induce the differentiation of B-cells into antibody-producing plasma-cells and to stimulate memory T cells proliferation [296]. To provide fast protective immunity, IgM antibodies are produced

early in the humoral immune response after vaccination. Following this, IgG antibodies, with high affinity for S protein, are released to confer immunological memory into immunized subjects [296, 297].

mRNA-based vaccines showed some advantages over other vaccines: a) there is no risk of infection during vaccination, b) examination of mouse models has shown that repeated immunizations with mRNA-vaccines are associated with long-term immunity, and c) there is no possibility of insertional mutations in them [298]. COVID-19 mRNA vaccines currently available are Moderna/NIAID and Pfizer/BioNTech, that contains mRNA-1273 and BNT162b2 molecules, respectively. mRNA-1273 of Moderna vaccine encodes the S2-portion, while BNT162b2 of Pfizer encode the membrane-anchored full-length S-protein and the secreted RBD (BNT162b1) of SARS-CoV-2. Both Moderna/NIAID and Pfizer/BioNTech vaccines require booster doses, to ensure high antibody titration and long-term safety [299].

In addition, also protein-based vaccines against SARS-CoV-2 have been designed. Peptides, like RNAs, are usually unstable and are therefore located within nanoparticles adsorbed into adjuvants [290]. Among these candidates, the NVX-CoV2373 by Novavax has gone through various phases of clinical trial. This vaccine contains a recombinant full-length S protein, that has been engineered to resist against proteolytic degradation, and present a high binding to ACE2. Protein-based vaccines present several advantages, such as safety and cost effectiveness, but the needing of adjuvants (to produce a long-term immune response) is an important limitation [300].

The widespread use of the different kinds of available vaccines in the population resulted to be the most successful strategy in controlling the spread of SARS-CoV-2 and COVID-19 outcome.

5. Methods and results

5.1. Evaluation of SARS-CoV-2 infection effect on host immune system

Both innate and adaptive immune systems play a crucial role in the protection against SARS-CoV-2 infection.

Host innate immune response is the first to be activated to control viral infections and serves four main purposes [301]:

- a) restriction of viral replication within infected cells,
- b) creation of an antiviral state in the local tissue environment, including recruitment of effector cells,
- c) soliciting the adaptive immune response,
- d) protect the host from potential dangerous non-self antigens.

Innate immunity is fundamental to activate rapid and non-specific response against pathogens. During a viral infection, host innate immunity represents the first line of defense, in which participate macrophages, monocytes, dendritic cells, neutrophils and natural killer (NK) cells [302]. These effectors have a central role in the activation of adaptive immune response, which in turn is essential for the development of immunological memory [303].

During SARS-CoV-2 infection, viral recognition by lung-resident immune cells provides a local immune response, resulting in the recruitment of neutrophils from the blood, which drive hyperinflammation [172]. Together with monocytes, macrophages, and NK cells [302].

The activation of those immune effectors is triggered by SARS-CoV-2 structural components, identified by immune system cells as “non self”, such as the viral genome [302].

This sensing process involves a complex system of receptors, named Pattern Recognition Receptors (PRRs) expressed by host cells, that recognize pathogen-associated molecular patterns (PAMPs) or damage-associated molecular patterns (DAMPs), to induce inflammatory pathways with the aim to control the infection [304].

The PRRs system comprises several surface and intracellular receptors, including Toll-like receptors (TLRs), C-type lectin receptors (CLRs), nucleotide-binding oligomerization domain (NOD)-like receptors, retinoic acid-inducible gene-I (RIG-I)-like receptors (RLRs), and a group of intracellular DNA sensors, such as cyclic GMP-AMP synthase (cGAS) and IFN γ -inducible protein [305, 306].

Focusing on RNA virus sensing, including SARS-CoV-2, their RNA genome induces the activation of two main RNA sensing systems able to recognize viral RNAs: the cytosolic RLRs system, composed by cytoplasmatic RNA helicases, which include the melanoma differentiation-associated protein 5 (MDA5) and the retinoic acid-inducible gene-I protein (RIG-I) [307, 308], and endosome-associated TLRs, that are TLR3, TLR7 and TLR8 [309] (Figure 12).

The interaction between viral RNA genomes and these PRRs triggers an intracellular signaling cascade which induces cytokine and interferon production and expression of IFN-stimulated genes (ISGs) [310] (Figure 12).

Among the main transcriptional factors involved in the instauration of the antiviral status associated to RNA sensing systems, Interferon Regulatory transcription Factor 3 (IRF3) and Nuclear Factor kappa-light-chain-enhancer of activated B-cells (NF- κ B) are the most studied.

In particular, IRF3 is involved in the regulation of interferon expression, while NF- κ B is mainly employed in the induction of proinflammatory response [311] (Figure 12).

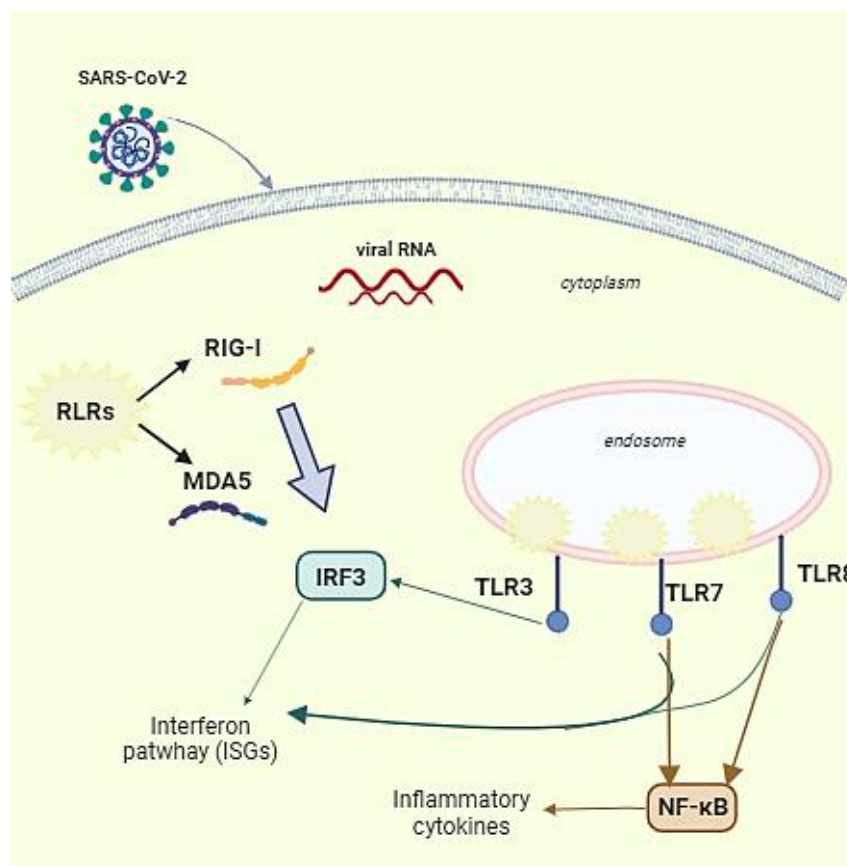


Figure 12. Schematic representation of TLR and RLR pathways. TLR3, TLR7 and TLR8 are typically localized into endocytic compartments, in particular TLR3 activate IRF3 to stimulate IFN pathway. TLR7 and TLR8 trigger inflammatory cytokine secretion via NF- κ B, and directly the IFN pathway [311].

In particular, the potential role of endosomal TLRs in COVID-19 disease was demonstrated by Conti et al., that correlated the activation of TLRs to the overproduction of pro-inflammatory cytokines observed during the infection [312]. Interestingly, it has been reported \ the existence of genetic defective variants of these TLRs have been linked to a less effective IFN-I and IFN-II response [313, 314].

Given the importance of TLRs sensing in SARS-CoV-2 antiviral response, we further investigate the involvement of TLRs activation in SARS-CoV-2 sensing ([315], paper attached). We confirmed the activation of both TLR3 and TLR7 during SARS-CoV-2 infection, which follows a peculiar order. Firstly, TLR3 is activated during the early phase of infection, triggering IRF3 phosphorylation and consequent IFN- α and IFN- β expression. Then, NF κ B pathway is induced, leading to pro-inflammatory cytokine secretion (IL-1 α , IL-1 β , IL-4, IL-6). Later, also TLR7 participates in the signaling, inducing IFN-I, IFN- γ and IFN- λ 3 expression, via NF κ B ([315], paper attached).

This peculiar time-dependent activation observed for TLR3 and TLR7, characterized by an early induction of a pro-inflammatory environment, could represent a key step in the setting of cytokine storm condition reported in COVID-19, suggesting TLRs as a potential therapeutic target.



Article

TLR3 and TLR7 RNA Sensor Activation during SARS-CoV-2 Infection

Daria Bortolotti ^{1,†}, Valentina Gentili ^{1,†}, Sabrina Rizzo ¹, Giovanna Schiuma ¹, Silvia Beltrami ¹, Giovanni Strazzabosco ¹, Mercedes Fernandez ¹, Francesca Caccuri ², Arnaldo Caruso ² and Roberta Rizzo ^{1,3,*}

¹ Department of Chemical, Pharmaceutical and Agricultural Science, University of Ferrara, 44121 Ferrara, Italy; daria.bortolotti@unife.it (D.B.); valentina.gentili@unife.it (V.G.); sabrina.rizzo@unife.it (S.R.); giovanna.schiума@unife.it (G.S.); silvia.beltrami@unife.it (S.B.); giovanni.strazzabosco@unife.it (G.S.); mercedes.fernandez@unife.it (M.F.)

² Department of Microbiology and Virology, "Spedali Civili," 25126 Brescia, Italy; francesca.caccuri@unibs.it (F.C.); arnaldo.caruso@unibs.it (A.C.)

³ LTTA, University of Ferrara, 44121 Ferrara, Italy

* Correspondence: rbr@unife.it; Tel.: +39-0532-455382

† These authors contributed equally to this work.



Citation: Bortolotti, D.; Gentili, V.; Rizzo, S.; Schiuma, G.; Beltrami, S.; Strazzabosco, G.; Fernandez, M.; Caccuri, F.; Caruso, A.; Rizzo, R. TLR3 and TLR7 RNA Sensor Activation during SARS-CoV-2 Infection. *Microorganisms* **2021**, *9*, 1820. <https://doi.org/10.3390/microorganisms9091820>

Academic Editor: Andrea Marzi

Received: 23 July 2021

Accepted: 23 August 2021

Published: 26 August 2021

Publisher's Note: MDPI stays neutral with regard to jurisdictional claims in published maps and institutional affiliations.



Copyright: © 2021 by the authors. Licensee MDPI, Basel, Switzerland. This article is an open access article distributed under the terms and conditions of the Creative Commons Attribution (CC BY) license (<https://creativecommons.org/licenses/by/4.0/>).

Abstract: (1) Background: Acute respiratory syndrome coronavirus 2 (SARS-CoV-2) is the etiological agent for the coronavirus disease (COVID-19) that has led to a pandemic that began in March 2020. The role of the SARS-CoV-2 components on innate and adaptive immunity is still unknown. We investigated the possible implication of pathogen-associated molecular patterns (PAMPs)–pattern recognition receptors (PRRs) interaction. (2) Methods: We infected Calu-3/MRC-5 multicellular spheroids (MTCs) with a SARS-CoV-2 clinical strain and evaluated the activation of RNA sensors, transcription factors, and cytokines/interferons (IFN) secretion, by quantitative real-time PCR, immunofluorescence, and ELISA. (3) Results: Our results showed that the SARS-CoV-2 infection of Calu-3/MRC-5 multicellular spheroids induced the activation of the TLR3 and TLR7 RNA sensor pathways. In particular, TLR3 might act via IRF3, producing interleukin (IL)-1 α , IL-1 β , IL-4, IL-6, and IFN- α and IFN- β , during the first 24 h post-infection. Then, TLR3 activates the NF κ B transduction pathway, leading to pro-inflammatory cytokine secretion. Conversely, TLR7 seems to mainly act via NF κ B, inducing type 1 IFN, IFN- γ , and IFN- λ 3, starting from the 48 h post-infection. (4) Conclusion: We showed that both TLR3 and TLR7 are involved in the control of innate immunity during lung SARS-CoV-2 infection. The activation of TLRs induced pro-inflammatory cytokines, such as IL-1 α , IL-1 β , IL-4, and IL-6, as well as interferons. TLRs could be a potential target in controlling the infection in the early stages of the disease.

Keywords: SARS-CoV-2; TLR; RNA sensors

1. Introduction

SARS-CoV-2 is a new strain of the positive ssRNA coronavirus family, the cause of the coronavirus disease (COVID-19), which shares high homology with the previous severe disease-associated coronaviruses MERS (Middle East respiratory syndrome) and SARS (severe acute respiratory syndrome). The SARS-CoV-2 outbreak emerged firstly in Wuhan in December 2019, and then rapidly spread worldwide, becoming a pandemic in January 2020 [1–3].

As reported by different published works, COVID-19 is associated with a peculiar clinical case history, characterized by an inefficient immune system response and high levels of inflammatory cytokines, known as “cytokine storm”, including IL-1, IL-6, IL-4, IL-10, and INF- γ [4]. In particular, the presence of high serum levels of these cytokines has been associated with severe COVID-19 [5], reported to be possibly associated with the increased expression of angiotensin converting enzyme 2 (ACE2), which is the cellular

receptor bound by SARS-CoV-2 spike (S) protein. The ACE2 receptor is essential for viral entry into the target cells [6]. Simultaneously, the interaction between ACE2 and SARS-CoV-2 increases the secretion of soluble ACE2 in the blood and urine [7], leading to the release of a massive quantity of cytokines (cytokine storm), which includes the production of IL-6 by macrophages [8,9]. This condition is related to severe lymphocytopenia [10], hypercoagulation [11], increased mortality [12], and a poor clinical follow-up [13]. The typical inflammatory environment triggered by SARS-CoV-2 infection is the result of the initial recruitment of the innate immune response, which represents the first line of protection against pathogens and that, in turn, stimulates acquired immunity activation [14].

For this reason, to achieve efficient control of the infection, it is crucial that the host immune response is balanced, in order to avoid both excessive inflammation that could damage the host system, as observed in COVID-19 patients' lungs, and low activation of the immune system, which could facilitate viral spread [15,16].

During a viral infection, both the infected cells and the innate immune system are aware of the presence of an infection, by the recognition of specific pathogen portions, called "pathogen-associated molecular patterns" (PAMPs), which are recognized by specific pattern recognition receptors (PRRs) [17]. The PAMPs-PRRs interaction leads to an intracellular signaling cascade that is essential for both the antiviral activity by interferons production, and immune system activation by cytokine secretion [17]. The PRRs family includes different components that are involved in the sensing of RNA virus infections, such as RIG-I-like receptors (RLRs), e.g., RIG-I and MDA5, and Toll-like receptors (TLRs) [18]. RLRs consist of cytoplasmic RNA helicases that recognize intracellular double-stranded RNA (dsRNA), while TLRs are membrane-associated receptors that are able to recognize PAMPs [19,20]. Anti-viral TLRs include TLR3, which recognizes dsRNA, TLR7 and TLR8 that engage single-stranded RNA (ssRNA), while TLR9 detects unmethylated CpG DNA. In particular, TLRs 3, 7, and 8 are all localized on the endosomal membrane, and could recognize ssRNA [21]. TLR3 engagement by viral dsRNA activates the TRIF-dependent pathway and induces proinflammatory cytokines, chemokines, and type I and type III interferons via NF- κ B and IRF3. TLR7/8, located on the X-chromosome, as tandem duplicated genes, are expressed on the endosome membranes. The interaction between TLR7/8 and ssRNA enhances immune activation and the release of pro-inflammatory molecules, which might be connected with disease outcome [21]. Recently, TLR7 has been reported to be implicated in the sensing of SARS-CoV-2 infection, and the presence of TLR7-deficient genetic variants have been associated with a less-efficient control of the infection [22]. This central role of TLR7 in the antiviral response towards SARS-CoV-2 has been considered to be a potential target for therapy with the immune-stimulator imiquimod, in order to increase TLR7 activation and, consequently, its antiviral effect [22]. Once the viral RNA sensors are activated, downstream signaling is engaged to induce the transcription factors in the nucleus, which, in turn, promote the expression of target genes, including types I and III IFNs, and a number of other important pro-inflammatory cytokines [23]. Among the transcriptional factors involved, IRF3 and NF- κ B play a central role [24], with the IRF3 protein being involved in the production of interferons [25], while NF- κ B is mainly employed in the induction of the proinflammatory response [26]. Even if both IRF3 and NF- κ B are reported to be crucial in RNA sensing signaling, they are differentially induced by endosomal TLRs-3 and -7. In fact, while TLR7 activation leads mainly to NF- κ B recruitment, TLR3 typically activates both NF- κ B and the IRF3 signal [27]. This differential signaling is possible because both TLR3 and TLR7 involve the kinase TBK1, which is responsible for IRF3 and NF- κ B phosphorylation. This first signal is followed by a second one that is addressed to all the surrounding cells, which are led to express a great number of interferon-stimulated genes, in order to establish the antiviral state [28].

In this study, we used Calu-3/MRC-5 multicellular spheroids as an *in vitro* lung model. The choice to use MTCs lung model was supported by the evidence that both epithelial and fibroblast components could participate in the inflammatory response observed during lung damage [29], contributing to both the cytokine storm and antiviral response.

Our aim was to investigate how PRRs activation during the SARS-CoV-2 infection may affect the innate immune response in the lung cell environment.

2. Materials and Methods

2.1. Cell Cultures

African green monkey kidney epithelial Vero E6 (ATCC CRL-1586), human lung fibroblast MRC-5 cells (ATCC CCL-171) (LGC Standards S.r.l., Milan, Italy) and human lung adenocarcinoma Calu-3 cells (ATCC, HTB-55), were grown in EMEM (ThermoFisher Scientific, Milan, Italy) with 1% penicillin–streptomycin (ThermoFisher Scientific, Milan, Italy), 1% L-glutamin (ThermoFisher Scientific, Milan, Italy) and 10% fetal bovine (ThermoFisher Scientific, Milan, Italy), and cultured at 37 °C in presence of 5.0% CO₂.

2.2. 3D Cultures: Multicellular Spheroids Formation

Calu-3/MRC-5 multicellular spheroids (MTCs) were obtained using the liquid overlay method [30]. Briefly, Calu-3 and MRC-5 cells were seeded in 1:5 ratio to obtain a total of 5000 cells/well in 200 uL of complete EMEM (ThermoFisher Scientific, Milan, Italy) into a 96-well plate (Nunc, ThermoFisher Scientific, Milan, Italy) previously filled with 1.5% sterile agarose (ThermoFisher Scientific, Milan, Italy). In order to check cell distribution into MTCs, Calu-3 and MRC-5 single-cell suspensions were stained, respectively, with Syto9 (green fluorescent nucleic acid stain) and Syto59 (red fluorescent nucleic acid stain) (ThermoFisher Scientific, Milan, Italy). After seeding, the plate was briefly centrifuged (200g × 1min) and the plate was incubated at 37 °C in presence of 5.0% CO₂ to allow cell aggregation and spheroids formation. After 3–4 days of culture, a single spheroid was formed into each well and checked by immunofluorescence for cell distribution into spheroids. The MTCs obtained were, on average, 250–300 um in diameter.

2.3. MTT Assay for Cell Viability

Cell viability of MTCs was assessed by MTT assay (Roche Diagnostics, Milan, Italy) after SARS-CoV-2 infection as previously described [30]. Briefly, 10 uL of MTT solution was added to each well overnight. The day after, 100 uL of solvent was added and after 4 h the absorbance at 570 nm was measured. Results are expressed as mean value ± SD percent optical density (OD) derived from three independent experiments.

2.4. SARS-CoV-2 Propagation and Infection

SARS-CoV-2 was isolated from a nasopharyngeal swab retrieved from a patient with COVID-19 (Caucasian man of Italian origin, genome sequences available at GenBank (SARS-CoV-2-UNIBS-AP66: ERR4145453). This SARS-CoV-2 isolate clustered in the B1 clade, which includes most of the Italian sequences, together with sequences derived from other European countries and the United States. As previously described, the viral titer was determined by plaque assay in Vero E6 cells [30]. SARS-CoV-2 manipulation was performed in the BSL-3 laboratory of the University of Ferrara, following the biosafety requirements and accordingly with the Institutional Biosafety Committee. Both Calu-3 and MRC-5's susceptibility to SARS-CoV-2 infection was assayed by infecting single-type cell with an MOI of 1 for 2 h at 37 °C, as previously reported (approx. 2×10^5 infectious virus particles per well) [30]. SARS-CoV-2 infection in Calu-3/MRC-5 MTCs was performed by transferring the spheroids into a new U-bottom 96 well, using a multiplicity of infection (MOI) of 1.0 for 1 h at 37 °C on a shaker. Then, 24, 48, 72 and 96 h after infection, the infected spheroids were collected and used for the different assays.

2.5. Viral RNA Detection

RNA extraction was performed 24 and 48 h post-infection (hpi) with MagMAX viral/pathogen nuclei acid isolation kit (Thermo Fisher, Milan, Italy), a kit for the recovery of RNA and DNA from virus, as previously described [14]. SARS-CoV-2 titration was obtained by TaqMan 2019nCoV assay kit v1 real-time qPCR (Thermo Fisher, Milan, Italy).

2.6. MTCs Treatment for RNA Sensor Pathways Analysis

The evaluation of RLRs and TLRs inducible expression was performed using the following RLRs and TLRs agonists: RIG-I/MDA5 agonist 5' triphosphate hairpin RNA complexed with transfection reagent LyoVec (1 µg/mL) (Invivogen, San Diego, CA, USA); TLR3 agonist Poly(I:C) (HMW) (2 µg/mL) (Invivogen, San Diego, CA, USA); TLR7/8 agonist—imidazoquinoline compound R848 (2 µg/mL) (Invivogen, San Diego, CA, USA); TLR4 agonist lipopolysaccharides LPS-B5 (LPS from *E. coli* 055:B5) (1 µg/mL) (Invivogen, San Diego, CA, USA). RNA sensors inhibition was performed using the following RLRs antagonists: TLR3/dsRNA complex inhibitor (30 µM) (Sigma-Aldrich, Merck Life Science S.r.l., Milan, Italy); TLR7 inhibitor Pepinh-MYD (50 µM) (Invivogen, San Diego, CA, USA). For the evaluation of the role of IRF3 and NF-κB we used MRT67307 (20 nM) (Sigma-Aldrich, Merck Life Science S.r.l., Milan, Italy), which prevents IRF3 phosphorylation, and helenalin (10 µM) (Cayman Chemicals, Ann Arbor, MI, USA), an inhibitor of NF-κB.

Further, siRNAs specific to human TLR3 (assay ID 107054; Thermo Fisher, Milan, Italy) and human TLR7 (assay ID 108895; Thermo Fisher, Milan, Italy), and the non-specific control siRNA (Ambion Silencer Negative Control) (Thermo Fisher, Milan, Italy), were transfected to Calu-3/MRC5 cells cultured on a 6-well plate (6×10^5 /well) using the Lipofectamine RNAiMAX reagent (Thermo Fisher, Milan, Italy) according to the manufacturer's instructions.

2.7. Gene Expression Analysis

RNA sensors pathway genes expression was evaluated on RNA extracted by using the RNeasy kit (Qiagen, Milan, Italy). DNase treatment was used to check for contaminant DNA presence, using β-actin PCR as a control. RT2 first strand kit (Qiagen, Milan, Italy) was used for RNA reverse transcription and cDNAs were immediately used or stored at -20 °C. Gene expression analysis on extracted RNA was performed by real-time quantitative PCR using PowerUp SYBR Green Master Mix (Thermo Fisher, Milan, Italy) and the primer sets reported in Table 1.

Table 1. PrimeTime qPCR assays used for gene expression analysis.

Target Gene	PrimeTime qPCR Primer Assay *
RIG-I	Hs.PT.58.4273674
MDA5	Hs.PT.58.1224165
TLR3	Hs.PT.58.25887499.g
TLR4	Hs.PT.58.38700156.g
TLR7	Hs.PT.58.39183219.g
TLR8	Hs.PT.58.15023918.g
IRF3	Hs.PT.58.27933933.g
NF-κB	Hs.PT.58.20344216
GAPDH	Hs.PT.58.25887499.g

* PrimeTime qPCR primer assays provide a primer pair designed for real-time PCR using intercalating dyes, such as SYBR®Green (IDT, Leuven, Belgium).

Amplification followed this fast protocol, as follows: 1 cycle at 50 °C for 2 min, 1 cycle at 95 °C for 2 min and 40 cycles at 95 °C for 1 s and 60 °C for 30 s. Quantitative PCR analysis was performed using QuantStudio3 real-time PCR detection system (Applied Biosystems, Thermo Fisher, Milan, Italy). Relative quantification of given mRNA levels for the samples was conducted using the $2^{-\Delta\Delta CT}$, 2 (Delta Delta CT) method [31] normalized to the constitutively expressed housekeeping gene GAPDH. Relative fold changes were generated comparing the non-infected control (NT) to the samples.

2.8. Immunofluorescence Analysis

Spheroids were air-dried, fixed in cool methanol at $-20\text{ }^{\circ}\text{C}$ for 10 min. After rehydration in PBS, MTCS were permeabilized with PBS—3%, BSA—0.1%, TritonX for 30 min at RT and then incubated with a specific antibody directed against SARS-CoV-2 nucleocapsid protein (NP) (MA1-7404, Thermo Fisher, Milan, Italy) or against human angiotensin-converting enzyme 2 (ACE2) (SN0754 Thermo Fisher; Italy) as previously described [32], followed by incubation with FITC goat anti-mouse IgG (H + L) secondary antibody (Thermo Fisher, Milan, Italy). Immunofluorescence was visualized by fluorescent microscopy (Nikon Eclipse Nikon Eclipse TE2000S, Milan, Italy). DNA was stained using DAPI (Thermo Fisher, Milan, Italy).

All MCTS measured $500\text{ }\mu\text{m} \pm 20\text{ }\mu\text{m}$ in diameter and were subdivided into seven parts (40, 80, 120, 160, 200, 240, 290 μm) on the basis of the distance from the surface of the spheroid. The number of NP-positive cells was determined in each part of the spheroid and expressed as percentage of NP-positive cells in the spheroid area.

2.9. Wesern Blot Analysis

TLR3 and TLR7 protein expression were quantified by Western blot assay. Whole cell lysates were treated with RIPA buffer containing proteinase inhibitor cocktail (Sigma-Aldrich, Merck Life Science S.r.l., Milan, Italy). Protein contents were evaluated by means of the Bradford assay (Bio-Rad, Milan, Italy) using bovine albumin (Sigma-Aldrich) as standard. Then, 20 μg of total proteins were loaded in each well and evaluated in denaturing conditions in 10% TGX pre-cast gel (Bio-Rad, Milan, Italy), with subsequent electroblotting transfer onto a PVDF membrane (Millipore, Merck Life Science S.r.l., Milan, Italy). The membrane was incubated with a specific antibody for the protein to be analyzed, then with a horseradish peroxidase (HRP)-conjugated anti-mouse antibody (1:5000; Amersham Biosciences, Piscataway, NJ, USA) and developed with the ECL kit (Amersham Biosciences, NJ, USA). The images were acquired by Geliance 600 (Perkin Elmer, Milan, Italy). The specific antibodies used were as follows: anti-TLR3 (clone 27N3D4), anti-TLR7 (clone NBP2-24905) (Novus Biologics, Milan, Italy). The complete Western blots are reported in Supplementary Figure S2.

2.10. IRF3 and NF- κ B Expression and Phosphorylation Analysis

The evaluation of IRF3 and NF κ B expression and phosphorylation status was performed using the detection kit human total IRF-3 and phospho-IRF-3 (S386) ELISA kit (RayBiotech, Peachtree Corners, GA, USA), and total NF- κ B p65 and phospho-NF- κ B p65 (S536) (Abcam, Cambridge, UK) on MTSC cell lysates. MTCS were lysed for 30 min on ice in modified RIPA buffer with 150 mM NaCl, 1% Nonidet P-40, 50 mM Tris-HCl, pH 7.4, 1 mM Na₃VO₄, 0.25% sodium deoxycholate, and 1 mM NaF supplemented with protease inhibitor cocktails (Roche Diagnostics Corporation, Mannheim, Germany). Total protein extract was collected from supernatant after centrifugation at $12.000\times g$ for 20 min at $4\text{ }^{\circ}\text{C}$. Protein content was evaluated by Bradford's method, with bovine serum albumin as calibrator.

2.11. Soluble Factors Quantification by ELISA Assay

IL-1 α , IL-1 β , IL-4, IL-6, IL-10, interferon- α (IFN- α), interferon- β (IFN- β), interferon- γ (INF- γ), interferon-lambda1 (IL-29), interferon- λ 2 (IL28A), interferon- λ 3 (IL-28B) levels were evaluated in MTCSs culture supernatants by single ELISA kit assays (myBiosource, San Diego, CA, USA) following the customer's protocols.

2.12. Statistical Analysis

Two-tailed Student's *t*-test was used for comparative analysis between individual parameters, relative expression of target genes normalized to the expression of GADPH and for soluble factors evaluation, expressed as fold change relative to the corresponding control group. The data were analyzed by paired Student's *t*-test. *P* values < 0.05 were

considered significant. The statistical analyses were performed with GraphPad Prism version 9 software (GraphPad, La Jolla, CA, USA).

3. Results

3.1. Calu-3/MRC-5 Multicellular Spheroids Are Efficiently Infected by SARS-CoV-2

The main structural cell types of the lung, epithelial and fibroblast cells were cultured in a 3D in vitro model, which was obtained 4 days after seeding the Calu3 and MRC-5 cells in a ratio of 1:5 (Figure 1a). In order to check the cell distribution in the multicellular spheroid (MTCS), Calu-3 and MRC-5 single-cell suspensions were pre-stained with Syto9 and Syto59, respectively. We observed the localization of the MRC-5 cells in the core of the spheroid, while the Calu-3 cells were in the outer region. This peculiar cellular distribution is in line with the results reported in the literature [32], and is consistent with the structure of the airway epithelium. We observed a high viability rate until 72 h of culturing (Figure 1b), while at 96 h of culturing, the spheroids presented a reduced viability (Figure 1b; $p < 0.001$; Student's *t*-test). We used these MTCSs as an in vitro model for lung SARS-CoV-2 infection.

MTCSs were infected with 1.0 MOI of SARS-CoV-2 for 2 h and viral titration was performed by real-time qPCR. We observed susceptibility and permissivity to the SARS-CoV-2 infection, with a significant increase in the viral load 48 h after the infection (Figure 1c,d; $p < 0.0001$; Student's *t*-test). At 96 h post-infection, we had a significant decrease in the viral titration (Figure 1d), due to the senescence of the spheroids, as previously observed (Figure 1b). Figure 1c shows the expression of the SARS-CoV-2 NP protein in MTCS. We estimated the percentage of SARS-CoV-2 NP-positive cells on the basis of the distance to the spheroid surface. The MCTS measured $500 \mu\text{m} \pm 20 \mu\text{m}$ in diameter, and we subdivided the spheroid into seven parts, on the basis of the distance from the surface of the spheroid. We observed a progressive decrease in the proportion of NP-positive cells from the surface (40, 80, 120 μm) to the center of the spheroid (160, 200, 240, 290 μm) (Figure 1c,e). Approximately 60% of cells were positive for NP in the outer 40 μm of the spheroid, and 50% in the outer 80 μm of the spheroid, 48 h post-infection (Figure 1c,e). Conversely, we observed that only 20% of the cells were infected in the outer 200 μm of the spheroid, and there was almost the same absence of NP positivity in the center of the spheroid. The observed regionalization of SARS-CoV-2 infection in the spheroids might depend on the cell position to the spheroid surface and/or their differential permissivity to the virus.

3.2. Calu-3 and MRC-5 Permissivity to SARS-CoV-2 Infection

To evaluate the possible different permissivity of these two cell types, the Calu-3 and MRC-5 cells were infected with 1.0 MOI of SARS-CoV-2 inoculum. We assayed the viral infection in the culture supernatants 48 h post-infection (pi), by real-time qPCR. We observed that both the cell lines are susceptible and permissive to the SARS-CoV-2 infection (Figure 1f), as already reported [33]. The MRC-5 cell line presented a lower permissivity in comparison with the Calu-3 cell line, as demonstrated by the difference of more than 1 log viral load in the infected cell supernatants (Figure 1f; $p < 0.001$; Student's *t*-test). To account for this difference, we evaluated the expression of the SARS-CoV-2 receptor human ACE2 (hACE2) on both cell lines. As reported in Figure 1g,h, both the cell lines express hACE2 on the cell surface. The relative intensity measurement of immunofluorescence showed that Calu-3 expressed higher levels of hACE2 in comparison with the MRC-5 cell line (Figure 1h). This difference might influence the different SARS-CoV-2 permissivity of these two cell lines, together with their positions in the MTCS, which resemble the in vivo condition.

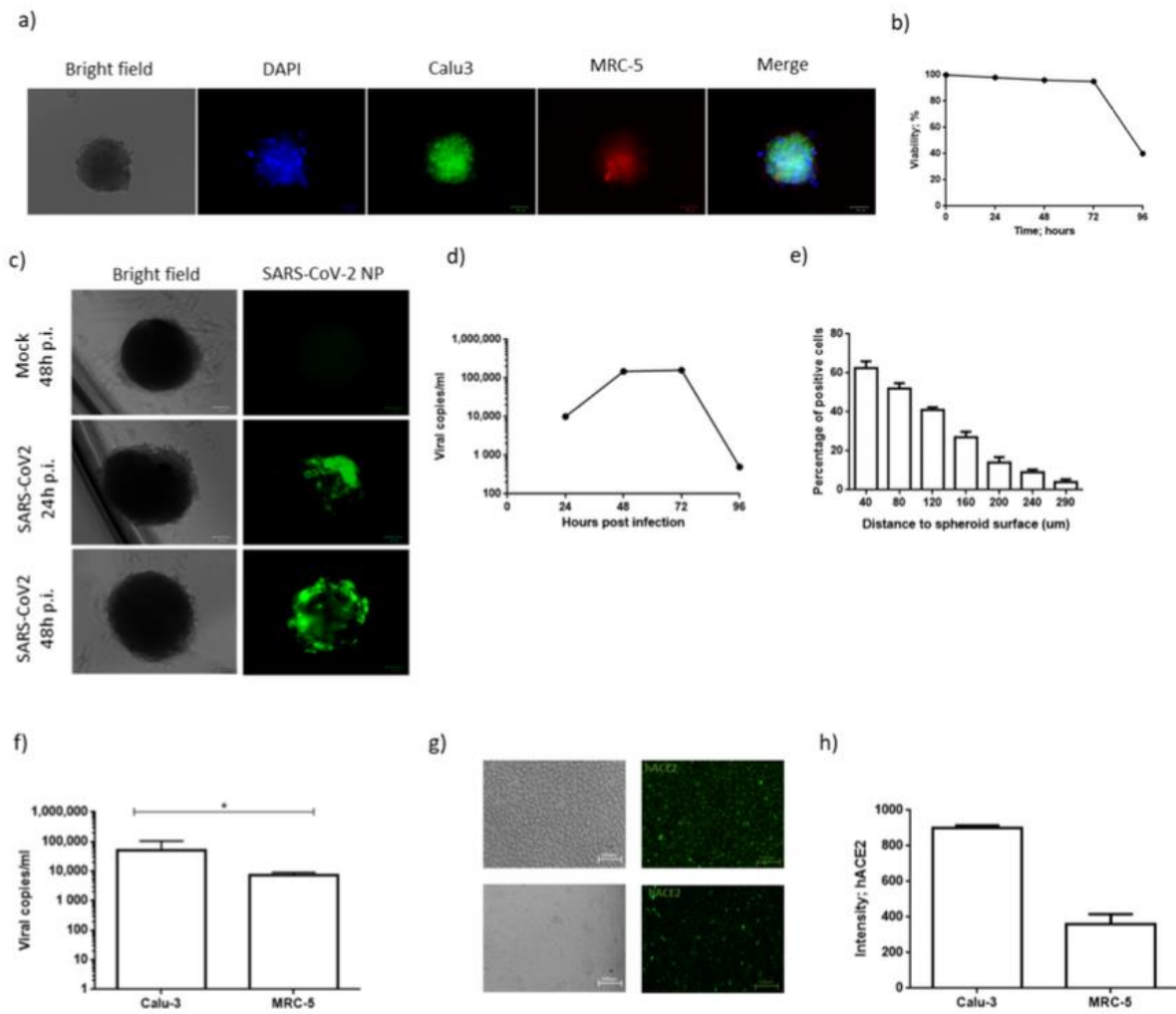


Figure 1. (a) A representative Calu-3/MRC-5 multicellular spheroid, 48 h after culture. Calu-3 and MRC-5 single-cell suspensions were pre-stained with Syto9 and Syto59, respectively. DAPI was used for nuclear staining. Scale bar 100 μ m. (b) Graphic representation of the percentage of viable cells during a time lapse of 96 h. Cell viability was measured by MTT assay. (c) Representative Calu-3/MRC-5 multicellular spheroids stained with anti-SARS-CoV-2 nucleoprotein. UV-inactivated SARS-CoV-2 (mock) was used as negative control. Scale bar 100 μ m. (d) Calu-3/MRC-5 multicellular spheroids were infected with SARS-CoV-2 at a multiplicity of infection (MOI) of 1.0 for 1 h at 37 $^{\circ}$ C. Thereafter, the cells were washed and cultured for 24, 48, 72 or 96 h. Viral yield was quantified in the cell supernatant using quantitative reverse-transcription PCR (RT-qPCR). At least three independent replicates were tested. Data represent three independent experiments. (e) Percentage of NP-positive cells, subdivided according to the distance to spheroid surface. Data are expressed as mean \pm standard deviation. (f) Calu-3 or MRC-5 cells were SARS-CoV-2 at a multiplicity of infection (MOI) of 1.0. Viral yield was quantified in the cell supernatant using quantitative reverse-transcription PCR (RT-qPCR). At least three independent replicates were tested. Data are representative of three independent experiments. (g) hACE2 staining of Calu-3 (upper panel) and MRC-5 (lower panel) cells. Scale bar 100 μ m. (h) Levels of hACE2 staining in Calu-3 and MRC-5 cells. Data correspond to the mean \pm standard deviation. * p value < 0.05, calculated with Student's t -test.

3.3. Calu-3/MRC-5 MTCS Response to SARS-CoV-2 Infection

One of the main cellular response systems to the coronavirus infection might be the activation of the RNA sensor pathways. We selected to evaluate the most important RNA sensors (TLR3, TLR7, TLR8, RIG-I, MDA5) in MTCS infected with SARS-CoV-2. TLR4 was used as a control, as implicated in bacterial lipopolysaccharide sensing. To be

sure that all these pathways are expressed in the in vitro system, we treated the MTCS with RNA sensors agonists. We obtained the activation of all the evaluated RNA sensors (Supplementary Figure S1). After 48 h of infection, we observed a predominant induction of both TLR7 and TLR3 expression (Figure 2a,b; $p < 0.001$; Student's *t*-test). On the contrary, the TLR4, TLR8 and RLRs genes (RIG-I, MDA5) expression was not significantly modified by the SARS-CoV-2 infection (Figure 2a). The TLR3 and TLR7 protein expression was similarly increased in the presence of SARS-CoV-2 infection (Figure 2b,c; $p < 0.01$; Student's *t*-test). These data support an induction of both TLR7 and TLR3 RNA sensing during SARS-CoV-2 infection.

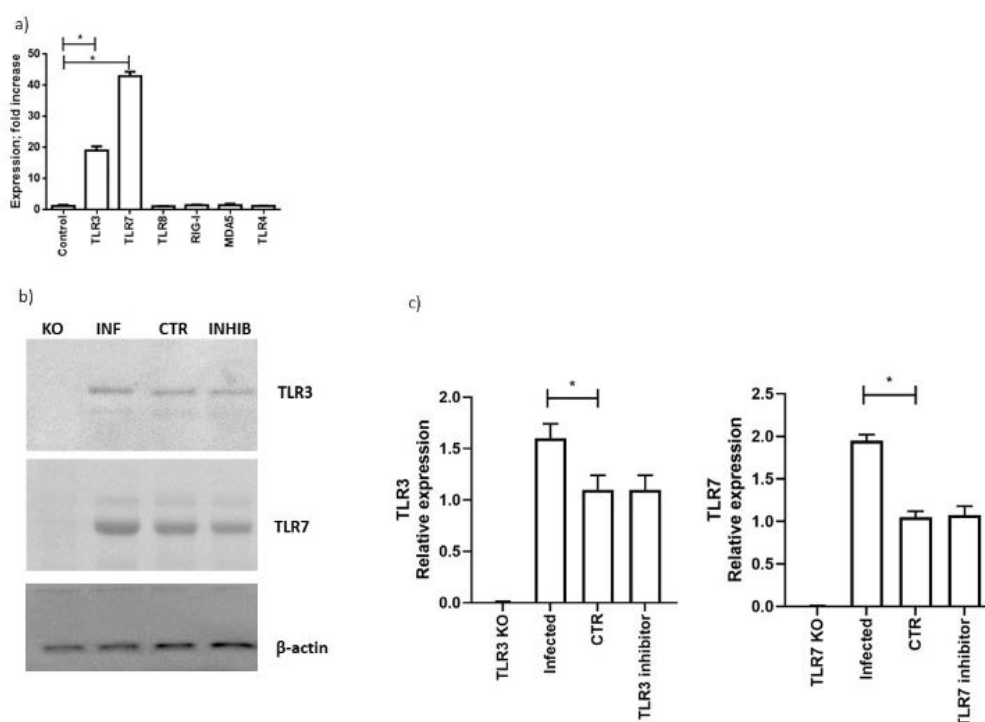


Figure 2. (a) Calu-3/MRC-5 multicellular spheroids were infected with SARS-CoV-2 at a multiplicity of infection (MOI) of 1.0 for 1 h at 37 °C. Thereafter, the cells were washed and cultured for 48 h. Levels of expression, quantified as fold increase in comparison with uninfected cells of TLR3, TLR7, TLR8, RIG-1, MAD5 and TLR4 are reported and are representative of three independent experiments. (b) Western blot analysis of TLR3, TLR7 and β -actin protein expression in Calu-3/MRC-5 multicellular spheroids (CTR), silenced for TLR3 (TLR3 KO), TLR7 (TLR7 KO) with RNA silencing technology; infected with SARS-CoV-2 with at a multiplicity of infection (MOI) of 1.0 (INF: infected) and treated with TLR3 or TLR7 inhibitors (INHIB: inhibitor). The molecular weights were determined by protein ladder (Bio-Rad, Milan, Italy). Actin was evidenced at 44 kDa, TLR3 and TLR7 at 116 kDa. The images were acquired by Geliance 600 (Perkin Elmer, Milan, Italy). The complete Western blots are reported in Supplementary Figure S2. (c) Evaluation of protein expression by densitometry (GelDoc software; Biorad, Italy), normalized on β -actin content. Data are representative of three independent experiments. Data correspond to the mean \pm standard deviation. * p value < 0.05 , calculated with Student's *t*-test.

3.4. SARS-CoV-2 Infection Induced an Increase in Cytokines and Interferon Secretion

One of the critical points in SARS-CoV-2 infection is the establishment of a strong pro-inflammatory environment, the so-called cytokine storm. The cytokine storm might also be induced by the RNA sensing activation. We selected the most important cytokines involved in the COVID19-associated cytokine storm, including IL-1 α , IL-1 β , IL-4, IL-6, IL-10, and interferons, in order to evaluate the effect of SARS-CoV-2 infection on their induction in MTCS [34]. We observed an increase in IL-1 α , IL-1 β , IL-4, and IL-6 levels in SARS-CoV-2 48 h-infected cells, in comparison with uninfected MTCS (Figure 3a–d) ($p < 0.001$; Student's

t-test). The levels of these inflammatory cytokines are reduced in the presence of the TLR3 inhibitor (Figure 3a–d) ($p < 0.001$; Student's *t*-test). On the contrary, the IL-10 levels were not affected by the SARS-CoV-2 infection (Figure 3e). Then, we evaluated the expression of type I and type II interferons. IFN- α and IFN- β were induced 24 h post-infection and also maintained a high secretion 48 h post-infection (Figure 3f,g) ($p < 0.001$; Student's *t*-test). Meanwhile, the addition of the TLR3 inhibitor reduced the secretion of IFN- α and IFN- β 24 h post-infection, while the addition of the TLR7 inhibitor reduced the expression of these type I IFNs 48 h post-infection (Figure 3f,g) ($p < 0.001$; Student's *t*-test). IFN- γ was induced by SARS-CoV-2 48 h post-infection (Figure 3h) ($p < 0.001$; Student's *t*-test) and reduced by the TLR7 inhibitor (Figure 3h) ($p < 0.001$; Student's *t*-test). IFN- λ 1 and IFN- λ 2 were not modified by SARS-CoV-2 infection (Figure 3i,j), while IFN- λ 3 was induced after 48 h of SARS-CoV-2 infection (Figure 3k) ($p < 0.001$; Student's *t*-test) and reduced by the TLR7 inhibitor (Figure 3k) ($p < 0.001$; Student's *t*-test).

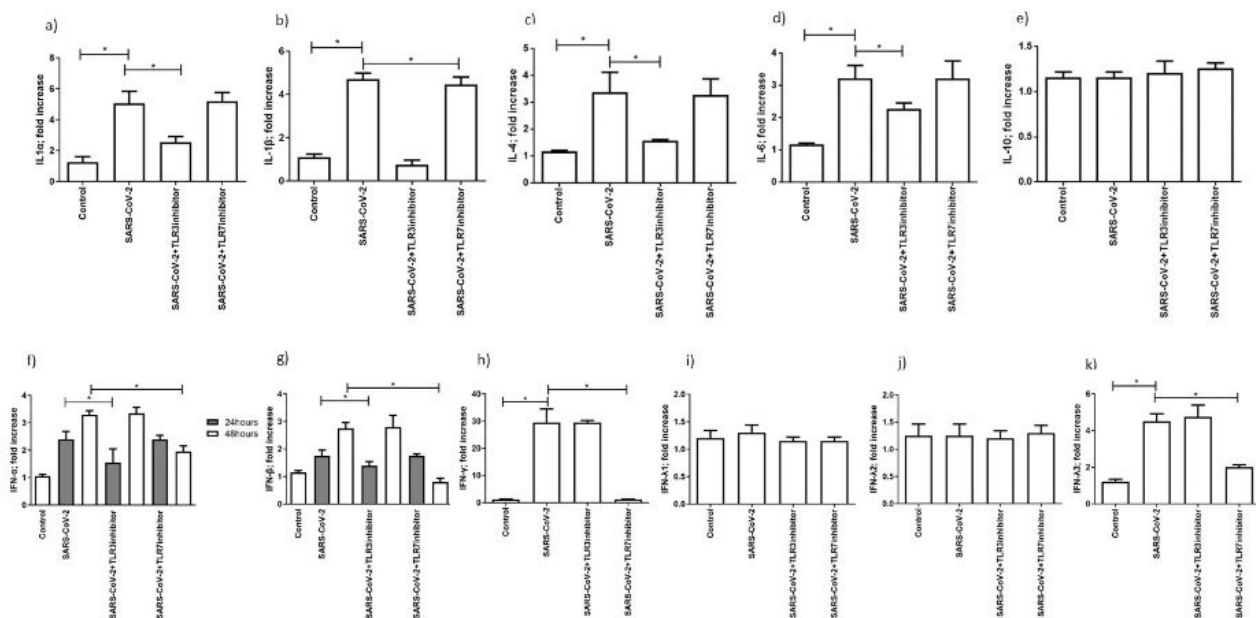


Figure 3. Levels of expression of cytokines (a) IL-1 α , (b) IL-1 β , (c) IL-4, (d) IL-6 and (e) IL-10 are reported after 48 h post-infection. The levels after 24 h post-infection were under the detection limit of the assays. Levels of (f) IFN- α , (g) IFN- β are reported 24 and 48 h post-infection. Data correspond to the mean \pm standard deviation. * p value < 0.05 , calculated with Student's *t*-test. Levels of (h) IFN- γ , (i) IFN- λ 1, (j) IFN- λ 2, (k) IFN- λ 3 are reported 48 h post-infection. The levels after 24 h post-infection were under the detection limit of the assays. Data correspond to the mean \pm standard deviation. * p value < 0.05 , calculated with Student's *t*-test.

These results suggest that TLR3 is mainly implicated in cytokine secretion control and type 1 IFN expression 24 h post-infection; TLR7 controls the expression of type 1 IFN, IFN- γ , and IFN- λ 3 expression in the late phases of SARS-CoV-2 infection.

3.5. TLR3 and TLR7 Activation Followed Different Signal Pathways after SARS-CoV-2 Infection

To evaluate the proposed effect of SARS-CoV-2 on TLR3- and TLR7-mediated gene expression, we assessed the expression of the following TLR3- and TLR7-associated key transcription factors: NF- κ B, which induces TLR-dependent gene activation, and IRF3, which mediates TLR3-dependent gene expression [35]. In SARS-CoV-2-infected cells, there was a significant increase in IRF3 expression 24 h post-infection, and of NF- κ B 48 h post-infection, which was maintained until 72 h post-infection (Figure 4a).

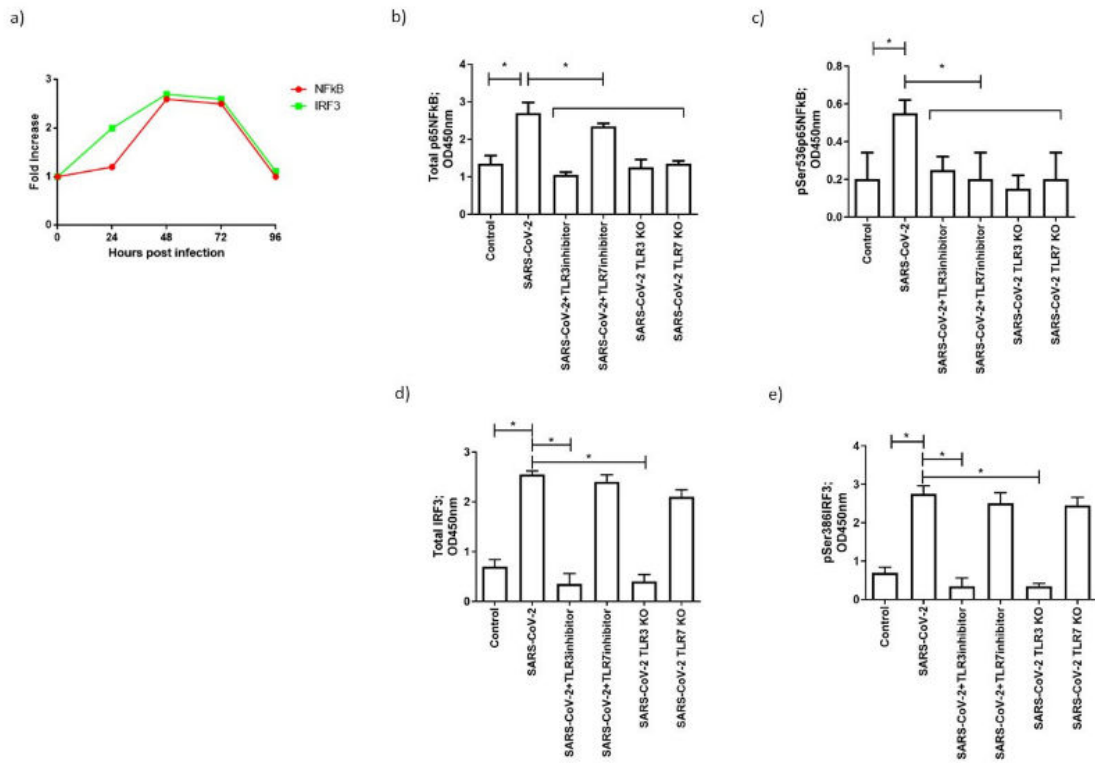


Figure 4. (a) Levels of expression, quantified as fold increase in comparison to uninfected cells, of NF-κB and IRF3, are reported and are representative of three independent experiments. Levels of (b) total and (c) phosphorylated NF-κB and of (d) total and (e) phosphorylated IRF3 in Calu-3/MRC-5 multicellular spheroids infected with SARS-CoV-2 and analyzed 48 h post-infection, with or without inhibitor (inhibitor) or silencing (KO) treatment. Data correspond to the mean \pm standard deviation. * p value < 0.05, calculated with Student's t -test.

To evaluate the effective activation of IRF3 and NF-κB, we assessed IRF3 Ser386 phosphorylation, which induces dimerization and association with the coactivators CREB-binding protein/p300, and the NF-κB p65 Ser536 phosphorylation that leads to the nuclear localization of the transcriptionally active complex. Both NF-κB and IRF3 presented an increased phosphorylation 48 h post-infection (Figure 4b,e; $p < 0.001$; Student's t -test). To assess the specificity of NF-κB and IRF3 induction by TLR3 and TLR7, we treated MTCs with TLR3 and TLR7 inhibitors, or RNA silencing. The TLR3/dsRNA complex inhibitor and TLR7 inhibitor Pepinh-MYD did not affect TLRs protein expression (Figure 2b,c), but blocked their activation and, consequently, NF-κB and/or IRF3 phosphorylation. In particular, NF-κB phosphorylation was reduced after TLR3 and TLR7 inhibition (Figure 4c) ($p < 0.001$; Student's t -test), while IRF3 phosphorylation was decreased only after TLR3 inhibition (Figure 4e) ($p < 0.001$; Student's t -test). TLR3- and TLR7-specific siRNA transfection resulted in the absence of RNA (Supplementary Figure S3) and protein expression (Figure 2b,c). Similarly, NF-κB phosphorylation was reduced after TLR3 and TLR7 silencing (Figure 4c) ($p < 0.001$; Student's t -test), while IRF3 phosphorylation was decreased only after TLR3 silencing (Figure 4e) ($p < 0.001$; Student's t -test).

Summarizing these results, TLR3 might act via NF-κB and IRF3, while TLR7 mainly acts via NF-κB activation. To investigate the role of NF-κB and IRF3 activation in TLR3- and TLR7-mediated inflammatory cytokine and interferons gene expression, during SARS-CoV-2 infection, we used MRT67307, which prevents IRF3 phosphorylation and expression of interferon-stimulated genes, and helenalin, an inhibitor of NF-κB (Figure 5). The pre-treatment of MTCs with MRT67307 reduced IFN- α and IFN- β gene expression (Figure 5e; $p < 0.001$; Student's t -test), and slightly reduced IL-6 and IL-4 (Figure 5c, d; $p < 0.012$,

$p = 0.023$, respectively; Student's t -test), while NF- κ B inhibition, by helenalin, completely abrogated the IL-1 α , IL-1 β , IL-4, and IL-6 gene expression (Figure 5a–d; $p < 0.001$; Student's t -test), and reduced type 1 IFN, IFN- γ and IFN- λ gene expression (Figure 5f; $p < 0.0001$; Student's t -test).

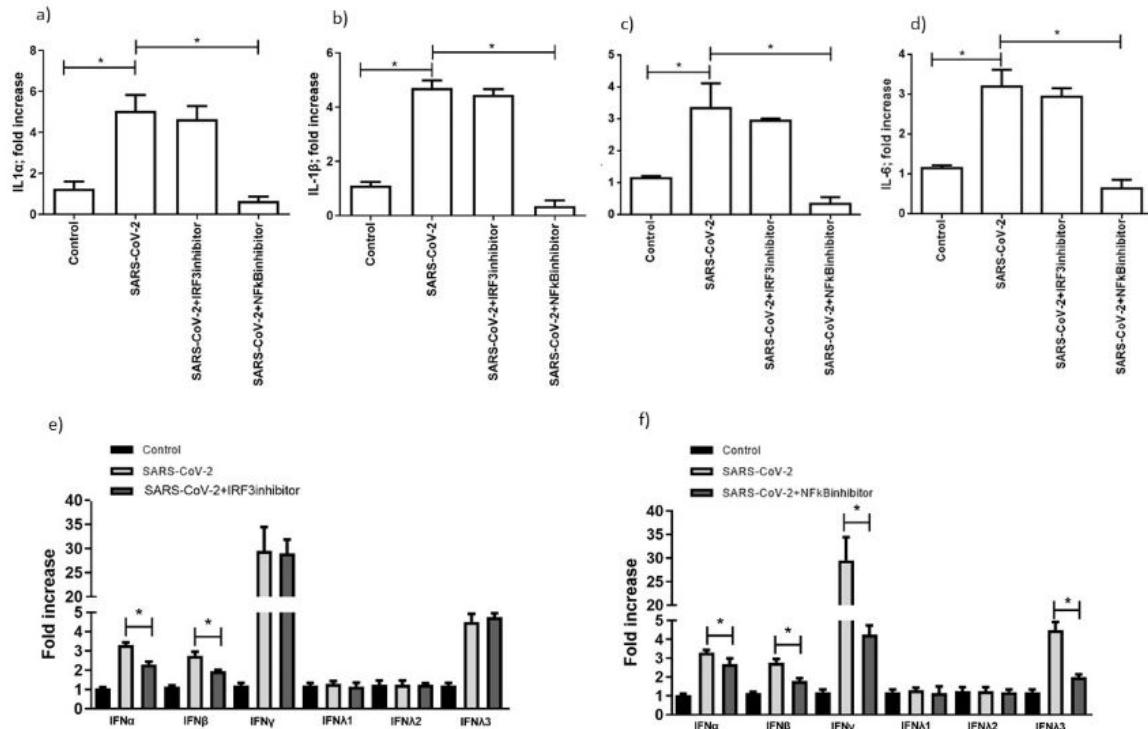


Figure 5. Levels of expression of cytokines (a) IL-1 α , (b) IL-1 β , (c) IL-4, (d) IL-6, (e), (f) IFN- α , IFN- β , IFN- γ , IFN- λ 1, IFN- λ 2, IFN- λ 3 are reported, in the presence or absence of NF κ B or IRF3 inhibitors. The levels of IFNs in the presence of IRF3 inhibitor were evaluated 24 h post-infection. Data correspond to the mean \pm standard deviation. * p value < 0.05 , calculated with Student's t -test.

4. Discussion

The role of the RNA sensor pathways during SARS-CoV-2 infection is of extreme interest, as TLRs are the innate mediators of the anti-viral response and might influence the pathogenesis of SARS-CoV-2 infection. TLR3 pathway activation is associated with the production of IFN- β by macrophages in murine coronavirus infection [36]; TLR7 and TLR8 activation enhances a cytokine storm in SARS-CoV-1 infection, causing several side effects [37].

Our results showed that the SARS-CoV-2 infection of Calu-3/MRC-5 multicellular spheroids induces the activation of TLR3 and TLR7 RNA sensor pathways. In particular, TLR3 might act via IRF3-producing IFN- α and IFN- β during the first 24 h post-infection. Then, TLR3 activates the NF κ B transduction pathway, leading to pro-inflammatory cytokine secretion (IL-1 α , IL-1 β , IL-4, IL-6). Conversely, TLR7 seems to act mainly via NF κ B, inducing type 1 IFN, IFN- γ , and IFN- λ 3, starting from the 48 h post-infection.

These data suggest a differential timing of TLRs activation, which, on one hand, might interfere with SARS-CoV-2 infection, activating the host immune response, or, on the other hand, might lead to a cytokine storm, with an adverse effect on disease follow-up. Totura et al. observed that the induction of TRIF-driven and MyD88-driven pathways by TLRs are essential in the control of SARS-CoV infection [38]. As a proof of concept, TLR3/TLR4 double-negative mice were more susceptible to SARS-CoV infection,

and the deletion of TRIF increased the SARS-CoV-dependent risk of mortality. Further, van der Made et al. showed a TLR7 loss-of-function variant in four male patients with severe COVID-19 infection that presented an impaired type I and type II IFNs response. Interestingly, SARS-CoV-2 has more ssRNA motifs that could be recognized by TLR7 [39], inducing a strong pro-inflammatory response [40,41].

These data support the harmful and beneficial role of TLRs in SARS-CoV-2 infection. Our data clarify the role of the TLR components, supporting the potential use of TLRs antagonists and agonists as therapeutic tools in SARS-CoV-2 infection. Not only are TLRs important, but also the related pathways. A study on SARS-CoV, which was responsible for the worldwide outbreak of SARS in 2003, showed that the SARS-CoV nucleocapsid protein (N protein) activates NF- κ B in Vero E6 cells, in a dose-dependent manner [42]. DeDiego et al. proved that inhibitors of the NF κ B pathway increased the survival rate in both in vitro and in vivo studies, using mice with reduced lung pathology [43]. In vitro studies in the previous SARS epidemic have shown that the spike (S) protein induces a strong cytokine response in infected mononuclear cells, through the NF κ B pathway. SARS-CoV-2 is more sensitive to interferon treatment [44], less efficient in suppressing cytokine induction via IRF3 nuclear translocation [45], and permissive of a higher level of induction of interferon-stimulated genes, in comparison with SARS-CoV [46]. Our data support an implication of both the transcription factors, which have an important role in controlling cytokine and IFN expression during SARS-CoV-2 infection. In conclusion, our data suggest an important role for TLR3 and TLR7 in COVID-19 disease, with a definition of the possible transduction pathways and activation timing. The suppression of excessive activation of TLRs seems to have a role in SARS-CoV-2 infection, as supported by several clinical trials [37], with the purpose of controlling TLRs activation and, consequently, SARS-CoV-2 infection.

This was confirmed by the recent findings on the contribution of both TLR3 and TLR7 in the antiviral signal against SARS-CoV-2 and that, in presence of genetic loss-of-function variants of TLR7, the TLR3 signal was not affected [22].

Supplementary Materials: The following are available online at <https://www.mdpi.com/article/10.3390/microorganisms9091820/s1>; Figure S1: Calu-3/MRC-5 multicellular spheroids were treated with TLR3, TLR7, TLR8, RIG-1, MAD5, and TLR4 agonists, and the levels of expression of TLR3, TLR7, TLR8, RIG-1, MAD5, and TLR4 are reported as fold-increased in comparison with untreated cells, and are representative of three independent experiments. Data correspond to the mean \pm standard deviation; Figure S2: Western blot analysis of TLR3 and TLR7 protein expression in Calu-3/MRC-5 multicellular spheroids (CTR), silenced for TLR3 (TLR3 KO), TLR7 (TLR7 KO) with RNA silencing technology, infected with SARS-CoV-2 with a multiplicity of infection (MOI) of 1.0 (infected) and treated with TLR3 or TLR7 antagonists (antagonist). The molecular weights were determined by protein ladder (BioRad). TLR3 and TLR7 were evidenced at 116 kDa. The images were acquired by GelDoc (BioRad, Italy); Figure S3: Calu-3/MRC-5 multicellular spheroids were treated with TLR3, TLR7 agonist; TLR3, TLR7 siRNA (TLR3 KO, TLR7 KO); TLR3, TLR7 siRNA and agonist-treated; siRNA control and siRNA control with agonist treatment. The levels of RNA expression of TLR3 and TLR7 are reported as fold-increased in comparison with untreated cells, and are representative of three independent experiments. The results showed that TLR3 and TLR7 agonists induce RNA expression, which is inhibited by siRNA transfection, also in the presence of agonists treatment (TLR3 KO agonist; TLR7 agonist). Control siRNA did not affect TLR3 and TLR7 RNA expression (siRNA CTR) and maintained the induction of RNA expression after agonist treatment (siRNA control agonist). Data correspond to the mean \pm standard deviation.

Author Contributions: D.B., V.G.: project administration, supervision, writing—original draft; S.R., G.S. (Giovanni Strazzabosco), S.B., G.S. (Giovanna Schiuma), M.F.: investigation, methodology; F.C.: writing—review and editing; A.C., R.R.: research conceptualization; writing—original draft. All authors have read and agreed to the published version of the manuscript.

Funding: This work was supported by University of Ferrara crowdfunding; 5X1000 University of Ferrara grant; University of Ferrara FAR (2019; 2020).

Data Availability Statement: The data presented in this study are all available upon request.

Acknowledgments: We thank Iva Pivanti for the technical support.

Conflicts of Interest: The authors declare no conflict of interest.

References

- Huang, C.; Wang, Y.; Li, X.; Ren, L.; Zhao, J.; Hu, Y.; Zhang, L.; Fan, G.; Xu, J.; Gu, X.; et al. Clinical features of patients infected with 2019 novel coronavirus in Wuhan, China. *Lancet* **2020**, *395*, 497–506. [CrossRef]
- National Health Commission of the People's Republic of China. Update on the Novel Coronavirus Pneumonia Outbreak. Available online: <http://www.nhc.gov.cn/xcs/yqtb/202002/18546da875d74445bb537ab014e7a1c6.shtml> (accessed on 16 February 2020).
- WHO. A Public Health Emergency of International Concern Over the Global Outbreak of Novel Coronavirus Declared. WHO. Available online: [https://www.who.int/news-room/detail/30-01-2020-statement-on-the-second-meeting-of-the-international-health-regulations-\(2005\)-emergency-committee-regarding-the-outbreak-of-novel-coronavirus-\(2019-ncov\)](https://www.who.int/news-room/detail/30-01-2020-statement-on-the-second-meeting-of-the-international-health-regulations-(2005)-emergency-committee-regarding-the-outbreak-of-novel-coronavirus-(2019-ncov)) (accessed on 23 July 2021).
- Gao, C.; Zhu, L.; Jin, C.C.; Tong, Y.X.; Xiao, A.T.; Zhang, S. Proinflammatory cytokines are associated with prolonged viral RNA shedding in COVID-19 patients. *Clin. Immunol.* **2020**, *221*, 108611. [CrossRef]
- Shaw, A.C.; Goldstein, D.R.; Montgomery, R.R. Age-dependent dysregulation of innate immunity. *Nat. Rev. Immunol.* **2013**, *13*, 875–887. [CrossRef]
- Bitker, L.; Burrell, L.M. Classic and Nonclassic Renin-Angiotensin Systems in the Critically Ill. *Crit. Care Clin.* **2019**, *35*, 213–227. [CrossRef]
- Osman, I.O.; Melenotte, C.; Brouqui, P.; Million, M.; Lagier, J.-C.; Parola, P.; Stein, A.; La Scola, B.; Meddeb, L.; Mege, J.-L.; et al. Expression of ACE2, Soluble ACE2, Angiotensin I, Angiotensin II and Angiotensin-(1-7) Is Modulated in COVID-19 Patients. *Front. Immunol.* **2021**, *12*, 625732. [CrossRef] [PubMed]
- Tanaka, T.; Narazaki, M.; Kishimoto, T. IL-6 in inflammation, immunity, and disease. *Cold Spring Harb. Perspect. Biol.* **2014**, *6*, a016295. [CrossRef] [PubMed]
- Diao, B.; Wang, C.; Tan, Y.; Chen, X.; Liu, Y.; Ning, L.; Chen, L.; Li, M.; Liu, Y.; Wang, G.; et al. Reduction and Functional Exhaustion of T Cells in Patients with Coronavirus Disease 2019 (COVID-19). *Front. Immunol.* **2020**, *11*, 827. [CrossRef] [PubMed]
- Mehta, P.; McAuley, D.F.; Brown, M.; Sanchez, E.; Tattersall, R.S.; Manson, J.J. HLH Across Speciality Collaboration, UK. COVID-19: Consider cytokine storm syndromes and immunosuppression. *Lancet* **2020**, *395*, 1033–1034. [CrossRef]
- Wu, C.; Chen, X.; Cai, Y.; Xia, J.; Zhou, X.; Xu, S.; Huang, H.; Zhang, L.; Zhou, X.; Du, C.; et al. Risk Factors Associated with Acute Respiratory Distress Syndrome and Death in Patients with Coronavirus Disease 2019 Pneumonia in Wuhan, China. *JAMA Intern. Med.* **2020**, *180*, 934–943. [CrossRef]
- Biasucci, L.M.; Liuzzo, G.; Fantuzzi, G.; Caligiuri, G.; Rebuffi, A.G.; Ginnetti, F.; Dinarello, C.A.; Maseri, A. Increasing levels of interleukin (IL)-1Ra and IL-6 during the first 2 days of hospitalization in unstable angina are associated with increased risk of in-hospital coronary events. *Circulation* **1999**, *99*, 2079–2084. [CrossRef] [PubMed]
- Cortinovis, M.; Perico, N.; Remuzzi, G. Long-term follow-up of recovered patients with COVID-19. *Lancet* **2021**, *397*, 173–175. [CrossRef]
- Bortolotti, D.; Gentili, V.; Rizzo, S.; Rotola, A. Rizzo R SARS-CoV-2 Spike 1 Protein Controls Natural Killer Cell Activation via the HLA-E/NKG2A Pathway. *Cells* **2020**, *9*, 1975. [CrossRef]
- De la Rica, R.; Borges, M.; Gonzalez-Freire, M. COVID-19: In the Eye of the Cytokine Storm. *Front. Immunol.* **2020**, *11*, 558898. [CrossRef] [PubMed]
- Said, E.A.; Tremblay, N.; Al-Balushi, M.S.; Al-Jabri, A.A.; Lamarre, D. Viruses Seen by our cells: The role of Viral RNA sensors. *J. Immunol. Res.* **2018**, *2018*, 9480497. [CrossRef] [PubMed]
- Mogensen, T.H. Pathogen Recognition and Inflammatory Signaling in Innate Immune Defenses. *Clin. Microbiol. Rev.* **2009**, *22*, 240–273. [CrossRef] [PubMed]
- Nazmi, A.; Dutta, K.; Hazra, B.; Basu, A. Role of pattern recognition receptors in flavivirus infections. *Virus Res.* **2014**, *185*, 32–40. [CrossRef]
- Lee, L.B.; Barton, G.M. Trafficking of endosomal Toll-like receptors. *Trends Cell Biol.* **2014**, *24*, 360–369. [CrossRef]
- Kawasaki, T.M.; Kawai, T. Toll-like receptor signaling pathways. *Front Immunol.* **2014**, *5*, 461. [CrossRef]
- Cervantes-Barragan, L.; Züst, R.; Weber, F.; Spiegel, M.; Lang, K.S.; Akira, S.; Thiel, V.; Ludewig, B. Control of coronavirus infection through plasmacytoid dendritic-cell-derived type I interferon. *Blood* **2007**, *109*, 1131–1137. [CrossRef]
- Poulas, K.; Farsalinos, K.; Zanidis, C. Activation of TLR7 and Innate Immunity as an Efficient Method Against COVID-19 Pandemic: Imiquimod as a Potential Therapy. *Front Immunol.* **2020**, *11*, 1373. [CrossRef]
- Takaoka, A.; Yamada, T. Regulation of signaling mediated by nucleic acid sensors for innate interferon-mediated responses during viral infection. *Int. Immunol.* **2019**, *31*, 477–488. [CrossRef]
- Schmitz, M.L.; Kracht, M.; Saul, V.V. The intricate interplay between RNA viruses and NF- κ B. *Biochim. Biophys. Acta Mol. Cell Res.* **2014**, *1843*, 2754–2764. [CrossRef]
- Yanai, H.; Chiba, S.; Hangai, S.; Kometani, K.; Inoue, A.; Kimura, Y.; Abe, T.; Kiyonari, H.; Nishio, J.; Taguchi-Atarashi, N.; et al. Revisiting the role of IRF3 in inflammation and immunity by conditional and specifically targeted gene ablation in mice. *Proc. Natl. Acad. Sci. USA* **2018**, *115*, 5253–5258. [CrossRef] [PubMed]

26. Liu, T.; Zhang, L.; Joo, D.; Sun, S. NF- κ B signaling in inflammation. *Signal. Transduct. Target. Ther.* **2017**, *2*, 17023. [[CrossRef](#)] [[PubMed](#)]
27. Nguyen, H.; Gazy, N.; Venketaraman, V. A Role of Intracellular Toll-Like Receptors (3, 7, and 9) in Response to Mycobacterium tuberculosis and Co-Infection with HIV. *Int. J. Mol. Sci.* **2020**, *21*, 6148. [[CrossRef](#)] [[PubMed](#)]
28. Kikkert, M. Innate immune evasion by human respiratory RNA viruses. *J. Innate. Immun.* **2020**, *12*, 4–20. [[CrossRef](#)]
29. Suwara, M.I.; Green, N.J.; Borthwick, L.A.; Mann, J.; Mayer-Barber, K.D.; Barron, L.; Corris, P.A. IL-1 α released from damaged epithelial cells is sufficient and essential to trigger inflammatory responses in human lung fibroblasts. *Mucosal Immunol.* **2014**, *7*, 684–693. [[CrossRef](#)]
30. Bortolotti, D.; Gentili, V.; Rotola, A.; Cultrera, R.; Marci, R.; di Luca, D.; Rizzo, R. HHV-6A infection of endometrial epithelial cells affects immune profile and trophoblast invasion. *Am. J. Reprod. Immunol.* **2019**, *82*, e13174. [[CrossRef](#)]
31. Livak, K.J.; Schmittgen, T.D. Analysis of relative gene expression data using real-time quantitative PCR and the 2(-Delta Delta C(T)) Method. *Methods* **2001**, *25*, 402–408. [[CrossRef](#)] [[PubMed](#)]
32. Mizukami, Y.; Takahashi, Y.; Shimizu, K.; Konishi, S.; Takakura, Y.; Nishikawa, M. Regulation of the Distribution of Cells in Mixed Spheroids by Altering Migration Direction. *Tissue Eng.* **2019**, *25*, 5–6. [[CrossRef](#)]
33. Shang, J.; Wan, Y.; Luo, C.; Ye, G.; Geng, Q. Cell entry mechanisms of SARS-CoV-2. *Proc. Natl. Acad. Sci. USA* **2020**, *117*, 11727–11734. [[CrossRef](#)] [[PubMed](#)]
34. Hsin, F.; Chao, T.; Chan, Y.; Kao, H.; Liu, W.; Wang, J.; Pang, Y.; Lin, C.; Tsai, Y.; Lin, J.; et al. Distinct Inductions of and Responses to Type I and Type III Interferons Promote Infections in Two SARS-CoV-2 Isolates. *bioRxiv* **2020**. [[CrossRef](#)]
35. Doyle, S.E.; Vaidya, S.A.; O'Connell, R.; Dadgostar, H.; Dempsey, P.W.; Wu, T.; Rao, G.; Sun, R.; Haberland, M.E.; Modlin, R.L.; et al. IRF3 Mediates a TLR3/TLR4-Specific Antiviral Gene Program. *Immunity* **2002**, *17*, 251–263. [[CrossRef](#)]
36. Mazaleuskaya, L.; Veltrop, R.; Ikpeze, N.; Martin-Garcia, J.; Navas-Martin, S. Protective role of Toll-like receptor 3-induced type I interferon in murine coronavirus infection of macrophages. *Viruses* **2012**, *4*, 901–923. [[CrossRef](#)]
37. Khanmohammadi, S.; Rezaei, N. Role of Toll-like receptors in the pathogenesis of COVID-19. *J. Med. Virol.* **2021**, *93*, 2735–2739. [[CrossRef](#)]
38. Totura, A.L.; Whitmore, A.; Agnihothram, S.; Schäfer, A.; Katze, M.G.; Heise, M.T.; Baric, R.S. Toll-Like Receptor 3 Signaling via TRIF Contributes to a Protective Innate Immune Response to Severe Acute Respiratory Syndrome Coronavirus Infection. *mBio* **2015**, *6*, e00638–15. [[CrossRef](#)]
39. Van der Made, C.I.; Simons, A.; Schuurs-Hoeijmakers, J.; van den Heuvel, G.; Mantere, T.; Kersten, S.; van Deuren, R.C.; Steehouwer, M.; van Reijmersdal, S.V.; Jaeger, M.; et al. Presence of genetic variants among young men with severe COVID-19. *JAMA* **2020**, *324*, 663–673. [[CrossRef](#)]
40. Moreno-Eutimio, M.A.; López-Macías, C.; Pastelin-Palacios, R. Bioinformatic analysis and identification of single-stranded RNA sequences recognized by TLR7/8 in the SARS-CoV-2, SARS-CoV, and MERS-CoV genomes. *Microb. Infect.* **2020**, *22*, 226–229. [[CrossRef](#)]
41. Veras, F.P.; Pontelli, M.C.; Silva, C.M.; Toller-Kawahisa, J.E.; de Lima, M.; Nascimento, D.C.; Schneider, A.H.; Caetité, D.; Tavares, L.A.; Paiva, I.M.; et al. SARS-CoV-2-triggered neutrophil extracellular traps mediate COVID-19 pathology. *J. Exp. Med.* **2020**, *217*, e20201129. [[CrossRef](#)]
42. Liao, Q.-J.; Ye, L.-B.; Timani, K.A.; Zeng, Y.-C.; She, Y.-L.; Ye, L.; Wu, Z.-H. Activation of NF- κ B by the Full-length Nucleocapsid Protein of the SARS Coronavirus. *Acta Biochim. Biophys. Sin.* **2005**, *37*, 607–612. [[CrossRef](#)]
43. DeDiego, M.L.; Nieto-Torres, J.L.; Jimenez-Guardeño, J.M.; Regla-Nava, J.A.; Castaño-Rodríguez, C.; Fernandez-Delgado, R.; Usera, F.; Enjuanes, L. Coronavirus virulence genes with main focus on SARS-CoV envelope gene. *Virus Res.* **2014**, *194*, 124–137. [[CrossRef](#)] [[PubMed](#)]
44. Khan, S.; Shafiei, M.S.; Longoria, C.; Schoggins, J.; Savani, R.C.; Zaki, H. SARS-CoV-2 spike protein induces inflammation via TLR2-dependent activation of the NF- κ B pathway. Version 1. *bioRxiv* **2021**. [[CrossRef](#)]
45. Fung, S.-Y.; Siu, K.-L.; Lin, H.; Yeung, M.L.; Jin, D.-Y. SARS-CoV-2 main protease suppresses type I interferon production by preventing nuclear translocation of phosphorylated IRF3. *Int. J. Biol. Sci.* **2021**, *17*, 1547–1554. [[CrossRef](#)] [[PubMed](#)]
46. Schroeder, S.; Pott, F.; Niemeyer, D.; Veith, T.; Richter, A.; Muth, D.; Goffinet, C.; Müller, M.A.; Drosten, C. Interferon antagonism by SARS-CoV-2: A functional study using reverse genetics. *Lancet Microbe* **2021**, *5*, e210–e218. [[CrossRef](#)]

It is known that innate immunity is essential to determine the activation of an efficient acquired immune response.

This is possible thanks to the loading of peptides synthesized during viral replication on Major Histocompatibility Complex (MHC) molecules, which present the viral peptides on the surface of infected cells, in order to be recognized by lymphocytes [316], inducing lymphocytes expansion and the development of immune memory [317].

It can be deduced that the MHC molecules, also known as Human Leukocyte antigens (HLAs), permit the communication between innate and adaptive immune system. HLAs can be subdivided into three classes: HLA class-I (HLA-A, B and C), which present peptides synthesized inside the cell [318], HLA class-II (DP, DM, DO, DQ and DR), involved in the presentation of extracellular antigens, and HLA class-III, which encode components of the complement system [319]. HLA-I molecules are also divided into “non-classical” and “classical” molecules. While the main function of classical HLA-I consists in presenting antigenic peptide to CD8+ T cells [320], non-classical HLAs act as immunomodulatory molecules [319]. The non-classical HLA-I include HLA-E, -G, -F and -H, characterized by a lower polymorphism compared to the classical group [319].

Immune-escape strategies used by viruses also include HLA molecules modulation. For example, the alteration of specific HLA class-II (HLA-DR) affects monocyte and macrophage function. In fact, an association between low expression of HLA-DR on monocytes and ICU needing were observed in serious COVID-19 subjects [321], representing a marker of immune suppression typical of SARS-CoV-2 infection. Moreover, Spike protein mutations can evade *in vitro* CD8+ T cell responses, since the Spike-derived peptides loaded on HLA-I molecules result less efficient in T cell stimulation [322].

Again, the modulation of HLA-I molecules expression is also used by viruses to avoid host immune recognition ([323], paper attached).

For instance, HBV, CMV, HP, HIV and also SARS-CoV-2 exploit the modulation of the non-classical HLA-E and HLA-G molecules as an immune evasion strategy ([323], paper attached), resulting in over-activated and/or decreased immune response [324], as summarized in the work below ([323], paper attached).



Contents lists available at ScienceDirect

journal homepage: www.elsevier.com/locate/humimm

Review

Non-classical HLA class I molecules and their potential role in viral infections

Silvia Beltrami^{a,1}, Sabrina Rizzo^{a,1}, Giovanni Strazzabosco^a, Valentina Gentili^a, Andrea Alogna^a, Marco Narducci^{a,b}, Daria Bortolotti^a, Giovanna Schiuma^{a,2}, Roberta Rizzo^{a,c,*}

^a Department of Chemical, Pharmaceutical and Agricultural Sciences, University of Ferrara, Ferrara, Italy - Via Luigi Borsari, 46, 44121 Ferrara, Italy

^b Temple University, Japan Campus, 1 Chome-14-29 Taishido, Setagaya City, Tokyo 154-0004, Italy

^c LTTA, University of Ferrara, Via Luigi Borsari, 46, 44121 Ferrara, Italy

ARTICLE INFO

Keywords:

HLA-E
HLA-G
Viral infection
SARS-CoV-2
NK cells

ABSTRACT

Human Leukocyte Antigens (HLA) are classified in three different classes I, II and III, and represent the key mediators of immune responses, self-tolerance development and pathogen recognition. Among them, non-classical subtypes (HLA-Ib), e.g. HLA-E and HLA-G, are characterized by tolerogenic functions that are often exploited by viruses to evade the host immune responses.

In this perspective, we will review the main current data referred to HLA-G and HLA-E and viral infections, as well as the impact on immune response. Data were selected following eligibility criteria accordingly to the reviewed topic. We used a set of electronic databases (Medline/PubMed, Scopus, Web of Sciences (WOS), Cochrane library) for a systematic search until November 2022 using MeSH keywords/terms (i.e. HLA, HLA-G, HLA-E, viral infection, SARS-CoV-2, etc...).

Recent studies support the involvement of non-classical molecules, such as HLA-E and HLA-G, in the control of viral infection. On one side, viruses exploit HLA-G and HLA-E molecule to control host immune activation. On the other side, the expression of these molecules might control the inflammatory condition generated by viral infections. Hence, this review has the aim to summarize the state of art of literature about the modulation of these non-classical HLA-I molecules, to provide a general overview of the new strategies of viral immune system regulation to counteract immune defenses.

Contents

1. Introduction	00
2. Methods	00
3. Role of non-classical HLA-I molecules in viral infections	00
3.1. HLA-E modulation during viral infections	00
3.2. HLA-G modulation during viral infections	00
3.3. Non classical HLA-I molecules and SARS-CoV-2 infection	00
3.4. HLA-E and SARS-CoV-2	00
3.5. Role of HLA-G during SARS-CoV-2 infection	00
4. Conclusions	00
Declaration of Competing Interest	00
References	00

* Corresponding author.

E-mail address: rbr@unife.it (R. Rizzo).

¹ Equally contributed to the manuscript.

² Equally contributed to the manuscript.

<https://doi.org/10.1016/j.humimm.2023.03.007>

Received 1 December 2022; Revised 14 March 2023; Accepted 27 March 2023

Available online xxx

0198-8859/© 2023 Published by Elsevier Inc. on behalf of American Society for Histocompatibility and Immunogenetics.

Please cite this article in press as: S Beltrami et al. Non-classical HLA class I molecules and their potential role in viral infections. Hum. Immunol. (2023), <https://doi.org/10.1016/j.humimm.2023.03.007>

1. Introduction

Nearly 60 years ago, Human Leukocyte Antigen (HLA) system, the major histocompatibility complex (MHC) in humans has been discovered and its role was identified in the activation of the immune system against several pathogens [1]. HLAs are encoded by a gene family clustered in a region of chromosome 6 and their main function is to present intracellular and extracellular peptide antigens to immune cells, regulating both innate and adaptive immune responses [2]. Basing on their function and expression, HLA molecules are classified into three different groups: class I, class II and class III.

HLA-III proteins are involved in both indirect and direct activation of immune system, involving for example complement activation, for example by the encode of TNFbeta (TNF β) or Lymphocyte antigen 6 (Ly6)[3]. Conversely, HLA-I and -II are involved in immune response activation. In particular, while HLA-II proteins are mainly expressed by professional antigen-presenting cells (APCs), such as macrophages, dendritic cells and B cells, enabling antigen presentation to CD4 + helper T cells [4], HLA-I proteins are expressed ubiquitously on all nucleated cells, in order to present intracellular self/non-self antigens to CD8 + cytotoxic T cell receptors and regulate Natural Killer cells (NK) activation mainly by killer-cell immunoglobulin-like receptors (KIR) engagement [1].

Furthermore, HLA-I molecules can be broadly divided into classical HLA-Ia (HLA-A, B and C) and non-classical subtypes HLA-Ib (including HLA-E, F, G and H).

The major difference between HLA-Ia and -Ib is that non-classical HLA-I molecules are less polymorphic than classical ones [1]. Moreover, HLA-Ib exert functions in both the innate and adaptive immune system but, importantly, they appear to have mostly inhibitory effects on immune cells compared to HLA-Ia, due to their capability to interact with several inhibitory receptors [1].

Among the HLA-I molecules, the most studied for their tolerogenic effect are HLA-E and HLA-G.

HLA-E is mainly expressed by endothelial and immune cells, where HLA-E exhibits a dual role since it can both activate or inhibit immune responses, by interacting with activating or inhibitory receptors, respectively [5]. The immune-regulatory function of HLA-E appears to be particularly crucial in NK cells, which could be both activated or inhibited by HLA-E interaction depending by its interaction with stimulatory CD94/NKG2C and inhibitory CD94/NKG2A receptors, respectively (Fig. 1) [6]. The interaction of HLA-E with the respective immune effector cell depends considerably on the peptide presented on HLA-E, which is an essential condition for its stable expression, which include specific peptides derived from HLA-G and other HLA-class I molecules [7]. HLA-E molecule loaded with the HLA-G leader sequence-derived peptide binds CD94/NKG2A with a high affinity, even if HLA-E molecule loaded with a leader sequence-derived non-amer peptide from either HLA-B58, HLA-Cw*0702 or HLA-Cw*0402 also binds the same receptor (Fig. 1) [8]. On the contrary, only the HLA-E-G leader sequence-derived peptide binds CD94/NKG2C with an affinity (~10 μ M) that is able to trigger a response by the NK cell (Fig. 1) [8].

HLA-E molecules are one of the least polymorphic members of the HLA-I family. It has been proposed that eight alleles are involved in coding three known proteins, but only HLA-E*01:01 and HLA-E*01:03 alleles occur in significant frequencies (nearly 50% each). These two HLA-E alleles vary in peptide binding affinity and level of expression, with HLA-E*01:03 reported to show the higher affinity and the lower cell surface expression [9]. Between these two main alleles, it has been demonstrated that HLA-E*01:01 also appears to bind CD94/NKG2A (Fig. 1), supporting the evidence that HLA-E affinity to the inhibitory CD94/NKG2A receptor is sixfold higher than the other receptor.

HLA-G was firstly described expressed during pregnancy, where it is fundamental to induce maternal immune system tolerance towards the semi-allogenic fetus [10]. The alternative splicing of the primary HLA-G mRNA leads to 7 different isoforms of the protein (G1-G7): G1-G4 isoforms are membranous proteins, while G5-G7 are soluble molecules (sHLA-G). Besides the 7 different isoforms, HLA-G is the most polymorphic of the non-classical molecules, several polymorphisms, including Single Nucleotide Polymorphisms (SNPs), have been identified as implicated in HLA-G stability and expression. For instance, referring specifically at the 3'UTR region, several polymorphisms have been reported to influence mRNA stability, turnover, mobility, and splicing pattern. In particular, a 14 base pair (14 bp) insertion/deletion (INS/DEL) polymorphism (rs66554220) in 3'UTR involves mRNA stability and expression, since the DEL allele stabilizes the mRNA with a consequent higher HLA-G expression [11]. Conversely, in 3'UTR the presence of an adenine at position + 3187, decreases mRNA stability and the + 3142C > G SNP could influence HLA-G expression by increasing mRNA degradation [12]. HLA-G expression shows a limited tissue-specific distribution [13], which includes cytotrophoblast cells at the maternal-fetal interface of the placenta, corneal, nail matrix, embryonic mesenchymal stem cells and pancreatic islet β cells. HLA-G main function consists in modulating immune system by interaction with its specific receptors, including ILT-2, ILT-4, and KIR2DL4 [14] (Fig. 1), which results in the inhibition of a wide range of immune functions, including the cytolytic function of cytotoxic T cells, as well as the allo-proliferative response of CD4 + T cells, the ongoing proliferation of NK and T cells and the maturation of dendritic cells [15]. Moreover, the engagement of HLA-G receptors depends on HLA-G alleles expressed on cell surface. For example, it has been demonstrated that the most common allelic subtypes HLA-G*01:01/01:03 and 01:04 differ in peptide repertoire and consequently in receptors engagement on NK cells. Particularly, several studies have shown that the affinity of NKG2A/CD94 for G*01:04 seems to be the highest, followed by G*01:03, while the NKG2A/CD94-G*01:01 binding has been reported to be marginal (Fig. 1) [16].

Moreover, HLA-G was also reported to be able to modulate HLA-E expression. In particular, the expression of different isoforms of HLA-G can generate different kind of peptides which bind by HLA-E pocket, affecting its expression on cell surface. Furthermore, HLA-G and HLA-E are physiologically co-expressed on different cell populations establishing an immune-suppressive microenvironment in different physiological and pathological conditions [17].

In fact, these non-classical molecules can be altered in particular conditions, resulting in pathological alterations leading to diseases such as inflammatory and autoimmune diseases [18], pregnancy disorders and abortions [19] and coronary artery diseases [20].

In particular, HLA-E*01:01 allele was found to be associated with type 1 diabetes mellitus, an impaired glucose metabolism disease which could be also related to higher levels of sHLA-G [21].

On the other hand, while HLA-E*01:01/HLA-E*01:01 genotype is associated with reduced risk of rheumatoid arthritis [22], the HLA-G gene expression has been shown to be up-regulated in bone marrow-derived mononuclear cells of these patients [23].

Moreover, HLA-E*01:03 homozygous individuals are associated to a lower risk of psoriatic arthritis, supporting the result obtained analyzing patients with psoriasis, in which the HLA-E*01:01 homozygous leads to a higher risk of this disease. Again, HLA-G can be detected in psoriatic skin lesions, although, significantly lower sHLA-G plasma levels have been found in psoriatic patients compared with controls [24], suggesting a difference in systemic HLA-G expression that could be associated with the IL-10 deficiency typical of psoriasis.

Torres et al. have also shown the presence of higher sHLA-G levels in biopsies from celiac patients, and an increased frequency of the 14 bp INS/INS genotype among celiac patients has been stated [25].

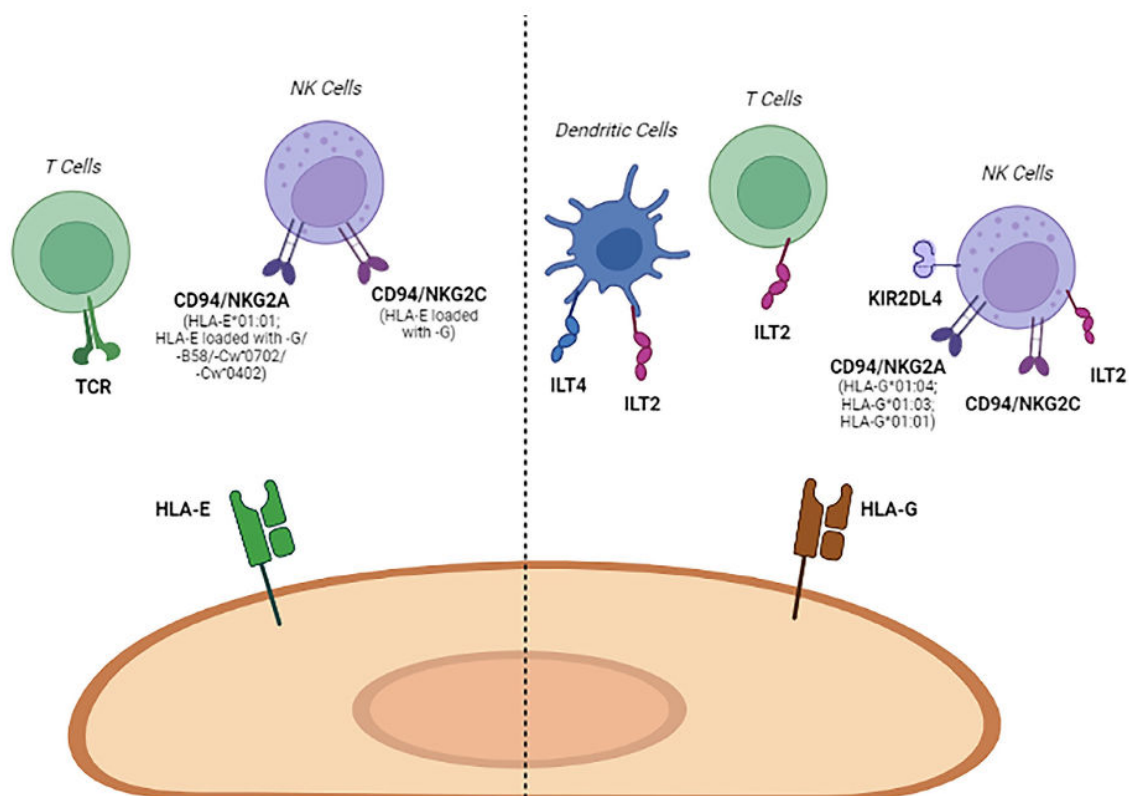


Fig. 1. HLA-E and HLA-G receptors expressed by immune cells.

In addition, several studies of pre-eclampsia, recurrent spontaneous abortions (RSA) and blastocyst implantation also suggest that HLA-G expression and genetics, in both woman and embryo/fetus, may be important for pregnancy and its outcome [14].

Accordingly, the tolerogenic effect exerted by both HLA-G and HLA-E molecules towards both the innate and adaptive immune system is often exploited by pathogens as an immune-escape mechanism [15].

2. Methods

In this perspective, we have reviewed the main current data referred to non classical HLA class I molecules and viral infections. Data were selected following eligibility criteria accordingly to the reviewed topic. We used a set of electronic databases (Medline/PubMed, Scopus, Web of Sciences (WOS), Cochrane library) for a systematic search until November 2022 using MeSH keywords/terms, such as “HLA”, “HLA-G”, “HLA-E”, “viral infection”, “SARS-CoV-2”. We applied no date or language restriction. We followed the Preferred Reporting Items for the Systematic Review and Meta-Analysis (PRISMA) statement [26]. Two independent reviewers performed title-abstract screening on all selected studies, then the full-text of the selected articles was reviewed. In cases of duplicate information, the data were checked and combined. Studies reporting HLA-G, HLA-E as well as viral infection were selected. Publications were selected using specific keywords (i.e. HLA, HLA-G, HLA-E, viral infection, SARS-CoV-2, etc...) also according to the date of publication (not older than 1999) and for the fulfillment with the topic of this review. Studies that were just case reports and commentaries were excluded. The extraction of the data from included studies was performed by

Table 1

HLA-E and HLA-G expression modifications during viral infections and their effect on immune system.

Virus	Expression	Effects	References
HCV	HLA-E up-regulation HLA-G up-regulation	Decreased cytotoxicity of effector cells	22, 23 27, 32, 33, 34, 35
HIV	HLA-E/HIV-1 peptide	NK cell activation – viral spreading NK cell inhibition	26 36, 37
CMV	HLA-G up-regulation HLA-E up-regulation HLA-G up-regulation	Inhibitory signal	24 29, 30, 31
HPV	HLA-E up-regulation HLA-G up-regulation	NK inhibition Immune escape	25 38
HBV	HLA-G up-regulation	Immune escape	32, 33
HHV-6	HLA-G up-regulation	Immune escape	41
HSV-1	HLA-G up-regulation	Immune escape	42
SARS-CoV-2	HLA-E up-regulation HLA-G: Early phase Replication phase Remission phase	NK cell inhibition Hyper-inflammation MMPs activation Immune response control	50, 51, 54, 55 60, 61 61, 63 60

two reviewers separately, considering key characteristics including publication year, author, type of study, country, sample size, and laboratory findings. The funnel plot and Egger's regression test were used to assess publication bias [27].

3. Role of non-classical HLA-I molecules in viral infections

Due to the opposite role of classical and non-classical HLA-I molecules in regulating host immune response, a fine balance between the downregulation of classical HLA-I and the upregulation of non-classical HLA-I is observed during viral infections [28].

In humans, CD8 + cytotoxic T lymphocytes (CTLs) control viral infections via recognition of HLA-I antigens loaded with viral peptides by T cell receptor (TCR). Therefore, the expression of HLA-I molecules is extremely important for the immune response activation during infections, and several viruses have developed strategies to decrease the expression of HLA-I antigens to avoid T-cell recognition [28].

Conversely, the down-modulation of HLA-I molecules, induced by viral infections, triggers NK cells activation [29], that sense the absence of HLA-I on the surface on infected cells. Thus, to also avoid NK cell activation, several viruses have developed mechanism to modulate both HLA-E and HLA-G molecules expression, in order to inhibit NK cells through the binding with inhibitory receptors.

3.1. HLA-E modulation during viral infections

Although HLA-E presents a restricted number of antigens, it can present pathogen-derived peptides eliciting specific T cell responses [30] (Fig. 1). However, as previously mentioned, during viral infections the balance between inhibitory and stimulatory signals could be altered, including HLA-E expression [5] (Table 1).

Hepatitis C virus (HCV) is a positive-sense single-stranded RNA enveloped virus of the family *Flaviviridae*. HCV is the cause of hepatitis C and some cancers such as liver cancer (hepatocellular carcinoma) and lymphomas in humans. HCV viral core protein stabilizes HLA-E surface expression resulting in impaired NK cell-mediated cytotoxicity via interaction with NKG2A receptor [31]. Cytomegalovirus (CMV), or Human Herpesvirus 5, is a genus of viruses in the order *Herpesvirales*, in the family *Herpesviridae*, in the subfamily *Betaherpesvirinae*. Diseases associated with CMV include mononucleosis and pneumonia. CMV glycoprotein UL40 (gpUL40) upregulates and stabilizes HLA-E expression in infected cells, inhibiting NK cells activation through CD94/NKG2 receptor signaling [32]. A similar effect is observed for UL18 glycoprotein, representing a homologous of HLA-I molecules which can bind ILT2 (LIR-1, CD85j) inhibitory receptors on the surface of NK cells, favoring viral immune-escape. Human papillomavirus (HPV), a DNA virus from the *Papillomaviridae* family, can affect humans and results in either warts or precancerous lesions. HPV infection decreases the surface expression of HLA-Ia proteins along with an increased HLA-E expression [33] and NK cells inhibition [33], allowing viral immune escape. Human immunodeficiency virus (HIV) is a *Lentivirus* of the family of *Retrovirus*, that infect humans and causes acquired immunodeficiency syndrome (AIDS), a condition in which progressive failure of the immune system allows life-threatening opportunistic infections and cancers. HIV highly conserved peptide is presented by HLA-E molecules but it is not recognized by CD94-NKG2A receptor, resulting in NK cell mediated lysis of HIV infected T cells, promoting viral spreading [34].

3.2. HLA-G modulation during viral infections

HLA-G expression is modulated by several viruses. Commonly, soluble HLA-G levels are increased during viral infections, such as HIV, CMV and Hepatitis B virus (HBV) (Table 1) [35], due to the high levels of cytokine production that stimulates HLA-G shedding from cell sur-

face by metalloproteases (MMP) activation [35]. In fact, viral infections induce Interleukin-10 (IL-10) secretion, leading to the activation of MMP2 which in turn cleaves HLA-G from cell surface, resulting in increased sHLA-G levels [36].

The CMV-encoded homologs IL-10 (cmvIL-10) is able to induce HLA-G expression, similarly to human IL-10 [37], preventing NK cell recognition of CMV infected cells.

Hepatitis C virus (HCV) and Hepatitis B virus (HBV), a partially double-stranded DNA virus of the genus *Orthohepadnavirus* of the *Hepadnaviridae* family, induce HLA-G expression to control host immune response as well (Table 1) [38]. During HBV and HCV infections, IL-10 and interferon-dependent MMPs induction leads to increased sHLA-G levels [35]. Furthermore, HLA-G expression is higher during chronic HBV infection [39]. Patients affected by HCV infection and increased levels of HLA-G molecules, mainly in liver fibrotic areas, showed a lower viral clearance and a defective response to therapy [40].

HLA-G serum levels increase during the first phases of HIV infection and lower to normal when infection progresses to a chronic stage (Table 1) [41], suggesting HLA-G detection as a biomarker for disease progression.

HLA-G expression correlates with HPV-associated nasal polyposis development [42] (Table 1). The host HLA-G genotypes appear to impact the outcomes of oral HPV infections in women [43] and men [44] but have little if any effect on genital HPV status or infection outcomes.

HLA-G is physiologically expressed during pregnancy and several viruses involved in congenital infection exploit HLA-G expression as an immune-escape mechanism, causing impairment of pregnancy as well. Human Herpesvirus 6 (HHV-6) is the common collective name for human betaherpesvirus 6A (HHV-6A) and human betaherpesvirus 6B (HHV-6B), double-stranded DNA viruses within the *Betaherpesvirinae* subfamily and of the genus *Roseolovirus*. HHV-6A has been associated with late-onset intrauterine growth restriction (IUGR), resulting in impaired growth and development of the fetus [45]. In fact, the presence of HHV-6 in a high percentage of IUGR placenta samples has been detected, together with a higher HLA-G expression (Table 1), suggesting a correlation between the presence of this virus and the increase of HLA-G at endometrial level [45].

Herpes Simplex Virus-1 (HSV-1), a member of the *Betaherpesvirinae* subfamily of the *Herpesviridae* family, induces the up-regulation of membrane and soluble HLA-G molecules in actively infected neurons, with a consequent protection toward host NK cells response (Table 1) [46].

3.3. Non classical HLA-I molecules and SARS-CoV-2 infection

SARS-CoV-2 is a new Betacoronavirus, emerged in December 2019 in Wuhan, China, associated with a severe respiratory syndrome called COVID-19. Its rapid spread around the world has led the World Health Organization (WHO) to declare the state of pandemic in the month of March 2020 [47]. SARS-CoV-2, in addition to lung tissue, is also able to infect numerous other tissues thanks to the high expression of receptors recognized by viral Spike protein 1 (SP1), including ACE2 (Angiotensin-converting enzyme 2) and CD147, which mediate their entry into the host cell [48]. SARS-CoV-2 evades the recognition of immune system to promote its replication, developing asymptomatic infection or severe and lethal COVID-19 pathology. Several risk factors have been described to participate in COVID-19 severity, including age, male gender and comorbidities [49], but did not explain the differences in severity of COVID-19 observed among individuals, suggesting that also patient's genetic background may contribute to severity and clinical outcome of COVID-19 [50]. This hypothesis is supported by the observation that some COVID-19 patients develop macrophages and monocytes hyperactivation [51] that promote cytokine storm and functional lymphopenia [52]. The immunological mechanisms associ-

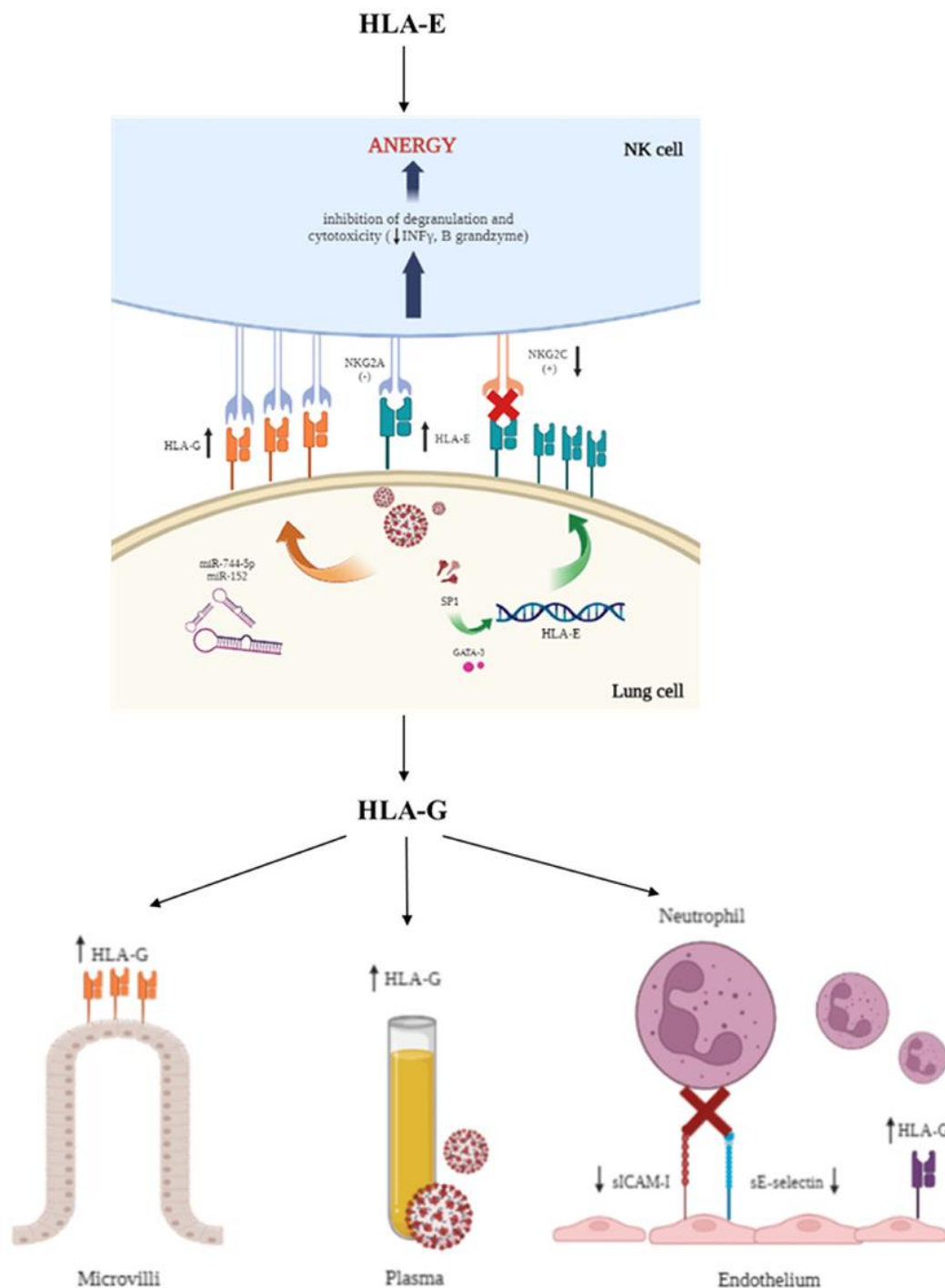


Fig. 2. HLA-E and HLA-G role during SARS-CoV-2 infection and immunological features in COVID-19.

ated with SARS-CoV-2 infection are complex and not entirely clear and recent studies suggested that non-classical HLA-I molecules, including HLA-G and HLA-E, are involved in SARS-CoV-2 infection.

3.4. HLA-E and SARS-CoV-2

NK cells are important effectors in anti-viral immunity and their activation is partly controlled by the expression of HLA molecules,

via the interaction with specific receptors on cell surface [53]. Among the NK cells ligands, HLA-E represents one of the most studied, in particular for its interaction with the inhibitory receptor CD94/NKG2A, described as involved in promoting functional resistance to NK cell killing [6]. During SARS-CoV-2 lung infection, the S1 spike protein generates S1-derived HLA-E binding peptides, leading to increased HLA-E stabilization on cell membrane [54] (Fig. 2). In addition, NKG2A/CD94 inhibitory receptor was found up-modulated on NK

cells when S1 was expressed in lung epithelial cells. Thus, the increased expression of both HLA-E and NKG2A/CD94 on infected cells and NK cells, respectively, trigger NK cell cytotoxicity, secretion, and degranulation suppression [55]. In vivo evaluations reported an increase in positive-NKG2A/CD94 circulating lymphocytes (NK and T cells) with IFN- γ secretion and cytotoxicity reduction from the 16% to 80% in COVID-19 patients in comparison with controls, confirming the potential role of HLA-E/NKG2A binding in the final exhaustion of NK cells [10] (Fig. 2), partially explaining the anergic status observed in patients with severe COVID-19 [56].

The decrease in NK cells percentage in COVID-19 patients involves the non-structural protein 13₂₃₂₋₂₄₀ (Nsp13₂₃₂₋₂₄₀) of SARS-CoV-2, the helicase of the replication and transcription complex of the virion [57]. Viral Nsp13 is presented by HLA-E, forming a stable complex HLA-E/Nsp13₂₃₂₋₂₄₀. As demonstrated by Hammer et al., this HLA-E/Nsp13₂₃₂₋₂₄₀ complex elicits NK cells inhibition interfering with HLA-E binding to NKG2A receptor, thereby blocking NKG2A-positive NK cell effector functions [58]. On the contrary, HLA-E interaction with the receptor CD94/NKG2C seems to be crucial in NK cell hyperactivation during COVID-19 disease [59]. NKG2C activation by HLA-E mediates NK cell cytotoxicity and release of pro-inflammatory effectors during viral infections [60]. As a proof-of-concept, patients which experience severe or fatal COVID-19 outcomes showed an increased frequency of both circulating and lung-resident positive-NKG2C NK, characterized by increased proliferation and activation [61] and deletion of NKG2C gene was described in severe COVID-19 patients in association to a significant decreased NK cell activation, due to the lack of interaction between the receptor and HLA-E [61] (Fig. 2).

HLA-E genetic alleles seem to have a role in COVID-19 severity. The frequency of both homozygous and heterozygous HLA-E*0101 allele is higher in patients with severe COVID-19 disease, compared to those with mild disease condition [59]. Moreover, S1 peptide shows higher affinity with HLA-E*0101 than with HLA-E*0103 allele, supporting its involvement in the production of HLA-E/S1 peptide complex that enhances NK cells anergy and COVID-19 severity [59]. These results confirm the role of HLA-E in SARS-CoV-2 infection, due to the direct modulation of NK cells activation. The cell surface expression of HLA-E*0101 allele results in delayed or decreased positive-NKG2C NK cell response [9], promoting viral replication and infection.

3.5. Role of HLA-G during SARS-CoV-2 infection

A recent study by Zhang et al. described the modulation of HLA-G expression in patients with COVID-19, during the different infection stages [62]. Based on the three main stages of SARS-CoV-2 infection, early stage, progression and recovery, HLA-G levels can be described as depicted in (Fig. 3). The early infection stage is characterized by a high membrane expression of HLA-G, mainly at the surface of immune cells including T cells, B cells and monocytes. The increase in HLA-G expression might be triggered by the hyperinflammation induced by the SARS-CoV-2, and the consequent increase of IL-10, one of the main inducer of HLA-G expression. The replication stage is characterized by a decrease in HLA-G expression in immune cells, that inversely correlates with an increase of plasma sHLA-G [63]. The membrane-bound HLA-G might decrease for the delocalization into plasma after cleavage by MMPs [64], massively produced by connective tissue and pro-inflammatory cells including activated neutrophils during SARS-CoV-2 infection [53] (Fig. 3). In the replication stage of SARS-CoV-2, the total number of NK and CD8 + T cells is markedly decreased thus favouring the spread of the virus [62]. During convalescence, HLA-G expression is increased at surface of immune cells, with a concomitant decrease of plasma sHLA-G [65], significative of a reinforced immune response.

A recent genome-wide association study, with a larger case/control cohort (2244/10220) showed that HLA-G (rs9380142) polymorphism is strongly associated with severe COVID-19 [66], suggesting a possi-

ble association between HLA-G expression during COVID19 and genetic variants. The ability of SARS-CoV-2 to affect HLA-G expression might impair the function of host immune system, in particular decreasing NK cells activation during the acute phase of infection. In fact, during SARS-CoV-2 replication, the total number of NK cells decreases significantly in concomitance to high NKG2A/CD94 inhibitory receptor expression, causing a reduction of CD107a and granzyme B release [67]. Seliger et al. showed an increased expression of SARS-CoV-2 nucleocapsid antigen and spike protein in COVID-19 patients' lung tissues, that was associated with high HLA-G expression levels [68] and low levels of miR-744-5p and miR-152, involved in HLA-G regulation [68], suggesting that SARS-CoV-2 might control HLA-G via specific miRNA expression. In addition to miR-744-5p and miR-152, the transcriptome sequencing of whole blood of moderate and severe COVID-19 patients reveals that several miRNAs are affected during infection. In particular, miR-146a-5p, miR-21-5p, miR-142-3p, miR-181a-2-3p, miR-31-5p and miR-99a-5p were downregulated, while miR-3605-3p, miR-15b-5p, miR-486-3p and miR-486-5p were consistently upregulated. Thus, the presence of these molecular features constitutes an important suggestion of the role of miRNA encoded during SARS-CoV-2 in inhibiting or activating immune-related genes that could affect HLA-G expression, impairing firstly the pulmonary defence [69].

Although COVID-19 is primarily considered a respiratory disease, it is now clear that SARS-CoV-2 infection could also affect other body compartments, including the gastrointestinal system. In a study conducted on a patient with persistently negative swab test hospitalized intestinal ulceration [70], the presence of SARS-CoV-2 nucleoprotein (NP) was reported in the damaged intestinal mucosa in association to morphological alteration of microvilli, in concomitance to HLA-G expression at the site of SARS-CoV-2 infection. The induction of HLA-G expression, known to be involved in both viral immune-escape mechanism and neoangiogenesis processes, at the site of SARS-CoV-2 infection might be a cause of the COVID-19-dependent bleeding [70]. This evidence was confirmed also by a similar study conducted on three patients with acute abdominal symptoms, that on admission did not show any usual COVID-19 clinical signs but presented HLA-G gut expression and in situ viral infection [71].

A recent work reported higher levels of sHLA-G in plasma samples from COVID-19 patients in comparison with controls. The highest concentration of sHLA-G in plasma samples might be related to a better inflammation resolution, as it was found in patients who had better clinical course [63]. As a proof of concept for the potential role of sHLA-G levels in COVID-19 severity, the authors assessed the levels of endothelial activation biomarkers and correlated them with sHLA-G levels, reporting an inverse correlation between sHLA-G levels and sICAM-1 and E-selectin levels in COVID-19 patients, but not in controls. The ability of HLA-G molecules to control sICAM-1 and sE-selectin expression via CD160 interaction and subsequent FGF2 induction, might affect neutrophil adhesion, as confirmed by in vitro experiments. Thus, these findings suggested a possible role for sHLA-G in the regulation of neutrophil adhesion to activated endothelium in COVID-19 patients, which is associated to disease improvement [63]. The critical role of sHLA-G plasmatic levels was confirmed also by other studies. Bayatee et al. found significantly increased sHLA-G levels in serum samples from COVID-19 patients compared to controls [72] and Cordeiro et al. showed a correlation between disease severity and sHLA-G levels, that are significantly reduced in critically ill patients, suggesting an immune exhaustion phenomena [73].

Recent studies have reported the ability of SARS-CoV-2 to infect placenta, which is a specialized organ that supports the normal growth and development of the fetus, due to the high tissue expression of ACE2 and CD147 receptors [74]. Since HLA-G is involved in promoting fetus tolerance [75], its physiological expression during pregnancy could be exploited by several viruses, such as SARS-CoV-2. In particular, non-classical HLA-G molecules are expressed by the extravillous

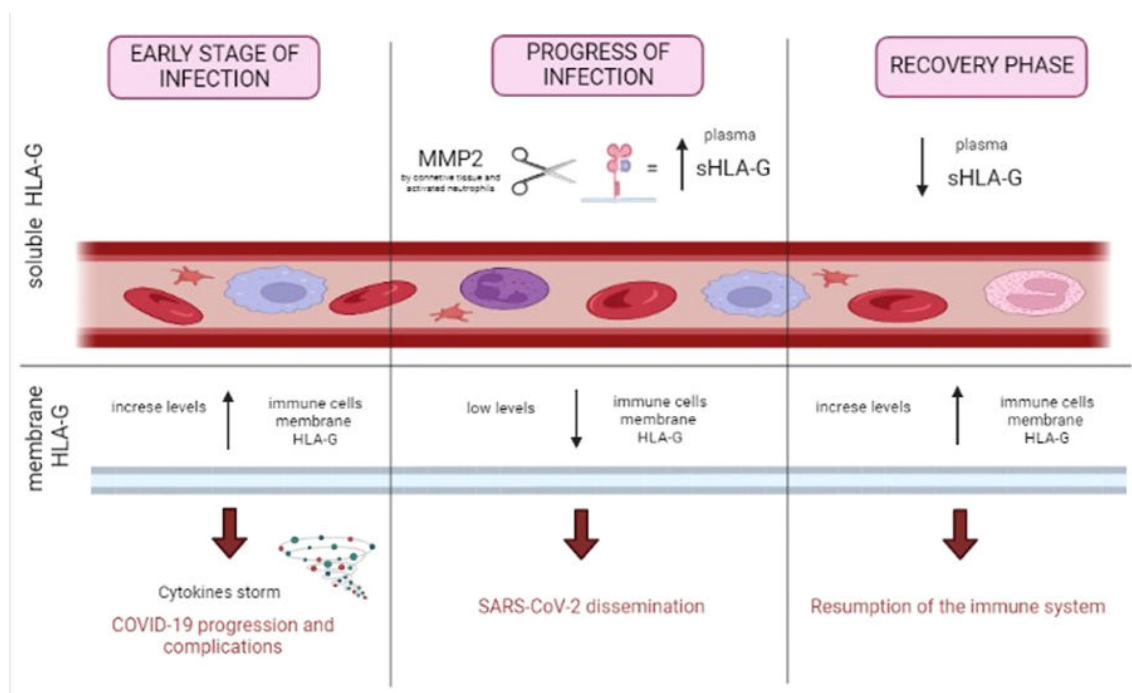


Fig. 3. Membrane and soluble HLA-G expression modification during SARS-CoV-2 infection.

trophoblast (EVT) cells of placenta and interact with their specific receptors expressed by immune cells, including T lymphocytes and uterine NK cells, in order to ensure immune tolerance between mother and fetus, inhibiting NK cell activity [75]. It has been suggested a possible role of HLA-G expression in COVID-19 pathogenesis during pregnancy. Expression and cluster analysis of placental cell type specific markers in COVID-19 patients showed a decrease in the expression of trophoblast markers, as HLA-G, compared with control samples, and an increased expression of chemokines and pathways associated with viral infection and inflammation [76]. As previously reported, during viral infection there is an up-regulation of NKG2A/CD94 receptor, that binds HLA-G leading to NK cells exhaustion [67], that might present an altered activation during pregnancy. The possible placental transmission of SARS-CoV-2 could follow a similar path to what observed for other pathogens, supported by the modification of HLA-G expression: (1) viral spreading from the maternal endothelial microvasculature to the endovascular extravillous trophoblasts; (2) spreading through the infected maternal immune cells; (3) transcytosis of virions via immune-mediated receptors; (4) transvaginal ascending infection; and (5) releasing of inflammatory mediators leading to increased permeability of placental barriers [77].

4. Conclusions

HLA system is a key mediator of immune responses to pathogens [1]. In this review we focused on non-classical HLA class I molecules, a group of antigen-presenting proteins characterized by a tissue/cell specific expression and a peculiar role during viral infections. Among these, both HLA-E and HLA-G exhibit immunomodulatory functions, and their immune tolerogenic effect is often exploited by viral pathogens as an immune-escape mechanism [5]. Several studies demonstrate that in HCV [31], HIV [78], CMV [32] and HPV [33] infections, the viral proteins stabilize HLA-E expressing cells, resulting

in impaired NK cell-mediated cytotoxicity due to its interaction with inhibitory NKG2A receptor. Also, HLA-G levels are up-regulated during viral infections, such as during HIV [79], CMV [37], HBV [35] and HCV [80] infections.

SARS-CoV-2 promotes its replication through HLA-G and HLA-E modulation, supporting their implication in infection susceptibility and severity of COVID-19. Regarding HLA-G, a recent study described its modulation during the various stages of SARS-CoV-2 infection, with high levels in early stage and recovery phases, while it decreases during replication phase [63]. HLA-G expression was also observed in the sites of intestinal SARS-CoV-2 infection [70,71]. SARS-CoV-2 controls NK cell functions modulating the levels of HLA-E on lung epithelial cells, that results in NK cells anergy. During infection, the virus encodes a S1-derived HLA-E binding peptide, which stabilize and upregulate HLA-E levels on lung epithelial cells. The peptide-loaded HLA-E binds to NKG2A receptor and transduces inhibitory signaling to NK cells, suppressing their cytotoxicity [54] (Fig. 1). The peptide-loaded HLA-E is unable to recognize the activating NKG2C/HLA-E receptor, leading to NK cells exhaustion (Fig. 1). In this scenario is mainly involved HLA-E*0101 allele, suggesting a genetic background implicated in severe COVID-19 cases [61].

These data on HLA-G and HLA-E molecules during viral infections suggest a possible use as biomarkers to monitoring viral susceptibility and disease outcome. New approaches, based on HLA-G and HLA-E targeting, might provide opportunities for developing novel anti-viral therapies, to control immune response to viral infections.

This review was funded by HHV-6 foundation, FISM - Fondazione Italiana Sclerosi Multipla onlus grant no° Cod 2019/R-Single/004.

Declaration of Competing Interest

The authors declare that they have no known competing financial interests or personal relationships that could have appeared to influence the work reported in this paper.

References

- [1] R.C. Wyatt et al, What the HLA-II-classical and non-classical HLA class I and their potential roles in type 1 diabetes, *Curr. Diab. Rep.* 19 (12) (2019) 159.
- [2] G. Bodis, V. Toth, A. Schwarting, Role of human leukocyte antigens (HLA) in autoimmune diseases, *Rheumatol. Ther.* 5 (1) (2018) 5–20.
- [3] C.A. Sargent et al, Human major histocompatibility complex contains genes for the major heat shock protein HSP70. *Proceedings of the National Academy of Sciences*, 1989. **86**(6): p. 1968-1972.
- [4] P. Innerhofer, G. Kühbacher, Immunomodulation mechanisms following transfusion of allogeneic und autologous erythrocyte concentrates, *Transfus. Med. Hemother.* 29 (3) (2002) 118–121.
- [5] F. Morandi et al, The role of HLA-class Ib molecules in immune-related diseases, tumors, and infections, *J. Immunol. Res.* 2014 (2014) 231618.
- [6] S. Rizzo et al, Role of KIR receptor in NK regulation during viral infections, *Immuno 1* (3) (2021) 305–331.
- [7] N. Lee et al, HLA-E surface expression depends on binding of TAP-dependent peptides derived from certain HLA class I signal sequences, *J. Immunol.* 160 (10) (1998) 4951–4960.
- [8] M. Vales-Gomez et al, Kinetics and peptide dependency of the binding of the inhibitory NK receptor CD94/NKG2-A and the activating receptor CD94/NKG2-C to HLA-E, *EMBO J.* 18 (15) (1999) 4250–4260.
- [9] R.K. Strong et al, HLA-E allelic variants. Correlating differential expression, peptide affinities, crystal structures, and thermal stabilities, *J. Biol. Chem.* 278 (7) (2003) 5082–5090.
- [10] A. Jewett, The potential effect of novel coronavirus SARS-CoV-2 on NK Cells; A perspective on potential therapeutic interventions, *Front. Immunol.* 11 (2020) 1692.
- [11] T.V. Hviid et al, HLA-G allelic variants are associated with differences in the HLA-G mRNA isoform profile and HLA-G mRNA levels, *Immunogenetics* 55 (2) (2003) 63–79.
- [12] E.C. Castelli et al, In silico analysis of microRNAs targeting the HLA-G 3' untranslated region alleles and haplotypes, *Hum. Immunol.* 70 (12) (2009) 1020–1025.
- [13] DISCORDE JEANDAUSSET†NATHALIEROUAS-FREISS, E.D.P.J.M.M., *HLA-G Molecules: from Maternal-Fetal Tolerance to Tissue Acceptance. Advances in Immunology*, 2003. **Volume 81**.
- [14] E. Alegre et al, Some basic aspects of HLA-G biology, *J. Immunol. Res.* 2014 (2014) 657625.
- [15] A. Gonzalez et al, The immunosuppressive molecule HLA-G and its clinical implications, *Crit. Rev. Clin. Lab. Sci.* 49 (3) (2012) 63–84.
- [16] G.T. Ho et al, NKG2A/CD94 is a new immune receptor for HLA-G and distinguishes amino acid differences in the HLA-G heavy chain, *Int. J. Mol. Sci.* 21 (12) (2020).
- [17] F. Morandi, V. Pistoia, Interactions between HLA-G and HLA-E in Physiological and Pathological Conditions, *Front. Immunol.* 5 (2014) 394.
- [18] F. Morandi, V. Pistoia, Interactions between HLA-G and HLA-E in physiological and pathological conditions, *Front. Immunol.* 5 (2014).
- [19] I. Zidi et al, sHLA-G1 and HLA-G5 levels are decreased in Tunisian women with multiple abortion, *Hum. Immunol.* 77 (4) (2016) 342–345.
- [20] I. Zidi et al, Nonclassical human leukocyte antigen (HLA-G, HLA-E, and HLA-F) in coronary artery disease, *Hum. Immunol.* 77 (4) (2016) 325–329.
- [21] A.D. Hodgkinson, B.A. Millward, A.G. Demaine, The HLA-E locus is associated with age at onset and susceptibility to type 1 diabetes mellitus, *Hum. Immunol.* 61 (3) (2000) 290–295.
- [22] M. Iwaszko et al, Polymorphisms within the human leukocyte antigen-E gene and their associations with susceptibility to rheumatoid arthritis as well as clinical outcome of anti-tumour necrosis factor therapy, *Clin. Exp. Immunol.* 182 (3) (2015) 270–277.
- [23] H.M. Lee et al, Abnormal networks of immune response-related molecules in bone marrow cells from patients with rheumatoid arthritis as revealed by DNA microarray analysis, *Arthritis Res. Ther.* 13 (3) (2011) R89.
- [24] A. Borghi et al, Soluble human leukocyte antigen-G and interleukin-10 levels in plasma of psoriatic patients: preliminary study on a possible correlation between generalized immune status, treatments and disease, *Arch. Dermatol. Res.* 300 (10) (2008) 551–559.
- [25] M.I. Torres et al, New advances in coeliac disease: serum and intestinal expression of HLA-G, *Int. Immunol.* 18 (5) (2006) 713–718.
- [26] D. Moher et al, Preferred reporting items for systematic review and meta-analysis protocols (PRISMA-P) 2015 statement, *Syst. Rev.* 4 (1) (2015) 1.
- [27] W.A. van Enst et al, Investigation of publication bias in meta-analyses of diagnostic test accuracy: a meta-epidemiological study, *BMC Med. Res. Method.* 14 (2014) 70.
- [28] B. Seliger, U. Ritz, S. Ferrone, Molecular mechanisms of HLA class I antigen abnormalities following viral infection and transformation, *Int. J. Cancer* 118 (1) (2006) 129–138.
- [29] E.O. Long et al, Controlling natural killer cell responses: integration of signals for activation and inhibition, *Annu. Rev. Immunol.* 31 (2013) 227–258.
- [30] S.A. Joosten, L.C. Sullivan, T.H. Ottenhoff, Characteristics of HLA-E restricted T-cell responses and their role in infectious diseases, *J. Immunol. Res.* 2016 (2016) 2695396.
- [31] J. Nattermann et al, Surface expression and cytolytic function of natural killer cell receptors is altered in chronic hepatitis C, *Gut* 55 (6) (2006) 869–877.
- [32] M. Llano et al, Differential effects of US2, US6 and US11 human cytomegalovirus proteins on HLA class Ia and HLA-E expression: impact on target susceptibility to NK cell subsets, *Eur. J. Immunol.* 33 (10) (2003) 2744–2754.
- [33] M.A. Goncalves et al, Classical and non-classical HLA molecules and p16(INK4a) expression in precursors lesions and invasive cervical cancer, *Eur. J. Obstet. Gynecol. Reprod. Biol.* 141 (1) (2008) 70–74.
- [34] Z.B. Davis et al, A conserved HIV-1-derived peptide presented by HLA-E renders infected T-cells highly susceptible to attack by NKG2A/CD94-bearing natural killer cells, *PLoS Pathog.* 12 (2) (2016) e1005421.
- [35] L. Amiot, N. Vu, M. Samson, Immunomodulatory properties of HLA-G in infectious diseases, *J. Immunol. Res.* 2014 (2014) 298569.
- [36] R. Rizzo et al, Matrix metalloproteinase-2 (MMP-2) generates soluble HLA-G1 by cell surface proteolytic shedding, *Mol. Cell. Biochem.* 381 (1–2) (2013) 243–255.
- [37] M. Onno et al, Modulation of HLA-G antigens expression by human cytomegalovirus: specific induction in activated macrophages harboring human cytomegalovirus infection, *J. Immunol.* 164 (12) (2000) 6426–6434.
- [38] Q. Han et al, Association of serum soluble human leukocyte antigen-G levels with chronic hepatitis B virus infection, *Clin. Exp. Med.* 14 (1) (2014) 35–43.
- [39] L. Amiot et al, Expression of HLA-G by mast cells is associated with hepatitis C virus-induced liver fibrosis, *J. Hepatol.* 60 (2) (2014) 245–252.
- [40] S. Khorrami et al, The relationship between HLA-G and viral loads in non-responder HCV-infected patients after combined therapy with IFN-alpha2alpha and ribavirin, *Hum. Immunol.* 76 (2–3) (2015) 181–186.
- [41] J. Huang et al, Soluble HLA-G inhibits myeloid dendritic cell function in HIV-1 infection by interacting with leukocyte immunoglobulin-like receptor B2, *J. Virol.* 84 (20) (2010) 10784–10791.
- [42] R. Rizzo et al, Infection and HLA-G molecules in nasal polyposis, *J. Immunol. Res.* 2014 (2014) 407430.
- [43] N.T. Suominen et al, The association of HLA-G polymorphism with oral and genital HPV infection in men, *Eur. J. Clin. Microbiol. Infect. Dis.* 41 (2) (2022) 219–226.
- [44] A. Jaakola et al, HLA-G polymorphism impacts the outcome of oral HPV infections in women, *BMC Infect. Dis.* 21 (1) (2021) 419.
- [45] D. Bortolotti et al, Late-onset intrauterine growth restriction and HHV-6 infection: a pilot study, *J. Med. Virol.* 93 (11) (2021) 6317–6322.
- [46] F. Megret et al, Modulation of HLA-G and HLA-E expression in human neuronal cells after rabies virus or herpes virus simplex type 1 infections, *Hum. Immunol.* 68 (4) (2007) 294–302.
- [47] D. Wu et al, The SARS-CoV-2 outbreak: what we know, *Int. J. Infect. Dis.* 94 (2020) 44–48.
- [48] J. Shang et al, Cell entry mechanisms of SARS-CoV-2, *PNAS* 117 (21) (2020) 11727–11734.
- [49] J. Yang et al, Prevalence of comorbidities and its effects in patients infected with SARS-CoV-2: a systematic review and meta-analysis, *Int. J. Infect. Dis.* 94 (2020) 91–95.
- [50] I.G. Ovsyannikova et al, The role of host genetics in the immune response to SARS-CoV-2 and COVID-19 susceptibility and severity, *Immunol. Rev.* 296 (1) (2020) 205–219.
- [51] S.F. Pedersen, Y.C. Ho, SARS-CoV-2: a storm is raging, *J. Clin. Invest.* 130 (5) (2020) 2202–2205.
- [52] L. Tan et al, Lymphopenia predicts disease severity of COVID-19: a descriptive and predictive study, *Signal Transduct. Target. Ther.* 5 (1) (2020) 33.
- [53] N. Anfossi et al, Human NK cell education by inhibitory receptors for MHC class I, *Immunity* 25 (2) (2006) 331–342.
- [54] D. Bortolotti et al, SARS-CoV-2 spike 1 protein controls natural killer cell activation via the HLA-E/NKG2A pathway, *Cells* 9 (9) (2020).
- [55] S. Nguyen et al, HLA-E upregulation on IFN-gamma-activated AML blasts impairs CD94/NKG2A-dependent NK cytotoxicity after haplo-mismatched hematopoietic SCT, *Bone Marrow Transplant.* 43 (9) (2009) 693–699.
- [56] F. Ahmed, D.H. Jo, S.H. Lee, Can natural killer cells be a principal player in anti-SARS-CoV-2 immunity?, *Front Immunol.* 11 (2020) 586765.
- [57] P. V.Kovski et al, Coronavirus biology and replication: implications for SARS-CoV-2, *Nat. Rev. Microbiol.* 19 (3) (2021) 155–170.
- [58] Q. Hammer et al, SARS-CoV-2 Nsp13 encodes for an HLA-E-stabilizing peptide that abrogates inhibition of NKG2A-expressing NK cells, *Cell Rep.* 38 (10) (2022) 110503.
- [59] H. Vietzen et al, Deletion of the NKG2C receptor encoding KLRC2 gene and HLA-E variants are risk factors for severe COVID-19, *Genet. Med.* 23 (5) (2021) 963–967.
- [60] M. Della Chiesa et al, Activating KIRs and NKG2C in viral infections: toward NK cell memory?, *Front Immunol.* 6 (2015) 573.
- [61] C. Maucourant et al, Natural killer cell immunotypes related to COVID-19 disease severity, *Sci. Immunol.* 5 (50) (2020).
- [62] S. Zhang et al, Dynamics of peripheral immune cells and their HLA-G and receptor expressions in a patient suffering from critical COVID-19 pneumonia to convalescence, *Clin. Transl. Immunol.* 9 (5) (2020) e1128.
- [63] D. Bortolotti et al, Increased sHLA-G is associated with improved COVID-19 outcome and reduced neutrophil adhesion, *Viruses* 13 (9) (2021).
- [64] I. Zidi, Puzzling out the COVID-19: therapy targeting HLA-G and HLA-E, *Hum. Immunol.* 81 (12) (2020) 697–701.
- [65] S. Zhang et al, Dynamics of peripheral immune cells and their HLA-G and receptor expressions in a patient suffering from critical COVID-19 pneumonia to convalescence, *Clin. Transl. Immunol.* 9 (5) (2020).
- [66] A. Lin, W.H. Yan, Perspective of HLA-G Induced Immunosuppression in SARS-CoV-2 Infection, *Front. Immunol.* 12 (2021) 788769.
- [67] M. Zheng et al, Functional exhaustion of antiviral lymphocytes in COVID-19 patients, *Cell. Mol. Immunol.* 17 (5) (2020) 533–535.
- [68] B. Seliger et al, Induction of pulmonary HLA-G expression by SARS-CoV-2 infection, *Cell. Mol. Life Sci.* 79 (11) (2022) 582.
- [69] S. Zhang et al, The miRNA: a small but powerful RNA for COVID-19, *Brief. Bioinform.* 22 (2) (2021) 1137–1149.

- [70] R. Rizzo et al, SARS-CoV-2 nucleocapsid protein and ultrastructural modifications in small bowel of a 4-week-negative COVID-19 patient, *Clin. Microbiol. Infect.* 27 (6) (2021) 936–937.
- [71] D. Bortolotti et al, Relevance of VEGF and CD147 in different SARS-CoV-2 positive digestive tracts characterized by thrombotic damage, *FASEB J.* 35 (12) (2021) e21969.
- [72] N.T. Al-Bayatee, A.H. Ad'hiah, Soluble HLA-G is upregulated in serum of patients with severe COVID-19, *Hum. Immunol.* 82 (10) (2021) 726–732.
- [73] J.F.C. Cordeiro et al, The severity of COVID-19 affects the plasma soluble levels of the immune checkpoint HLA-G molecule, *Int. J. Mol. Sci.* 23 (17) (2022).
- [74] T. Behl et al, CD147-spike protein interaction in COVID-19: Get the ball rolling with a novel receptor and therapeutic target, *Sci. Total Environ.* 808 (2022) 152072.
- [75] C. Ober, HLA and pregnancy: the paradox of the fetal allograft, *Am. J. Hum. Genet.* 62 (1) (1998) 1–5.
- [76] L.B. Argueta et al, Inflammatory responses in the placenta upon SARS-CoV-2 infection late in pregnancy, *iScience* 25 (5) (2022) 104223.
- [77] E. Delorme-Axford, Y. Sadovsky, C.B. Coyne, The placenta as a barrier to viral infections, *Annu Rev Virol* 1 (1) (2014) 133–146.
- [78] C.M. Mela et al, Switch from inhibitory to activating NKG2 receptor expression in HIV-1 infection: lack of reversion with highly active antiretroviral therapy, *AIDS* 19 (16) (2005) 1761–1769.
- [79] A. Cabello et al, HAART induces the expression of HLA-G on peripheral monocytes in HIV-1 infected individuals, *Hum. Immunol.* 64 (11) (2003) 1045–1049.
- [80] P.J. Weng et al, Elevation of plasma soluble human leukocyte antigen-G in patients with chronic hepatitis C virus infection, *Hum. Immunol.* 72 (5) (2011) 406–411.

In particular, HLA-G was firstly described during pregnancy, where it acts to protect the semi-allogenic fetus from maternal immune system, characterized by tolerogenic functions and frequently reported to be induced during viral infection [325]. HLA-G exists in seven isoforms, four membrane-bound (G1, G2, G3 and G4) and three soluble (G5, G6, and G7), and its synthesis is finely controlled by specific polymorphisms located in the regulatory regions (UTRs) of HLA-G gene [326], which include a deletion/insertion of 14bp polymorphism (rs371194629) and a C>G single-nucleotide polymorphism (snp) at the +3142bp position (rs1063320) [326].

HLA-G is known to have suppressive effects on the immune system, provided through its interaction with at least four specific receptors (ILT2, ILT4, KIR2DL4 and CD160) expressed on T and B lymphocytes, NK cells, neutrophils and APCs [327].

Thus, HLA-G immune-modulatory functions include [325]:

- reduction of inflammatory and immune responses;
- preservation of immune tolerance;
- modulation of tumoral processes;
- promotion of viral immune escape.

A study conducted by Seliger et al. revealed that the abundance of T cells and macrophages infiltration observed during SARS-CoV-2 infection is associated to high HLA-G and IFN γ expression at lung level [328]. In addition, high HLA-G expression has also been found at peripheral level on monocytes and B cells, in association with decreased CD8+ T cells count [328].

Besides HLA-G expression by immune cells, also endothelial cells are reported to express this molecule [329]. In fact, HLA-G mediates the antiangiogenic and vascular remodeling processes through its interaction with CD160 receptors expressed at vascular level [330], also inhibiting neutrophil adhesion to endothelial cells. For this reasons, it is possible that HLA-G imbalance could lead to an increased infiltration of immune cells, such as neutrophil [330].

As a matter of fact, HLA-G modulation seems to be related to immune dysfunctions occurring in SARS-CoV-2 infection, particularly affecting neutrophils adhesion [330].








To investigate this aspect, we analyzed soluble HLA-G (sHLA-G) levels in blood samples collected from hospitalized COVID-19 patients, in correlation to endothelial and neutrophil activation ([331], paper attached), in terms of E-selectin and of Intercellular Adhesion Molecule-1 (ICAM-1) expression, known to be two key molecules involved in the adhesion of neutrophils to inflammatory endothelium [332].

According to the data obtained, the levels of sHLA-G were significantly higher in COVID-19 patients with respiratory failure at admission time, compared to controls. Interesting, in those subjects was identified an inverse correlation among both soluble ICAM-1 and sE-selectin levels with plasma sHLA-G values ([331], paper attached). This result was confirmed by *in-vitro* experiments, showing the ability of HLA-G molecules to control sICAM-1 and sE-selectin expression on endothelium, involving CD160 receptor and activating neutrophil adhesion ([331], paper attached).

Thus, this study corroborates the association of COVID-19 clinical onset with increased sHLA-G plasma levels, establishing HLA-G molecule as a possible prognostic and therapeutical marker in ARDS condition.

Article

Increased sHLA-G Is Associated with Improved COVID-19 Outcome and Reduced Neutrophil Adhesion

Daria Bortolotti ¹ , Valentina Gentili ¹ , Sabrina Rizzo ¹, Giovanna Schiuma ¹ , Silvia Beltrami ¹ , Savino Spadaro ² , Giovanni Strazzabosco ¹, Gianluca Campo ³, Edgardo D. Carosella ⁴, Alberto Papi ^{5,6}, Roberta Rizzo ^{1,7,*}  and Marco Contoli ^{5,6,†} 

¹ Department of Chemical, Pharmaceutical and Agricultural Science, University of Ferrara, 44121 Ferrara, Italy; daria.bortolotti@unife.it (D.B.); valentina.gentili@unife.it (V.G.); sabrina.rizzo@unife.it (S.R.); giovanna.schiума@unife.it (G.S.); silvia.beltrami@unife.it (S.B.); giovanni.strazzabosco@unife.it (G.S.)

² Intensive Care Unit, Department of Translational Medicine, University of Ferrara, 44121 Ferrara, Italy; savino.spadaro@unife.it

³ Cardiology Unit, Azienda Ospedaliera Universitaria di Ferrara, Cona, 44124 Ferrara, Italy; gianluca.campo@unife.it

⁴ CEA, Institute of Emerging Diseases and Innovative Therapies (iMETI), Research Division in Hematology and Immunology (SRHI), Saint-Louis Hospital, 75001 Paris, France; edgardo.carosella@cea.fr

⁵ Respiratory Section, Department of Translational Medicine, University of Ferrara, 44121 Ferrara, Italy; alberto.papi@unife.it (A.P.); marco.contoli@unife.it (M.C.)

⁶ Respiratory Unit, Azienda Ospedaliera Universitaria Ferrara, Cona, 44124 Ferrara, Italy

⁷ Industrial Research and Technology Transfer Laboratory (LTTA), University of Ferrara, 44121 Ferrara, Italy

* Correspondence: rbr@unife.it; Tel.: +39-0532455382

† These authors contributed equally to this work.



Citation: Bortolotti, D.; Gentili, V.; Rizzo, S.; Schiuma, G.; Beltrami, S.; Spadaro, S.; Strazzabosco, G.; Campo, G.; Carosella, E.D.; Papi, A.; et al. Increased sHLA-G Is Associated with Improved COVID-19 Outcome and Reduced Neutrophil Adhesion. *Viruses* **2021**, *13*, 1855. <https://doi.org/10.3390/v13091855>

Academic Editor: Bernd Lepenies

Received: 13 August 2021

Accepted: 14 September 2021

Published: 17 September 2021

Publisher's Note: MDPI stays neutral with regard to jurisdictional claims in published maps and institutional affiliations.



Copyright: © 2021 by the authors. Licensee MDPI, Basel, Switzerland. This article is an open access article distributed under the terms and conditions of the Creative Commons Attribution (CC BY) license (<https://creativecommons.org/licenses/by/4.0/>).

Abstract: Human leukocyte antigen (HLA) is a group of molecules involved in inflammatory and infective responses. We evaluated blood sHLA-E and sHLA-G levels in hospitalized COVID-19 patients with respiratory failure and their relationship with clinical evolution, changes in endothelial activation biomarker profile, and neutrophil adhesion. sHLA-E, sHLA-G, and endothelial activation biomarkers were quantified by ELISA assay in plasma samples. Neutrophil adhesion to endothelium was assessed in the presence/absence of patients' plasma samples. At admission, plasma levels of sHLA-G and sHLA-E were significantly higher in COVID-19 patients with respiratory failure compared to controls. COVID-19 clinical improvement was associated with increased sHLA-G plasma levels. In COVID-19, but not in control patients, an inverse correlation was found between serum sICAM-1 and E-selectin levels and plasma sHLA-G values. The in vitro analysis of activated endothelial cells confirmed the ability of HLA-G molecules to control sICAM-1 and sE-selectin expression via CD160 interaction and FGF2 induction and consequently neutrophil adhesion. We suggest a potential role for sHLA-G in improving COVID-19 patients' clinical condition related to the control of neutrophil adhesion to activated endothelium.

Keywords: HLA-G; COVID-19; E-selectin; ICAM-1; CD160; neutrophil

1. Introduction

Human leukocyte antigen (HLA)-E and HLA-G belong to 'non-classical' HLA-class Ib molecules, which also includes -F and -H [1,2]. In contrast with highly polymorphic HLA-class Ia molecules (HLA-A, -B, and -C), HLA-Ib molecules display a low degree of polymorphism and different immunoregulatory properties [3]. Several results supported a correlation between HLA-E and HLA-G expression in physiological and pathological conditions [4,5]. HLA-G molecules interact with immune inhibitory receptors (ILT2, ILT4, KIR2DL4), modulating the functions of NK (Natural Killer) cells, T cells, B cells, and [6,7]. Thus, HLA-G molecules are involved in the control of infective and inflammatory conditions [8]. Moreover, HLA-G interact with endothelial cells via the CD160 receptor [9],

a glycosylphosphatidylinositol-anchored member of the immunoglobulin superfamily. The interaction between soluble (s)HLA-G and CD160 on the surface of endothelial cells induces the apoptosis of endothelial cells, inhibiting the angiogenic process via down-regulation of fibroblast growth factor 2 (FGF2) [9]. The expression of HLA-G molecules is partly controlled by genetic background, with HLA-G*0105N alleles presenting significantly reduced sHLA-G expression levels in comparison with HLA-G*0101 alleles [10].

HLA-E expression on the cell surface needs interaction with nonapeptides derived from leader peptides from HLA-I molecules and beta2 microglobulin [11]. HLA-E interacts with the NKG2A/CD94 inhibitory receptor, exerting immunosuppressive functions on NK cell and CD8+ T cell-mediated lysis [12,13]. Recently, the increased expression of soluble (s)HLA-E, generated by metalloproteases-dependent shedding of the membrane-bound molecule, has been observed in pathological conditions, such as multiple sclerosis, melanoma, and juvenile idiopathic arthritis [14]. sHLA-E is secreted by activated endothelial cells [15,16] and the levels might be controlled by genetic background, with a higher expression in the HLA-E*0103 allele in comparison with the HLA-E*0101 allele [17]. Recently, it has been suggested that there is a role for these molecules in the SARS-COV2 infection [18], supporting our data on the expression of HLA-G molecules by epithelial cells of the intestinal mucosa and in some lymphocytes, in correspondence with SARS-COV2-positive sites [19].

The coronavirus disease 2019 (COVID-19) is a global public health issue. Approximately 170 million cases have been globally confirmed so far, with 3.5 million deaths (<https://covid19.who.int>; accessed on 5 August 2021) [20]. COVID-19 is a heterogeneous disease associated with SARS-COV2 infection with a range of severity spanning from paucisymptomatic manifestations characterized by fever, cough, dyspnea, anosmia, ageusia, and fatigue up to respiratory distress syndrome (ARDS) and multiple organ failure with poor prognosis. Emerging evidence suggests that endothelial activation plays a central role in the pathogenesis of ARDS and multi-organ failure in patients with COVID-19. However, the molecular mechanisms underlying endothelial activation in COVID-19 patients remain unclear. Both HLA-E and HLA-G are involved in endothelial cells remodeling. HLA-G/CD160-mediated antiangiogenic property may participate in the vascular remodeling [9]. HLA-E expression and release of sHLA-E are features of endothelial cells activation and emphasize immunoregulatory functions of the endothelium [16]. The endothelial cells response to immune stimulation consists of the up-modulation of molecules such as E-selectin and ICAM-1 (Intercellular Adhesion Molecule 1). E-selectin and ICAM-1 are probably the most specific, inducible endothelial cell- surface molecules which are involved in the adhesion of neutrophils to inflammatory endothelium [21]. On the contrary, HLA-G is a potent inhibitor of neutrophil adhesion to endothelial cells [15]. The modification in the expression of these molecules on the surface of endothelial cells might affect the adhesion of neutrophils during the COVID-19 inflammatory cascade. The increased infiltration of immature and/or dysfunctional neutrophil contributes to the imbalance of the lungs' immune response and has been observed in severe COVID-19 cases [22,23].

Understanding the immune-inflammatory mechanisms that pave the way to disease manifestations can identify potential targets for pharmacological interventions. Here we evaluated blood sHLA-E and sHLA-G in hospitalized COVID-19 patients with respiratory failure in relation with the evolution of the clinical conditions and in relation with endothelial activation biomarker profile variations and neutrophil cells/endothelium interaction. In parallel, blood sHLA-G and sHLA-E were assessed and compared in a group of control hospitalized subjects with respiratory failure and healthy controls not associated with SARS-COV2 infection.

2. Materials and Methods

2.1. Patients

The study was an investigator-initiated, prospective, single-center study recruiting consecutive patients admitted to the Respiratory and Intensive Care Units of the Azienda

Ospedaliera Universitaria di Ferrara (Ferrara, Italy) (Supplementary Material File S1). The study aimed to prospectively evaluate the pro-thrombotic status and systemic inflammatory biomarkers in moderate-to-severe COVID-19 patients and to correlate these biomarkers with clinical outcomes (Clinicaltrials.gov identifier NCT04343053). The design of the study has been described in detail in previous reports [24–26]. Briefly, patients were included if they had SARS-COV2 infection (confirmed by PCR-positive nasopharyngeal swab specimens) and respiratory failure (defined as arterial oxygen tension of <8.0 kPa (60 mmHg) at room air and oxygen saturation < 90%). All the patients were infected by the SARS-COV2 isolate clustered in the B1 clade, which included most of the Italian sequences during the enrollment period. Patients were recruited from April 1 until the end of May 2020. After enrollment (T1; Baseline), COVID-19 patients were assessed every 7 ± 2 days for an additional 2 consecutive visits (T2 and T3). A detailed description of study procedures has been previously published [24–26] and is also available in the online supplement. Two control groups were recruited: a group of patients hospitalized in the same period at the same hospital with acute respiratory failure due to respiratory/cardiovascular acute conditions and not related to SARS-COV2; a group of healthy controls. For plasma preparation, the blood samples were collected using 6 mL EDTA-containing tubes. The tubes were centrifuged for 15 min at 2200 rpm. All blood specimens were processed immediately for plasma collection and aliquots were stored at -80 °C.

2.2. sHLA-G Specific ELISA

As described previously [27,28], serum levels of sHLA-G (sHLA-G1/HLA-G5) were measured by enzyme-linked immunosorbent assay (ELISA) using monoclonal antibodies MEM-G/9 (Exbio; Vestec, CZ) as capture antibodies, respectively. The intra-assay coefficient of variations (CV), the inter-assay CV, and the limit of sensitivity were 1.4%, 4%, and 1 ng/mL.

2.3. sHLA-E Specific ELISA

ELISA for soluble HLA-E were performed as previously described [28]. Briefly, MaxiSorp Nunc-Immuno 96 microwell plates (Nunc A/S; Roskilde, Denmark) were coated overnight at 4 °C with 3D12 mAb, specific for HLA-E HC (eBioscience; Science Center Drive, San Diego, CA, USA). After three washes with PBS 0.05% Tween 20 (washing buffer), plates were saturated with 200 μ L/w of PBS 2% BSA (Sigma; St. Louis, MO, USA) for 30 min at RT. 100 μ L of test samples (plasma) or standard (serial dilutions of total extract from normal peripheral blood mononuclear cells) were added to each well and incubated at RT for 2 h. After three washes, 100 μ L of detection reagent (HRP-conjugated anti-beta2 microglobulin mAb, Exbio; Vestec, CZ) was added, and plates were incubated for 2 h at RT. After three washes, 100 μ L of TMB (substrate for HRP) was added, and the reaction was stopped after approximately 10' by adding H₂SO₄ 5N. Absorbance at 450 nm was measured using Infinite 200 PRO spectrometer (Tecan Group Ltd.; Seestrasse, Männedorf, Switzerland). Results are expressed as arbitrary units/mL (1 unit = quantity of sHLA-E in 1 μ g of total extract).

2.4. HLA-E Allele Assignment

Genomic DNA was extracted from peripheral blood samples using the TIANamp Blood DNA Kit (Tiangen Biotech; Beijing, China). Allele-specific quantitative real-time PCR (qRT-PCR) with two forward primers, respectively, was used to discriminate HLA-E*0101 and HLA-E*0103 alleles: E*0101F (5'-GCG-AGC-TGG-GGC-CCG-CCA-3') and E*0103F (5'-GCG-AGC-TGG-GGC-CCG-CCG-3'). Each of the forward primers was combined with a common HLA-E-specific reverse primer: 5'-CCG-CCT-CAG-AGG-CAT-CAT-TTG-3'. Two PCR reactions for each sample were carried out in a 10 μ L reaction solution containing 20 ng genomic DNA, 0.2 μ mol/L allele-specific forward primer, 0.2 μ mol/L common reverse primer, and 5 μ L 2 \times SYBR Premix Ex Taq (TaKaRa; Shiga, Japan). The PCR amplification was carried out at 95 °C for 10 min, 40 cycles at 95 °C for 15 s, and 65 °C for 40 s, followed

by a final stage of product dissociation cycle, using Mastercycler ep realplex (Eppendorf; Hamburg, Germany). Allele discrimination was manually performed according to the different PCR amplification efficiencies for different alleles, which can be shown by the cycle of threshold (Ct) [17].

2.5. HLA-G Allele Assignment

HLA-G allele assignment was carried out using polymerase chain reaction (PCR) followed by sequencing analysis. Briefly exon 2, 3, and intron 2 were amplified with a primer pair: forward 5'-GGCTGA GAG GTC TAC AGG AGA T-3' and reverse 5'-GCT CCC ACT CCA TGA GGT ATT-3' and amplification of exon 4 was performed using the primers: forward 5'-GTA TCT GGT TCA TTC TTA GGA TGG-3' and reverse 5'-AAG ACT GCT CTG GGA AAG G-3'. PCR product of exon 2, 3, and intron 2 was 822 bp, and 502 bp for exon 4. The polymerase chain reaction (PCR) program for exon 2, 3, and intron 2 was: after 95 °C for 10 min, 30 cycles of 94 °C for 1 min, and 60 °C for 45 s followed by 72 °C for 45 s, and for exon 4 was: after 95 °C for 5 min, 30 cycles of 94 °C for 1 min and 59 °C for 45 s followed by 72 °C for 45 s [29]. The products were then sequenced with capillary sequencing using the Applied Biosystems 3500 XL sequencer (ThermoFisher Scientific; Milan; Italy) and 'plink' software was used (<http://pngu.mgh.harvard.edu/~purcell/plink/index.shtml>; accessed on 10 September 2021) for allelic haplotyping.

2.6. Endothelial Activation Biomarkers Levels Assay

Plasma samples were analyzed for Angiopoietin-2, Endoglin, Endothelin-1, IL-33, vWF, s-RAGE, sICAM-1, P-SELECTIN, sVCAM-1, PAI-1, sE-Selectin, Tissue Factor, Thrombomodulin, sCD40L by Multipore multiplex immunoassay-based (Merck; Milan, Italy) using Luminex instrument (Luminex; Austin, TX, USA).

2.7. Cell Cultures

HUVEC were obtained by collagenase treatment of the umbilical vein as described previously [30]. The cells were cultured in fibronectin-coated tissue culture flasks (Costar; Cambridge, MA; USA) in RPMI-1640 (Gibco, Paisley, UK), supplemented with 10% heat-inactivated human serum and 10% bovine calf serum (BCS), 50 pg/mL heparin, 30 pg/mL endothelial growth factor (Collaborative Research Incorporated; Bedford, MA; USA), and antibiotics. HUVEC of passage 3 or 4 were grown to confluence in 75 cm² (approximately 3 × 10⁶ cells/flask) cell culture flasks (Costar) or in 24 macro wells (Costar) and activated with TNF-alpha (0.625–5 ng/mL) for 4 h [31]. Anti-E-selectin (CD62E; Diaclone; Besançon cedex; France) (20 ng/mL), anti ICAM-1 (EP14442Y; Abcam; Milan, Italy) (20 ng/mL), anti-HLA-G (Exbio; Vestec, CZ) (10 ng/mL), and anti-CD160 (EPR23644-24; Abcam; Milan, Italy) (20 ng/mL) azide-free antibodies were added to cell cultures for 24 h. An anti-dinitrophenyl hapten mAb (Rat IgG1, DakoCytomation, Denmark) (10 ng/mL) was used as a negative control [32]. PD 166866 FGF2 inhibitor (Santa Cruz; Dallas, TX, USA) (50 nM) was used to inhibit FGF2 in endothelial cells. Each treatment was maintained for 24 h.

2.8. Neutrophil Binding Assay

Neutrophils were isolated from peripheral blood of COVID-19-negative control subjects by Polymorphprep (Progen; Heidelberg, Germany) [33]. Isolated neutrophil was stained with BioTracker 488 Green Nuclear Dye (Sigma-Aldrich; Milan, Italy) and added to HUVEC culture (6 × 10⁵). Cells were incubated for 20 min in a 37 °C, 5% CO₂ incubator. PRE-wash total neutrophil fluorescence was measured by fluorescence intensity of each well with an excitation wavelength of 500 nm and an emission wavelength of 515 nm (fluorescein filter set) in a FLUOstar spectrophotometer (BMG Labtech; ThermoFisher; Milan, Italy). The co-cultures were washed and the POST-wash total neutrophil fluorescence was determined. The percent adherence per well was determined.

2.9. sE-Selectin and sICAM1 Assay

Levels of E-selectin and sICAM-1 in cell culture supernatants were detected using the Human sE-Selectin/CD62E Quantikine and sICAM-1/CD54 ELISA Kit (ReDsystems; Minneapolis, MN, USA) according to manufacturer's instructions and using a Multiskan Ascent ELISA plate reader (ThermoFischer Scientific; Milan, Italy).

2.10. FGF2 Expression Assay

FGF2 gene expression was assessed by ready-to-use assay (Hs00266645_m1; Applied Biosystems, ThermoFischer Scientific; Milan, Italy) following manufacturer instructions [34].

2.11. Statistical Analysis

The normality of each variable was checked by using the Kolmogorov-Smirnov test. Statistical analysis was performed by a parametric approach for several variables with normal distribution. Fisher's exact test was used to compare allelic frequencies. Student's *t*-test was used to compare plasma mean levels of sHLA-E, sHLA-G, sE-selectin, and sICAM-1 among the various groups. The Spearman rank correlation coefficient test was used to identify possible relationships among different variables. A value of $p < 0.05$ was accepted as statistically significant. The statistical analysis was performed by GraphPad software version 9.

3. Results

3.1. Study Population

Patients' characteristics were previously reported [24–26]. We enrolled fifty-four COVID-19 patients, 11 control patients that presented respiratory failure [24–26], and 100 healthy control subjects. The hospitalization of the control group was necessary for cardiovascular (heart failure) or respiratory (pulmonary infiltrates/pneumonia) problems. The three groups of patients were matched for gender, age, BMI, and smoking history. The hospitalized patients were matched for number of comorbidities per patient, need of respiratory support at recruitment, and clinical improvement (Table 1). At baseline, no differences were found in blood cell counts (Table 2) between the two groups of patients, while healthy controls showed lower total blood leukocytes and neutrophils (Table 2). We did not find any difference for treatments between patients who died compared to patients who survived during the study follow-up [24]. At variance with COVID-19 patients, none of the patients in the control group received antiviral treatments or hydroxychloroquine.

Table 1. Demographic and clinical characteristics of the study population.

	Study Population (n = 165)			p-Value *	COVID-19 Patients (n = 54)		p-Value
	COVID-19 Patients, n = 54	Control Patients' Respiratory Failure n = 11	Control Patients n = 100		Non-Survivor n = 16	Survivors n = 38	
Gender N (%)				>0.9			>0.9
Male	40 (74%)	8 (73%)	74 (74%)		12 (75%)	28 (74%)	
Female	14 (26%)	3 (27%)	26 (26%)		4 (25%)	10 (26%)	
Age	65 (57, 73)	70 (66, 76)	67 (56, 74)	0.2	72 (65, 78)	62 (55, 71)	0.004
Smoking habit N (%)							
Active smoker	0 (0)	3 (27%)	1 (1%)	0.003	0 (0)	0 (0)	NA
Former smoker	16 (30%)	4 (36%)	29 (29%)	0.725	7 (44%)	9 (24%)	0.2
BMI (kg/m ²)	26.4 (24.2, 30.0)	24.8 (22.0, 27.1)	25.3 (23.1, 28.6)	0.13	28.5 (26.4, 30.9)	26.0 (24.1, 29.4)	0.2
Number of Comorbidities/patients	1.00 (0.00, 3.00)	2.00 (1.50, 3.00)	0 (0.00, 0.00)	0.12	3.00 (1.75, 4.00)	1.00 (0.00, 2.00)	0.004

Table 1. Cont.

	Study Population (n = 165)			p-Value *	COVID-19 Patients (n = 54)		p-Value
	COVID-19 Patients, n = 54	Control Patients' Respiratory Failure n = 11	Control Patients n = 100		Non-Survivor n = 16	Survivors n = 38	
Respiratory support at recruitment N (%)							
O ₂ only	11 (20%)	2 (18%)	NA		2 (12%)	9 (24%)	
HFNC or NIV	16 (30%)	6 (54%)	NA		4 (25%)	12 (31%)	
IV	27 (50%)	3 (27%)	NA		10 (62%)	17 (45%)	
Days from symptoms onset to recruitment	9 (5–14)	5 (2–8)	NA		10 (5–14)	8 (5–15)	0.60
Treatments N (%)							
Low molecular weight heparin	54 (100%)	11 (100%)	NA	>0.9	16 (100%)	38 (100%)	>0.9
Antibiotics	47 (87%)	10 (90%)	NA	>0.9	14 (88%)	33 (87%)	>0.9
Systemic corticosteroids	37 (69%)	9 (81%)	NA	>0.9	12 (75%)	25 (66%)	0.7
Antivirals	29 (54%)	NA	NA	NA	7 (44%)	22 (58%)	0.5
Hydroxychloroquine	40 (74%)	NA	NA	NA	11 (69%)	29 (76%)	0.7

BMI, body mass index; HFNC, high flow nasal canula; NIV, non-invasive ventilation; IV, invasive ventilation. * p-value: COVID-19 patients vs. control patients' respiratory failure.

Table 2. sHLA-G and sHLA-E levels and blood inflammatory cell counts at baseline (T1) in COVID-19 patients and controls.

	COVID-19 Patients, n = 54	Control Patients' Respiratory Failure, n = 11	Control Patients, n = 100	p-Value *	p-Value **	p-Value ***
sHLA-G (ng/mL)	165.87 (44.3, 218.03)	49.54 (18.3, 54.9)	20.51 (0.0, 43.53)	0.01	<0.001	0.01
sHLA-E (ng/mL)	672.22 (173.9, 890.9)	224.63 (98.6, 310.4)	10.23 (0.0, 21.51)	0.001	<0.001	<0.001
Total blood leucocytes (cells × 10 ³ /μL)	9.1 (6.8, 12.6)	12.0 (9.1, 14.7)	5.0 (4.1, 11.0)	0.2	0.023	0.021
Blood lymphocytes (cells × 10 ³ /μL)	0.83 (0.59, 1.04)	1.12 (0.52, 1.73)	0.96 (0.54, 1.29)	0.3	0.23	0.12
Blood Neutrophils (cells × 10 ³ /μL)	7.9 (5.6, 10.2)	10.1 (5.8, 12.1)	3.2 (2.0–7.4)	0.2	0.01	0.01
Blood eosinophils (cells × 10 ³ /μL)	0.04 (0.00, 0.14)	0.00 (0.00, 0.06)	0.00 (0.00, 0.02)	0.074	0.069	0.12

(Data are expressed as Median (IQR)). * p-value: COVID-19 patients vs. control patients' respiratory failure. ** p-value: COVID-19 patients vs. control patients. *** p-value: Control patients vs. control patients' respiratory failure.

3.2. Immunological Parameters Evaluation

At baseline (T1), we found higher blood levels of both sHLA-G and sHLA-E in COVID-19 patients compared to controls with respiratory failure (sHLA-G: Median (IQR) 11 (49.54) vs. 54 (165.87) ng/mL $p < 0.01$; sHLA-E: 11 (224.63) vs. 54 (672.22) ng/mL $p < 0.001$) and healthy controls (sHLA-G: Median (IQR) 100 (20.51) vs. 54 (165.87) ng/mL $p < 0.001$; sHLA-E: 100 (10.23) vs. 54 (672.22) ng/mL $p < 0.001$) (Table 2). Similarly, controls with respiratory failure presented higher levels of sHLA-G and sHLA-E in comparison with healthy controls (sHLA-G: Median (IQR) 11 (49.54) vs. 100 (20.51) ng/mL $p = 0.01$; sHLA-E: 11 (224.63) vs. 100 (10.23) ng/mL $p < 0.001$) (Table 2).

Although baseline levels of sHLA-G did not differ between survivors and non survivors for COVID-19 patients, the values significantly decreased over time in non-survivors

(Figure 1A) ($p = 0.036$ at T2; $p = 0.04$ at T3). In control patients, sHLA-G levels decreased in both survivors and non-survivors over time (Figure 1E) with no statistical differences.

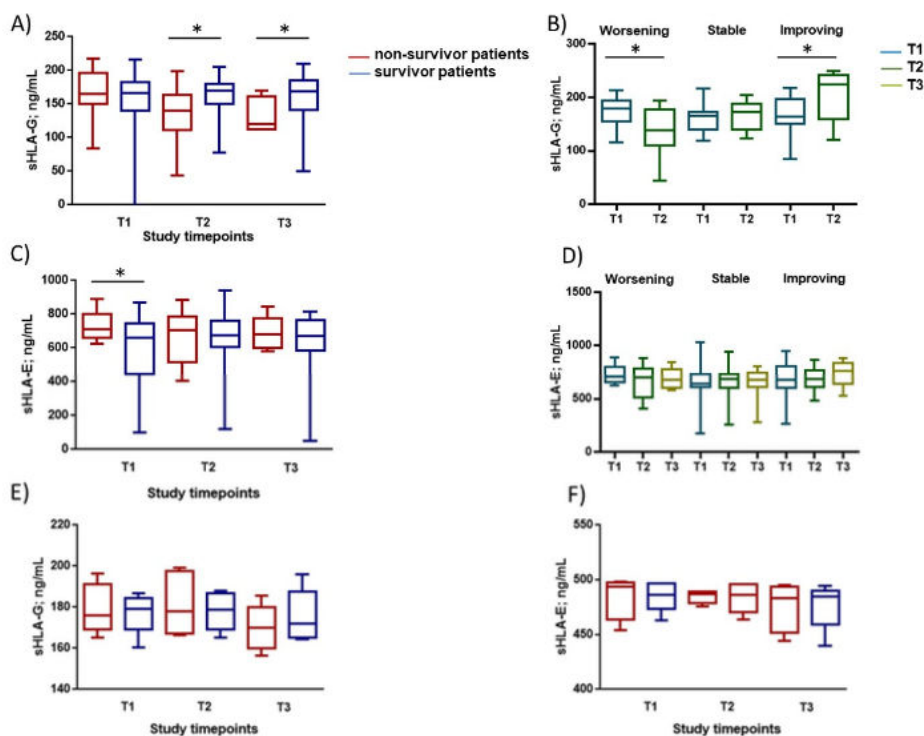


Figure 1. sHLA-G and sHLA-E concentration in blood of COVID-19 patients and controls. Blood sHLA-G and sHLA-E levels in COVID-19 patients and relationships with disease progression and clinical outcome: (A,C) Plasma sHLA-G and sHLA-E levels at baseline (T1) and at follow-up (T2 and T3; 7 ± 2 day interval between assessments) in non-survivor patients (red histograms) or survivor patients (blue histograms) during the study period. (B,D) Plasma sHLA-G and sHLA-E levels at baseline (T1) and after 7 ± 2 days (T2 and T3) on the basis of worsening, stability, or improving of the clinical manifestation of the disease ($* p < 0.05$, Student's *t*-test). (E,F) Plasma sHLA-G and sHLA-E levels at baseline (T1) and at follow-up (T2 and T3; 7 ± 2 day interval between assessments) in non-survivor (red dots) or survivor (blue dots) control patients during the study period.

The increase of severity of COVID-19 from T1 to T2 (but not T2 to T3) was paralleled by a significant decrease of blood sHLA-G levels (Figure 1B) ($p = 0.012$; Student's *t*-test). On the contrary, improved clinical conditions were paralleled by an increase in sHLA-G levels between T1 and T2 ($p = 0.01$; Student's *t*-test).

Overall, blood sHLA-E was higher in non-survivors compared with survivors for COVID-19 patients (Figure 1C), ($p = 0.016$ at T1). The severity of the manifestation of COVID-19 did not affect the levels of sHLA-E (Figure 1D). In control patients, sHLA-E levels did not change over time in both survivors and non-survivors (Figure 1F).

3.3. Allelic Frequencies of HLA-G and HLA-E Genes

Since HLA-G and HLA-E molecules expression might be influenced by genetic background, we evaluated the distribution of *HLA-G* and *HLA-E* genes in the three groups. As reported in Table 3, we observed no differences in the allelic distribution between the three groups.

Table 3. HLA-G and HLA-E allelic distribution in COVID-19 patients and controls.

	COVID-19 Patients n = 54	Control Patients' Respiratory Failure n = 11	Control Patients n = 100	p-Value **	p-Value ***
<i>HLA-E* alleles</i>					
0101 N (%)	25 (47)	5 (46)	48 (48)	0.59	0.53
0103	28 (53)	6 (54)	52 (52)		
<i>HLA-G* alleles</i>					
0101 N (%)	47 (87)	9 (86)	85 (85)	0.63	0.76
0103	1 (1)	0 (0)	1 (1)		
0104	4 (8)	1 (7)	8 (8)		
0105N	2 (4)	1 (6)	6 (6)		

** p-value: COVID-19 patients vs. control patients' respiratory failure. *** p-value: COVID-19 patients vs. Control patients.

3.4. Correlations between Blood sHLA-G Levels and Endothelial Activation Biomarkers in COVID-19 Patients

When all time points were considered, no correlations were found between sHLA-G and sHLA-E levels and blood inflammatory cell counts in COVID-19 patients and controls. Among the tested biomarkers, only E-selectin levels ($r_2 = 0.84$; $p < 0.0001$, Figure 2A) and soluble intercellular adhesion molecule-1 (sICAM-1) levels ($r_2 = 0.83$; $p < 0.0001$ Figure 2B) significantly and inversely correlated with blood baseline sHLA-G levels in COVID-19 patients. The tested biomarkers did not correlate with sHLA-G in control patients.

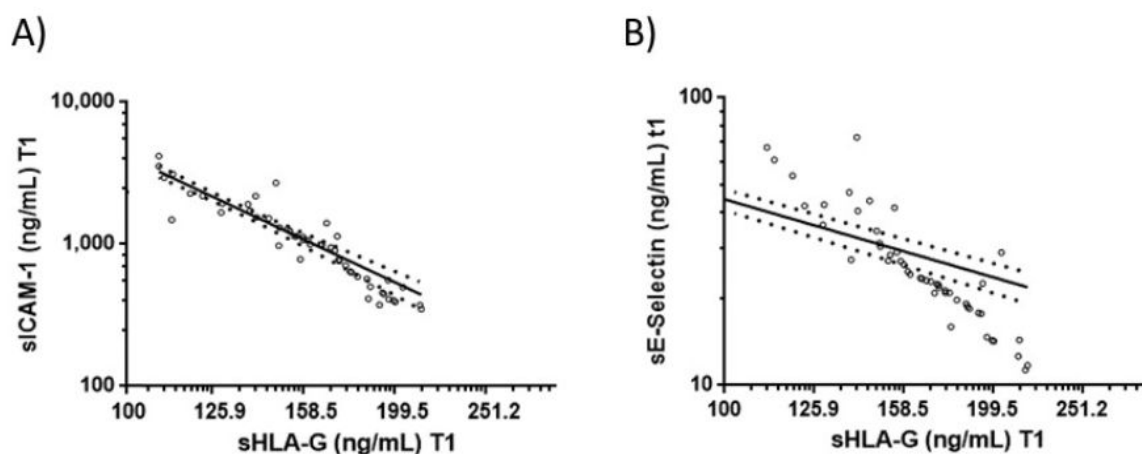


Figure 2. Correlations between sHLA-G concentration and sICAM and E-Selectin levels. Correlations between blood sHLA-G and (A) sICAM and (B) sE-Selectin levels in COVID-19 patients. Circles: single samples' values; Line: fitted linear regression line; Dots: data distribution.

3.5. Endothelial Cell Response to HLA-G Molecules and Neutrophil Adhesion

In COVID-19 patients, we observed an inverse correlation between baseline sHLA-G and the levels of these two adhesion molecules. Thus, as a proof of concept, we treated HUVEC cells with tumor necrosis factor alpha (TNF-alpha) and evaluated the levels of E-selectin and ICAM-1 molecules secretion in the presence or absence of HLA-G molecules. We observed an increase in both sE-selectin and sICAM-1 molecule secretion after TNF-alpha stimulation (Figure 3A) that decreased by the addition of HLA-G molecules (Figure 3B–D). The decrease in E-selectin and ICAM-1 molecules secretion was dose-dependent to HLA-G concentration. To evaluate the molecular mechanisms impli-

cated in HLA-G control of E-selectin and ICAM-1 molecules secretion, we considered the HLA-G receptor CD160, expressed by endothelial cells [9]. HUVEC cells were treated with anti-HLA-G or anti-CD160 antibodies before HLA-G treatment. The addition of both anti-HLA-G and anti-CD160 antibodies restored E-selectin and ICAM-1 molecule secretion (Figure 3B–D). Since HLA-G/CD160 interaction is known to downregulate fibroblast growth factor 2 (FGF2) [9] and the expression of the endothelial cell adhesion molecules, as E-selectin and ICAM-1, are significantly up-regulated in the inflamed tissue by FGF2 [30], we evaluated its possible different expression. As a proof of the implication of FGF2 in E-selectin and ICAM-1 expression, we treated TNF-alpha-activated endothelial cells with a FGF2 inhibitor and we observed a reduction in both E-selectin and ICAM-1 induction (Figure 3A) ($p < 0.0001$; Student's *t*-test). TNF-alpha treatment induced a significant increase in FGF2 expression which was reduced by HLA-G treatment (Figure 3E) ($p < 0.0001$; Student's *t*-test). On the contrary, the pretreatment with anti-HLA-G or anti-CD160 antibodies reverted the decrease in FGF2 expression induced by HLA-G treatment (Figure 3E).

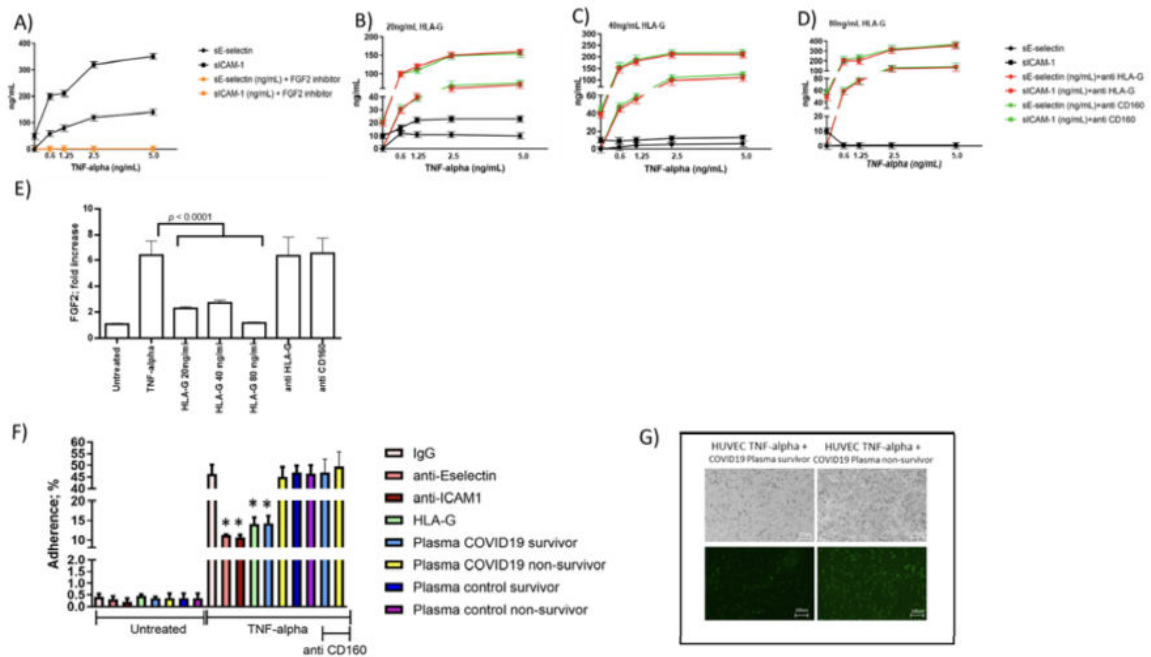


Figure 3. Endothelial cell in vitro assays. HUVEC endothelial cells were treated with TNF-alpha (0.625, 1.25, 2.5, 5.0 ng/mL) for 4 h and cultured overnight. (A) The levels of sICAM and sE-Selectin were assessed in culture supernatants in the absence or presence of FGF2 inhibitor. HUVEC endothelial cells were treated with TNF-alpha (0.625, 1.25, 2.5, 5.0 ng/mL) for 4 h and treated overnight with HLA-G molecules (20, 40, 80 ng/mL). (B–D) The levels of sICAM and sE-Selectin were assessed in culture supernatants in the absence or presence of anti-HLA-G (10 ng/mL) or anti-CD160 (20 ng/mL) antibodies. (E) Fold increase expression of FGF2 in TNF-alpha (2.5 ng/mL) activated HUVEC in the presence of HLA-G or anti-HLA-G, anti-CD160 antibodies in comparison with untreated HUVEC. (F) HUVEC endothelial cells were treated with TNF-alpha (2.5 ng/mL) for 4 h and cultured overnight in the presence of anti-E-Selectin (20 ng/mL), anti-ICAM1 (10 ng/mL), HLA-G molecule (40 ng/mL), and plasma samples (100 µL) from survivor and non-survivor patients in the absence (untreated) or presence of TNF-alpha treatment (2.5 ng/mL). The cells were then co-cultured with peripheral blood neutrophils from non-COVID-19 healthy controls and analyzed for neutrophil cells adhesion. anti-CD160 (10 ng/mL) was used to confirm the effect of interaction between plasmatic sHLA-G and CD160 in controlling neutrophil cells adhesion. A control IgG was used. * $p < 0.05$; Student's *t*-test. (G) Images of BioTracker 488 Green Nuclear Dye-labeled neutrophils bound to untreated and TNF α -treated HUVEC monolayers incubated with plasma sample (100 µL) from survivor (left panel) and non-survivor (right panel) patients.

3.6. Correlations between Blood sHLA-G Levels and Neutrophil Adhesion to Activated Endothelial Cells

Since the modification of the expression of ICAM-1 and E-selectin might affect the adhesion of neutrophils during the inflammatory cascade [21], we tested the efficiency of neutrophil adhesion to endothelial cells in the presence of HLA-G molecules. We treated TNF-alpha activated endothelial cells with HLA-G molecules (40 ng/mL) and observed a reduction of the neutrophil adhesion to the endothelial cells comparable to the addition of anti-ICAM-1 and anti-E-selectin treatment (Figure 3F). Since the plasma samples from COVID-19 patients and controls differ for sHLA-G levels, we used them to treat endothelial cells. We observed that the plasma samples from survivor COVID-19 patients with the highest sHLA-G levels had a higher ability to inhibit neutrophil adhesion to endothelial cells, in comparison with COVID-19 non-survivor plasma samples (Figure 3F,G) ($p < 0.001$; Student's *t*-test). Plasma samples from both survivor and non-survivor control patients behaved as COVID-19 non-survivor plasma samples, with no effect on neutrophil adhesion to endothelial cells (Figure 3F). The inhibition of neutrophil adhesion to endothelial cells obtained with plasma samples from survivor COVID-19 patients was significantly inhibited by anti-CD160 treatment (Figure 3F) ($p < 0.001$; Student's *t*-test). Interestingly, the survivors' plasma samples presented the highest levels of sHLA-G molecules in comparison with COVID-19 non-survivor plasma samples and control survivors and non-survivors.

4. Discussion

We report here for the first time the increased levels of sHLA-G and sHLA-E in plasma samples from hospitalized COVID-19 patients with respiratory failure.

We have demonstrated that sHLA-G and sHLA-E levels were higher in plasma samples from COVID-19 patients than in hospitalized control patients with respiratory failure at the time of admission and healthy controls. Hospitalized control patients with respiratory failure at the time of admission presented higher levels of sHLA-G and sHLA-E in comparison with healthy controls, showing the clinical condition as suggestive of an increase in the secretion of both molecules. Since the therapeutic treatment started after the admission, no confounding effect might be ascribed to therapeutic procedures. Moreover, no differences were found in terms of treatments between patients who died compared to patients who survived during the study follow-up. The evaluation of the genetic background did not show any differences in the three groups in terms of allelic frequencies. sHLA-G was increased in patients with improved clinical outcomes, thus suggesting that the increased concentration of sHLA-G in plasma samples may be related to inflammation and might reflect a peculiar feature of COVID-19 evolution. In fact, control patients showed a decrease in sHLA-G levels over time in both survivor and non-survivor patients. On the contrary, no correlation was found between serum sHLA-E levels and clinical outcomes of COVID-19 patients. HLA-G is known to have suppressive effects on the immune system [3]. Its deregulation has been implicated in both autoimmune and infectious diseases. In many autoimmune disorders, including celiac disease, rheumatoid arthritis, lupus, psoriasis, and diabetes, HLA-G upregulation is related to disease onset and progression [7]. Likewise, increased HLA-G levels have been found in infections of HIV-1, human cytomegalovirus, HPV, and herpes simplex virus-1, likely as a way to avoid immune detection of infected cells [7], and recently in patients with severe COVID-19 [35]. Thus, HLA-G upregulation might have a similar role in SARS-COV2 related immune dysfunction [36]. A case study by Zhang et al. reported the immune cell, cytokine, and HLA-G (including receptor) levels of a COVID-19 patient during hospitalization [37]. Overall, HLA-G levels decreased during the replication phase of COVID-19 and increased again after clearance, likely relating to corresponding cytokine levels. These data are in line with our findings of increased sHLA-G levels when clinical outcomes improve in COVID-19. We have previously reported that Natural Killer cells are affected by SARS-COV2 SP1 protein expression in lung epithelial cells via HLA-E/NKG2A interaction [38]. The resulting NK cells' exhaustion might contribute to immunopathogenesis in SARS-COV2 infection.

As a proof of concept of the possible implication of sHLA-G levels in the COVID-19 course, we evaluated the levels of biomarkers of endothelial activation and correlated them with sHLA-G levels. Indeed, the endothelial compartment is a relevant target of SARS-COV2 infection which expresses ACE2 [39,40]. Endothelial dysfunction may play a major contribution to COVID-19 pathophysiology, leading to loss of physiological properties of the endothelium, including the ability to stimulate vasodilation, fibrinolysis, and anti-aggregation [41]. Previous studies found that endothelial dysfunction plays an important role in critical illness, especially in sepsis [42].

We observed an inverse correlation between sHLA-G levels and sICAM-1 and E-selectin levels in COVID-19 patients, but not in controls. We are aware that the main limitation of this research is the low number of control patients with respiratory failure. However, in the control group we recruited patients with similar presentation to COVID-19 patients admitted to hospital in the same clinical settings and over the same period of time. It is well known that during the first wave of the COVID-19 outbreak a significant reduction in hospitalization and admission for non-COVID-19 acute conditions occurred, leading to a limited number of patients suitable for the control group. However, we confirmed the *ex vivo* data in an *in vitro* setting. The *in vitro* analysis of activated endothelial cells confirmed the ability of HLA-G molecules to control sICAM-1 and sE-selectin expression via CD160 interaction and consequent FGF2 induction. Endothelial cells as well as leucocytes express adhesion molecules that are induced by transcription factors such as FGF2 [34], which mediate the adhesion and subsequent migration of leucocytes into tissue. *De novo* expression or enhanced expression of E-selectin and ICAM-1 has been described in inflammatory conditions [43–45]. The regulation of expression of these adhesion molecules is considered to play a major role in the localization and development of an inflammatory reaction. E-selectin and ICAM-1 are structurally unrelated adhesion molecules for granulocytes, monocytes, and T lymphocytes [46]. The inflammatory cytokines tumor necrosis factor (TNF), interleukin-1 (IL-1), interferon- γ (IFN- γ), and bacterial endotoxins (lipopolysaccharides (LPS)) α , and LPS are known inducers and enhancers of E-selectin and ICAM-1 [46]. Circulating leukocytes enter inflamed tissues through sequential adhesive and signaling events [47]. Neutrophils first tether to and roll on E-selectin expressed on activated endothelial cells, which enables interactions with ICAM-1 that promote arrest, adhesion strengthening, intraluminal crawling, and trans-endothelial migration. Importantly, E-selectin directly triggers signals in rolling neutrophils that cooperate with chemokine signals to maximize neutrophil recruitment during inflammation [48]. When we evaluated the effect of HLA-G molecules on neutrophil adhesion to activated endothelial cells, we observed that the addition of HLA-G molecules reduced the neutrophil adhesion to the endothelial cells with a comparable efficiency to that obtained with the addition of anti-ICAM-1 and anti-E-selectin treatment. As a proof of concept, we showed that the plasma samples from survivor COVID-19 patients had a higher ability to inhibit neutrophil adhesion to endothelial cells in comparison with COVID-19 non-survivor plasma samples. The inhibition of neutrophil adhesion to endothelial cells obtained with plasma samples from survivor COVID-19 patients was significantly inhibited by anti-CD160 treatment, suggesting a role of HLA-G/CD160 interaction in regulating neutrophil adhesion to endothelial cells. With less adhesion factors on endothelial cells, fewer neutrophils adhere to vessel walls and transmigrate into tissues, decreasing the overall detrimental effects observed in severe COVID-19 patients [49]. Although the role of HLA-G as an adhesion inhibitor has not been extensively studied, a study revealed the ability of HLA-G to block human natural killer rolling adhesion on porcine endothelial cells [50]. This is in agreement with our results on neutrophil cells and is of particular interest because the rolling adhesion of neutrophils represents the main mechanism of their recruitment to the injury site where they adhere tightly and migrate through the endothelium, causing inflammatory effects. The recognition of the possible mechanisms by which HLA-G might inhibit neutrophil adhesion to activated endothelial cells and may have significant anti-inflammatory properties [15]. Notably, the plasma levels of adhesion molecules, such as ICAM-1, fractalkine, vascular

cell adhesion molecule-1 (VCAM-1), vascular adhesion protein-1 (VAP-1), and vascular endothelial growth factor (VEGF), have been reported to be elevated among COVID-19 patients, especially in severe cases [51]. These data, together with our results, suggest HLA-G and adhesion molecules are molecular mechanisms underlying COVID-19-induced endothelial injury, vascular permeability to neutrophil accumulation, angiogenesis, and pro-coagulation in COVID-19 pathogenesis.

In conclusion, our data suggest a potential role for sHLA-G in the control of neutrophil adhesion to activated endothelium in COVID-19 patients that is related to improvement of the disease (Figure 4). Thus, increased levels of sHLA-G in the blood may represent a novel, promising biomarker of disease activity in COVID-19. Further investigations are needed to assess HLA-G mechanisms to control ICAM-1 and E-selectin expression by activated endothelial cells and the neutrophil adhesion.

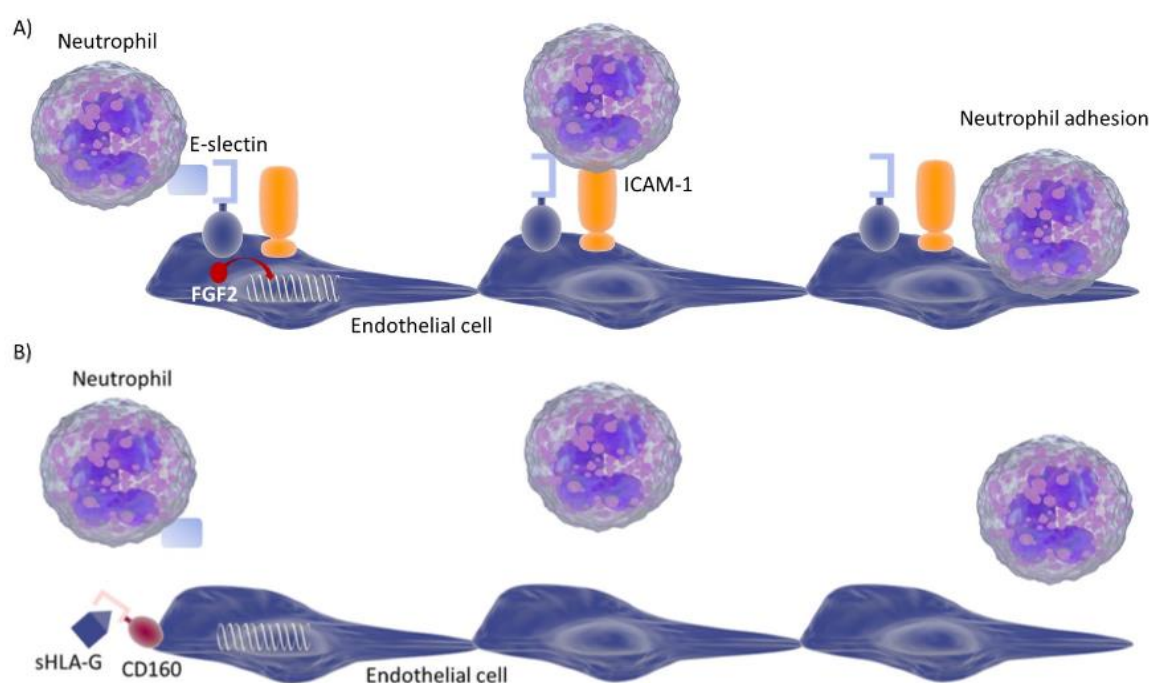


Figure 4. Representation of the molecular interaction on the basis of neutrophil cell adhesion to endothelial cells. **(A)** Neutrophils interact with E-selectin, enhancing ICAM-1 recognition and adhesion to endothelial cells. Both these molecules are induced by FGF2 (fibroblast growth factor 2). **(B)** In the presence of COVID-19 there is an increase in sHLA-G molecules interacting with CD160, which inhibits FGF2-dependent induction of E-selectin and ICAM-1. The reduction of E-selectin and ICAM-1 expression reduces neutrophil adhesion to endothelial cells. This condition might improve clinical conditions, reducing neutrophils activation.

Supplementary Materials: The following are available online at <https://www.mdpi.com/article/10.3390/v13091855/s1>, File S1: Data collection.

Author Contributions: D.B.: Project administration, supervision, writing—original draft; V.G., S.R., G.S. (Giovanna Schiuma), S.B., G.S. (Giovanni Strazzabosco): investigation, methodology; S.S., G.C.: sample collection, clinical data collection; E.D.C., A.P.: Writing—review & editing; M.C., R.R.: Research conceptualization; writing—original draft. All authors have read and agreed to the published version of the manuscript.

Funding: This research was funded by University of Ferrara crowdfunding and a 5 × 1000 grant.

Institutional Review Board Statement: Approval was granted by the ethics committee of Hospital General Universitario de Elche (PI 46/2020). The procedures used in this study adhere to the principles of the Declaration of Helsinki.

Informed Consent Statement: Informed consent was obtained from all subjects involved in the study.

Data Availability Statement: Data and statistical code are available from the corresponding author upon reasonable request.

Acknowledgments: We thank Iva Pivanti and Mercedes Fernandez for the technical support.

Conflicts of Interest: The authors declare no conflict of interest.

References

- Carosella, E.D.; Paul, P.; Moreau, P.; Rouas-Freiss, N. HLA-G and HLA-E: Fundamental and pathophysiological aspects. *Immunol. Today* **2000**, *21*, 532–534. [CrossRef]
- Le Bouteiller, P.; Lenfant, F. Antigen-presenting function(s) of the non-classical HLA-E, -F and -G class I molecules: The beginning of a story. *Res. Immunol.* **1996**, *147*, 301–313. [CrossRef]
- O’Callaghan, C.A.; Bell, J.I. Structure and function of the human MHC class Ib molecules HLA-E, HLA-F and HLA-G. *Immunol. Rev.* **1998**, *163*, 129–138. [CrossRef]
- Kren, L.; Slaby, O.; Muckova, K.; Lzicarova, E.; Sova, M.; Vybihal, V.; Svoboda, T.; Fadrus, P.; Lakomy, R.; Vanhara, P.; et al. Expression of immune-modulatory molecules HLA-G and HLA-E by tumor cells in glioblastomas: An unexpected prognostic significance? *Neuropathology* **2011**, *31*, 129–134. [CrossRef] [PubMed]
- Rabot, M.; Tabiasco, J.; Polgar, B.; Aguerre-Girr, M.; Berrebi, A.; Bensussan, A.; Strbo, N.; Rukavina, D.; Le Bouteiller, P. HLA Class I/NK Cell Receptor Interaction in Early Human Decidua basalis: Possible Functional Consequences. *Food Allergy Mol. Basis Clin. Pract.* **2005**, *89*, 72–83. [CrossRef]
- Amiot, L.; Vu, N.; Samson, M. Biology of the immunomodulatory molecule HLA-G in human liver diseases. *J. Hepatol.* **2015**, *62*, 1430–1437. [CrossRef] [PubMed]
- Rizzo, R.; Fainardi, E.; Rouas-Freiss, N.; Morandi, F. The Role of HLA-Class Ib Molecules in Immune-Related Diseases, Tumors, and Infections 2016. *J. Immunol. Res.* **2017**, *2017*, 1–2. [CrossRef]
- Rizzo, R.; Bortolotti, D.; Bolzani, S.; Fainardi, E. HLA-G Molecules in Autoimmune Diseases and Infections. *Front. Immunol.* **2014**, *5*, 592. [CrossRef]
- Fons, P.; Chabot, S.; Cartwright, J.E.; Lenfant, F.; L’Faqihi, F.; Giustiniani, J.; Herault, J.-P.; Gueguen, G.; Bono, F.; Savi, P.; et al. Soluble HLA-G1 inhibits angiogenesis through an apoptotic pathway and by direct binding to CD160 receptor expressed by endothelial cells. *Blood* **2006**, *108*, 2608–2615. [CrossRef]
- Rebmann, V.; van der Ven, K.; Pässler, M.; Pfeiffer, K.; Krebs, D.; Grosse-Wilde, H. Association of soluble HLA-G plasma levels with HLA-G alleles. *Tissue Antigens* **2001**, *57*, 15–21. [CrossRef]
- Braud, V.M.; Allan, D.S.J.; O’Callaghan, C.A.; Söderström, K.; D’Andrea, A.; Ogg, G.S.; Lazetic, S.; Young, N.T.; Bell, J.I.; Phillips, J.H.; et al. HLA-E binds to natural killer cell receptors CD94/NKG2A, B and C. *Nat. Cell Biol.* **1998**, *391*, 795–799. [CrossRef] [PubMed]
- Braud, V.M.; Allan, D.S.; Wilson, D.; McMichael, A.J. TAP- and tapasin-dependent HLA-E surface expression correlates with the binding of an MHC class I leader peptide. *Curr. Biol.* **1998**, *8*, 1–10. [CrossRef]
- Llano, M.; Lee, N.; Navarro, F.; Garcia, P.; Albar, J.P.; Geraghty, D.E.; López-Botet, M. HLA-E-bound peptides influence recognition by inhibitory and triggering CD94/NKG2 receptors: Preferential response to an HLA-G-derived nonamer. *Eur. J. Immunol.* **1998**, *28*, 2854–2863. [CrossRef]
- Allard, M.; Oger, R.; Vignard, V.; Percier, J.-M.; Fregni, G.; Perier, A.; Caignard, A.; Charreau, B.; Bernardeau, K.; Khammari, A.; et al. Serum Soluble HLA-E in Melanoma: A New Potential Immune-Related Marker in Cancer. *PLoS ONE* **2011**, *6*, e21118. [CrossRef]
- Mociornita, A.G.; Adamson, M.B.; Tumiati, L.C.; Ross, H.J.; Rao, V.; Delgado, D.H. Effects of everolimus and HLA-G on cellular proliferation and neutrophil adhesion in an in vitro model of cardiac allograft vasculopathy. *Arab. Archaeol. Epigr.* **2018**, *18*, 3038–3044. [CrossRef]
- Coupe, S.; Moreau, A.; Hamidou, M.; Horejsi, V.; Soullou, J.-P.; Charreau, B. Expression and release of soluble HLA-E is an immunoregulatory feature of endothelial cell activation. *Blood* **2007**, *109*, 2806–2814. [CrossRef] [PubMed]
- Zheng, H.; Lu, R.; Xie, S.; Wen, X.; Wang, H.; Gao, X.; Guo, L. Human leukocyte antigen-E alleles and expression in patients with serous ovarian cancer. *Cancer Sci.* **2015**, *106*, 522–528. [CrossRef]
- Zidi, I. Puzzling out the COVID-19: Therapy targeting HLA-G and HLA-E. *Hum. Immunol.* **2020**, *81*, 697–701. [CrossRef] [PubMed]
- Rizzo, R.; Neri, L.M.; Simioni, C.; Bortolotti, D.; Occhionorelli, S.; Zauli, G.; Secchiero, P.; Semprini, C.M.; Laface, I.; Sanz, J.M.; et al. SARS-CoV2 nucleocapsid protein and ultrastructural modifications in small bowel of a 4-week-negative COVID19 patient. *Clin. Microbiol. Infect.* **2021**, *27*, 936–937. [CrossRef] [PubMed]
- Available online: <https://covid19.who.int> (accessed on 5 August 2021).

21. Leeuwenberg, J.F.; Smeets, E.F.; Neeffjes, J.; Shaffer, M.A.; Cinek, T.; Jeunhomme, T.M.; Ahern, T.J.; Buurman, W.A. E-selectin and intercellular adhesion molecule-1 are released by activated human endothelial cells in vitro. *Immunology* **1992**, *77*, 543–549. [[PubMed](#)]
22. Barnes, B.J.; Adrover, J.M.; Baxter-Stoltzfus, A.; Borczuk, A.; Cools-Lartigue, J.; Crawford, J.M.; Daßler-Plenker, J.; Guerci, P.; Huynh, C.; Knight, J.S.; et al. Targeting potential drivers of COVID-19: Neutrophil extracellular traps. *J. Exp. Med.* **2020**, *6*, 217. [[CrossRef](#)] [[PubMed](#)]
23. Parackova, Z.; Zentsova, I.; Bloomfield, M.; Vrabcova, P.; Smetanova, J.; Klocperk, A.; Mesežnikov, G.; Mendez, L.F.C.; Vymazal, T.; Sediva, A. Disharmonic Inflammatory Signatures in COVID-19: Augmented Neutrophils' but Impaired Monocytes' and Dendritic Cells' Responsiveness. *Cells* **2020**, *9*, 2206. [[CrossRef](#)] [[PubMed](#)]
24. Contoli, M.; Papi, A.; Tomassetti, L.; Rizzo, P.; Sega, F.V.D.; Fortini, F.; Torsani, F.; Morandi, L.; Ronzoni, L.; Zucchetti, O.; et al. Blood Interferon- α Levels and Severity, Outcomes, and Inflammatory Profiles in Hospitalized COVID-19 Patients. *Front. Immunol.* **2021**, *12*, 648004. [[CrossRef](#)]
25. Spadaro, S.; Fogagnolo, A.; Campo, G.; Zucchetti, O.; Verri, M.; Ottaviani, I.; Tunstall, T.; Grasso, S.; Scaramuzzo, V.; Murgolo, F.; et al. Markers of endothelial and epithelial pulmonary injury in mechanically ventilated COVID19 ICU patients. *Crit. Care.* **2021**, *25*, 74. [[CrossRef](#)] [[PubMed](#)]
26. Campo, G.; Contoli, M.; Fogagnolo, A.; Sega, F.V.D.; Zucchetti, O.; Ronzoni, L.; Verri, M.; Fortini, F.; Pavasini, R.; Morandi, L.; et al. Over time relationship between platelet reactivity, myocardial injury and mortality in patients with SARS-COV2-associated respiratory failure. *Platelets* **2021**, *32*, 560–567. [[CrossRef](#)]
27. Fainardi, E.; Rizzo, R.; Melchiorri, L.; Stignani, M.; Castellazzi, M.; Caniatti, M.L.; Baldi, E.; Tola, M.R.; Granieri, E.; Baricordi, O.R. Soluble HLA-G molecules are released as HLA-G5 and not as soluble HLA-G1 isoforms in CSF of patients with relapsing–remitting Multiple Sclerosis. *J. Neuroimmunol.* **2007**, *192*, 219–225. [[CrossRef](#)]
28. Morandi, F.; Venturi, C.; Rizzo, R.; Castellazzi, M.; Baldi, E.; Caniatti, M.L.; Tola, M.R.; Granieri, E.; Fainardi, E.; Uccelli, A.; et al. Intrathecal Soluble HLA-E Correlates with Disease Activity in Patients with Multiple Sclerosis and may Cooperate with Soluble HLA-G in the Resolution of Neuroinflammation. *J. Neuroimmune Pharmacol.* **2013**, *8*, 944–955. [[CrossRef](#)]
29. Nishizawa, A.; Kumada, K.; Tateno, K.; Wagata, M.; Saito, S.; Katsuoka, F.; Mizuno, S.; Ogishima, S.; Yamamoto, M.; Yasuda, J.; et al. Analysis of HLA-G long-read genomic sequences in mother–offspring pairs with preeclampsia. *Sci. Rep.* **2020**, *10*, 1–10. [[CrossRef](#)]
30. Rizzo, R.; D'Accolti, M.; Bortolotti, D.; Caccuri, F.; Caruso, A.; Di Luca, D.; Caselli, E. Human Herpesvirus 6A and 6B inhibit in vitro angiogenesis by induction of Human Leukocyte Antigen G. *Sci. Rep.* **2018**, *8*, 17683. [[CrossRef](#)]
31. Kjaergaard, A.G.; Dige, A.; Krog, J.; Tønnesen, E.; Wogensen, L. Soluble Adhesion Molecules Correlate with Surface Expression in an In Vitro Model of Endothelial Activation. *Basic Clin. Pharmacol. Toxicol.* **2013**, *113*, 273–279. [[CrossRef](#)]
32. Rizzo, R.; Hviid, T.V.F.; Stignani, M.; Balboni, A.; Grappa, M.T.; Melchiorri, L.; Baricordi, O.R. The HLA-G genotype is associated with IL-10 levels in activated PBMCs. *Immunogenetics* **2005**, *57*, 172–181. [[CrossRef](#)] [[PubMed](#)]
33. Wilhelmsen, K.; Farrar, K.; Hellman, J. Quantitative In vitro Assay to Measure Neutrophil Adhesion to Activated Primary Human Microvascular Endothelial Cells under Static Conditions. *J. Vis. Exp.* **2013**, *78*, e50677. [[CrossRef](#)]
34. Zittermann, S.I.; Issekutz, A.C. Basic Fibroblast Growth Factor (bFGF, FGF-2) Potentiates Leukocyte Recruitment to Inflammation by Enhancing Endothelial Adhesion Molecule Expression. *Am. J. Pathol.* **2006**, *168*, 835–846. [[CrossRef](#)]
35. Al-Bayatee, N.T.; Ad'hiah, A.H. Soluble HLA-G is upregulated in serum of patients with severe COVID19. *Human Immunol* **2021**. [[CrossRef](#)]
36. Morandi, F.; Rizzo, R.; Fainardi, E.; Rouas-Freiss, N.; Pistoia, V. Recent Advances in Our Understanding of HLA-G Biology: Lessons from a Wide Spectrum of Human Diseases. *J. Immunol. Res.* **2016**, *2016*, 4326495. [[CrossRef](#)]
37. Zhang, S.; Gan, J.; Chen, B.; Zheng, D.; Zhang, J.; Lin, R.; Zhou, Y.; Yang, W.; Lin, A.; Yan, W. Dynamics of peripheral immune cells and their HLA-G and receptor expressions in a patient suffering from critical COVID-19 pneumonia to convalescence. *Clin. Transl. Immunol.* **2020**, *9*, e1128. [[CrossRef](#)]
38. Bortolotti, D.; Gentili, V.; Rizzo, S.; Rotola, A.; Rizzo, R. SARS-COV2 Spike 1 Protein Controls Natural Killer Cell Activation via the HLA-E/NKG2A Pathway. *Cells* **2020**, *9*, 1975. [[CrossRef](#)] [[PubMed](#)]
39. Lovren, F.; Pan, Y.; Quan, A.; Teoh, H.; Wang, G.; Shukla, P.C.; Levitt, K.S.; Oudit, G.Y.; Al-Omran, M.; Stewart, D.J.; et al. Angiotensin converting enzyme-2 confers endothelial protection and attenuates atherosclerosis. *Am. J. Physiol. Circ. Physiol.* **2008**, *295*, H1377–H1384. [[CrossRef](#)]
40. Sluimer, J.; Gasc, J.M.; Hamming, I.; van Goor, H.; Michaud, A.; Akker, L.H.V.D.; Jutten, B.; Cleutjens, J.; Bijmens, A.P.J.; Corvol, P.; et al. Angiotensin-converting enzyme 2 (ACE2) expression and activity in human carotid atherosclerotic lesions. *J. Pathol.* **2008**, *215*, 273–279. [[CrossRef](#)] [[PubMed](#)]
41. Godo, S.; Shimokawa, H. Endothelial Functions. *Arter. Thromb. Vasc. Biol.* **2017**, *37*, e108–e114. [[CrossRef](#)]
42. Aird, W.C. The role of the endothelium in severe sepsis and multiple organ dysfunction syndrome. *Blood* **2003**, *101*, 3765–3777. [[CrossRef](#)]
43. Vejlsgaard, G.L.; Ralfkiaer, E.; Avnstorp, C.; Czajkowski, M.; Marlin, S.D.; Rothlein, R. Kinetics and characterization of intercellular adhesion molecule-1 (ICAM-1) expression on keratinocytes in various inflammatory skin lesions and malignant cutaneous lymphomas. *J. Am. Acad. Dermatol.* **1989**, *20*, 782–790. [[CrossRef](#)]

Host immune system confers protection against SARS-CoV-2, but at the same time, its aberrant activation is the main causes of the hyperinflammatory environment associated to COVID-19 [278]. As a consequence of cytokine overproduction, COVID-19 patients often present aggregates of extracellular DNA fibers and proteases released from the recruited neutrophils, named as extracellular traps (NETs) [333], which amplify the innate immune response, prolonging the recruitments of monocyte, macrophages, neutrophils, eosinophils and NK cells at the site of infection [334].

This imbalanced immune activation is typical of COVID-19: on one side, the infection warns and recruits innate effectors, while on the other side, excessive immune activation leads to hyperinflammation and tissue damage. In addition, during SARS-CoV-2 host driven immune response, IFNs production is suppressed, while elevated levels of chemokines are reported, above all IL-6, that usually stimulate T cell proliferation [278].

In particular, the lack of IFNs was associated with a high risk of severe and fatal COVID-19 [240], due to an impairment of T cell function, that leads to a negative outcome of disease and to a reduction of NK cell activation, which show functional exhaustion [335].

As before mentioned, in COVID-19 patients IFN- γ secretion and NK cytotoxicity were reduced from the 16% to 80%. NK cells represent nearly the 10-15% of the circulating white cells and could be also found associated to tissues. Circulating and tissue resident NK cells display different behaviors, in association with peculiar immunophenotypes. In particular, CD56, the archetypal phenotypic marker of NK cells, is used to identify CD56^{bright} and CD56^{dim} cells [336]. CD56^{bright} NK cells are more abundant in tissues (for example in endometrial tissue [337]), lack the expression of CD16 (Fc γ -receptor, marker of NK cell activation) and exert a secretory function, while CD56^{dim} NK cells are predominant in peripheral blood, express CD16 and present cytotoxic activity [338].

NK cells activation is mainly due to HLA-I molecules expression detection on nucleated cells, which interact with specific inhibitory and activating receptors expressed on NK cell surface. In fact, the lack of HLA-I expression, as usually observed on infected cells, triggers NK cell activation, which consists in cytokine release and cell killing [339].

NK cell receptors can be classified into four major families, which include both activating and inhibitory members [340]:

- Natural Cytotoxicity Receptors (NCRs);
- C-type lectin receptors, including CD94/NKG2A, CD94/NKG2C, CD94/NKG2E, NKG2D;
- Leukocyte Immunoglobulin-Like Receptors (LILR);

- Killer Immunoglobulin-like Receptors (KIR).

The peculiar combination of these receptors in NK cell subclones affects NK cell activation efficiency and consequently is strictly connected to host ability to control viral infections.

Several studies reported that NK cell depletion or anergy result in increased susceptibility to viral infection, such as to Human Cytomegalovirus (HCMV) [341], Herpes Simplex Virus (HVS) [342] and HIV [343].

Notably, NK cell activation status has been reported to be affected also during SARS-CoV-2 infection. In fact, COVID-19 patients often develop circulating NK cells functional exhaustion, that facilitates viral spread, together with tissue-associated NK cells hyperactivation, that potentially contribute to local inflammation and injury [344, 345]. [346].

NK cells activation during viral infection depends mainly to their clonal expression of activating or inhibitory KIRs ([347], paper attached) and, for this reason, their expression is often modulated by viruses, as already described for HIV and Herpesviruses ([347], paper attached). Similarly, SARS-CoV-2 interact with KIR receptors on NK cells to activate both inhibitory [348] or activator signaling, causing lymphocytes and NK cells exhaustion observed in severe COVID-19 patients.

Thus, in the following review, we summarized the importance of KIRs in the antiviral defense ([347], paper attached).

Review

Role of KIR Receptor in NK Regulation during Viral Infections

Sabrina Rizzo [†], Giovanna Schiuma [†], Silvia Beltrami, Valentina Gentili, Roberta Rizzo * and Daria Bortolotti *

Department of Chemical, Pharmaceutical and Agricultural Sciences, University of Ferrara, 44121 Ferrara, Italy; sabrina.rizzo@unife.it (S.R.); giovanna.schiuma@unife.it (G.S.); silvia.beltrami@unife.it (S.B.); valentina.gentili@unife.it (V.G.)

* Correspondence: rbr@unife.it (R.R.); brtdra@unife.it (D.B.)

† These authors contributed equally to this work.

Abstract: Natural Killer (NK) cells are key effectors of the innate immune system which represent the first line of defense against viral infections. NK cell activation depends on the engagement of a complex receptor repertoire expressed on their surface, consisting of both activating and inhibitory receptors. Among the known NK cell receptors, the family of killer Ig-like receptors (KIRs) consists in activating/inhibitory receptors that interact with specific human leukocyte antigen (HLA) molecules expressed on target cells. In particular, the expression of peculiar KIRs have been reported to be associated to viral infection susceptibility. Interestingly, a significant association between the development and onset of different human pathologies, such as tumors, neurodegeneration and infertility, and a clonal KIRs expression on NK cells has been described in presence of viral infections, supporting the crucial role of KIRs in defining the effect of viral infections in different tissues and organs. This review aims to report the state of art about the role of KIRs receptors in NK cell activation and viral infection control.

Keywords: NK cells; KIR receptors; viral infections



Citation: Rizzo, S.; Schiuma, G.; Beltrami, S.; Gentili, V.; Rizzo, R.; Bortolotti, D. Role of KIR Receptor in NK Regulation during Viral Infections. *Immuno* **2021**, *1*, 305–331. <https://doi.org/10.3390/immuno1030021>

Academic Editor:
Alessandra Fierabracci

Received: 30 July 2021
Accepted: 2 September 2021
Published: 6 September 2021

Publisher's Note: MDPI stays neutral with regard to jurisdictional claims in published maps and institutional affiliations.



Copyright: © 2021 by the authors. Licensee MDPI, Basel, Switzerland. This article is an open access article distributed under the terms and conditions of the Creative Commons Attribution (CC BY) license (<https://creativecommons.org/licenses/by/4.0/>).

1. Introduction

Natural Killer (NK) cells are large granular lymphocytes belonging to the innate immune system present at both systemic level, where they constitute nearly 10–15% of the circulating lymphocytes [1], and in association to tissues [2,3]. Peripheral or tissue-associated NK cells display different behaviors: circulating NK cells are characterized by a cytotoxic profile, while tissue NK cells are typically secretory cells [4]. In particular, this latter type of NK cells has been reported in secondary lymphoid organs [5], inflammatory sites [6], and also in endometrium [7], where they are the predominant lymphocyte population playing important roles in reproduction [8,9], particularly during implantation and decidualization.

In general, NK cells are described as large lymphocytes that lack the expression of canonical T cell receptors (i.e., CD3 negative), thus human NK cells have been classically defined as CD3[−]CD56⁺. Besides these classical NK cells, later evidence has identified another set of NK cells, called NKT cells, that have been found within T cell populations and express both TCR molecules and NK cell markers [10]. Nevertheless, NKT cells show a restricted TCR repertoire and constitute a small percentage of cells found in thymus and spleen, but they are significantly present in the liver [10]. An additional NK cell population, showing both T cell and NK cell phenotypes, has been identified as Cytokine-induced killer (CIK) cells. These cells express either the T cell marker CD3 or NK-cell marker CD56 and exert a peculiar strong cytotoxic activity [11]. CIK cells are expandable from peripheral blood mononuclear cells and differentiate in presence of specific cytokines, like IL-15 and IL-2 [11,12].

However, classical NK cells are generally further subdivided into CD56^{bright} and CD56^{dim} NK cells. The substantial difference between the two groups is that CD56^{bright} NK

cells are much more abundant in tissues and lack the expression of CD16 (Fc γ -receptor) and typically exert a secretory function, while CD56^{dim} NK cells are predominant in peripheral blood, express CD16, and are characterized by a peculiar cytotoxic activity [13]. The presence of CD16 allows circulating NK cells to recognize the constant fraction (Fc) of antibodies and to engage cell lysis [14].

In addition to CD56^{bright} and CD56^{dim} classification, a subset of CD56⁻CD16⁺ NK cells appear to be expanded in the presence of chronic viral infections, for example, HIV-1 (human immunodeficiency virus-1), and they seem to represent an exhausted/aneergic subset of NK cells [15,16].

NK cells have also been classified into NK1 and NK2 subsets, based on their cytokine release [17] and on their chemokine receptors expression [18]. NK1 and NK2 produce both T helper type 1 (Th1) and Th2 cytokines, through which they can exert beneficial, as well as deleterious, effects in a variety of inflammatory diseases, playing an immunomodulatory role in cellular response [19]. Later studies have further investigated another NK1 subset, that secretes Th17-related cytokines, such as IL-17, called NKTh17 [19]. This novel subset of human NK cells is phenotypically characterized by the presence of CD56, CCR4, and IL-23 receptors and by the ability to produce IL-17 [20]. In particular, Rizzo et al. have observed that, during Herpes simplex virus (HSV)-1 infection, NKTh17 KIR2DL2+ cells produced high levels of Th17 cytokines, mainly IL-17A [21]. The production of IL-17 by NKTh17 might induce the upregulation of anti-apoptotic molecules, consequently increasing persistent infection by blocking cytotoxic T cells action [22].

NK cells represent the first line of defense against viral infections and their relevance is confirmed by the several mechanisms used by viruses to evade NK cell-mediated immune responses [23], that is characterized also by a memory-like status [14]. Even if immunological memory is a characteristic hallmark of the adaptive immune system, NK cells have been shown to mediate Ag-specific recall responses too. NK cell memory is the consequence of a clonal-like expansion during viral infection that generates a long-lived progeny (i.e., memory cells) that triggers a more efficacious secondary response against previously encountered pathogens [24].

The contribution of NK cells to the antiviral immune response has been extensively studied in mouse models of viral infections, demonstrating that these types of cells not only control viral replication by killing infected cells during the earliest stages of infection, prior to the development of adaptive immunity, but play a crucial immunoregulatory role during the development of adaptive immune response as well [25,26]. The ability of NK cells to modulate adaptive immunity is mediated by the secretion of cytokines, such as interferons and interleukins, able to stimulate adaptive immunity cells, as T- and B-cells, triggering their activation.

Several works found that an impairment in NK cell activity, for example due to NK cell deficiencies in humans [27,28], could enhance viral infections, including multiple infections by herpesviruses. The authors first reported a case of a young girl who lacked functional NK cells and experienced a series of viral infections during childhood and adolescence, including infections by multiple herpesviruses, highlighting the importance of NK cells contribution to the antiviral immune response [27].

In particular, during viral infections, both cytotoxic and secretory NK cells activation can be stimulated by specific cytokines upregulated during viral replication (Figure 1). For example, type-I interferons (IFN- α/β), secreted by infected cells, induce NK cells cytotoxicity [10]; the expression of IL-12 (interleukin-12) stimulates NK cells IFN- γ (interferon- γ) secretion [29]. This latter can activate multiple important pathways associated with direct antiviral functions and/or immunoregulatory effects on downstream immune response. Meanwhile, NK cells can also produce TNF- α (tumor necrosis factor- α) that mediates antiviral and immunoregulatory effects [10,30].

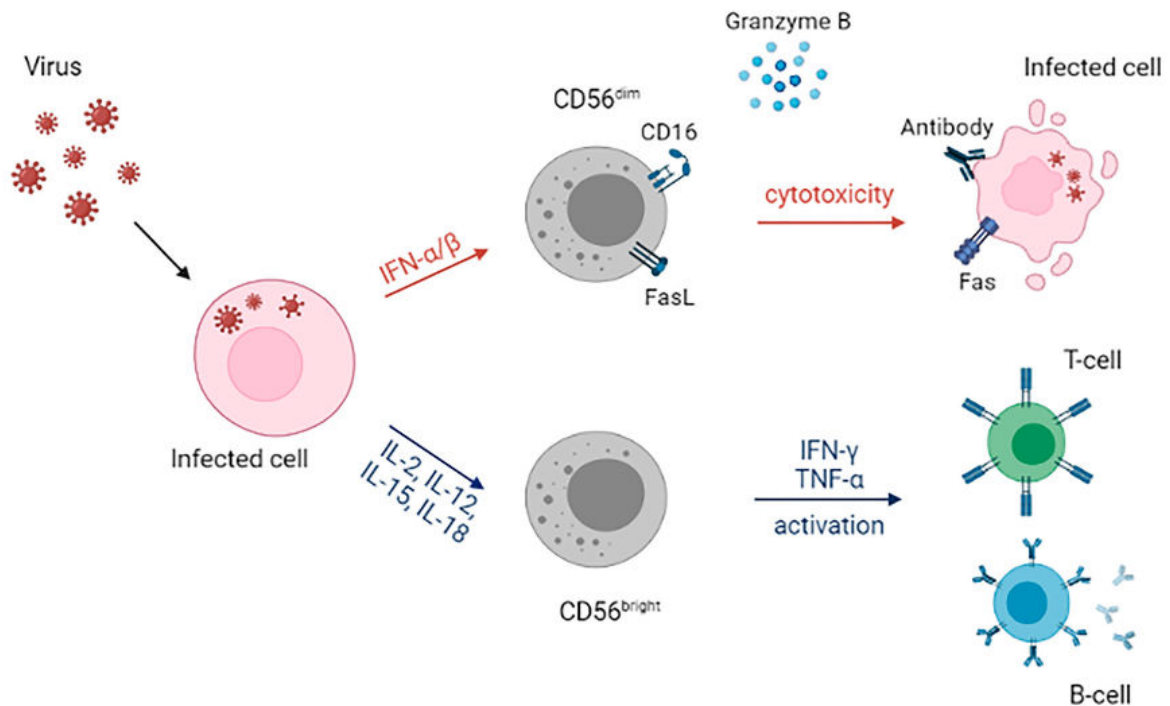


Figure 1. NK cell activation during infection. Virus can induce the production of $IFN-\alpha/-\beta$ (interferon- $\alpha/-\beta$) and IL (interleukin)-2, IL-12, IL-15, and IL-18 by infected cells, which respectively stimulate NK cells cytotoxicity and adaptive immunity activation. $CD56^{dim}$ NK cells have a cytotoxic function that can be mediated by Granzyme-B production, Fas/FasL (Fas ligand) interaction and CD16 binding with the Fc (constant fraction) of antibodies. Adaptive immunity modulation is mediated by $CD56^{bright}$ NK cells through the secretion of $IFN-\gamma$ (interferon- γ)/TNF- α (tumor necrosis factor- α), that affect T- and B-cells.

Besides the aforementioned IFNs and IL-12, also IL-2, IL-15, and IL-18 participate in NK cells early activation. During inflammation or viral infection, secreted IL-2, IL-12, and IL-18 drive NK cell activation inducing target cell killing and the release of cytotoxic cytokines [31–33]. IL-2 and IL-15 are mainly involved in NK cell “priming”. Both IL-2 and the “IL-2-like” IL-15 achieve their functions by binding the heterotrimeric receptor composed of CD132, CD122, and IL-2R α (CD25) for IL-2 [34] or IL-15R α for IL-15 binding [35]. Interestingly, IL-15 can activate NK cells with relatively lower concentrations compared to IL-2, thanks to its higher affinity for IL-15R α [35]. Moreover, it was found that prior exposure to IL-15 sensitizes NK cells to secondary stimuli, thereby resulting in exaggerated responses [36,37]. In fact, IL-15-primed NK cells produce elevated levels of IL-12-induced $IFN-\gamma$ [38]. Consequently, IL-15 promotes NK cells to be fully equipped to counteract viral infections through the rapid induction of granzymes and perforin [39]. IL-12 and IL-18 stimulate cytokine-induced memory-like NK cells [40], effective in response to viral infection reactivation.

After the initial activation triggered by cytokines, NK cell later activation involves specific receptors engagements and leads to their cytotoxic effect.

NK cells cytotoxicity during viral infections is mediated by different mechanisms, depending on the NK cell phenotype. Phenotypically immature $CD161^+/CD56^-$ NK cells mediate TRAIL (TNF-related apoptosis-inducing ligand)-dependent but not FasL- or granule release-dependent cytotoxicity, whereas mature $CD56^+$ NK cells mediate the latter two [41], as exocytosis of cytoplasmatic granules containing perforin and Granzyme-B, Fas ligand-mediated induction of apoptosis and antibody-dependent cellular cytotoxicity (ADCC) through CD16 binding with the Fc of antibodies (Figure 1) [23].

NK cells effector functions are regulated by the combination of activating and inhibitory signals triggered by specific receptor/ligand interactions [14] that determine infected cells killing and regulation of antigen presenting cells (APC) and T cells responses through soluble factors secretion (such as IFN- γ and TNF- α), as represented in Figure 2 [14].

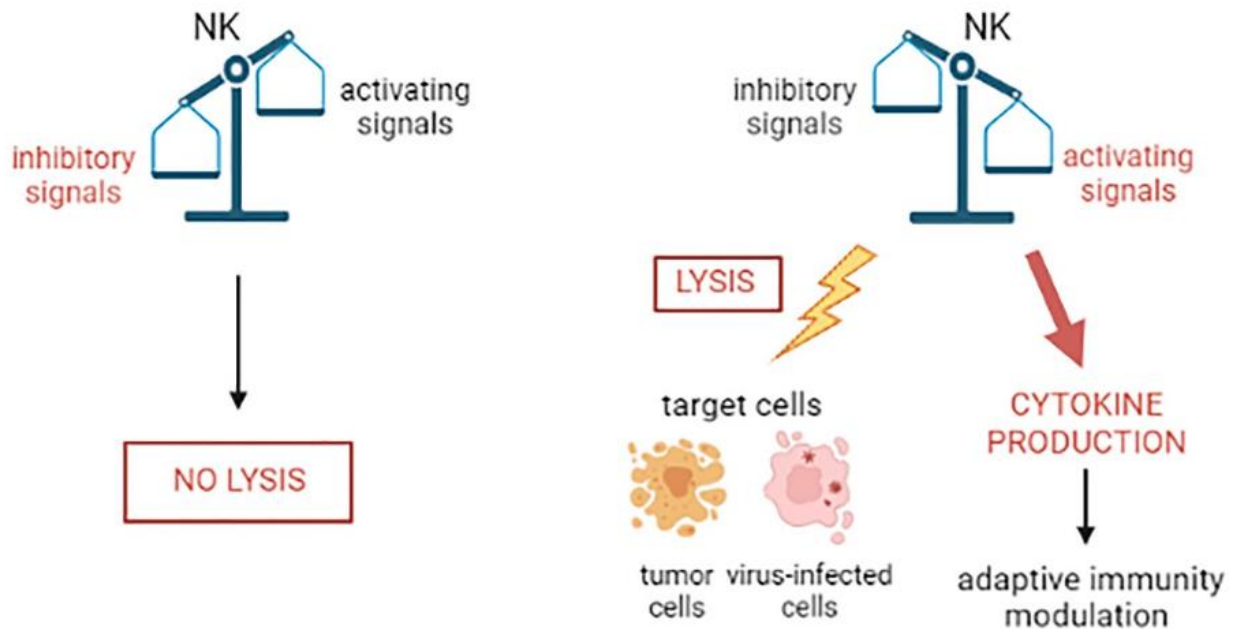


Figure 2. NK cells effector functions regulation by activating and inhibitory signals combination. Depending on the prevalence of inhibitory or activating environmental signals, NK cells can be respectively inhibited or stimulated to lyse target cells (tumor or infected) or to produce cytokine.

Both innate and adaptive immune system exert their function engaging specific receptors which are genetically determined. Unlike adaptive lymphocytes, wherein receptor diversity is generated by DNA rearrangements, NK cells express an array of germ-line encoded receptors capable of triggering their activation [42–45]. Despite this difference, NK cells display some features of adaptive immunity, placing these cells in the middle of the two types of immune system [46]. This peculiarity is due to NK cell cytotoxic/cytolytic activity towards tumor or infected cells typically via perforin or Granzyme-B secretion [23,47], that resembles CD8+ T lymphocytes killing, regulated by specific receptor engagement [11].

In this review we are going to analyze the important role of these receptors in NK cells regulation during viral infections, with particular attention to Killer immunoglobulin-like receptors (KIRs).

2. NK Receptors

The mechanisms by which NK cells recognize virally infected target cells are complex and still not entirely understood. Unlike B and T cells, NK cells do not express unique clonally distributed receptors for specific antigens, but they express on their surface an arsenal of different stimulatory and inhibitory receptors, whose engagement enables NK cells activity [43].

Membrane receptors invoked during NK cells regulation can be classified into five major families of molecules: natural cytotoxicity receptors (NCRs), C-type lectin, killer immunoglobulin-like receptors (KIR), leukocyte immunoglobulin-like receptors (LILR), and CD2.

The main molecular families, ligands, and regulatory functions of NK cell activating/inhibitory receptors are described below in Table 1.

Table 1. Principal NK cell receptors (activating and inhibitory) and ligands.

Receptor Family	Receptor	Known Ligand	Function
NCR	NKp46	Viral HA, HSPG, PfEMP-1	Activating
	NKp30	BAT-3, HCMV pp65, B7-H6,	Activating
	NKp44	HSPG, PfEMP-1, Viral HA, HSPG	Activating
C-type lectin	CD94/NKG2A	HLA-E	Inhibitory
	CD94/NKG2C	HLA-E	Activating
	CD94/NKG2E	HLA-E	Activating
	NKG2D	MICA/B, ULBPs	Activating
	NKR-P1A	LLT1	Inhibitory
KIR	KIR2DL1	HLA-C2 (Lys 80)	Inhibitory
	KIR2DL2/3	HLA-C1 (Asn 80)	Inhibitory
	KIR2DL4	HLA-G	Activating
	KIR2DL5	Unknown	Inhibitory
	KIR2DS1	HLA-C2 (Lys 80)	Activating
	KIR2DS2	HLA-C1 (Asn 80)	Activating
	KIR2DS3	Unknown	Activating
	KIR2DS4	HLA-Cw4	Activating
	KIR2DS5	Unknown	Activating
	KIR3DL1	HLA-Bw4	Inhibitory
	KIR3DS1	HLA-Bw4 (possible)	Activating
KIR3DL2	HLA-A3/A11	Inhibitory	
LILR	LILRB1/ILT2/LIR-1	HLA class I, UL18	Inhibitory
CD2	2B4	CD48	Activating/Inhibitory
	CD2	CD58	Activating
	NTB-A	NTB-A	Activating
	CRACC	CRACC	Activating
	DNAM-1	PVR, CD122	Activating
CEACAM	CEACAM1	NKG2D receptor–ligand system	Inhibitory
TIGIT	CD96	CD155	Inhibitory
	TIGIT	CD112, CD113, CD155	Inhibitory
TIM	Tim-3	Ceacam-1, PtdSer, Galectin-9	Inhibitory
DC-SIGN	Lag-3	HLA class II, IL-2R, IL-15R	Inhibitory
Type I cytokine receptor	IL-2R α	IL-2	Activating
	IL-15R α	IL-15	Activating

Abbreviations: NCR (natural cytotoxicity receptors); KIR (killer immunoglobulin-like receptors); LILR (leukocyte immunoglobulin-like receptors); CEACAM (carcinoembryonic antigen-related cell adhesion molecules); TIGIT (T cell immunoreceptor with Ig and ITIM domains); TIM (T cell/transmembrane, immunoglobulin, and mucin); DC-SIGN (dendritic cell-specific ICAM-3-grabbing non-integrin); HLA (human leukocyte antigen); BAT-3 (HLA-B-associated transcript 3); HA for hemagglutinin; HSPG for heparan sulfate proteoglycan; PfEMP-1 for Duffy-binding-like (DBL)-1 α of Plasmodium falciparum erythrocyte membrane protein-1; ULBP for UL16-binding protein; PtdSer for phosphatidyl serine.

Most human NK cells constitutively express the activating receptors NKp46 and NKp30, which belong to NCRs family. NCRs include NKp44 receptor as well, which is only detected on cell surface upon IL-2 mediated NK cell activation [48]. The precise ligands for these receptors remain largely undefined, even if several viral- or tumor-associated molecules that can interact with NCRs have been identified [49]. Interestingly, NKp46 and NKp44 can interact with influenza hemagglutinin (HA) and mediate NK cytolysis of infected cells expressing viral glycoproteins [50,51].

CD94-NKG2A/C/E heterodimers are highly conserved NK receptors which belong to the family of C-type lectins, involved in both activating and inhibitory signals. Inhibitory CD94-NKG2A and activating CD94-NKG2C/E heterodimers bind the non-classical HLA (Human Leukocyte Antigen) E molecule loaded with peptides derived from other HLA class I molecules, thereby monitoring the overall expression level of HLA class I antigens. Concerning NKG2D receptor, it recognizes ligands typically expressed by stressed, malignant, or infected cells, as for example cytomegalovirus (CMV) glycoprotein UL16-binding proteins (ULBPs) and the HLA class I chain-related molecules MIC (MHC class I chain-related protein) A and B. Nevertheless, viruses have evolved multiple mechanisms to evade recognition by NKG2D+ positive NK cells [23], including Epstein Barr virus (EBV), adenovirus, and HIV [52]. Interestingly, Carcinoembryonic antigen-related cell adhesion molecule 1 (CEACAM1) was found expressed on activated NK cells where it acts as an inhibitory receptor for NKG2D-mediated cytolysis.

NK cells are characterized by a plethora of activating/inhibitory receptors such as CD96 and TIGIT (T cell immunoreceptor with Ig and ITIM domains), that interact with CD155, CD112, and CD113; Tim-3 (T cell immunoglobulin-3), an NK cell coreceptor; Lag-3 (lymphocyte activation gene 3 protein), a negative co-inhibitory receptor that binds HLA-II molecules [53]; cytokine receptors such as IL-2R and IL-15R, as previously reported.

However, among all the reported receptors involved in NK cell regulation, the family of killer Ig-like receptors (KIRs) is one of the most studied, consisting in both activating and inhibitory receptors that bind to specific HLA-I molecules and act as key regulators of human NK cell function [54].

3. Killer Immunoglobulin-like Receptors (KIRs)

Killer immunoglobulin-like receptors (KIRs) are a family of transmembrane glycoproteins encoded by 15 highly polymorphic genes, whose members are characterized by distinct structural domains that determine distinct functions by providing different docking sites for ligands or signaling proteins [54]. The KIRs nomenclature was designed to reflect the structure and the function of the molecules, as well as the nucleotide sequence similarity among the different KIR family members. Thus, the first two digits following the acronym "KIR" correspond to the number of the extracellular domains (2D and 3D), while the third digit provides information on the length of the cytoplasmic tail (L or S) and consequently reveals details about protein function (inhibitory or activating, respectively) [55]. The only exception to this short/long-tailed rule is KIR2DL4, which is a unique long-tailed activating KIR (Figure 3).

The two-(2D) and three-(3D) immunoglobulin domain KIR isoforms with a long cytoplasmic tail are characterized by two sequences called immunoreceptor tyrosine-based inhibitory motifs (ITIMs), separated by 26–28 aminoacids (Figure 3) [56,57]. Molecular analysis of several membrane receptors with inhibitory function revealed the presence of a common ITIM motif (I/VxYxxL/V), which recruits the SHP-1 tyrosine phosphatase and arrests positive signals transduced via other receptors [58].

In contrast, KIRs with short cytoplasmic domains and with activating function associate with a transmembrane signalling adaptor protein which is called DAP12 (also called KARAP) [54]. DAP12-dependent activation occurs through the recruitment of Syk/ZAP-70 tyrosine kinases by immunoreceptor tyrosine-based activation motifs [ITAM; Yxx(L/I/V)x-Yxx(L/I/V)] (Figure 3) [54]. An exception to these two classification is represented by KIR2DL4, which compared with other long cytoplasmic tail KIR family members, behaves

like an activating receptor, inducing cytokines production [59] due to the association with ITAM-containing Fc ϵ RI- γ adaptor instead of DAP12 (Figure 3) [60].

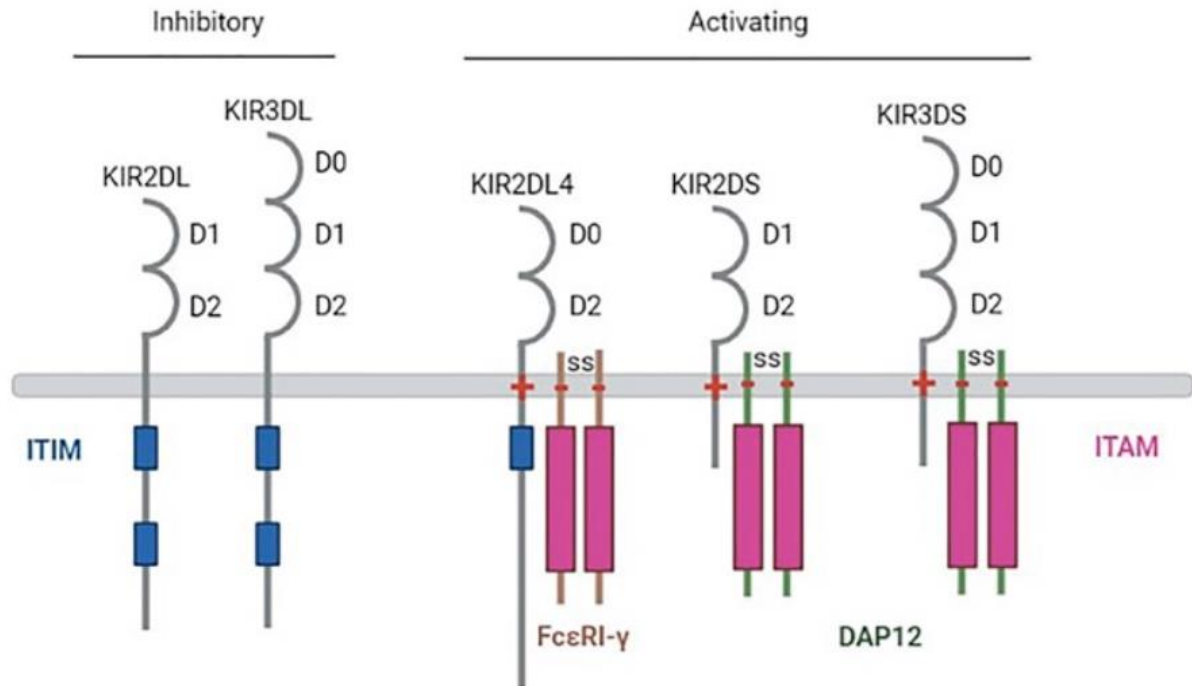


Figure 3. Representation of inhibitory and activating KIRs structure. Receptors with long cytoplasmic domains contain one or two immunoreceptor tyrosine-based inhibitory motif sequences (ITIMs), represented in blue, that provide inhibitory function. The short cytoplasmic KIR and the long-tailed KIR2DL4 are activating receptors, which contain a basic amino acid (+) within the transmembrane domain that interacts with an acidic amino acid (−) within the transmembrane domains of signaling adaptor proteins DAP12 (green) or Fc ϵ RI-c (brown), respectively. These adaptors provide intracellular immunoreceptor tyrosine-based activator motif sequences (ITAMs), in purple, that allow activating function.

To date, little is known about the tyrosine kinases and phosphatases implicated in KIRs ITIM domain phosphorylation. A potential role for the *lck* src tyrosine kinase family in KIRs function is suggested, since *lck* overexpression in NK cells has been reported to enhance KIR phosphorylation [61]. Literature also indicates that a critical substrate of the SHP-1 phosphatase recruited by KIR receptors is the p36 adapter protein [62].

The engagement of activating or inhibitory KIRs depends on both their ability to recognize and their strength in binding specific ligands expressed on target cells (Table 1) [63].

Interestingly, KIRs expression on NK cell surface is not only dependent on the genetic background but also seems to be influenced by the presence of specific HLA-I ligands [64].

HLA-I genes are located on the short arm of chromosome 6 [65] and are found on the surface of all nucleated cells. HLA-I are subdivided into “classical proteins”, that include HLA-A, -B and -C, and “non classical proteins”, referring to HLA-E, -F, and -G molecules. The level of HLA-I expression is modified by proinflammatory cytokines [66,67]. Thus, during viral infection, a general upregulation of HLA-I molecules normally occurs in order to trigger immune system activation, even if viruses have developed different strategies to decrease HLA-I expression and consequently viral epitopes exposure on infected cells, avoiding CD8+ T lymphocyte killing but consequently inducing NK cell killing activation.

Once engaged by HLA-I ligands, inhibitory KIRs transduction signal is triggered by tyrosine kinases and phosphatases activation, in order to induce NK cell inhibition.

Inhibitory KIRs have been described as three distinct protein isoforms. KIRs involved in HLA-C recognition (KIR2DL1, KIR2DL2, KIR2DL3) are usually monomeric glycopro-

teins of ~58 kDa containing two immunoglobulin-like domains (KIR-2D) in the extracellular region [56]. KIR2DL2/3 preferentially bind HLA-C1, while KIR2DL1 preferentially binds HLA-C2, showing a stronger affinity than the former. Nevertheless, HLA-C1 is also ligand for the activating KIR2DS1 receptor, while ligands for the remaining activating KIRs still remain to be identified [68]. KIRs reactive with HLA-B (KIR3DL1) are ~70 kDa monomeric glycoproteins with three immunoglobulin-like domains (KIR-3D) [56]. KIRs reactive with HLA-A ligands (KIR3DL2) possess three immunoglobulin domains in the extracellular region [69,70] and are expressed on the cell surface as bisulfide-linked homodimers composed of two ~70 kDa subunits [70].

Members of the KIR gene family are tightly clustered on human chromosome 19q13.4 and consist in 15 gene loci [71], clustered in the Leukocyte Receptor Complex (LRC) region [72]. The KIR gene family also included 2 pseudogenes, KIR2DP1 and KIR3DP1, which are part of the KIR2D genes [73] and include an inactivated pseudoexon 3 sequence [74]. These two pseudogenes are not transcribed because of sequence defects [71]; therefore, they are not involved in encoding a functional KIR molecule. However, the non-functional KIR pseudogene, KIR3DP1, can be activated through non-reciprocal recombination with functional KIR genes [73,75]. About 4.5% of the individuals of a Caucasoid population own a recombinant allele of KIR3DP1, named KIR3DP1*004, that associates tightly with gene duplications of KIR3DP1, KIR2DL4, and KIR3DL1/KIR3DS1. Despite KIR3DP1 gene being normally silent, the recombinant allele KIR3DP1*004 contains a novel promoter sequence that, consequently, allows KIR3DP1 transcription [73].

KIR genes are organized into two haplotypes defined as A and B haplotypes, which differ in number and kind of KIR genes, as shown in Figure 4 [76].

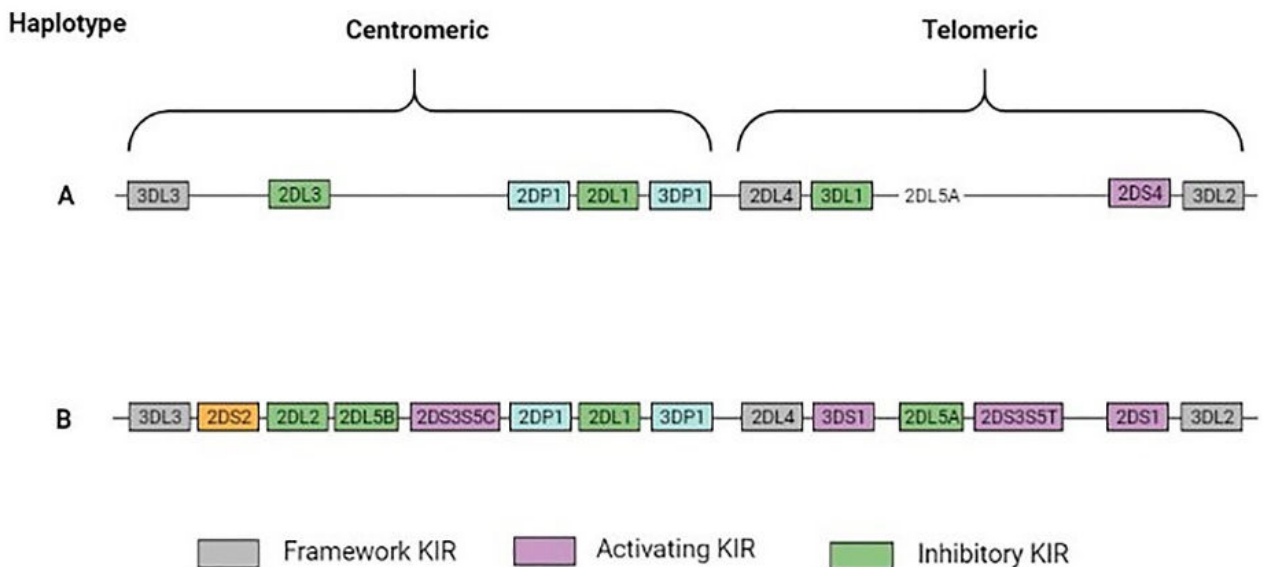


Figure 4. Genomic organization of KIR A haplotype and B representative haplotype. Activating KIRs are indicated in violet, inhibitory KIRs in green, framework KIRs in grey, and pseudogenes in blue.

The A haplotype is characterized by an extensive variability at allelic level [77], while B haplotype exhibits substantial variation in gene content but low allelic polymorphism [78]. B haplotypes generally possess more KIR genes than group A, including mainly activating KIRs, except the haplotype B1, which is intermediate between A and B haplotypes gene content [73].

More precisely, A haplotypes are devoid of activating KIR genes, except for KIR2DS4 (even if it is frequently deleted of transmembrane and cytoplasmic tail), and mainly encode inhibitory KIRs, such as KIR2DL1, KIR2DL3, KIR3DL1, KIR2DS4, and KIR2DP1 [79]. On

the contrary, B haplotypes present a higher KIRs variability and are characterized by the presence of at least one gene among KIR2DL2, KIR2DL5A/B, KIR2DS1, KIR2DS2, KIR2DS3, KIR2DS5, and KIR3DS1. The remaining four KIR genes, termed framework genes, are shared by both haplotypes.

Interestingly, there are several pieces of evidence in literature demonstrating that there are some associations between inheritance of certain combinations of KIRs, into A or B haplotypes, and HLA genes and susceptibility to several diseases, including viral infections [54].

4. Modulation of KIRs/Ligands during Viral Infections and Associated Diseases

Viruses have developed several mechanisms to counteract host immune response. Several viruses (such as herpesvirus, papillomavirus, retrovirus, poxvirus, human immunodeficiency virus, and flavivirus) are able to evade NK cell effector functions [80].

In particular, since NK cell activation depends on the loss of inhibitory signals provided by HLA-I molecules and on the expression of stress or virally induced ligands of NK cell receptors [81], modulation of KIRs expression and of their HLA-I ligands represent a key mechanism exploited during viral immune escape. In particular, KIRs modulation by viruses may involve both direct and/or indirect strategies: the direct mechanisms mainly refer to epigenetic modulation of KIR receptors, while indirect KIRs modulation is essentially based on the selective expression of KIRs main ligands, that is HLA-I molecules [80,82].

It is known that the distribution pattern of KIR receptors is entirely maintained by CpG DNA methylation and consequently their expression is controlled by DNA methyltransferase enzyme [83]. In this context, viruses, especially those which have latency characteristic as Herpesviruses and Retroviruses, could affect KIRs expression at epigenetic level as a consequence of the modifications that occur during virus life cycle and immune system activity [84]. In fact, integrated viruses with latent cycle, as Human Immunodeficiency Virus (HIV), induce a peculiar epigenetic configuration in the infected cell with the aim to maximize virus integration [85]. In this way, viruses can take advantage by epigenetic modifications to up- or downmodulate KIRs expression on NK surface [86–88].

Otherwise, indirect processes of KIRs modulation are represented by the up-/downregulation of HLA molecules as well, that are known ligands of these receptors and particularly targeted by viruses.

In fact, the selective modulation of HLA-I expression is used by several viruses to evade immune recognition and is represented in Figure 5 [89].

This mechanism enables pathogens to escape recognition by CD8+ cytotoxic T cells (CTLs) which recognizes virus-encoded peptides presented on the surface of infected cells by class I HLA molecules, such as HLA-A and HLA-B [90].

Many viruses, such as HIV [91] and herpesviruses [92], are able to interfere with HLA-I presentation of viral peptides, for example downregulating HLA-I surface expression by increasing HLA-I retention in the endoplasmic reticulum [93] or the endocytosis from the cell surface, in order to block CTL killing (Figure 5) [94].

The interplay between activating and inhibitory KIRs and their corresponding HLA ligands is likely to play a role in both viral infection susceptibility and outcome [87,95], leading to chronic viremia [96] and possibly correlated pathologies [90], as summarized in Figure 6 and Table 2.

We will report the summary on the main viral infections reported to exploit KIRs/HLA-I modulation and on their possible implication in human diseases.

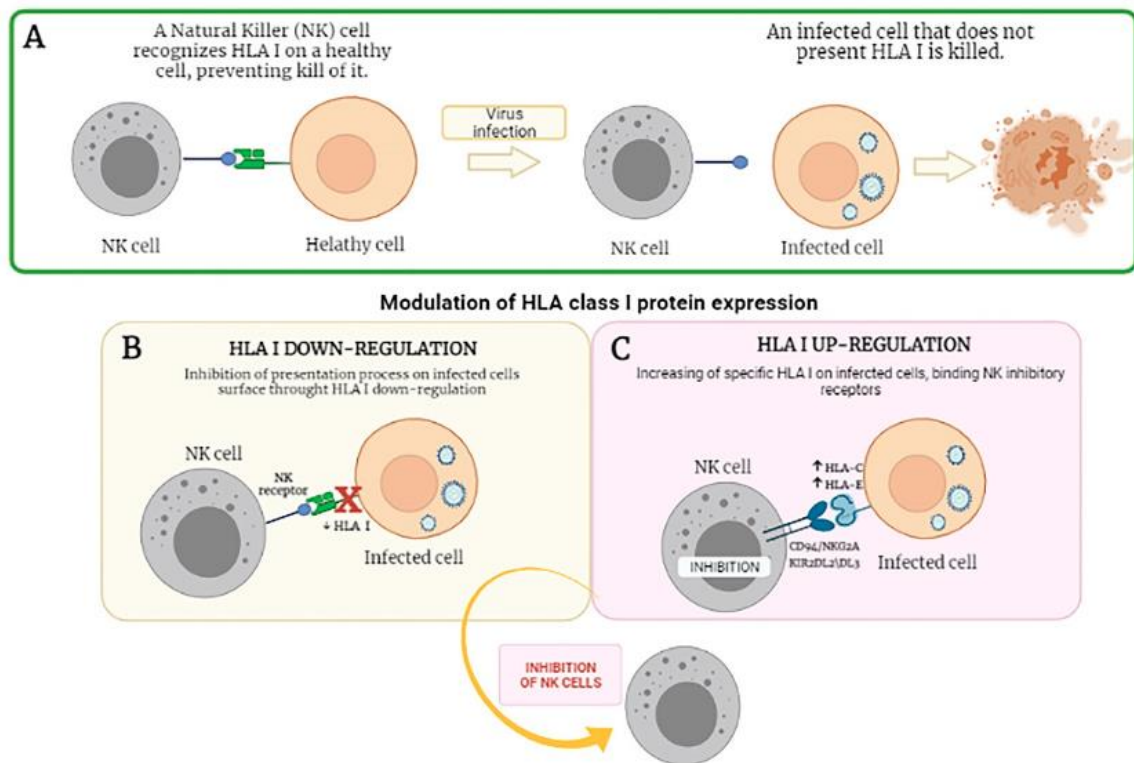


Figure 5. Representation of HLA-I dependent NK cells activation. NK cell response in presence of healthy and infected cells (A); NK cells response in presence of selective downmodulation (B) and upmodulation (C) of HLA-I protein expression by virus.

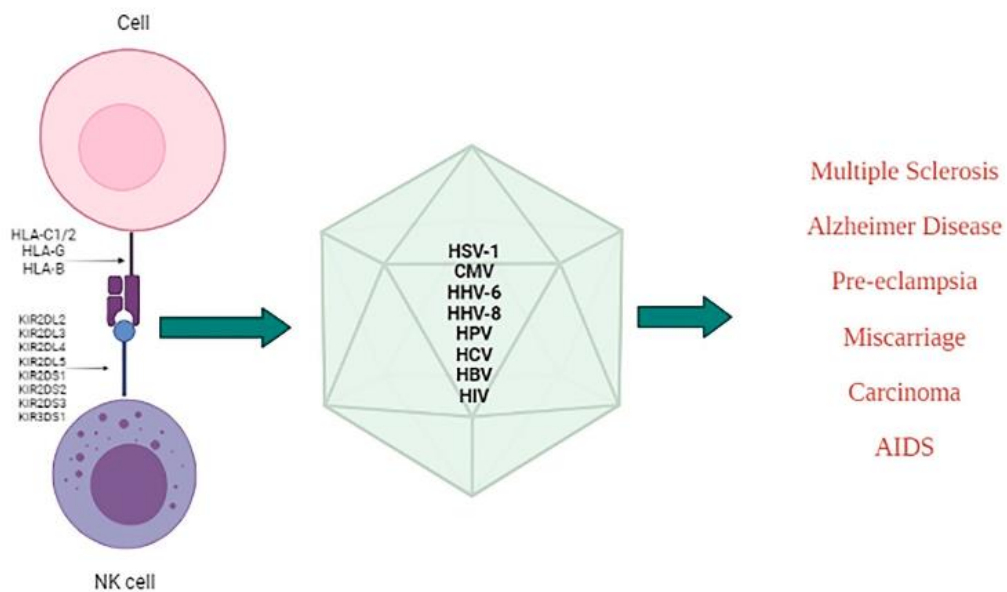


Figure 6. Schematic representation of KIR/HLA class I association to viral susceptibility and diseases. The presence of particular activating (KIR2DL4, KIR2DS1, etc.) and inhibitory (KIR2DL2, KIR2DL3, etc.) KIRs, together with their specific ligands (HLA-C, HLA-G, and HLA-B), is involved in some viral infections' susceptibility and outcome (HSV-1, CMV, HIV, etc.), leading to multiple diseases like Multiple sclerosis, Alzheimer disease, Pre-eclampsia, Miscarriage, Carcinoma, AIDS.

Table 2. Virus and KIRs/HLA association and possibly related diseases.

Virus	KIRs/HLA	KIRs/HLA Frequency	System/Disease or Effect on Infection Outcome	References
CMV	KIR2DL2	increased	Increased susceptibility to herpetic infections	[97]
	HLA class I	decreased	Viral immune-escape	[81,98]
	HLA-C	increased	Viral immune-escape	[89,99–101]
	KIR2DS1	increased	Control of placental CMV infection	[102]
	KIR2DS1, KIR2DS5	decreased	Lower CMV infection control; abortion, pre-term delivery	[102,103]
	HLA-G/KIR2DL4	increased	Trophoblast cells; viral immune-escape	[104]
	KIR2DL1 /HLA-C2	increased	immunodeficiency syndrome, recurrent CMV reactivation	[105]
	KIR2DS2, KIR2DL3, HLA-C1	increased	organ transplant; protection from CMV reactivation	[106]
	KIR2DL2, KIR2DS1	increased	SLE	[107]
KIR2DS2	decreased	SLE	[108]	
KIR2DS2, KIR2DL3	increased	Rheumatoid Arthritis; worst prognosis	[109]	
EBV	HLA class I	decreased	Reduced NK cell killing	[93]
	KIR2DS5, KIR2DS4	increased	Increased risk of lymphoproliferative diseases	[110]
	KIR2DS2, KIR2DL3	increased	Rheumatoid Arthritis; worst prognosis	[109]
	KIR2DL2	increased	Multiple Sclerosis, increased susceptibility to herpetic infections	[97]
HHV-8	HLA class I	decreased	Viral immune-escape	[111–113]
	KIR2DL2/HLA-C1	increased	type-2 diabetes	[114]
	KIR2DL2, KIR2DS2	increased	Cutaneous vascular lesions	[115]
	KIR2DS1, KIR3DS1	increased	Kaposi Sarcoma	[116]
HHV-6	KIR2DL2/HLA-C1	increased	Alzheimer’s Disease, NK cell inhibition	[117,118]
	KIR2DL2/HLA-C1	increased	Multiple Sclerosis, worst disease outcome, NK cell inhibition, herpetic reactivation	[97,119,120]
	HLA-G	increased	IUGR, altered KIR2DL4+ dNK cell function	[121,122]
	HLA-G/KIR2DL4	decreased	Infertility; KIR2DL4+ dNK cell function	[123–127]
	KIR2DL2	increased	Infertility, Multiple Sclerosis, increased susceptibility to herpetic infections	[97,128]
	KIR2DL5	decreased	infertility	[128]
HSV-1	KIR2DL2/HLA-C	increased	infertility	[129,130]
	KIR2DL2/HLA-C	increased	Multiple Sclerosis	[119,120]
HIV	KIR2DL5, KIR2DS5	increased	Protection from HIV transmission	[95]
	HLA-C	increased	Protection from HIV transmission	[131]
	HLA-C	increased	Viral immune-escape (via Nef protein)	[132]
	HLA-A, HLA-B	decreased	Viral immune-escape (via Nef protein)	[133]
	KIR2DL2, HLA-Cw*0102	increased	Viral immune-escape (via Gag protein)	[134]
	HLA-C	increased	Viral immune-escape (via Env protein)	[135,136]
	KIR3DS1	decreased	Higher NK cell function, reduced perinatal transmission	[137,138]
	KIR3DL1, KIR2DL2, KIR2DL3, KIR2DL5, KIR2DS5, HLA-C	increased	Reduced perinatal transmission	[139,140]
	KIR2DL2, KIR2DS2, KIR2DS3, KIR2DS4, KIR3DS1	increased	Higher susceptibility in the newborn	[138]
	KIR3DS1/HLA-Bw4-80I	increased	Decreased AIDS progression; protective effect	[141–144]

Table 2. Cont.

Virus	KIRs/HLA	KIRs/HLA Frequency	System/Disease or Effect on Infection Outcome	References
HBV	KIR2DS1, KIR2DS2	increased	HBV recovered subjects, lower NK cell activation	[145]
	KIR2DL3/HLA-C1	increased	Protective toward HBV susceptibility	[146]
	KIR2DL3	decreased	CHB	[147]
	KIR2DL1/HLA-C2	increased	Higher HBV infection rate	[146]
	KIR2DS2, KIR2DS3	increased	CHB, increased HBV susceptibility	[148]
	KIR2DS1, KIR3DS1, KIR2DL5, KIR2DL3	increased	CHB, protective effect, HBV clearance	[147–149]
	HLA-C1	increased	Increased risk of HCC progression in HBV-infected patients	[150]
HCV	HLA-C2, HLA-A-Bw4	increased	Increased risk for CHB development	[147]
	KIR3DL2, KIR2DL1, KIR2DL2, KIR2DL3, HLA-C2	increased	Poor HCV clearance after treatment	[151,152]
	HLA-C*03:04, KIR2DL3	increased	Viral immune-escape	[153]
	HLA-B*27/KIR3DL1	decreased	Viral immune-escape	[154–156]
	KIR3DL1	decreased	Increased risk for chronic HCV infection	[157]
	KIR2DS3	increased	Protective against liver disease in HCV patients	[158]
	HLA-Bw4/KIR3DS1	increased	Spontaneous infection resolution and sustained response to HCV antiviral therapy	[159]
Enterovirus	HLA-C1/KIR2DL3	increased		[160,161]
	KIR3DL1	decreased	Type-1 diabetes	[162]
Parvovirus	HLA class I	increased	Induction of antiviral response that triggers Hashimoto's Thyroiditis condition	[163]
	HLA-I	increased	SLE, persistent viral infection	[164,165]
HPV	KIR2DL2/HLA-C1, KIR2DL3/HLA-C1	increased	Cervix cancer, risk factor for HPV high-risk infection and neoplastic transformation	[166]
	HLA-C2	increased	Cervix cancer, no increased risk for HPV high-risk infection and neoplastic transformation	[166]
	KIR2DL1	increased	Cervix cancer	[166]
	KIR2DL2/HLA-C2	decreased	Cervix cancer	[166]

Abbreviations: SLE (Systemic Lupus Erythematosus), HHV-8 (Human Herpesvirus 8), HHV-6 (Human Herpesvirus 6), IUGR (intrauterine growth restriction), AIDS (Acquired Immune Deficiency Syndrome), HBV (Hepatitis B virus), HCC (hepatocellular carcinoma), CHB (chronic hepatitis B), HCV (Hepatitis C virus), HPV (Human Papillomavirus).

4.1. Herpesviruses

Herpesviruses have developed several strategies that inhibit NK cell activation by blocking the expression of ligands of activating receptors or preserving the expression of ligands of inhibitory receptors, including HLA-I.

Human Cytomegalovirus (HCMV) viral proteins US2 and US11 have been reported to shuttle HLA-I from the endoplasmic reticulum to the cytoplasm, resulting in HLA-I degradation [81,98], while UL16, UL18, and UL40 maintain a locus-restricted surface expression of HLA molecules, including HLA-C, that act as ligands for NK cells inhibitory receptors [89,99] (Table 2; Figure 7). Interestingly, HCMV-induced HLA-C expression includes specific HLA-C modification, as glycosylation [100] and formation of heterodimers with other HLA-I molecules [167–169] or with viral protein [101], that sustain a differential KIRs recruitment.

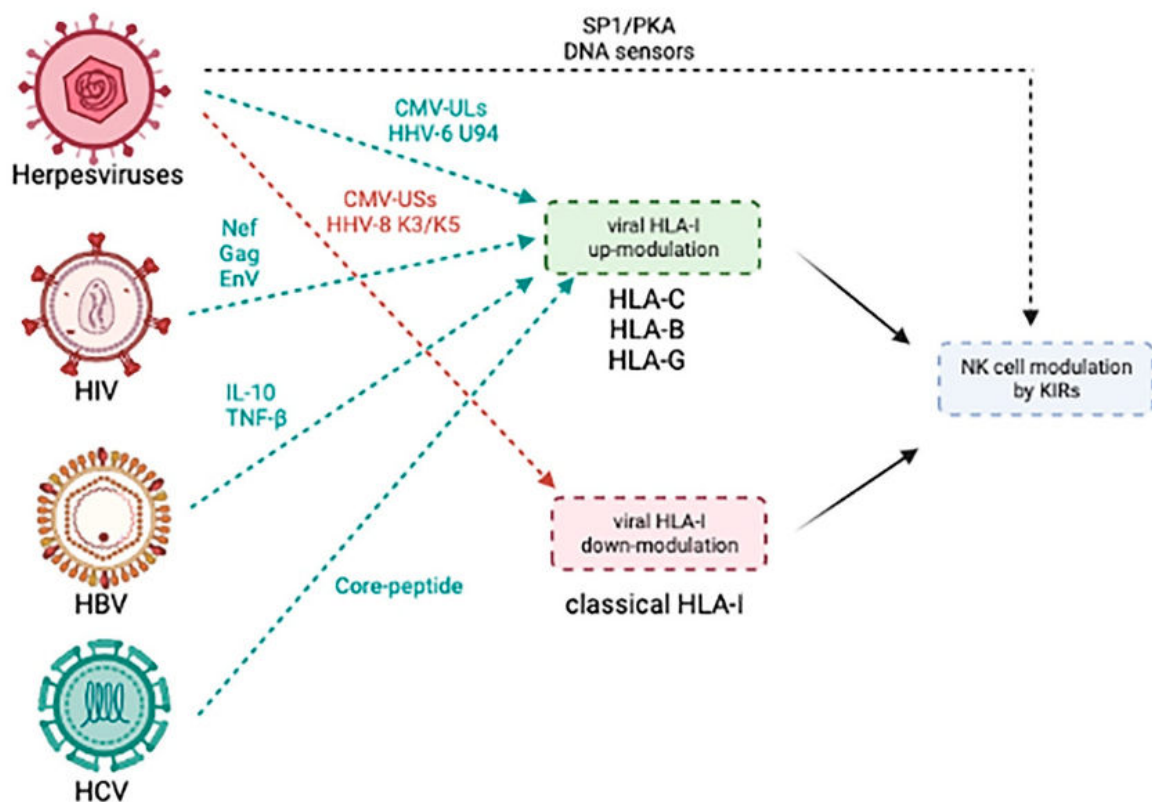


Figure 7. Schematic representation of the main viral strategy to modulate KIRs/HLA-I ligands described in the text. Viruses (e.g., Herpesviruses, HIV, HBV, and HCV) have evolved different mechanisms to modulate HLA-I molecules or induce/exploit specific KIRs expression, for example, by production of specific viral proteins to modify NK cell activation and evade host immune response.

KIRs also play a role in NK cells-mediated clearance of HCMV infection associated to congenital disorders such as spontaneous abortion or pre-term delivery (Table 2) [103]. The expression of KIR2DS1 by decidual NK (dNK) cells increases their ability to control placental HCMV infection, reducing or preventing virus-induced pathology of the placenta and improving its function. In contrast, pregnant women who lack KIR2DS1, or similarly KIR2DS5, showed a lower ability to control placental HCMV infection and developed complications (Table 2) [102].

Again, HCMV infection modifies the expression of HLA class I molecules at the surface of placental extravillous trophoblast (EVT) cells, which typically do not express HLA-A and HLA-B molecules but do express an unusual combination of HLA-E, HLA-F, and HLA-G, in addition to low levels of HLA-C. Schust et al. addressed that unlike HLA-A and -B, both HLA-C and HLA-G expressed in a human trophoblast cell line were fully resistant to the rapid degradation associated with HCMV proteins US2 and US11 [104], mounting evidence that HLA-G could interact with KIR2DL4 expressed by decidual NK cells inducing IFN- γ and TNF- α secretion and promoting viral immune escape (Table 2).

In a case study of a child with a novel immunodeficiency syndrome and recurrent HCMV infection [105], the entire population of NK cells from this patient expressed KIR2DL1 in the presence of KIR2DL1 ligand, HLA-C2, raising the possibility that the strongly inhibitory KIR2DL1/HLA-C2 combination crippled NK cell activity and prevented a protective NK cell response against HCMV (Table 2). Activating KIR expression improves the protection during HCMV reactivation in stem cell transplantation [170] and solid organ transplant, where a combination of the activating KIR2DS2 and weak inhibitory KIR2DL3,

which share the ligand HLA-C1, in the recipient was associated with a decreased risk of CMV viremia when both donor and recipient were homozygous for HLA-C1 (Table 2) [106].

CMV has also been described associated to Systemic Lupus Erythematosus (SLE) susceptibility [171], possibly involving specific KIRs/HLA-I combinations. Hou et al. have suggested that KIR genotype and HLA ligand interaction may potentially influence the threshold for NK cells activation mediated by activating receptors, thereby contributing to the pathogenesis of SLE [172] and also to viral susceptibility. In this study an increased frequency of KIR2DL2 and KIR2DS1 has been observed among SLE cases compared to controls [107], while a controversial study by Pellet et al. has observed the absence of KIR2DS2 in SLE cases (Table 2) [108]. Since KIR2DL2 has been associated to increased susceptibility to herpetic infections [97], the presence of this KIR gene may represent a common feature for SLE development in the presence of herpesvirus infections (Table 2).

A recent clinical study has evaluated the involvement of KIR genes in Rheumatoid Arthritis (RA), in the presence of EBV and HCMV infections. The study found that the presence of activating KIR2DS2 and inhibitory KIR2DL3 receptors, in the presence of EBV and HCMV infections, might be associated with a worst RA prognosis [109] (Table 2).

EBV encode an miRNA that targets MICB, miR-BART2-5p, resulting in reduced NK cell-mediated killing (Table 2) [93,173]. Moreover, in the specific case of EBV infection, KIR2DS5 and KIR2DS4 were associated with increased risk of lymphoproliferative diseases (Table 2) [110].

Human Herpesvirus 8 (HHV-8), also called Kaposi's Sarcoma-associated Herpesvirus (KSHV), exploits an immune-escape mechanism consisting in the acceleration of HLA-I molecule endocytosis which involves K3 and K5 viral proteins (Figure 7). Interestingly, K3 downregulates the expression of both canonical and non-canonical HLA class I molecules in humans (HLA-A, -B, -C, and -E), whereas K5 primarily downregulates HLA-A and -B alleles (Table 2) [111–113]. HHV-8 infection is notably associated to autoimmune and neoplastic disorders and KIRs profile seems to play a role in the development of correlated diseases. In particular, HHV-8 infected type-2 diabetes subjects showed an increased frequency of KIR2DL2/HLA-C1 pair in comparison with uninfected patients (Table 2) [114], HHV-8 positive cutaneous vascular lesions were significantly associated with KIR2DL2/DS2 homozygosity (Table 2) [115], and patients affected by classic Kaposi Sarcoma, typically positive for HHV-8 infection, showed a higher frequency of KIR2DS1 and KIR3DS1 compared to controls (Table 2) [116].

Human Herpes Virus-6 (HHV-6) susceptibility association to peculiar KIR\HLA-I expression has been widely described. HHV-6 has been recently distinguished in two different viruses, HHV-6A and -6B, characterized by different biological features [123]. In particular, while HHV-6B tropism is more aimed at T cells, HHV-6A is able to infect a wide range of tissues and differently affects NK cell activation. This peculiarity involves a differential viral DNA sensing [118] and KIRs modulation and leads to a mechanism of anti-viral activation, characterized by a Th2 type response and a non-cytotoxic profile. HHV-6A infection induced PKA activity and phosphorylation of Sp1 in the NK cells, which may increase expression of KIR2DL2 and thereby inhibit NK cell cytotoxicity (Figure 7). These findings were reported associated to Alzheimer's Disease (AD), where the authors noted that the HHV-6A-induced expression of apolipoprotein E e4, a known marker for AD, may further inhibit NK cell function, in part by increasing PKA activity, Tau hyperphosphorylation, and amyloid-beta deposition (Table 2) [117].

Herpesviruses, and in particular HHV-6, were found to have a possible association with neural pathologies because of their peculiar neurotropism and the ability to establish latent infections [174], as supported also by the presence of HHV-6 infection in AD post-mortem brain tissue [175,176] and in Multiple Sclerosis (MS) plaques [177,178]. The increased susceptibility to herpesviruses infection in neurological subjects seems to be associated to KIR2DL2/HLA-C1 expression on the surface of NK cells in both AD and MS patients [118,119]. This was confirmed by the evidence that patients expressing KIR2DL2 are characterized by impaired NK cells response against herpesviruses, favoring the in-

fection and possibly disease outcome [97,118]. The ability of herpesviruses to establish a lifelong latency in CNS, with the potential to reactivate, suggests these viruses as co-factors in the relapsing-remitting course of MS, particularly in association to KIR2DL2 presence, since KIR2DL2 expression on NK cells enhances viral reactivations, concomitantly with the typical relapses of the disease (Table 2) [120]. HHV-6 infection and KIRs are also possibly implicated in reproductive pathologies, including intrauterine growth restriction (IUGR) and infertility.

One of the most important KIRs expressed mostly on dNK cells is KIR2DL4. This receptor is engaged by HLA-G expressing trophoblast cells during placental development, where it triggers vascular remodeling. Its role during placentation is supported by the highest KIR2DL4 gene expression in healthy pregnant women compared to patients with recurrent spontaneous miscarriage [179]. In IUGR placentas, HHV-6 infection has been reported together with increased HLA-G expression which possibly affect dNK cell function engaging KIR2DL4 (Table 2) [121,123]. It was suggested that this effect on HLA-G expression and might be due the expression the U94 viral protein [122] (Figure 7). Moreover, the presence of HHV-6A infection in endometrial cells was reported to be associated with primary idiopathic infertility in women [123–126], together with altered basal sHLA-G levels and CD56⁺KIR2DL4⁺ endometrial NK cell percentages (Table 2) [127]. Furthermore, HHV-6 endometrial infection in idiopathic infertile women seems to be correlated to the presence of the inhibitory receptor KIR2DL2, while, on the contrary, the inhibitory receptor KIR2DL5 was found with lower frequency in comparison to the fertile cohort (Table 2) [128].

The possible implication of KIR2DL2 in infertility in presence of herpetic infections was also confirmed by El Borai et al., who reported the association between Herpes simplex virus (HSV)-1 and male infertility. The authors found HSV-1 DNA in 24% of semen samples obtained from infertile males [129], in correspondence to high frequency of KIR2DL2/HLA-C combination, compared to healthy controls (Table 2) [130].

4.2. Human Immunodeficiency Virus (HIV)

Concerning HIV infection, HLA/KIR combinations have been associated with virus-associated disease progression and protection against disease acquisition. The mechanisms conferring this protection may include the direct interaction of KIRs with HIV-derived peptide motifs presented on HLA molecules and confirmed by *in vitro* experiments reporting that specific viral variant/KIR combinations associate with differences in NK cell viral inhibition [23] and that distinct HLA/KIR combinations confer differences in HIV control [180] and susceptibility [141,181]. In particular, KIR2DL5 and KIR2DS5 have been associated with decreased odds of HIV transmission [95], in concordance with a study on cell surface expression levels of all common HLA-C allotypes in African and European Americans [131], which reported an increased HLA-C expression associated with protection from infection (Table 2).

HIV has the distinctive ability to selectively downregulate HLA-A and HLA-B on the surface of infected cells through Nef protein (Figure 7; Table 2), without affecting HLA-C and HLA-E expression [133], controlling in this way both CTL and NK cell activation. To disrupt the cell surface expression of HLA-A and HLA-B molecules, Nef binds to the cytoplasmic tail domain and promotes the association of the conserved HLA-I cytoplasmic tail tyrosine residue with the clathrin adaptor protein 1 (AP-1) [182,183]. Significantly, HLA-C cytoplasmic tails lack two amino acids necessary for this interaction. As a result, the HIV-1 Nef protein does not downmodulate HLA-C molecules from the cell surface (Table 2) [132].

Besides Nef protein, also HIV Gag and Env proteins participate in NK cell regulation via KIRs engagement by modulating HLA-C expression (Figure 7).

Fedda et al. identified one HLA-Cw*0102-presented peptide (p24 Gag209–218) that was recognized by the inhibitory NK cell receptor KIR2DL2 leading to functional inhibition of KIR2DL2-expressing NK cells, suggesting that selections of sequence polymorphisms that increase avidity to KIR2DL2 might provide a mechanism for HIV-1 to escape NK cell-mediated immune pressure (Table 2) [134].

Again, it was found that the presence of HLA-C, particularly as free heavy chains, positively modulates the infectivity of HIV-1 [135] as a result of the association with HIV-1 Env protein at the cell membrane level [136]. This work suggested that HIV-1 envelope may facilitate dissociation of β 2M from HLA-C, leading to higher levels of HLA-C free chain molecules at the cell surface influencing HIV-1 infectivity.

HIV infection is notably associated to pregnancy problems, due to viral-related immune system dysfunctions [184] and the role of KIRs concerning HIV mother-child transmission during pregnancy has been investigated. In particular, KIR3DS1 has been associated with higher NK cells effector functions in early HIV-1 disease, which may lead to better clinical outcomes reducing perinatal transmission (Table 2) [137,138]. In addition, KIR3DL1, KIR2DL2, KIR2DL3, KIR2DL5, KIR2DS5, and HLA-C ligands were associated with newborn protection against HIV-1 infection (Table 2) [139,140].

On the contrary, KIR2DL2, KIR2DS2, KIR2DS3, KIR2DS4, KIR3DS1 receptors have been associated with higher susceptibility to HIV-1 infection in the child (Table 2) [138].

A role for HIV infection in immune disorders has also been described in association with particular KIRs.

HIV positive patients expressing KIR3DS1 and HLA-Bw4-80I showed a decrease AIDS (Acquired Immune Deficiency Syndrome) progression, compared to KIR3DS1 and HLA-Bw4-80I negative subjects [141], possibly due to a protective effect toward HIV infection [142]. In individuals infected with HIV, this effect is confirmed by a lower viral load and the protection against opportunistic infections [185,186]. Moreover, a study conducted on HIV exposed intravenous drug users from Vietnam showed an increased KIR3DS1 homozygosity and a high prevalence of B haplotypes in HIV exposed seronegative intravenous drug users [143,144] which could explain the resistance to HIV infection observed in these subjects (Table 2).

4.3. Hepatitis Viruses (HBV and HCV)

Hepatitis B virus (HBV) and hepatitis C virus (HCV) account for 70% of the global burden of liver disease [187], often involved in neoplastic transformation processes. The clinical outcomes following infection with both HBV and HCV viruses vary considerably, from clearance of infection to chronic viral persistence, cirrhosis, and hepatocellular carcinoma (HCC) [188]. Since the interaction between virus and immune system plays an important role in pathogenesis, inflammation, necrosis, and fibrosis of the liver tissue [189], different candidate gene association studies have identified specific immune receptors associations for both HBV and HCV susceptibility and outcome. Among these receptors, specific KIR genes have been reported to affect the immune response against viral infections in liver.

Liver NK cells show phenotypic and functional characteristics that are distinct from their circulating counterparts. In particular, even if the majority of intrahepatic NK cells have a CD56^{bright} phenotype, their CD56^{dim}CD16⁺ fraction express lower levels of KIRs than NK cell subset in the periphery, which may limit their capacity to be adequately licensed [190].

This hepatic NK cell enrichment is maintained in the inflammatory infiltrate characteristic of HBV infection. In fact, in order to understand the role of NK cells in HBV infection it is necessary to first consider the liver microenvironment, well known for its tolerogenic properties due to the local immunological environment including the cytokine and nutrient milieu [191,192]. For example, Kupffer cells are able to produce immunosuppressive cytokines such as IL-10 and TGF- β that can tolerize local intrahepatic NK cells also affecting HLA-I and stress ligands expression [193,194]. These modulations, together with KIRs profile, participate in infection resolution and outcome.

A genetic tendency towards lower activation of NK cells in HBV recovered subjects was described in presence of activating KIRs-phenotype, characterized, for example, by KIR2DS1, KIR2DS2 expression, during HBV infection (Table 2) [145]. Other studies reported that KIR2DL3/HLA-C1 homozygosity is protective toward susceptibility to HBV infection,

while KIR2DL1/HLA-C2 is associated to high HBV infection rate (Table 2) [146]. In addition, KIR2DS2 and KIR2DS3 act as HBV susceptibility genes in the presence of chronic hepatitis B, whereas KIR2DS1, KIR3DS1, and KIR2DL5 may be protective genes facilitating the clearance of HBV, consequently protecting from cancer development (Table 2) [148].

This latter evidence was supported also by a study on a Turkish cohort that showed a higher rate of inhibitory KIR2DL3 and KIR3DS1 in the healthy group than in the group composed of chronic HBV patients and patients with spontaneous remission [149]. Moreover, a case-control study showed that HLA-C1 was associated with disease progression towards hepatocellular carcinoma (HCC) in HBV-infected patients (Table 2). In particular, one copy of HLA-C1 alleles was associated with cirrhosis, while two copies were associated with HCC (Table 2) [150].

In a later study, the frequencies of KIR and HLA genes were compared in subjects with chronic hepatitis B (CHB) and subjects with resolved infection [147]. Once again, the inhibitory KIR2DL3 gene was less frequent in CHB (81%) than in subjects with resolved infection (98%), suggesting the protective role of this KIR in CHB development. Moreover, the authors found higher frequency of both HLA-C2 and HLA-A-Bw4 alleles in CHB group compared to subjects with resolved infection and controls (Table 2). No difference was reported in the frequency of KIR haplotypes between the groups, suggesting that activating receptors might do not play a role in controlling the infection. The results obtained by these studies suggest that KIR/HLA combination is able to predict the outcome of HBV infection and consequently cancer progression.

As well as HBV, HCV can exploit KIR receptors to modulate NK cell response [195], increasing viral spread and inducing the neoplastic process. Thus, KIR/HLA combination might influence HCV infection outcome, influencing HCV viral load and the risk of hepatocellular carcinoma progression [159,196]. NK cells were demonstrated to mediate the inhibition of HCV-replication and to exert a targeted cytotoxic action against infected cells [197,198].

Several KIRs have been identified as relevant to the outcome of HCV infection and treatment efficacy, including KIR2DL2, KIR2DL3, KIR2DL1, KIR2DS2, and KIR3DL1, together with HLA-C2 expression (Table 2) [151,152].

In particular, Lunemann and coauthors identified a core-derived epitope that dampens NK cell responses, and thereby possibly prevents killing of infected cells through this part of the innate immune system. This 9mer HCV peptide, YIPLVGAPL, is facilitated via presentation of the viral peptide on HLA-C*03:04 to the inhibitory KIR receptor KIR2DL3 on NK cells [153]. In fact, this HCV peptide resulted in significantly higher KIR2DL3 binding to HLA-C*03:04 suggesting that HCV genotype 1 binding to HLA-C*03:04 results in a sequence-dependent engagement of the inhibitory NK cell receptor KIR2DL3, showing that sequence variations within HCV can modulate NK cell function, providing potential pathways for viral escape (Figure 7; Table 2).

Another strategy used in HCV escape consists in mutations at the HLA-B*27 binding anchor of the epitope [154]. This epitope is present in the viral RNA-dependent RNA polymerase. The ability to mutate at the main HLA-B*27-binding anchor is dependent on viral fitness [199]. Misfolded HLA-B*27 may also be unable to engage KIR3DL1, resulting in increased NK cell activation (Table 2) [155,156]. Moreover, another study reported that the expression of KIR3DL1 was decreased in individuals with HCV infection, supporting the role of this receptor in the regulation of chronic HCV infection (Table 2) [157].

HCV patients were found with high frequency of KIR2DS3 receptor [158] and a protective role for HLA-Bw4/KIR3DS1 against liver disease progression has been also proposed (Table 2) [159].

Another study has shown that KIR2DL3 was associated with spontaneous resolution of HCV infection, in presence of HLA-C1 homozygous genotype [160]. At the same time, HLA-C1/KIR2DL3 has also been associated with sustained virus response to anti-HCV therapy (Table 2), even if previous data have also suggested that KIR2DL1/HLA-C2 combination may confer stronger inhibitory responses than KIR2DL3/HLA-C1 [161].

4.4. Other Viruses

In addition, other viral infections have been reported to be associated to characteristic KIRs asset, including enterovirus, Parvoviruses, and Human Papillomavirus (HPV).

Enteroviruses represent risk factors for T1D and have been reportedly associated to peculiar KIRs [171]; enteroviruses have been reported to possibly directly affect pancreatic islets, together with low expression level of the inhibitory receptor KIR3DL1, in TD1 patients (Table 2) [162].

Hashimoto's Thyroiditis (HT) is another autoimmune disease in which an increased susceptibility to enterovirus was reported [163], in association with upregulation of HLA-I molecules (Table 2). The colocalization of HLA class I with STAT1 and VP1 with PKR indicates an intracellular, antiviral host response, supporting a firm link between viral infection and autoimmune thyroid diseases which possibly also affects NK cell function via KIRs engagement.

Parvovirus 9, similarly to CMV and HCV, have been reported implicated in SLE susceptibility [171], possibly in concomitance to the presence of KIR2DL2 and KIR2DS1 (Table 2) [107,172]. In addition, Parvovirus B19 has been reported in SLE to be responsible for an aberrant immune activation [164] involving HLA molecules upregulation which allows a persistent viral infection (Table 2) [165].

HPV infection is known to be the main risk factor for the development of premalignant and malignant epithelial lesions of the cervix [200]. Besides HPV infection, there are other factors participating in increasing cervix cancer susceptibility. Rizzo et al. demonstrated that KIR2DL2/HLA-C1 and KIR2DL3/HLA-C1 pairs constitute a risk factors for HPV high-risk infection, while the increased frequency of HLA-C2 alleles in HPV-positive patients did not increase risk [166]. In this study, HPV-positive subjects with cervix cancer presented a decreased KIR2DL2/HLA-C2 frequency, while KIR2DL1 was found in most of the subjects. In particular, it has been hypothesized that KIR2DL2/HLA-C1 and KIR2DL3/HLA-C1 presence could induce NK cells inhibition toward HPV infection, sustaining the high-risk HPV-associated transformation and the development of pre-neoplastic lesions (Table 2) [166].

5. Conclusions

The role of NK cells in controlling viral infection is known and the efficiency in the control of viral spread and host outcomes is due to the crosstalk between intracellular signals received from a large repertoire of germ-line-encoded surface receptors.

Among NK receptors, the family of killer immunoglobulin-like receptors (KIR) is characterized by highly polymorphic activating and inhibitory receptors, involved in the regulation of NK cell functions. Specific ligands for KIRs are Human Leukocyte Antigen (HLA) molecules expressed on target cells, whose binding induces NK cells activation/inhibition.

In this review we have reported the role of KIR receptors in viral infection control by NK cells. In particular, we reported several strategies developed by viruses to alter NK cell activation affecting KIRs/ligands expression (Figure 7) and that peculiar KIR assets have been found possibly correlated to viral infection susceptibility and human disease development and progression.

In conclusion, the crucial role of KIRs in the control of viral infection suggests these receptors, together with their ligands, as possible targets for new therapeutical strategies for viral infections' clearance and as putative biomarkers for disease prognosis.

Author Contributions: Conceptualization, D.B. and R.R.; data curation, S.R., G.S. and S.B.; writing—original draft, S.R., V.G. and G.S.; writing—review and editing, D.B. and R.R.; supervision, D.B.; funding acquisition, R.R. All authors have read and agreed to the published version of the manuscript.

Funding: This work was supported by FISM-Fondazione Italiana Sclerosi Multipla grant (cod 2015/R/20; 2020-FOND-RR_001 to R.R.).

Institutional Review Board Statement: Not applicable.

Informed Consent Statement: Not applicable.

Data Availability Statement: Not applicable.

Conflicts of Interest: None of the authors have any conflicts of interest in association with this manuscript.

References

1. Lanier, L.L. NK cell recognition. *Annu. Rev. Immunol.* **2005**, *23*, 225–274. [[CrossRef](#)] [[PubMed](#)]
2. Sojka, D.K.; Tian, Z.; Yokoyama, W.M. Tissue-resident natural killer cells and their potential diversity. In *Seminars in Immunology*; Academic Press: Cambridge, MA, USA, 2014; pp. 127–131.
3. Yokoyama, W.M.; Sojka, D.K.; Peng, H.; Tian, Z. Tissue-resident natural killer cells. In *Cold Spring Harbor Symposia on Quantitative Biology*; Cold Spring Harbor Laboratory Press: Long Island, NY, USA, 2013; pp. 149–156.
4. Poli, A.; Michel, T.; Theresine, M.; Andres, E.; Hentges, F.; Zimmer, J. CD56bright natural killer (NK) cells: An important NK cell subset. *Immunology* **2009**, *126*, 458–465. [[CrossRef](#)] [[PubMed](#)]
5. Ferlazzo, G.; Thomas, D.; Lin, S.L.; Goodman, K.; Morandi, B.; Muller, W.A.; Moretta, A.; Munz, C. The Abundant Nk Cells in human secondary lymphoid tissues require activation to express killer cell Ig-like receptors and become cytolytic. *J. Immunol.* **2004**, *172*, 1455–1462. [[CrossRef](#)]
6. Perussia, B.; Chen, Y.; Loza, M.J. Peripheral NK cell phenotypes: Multiple changing of faces of an adapting, developing cell. *Mol. Immunol.* **2005**, *42*, 385–395. [[CrossRef](#)] [[PubMed](#)]
7. Loke, Y.; King, A. *Human Implantation: Cell Biology and Immunology*; Cambridge University Press: Cambridge, UK, 1995.
8. Moffett-King, A. Natural killer cells and pregnancy. *Nat. Rev. Immunol.* **2002**, *2*, 656–663. [[CrossRef](#)] [[PubMed](#)]
9. Moffett-King, A.; Entrican, G.; Ellis, S.; Hutchinson, J.; Bainbridge, D. Natural killer cells and reproduction. *Trends Immunol.* **2002**, *23*, 332–333. [[CrossRef](#)]
10. Biron, C.A.; Brossay, L. NK cells and NKT cells in innate defense against viral infections. *Curr. Opin. Immunol.* **2001**, *13*, 458–464. [[CrossRef](#)]
11. Schmeel, L.C.; Schmeel, F.C.; Coch, C.; Schmidt-Wolf, I.G. Cytokine-induced killer (CIK) cells in cancer immunotherapy: Report of the international registry on CIK cells (IRCC). *J. Cancer Res. Clin. Oncol.* **2015**, *141*, 839–849. [[CrossRef](#)]
12. Li, Y.; Schmidt-Wolf, I.G.; Wu, Y.F.; Huang, S.L.; Wei, J.; Fang, J.; Huang, K.; Zhou, D.H. Optimized protocols for generation of cord blood-derived cytokine-induced killer/natural killer cells. *Anticancer Res.* **2010**, *30*, 3493–3499.
13. Cooper, M.A.; Fehniger, T.A.; Caligiuri, M.A. The biology of human natural killer-cell subsets. *Trends Immunol.* **2001**, *22*, 633–640. [[CrossRef](#)]
14. Kumar, S. Natural killer cell cytotoxicity and its regulation by inhibitory receptors. *Immunology* **2018**, *154*, 383–393. [[CrossRef](#)] [[PubMed](#)]
15. Mavilio, D.; Benjamin, J.; Daucher, M.; Lombardo, G.; Kottlilil, S.; Planta, M.A.; Marcenaro, E.; Bottino, C.; Moretta, L.; Moretta, A.; et al. Natural killer cells in HIV-1 infection: Dichotomous effects of viremia on inhibitory and activating receptors and their functional correlates. *Proc. Natl. Acad. Sci. USA* **2003**, *100*, 15011–15016. [[CrossRef](#)] [[PubMed](#)]
16. Alter, G.; Teigen, N.; Davis, B.T.; Addo, M.M.; Suscovich, T.J.; Waring, M.T.; Streeck, H.; Johnston, M.N.; Staller, K.D.; Zaman, M.T.; et al. Sequential deregulation of NK cell subset distribution and function starting in acute HIV-1 infection. *Blood* **2005**, *106*, 3366–3369. [[CrossRef](#)]
17. Peritt, D.; Robertson, S.; Gri, G.; Showe, L.; Aste-Amezaga, M.; Trinchieri, G. Cutting edge: Differentiation of human NK cells into NK1 and NK2 subsets. *J. Immunol.* **1998**, *161*, 5821–5824.
18. Berahovich, R.D.; Lai, N.L.; Wei, Z.; Lanier, L.L.; Schall, T.J. Evidence for NK cell subsets based on chemokine receptor expression. *J. Immunol.* **2006**, *177*, 7833–7840. [[CrossRef](#)]
19. Michel, M.L.; Keller, A.C.; Paget, C.; Fujio, M.; Trottein, F.; Savage, P.B.; Wong, C.H.; Schneider, E.; Dy, M.; Leite-de-Moraes, M.C. Identification of an IL-17-producing NK1.1(neg) iNKT cell population involved in airway neutrophilia. *J. Exp. Med.* **2007**, *204*, 995–1001. [[CrossRef](#)]
20. Pandya, A.D.; Al-Jaderi, Z.; Hoglund, R.A.; Holmoy, T.; Harbo, H.F.; Norgauer, J.; Maghazachi, A.A. Identification of human NK17/NK1 cells. *PLoS ONE* **2011**, *6*, e26780. [[CrossRef](#)] [[PubMed](#)]
21. Rizzo, R.; Bortolotti, D.; Fainardi, E.; Gentili, V.; Bolzani, S.; Baldi, E.; Casetta, I.; Granieri, E.; Rotola, A.; Furlan, R.; et al. KIR2DL2 inhibitory pathway enhances Th17 cytokine secretion by NK cells in response to herpesvirus infection in multiple sclerosis patients. *J. Neuroimmunol.* **2016**, *294*, 1–5. [[CrossRef](#)] [[PubMed](#)]
22. Hou, W.; Kang, H.S.; Kim, B.S. Th17 cells enhance viral persistence and inhibit T cell cytotoxicity in a model of chronic virus infection. *J. Exp. Med.* **2009**, *206*, 313–328. [[CrossRef](#)]
23. Jost, S.; Altfeld, M. Control of human viral infections by natural killer cells. *Annu. Rev. Immunol.* **2013**, *31*, 163–194. [[CrossRef](#)]
24. Sun, J.C.; Lopez-Verges, S.; Kim, C.C.; DeRisi, J.L.; Lanier, L.L. NK cells and immune “memory”. *J. Immunol.* **2011**, *186*, 1891–1897. [[CrossRef](#)]
25. Altfeld, M.; Fadda, L.; Frleta, D.; Bhardwaj, N. DCs and NK cells: Critical effectors in the immune response to HIV-1. *Nat. Rev. Immunol.* **2011**, *11*, 176–186. [[CrossRef](#)] [[PubMed](#)]

26. Vivier, E.; Tomasello, E.; Baratin, M.; Walzer, T.; Ugolini, S. Functions of natural killer cells. *Nat. Immunol.* **2008**, *9*, 503–510. [[CrossRef](#)] [[PubMed](#)]
27. Biron, C.A.; Byron, K.S.; Sullivan, J.L. Severe herpesvirus infections in an adolescent without natural killer cells. *N. Engl. J. Med.* **1989**, *320*, 1731–1735. [[CrossRef](#)] [[PubMed](#)]
28. Orange, J.S. Human natural killer cell deficiencies and susceptibility to infection. *Microbes Infect.* **2002**, *4*, 1545–1558. [[CrossRef](#)]
29. Biron, C.A.; Dalod, M.; Salazar-Mather, T.P. Innate immunity and viral infections. *Immunol. Infect. Dis.* **2001**, *11*, 139–160. [[CrossRef](#)]
30. Solerte, S.B.; Cravello, L.; Ferrari, E.; Fioravanti, M. Overproduction of IFN-gamma and TNF-alpha from natural killer (NK) cells is associated with abnormal NK reactivity and cognitive derangement in Alzheimer's disease. *Ann. N. Y. Acad. Sci.* **2000**, *917*, 331–340. [[CrossRef](#)]
31. Fehniger, T.A.; Cooper, M.A.; Nuovo, G.J.; Cella, M.; Facchetti, F.; Colonna, M.; Caligiuri, M.A. CD56bright natural killer cells are present in human lymph nodes and are activated by T cell-derived IL-2: A potential new link between adaptive and innate immunity. *Blood* **2003**, *101*, 3052–3057. [[CrossRef](#)]
32. Walzer, T.; Dalod, M.; Robbins, S.H.; Zitvogel, L.; Vivier, E. Natural-killer cells and dendritic cells: "l'union fait la force". *Blood* **2005**, *106*, 2252–2258. [[CrossRef](#)]
33. Long, E.O. Ready for prime time: NK cell priming by dendritic cells. *Immunity* **2007**, *26*, 385–387. [[CrossRef](#)]
34. Sim, G.C.; Radvanyi, L. The IL-2 cytokine family in cancer immunotherapy. *Cytokine Growth Factor Rev.* **2014**, *25*, 377–390. [[CrossRef](#)]
35. Giri, J.G.; Kumaki, S.; Ahdieh, M.; Friend, D.J.; Loomis, A.; Shanebeck, K.; DuBose, R.; Cosman, D.; Park, L.S.; Anderson, D.M. Identification and cloning of a novel IL-15 binding protein that is structurally related to the alpha chain of the IL-2 receptor. *EMBO J.* **1995**, *14*, 3654–3663. [[CrossRef](#)]
36. Fehniger, T.A.; Shah, M.H.; Turner, M.J.; VanDeusen, J.B.; Whitman, S.P.; Cooper, M.A.; Suzuki, K.; Wechsler, M.; Goodsaid, F.; Caligiuri, M.A. Differential cytokine and chemokine gene expression by human NK cells following activation with IL-18 or IL-15 in combination with IL-12: Implications for the innate immune response. *J. Immunol.* **1999**, *162*, 4511–4520.
37. Lucas, M.; Schachterle, W.; Oberle, K.; Aichele, P.; Diefenbach, A. Dendritic cells prime natural killer cells by trans-presenting interleukin 15. *Immunity* **2007**, *26*, 503–517. [[CrossRef](#)]
38. Nandagopal, N.; Ali, A.K.; Komal, A.K.; Lee, S.H. The critical role of IL-15-PI3K-mTOR pathway in natural killer cell effector functions. *Front. Immunol.* **2014**, *5*, 187. [[CrossRef](#)] [[PubMed](#)]
39. Fehniger, T.A.; Cai, S.F.; Cao, X.; Bredemeyer, A.J.; Presti, R.M.; French, A.R.; Ley, T.J. Acquisition of murine NK cell cytotoxicity requires the translation of a pre-existing pool of granzyme B and perforin mRNAs. *Immunity* **2007**, *26*, 798–811. [[CrossRef](#)]
40. Cooper, M.A.; Elliott, J.M.; Keyel, P.A.; Yang, L.; Carrero, J.A.; Yokoyama, W.M. Cytokine-induced memory-like natural killer cells. *Proc. Natl. Acad. Sci. USA* **2009**, *106*, 1915–1919. [[CrossRef](#)] [[PubMed](#)]
41. Zamai, L.; Ahmad, M.; Bennett, I.M.; Azzoni, L.; Alnemri, E.S.; Perussia, B. Natural killer (NK) cell-mediated cytotoxicity: Differential use of TRAIL and Fas ligand by immature and mature primary human NK cells. *J. Exp. Med.* **1998**, *188*, 2375–2380. [[CrossRef](#)]
42. Bryceson, Y.T.; Chiang, S.C.; Darmanin, S.; Fauriat, C.; Schlums, H.; Theorell, J.; Wood, S.M. Molecular mechanisms of natural killer cell activation. *J. Innate Immun.* **2011**, *3*, 216–226. [[CrossRef](#)]
43. Lanier, L.L. Up on the tightrope: Natural killer cell activation and inhibition. *Nat. Immunol.* **2008**, *9*, 495–502. [[CrossRef](#)]
44. Veillette, A. SLAM-family receptors: Immune regulators with or without SAP-family adaptors. *Cold Spring Harb. Perspect. Biol.* **2010**, *2*, a002469. [[CrossRef](#)]
45. Wu, N.; Veillette, A. SLAM family receptors in normal immunity and immune pathologies. *Curr. Opin. Immunol.* **2016**, *38*, 45–51. [[CrossRef](#)] [[PubMed](#)]
46. Cerwenka, A.; Lanier, L.L. Natural killer cell memory in infection, inflammation and cancer. *Nat. Rev. Immunol.* **2016**, *16*, 112–123. [[CrossRef](#)] [[PubMed](#)]
47. Afonina, I.S.; Cullen, S.P.; Martin, S.J. Cytotoxic and non-cytotoxic roles of the CTL/NK protease granzyme B. *Immunol. Rev.* **2010**, *235*, 105–116. [[CrossRef](#)] [[PubMed](#)]
48. Arnon, T.I.; Markel, G.; Mandelboim, O. Tumor and viral recognition by natural killer cells receptors. In *Seminars in Cancer Biology*; Academic Press: Cambridge, MA, USA, 2006; pp. 348–358.
49. Jost, S.; Altfield, M. Evasion from NK cell-mediated immune responses by HIV-1. *Microbes Infect.* **2012**, *14*, 904–915. [[CrossRef](#)]
50. Arnon, T.I.; Lev, M.; Katz, G.; Chernobrov, Y.; Porgador, A.; Mandelboim, O. Recognition of viral hemagglutinins by NKp44 but not by NKp30. *Eur. J. Immunol.* **2001**, *31*, 2680–2689. [[CrossRef](#)]
51. Mandelboim, O.; Lieberman, N.; Lev, M.; Paul, L.; Arnon, T.I.; Bushkin, Y.; Davis, D.M.; Strominger, J.L.; Yewdell, J.W.; Porgador, A. Recognition of haemagglutinins on virus-infected cells by NKp46 activates lysis by human NK cells. *Nature* **2001**, *409*, 1055–1060. [[CrossRef](#)]
52. Baugh, R.; Khalique, H.; Seymour, L.W. Convergent evolution by cancer and viruses in evading the NKG2D immune response. *Cancers* **2020**, *12*, 3827. [[CrossRef](#)] [[PubMed](#)]

53. Sun, H.; Sun, C. The rise of NK cell checkpoints as promising therapeutic targets in cancer immunotherapy. *Front. Immunol.* **2019**, *10*, 2354. [[CrossRef](#)] [[PubMed](#)]
54. Campbell, K.S.; Purdy, A.K. Structure/function of human killer cell immunoglobulin-like receptors: Lessons from polymorphisms, evolution, crystal structures and mutations. *Immunology* **2011**, *132*, 315–325. [[CrossRef](#)] [[PubMed](#)]
55. Pende, D.; Falco, M.; Vitale, M.; Cantoni, C.; Vitale, C.; Munari, E.; Bertaina, A.; Moretta, F.; Del Zotto, G.; Pietra, G.; et al. Killer Ig-like receptors (KIRs): Their role in NK cell modulation and developments leading to their clinical exploitation. *Front. Immunol.* **2019**, *10*, 1179. [[CrossRef](#)] [[PubMed](#)]
56. Colonna, M.; Samaridis, J. Cloning of immunoglobulin-superfamily members associated with HLA-C and HLA-B recognition by human natural killer cells. *Science* **1995**, *268*, 405–408. [[CrossRef](#)] [[PubMed](#)]
57. D'Andrea, A.; Chang, C.; Franz-Bacon, K.; McClanahan, T.; Phillips, J.H.; Lanier, L.L. Molecular cloning of NK1. A natural killer cell receptor for HLA-B allotypes. *J. Immunol.* **1995**, *155*, 2306–2310. [[PubMed](#)]
58. Scharenberg, A.M.; Kinet, J.P. The emerging field of receptor-mediated inhibitory signaling: SHP or SHIP? *Cell* **1996**, *87*, 961–964. [[CrossRef](#)]
59. Rajagopalan, S.; Fu, J.; Long, E.O. Cutting edge: Induction of IFN-gamma production but not cytotoxicity by the killer cell Ig-like receptor KIR2DL4 (CD158d) in resting NK cells. *J. Immunol.* **2001**, *167*, 1877–1881. [[CrossRef](#)]
60. Kikuchi-Maki, A.; Catina, T.L.; Campbell, K.S. Cutting edge: KIR2DL4 transduces signals into human NK cells through association with the fc receptor gamma protein. *J. Immunol.* **2005**, *174*, 3859–3863. [[CrossRef](#)] [[PubMed](#)]
61. Binstadt, B.A.; Brumbaugh, K.M.; Dick, C.J.; Scharenberg, A.M.; Williams, B.L.; Colonna, M.; Lanier, L.L.; Kinet, J.P.; Abraham, R.T.; Leibson, P.J. Sequential involvement of Lck and SHP-1 with MHC-recognizing receptors on NK cells inhibits FcR-initiated tyrosine kinase activation. *Immunity* **1996**, *5*, 629–638. [[CrossRef](#)]
62. Valiante, N.M.; Phillips, J.H.; Lanier, L.L.; Parham, P. Killer cell inhibitory receptor recognition of human leukocyte antigen (HLA) class I blocks formation of a pp36/PLC-gamma signaling complex in human natural killer (NK) cells. *J. Exp. Med.* **1996**, *184*, 2243–2250. [[CrossRef](#)]
63. Pegram, H.J.; Andrews, D.M.; Smyth, M.J.; Darcy, P.K.; Kershaw, M.H. Activating and inhibitory receptors of natural killer cells. *Immunol. Cell Biol.* **2011**, *89*, 216–224. [[CrossRef](#)]
64. Jonsson, A.H.; Yokoyama, W.M. Natural killer cell tolerance licensing and other mechanisms. *Adv. Immunol.* **2009**, *101*, 27–79. [[CrossRef](#)] [[PubMed](#)]
65. Carey, B.S.; Poulton, K.V.; Poles, A. Factors affecting HLA expression: A review. *Int. J. Immunogenet.* **2019**, *46*, 307–320. [[CrossRef](#)]
66. Van den Elsen, P.J. Expression regulation of major histocompatibility complex class I and class II encoding genes. *Front. Immunol.* **2011**, *2*, 48. [[CrossRef](#)]
67. Van den Elsen, P.J.; Holling, T.M.; Kuipers, H.F.; van der Stoep, N. Transcriptional regulation of antigen presentation. *Curr. Opin. Immunol.* **2004**, *16*, 67–75. [[CrossRef](#)]
68. Stewart, C.A.; Laugier-Anfossi, F.; Vely, F.; Saulquin, X.; Riedmuller, J.; Tisserant, A.; Gauthier, L.; Romagne, F.; Ferracci, G.; Arosa, F.A.; et al. Recognition of peptide-MHC class I complexes by activating killer immunoglobulin-like receptors. *Proc. Natl. Acad. Sci. USA* **2005**, *102*, 13224–13229. [[CrossRef](#)] [[PubMed](#)]
69. Dohring, C.; Colonna, M. Human natural killer cell inhibitory receptors bind to HLA class I molecules. *Eur. J. Immunol.* **1996**, *26*, 365–369. [[CrossRef](#)]
70. Pende, D.; Biassoni, R.; Cantoni, C.; Verdiani, S.; Falco, M.; di Donato, C.; Accame, L.; Bottino, C.; Moretta, A.; Moretta, L. The natural killer cell receptor specific for HLA-A allotypes: A novel member of the p58/p70 family of inhibitory receptors that is characterized by three immunoglobulin-like domains and is expressed as a 140-kD disulphide-linked dimer. *J. Exp. Med.* **1996**, *184*, 505–518. [[CrossRef](#)]
71. Tajik, N.; Shahsavari, F.; Mousavi, T.; Radjabzadeh, M.F. Distribution of KIR genes in the Iranian population. *Tissue Antigens* **2009**, *74*, 22–31. [[CrossRef](#)] [[PubMed](#)]
72. Martin, A.M.; Kulski, J.K.; Gaudieri, S.; Witt, C.S.; Freitas, E.M.; Trowsdale, J.; Christiansen, F.T. Comparative genomic analysis, diversity and evolution of two KIR haplotypes A and B. *Gene* **2004**, *335*, 121–131. [[CrossRef](#)] [[PubMed](#)]
73. Gomez-Lozano, N.; Estefania, E.; Williams, F.; Halfpenny, I.; Middleton, D.; Solis, R.; Vilches, C. The silent KIR3DP1 gene (CD158c) is transcribed and might encode a secreted receptor in a minority of humans, in whom the KIR3DP1, KIR2DL4 and KIR3DL1/KIR3DS1 genes are duplicated. *Eur. J. Immunol.* **2005**, *35*, 16–24. [[CrossRef](#)]
74. Gomez-Lozano, N.; Gardiner, C.M.; Parham, P.; Vilches, C. Some human KIR haplotypes contain two KIR2DL5 genes: KIR2DL5A and KIR2DL5B. *Immunogenetics* **2002**, *54*, 314–319. [[CrossRef](#)]
75. Uhrberg, M. The KIR gene family: Life in the fast lane of evolution. *Eur. J. Immunol.* **2005**, *35*, 10–15. [[CrossRef](#)]
76. Uhrberg, M.; Valiante, N.M.; Shum, B.P.; Shilling, H.G.; Lienert-Weidenbach, K.; Corliss, B.; Tyan, D.; Lanier, L.L.; Parham, P. Human diversity in killer cell inhibitory receptor genes. *Immunity* **1997**, *7*, 753–763. [[CrossRef](#)]
77. Shilling, H.G.; Guethlein, L.A.; Cheng, N.W.; Gardiner, C.M.; Rodriguez, R.; Tyan, D.; Parham, P. Allelic polymorphism synergizes with variable gene content to individualize human KIR genotype. *J. Immunol.* **2002**, *168*, 2307–2315. [[CrossRef](#)]

78. Yawata, M.; Yawata, N.; Abi-Rached, L.; Parham, P. Variation within the human killer cell immunoglobulin-like receptor (KIR) gene family. *Crit. Rev. Immunol.* **2002**, *22*, 463–482. [[CrossRef](#)] [[PubMed](#)]
79. Hsu, K.C.; Liu, X.R.; Selvakumar, A.; Mickelson, E.; O'Reilly, R.J.; Dupont, B. Killer Ig-like receptor haplotype analysis by gene content: Evidence for genomic diversity with a minimum of six basic framework haplotypes, each with multiple subsets. *J. Immunol.* **2002**, *169*, 5118–5129. [[CrossRef](#)] [[PubMed](#)]
80. Orange, J.S.; Fassett, M.S.; Koopman, L.A.; Boyson, J.E.; Strominger, J.L. Viral evasion of natural killer cells. *Nat. Immunol.* **2002**, *3*, 1006–1012. [[CrossRef](#)] [[PubMed](#)]
81. Machold, R.P.; Wiertz, E.J.; Jones, T.R.; Ploegh, H. The HCMV gene products US11 and US2 differ in their ability to attack allelic forms of murine major histocompatibility complex (MHC) class I heavy chains. *J. Exp. Med.* **1997**, *185*, 363–366. [[CrossRef](#)] [[PubMed](#)]
82. Früh, K.; Gruhler, A.; Krishna, R.M.; Schoenhals, G.J. A comparison of viral immune escape strategies targeting the MHC class I assembly pathway. *Immunol. Rev.* **1999**, *168*, 157–166. [[CrossRef](#)]
83. Chan, H.-W.; Kurago, Z.B.; Stewart, C.A.; Wilson, M.J.; Martin, M.P.; Mace, B.E.; Carrington, M.; Trowsdale, J.; Lutz, C.T. DNA methylation maintains allele-specific KIR gene expression in human natural killer cells. *J. Exp. Med.* **2003**, *197*, 245–255. [[CrossRef](#)]
84. Milavetz, B.I.; Balakrishnan, L. Viral epigenetics. *Methods Mol. Biol.* **2015**, *1238*, 569–596. [[CrossRef](#)]
85. Blazkova, J.; Trejbalova, K.; Gondois-Rey, F.; Halfon, P.; Philibert, P.; Guiguen, A.; Verdin, E.; Olive, D.; Van Lint, C.; Hejnar, J. CpG methylation controls reactivation of HIV from latency. *PLoS Pathog.* **2009**, *5*, e1000554. [[CrossRef](#)]
86. Chan, H.W.; Miller, J.S.; Moore, M.B.; Lutz, C.T. Epigenetic control of highly homologous killer Ig-like receptor gene alleles. *J. Immunol.* **2005**, *175*, 5966–5974. [[CrossRef](#)] [[PubMed](#)]
87. Rajagopalan, S.; Long, E.O. Understanding how combinations of HLA and KIR genes influence disease. *J. Exp. Med.* **2005**, *201*, 1025–1029. [[CrossRef](#)]
88. Snyder, M.R.; Weyand, C.M.; Goronzy, J.J. The double life of NK receptors: Stimulation or co-stimulation? *Trends Immunol.* **2004**, *25*, 25–32. [[CrossRef](#)]
89. López-Botet, M.; Llano, M.; Ortega, M. Human cytomegalovirus and natural killer-mediated surveillance of HLA class I expression: A paradigm of host–pathogen adaptation. *Immunol. Rev.* **2001**, *181*, 193–202. [[CrossRef](#)]
90. Miller, J.S. Biology of Natural Killer Cells in Cancer and Infection: Miniseries/Special Article. *Cancer Investig.* **2002**, *20*, 405–419. [[CrossRef](#)]
91. Hopfensperger, K.; Richard, J.; Stürzel, C.M.; Bibollet-Ruche, F.; Apps, R.; Leoz, M.; Plantier, J.-C.; Hahn, B.H.; Finzi, A.; Kirchhoff, F. Convergent Evolution of HLA-C Downmodulation in HIV-1 and HIV-2. *mBio* **2020**, *11*, e00782-20. [[CrossRef](#)] [[PubMed](#)]
92. Jugovic, P.; Hill, A.M.; Tomazin, R.; Ploegh, H.; Johnson, D.C. Inhibition of major histocompatibility complex class I antigen presentation in pig and primate cells by herpes simplex virus type 1 and 2 ICP47. *J. Virol.* **1998**, *72*, 5076–5084. [[CrossRef](#)] [[PubMed](#)]
93. Tortorella, D.; Gewurz, B.E.; Furman, M.H.; Schust, D.J.; Ploegh, H.L. Viral subversion of the immune system. *Annu. Rev. Immunol.* **2000**, *18*, 861–926. [[CrossRef](#)]
94. Collins, K.L.; Chen, B.K.; Kalams, S.A.; Walker, B.D.; Baltimore, D. HIV-1 Nef protein protects infected primary cells against killing by cytotoxic T lymphocytes. *Nature* **1998**, *391*, 397–401. [[CrossRef](#)] [[PubMed](#)]
95. Kulkarni, S.; Martin, M.P.; Carrington, M. The Yin and Yang of HLA and KIR in human disease. In *Seminars in Immunology*; Academic Press: Cambridge, MA, USA, 2008; pp. 343–352.
96. Romero, V.; Azocar, J.; Zúñiga, J.; Clavijo, O.P.; Terreros, D.; Gu, X.; Husain, Z.; Chung, R.T.; Amos, C.; Yunis, E.J. Interaction of NK inhibitory receptor genes with HLA-C and MHC class II alleles in Hepatitis C virus infection outcome. *Mol. Immunol.* **2008**, *45*, 2429–2436. [[CrossRef](#)]
97. Rizzo, R.; Gentili, V.; Casetta, I.; Caselli, E.; De Gennaro, R.; Granieri, E.; Cassai, E.; Di Luca, D.; Rotola, A. Altered natural killer cells' response to herpes virus infection in multiple sclerosis involves KIR2DL2 expression. *J. Neuroimmunol.* **2012**, *251*, 55–64. [[CrossRef](#)]
98. Gewurz, B.E.; Wang, E.W.; Tortorella, D.; Schust, D.J.; Ploegh, H.L. Human cytomegalovirus US2 endoplasmic reticulum-luminal domain dictates association with major histocompatibility complex class I in a locus-specific manner. *J. Virol.* **2001**, *75*, 5197–5204. [[CrossRef](#)] [[PubMed](#)]
99. Guma, M.; Angulo, A.; Lopez-Botet, M. NK cell receptors involved in the response to human cytomegalovirus infection. *Curr. Top Microbiol. Immunol.* **2006**, *298*, 207–223. [[CrossRef](#)] [[PubMed](#)]
100. Lanteri, M.; Giordanengo, V.; Hiraoka, N.; Fuzibet, J.G.; Auberger, P.; Fukuda, M.; Baum, L.G.; Lefebvre, J.C. Altered T cell surface glycosylation in HIV-1 infection results in increased susceptibility to galectin-1-induced cell death. *Glycobiology* **2003**, *13*, 909–918. [[CrossRef](#)]
101. Kielczewska, A.; Pyzik, M.; Sun, T.; Krmpotic, A.; Lodoen, M.B.; Munks, M.W.; Babic, M.; Hill, A.B.; Koszinowski, U.H.; Jonjic, S.; et al. Ly49P recognition of cytomegalovirus-infected cells expressing H2-Dk and CMV-encoded m04 correlates with the NK cell antiviral response. *J. Exp. Med.* **2009**, *206*, 515–523. [[CrossRef](#)]

102. Crespo, A.C.; Strominger, J.L.; Tilburgs, T. Expression of KIR2DS1 by decidual natural killer cells increases their ability to control placental HCMV infection. *Proc. Natl. Acad. Sci. USA* **2016**, *113*, 15072–15077. [[CrossRef](#)] [[PubMed](#)]
103. Kenneson, A.; Cannon, M.J. Review and meta-analysis of the epidemiology of congenital cytomegalovirus (CMV) infection. *Rev. Med. Virol.* **2007**, *17*, 253–276. [[CrossRef](#)]
104. Schust, D.J.; Tortorella, D.; Seebach, J.; Phan, C.; Ploegh, H.L. Trophoblast class I major histocompatibility complex (MHC) products are resistant to rapid degradation imposed by the human cytomegalovirus (HCMV) gene products US2 and US11. *J. Exp. Med.* **1998**, *188*, 497–503. [[CrossRef](#)]
105. Gazit, R.; Garty, B.Z.; Monselise, Y.; Hoffer, V.; Finkelstein, Y.; Markel, G.; Katz, G.; Hanna, J.; Achdout, H.; Gruda, R.; et al. Expression of KIR2DL1 on the entire NK cell population: A possible novel immunodeficiency syndrome. *Blood* **2004**, *103*, 1965–1966. [[CrossRef](#)]
106. Van Duin, D.; Avery, R.K.; Hemachandra, S.; Yen-Lieberman, B.; Zhang, A.; Jain, A.; Butler, R.S.; Barnard, J.; Schold, J.D.; Fung, J.; et al. KIR and HLA interactions are associated with control of primary CMV infection in solid organ transplant recipients. *Am. J. Transplant.* **2014**, *14*, 156–162. [[CrossRef](#)]
107. Hou, Y.F.; Zhang, Y.C.; Jiao, Y.L.; Wang, L.C.; Li, J.F.; Pan, Z.L.; Yang, Q.R.; Sun, H.S.; Zhao, Y.R. Disparate distribution of activating and inhibitory killer cell immunoglobulin-like receptor genes in patients with systemic lupus erythematosus. *Lupus* **2010**, *19*, 20–26. [[CrossRef](#)] [[PubMed](#)]
108. Pellett, F.; Siannis, F.; Vukin, I.; Lee, P.; Urowitz, M.; Gladman, D. KIRs and autoimmune disease: Studies in systemic lupus erythematosus and scleroderma. In *Tissue Antigens*; Wiley Online Library: Hoboken, NJ, USA, 2007.
109. Majorczyk, E.; Pawlik, A.; Luszczek, W.; Nowak, I.; Wisniewski, A.; Jasek, M.; Kusnierczyk, P. Associations of killer cell immunoglobulin-like receptor genes with complications of rheumatoid arthritis. *Genes Immun.* **2007**, *8*, 678–683. [[CrossRef](#)] [[PubMed](#)]
110. Hoteit, R.; Bazarbachi, A.; Antar, A.; Salem, Z.; Shammaa, D.; Mahfouz, R. KIR genotype distribution among patients with multiple myeloma: Higher prevalence of KIR 2DS4 and KIR 2DS5 genes. *Meta Gene* **2014**, *2*, 730–736. [[CrossRef](#)] [[PubMed](#)]
111. Coscoy, L.; Ganem, D. Kaposi's sarcoma-associated herpesvirus encodes two proteins that block cell surface display of MHC class I chains by enhancing their endocytosis. *Proc. Natl. Acad. Sci. USA* **2000**, *97*, 8051–8056. [[CrossRef](#)] [[PubMed](#)]
112. Ishido, S.; Wang, C.; Lee, B.S.; Cohen, G.B.; Jung, J.U. Downregulation of major histocompatibility complex class I molecules by Kaposi's sarcoma-associated herpesvirus K3 and K5 proteins. *J. Virol.* **2000**, *74*, 5300–5309. [[CrossRef](#)] [[PubMed](#)]
113. Wang, X.; Lybarger, L.; Connors, R.; Harris, M.R.; Hansen, T.H. Model for the interaction of gammaherpesvirus 68 RING-CH finger protein mK3 with major histocompatibility complex class I and the peptide-loading complex. *J. Virol.* **2004**, *78*, 8673–8686. [[CrossRef](#)]
114. Caselli, E.; Rizzo, R.; Ingianni, A.; Contini, P.; Pompei, R.; Di Luca, D. High prevalence of HHV8 infection and specific killer cell immunoglobulin-like receptors allotypes in Sardinian patients with type 2 diabetes mellitus. *J. Med. Virol.* **2014**, *86*, 1745–1751. [[CrossRef](#)]
115. Borghi, A.; D'Accolti, M.; Rizzo, R.; Virgili, A.; Di Luca, D.; Corazza, M.; Caselli, E. High prevalence of specific KIR types in patients with HHV-8 positive cutaneous vascular lesions: A possible predisposing factor? *Arch. Dermatol. Res.* **2016**, *308*, 373–377. [[CrossRef](#)]
116. Guerini, F.R.; Mancuso, R.; Agostini, S.; Agliardi, C.; Zanzottera, M.; Hernis, A.; Turlaki, A.; Calvo, M.G.; Bellinvia, M.; Brambilla, L.; et al. Activating KIR/HLA complexes in classic Kaposi's Sarcoma. *Infect. Agent. Cancer* **2012**, *7*, 9. [[CrossRef](#)]
117. Eimer, W.A.; Vijaya Kumar, D.K.; Navalpur Shanmugam, N.K.; Rodriguez, A.S.; Mitchell, T.; Washicosky, K.J.; Gyorgy, B.; Breakefield, X.O.; Tanzi, R.E.; Moir, R.D. Alzheimer's disease-associated beta-amyloid is rapidly seeded by herpesviridae to protect against brain infection. *Neuron* **2018**, *99*, 56–63. [[CrossRef](#)]
118. Rizzo, R.; Bortolotti, D.; Gentili, V.; Rotola, A.; Bolzani, S.; Caselli, E.; Tola, M.R.; Di Luca, D. KIR2DS2/KIR2DL2/HLA-C1 Haplotype is associated with Alzheimer's disease: Implication for the role of herpesvirus infections. *J. Alzheimers Dis.* **2019**, *67*, 1379–1389. [[CrossRef](#)] [[PubMed](#)]
119. Machado-Sulbaran, A.C.; Ramirez-Duenas, M.G.; Navarro-Zarza, J.E.; Munoz-Valle, J.F.; Mendoza-Carrera, F.; Banos-Hernandez, C.J.; Parra-Rojas, I.; Montoya-Buelna, M.; Sanchez-Hernandez, P.E. KIR/HLA gene profile implication in systemic sclerosis patients from Mexico. *J. Immunol. Res.* **2019**, *2019*, 6808061. [[CrossRef](#)] [[PubMed](#)]
120. Ben Fredj, N.; Rizzo, R.; Bortolotti, D.; Nefzi, F.; Chebel, S.; Rotola, A.; Frih-Ayed, M.; Di Luca, D.; Aouni, M. Evaluation of the implication of KIR2DL2 receptor in multiple sclerosis and herpesvirus susceptibility. *J. Neuroimmunol.* **2014**, *271*, 30–35. [[CrossRef](#)] [[PubMed](#)]
121. Bortolotti, D.; Gentili, V.; Santi, E.; Taliento, C.; Vitagliano, A.; Schiuma, G.; Beltrami, S.; Rizzo, S.; Lanza, G.; Rizzo, R.; et al. Late-onset intrauterine growth restriction and HHV-6 infection: A pilot study. *J. Med. Virol.* **2021**. [[CrossRef](#)] [[PubMed](#)]
122. Rizzo, R.; D'Accolti, M.; Bortolotti, D.; Caccuri, F.; Caruso, A.; Di Luca, D.; Caselli, E. Human herpesvirus 6A and 6B inhibit in vitro angiogenesis by induction of human leukocyte antigen G. *Sci. Rep.* **2018**, *8*, 17683. [[CrossRef](#)] [[PubMed](#)]
123. Komaroff, A.L.; Rizzo, R.; Ecker, J.L. Human herpesviruses 6A and 6B in reproductive diseases. *Front. Immunol.* **2021**, *12*, 648945. [[CrossRef](#)]
124. Caselli, E.; Bortolotti, D.; Marci, R.; Rotola, A.; Gentili, V.; Soffritti, I.; D'Accolti, M.; Lo Monte, G.; Siculo, M.; Barao, I.; et al. HHV-6A infection of endometrial epithelial cells induces increased endometrial NK cell-mediated cytotoxicity. *Front. Microbiol.*

125. Marci, R.; Gentili, V.; Bortolotti, D.; Lo Monte, G.; Caselli, E.; Bolzani, S.; Rotola, A.; Di Luca, D.; Rizzo, R. Presence of HHV-6A in endometrial epithelial cells from women with primary unexplained infertility. *PLoS ONE* **2016**, *11*, e0158304. [[CrossRef](#)] [[PubMed](#)]
126. Pegoraro, A.; Bortolotti, D.; Marci, R.; Caselli, E.; Falzoni, S.; De Marchi, E.; Di Virgilio, F.; Rizzo, R.; Adinolfi, E. The P2X7 receptor 489C>T gain of function polymorphism favors HHV-6A infection and associates with female idiopathic infertility. *Front. Pharmacol.* **2020**, *11*, 96. [[CrossRef](#)] [[PubMed](#)]
127. Rizzo, R.; Lo Monte, G.; Bortolotti, D.; Graziano, A.; Gentili, V.; Di Luca, D.; Marci, R. Impact of soluble HLA-G levels and endometrial NK cells in uterine flushing samples from primary and secondary unexplained infertile women. *Int. J. Mol. Sci.* **2015**, *16*, 5510–5516. [[CrossRef](#)]
128. Djulejic, E.; Petlickovski, A.; Trajkov, D.; Dimitrov, G.; Alabakovska, S. KIR Gene Frequencies in Women with Infertility Problems. *South East Eur. J. Immunol.* **2015**, *2015*, 1–5. [[CrossRef](#)]
129. El Borai, N.; Inoue, M.; Lefevre, C.; Naumova, E.N.; Sato, B.; Yamamura, M. Detection of herpes simplex DNA in semen and menstrual blood of individuals attending an infertility clinic. *J. Obstet. Gynaecol. Res.* **1997**, *23*, 17–24. [[CrossRef](#)]
130. Gimenes, F.; Souza, R.P.; Bento, J.C.; Teixeira, J.J.; Maria-Engler, S.S.; Bonini, M.G.; Consolaro, M.E. Male infertility: A public health issue caused by sexually transmitted pathogens. *Nat. Rev. Urol.* **2014**, *11*, 672–687. [[CrossRef](#)]
131. Apps, R.; Qi, Y.; Carlson, J.M.; Chen, H.; Gao, X.; Thomas, R.; Yuki, Y.; Del Prete, G.Q.; Goulder, P.; Brumme, Z.L.; et al. Influence of HLA-C expression level on HIV control. *Science* **2013**, *340*, 87–91. [[CrossRef](#)] [[PubMed](#)]
132. Le Gall, S.; Erdtmann, L.; Benichou, S.; Berlioz-Torrent, C.; Liu, L.; Benarous, R.; Heard, J.M.; Schwartz, O. Nef interacts with the mu subunit of clathrin adaptor complexes and reveals a cryptic sorting signal in MHC I molecules. *Immunity* **1998**, *8*, 483–495. [[CrossRef](#)]
133. Cohen, G.B.; Gandhi, R.T.; Davis, D.M.; Mandelboim, O.; Chen, B.K.; Strominger, J.L.; Baltimore, D. The selective downregulation of class I major histocompatibility complex proteins by HIV-1 protects HIV-infected cells from NK cells. *Immunity* **1999**, *10*, 661–671. [[CrossRef](#)]
134. Fadda, L.; Korner, C.; Kumar, S.; van Teijlingen, N.H.; Piechocka-Trocha, A.; Carrington, M.; Altfeld, M. HLA-Cw*0102-restricted HIV-1 p24 epitope variants can modulate the binding of the inhibitory KIR2DL2 receptor and primary NK cell function. *PLoS Pathog.* **2012**, *8*, e1002805. [[CrossRef](#)] [[PubMed](#)]
135. Parolini, F.; Biswas, P.; Serena, M.; Sironi, F.; Muraro, V.; Guizzardi, E.; Cazzoletti, L.; Scupoli, M.T.; Gibellini, D.; Ugolotti, E.; et al. Stability and expression levels of HLA-C on the cell membrane modulate HIV-1 infectivity. *J. Virol.* **2018**, *92*, e01711–e01717. [[CrossRef](#)] [[PubMed](#)]
136. Serena, M.; Parolini, F.; Biswas, P.; Sironi, F.; Blanco Miranda, A.; Zoratti, E.; Scupoli, M.T.; Ziglio, S.; Valenzuela-Fernandez, A.; Gibellini, D.; et al. HIV-1 Env associates with HLA-C free-chains at the cell membrane modulating viral infectivity. *Sci. Rep.* **2017**, *7*, 40037. [[CrossRef](#)]
137. Long, B.R.; Ndhlovu, L.C.; Oksenberg, J.R.; Lanier, L.L.; Hecht, F.M.; Nixon, D.F.; Barbour, J.D. Conferral of enhanced natural killer cell function by KIR3DS1 in early human immunodeficiency virus type 1 infection. *J. Virol.* **2008**, *82*, 4785–4792. [[CrossRef](#)]
138. Omosun, Y.O.; Blackstock, A.J.; Williamson, J.; van Eijk, A.M.; Ayisi, J.; Otieno, J.; Lal, R.B.; Ter Kuile, F.O.; Slutsker, L.; Shi, Y.P. Association of maternal KIR gene content polymorphisms with reduction in perinatal transmission of HIV-1. *PLoS ONE* **2018**, *13*, e0191733. [[CrossRef](#)]
139. Sorgho, P.A.; Djigma, F.W.; Martinson, J.J.; Yonli, A.T.; Nagalo, B.M.; Compaore, T.R.; Diarra, B.; Sombie, H.K.; Simpore, A.; Zongo, A.W.; et al. Role of killer cell immunoglobulin-like receptors (KIR) genes in stages of HIV-1 infection among patients from Burkina Faso. *Biomol. Concepts* **2019**, *10*, 226–236. [[CrossRef](#)]
140. Paximadis, M.; Minevich, G.; Winchester, R.; Schramm, D.B.; Gray, G.E.; Sherman, G.G.; Coovadia, A.H.; Kuhn, L.; Tiemessen, C.T. KIR-HLA and maternal-infant HIV-1 transmission in sub-Saharan Africa. *PLoS ONE* **2011**, *6*, e16541. [[CrossRef](#)]
141. Martin, M.P.; Gao, X.; Lee, J.-H.; Nelson, G.W.; Detels, R.; Goedert, J.J.; Buchbinder, S.; Hoots, K.; Vlahov, D.; Trowsdale, J. Epistatic interaction between KIR3DS1 and HLA-B delays the progression to AIDS. *Nat. Genet.* **2002**, *31*, 429–434. [[CrossRef](#)]
142. Khakoo, S.I.; Carrington, M. KIR and disease: A model system or system of models? *Immunol. Rev.* **2006**, *214*, 186–201. [[CrossRef](#)] [[PubMed](#)]
143. Ravet, S.; Scott-Algara, D.; Bonnet, E.; Tran, H.K.; Tran, T.; Nguyen, N.; Truong, L.X.; Theodorou, I.; Barre-Sinoussi, F.; Pancino, G.; et al. Distinctive NK-cell receptor repertoires sustain high-level constitutive NK-cell activation in HIV-exposed uninfected individuals. *Blood* **2007**, *109*, 4296–4305. [[CrossRef](#)] [[PubMed](#)]
144. Boulet, S.; Sharafi, S.; Simic, N.; Bruneau, J.; Routy, J.P.; Tsoukas, C.M.; Bernard, N.F. Increased proportion of KIR3DS1 homozygotes in HIV-exposed uninfected individuals. *AIDS* **2008**, *22*, 595–599. [[CrossRef](#)]
145. Shah-Hosseini, A.; Jafari, M.; Mohammadi, A.; Sanaei, R.; Alavian, S.M.; Doosti-Irani, A.; Nooradeh Keykavousi, M.; Tajik, N. The impact of KIR-HLA genotype on hepatitis B virus clearance in Iranian infected individuals. *Med. Microbiol. Immunol.* **2017**, *206*, 463–470. [[CrossRef](#)] [[PubMed](#)]
146. Jamil, K.M.; Khakoo, S.I. KIR/HLA interactions and pathogen immunity. *J. Biomed. Biotechnol.* **2011**, *2011*, 298348. [[CrossRef](#)] [[PubMed](#)]
147. Di Bona, D.; Aiello, A.; Colomba, C.; Bilancia, M.; Accardi, G.; Rubino, R.; Giannitrapani, L.; Tuttolomondo, A.; Cascio, A.; Caiaffa, M.F.; et al. KIR2DL3 and the KIR ligand groups HLA-A-Bw4 and HLA-C2 predict the outcome of hepatitis B virus infection. *J. Viral Hepat.* **2017**, *24*, 768–775. [[CrossRef](#)]

148. Lu, Z.; Zhang, B.; Chen, S.; Gai, Z.; Feng, Z.; Liu, X.; Liu, Y.; Wen, X.; Li, L.; Jiao, Y.; et al. Association of KIR genotypes and haplotypes with susceptibility to chronic hepatitis B virus infection in Chinese Han population. *Cell. Mol. Immunol.* **2008**, *5*, 457–463. [[CrossRef](#)]
149. Kibar, F.; Goruroglu Ozturk, O.; Ulu, A.; Erken, E.; Inal, S.; Dinkci, S.; Kurtaran, B.; Tasova, Y.; Aksu, H.S.; Yaman, A. Role of KIR genes and genotypes in susceptibility to or protection against hepatitis B virus infection in a Turkish cohort. *Med. Sci. Monit.* **2014**, *20*, 28–34. [[CrossRef](#)] [[PubMed](#)]
150. Pan, N.; Jiang, W.; Sun, H.; Miao, F.; Qiu, J.; Jin, H.; Xu, J.; Shi, Q.; Xie, W.; Zhang, J. KIR and HLA loci are associated with hepatocellular carcinoma development in patients with hepatitis B virus infection: A case-control study. *PLoS ONE* **2011**, *6*, e25682. [[CrossRef](#)] [[PubMed](#)]
151. Suppiah, V.; Gaudieri, S.; Armstrong, N.J.; O'Connor, K.S.; Berg, T.; Weltman, M.; Abate, M.L.; Spengler, U.; Bassendine, M.; Dore, G.J.; et al. IL28B, HLA-C, and KIR variants additively predict response to therapy in chronic hepatitis C virus infection in a European Cohort: A cross-sectional study. *PLoS Med.* **2011**, *8*, e1001092. [[CrossRef](#)] [[PubMed](#)]
152. Golden-Mason, L.; Bambha, K.M.; Cheng, L.; Howell, C.D.; Taylor, M.W.; Clark, P.J.; Afdhal, N.; Rosen, H.R.; Virahep, C.S.G. Natural killer inhibitory receptor expression associated with treatment failure and interleukin-28B genotype in patients with chronic hepatitis C. *Hepatology* **2011**, *54*, 1559–1569. [[CrossRef](#)]
153. Lunemann, S.; Martrus, G.; Holzemer, A.; Chapel, A.; Ziegler, M.; Korner, C.; Garcia Beltran, W.; Carrington, M.; Wedemeyer, H.; Altfeld, M. Sequence variations in HCV core-derived epitopes alter binding of KIR2DL3 to HLA-C *03:04 and modulate NK cell function. *J. Hepatol.* **2016**, *65*, 252–258. [[CrossRef](#)]
154. Schneidewind, A.; Brockman, M.A.; Yang, R.; Adam, R.I.; Li, B.; Le Gall, S.; Rinaldo, C.R.; Craggs, S.L.; Allgaier, R.L.; Power, K.A.; et al. Escape from the dominant HLA-B27-restricted cytotoxic T-lymphocyte response in Gag is associated with a dramatic reduction in human immunodeficiency virus type 1 replication. *J. Virol.* **2007**, *81*, 12382–12393. [[CrossRef](#)]
155. Marcilla, M.; Lopez de Castro, J.A. Peptides: The cornerstone of HLA-B27 biology and pathogenetic role in spondyloarthritis. *Tissue Antigens* **2008**, *71*, 495–506. [[CrossRef](#)]
156. Stewart-Jones, G.B.; di Gleria, K.; Kollnberger, S.; McMichael, A.J.; Jones, E.Y.; Bowness, P. Crystal structures and KIR3DL1 recognition of three immunodominant viral peptides complexed to HLA-B*2705. *Eur. J. Immunol.* **2005**, *35*, 341–351. [[CrossRef](#)]
157. Oliviero, B.; Varchetta, S.; Paudice, E.; Michelone, G.; Zaramella, M.; Mavilio, D.; De Filippi, F.; Bruno, S.; Mondelli, M.U. Natural killer cell functional dichotomy in chronic hepatitis B and chronic hepatitis C virus infections. *Gastroenterology* **2009**, *137*, 1151–1160. [[CrossRef](#)]
158. Njiomegnie, G.F.; Read, S.A.; Fewings, N.; George, J.; McKay, F.; Ahlenstiel, G. Immunomodulation of the natural killer cell phenotype and response during HCV infection. *J. Clin. Med.* **2020**, *9*, 1030. [[CrossRef](#)] [[PubMed](#)]
159. De Re, V.; Caggiari, L.; De Zorzi, M.; Repetto, O.; Zignego, A.L.; Izzo, F.; Tornesello, M.L.; Buonaguro, F.M.; Mangia, A.; Sansonno, D.; et al. Genetic diversity of the KIR/HLA system and susceptibility to hepatitis C virus-related diseases. *PLoS ONE* **2015**, *10*, e0117420. [[CrossRef](#)]
160. Knapp, S.; Warshow, U.; Hegazy, D.; Brackenbury, L.; Guha, I.N.; Fowell, A.; Little, A.M.; Alexander, G.J.; Rosenberg, W.M.; Cramp, M.E.; et al. Consistent beneficial effects of killer cell immunoglobulin-like receptor 2DL3 and group 1 human leukocyte antigen-C following exposure to hepatitis C virus. *Hepatology* **2010**, *51*, 1168–1175. [[CrossRef](#)] [[PubMed](#)]
161. Ahlenstiel, G.; Martin, M.P.; Gao, X.; Carrington, M.; Rehermann, B. Distinct KIR/HLA compound genotypes affect the kinetics of human antiviral natural killer cell responses. *J. Clin. Investig.* **2008**, *118*, 1017–1026. [[CrossRef](#)]
162. Qin, H.; Wang, Z.; Du, W.; Lee, W.H.; Wu, X.; Riggs, A.D.; Liu, C.P. Killer cell Ig-like receptor (KIR) 3DL1 down-regulation enhances inhibition of type 1 diabetes by autoantigen-specific regulatory T cells. *Proc. Natl. Acad. Sci. USA* **2011**, *108*, 2016–2021. [[CrossRef](#)] [[PubMed](#)]
163. Weider, T.; Richardson, S.J.; Morgan, N.G.; Paulsen, T.H.; Dahl-Jorgensen, K.; Hammerstad, S.S. Upregulation of HLA class I and antiviral tissue responses in Hashimoto's thyroiditis. *Thyroid* **2020**, *30*, 432–442. [[CrossRef](#)]
164. Aslanidis, S.; Pырpasopoulou, A.; Kontotasios, K.; Doumas, S.; Zamboulis, C. Parvovirus B19 infection and systemic lupus erythematosus: Activation of an aberrant pathway? *Eur. J. Intern. Med.* **2008**, *19*, 314–318. [[CrossRef](#)] [[PubMed](#)]
165. Gasser, S.; Raulet, D. The DNA damage response, immunity and cancer. In *Seminars in Cancer Biology*; Academic Press: Cambridge, MA, USA, 2006; pp. 344–347.
166. Rizzo, R.; Gentili, V.; Rotola, A.; Bortolotti, D.; Cassai, E.; Di Luca, D. Implication of HLA-C and KIR alleles in human papillomavirus infection and associated cervical lesions. *Viral Immunol.* **2014**, *27*, 468–470. [[CrossRef](#)]
167. Kollnberger, S.; Bird, L.; Sun, M.Y.; Retiere, C.; Braud, V.M.; McMichael, A.; Bowness, P. Cell-surface expression and immune receptor recognition of HLA-B27 homodimers. *Arthritis Rheum.* **2002**, *46*, 2972–2982. [[CrossRef](#)]
168. Garcia-Beltran, W.F.; Holzemer, A.; Martrus, G.; Chung, A.W.; Pacheco, Y.; Simoneau, C.R.; Rucevic, M.; Lamothe-Molina, P.A.; Pertel, T.; Kim, T.E.; et al. Open conformers of HLA-F are high-affinity ligands of the activating NK-cell receptor KIR3DS1. *Nat. Immunol.* **2016**, *17*, 1067–1074. [[CrossRef](#)]
169. Burian, A.; Wang, K.L.; Finton, K.A.; Lee, N.; Ishitani, A.; Strong, R.K.; Geraghty, D.E. HLA-F and MHC-I open conformers bind natural killer cell Ig-like receptor KIR3DS1. *PLoS ONE* **2016**, *11*, e0163297. [[CrossRef](#)]
170. Cook, M.; Briggs, D.; Craddock, C.; Mahendra, P.; Milligan, D.; Fegan, C.; Darbyshire, P.; Lawson, S.; Boxall, E.; Moss, P. Donor KIR genotype has a major influence on the rate of cytomegalovirus reactivation following T-cell replete stem cell transplantation. *Blood* **2006**, *107*, 1230–1232. [[CrossRef](#)] [[PubMed](#)]

171. Agrawal, S.; Prakash, S. Significance of KIR like natural killer cell receptors in autoimmune disorders. *Clin. Immunol.* **2020**, *216*, 108449. [[CrossRef](#)] [[PubMed](#)]
172. Hou, Y.; Zhang, C.; Xu, D.; Sun, H. Association of killer cell immunoglobulin-like receptor and human leucocyte antigen-C w gene combinations with systemic lupus erythematosus. *Clin. Exp. Immunol.* **2015**, *180*, 250–254. [[CrossRef](#)]
173. Beck, S.; Barrell, B.G. Human cytomegalovirus encodes a glycoprotein homologous to MHC class-I antigens. *Nature* **1988**, *331*, 269–272. [[CrossRef](#)] [[PubMed](#)]
174. Rizzo, R. Controversial role of herpesviruses in Alzheimer’s disease. *PLoS Pathog.* **2020**, *16*, e1008575. [[CrossRef](#)]
175. Itzhaki, R.F. Herpes simplex virus type 1 and Alzheimer’s disease: Increasing evidence for a major role of the virus. *Front. Aging Neurosci.* **2014**, *6*, 202. [[CrossRef](#)]
176. Readhead, B.; Haure-Mirande, J.V.; Funk, C.C.; Richards, M.A.; Shannon, P.; Haroutunian, V.; Sano, M.; Liang, W.S.; Beckmann, N.D.; Price, N.D.; et al. Multiscale analysis of independent Alzheimer’s cohorts finds disruption of molecular, genetic, and clinical networks by human herpesvirus. *Neuron* **2018**, *99*, 64–82.e67. [[CrossRef](#)]
177. Challoner, P.B.; Smith, K.T.; Parker, J.D.; MacLeod, D.L.; Coulter, S.N.; Rose, T.M.; Schultz, E.R.; Bennett, J.L.; Garber, R.L.; Chang, M.; et al. Plaque-associated expression of human herpesvirus 6 in multiple sclerosis. *Proc. Natl. Acad. Sci. USA* **1995**, *92*, 7440–7444. [[CrossRef](#)]
178. Alvarez-Lafuente, R.; De las Heras, V.; Bartolome, M.; Picazo, J.J.; Arroyo, R. Relapsing-remitting multiple sclerosis and human herpesvirus 6 active infection. *Arch. Neurol.* **2004**, *61*, 1523–1527. [[CrossRef](#)]
179. Gómez-Lozano, N.; de Pablo, R.; Puente, S.; Vilches, C. Recognition of HLA-G by the NK cell receptor KIR2DL4 is not essential for human reproduction. *Eur. J. Immunol.* **2003**, *33*, 639–644. [[CrossRef](#)]
180. Boulet, S.; Kleyman, M.; Kim, J.Y.; Kanya, P.; Sharafi, S.; Simic, N.; Bruneau, J.; Routy, J.P.; Tsoukas, C.M.; Bernard, N.F. A combined genotype of KIR3DL1 high expressing alleles and HLA-B*57 is associated with a reduced risk of HIV infection. *AIDS* **2008**, *22*, 1487–1491. [[CrossRef](#)] [[PubMed](#)]
181. Jennes, W.; Verheyden, S.; Demanet, C.; Menten, J.; Vuylsteke, B.; Nkengasong, J.N.; Kestens, L. Low CD4+ T cell counts among African HIV-1 infected subjects with group B KIR haplotypes in the absence of specific inhibitory KIR ligands. *PLoS ONE* **2011**, *6*, e17043. [[CrossRef](#)] [[PubMed](#)]
182. Roeth, J.F.; Williams, M.; Kasper, M.R.; Filzen, T.M.; Collins, K.L. HIV-1 Nef disrupts MHC-I trafficking by recruiting AP-1 to the MHC-I cytoplasmic tail. *J. Cell Biol.* **2004**, *167*, 903–913. [[CrossRef](#)]
183. Wonderlich, E.R.; Williams, M.; Collins, K.L. The tyrosine binding pocket in the adaptor protein 1 (AP-1) mu1 subunit is necessary for Nef to recruit AP-1 to the major histocompatibility complex class I cytoplasmic tail. *J. Biol. Chem.* **2008**, *283*, 3011–3022. [[CrossRef](#)]
184. Vidricaire, G.; Imbeault, M.; Tremblay, M.J. Endocytic host cell machinery plays a dominant role in intracellular trafficking of incoming human immunodeficiency virus type 1 in human placental trophoblasts. *J. Virol.* **2004**, *78*, 11904–11915. [[CrossRef](#)] [[PubMed](#)]
185. Martin, M.P.; Qi, Y.; Gao, X.; Yamada, E.; Martin, J.N.; Pereyra, F.; Colombo, S.; Brown, E.E.; Shupert, W.L.; Phair, J.; et al. Innate partnership of HLA-B and KIR3DL1 subtypes against HIV-1. *Nat. Genet.* **2007**, *39*, 733–740. [[CrossRef](#)]
186. Qi, Y.; Martin, M.P.; Gao, X.; Jacobson, L.; Goedert, J.J.; Buchbinder, S.; Kirk, G.D.; O’Brien, S.J.; Trowsdale, J.; Carrington, M. KIR/HLA pleiotropism: Protection against both HIV and opportunistic infections. *PLoS Pathog.* **2006**, *2*, 741–745. [[CrossRef](#)]
187. Singh, R.; Kaul, R.; Kaul, A.; Khan, K. A comparative review of HLA associations with hepatitis B and C viral infections across global populations. *World J. Gastroenterol.* **2007**, *13*, 1770–1787. [[CrossRef](#)] [[PubMed](#)]
188. Blackwell, J.M.; Jamieson, S.E.; Burgner, D. HLA and infectious diseases. *Clin. Microbiol. Rev.* **2009**, *22*, 370–385. [[CrossRef](#)] [[PubMed](#)]
189. Chen, Y.; Wei, H.; Gao, B.; Hu, Z.; Zheng, S.; Tian, Z. Activation and function of hepatic NK cells in hepatitis B infection: An underinvestigated innate immune response. *J. Viral Hepat.* **2005**, *12*, 38–45. [[CrossRef](#)] [[PubMed](#)]
190. Burt, B.M.; Plitas, G.; Zhao, Z.; Bamboat, Z.M.; Nguyen, H.M.; Dupont, B.; DeMatteo, R.P. The lytic potential of human liver NK cells is restricted by their limited expression of inhibitory killer Ig-like receptors. *J. Immunol.* **2009**, *183*, 1789–1796. [[CrossRef](#)]
191. Crispe, I.N. The liver as a lymphoid organ. *Annu. Rev. Immunol.* **2009**, *27*, 147–163. [[CrossRef](#)]
192. Protzer, U.; Maini, M.K.; Knolle, P.A. Living in the liver: Hepatic infections. *Nat. Rev. Immunol.* **2012**, *12*, 201–213. [[CrossRef](#)] [[PubMed](#)]
193. Tu, Z.; Bozorgzadeh, A.; Pierce, R.H.; Kurtis, J.; Crispe, I.N.; Orloff, M.S. TLR-dependent cross talk between human Kupffer cells and NK cells. *J. Exp. Med.* **2008**, *205*, 233–244. [[CrossRef](#)] [[PubMed](#)]
194. Chen, Y.; Wei, H.; Sun, R.; Dong, Z.; Zhang, J.; Tian, Z. Increased susceptibility to liver injury in hepatitis B virus transgenic mice involves NKG2D-ligand interaction and natural killer cells. *Hepatology* **2007**, *46*, 706–715. [[CrossRef](#)]
195. Parham, P.; Abi-Rached, L.; Matevosyan, L.; Moesta, A.K.; Norman, P.J.; Older Aguilar, A.M.; Guethlein, L.A. Primate-specific regulation of natural killer cells. *J. Med. Primatol.* **2010**, *39*, 194–212. [[CrossRef](#)] [[PubMed](#)]
196. Ursu, L.D.; Calenic, B.; Diculescu, M.; Dima, A.; Stoian, I.T.; Constantinescu, I. Clinical and histopathological changes in different KIR gene profiles in chronic HCV Romanian patients. *Int. J. Immunogenet.* **2021**, *48*, 16–24. [[CrossRef](#)] [[PubMed](#)]
197. Larkin, J.; Bost, A.; Glass, J.L.; Tan, S.L. Cytokine-activated natural killer cells exert direct killing of hepatoma cells harboring hepatitis C virus replicons. *J. Interferon Cytokine Res.* **2006**, *26*, 854–865. [[CrossRef](#)] [[PubMed](#)]

198. Stegmann, K.A.; Bjorkstrom, N.K.; Veber, H.; Ciesek, S.; Riese, P.; Wiegand, J.; Hadem, J.; Suneetha, P.V.; Jaroszewicz, J.; Wang, C.; et al. Interferon-alpha-induced TRAIL on natural killer cells is associated with control of hepatitis C virus infection. *Gastroenterology* **2010**, *138*, 1885–1897. [[CrossRef](#)] [[PubMed](#)]
199. Nitschke, K.; Barriga, A.; Schmidt, J.; Timm, J.; Viazov, S.; Kuntzen, T.; Kim, A.Y.; Lauer, G.M.; Allen, T.M.; Gaudieri, S.; et al. HLA-B*27 subtype specificity determines targeting and viral evolution of a hepatitis C virus-specific CD8+ T cell epitope. *J. Hepatol.* **2014**, *60*, 22–29. [[CrossRef](#)] [[PubMed](#)]
200. Hausen, H.z. Papillomavirus infections—a major cause of human cancers. *Biochim. Biophys. Acta Rev. Cancer* **1996**, *1288*, F55–F78. [[CrossRef](#)]

Despite the role of KIRs in regulate NK cells activation, another important mechanism that affect NK cell function involves the presence of the non-classical HLA-E molecule and its interaction with specific NK receptors [347].

In particular, NK cell anergy observed in severe COVID-19 has been reported to involve the expression of the inhibitory CD94/NK group 2 member A (NKG2A) receptor, a heterodimeric inhibitory receptor that binds HLA-E [349], suppressing NK cell cytotoxicity and secretion [350] as supported by the study of Zheng et al., reporting NKG2A significant overexpression in COVID-19 NK cells [335].

Basing on this evidence, we evaluated the mechanisms exploited by SARS-CoV-2 in affecting NK cell functions ([348], paper attached). We found that the intracellular expression of SARS-CoV-2 S Protein S1 (SP1) in lung epithelial cells resulted in NK cell-reduced degranulation, in concomitance with increased expression of the inhibitory NKG2A/CD94 receptor and HLA-E up-regulation and stabilization on lung epithelial cells ([348], paper attached). Thus, our study supported a role for HLA-E and NKG2A in NK cell anergy observed in COVID-19 condition, directly caused by SP1, validating the importance of NK cells depletion in COVID-19 immunopathogenesis.



Article

SARS-CoV-2 Spike 1 Protein Controls Natural Killer Cell Activation via the HLA-E/NKG2A Pathway

Daria Bortolotti [†] , Valentina Gentili [†] , Sabrina Rizzo, Antonella Rotola and Roberta Rizzo ^{*}

Department of Chemical and Pharmaceutical Science, University of Ferrara, 44121 Ferrara, Italy; daria.bortolotti@unife.it (D.B.); valentina.gentili@unife.it (V.G.); sabrina.rizzo@unife.it (S.R.); antonella.rotola@unife.it (A.R.)

* Correspondence: rbr@unife.it; Tel.: +39-0532-455382

† These authors contributed equally to this work.

Received: 7 August 2020; Accepted: 21 August 2020; Published: 26 August 2020



Abstract: Natural killer cells are important in the control of viral infections. However, the role of NK cells during severe acute respiratory syndrome coronavirus 2 (SARS-CoV-2) infection has previously not been identified. Peripheral blood NK cells from SARS-CoV and SARS-CoV-2 naïve subjects were evaluated for their activation, degranulation, and interferon-gamma expression in the presence of SARS-CoV and SARS-CoV-2 spike proteins. K562 and lung epithelial cells were transfected with spike proteins and co-cultured with NK cells. The analysis was performed by flow cytometry and immune fluorescence. SARS-CoV and SARS-CoV-2 spike proteins did not alter NK cell activation in a K562 in vitro model. On the contrary, SARS-CoV-2 spike 1 protein (SP1) intracellular expression by lung epithelial cells resulted in NK cell-reduced degranulation. Further experiments revealed a concomitant induction of HLA-E expression on the surface of lung epithelial cells and the recognition of an SP1-derived HLA-E-binding peptide. Simultaneously, there was increased modulation of the inhibitory receptor NKG2A/CD94 on NK cells when SP1 was expressed in lung epithelial cells. We ruled out the GATA3 transcription factor as being responsible for HLA-E increased levels and HLA-E/NKG2A interaction as implicated in NK cell exhaustion. We show for the first time that NK cells are affected by SP1 expression in lung epithelial cells via HLA-E/NKG2A interaction. The resulting NK cells' exhaustion might contribute to immunopathogenesis in SARS-CoV-2 infection.

Keywords: SARS-CoV-2; NK cell; NKG2A; HLA-E

1. Introduction

In December 2019, a novel coronavirus was isolated in Wuhan, China [1]. The severe acute respiratory syndrome coronavirus 2 (SARS-CoV-2) was the causative agent for coronavirus disease 2019 (COVID-19). SARS-CoV-2 is a β -coronavirus with a 79.5% sequence homology with SARS-CoV [2,3]. The CoVs have been demonstrated to be able to adapt quickly and cross the species barrier, as happened with SARS-CoV and Middle East respiratory syndrome CoV (MERS-CoV), with resulting epidemics or pandemics. The effect of these infections on humans often leads to severe clinical symptoms and high mortality [3]. The number of SARS-CoV-2-infected cases is more than 22 million, with typical clinical manifestations including fever, cough, diarrhea, and fatigue [4].

Several studies are currently investigating the potential response of the immune system during SARS-CoV-2 infection [5]. It has already been shown that, during the infection, patients develop an uncontrolled immune response and hyperactivation of macrophages and monocytes [6]. This immune dysregulation is associated with an increase in Interleukin-6 (IL-6), neutrophils, natural killer (NK) [7] cells, and reactive protein C (PCR) and in a decrease in the total number of lymphocytes [5,8]. Interestingly, NK cells showed a functional exhaustion with increased NKG2A expression [8]. NK cells

are important effectors in antitumor and anti-infection immunity [9]. The activity of NK cells is controlled by activating and inhibitory receptors [10]. The CD94/NK group 2 member A (NKG2A) is a heterodimeric inhibitory receptor expressed by NK cells [11]. It binds to the nonclassical HLA class I molecule (HLA-E), which presents peptides derived from leader peptide sequences of other HLA class I molecules, including HLA-G [12–14]. The ligation of the peptide-loaded HLA-E with NKG2A transduces inhibitory signaling through two inhibitory immune-receptor tyrosine-based inhibition motifs, which suppress NK cytokine cytotoxicity and secretion [11,12,15,16]. By now, no data are available on how SARS-CoV-2 might control NK cells. We evaluated the possible role of SARS-CoV-2 spike proteins in modifying NK cell functions.

2. Materials and Methods

2.1. NK Cells Purification

Human primary NK cells were obtained from the peripheral blood of four healthy blood donors. This study was approved by the “Ferrara Ethics Committee”. All subjects gave written informed consent in accordance with the Declaration of Helsinki.

Primary NK cells were separated from peripheral blood samples using the negative magnetic cell separation (MACS) system (Miltenyi Biotec, Gladbach, Germany) [17]. The analysis of purified cell fraction by flow cytometry with CD3-PerCp-Cy5.5, CD56-FITC moAbs (e-Bioscience, Frankfurt, Germany), demonstrated that the NK cell content was > 90% (Figure S1A).

2.2. Viral RNA Detection

RNA extraction was performed by using the MagMAX Viral/Pathigen Nuclei Acid Isolation kit (ThermoFisher, Milano, Italy) according to the manufacturer’s instructions. The RT-PCR was performed with the TaqMan 2019nCoV assay kit v1 (ThermoFisher, Milano, Italy).

2.3. Cell Culture

NK cell were supplemented with IL-12 (10 ng/mL) (Becton Dickinson, San Jose, CA, USA) to have a positive control for IFN-gamma secretion [18].

The Beas-2B (ATCC CRL-9609) bronchial epithelial cell line was grown in BEGM culture medium (BEGM Kit Catalog No. CC-3170; Lonza/Clonetics Corporation, USA). The K562 (ATC CCL-243) lymphoblastoid cell line was cultured in Roswell Park Memorial Institute medium (RPMI) (Gibco, Milano, Italy) supplemented with 10% of FCS (fetal calf serum, Euroclone, Pero, MI, Italy) and 100 U/mL penicillin and 100 µg/mL streptomycin. Cell cultures were maintained at 37 °C in a humidified atmosphere of 5% CO₂ in air.

The role of HLA-E and NKG2A was evaluated by incubating the cells with anti-HLA-E (clone MEM-E/08, Exbio, Praha, CZ) or anti-CD94/NKG2A (clone 131411, BD, Italy) antibodies (7.5 ng/mL).

GATA3 DNA-binding activity was inhibited by adding pyrrothiogatain (cat#sc-352288A, Santa Cruz, CA, USA) to cell cultures (10 µM) [19].

2.4. Flow Cytometry

In total, 1×10^5 eNK cells were labeled with fluorophore-conjugated antibodies: CD3-PE (clone SP34-2, CD16-APC (clone B73.1), CD56-PE-Cy7 (clone B159), NKG2A-APC (clone 131411), and matched isotype controls.

In total, 5×10^5 bronchial epithelial cells were stained specific Ab HLA-I (HLA-A, -B, -C)-PE (Becton Dickinson, San Jose, CA, USA), HLA-E (clone MEM-E/08)-FITC, and matched isotype controls.

GATA3 expression was evaluated in fixed and permeabilized cells with IntraPrep reagent (Beckman Coulter; Brea, CA, USA) and stained with anti-GATA3 (BV421; BD)-PE MoAb. CK8 expression was evaluated with anti-CK8 (TS1, Novus Biologicals, Milano, Italy)-PE MoAb.

SP1, SP2, and S proteins expression in K562 and Beas-2B transfected cells were evaluated with anti-spike 1 (clone 2C1), anti-spike 2, and anti Sars-Cov spike antibodies (myBiosource, San Diego, CA, USA).

Data were analyzed using FACS CantoII flow cytometer (BD, Milan, Italy) and FlowJo LLC analysis software (Tree Star Inc, Ashland, OR, USA). In total, 10,000 events were acquired.

2.5. Immunofluorescence Assay

HLA-E expression was analyzed by immunofluorescence with anti-HLA-E-PE antibody (MEM-E/08-PE), as previously described [20,21]. In particular, 10^5 cells were spotted onto glass slides and fixed by cold acetone for 30 min at 20 °C. Slides were air-dried and kept at 20 °C until use. For assay, slides were rehydrated by washings in PBS, and incubated with anti HLA-E-PE-labelled antibody diluted 1:100 in PBS for 35 min at 37 °C in a humidified chamber. Slides were washed twice with PBS for 10 min, once for 1 min with tap water, and once for 1 min with distilled water. After washings as described, slides were stained with 1:2000 in PBS diluted Hoechst stock solution (ThermoFisher, Milano, Italy) for 5–10 min, washed in distilled water, and finally mounted with 50% glycerol in PBS for fluorescence microscope observation. All samples were observed under a UV light microscope (Nikon Eclipse E600) equipped with a digital camera (DMX 1200).

2.6. Cell Migration Assay

The assay was performed using the Corning Transwell System, with inserts with 5- μ m pore polycarbonate membrane. Briefly, 1×10^6 cells were seeded in the upper chamber in 150 μ L of RPMI with the 0.5% of FBS and IL-2 (100 IU/mL; Sigma Biosciences, MO, USA). The inserts containing cells were positioned into a 24-well plate, which provides the lower reservoirs for the migration system. Each reservoir was filled with 650 μ L of medium (RPMI) containing SARS-CoV-2 proteins (spike protein S1 subunit, spike protein S2 subunit) (RayBiotech, Peachtree Corners, GA, USA) or control SARS-CoV spike protein (MyBiosource, San Diego, CA, USA) at the final concentration of 100 ng/mL. Medium with CXCL12 (100 ng/mL; BioLegend, San Diego, CA, USA) [22] was used as the positive. Migration was performed for 3 h at 37 °C and then the plate was briefly centrifuged at $300 \times g$ for 5 min in order to collect migrated cells in the lower reservoir for the cell count. Every condition was tested in triplicate and results were reported as the number of migrated cells compared to untreated NK cells.

2.7. Protein Transfection

K562 or Beas-2B cell lines were transfected using the Pierce Protein Transfection Kit (ThermoFisher, Milano, Italy) following the product instructions. A total of 4×10^5 cells were transfected with 1 μ g of protein (spike protein S1 subunit, spike protein S2 subunit) of SARS-CoV-2 or SARS-CoV spike protein. Transfection was performed for 3–4 h at 37 °C in 1 mL of medium without FBS. After transfection, a volume of complete medium with 20% FBS was added to each well. K562 or Beas-2B cells treated with transfection reagent alone or transfected with 0.5 μ g of control fluorescent antibody (provided in the kit) were used as the negative and efficiency control, respectively.

2.8. Lactate Dehydrogenase (LDH) Assay

The LDH assay was performed to evaluate the effect of the transfection with SARS-CoV-2 and SARS-CoV proteins in K562 or Beas-2B cells on cell viability. Transfected K562 or Beas-2B cells were suspended at 5×10^4 cells/mL and cultured for 4 h on a 96-well microplate at 37 °C with 5% CO₂. A colorimetric-based lactate dehydrogenase (LDH) assay (Cytotoxicity Detection KitPLUS; Switzerland) was used, according to the manufacturer's instructions.

2.9. Degranulation Analysis

In vitro cytotoxicity experiments were performed using K562 or Beas-2B cells as the target and NK cells as effector cells. NK cells were added to K562 or Beas-2B cells with a 5:1 effector:target ratio [23]. NK cell degranulation was evaluated by CD107a staining (anti-CD107a-PE; clone H4A3; BD Biosciences) after 3 h of treatment with Golgi Stop solution (BD). Labeled cells were analyzed with a FACSCantoII flow cytometer (BD, Milano, Italy) and FlowJo software (Tree Star Inc., Ashland, OR, USA).

2.10. Carboxyfluorescein Diacetate Succinimidyl Ester (CFSE) Analysis

K562 or Beas-2B cells were labeled with carboxyfluorescein diacetate succinimidyl ester (CFSE) to assess cell-mediated cytotoxicity, using a 7AAD/CFSE Cell-mediated cytotoxicity assay kit (Ann Arbor, MI, USA). In total, 10^7 cells/mL were resuspended in CFSE staining solution and incubated for 15 min at 37 °C. Control target cells were resuspended in 0.1% BSA. Then, cells were washed two times with culture medium and incubated for 30 min at 37 °C. NK cells were put in co-culture with CFSE-labeled infected cells at a 1:5 ratio. The cell mixture was incubated for 4 h, centrifuged, and resuspended in 7-AAD staining solution. Control target cells were resuspended in assay buffer. Cells were incubated for 15 min in the dark at 4 °C. Then cells were centrifuged and resuspended in assay buffer. Cells were analyzed with a FACSCantoII flow cytometer and FlowJo software.

2.11. IFN- γ ELISA Assay

IFN- γ levels were detected by an IFN- γ ELISA kit (MyBiosource, San Diego, CA, USA) following the instructions. In particular, standards and samples were pipetted into the wells and IFN γ present in a sample was bound to the wells by the immobilized antibody. The wells were washed and biotinylated anti-Human IFN γ antibody was added. After washing away unbound biotinylated antibody, HRP-conjugated streptavidin was pipetted to the wells. The wells were again washed, a TMB substrate solution was added to the wells, and color developed in proportion to the amount of IFN γ bound. The Stop Solution changed the color from blue to yellow, and the intensity of the color was measured at 450 nm (ThermoFisher ELISA Reader).

2.12. Real-Time PCR

RNA extraction was performed by using the RNeasy kit (Qiagen, Hilden, Germany) according to the manufacturer's instructions. The Real-Time PCR was performed with the TaqMan 2019nCoV assay TaqMan gene expression assays for HLA- E (Hs00428366_m1), GATA3 (Hs00231122_m1), Eotaxin3 (Hs00171146_m1), and NKG2A (Hs00970273_g1) (ThermoFisher).

2.13. HLA-E Binding Prediction

The HLA-E binding prediction was made using the IEDB analysis resource ANN aka NetMHC (ver. 4.0) tool at the <http://tools.iedb.org/mhci/help/>, using the viral spike 1 protein from the SARS-CoV-2 sequence (QHO62112.1).

2.14. Statistical Analysis

Since the biological variables presented a normal distribution (Kruskal–Wallis test, $p > 0.05$), they were evaluated by Student t test by Graph Pad Prism 6 software (<https://www.graphpad.com/scientific-software/prism/>). A p -value < 0.05 was defined statistically significant.

2.15. Data Availability

All relevant data are within the manuscript.

3. Results

3.1. Spike Proteins Induce NK Cell Migration

Although the role of NK cells in the immune response towards viral infections is generally accepted, there are few data on the early NK cell trafficking in response to coronavirus infections [5]. The evaluation of NK response to SARS-CoV-2 infection is important to determining the innate immune response per se and for the cross-talk with adaptive immune cells [24]. We explored the migration, interferon-gamma (IFN-gamma) secretion, and degranulation of NK cells in the presence of spike 1 (SP1) and spike 2 (SP2) SARS-CoV-2 proteins and SARS-CoV spike proteins (S). We used a cell migration system in a 5- μ m transwells w/polycarbonate filter, without a cell barrier. We purified NK cells from the peripheral blood of control subjects (Figure S1A) negative for both SARS-CoV-2 and SARS-CoV viremia (data not shown). This condition ensured that NK cells were naïve for spike proteins. We cultured NK cells in the presence of SP1, SP2 from SARS-CoV-2, or spike protein (S) from SARS-CoV and we observed no effect on cell viability (Figure S1B). We used CXCL12 as a positive control for NK cell migration [22]. We observed an increase in NK cell migration in the presence of both SP1 and SP2 (SP1 $p = 0.021$; SP2 $p = 0.013$ Student t test) (Figure 1A). Similarly, NK cell migration was induced by the SARS-CoV S protein ($p < 0.01$; Student t test) (Figure 1A). No modifications in cell viability were observed (Figure S1B). These data suggest that both SARS-CoV-2 and SARS-CoV spike proteins are able to chemo-attract NK cells. To evaluate if spike proteins are able to also induce NK cells' activation, we analyzed the secretion of IFN-gamma. We observed an increase in IFN-gamma secretion in the presence of SP1, SP2, and S-protein ($p < 0.001$; Student t test) (Figure 1B). The basal IFN-gamma secretion might be enhanced by the IL-2 treatment of NK cells, which is necessary for the in vitro maintenance of primary NK cells.

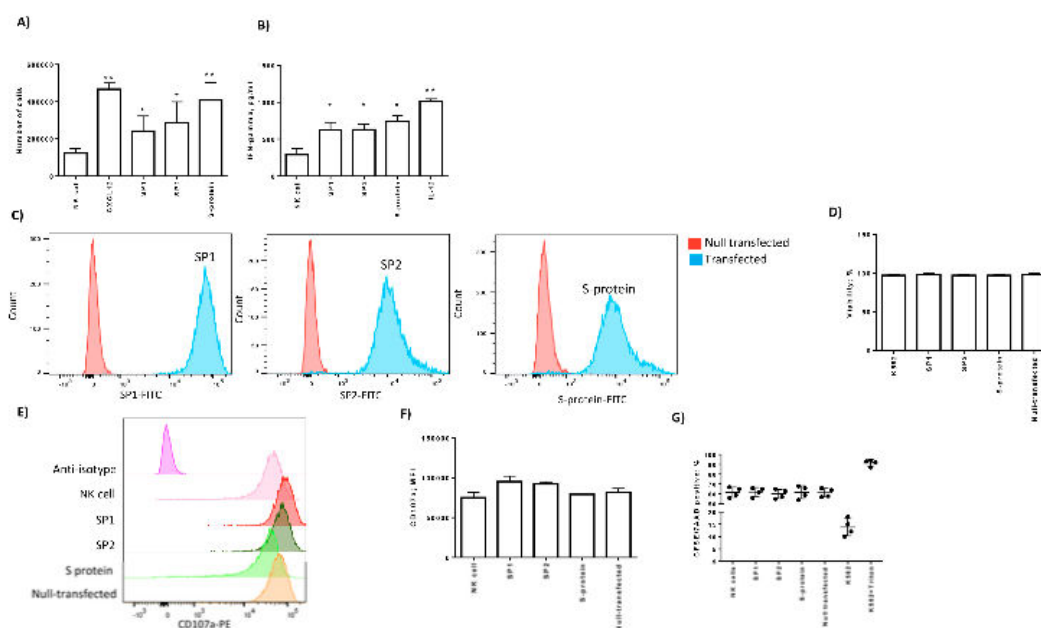


Figure 1. Peripheral blood NK cells from four control subjects negative for both SARS-CoV-2 and SARS-CoV viremia were cultured NK cells in the presence of SP1, SP2 from SARS-CoV-2, or spike protein (S) from SARS-CoV. (A) NK cell migration is reported as the cell number. We used CXCL12 as a positive control for NK cell migration. NK cells with no treatment were used as negative control (NK cells). (B) Secretion of IFN-gamma evaluated by ELISA. IL-12 treatment was used as the control of IFN-gamma secretion. (C) Representative intracellular expression of SP1, SP2, and S proteins in K562 cells after transfection. (D) K562 viability, assessed by the LDH assay, in basal and transfected conditions. The transfection with 0.5 μ g of control fluorescent antibody was used as a positive control

(null-transfected). (E) Representative histograms of NK cell degranulation towards the K562 cell target. NK cells were marked with CD56-PECy7 (see Figure S1C). The degranulation was assessed by CD107a-PE expression. (F) Mean fluorescence intensity (MFI) of CD107a-positive NK cells after the co-culture with K562 target cells. (G) CFSE+/7-AAD+ cell percentage in NK cell/K562 co-cultures. K562 alone and treated with Triton x-100 (0.8%) were used as negative and positive controls, respectively. The values are presented as mean \pm standard deviation. *, ** significant p values Student t test.

3.2. Spike Proteins Did Not Modify NK Cell Cytotoxicity

Then, we evaluated the cytotoxicity of NK cells in the presence of spike proteins, using CD107a staining, a marker of degranulation [23]. We mimicked the expression of spike proteins inside NK target cells, the K562 cell line, transfecting directly the proteins. We obtained a mean transfection efficiency of 95% for SP1, SP2, and S proteins (Figure 1C). The K562 cell viability, evaluated by the LDH assay, was not affected by protein transfection (Figure 1D). We incubated NK cells for four hours with K562 and evaluated the expression of CD107a on CD56-gated NK cells (Figure S1C). We observed an increase in CD107a staining in all the culture conditions, with no difference in the presence of SP1, SP2, and S proteins in comparison with the untreated co-culture (S1 $p = 0.078$; S2 $p = 0.087$; S $p = 0.081$; Student t test) (Figure 1E,F). To be sure that NK cells expressing CD107a were able to kill K562 cells, CFSE (carboxyfluorescein diacetate succinimidyl ester), the staining of target cells was detected by flow cytometry [20]. We observed an increase in the K562 CFSE+/7-AAD+ cell percentage in all the co-culture conditions comparable with the killing observed in the untreated co-culture ($p < 0.001$; Student t test) (Figure 1G), confirming the results observed with CD107a staining (Figure 1E,F).

3.3. SARS-CoV-2 Spike 1 Protein Modifies NK Cell Cytotoxicity When Presented by Lung Epithelial Cells

Since the target cells for SARS-CoV-2 replication are lung epithelial cells [4], we considered the activation status of NK cells in this context. We mimicked the expression of SP1, SP2, and S proteins inside Beas-2B lung epithelial cells, transfecting directly the proteins. We obtained an average 95% efficiency of transfection with all the proteins (Figure 2A). The transfection did not affect cell viability (Figure 2B) and the expression of CK8 epithelial cell markers (Figure 2A).

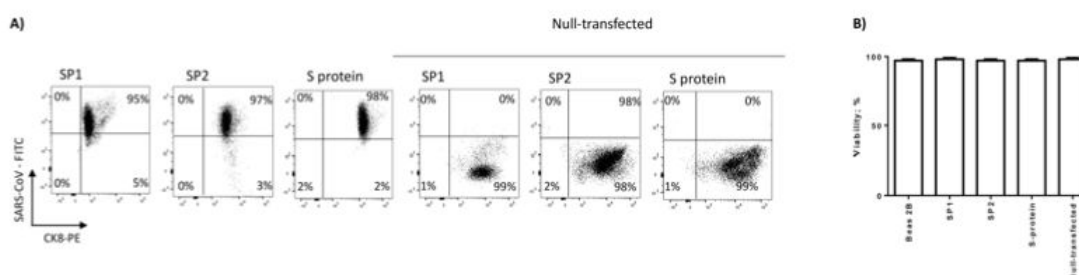


Figure 2. (A) Representative intracellular expression of SP1, SP2, and S proteins and surface expression of the epithelial marker CK8-PE in Beas-2B cells after transfection. (B) Beas-2B viability, assessed by the LDH assay, in basal and transfected conditions. The transfection with 0.5 μ g of control fluorescent antibody was used as a positive control (null-transfected). The values are presented as mean \pm standard deviation.

We incubated NK cells for four hours with lung epithelial cells and evaluated the expression of the CD107a degranulation marker. We observed a decrease in CD107a staining in the culture condition with SP1-transfected Beas-2B cells ($p < 0.001$; Student t test) (Figure 3A,B). On the contrary, we observed an increase in CD107a expression in the co-culture conditions with SP2 and S protein-transfected Beas-2B cells, which is similar to that observed with the control of the transfection condition (null-transfected) and untreated co-culture ($p = 0.079$; $p = 0.085$, respectively; Student t test) (Figure 3A,B).

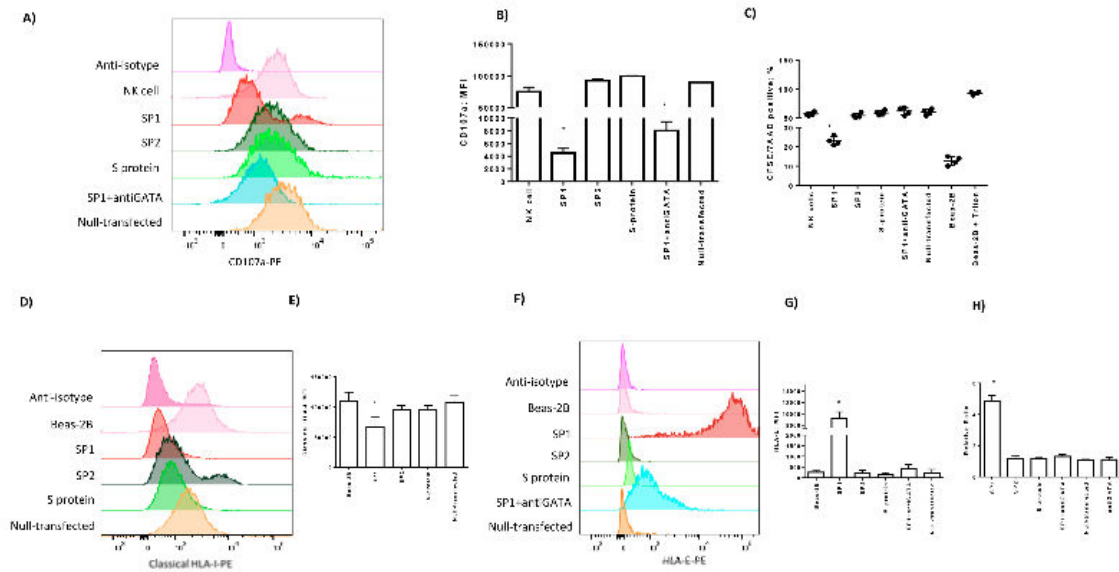


Figure 3. (A) Representative histograms of NK cell degranulation towards the Beas-2B cell target. NK cells were marked with CD56 and gated as reported in Figure S1C. The degranulation was assessed by CD107a-PE expression. Beas-2B was transfected with SP1, SP2, and S proteins or control fluorescent antibody was used as the positive control (null-transfected), or treated with GATA3 inhibitor (anti-GATA). (B) MFI of CD107a-PE-positive NK cells after the co-culture with Beas-2B cells. (C) CFSE+/7-AAD+ cell percentage in NK cell/Beas-2B co-cultures. Beas-2B alone and treated with Triton-x100 (0.8%) were used as negative and positive controls, respectively. The values are presented as mean \pm standard deviation. (D) Representative histograms of HLA-I expression on the surface of transfected Beas-2B. (E) The histograms showed the mean \pm standard deviation MFI (mean fluorescence intensity) values of HLA-I expression in three independent experiments. * significant p values Student t test; (F) Representative histograms of HLA-E expression on the surface of transfected Beas-2B cells. (G) The histograms showed the mean \pm standard deviation MFI (mean fluorescence intensity) values of HLA-E expression in three independent experiments. * significant p values t test. (H) Relative ratio of Real-Time PCR of HLA-E expression in transfected Beas-2B cells. SP1 transfected Beas-2B cells were also treated with GATA inhibitor (anti-GATA). * significant p values Student t test.

To be sure that NK cells expressing CD107a were able to kill Beas2B cells, CFSE staining of target cells was detected by flow cytometry. We observed an increase in the Beas-2B CFSE+/7-AAD+ cell percentage in the co-culture with NK cells in SP2 and S protein-transfected Beas2B cells (Figure 3C), while there was a decrease in the Beas-2B CFSE+/7-AAD+ cell percentage in the co-culture with NK cells in SP1-transfected Beas-2B cells ($p < 0.001$; Student t test) (Figure 3C), confirming the results observed with CD107a staining (Figure 3A,B).

3.4. Spike 1 Peptide Is Presented by Lung Epithelial Cells via HLA-E Molecules

Since the presence of intracellular SP1 protein in lung epithelial cells induced a decrease in the cytotoxic activity of NK cells, we analyzed the possible factors involved in the modification of NK cell status.

Since viral proteins are commonly recognized and degraded by the proteasome inside the infected cells [25], we hypothesized that SP1 peptides might be presented to NK cells. Intracellular peptide presentation is performed by human leukocyte antigen (HLA) class I molecules, which are expressed by all nucleated cells. Firstly, we evaluated the expression of HLA class I molecules in Beas-2B cells transfected with SP1, SP2, and S proteins. When we stained the cells with anticlassical HLA class I molecules (HLA-A, HLA-B, HLA-C) antibody, we recognized a significant decrease in their membrane expression when lung epithelial cells were transfected with SP1 protein ($p < 0.001$; Student t test)

(Figure 3D,E). SP2 and S protein slightly inhibited HLA-I expression ($p = 0.039$; $p = 0.041$, respectively; Student *t* test). Epithelial lung cells can express also non-classical HLA-E molecule [7]. HLA-E binds peptides primarily derived from specific signal sequences [26] and interacts with NKG2A/CD94 NK cell inhibitory receptors [15]. When we performed the lung epithelial cell staining with MEM-E/06 anti-HLA-E antibody, we observed no expression in basal conditions, which was not affected by SP2 and S transfection (Figure 3F,H). On the contrary, there was a significant increase in HLA-E protein ($p = 0.011$; Student *t* test) (Figure 3F,G) and mRNA expression ($p < 0.001$; Student *t* test) (Figure 3H), in the presence of SP1 protein. HLA-E expression is controlled by the GATA3 transcription factor [12], which is known to also be expressed by lung epithelial cells [27,28]. We observed an increase in GATA3 protein ($p < 0.001$; Student *t* test) (Figure 4A,B) and mRNA ($p < 0.01$; Student *t* test) (Figure 4C) expression only in the presence of SP1. To confirm the transcriptional activity of GATA3 induced by SP1, we analyzed the expression levels of a target gene for GATA3, the Eotaxin3/CCL26 [29]. We observed the induction of CCL26 transcription only in the presence of SP1 ($p < 0.001$; Student *t* test) (Figure 4D). The treatment with a GATA inhibitor, the pyrrothiogatain [19], reduced both GATA3 protein (Figure 4A,B) and mRNA (Figure 4C) expression. To be sure that the increase in HLA-E expression in lung epithelial cells transfected with SP1 protein is controlled by GATA3 transcription factor, we treated the cells with pyrrothiogatain. This inhibitory molecule reduced the expression and transcription of the HLA-E gene in Beas-2B cells (Figure 3F,H).

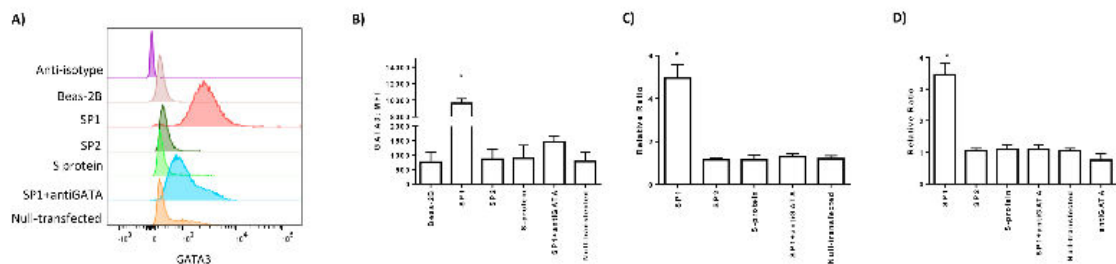


Figure 4. (A) Representative histograms of GATA3 expression on the surface of Beas-2B cells after transfection with SP1, SP2, and S proteins or control fluorescent antibody was used as a positive control (null-transfected) or treated with GATA inhibitor (anti-GATA). (B) The histograms showed the mean \pm standard deviation MFI (mean fluorescence intensity) values of GATA3 expression in three independent experiments. * significant *p* values Student *t* test. (C) Relative ratio of real-time PCR of GATA3 expression in transfected Beas-2B cells. SP1-transfected Beas-2B cells were also treated with GATA inhibitor (anti-GATA). (D) Relative ratio of real-time PCR of GATA3 target gene Eotaxin3/CCL26 in transfected Beas-2B cells. SP1-transfected Beas-2B cells were also treated with GATA inhibitor (anti-GATA). * significant *p* values Student *t* test.

The immune-fluorescence staining showed increased modulation of the expression of HLA-E molecules in the presence of intracellular SP1, which was reduced with the addition of GATA inhibitor (Figure 5A,B). To evaluate if SP1 peptides might be presented by HLA-E molecules, we performed MHC I (Major histocompatibility Class I) binding predictions, made on 26 April 2020 using the IEDB analysis resource ANN aka NetMHC (ver. 4.0) tool. We observed that an 8mer peptide in the SP1 domain (270-277, LQPRTFLL) showed a high affinity mainly for the HLA-E*0101 binding groove (IC50: 0.02) and in a lower extent for the HLA-E*0301 allele (IC50: 0.76), with a similar consensus motif with HLA-E binding (VMAPRTVLL) [14]. We might speculate that the induction of GATA3 and the binding of SP1 peptide might induce HLA-E membrane expression on lung epithelial cells.

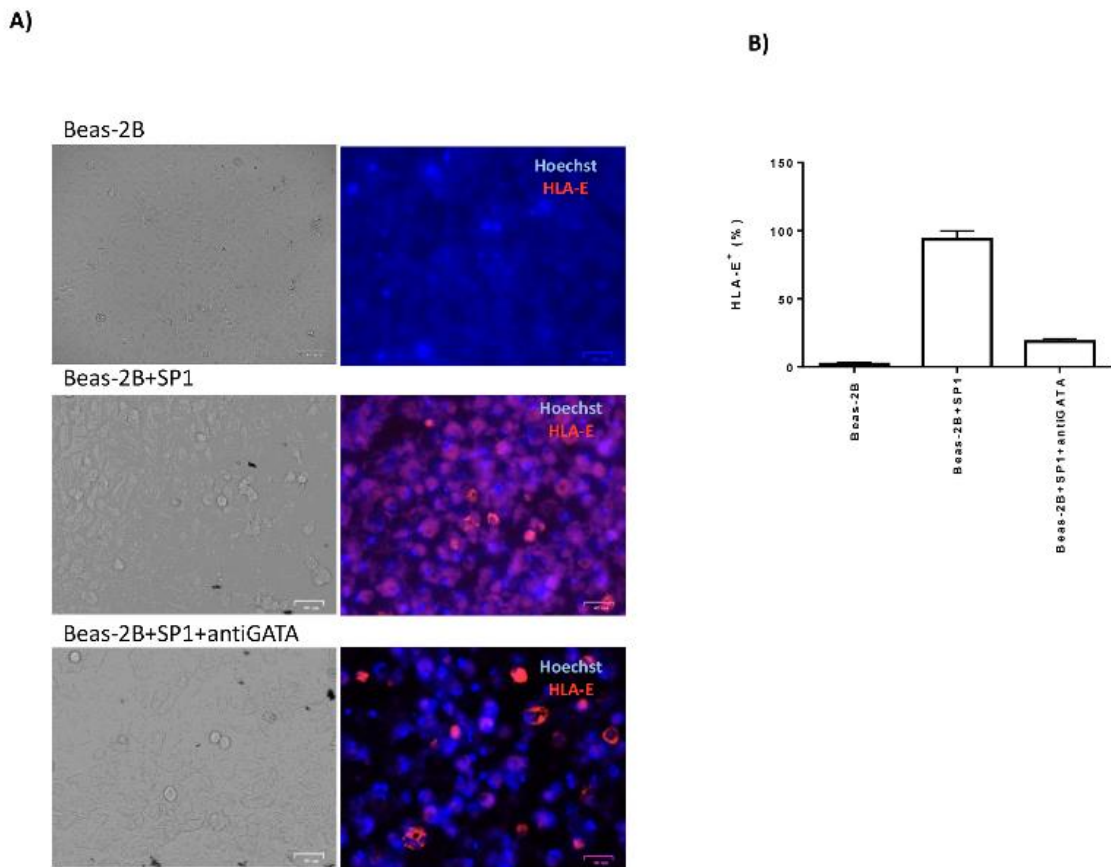


Figure 5. HLA-E expression in Beas-2B cells was characterized by immunofluorescence (Nikon Eclipse TE2000S, equipped with a digital camera). The evaluation was assessed after SP1 transfection (SP1) without or with GATA inhibitor (antiGATA inhibitor). (A) The cells were stained with Hoechst for nuclear detection and anti-HLA-E-PE monoclonal antibody (clone MEM-E/08, Exbio, Praha, Czech Republic). Original magnification 40 \times . (B) Percentage of HLA-E positive (+) cells in the Beas-2B and after SP1 transfection (SP1) without or with GATA inhibitor (antiGATA).

3.5. HLA-E/NKG2A/CD94 Interaction Is Responsible for NK Cells' Exhaustion

Since the functional control of NK cells by HLA-E is possible in the presence of NKG2A/CD94 on NK cells, we evaluated the expression of this receptor on the surface of NK cells. When NK cells were co-cultured with SP1-transfected Beas-2B cells, we observed an increase in the protein ($p < 0.001$; Student t test) (Figure 6A,B) and mRNA ($p < 0.01$; Student t test) (Figure 6C) expression of the inhibitory receptor NKG2A/CD94. Interestingly, the percentage of NKG2A-positive NK cells increased from an average of 16% to 80%. Interestingly, a high percentage of NKG2A-positive NK cells were also CD107A negative (Figure 6A).

To be sure that the resulting inactivity of NK cells towards lung epithelial cells expressing SP1 was determined by HLA-E/NKG2A interaction, we treated the cell culture with anti-HLA-E or anti-NKG2A/CD94 antibodies. We incubated NK cells for four hours with the SP1-transfected Beas-2B cell line and evaluated the expression of CD107a in the presence or absence of anti-HLA-E or anti-NKG2A antibodies. We observed a decrease in CD107a-positive NK cells in the culture condition with SP1-transfected Beas-2B cells ($p < 0.001$; Student t test) (Figure 7A,B), which was recovered by the treatment with anti-HLA-E and anti-NKG2A/CD94 antibodies (Figure 7A,B). As a proof of concept, the secretion of IFN-gamma was reduced by SP1 treatment ($p < 0.01$; Student t test) (Figure 7C), while it was enhanced after the treatment with anti-HLA-E, anti-NKG2A/CD94 antibodies, and GATA inhibitor (Figure 7C).

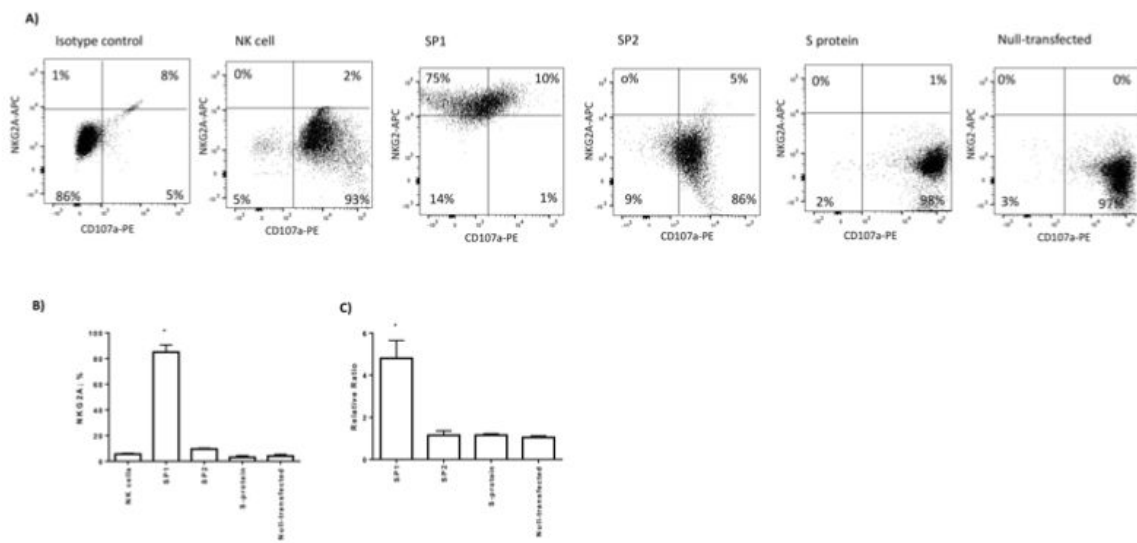


Figure 6. (A) Representative dot plots of NKG2A/CD94 and CD107a expression on the surface of NK cells after co-culture with Beas-2B transfected with SP1, SP2, and S proteins or control fluorescent antibody was used as a positive control (null-transfected). (B) The histograms show the mean \pm standard deviation percentage of NKG2A/CD94-positive cells in three independent experiments. * significant p values Student t test. (C) Relative ratio of real-time PCR of NKG2A expression in transfected Beas-2B cells. * significant p values Student t test.

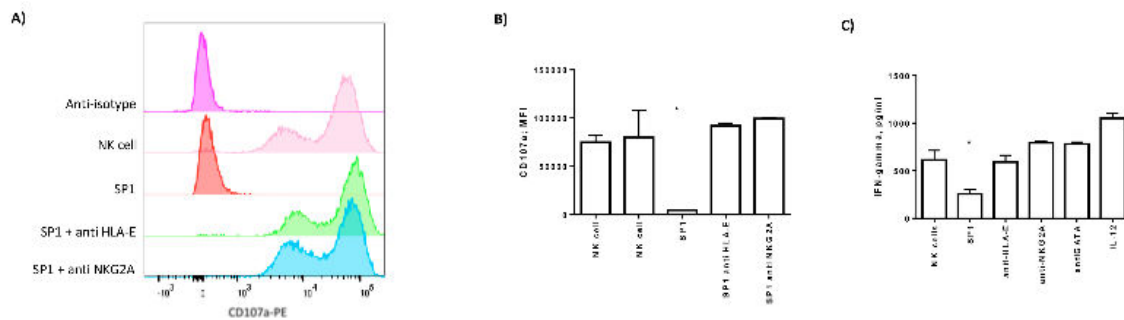


Figure 7. (A) Representative histograms of NK cell degranulation towards Beas-2B cells transfected with SP1 protein without or with anti-HLA-E, anti-NKG2A, or anti-isotype control. NK cells were marked with CD56 and gated as reported in Figure S1C. The degranulation was assessed by CD107a-PE expression. (B) MFI of CD107a in NK cells after the co-culture with Beas-2B cells transfected with SP1 protein without or with anti-HLA-E, anti-NKG2A, or anti-isotype control. The values are presented as mean \pm standard deviation. * significant p values Student t test. (C) Secretion of IFN-gamma evaluated by ELISA. IL-12 treatment was used as a control of IFN-gamma secretion.

4. Discussion

The gaps in the activation of the immune system during SARS-CoV-2 infection translate into the severity of the COVID19 disease. Recent studies have documented a modification in the NK cell number and phenotype [5,8,30]. The total number of NK cells decreased in patients with SARS-CoV-2 infection and the expression of NKG2A on the surface of NK cells was increased, suggesting an exhausted phenotype [31,32]. Interestingly, when the patients were rescued after the infection, NKG2A expression was decreased simultaneously with the increase in the number of NK cells [30]. These results suggest that SARS-CoV-2 infection might compromise the innate antiviral immunity exhausting NK cells' functions [33,34].

We evaluated the effect of SARS-CoV-2 spike proteins in the control of NK cell activation. We considered spike 1 protein, which is involved in the attachment of the virion to the cell membrane

by interacting with ACE2 receptor [35], and spike 2 protein that mediates the fusion of the virion. We observed that the extracellular spike proteins from SARS-CoV-2 and SARS-CoV are able to induce NK cell chemotaxis and activation, via the induction of IFN-gamma secretion in the K562 cell model. These results are interesting considering the efficacy of IFN-gamma in inhibiting SARS-CoV replication partly through the downregulation of ACE2 [36]. Our data sustain the role of the immune response of NK cells during SARS-CoV-2 infection [37]. They would migrate to the infected sites and respond to viruses producing IFN-gamma, killing virus-infected cells, and boosting the adaptive immune response with the production of innate proinflammatory cytokine and type I IFNs [5]. The spike proteins, per se, are not able to affect NK cell activation and IFN-gamma secretion.

Since SARS-CoV-2 infection is mainly localized to lung epithelial cells, where the detrimental effects of this infection are more evident [4], we evaluated the effect of SARS-CoV proteins on this cell type.

Surprisingly, we showed that the intracellular expression of S1 protein in lung epithelial cells reduces the activation of NK cells and their ability to degranulate, which is the opposite pattern to that observed in K562 cells. These results account for the in vivo observation of a break in the interplay of lung epithelial cells and immune cells during SARS-CoV-2 infection [37], with a consequent exhausted immune response [37].

To evaluate the possible mechanisms used by SARS-CoV proteins to control NK cells' activation, we considered that the activation of NK cells is partly controlled by the expression of HLA class molecules, via the interaction with specific NK cell receptors [38]. We evaluated the possible modification of surface HLA class I molecules on lung epithelial cells. The presentation of pathogen-derived peptides by HLA molecules and the genetic variability of HLA alleles in human populations account for their role in the individual responses to SARS-CoV-2 infection and/or progression. We showed that S1 protein on one side diminished classical HLA class I molecule expression but on the other side upregulated HLA-E expression. The protein HLA-E is a non-classical major histocompatibility complex molecule that binds peptides derived from a specific signal sequence [14]. We recognized an SP1-derived HLA-E binding peptide that might stabilize HLA-E expression on the surface of lung epithelial cells during SARS-CoV-2 infection. Interestingly, the highest affinity is demonstrated for the HLA-E*0101 allele. HLA-E surface expression conferred cell resistance to NK cell lysis, interacting with the NK cell inhibitory receptor CD94/NKG2A [14,38]. The involvement of HLA-E in the control of NK cell activation is confirmed also by the different results observed in K562 and lung cell models. K562 cells express no HLA molecules, providing no effective molecules to SARS-CoV spike 1 protein in order to control NK cells. For this, we observed IFN-gamma secretion and NK cell activation also in the presence of SARS-CoV spike 1 protein in the K562 cell model. On the contrary, lung cells, which express HLA-E molecules in the presence of SARS-CoV spike 1 protein, are able to inhibit IFN-gamma secretion and NK cell activation.

Since, it was shown earlier that HLA-E is tightly upregulated through GATA3 response elements [12], we evaluated the role of this transcription factor. We observed that *HLA-E* up-modulation by SP1 is controlled by GATA3 transcription factor. In fact, the treatment with GATA inhibitor reduced the expression of HLA-E even in the presence of SP1. GATA3 is a transcription factor that drives the differentiation of T helper (Th) 2 cells [28], immune regulation [27], and embryonic and adult non-hematopoietic cells' differentiation, including the lung [39]. The upregulation of GATA3 mRNA and protein by SP1 protein might have other important effects on lung epithelial cells that surely deserve to be evaluated. More interestingly, GATA3 is not only up-modulated, but it is transcriptional active, as showed by the induction of mRNA transcription of a GATA3 target gene, as *CCL26*. The induction of *CCL26* might modify NK cell status. In particular, it has been shown that *CCL26* is able induce the migration of NK cells infiltrated in the epithelial layers of nasal tissue [40]. We hypothesize that SP1 induction of GATA3 and the consequent secretion of *CCL26* might induce NK cell migration, as we previously observed (Figure 1A). Further experiments are necessary to prove this hypothesis.

Simultaneously, NK cells showed increased levels of NKG2A/CD94 inhibitory receptor in the presence of SP1 intracellular expression in lung epithelial cells. The percentage of NKG2A-positive cells increased from the 16% to 80%. These NKG2A-positive NK cells were also CD107a negative, supporting the role of this inhibitory receptor in the control of NK cell activation in the presence of SP1. These data are in agreement with the recognized crosstalk between HLA-E and NKG2A/CD94, that induces a higher surface level of HLA-E molecules concurrently with a prevalent expression of NKG2A receptor on the surface of NK cells [15]. Moreover, the maintenance of NK cell activation towards K562 cells, even in the presence of SP1, might be associated to the inability of K562 to express HLA-E molecules [41] and consequently to interact with NKG2A.

The internalization of viral SP1 might induce a cellular stress condition in lung epithelial cells [42], which can result in endoplasmic reticulum stress and consequent down-modulation of classical HLA class I molecules and upregulation of the GATA3 transcription factor. The processing of SP1 by proteasome might create HLA-E-specific peptides that enhance HLA-E surface expression and consequently stimulate NKG2A/CD94 receptors on the surface of NK cells. These aspects deserve further evaluation and more accurate analysis. Further experiments might also elucidate the possible interaction of NK cells with the regulation of adaptive immunity, in particular T cell activation.

These new aspects of interaction between SARS-CoV-2 S1 protein and the host cells might have important implications in the pathogenesis of COVID19, providing opportunities for developing new therapies against SARS-CoV-2. In particular, counteracting the cellular stress, targeting the S1 protein or using the anti-NKG2A monoclonal antibody monalizumab, currently in use for management of rheumatoid arthritis and several neoplastic disorders [43], might represent new anti-SARS-CoV-2 strategies to enhance the innate immune response at the early stage of the disease, inducing mucosal immunity that might lead to a long-term protection against SARS-CoV-2 infection [44].

Supplementary Materials: The following are available online at <http://www.mdpi.com/2073-4409/9/9/1975/s1>, Figure S1: (A) Representative dot plots of pre and post NK cell purification from peripheral blood, stained with CD56-PECy7 and CD3-FITC. (B) NK cell viability in the presence of SP1, SP2 from SARS-CoV-2 or spike protein (S) from SARS-CoV. (C) Gating strategy for the analysis of NK cell after the co-culture with K562 cells. Cells were gated for FSC and SSC parameters, selecting singlets and alive cells (7-AAD-). Cell were stained with CD56-PECy7 and CD3-FITC and NK cells were recognized as CD3-CD56+ cells, while K562 cells were CD3-CD56-cells.

Author Contributions: Conceptualization, D.B., V.G. and R.R.; Methodology, D.B. and V.G.; Formal Analysis, A.R.; Investigation, A.R. and S.R.; Data Curation, D.B., V.G. and R.R.; Writing—Original Draft Preparation, R.R.; Writing—Review & Editing, R.R., D.B. and V.G.; Supervision, R.R.; Funding Acquisition, R.R. All authors have read and agreed to the published version of the manuscript.

Funding: This research was funded by University of Ferrara COVID19 grant (RR), University of Ferrara FAR 2018 (RR), 2019 (RR). The funders had no role in study design, data collection and analysis, decision to publish, or preparation of the manuscript.

Acknowledgments: We thank Linda Sartor for writing assistance.

Conflicts of Interest: The authors declare no conflict of interest.

References

1. Zhu, N.; Zhang, D.; Wang, W.; Li, X.; Yang, B.; Song, J.; Zhao, X.; Huang, B.; Shi, W.; Lu, R.; et al. A Novel Coronavirus from Patients with Pneumonia in China, 2019. *N. Engl. J. Med.* **2020**, *382*, 727–733. [[CrossRef](#)] [[PubMed](#)]
2. Li, Q.; Guan, X.; Wu, P.; Wang, X.; Zhou, L.; Tong, Y.; Ren, R.; Leung, K.S.M.; Lau, E.H.Y.; Wong, J.Y.; et al. Early Transmission Dynamics in Wuhan, China, of Novel Coronavirus-Infected Pneumonia. *N. Engl. J. Med.* **2020**, *382*, 1199–1207. [[CrossRef](#)] [[PubMed](#)]
3. Zhou, P.; Yang, X.L.; Wang, X.G.; Hu, B.; Zhang, L.; Zhang, W.; Si, H.R.; Zhu, Y.; Li, B.; Huang, C.L.; et al. A pneumonia outbreak associated with a new coronavirus of probable bat origin. *Nature* **2020**, *579*, 270–273. [[CrossRef](#)]

4. Guan, W.J.; Ni, Z.Y.; Hu, Y.; Liang, W.H.; Ou, C.Q.; He, J.X.; Liu, L.; Shan, H.; Lei, C.L.; Hui, D.S.C.; et al. Clinical Characteristics of Coronavirus Disease 2019 in China. *N. Engl. J. Med.* **2020**, *382*, 1708–1720. [[CrossRef](#)] [[PubMed](#)]
5. Qin, C.; Zhou, L.; Hu, Z.; Zhang, S.; Yang, S.; Tao, Y.; Xie, C.; Ma, K.; Shang, K.; Wang, W.; et al. Dysregulation of immune response in patients with COVID-19 in Wuhan, China. *Clin. Infect. Dis.* **2020**. [[CrossRef](#)]
6. Pedersen, S.F.; Ho, Y.C. SARS-CoV-2: A storm is raging. *J. Clin. Investig.* **2020**, *130*, 2202–2205. [[CrossRef](#)] [[PubMed](#)]
7. Gornalusse, G.G.; Hirata, R.K.; Funk, S.E.; Riobobos, L.; Lopes, V.S.; Manske, G.; Prunkard, D.; Colunga, A.G.; Hanafi, L.A.; Clegg, D.O.; et al. HLA-E-expressing pluripotent stem cells escape allogeneic responses and lysis by NK cells. *Nat. Biotechnol.* **2017**, *35*, 765–772. [[CrossRef](#)]
8. Tan, L.; Wang, Q.; Zhang, D.; Ding, J.; Huang, Q.; Tang, Y.Q.; Wang, Q.; Miao, H. Lymphopenia predicts disease severity of COVID-19: A descriptive and predictive study. *Signal. Transduct. Target. Ther.* **2020**, *5*, 33. [[CrossRef](#)]
9. Vivier, E.; Tomasello, E.; Baratin, M.; Walzer, T.; Ugolini, S. Functions of natural killer cells. *Nat. Immunol.* **2008**, *9*, 503–510. [[CrossRef](#)]
10. Long, E.O.; Kim, H.S.; Liu, D.; Peterson, M.E.; Rajagopalan, S. Controlling natural killer cell responses: Integration of signals for activation and inhibition. *Annu. Rev. Immunol.* **2013**, *31*, 227–258. [[CrossRef](#)]
11. Houchins, J.P.; Lanier, L.L.; Niemi, E.C.; Phillips, J.H.; Ryan, J.C. Natural killer cell cytolytic activity is inhibited by NKG2-A and activated by NKG2-C. *J. Immunol.* **1997**, *158*, 3603–3609. [[PubMed](#)]
12. Nguyen, S.; Beziat, V.; Dhedin, N.; Kuentz, M.; Vernant, J.P.; Debre, P.; Vieillard, V. HLA-E upregulation on IFN-gamma-activated AML blasts impairs CD94/NKG2A-dependent NK cytotoxicity after haplo-mismatched hematopoietic SCT. *Bone Marrow Transplant.* **2009**, *43*, 693–699. [[CrossRef](#)] [[PubMed](#)]
13. Miller, J.D.; Weber, D.A.; Ibegbu, C.; Pohl, J.; Altman, J.D.; Jensen, P.E. Analysis of HLA-E peptide-binding specificity and contact residues in bound peptide required for recognition by CD94/NKG2. *J. Immunol.* **2003**, *171*, 1369–1375. [[CrossRef](#)] [[PubMed](#)]
14. Braud, V.; Jones, E.Y.; McMichael, A. The human major histocompatibility complex class Ib molecule HLA-E binds signal sequence-derived peptides with primary anchor residues at positions 2 and 9. *Eur. J. Immunol.* **1997**, *27*, 1164–1169. [[CrossRef](#)] [[PubMed](#)]
15. Lee, N.; Llano, M.; Carretero, M.; Ishitani, A.; Navarro, F.; Lopez-Botet, M.; Geraghty, D.E. HLA-E is a major ligand for the natural killer inhibitory receptor CD94/NKG2A. *Proc. Natl. Acad. Sci. USA* **1998**, *95*, 5199–5204. [[CrossRef](#)] [[PubMed](#)]
16. Lazetic, S.; Chang, C.; Houchins, J.P.; Lanier, L.L.; Phillips, J.H. Human natural killer cell receptors involved in MHC class I recognition are disulfide-linked heterodimers of CD94 and NKG2 subunits. *J. Immunol.* **1996**, *157*, 4741–4745.
17. Marci, R.; Gentili, V.; Bortolotti, D.; Lo Monte, G.; Caselli, E.; Bolzani, S.; Rotola, A.; Di Luca, D.; Rizzo, R. Presence of HHV-6A in Endometrial Epithelial Cells from Women with Primary Unexplained Infertility. *PLoS ONE* **2016**, *11*, e0158304. [[CrossRef](#)]
18. Mirjagic Martinovic, K.; Babovic, N.; Dzodic, R.; Jurisic, V.; Matkovic, S.; Konjevic, G. Favorable in vitro effects of combined IL-12 and IL-18 treatment on NK cell cytotoxicity and CD25 receptor expression in metastatic melanoma patients. *J. Transl. Med.* **2015**, *13*, 120. [[CrossRef](#)]
19. Nomura, S.; Takahashi, H.; Suzuki, J.; Kuwahara, M.; Yamashita, M.; Sawasaki, T. Pyrrothiogatain acts as an inhibitor of GATA family proteins and inhibits Th2 cell differentiation in vitro. *Sci. Rep.* **2019**, *9*, 17335. [[CrossRef](#)]
20. Bortolotti, D.; Gentili, V.; Rotola, A.; Cultrera, R.; Marci, R.; Di Luca, D.; Rizzo, R. HHV-6A infection of endometrial epithelial cells affects immune profile and trophoblast invasion. *Am. J. Reprod. Immunol.* **2019**, *82*, e13174. [[CrossRef](#)]
21. Bortolotti, D.; Gentili, V.; Caselli, E.; Siculo, M.; Soffritti, I.; D'Accolti, M.; Barao, I.; Rotola, A.; Di Luca, D.; Rizzo, R. DNA Sensors' Signaling in NK Cells During HHV-6A, HHV-6B and HHV-7 Infection. *Front. Microbiol.* **2020**, *11*, 226. [[CrossRef](#)] [[PubMed](#)]
22. Inngjerdingen, M.; Rolstad, B.; Ryan, J.C. Activating and inhibitory Ly49 receptors modulate NK cell chemotaxis to CXC chemokine ligand (CXCL) 10 and CXCL12. *J. Immunol.* **2003**, *171*, 2889–2895. [[CrossRef](#)]

23. Rizzo, R.; Gentili, V.; Casetta, I.; Caselli, E.; De Gennaro, R.; Granieri, E.; Cassai, E.; Di Luca, D.; Rotola, A. Altered natural killer cells' response to herpes virus infection in multiple sclerosis involves KIR2DL2 expression. *J. Neuroimmunol.* **2012**, *251*, 55–64. [[CrossRef](#)]
24. Zitvogel, L. Dendritic and natural killer cells cooperate in the control/switch of innate immunity. *J. Exp. Med.* **2002**, *195*, F9–F14. [[CrossRef](#)] [[PubMed](#)]
25. Mwimanzi, P.; Markle, T.J.; Ueno, T.; Brockman, M.A. Human leukocyte antigen (HLA) class I down-regulation by human immunodeficiency virus type 1 negative factor (HIV-1 Nef): What might we learn from natural sequence variants? *Viruses* **2012**, *4*, 1711–1730. [[CrossRef](#)] [[PubMed](#)]
26. Stevens, J.; Joly, E.; Trowsdale, J.; Butcher, G.W. Peptide binding characteristics of the non-classical class Ib MHC molecule HLA-E assessed by a recombinant random peptide approach. *BMC Immunol.* **2001**, *2*, 5. [[CrossRef](#)]
27. Caramori, G.; Lim, S.; Ito, K.; Tomita, K.; Oates, T.; Jazrawi, E.; Chung, K.F.; Barnes, P.J.; Adcock, I.M. Expression of GATA family of transcription factors in T-cells, monocytes and bronchial biopsies. *Eur. Respir. J.* **2001**, *18*, 466–473. [[CrossRef](#)]
28. Zheng, W.; Flavell, R.A. The transcription factor GATA-3 is necessary and sufficient for Th2 cytokine gene expression in CD4 T cells. *Cell* **1997**, *89*, 587–596. [[CrossRef](#)]
29. Sun, Q.; Yang, X.; Zhong, B.; Jiao, F.; Li, C.; Li, D.; Lan, X.; Sun, J.; Lu, S. Upregulated protein arginine methyltransferase 1 by IL-4 increases eotaxin-1 expression in airway epithelial cells and participates in antigen-induced pulmonary inflammation in rats. *J. Immunol.* **2012**, *188*, 3506–3512. [[CrossRef](#)]
30. Zheng, M.; Gao, Y.; Wang, G.; Song, G.; Liu, S.; Sun, D.; Xu, Y.; Tian, Z. Functional exhaustion of antiviral lymphocytes in COVID-19 patients. *Cell Mol. Immunol.* **2020**, *17*, 533–535. [[CrossRef](#)]
31. Antonioli, L.; Fornai, M.; Pellegrini, C.; Blandizzi, C. NKG2A and COVID-19: Another brick in the wall. *Cell Mol. Immunol.* **2020**. [[CrossRef](#)] [[PubMed](#)]
32. Yaqinuddin, A.; Kashir, J. Innate immunity in COVID-19 patients mediated by NKG2A receptors, and potential treatment using Monalizumab, Cholroquine, and antiviral agents. *Med. Hypotheses* **2020**, *140*, 109777. [[CrossRef](#)] [[PubMed](#)]
33. Jewett, A. The Potential Effect of Novel Coronavirus SARS-CoV-2 on NK Cells; A Perspective on Potential Therapeutic Interventions. *Front. Immunol.* **2020**, *11*, 1692. [[CrossRef](#)] [[PubMed](#)]
34. Market, M.A.L.; Martel, A.B.; Bastin, D.; Olanubi, O.; Tennakoon, G.; Boucher, D.M.; Ng, J.; Ardolino, M.; Auer, R.C. Flattening the COVID-19 Curve With Natural Killer Cell Based Immunotherapies. *Front. Immunol.* **2020**, *11*. [[CrossRef](#)] [[PubMed](#)]
35. Hoffmann, M.; Kleine-Weber, H.; Schroeder, S.; Kruger, N.; Herrler, T.; Erichsen, S.; Schiergens, T.S.; Herrler, G.; Wu, N.H.; Nitsche, A.; et al. SARS-CoV-2 Cell Entry Depends on ACE2 and TMPRSS2 and Is Blocked by a Clinically Proven Protease Inhibitor. *Cell* **2020**, *181*, 271–280.e8. [[CrossRef](#)] [[PubMed](#)]
36. de Lang, A.; Osterhaus, A.D.; Haagmans, B.L. Interferon-gamma and interleukin-4 downregulate expression of the SARS coronavirus receptor ACE2 in Vero E6 cells. *Virology* **2006**, *353*, 474–481. [[CrossRef](#)]
37. Frieman, M.; Heise, M.; Baric, R. SARS coronavirus and innate immunity. *Virus Res.* **2008**, *133*, 101–112. [[CrossRef](#)]
38. Anfossi, N.; Andre, P.; Guia, S.; Falk, C.S.; Roetyneck, S.; Stewart, C.A.; Bresó, V.; Frassati, C.; Reviron, D.; Middleton, D.; et al. Human NK cell education by inhibitory receptors for MHC class I. *Immunity* **2006**, *25*, 331–342. [[CrossRef](#)]
39. Grote, D.; Boualia, S.K.; Souabni, A.; Merkel, C.; Chi, X.; Costantini, F.; Carroll, T.; Bouchard, M. Gata3 acts downstream of beta-catenin signaling to prevent ectopic metanephric kidney induction. *PLoS Genet.* **2008**, *4*, e1000316. [[CrossRef](#)]
40. El-Shazly, A.E.; Doloriert, H.C.; Bisig, B.; Lefebvre, P.P.; Delvenne, P.; Jacobs, N. Novel cooperation between CX3CL1 and CCL26 inducing NK cell chemotaxis via CX3CR1: A possible mechanism for NK cell infiltration of the allergic nasal tissue. *Clin. Exp. Allergy* **2013**, *43*, 322–331. [[CrossRef](#)]
41. Hirano, N.; Butler, M.O.; Xia, Z.; Ansen, S.; von Bergwelt-Baildon, M.S.; Neuberg, D.; Freeman, G.J.; Nadler, L.M. Engagement of CD83 ligand induces prolonged expansion of CD8+ T cells and preferential enrichment for antigen specificity. *Blood* **2006**, *107*, 1528–1536. [[CrossRef](#)] [[PubMed](#)]
42. Ulianich, L.; Terrazzano, G.; Annunziatella, M.; Ruggiero, G.; Beguinot, F.; Di Jeso, B. ER stress impairs MHC Class I surface expression and increases susceptibility of thyroid cells to NK-mediated cytotoxicity. *Biochim. Biophys. Acta* **2011**, *1812*, 431–438. [[CrossRef](#)] [[PubMed](#)]

43. van Hall, T.; Andre, P.; Horowitz, A.; Ruan, D.F.; Borst, L.; Zerbib, R.; Narni-Mancinelli, E.; van der Burg, S.H.; Vivier, E. Monalizumab: Inhibiting the novel immune checkpoint NKG2A. *J. Immunother. Cancer* **2019**, *7*, 263. [[CrossRef](#)] [[PubMed](#)]
44. Masselli, E.V.M.; Carubbi, C.; Pozzi, G.; Presta, V.; Mirandola, P.; Vitale, M. NK cells: A double edge sword against SARS-CoV-2. *Adv. Biol. Regul.* **2020**, *77*. [[CrossRef](#)] [[PubMed](#)]



© 2020 by the authors. Licensee MDPI, Basel, Switzerland. This article is an open access article distributed under the terms and conditions of the Creative Commons Attribution (CC BY) license (<http://creativecommons.org/licenses/by/4.0/>).

5.1.1 SARS-CoV-2 vaccination effect on host immune system

The high rate of SARS-CoV-2 transmission in the population through both aerosol and droplets contaminated surfaces, was one of the main concerns during 2020 pandemic [187, 188].

The increasing need of efficient strategies able to counteract the rapid spread of SARS-CoV-2 infection, led to the identification of possible specific treatments against SARS-CoV-2 infection [351] and to the synthesis of anti-COVID-19 vaccines [299].

SARS-CoV-2 vaccination process reproduces SARS-CoV-2 infection in the host, inducing antibodies production and the develop of immune memory, to ameliorate infection associated adverse outcomes [352]. An effective humoral immune response to vaccination is characterized by the induction of high affinity and long-lasting protective antibody responses, consisting in IgM/IgG anti-Spike and IgM/IgG anti-Spike-RBD released by plasma cells [353]. Despite the evaluation of humoral immunity represents the gold standard in the determination of vaccination efficacy [354], also cellular-mediated immunity is fundamental [290].

Concerning the importance of vaccination in the SARS-CoV-2 defense, we evaluated the levels of Spike-binding and neutralizing antibodies against SARS-CoV-2 in healthy volunteers, at nine months after the second vaccination dose and one month after the booster dose with Comirnaty Pfizer vaccine ([355], paper attached), in association to IFN- γ secretion and T cells phenotype, when exposed to SARS-CoV-2 VOCs.

Thus, in our study we reported that the booster dose induced a significant increase in Spike-binding and neutralizing antibody amount one month after the booster dose and an early

activation of memory CD8+ T subset ([355], paper attached). Moreover, after the booster dose, we showed an increase of IFN- γ secretion by T lymphocyte when exposed to viral Spike variants. We reported that Wuhan Spike variant challenge induced the highest increase in both nine months after the second vaccination and booster dose, compared with Alpha, Delta and Omicron stimulation.

Our results suggested the importance of booster dose of vaccine. However, the Wuhan VOC efficacy in enhancing T cell activation suggests the presence of immune imprinting related to vaccine, that boost the initially immune responses ([355], paper attached).



Contents lists available at ScienceDirect

International Journal of Infectious Diseases

journal homepage: www.elsevier.com/locate/ijid

Short Communication

Humoral and adaptive immune responses to the SARS-CoV-2 vaccine

Roberta Rizzo^{1,*}, Daria Bortolotti¹, Luca Morandi², Sabrina Rizzo¹, Giovanna Schiuma¹, Silvia Beltrami¹, Alberto Papi², Marco Contoli^{2,**}¹ Department of Chemical, Pharmaceutical and Agricultural Sciences, University of Ferrara, Italy² Respiratory Section, Department of Translational Medicine, University of Ferrara, Italy

ARTICLE INFO

Article history:
Received 12 March 2022
Revised 2 June 2022
Accepted 13 June 2022

Keywords:
SARS-CoV-2
Vaccine
Humoral response
Adaptive immunity
Neutralizing antibody

ABSTRACT

Vaccines against SARS-CoV-2 ameliorate infection and adverse outcomes from SARS-CoV-2. Elicitation of high affinity and durable protective antibody responses is a hallmark of a successful humoral immune response to vaccination. To assess the relevance of serum levels of SARS-CoV-2 specific antibodies and to further characterize the immune response to SARS-CoV-2 vaccines, we report i) the levels of spike-binding and neutralizing antibodies to SARS-CoV-2 in the sera of 30 healthy volunteers at nine months after the second vaccination dose of mRNA vaccine and one month after the booster dose; ii) the levels of IFN- γ production by blood T cells exposed to SARS-CoV-2 spike antigen (Wuhan, Alpha B.1.1.7, Delta B.1.617.2, and Omicron B.1.1.529 variants); and iii) the specific phenotype of T cells related with exposure to SARS-CoV-2 spike antigen. We observed that the booster dose induced increased humoral and adaptive immune responses and led to early activation of the memory CD8⁺ T subset.

© 2022 The Authors. Published by Elsevier Ltd on behalf of International Society for Infectious Diseases. This is an open access article under the CC BY-NC-ND license (<http://creativecommons.org/licenses/by-nc-nd/4.0/>)

Introduction

Vaccines against SARS-CoV-2 prevent infection and adverse outcomes from SARS-CoV-2 (Olliaro et al., 2021). Elicitation of high affinity and durable protective antibody responses is a hallmark of a successful humoral immune response to vaccination (Turner et al., 2021). Antibody responses decline sharply at six months, particularly after SARS-CoV-2 mRNA vaccines (Collier et al., 2021). A recent study showed that after 20 weeks or more, the vaccination with two doses is effective against COVID-19-related hospitalization and death with a waning of the clinical protection in older adults and fragile/co-morbid patients (Andrews et al., 2022).

Methods

To assess the relevance of serum levels of SARS-CoV-2 specific antibodies and to further characterize the immune response to SARS-CoV-2 vaccines, we report i) the levels of spike-binding and

neutralizing antibodies to SARS-CoV-2 in the sera of 30 healthy volunteers at nine months after the second vaccination dose of mRNA vaccine (Comirnaty; Pfizer Australia Pty Ltd) and one month after the booster dose (Table 1); ii) the levels of Interferon- γ (IFN- γ) production by blood T cells exposed to SARS-CoV-2 spike antigen (Wuhan, Alpha B.1.1.7, Delta B.1.617.2, and Omicron B.1.1.529 variants); and iii) the specific phenotype of T cells induced by SARS-CoV-2 spike antigen presentation. The extensive methods are reported in the Supplementary Materials.

Results

High variability of spike-binding and neutralizing antibody levels was found in the sera of healthy donors nine months after the second vaccination (Figure 1A, B). Both spike-binding and neutralizing antibody levels significantly increased one month after the booster dose (Figure 1A, B). These data confirm that the booster dose is effective in enhancing the levels of spike-binding and neutralizing antibodies.

Because the specific adaptive immune response is a key element in the protective immune response to vaccines (Tejaro and Farber, 2021), we investigated the T cell responses to spike proteins from SARS-CoV-2 variants by measuring the percentage of T lymphocytes releasing IFN- γ when *ex-vivo* exposed to SARS-CoV-2 spike antigens. After the booster dose, we observed that the T lymphocytes

* Corresponding authors: Roberta Rizzo, University of Ferrara, Department of Chemical, Pharmaceutical and Agricultural Sciences; Via Luigi Borsari, 46 - 44121 Ferrara, Italy.

** Corresponding authors: Marco Contoli, University of Ferrara, Department of Translational Medicine; Via Luigi Borsari, 46 - 44121 Ferrara, Italy.

E-mail addresses: rbr@unife.it (R. Rizzo), marco.contoli@unife.it (M. Contoli).

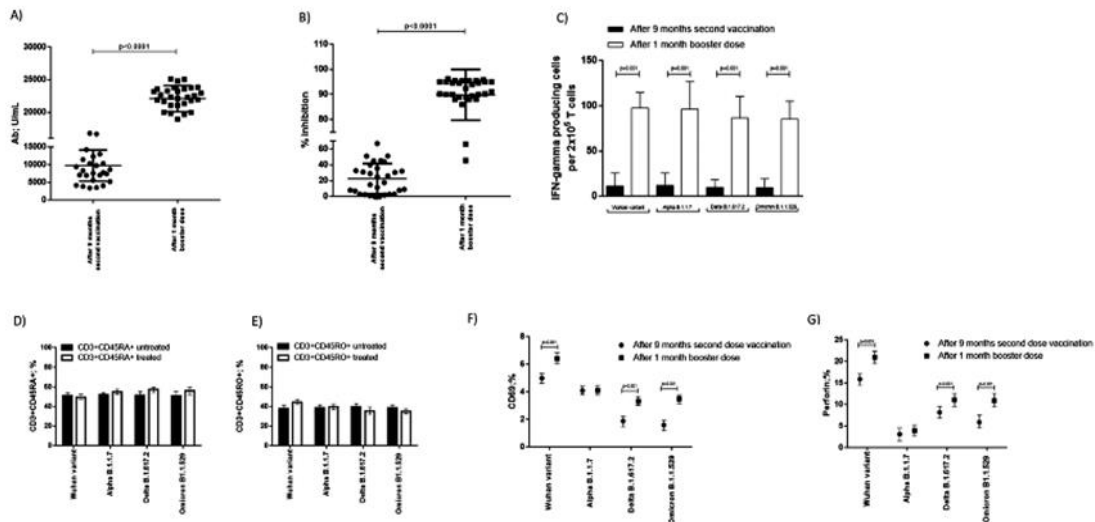


Figure 1. (A) Levels of anti-spike SARS-CoV-2 RBD IgG (Ab) in the plasma samples of 30 healthy individuals nine months after the second vaccination and one month after the booster dose. The results are reported as mean \pm SD. P-values were evaluated by Student's *t*-test. (B) Percentage of inhibition of SARS-CoV-2 infection of Calu-3 (ATCC HTB-55) human lung cell line in the presence of patients' plasma samples of 30 healthy individuals nine months after the second vaccination and one month after the booster dose. The results are reported as mean \pm SD. P-values were evaluated by Fisher's exact test. (C) Number of IFN- γ secreting T lymphocytes obtained from peripheral blood of 30 healthy individuals nine months after the second vaccination and one month after the booster dose, stimulated with Wuhan, Alpha B.1.1.7, Delta B.1.617.2, and Omicron B.1.1.529 variants. The results are reported as mean \pm SD. P-values were evaluated by Student's *t*-test. Percentage of (D) naive T cells (CD3+CD45RO+) and (E) memory T cells (CD3+CD45RO+) untreated or stimulated with Wuhan, Alpha B.1.1.7, Delta B.1.617.2, and Omicron B.1.1.529 variants. T lymphocytes were obtained from peripheral blood of 30 healthy individuals one month after the booster dose. The results are reported as mean \pm SD. P-values were evaluated by Fisher's exact test. Percentage of (F) CD69 and (G) perforin positive memory T cells lymphocytes obtained from peripheral blood of 30 healthy individuals nine months after the second vaccination and one month after the booster dose and stimulated with Wuhan, Alpha B.1.1.7, Delta B.1.617.2, and Omicron B.1.1.529 variants. The results are reported as mean \pm SD. P-values were evaluated by Fisher's exact test. IFN- γ = Interferon- γ ; IgG (Ab) = Immunoglobulin G Antibody; RBD = Receptor-Binding Domain; SARS-CoV-2 = severe acute respiratory syndrome coronavirus 2.

Table 1
Demographic and clinical characteristics of the study population.

Female, % (n)	50 (15)
Age (years), mean (SD)	38 (10)
Health care workers % (n)	100 (30)
Smoker, % (n)	0 (0)
Co-morbidities % (n)	0 (0)
mRNA vaccine ^a % (n)	100 (30)
Blood sampling after second immunization (months \pm SD)	9 \pm 0.2
Blood sampling after booster dose (months \pm SD)	1 \pm 0.1

SD = standard deviation.

^a All the subjects received three doses of Comirnaty (Pfizer Australia Pty Ltd).

phocyte IFN- γ production was significantly enhanced toward all four SARS-CoV-2 spike variants (Figure 1C). These data further emphasize the importance of the booster dose to reactivate humoral but also cellular-mediated immune response to the vaccine.

CD8+ T cells are recognized to have an important role in viral eradication, including SARS-CoV-2 (Rha and Shin, 2021), and the induction of memory CD8+ T cells (i.e., expressing CD45RO) (Tomiyama et al., 2002) is important for the effectiveness of vaccines (Turner et al., 2021). Therefore, we further evaluated T lymphocyte responses by measuring naive (CD45RA+) and memory (CD45RO+) CD3+CD8+ blood cells and the expression in these cells of surface CD69 and intracellular perforin as markers of early activation (Sancho et al., 2005) and cytotoxic activity (Voskoboinik et al., 2015), respectively. After stimulation of blood samples with spike variants, we found no difference in the proportion of naive versus memory cells one month after the booster dose compared with 9 months after the second vaccination (Figure 1D, E). However, when we looked at T cell activation, we

found differences in response to the different SARS-CoV-2 variants. Activated (CD69+) memory T cells percentage was increased after the booster dose when challenged with Wuhan, Delta B.1.617.2, and Omicron B.1.1.529 variants (Figure 1F; $P < 0.001$, Fisher's exact test). The Wuhan variant challenge induced the highest percentage of activated memory T cells, in both nine months after the second vaccination and booster dose time points, compared with the Delta B.1.617.2 and Omicron B.1.1.529 variants challenge (Figure 1F; $P < 0.001$; Fisher's exact test). Activated memory T cells percentage was not increased by the booster dose when challenged with the Alpha B.1.1.7 variant but maintained the levels reached nine months after the second vaccination dose (Figure 1F). Similarly, the perforin+ memory T cells percentage was increased after the booster dose when challenged with Wuhan, Delta B.1.617.2, and Omicron B.1.1.529 variants (Figure 1G; $P < 0.001$, Fisher's exact test). The Wuhan variant challenge induced the highest percentage of activated memory T cells, in both 9 months after the second vaccination and booster dose time points, compared with the Delta B.1.617.2 and Omicron B.1.1.529 variants challenge (Figure 1G; $P < 0.001$; Fisher's exact test). The perforin+ memory T cells percentage was slightly increased by the booster dose when challenged with the Alpha B.1.1.7 variant (Figure 1G). These data indicate that at one month after the booster dose, there are no increased levels of memory CD8+ cells, but the repeated doses lead to early activation of these cells toward SARS-CoV-2 spike variants.

Discussion

Vaccines are important for public health, and the World Health Organization estimates that SARS-CoV-2 vaccination is preventing millions of deaths (World Health Organization, 2021). However, vaccination always raises concerns about the real efficacy of the

immune response. We evaluated the levels of spike-binding and neutralizing antibodies to SARS-CoV-2 at nine months after the second vaccination dose of mRNA vaccine and one month after the booster dose (Comirnaty; Pfizer Australia Pty Ltd). We observed that both spike-binding and neutralizing antibody levels were significantly increased one month after the booster dose, confirming the efficacy of the booster dose in enhancing the levels of spike-binding and neutralizing antibodies.

Because the specific adaptive immune response is a key element in the protective immune response to vaccines (Tejaro and Farber, 2021), we investigated the T cell responses to spike proteins from SARS-CoV-2 variants by measuring the percentage of T lymphocytes releasing IFN- γ when *ex-vivo* exposed to spike antigens from different SARS-CoV-2 variants (Wuhan, Alpha B.1.1.7, Delta B.1.617.2, and Omicron B.1.1.529). We observed an increased production of IFN- γ by T lymphocytes obtained after the booster dose and challenged with the four SARS-CoV-2 variants.

The challenge with the different SARS-CoV-2 variants did not affect the percentage of naïve and memory T cells. Wuhan, Delta B.1.617.2, and Omicron B.1.1.529 spike variants enhanced the activation (CD69+perforin+) of memory T cells obtained one month after the booster dose. The Wuhan variant challenge induced the highest increase in the percentage of activated T cells, in both 9 months after the second vaccination and booster dose time points, compared with the Delta B.1.617.2 and Omicron B.1.1.529 variants challenge. The Alpha B.1.1.7 variant challenge slightly induced memory T cell activation.

In conclusion, the mRNA booster vaccine expressing Wuhan-Hu-1-like antigens induces increased neutralizing antibodies and enhanced memory T cell activation toward all the analyzed variants (Wuhan, Alpha B.1.1.7, Delta B.1.617.2, and Omicron B.1.1.529). The efficacy of the Wuhan variant in enhancing memory T cell activation suggests the presence of a vaccine-related immune imprinting, which boost the immune responses to the viral variant initially encountered by the immune system. These data are of extreme importance, suggesting a decreased efficacy of the Wuhan-Hu-1-like antigens-based vaccine toward the new viral variants, sustaining the need for updated vaccine-encoding sequences from one or more circulating variants. These data are still optimistic, as most vaccine-elicited T cell responses remain capable of recognizing all known SARS-CoV-2 variants. Nevertheless, it is of extreme importance to maintain strict surveillance of the variant evolution that could result in further reduction of T cell responses.

Funding

This research was funded by University of Ferrara grants (5 × 1000; Crowdfunding, 2021; FIR2021).

Ethical approval

The research was approved by the Ethics Committee of the Area Vasta Emilia Centro della Regione Emilia-Romagna (CE-AVEC) with the number 122/2021/Oss/AOUFe.

Author contribution

Study design: Roberta Rizzo and Marco Contoli.
Data and patient data collection: Luca Morandi.
Experimental analysis: Sabrina Rizzo, Giovanna Schiuma, and Silvia Beltrami.
Data analysis: Daria Bortolotti.
Writing: Alberto Papi, Roberta Rizzo, and Marco Contoli.

Data availability

All the data are available at request.

Declaration of Competing Interest

The authors have no competing interests to declare.

Supplementary materials

Supplementary material associated with this article can be found, in the online version, at doi:10.1016/j.ijid.2022.06.020.

References

- Andrews N, Tessier E, Stowe J, et al. Duration of protection against mild and severe disease by COVID-19 vaccines. *N Engl J Med* 2022;386:340–50.
- Collier AY, Yu J, McMahan K, et al. Differential kinetics of immune responses elicited by COVID-19 vaccines. *N Engl J Med* 2021;385:2010–12.
- Olliaro P, Torreale E, Vaillant M. COVID-19 vaccine efficacy and effectiveness—the elephant (not) in the room. *Lancet Microbe* 2021;2:e279–80.
- Rha MS, Shin EC. Activation or exhaustion of CD8+ T cells in patients with COVID-19. *Cell Mol Immunol* 2021;18:2325–33.
- Sancho D, Gómez M, Sánchez-Madrid F. CD69 is an immunoregulatory molecule induced following activation. *Trends Immunol* 2005;26:136–40.
- Tejaro JR, Farber DL. COVID-19 vaccines: modes of immune activation and future challenges. *Nat Rev Immunol* 2021;21:195–7.
- Tomiya H, Matsuda T, Takiguchi M. Differentiation of human CD8(+) T cells from a memory to memory/effector phenotype. *J Immunol* 2002;168:5538–50.
- Turner JS, O'Halloran JA, Kalaidina E, Kim W, Schmitz AJ, Zhou JQ, Lei T, Thapa M, Chen RE, Case JB, Amanat F, Raouf AM, Haile A, Xie X, Klebert MK, Suessen T, Middleton WD, Shi PY, Krammer F, Teefey SA, Diamond MS, Presti RM, Ellebedy AH. SARS-CoV-2 mRNA vaccines induce persistent human germinal centre responses. *Nature* 2021;596:109–13.
- Voskoboinik I, Whisstock JC, Trapani JA. Perforin and granzymes: function, dysfunction and human pathology. *Nat Rev Immunol* 2015;15:388–400.
- World Health Organization. Immunization coverage: 2021 <https://www.who.int/en/news-room/fact-sheets/detail/immunization-coverage> accessed 28 May 2022.

Although NK cells are traditionally considered as component of the innate immune system, they can also exhibit similar features to adaptive lymphocytes. In this terms, memory-like NK cells are a specific subset of innate cells, that can be generated after viral infectious diseases [356]. Similarly to T and B lymphocytes, activation of memory-NK cells during viral infection consists in an “education” process after the recognition of viral antigen [356]. This process interests CD56dim NK cells, that change their immunophenotype by the expression of maturation, activation and differentiation surface markers, namely CD57 [357], CD69 [358] and CD127 [359], respectively. Memory-NK cells maturation is also followed by the increase of NKG2C receptor expression, to encourage NK cells-mediated protection through the increase of their signaling, activation, proliferation and cytotoxicity [360].

In particular, SARS-CoV-2 vaccination might be effective in restoring NK cells functions to avoid immune depletion caused by virus. In fact, several studies have demonstrated that the BNT162b2 Comirnaty (Pfizer Australia Pty Ltd) vaccine promotes cellular and humoral immune activation, including the expansion of NK cells [361, 362].

These evidences are the basis of our study, in which we analyzed the correlation between the effect of Comirnaty (Pfizer Australia Pty Ltd) vaccine and the activation of circulating NK cells, especially one month after the booster dose ([363], paper attached). In vaccinated patients, we observed that one month following the booster dose there was an enriched in: a) NK cells with memory-like features (CD56dimCD57+ cells), b) differentiation marker CD127+ expression, and c) CD107a+ and/or Granzyme-B secreting cells. The increase in NK cells Granzyme-B secreting levels was revealed mostly after the stimulation with the Spike protein of Wuhan SARS-CoV-2 variant. In addition, NK CD56dim cells revealed a major expression of NKG2A, NKG2C, and NKG2D receptors ([363], paper attached).

Original Research

Natural Killer Cells in SARS-CoV-2-Vaccinated Subjects with Increased Effector Cytotoxic CD56^{dim} Cells and Memory-Like CD57⁺NKG2C⁺CD56^{dim} Cells

 Valentina Gentili^{1,†}, Daria Bortolotti^{1,†}, Luca Morandi², Sabrina Rizzo¹,
 Giovanna Schiuma¹, Silvia Beltrami¹, Fabio Casciano³, Alberto Papi³,
 Marco Contoli³, Giorgio Zauli^{4,‡}, Roberta Rizzo^{1,*}
¹Department of Chemical, Pharmaceutical and Agricultural Sciences, University of Ferrara, 44121 Ferrara, Italy²Pulmonology Unit, University Hospital of Ferrara, 44121, Ferrara, Italy³Department of Translational Medicine and LTTA Centre, University of Ferrara, 44121 Ferrara, Italy⁴Research Department, King Khaled Eye Specialistic Hospital, 11462 Riyadh, Saudi Arabia*Correspondence: rbr@unife.it (Roberta Rizzo)

†These authors contributed equally.

‡These authors contributed equally.

Academic Editor: Amedeo Amedei

Submitted: 7 May 2023 Revised: 15 May 2023 Accepted: 12 June 2023 Published: 31 July 2023

Abstract

Background: The infection and negative effects of the SARS-CoV-2 (severe acute respiratory syndrome coronavirus) virus are mitigated by vaccines. It is unknown whether vaccination has worked by eliciting robust protective innate immune responses with high affinity. **Methods:** Twenty healthy volunteers received three doses of Comirnaty (Pfizer Australia Pty Ltd.) and were evaluated 9 months after the second vaccination and 1 month after the booster dose. The exclusion criteria were the presence of adverse effects following the vaccination, a history of smoking, and heterologous immunization. The inclusion criteria were the absence of prior Coronavirus Disease (COVID)-19 history, the absence of adverse effects, and the absence of comorbidities. Specific phenotype and levels of CD107a and granzyme production by blood NK (natural killer) cells were analyzed after exposure to SARS-CoV-2 spike antigen (Wuhan, Alpha B.1.1.7, Delta B.1.617.2, and Omicron B.1.529 variants), and related with anti-SARS-CoV-2 antibody production. **Results:** The booster dose caused early NK CD56^{dim} subset activation and memory-like phenotype. **Conclusions:** We report the relevance of the innate immune response, especially NK cells, to SARS-CoV-2 vaccines to guarantee efficient protection against the infection following a booster dose.

Keywords: SARS-CoV-2; vaccine; innate response; NK cell

1. Introduction

The severe acute respiratory syndrome coronavirus, sometimes known as SARS-CoV-2 (severe acute respiratory syndrome coronavirus), is vaccine-preventable [1]. High affinity and persistent protective antibody responses indicate an efficient humoral immune response to vaccination [2]. By six months, there is a significant reduction in antibody responses, especially after vaccinations against SARS-CoV-2 mRNA [3].

A recent investigation found that the protection against Coronavirus Disease (COVID)-19-related hospitalization and death started to decrease in older adults and patients with weak or numerous medical conditions after 20 weeks [4]. Natural killer (NK) cells are essential for antiviral immunity. Virally infected host cells can be killed by NK cells by triggering apoptosis in various ways. Two of the proteins that it can first exocytose are perforin and granzymes, and when they interact, they can cause the target cell to undergo apoptosis [5]. By expressing the executioner molecules Fas cell surface death re-

ceptor (FAS) ligand (FasL) [6] and Tumor Necrosis Factor (TNF)-related apoptosis-inducing ligand (TRAIL) [7,8], NK cells can destroy the target. This stimulates the signaling of the extrinsic apoptotic pathway. NK cells can also release chemokines and pro-inflammatory cytokines such as Interferon (IFN)-gamma, TNF-beta, and granulocyte-macrophage colony-stimulating factor (GM-CSF) [9]. By encouraging pro- or anti-inflammatory tendencies as a disease progresses, NK cells exhibit functional plasticity [9].

Peripheral blood contains about 10–15% of human NK cells, which are recognized phenotypically by the presence of CD56 and CD16 on their surfaces and the absence of CD3. Based on the surface expression of CD56 and CD16, two subgroups of NK cells have been discovered in humans: CD56(+)bright/CD16(-) cells and CD56(+)bright/CD16(dim) cells. These categories are unique from one another in terms of function and homing abilities, in addition to physical characteristics. While CD56(+)bright/CD16(-) cells are mainly found in lymph nodes and inflammatory areas, CD56(+)dim/CD16(+)bright cells are principally cytotoxic and detected in peripheral blood [10].


 Copyright: © 2023 The Author(s). Published by IMR Press.
 This is an open access article under the [CC BY 4.0 license](https://creativecommons.org/licenses/by/4.0/).

Publisher's Note: IMR Press stays neutral with regard to jurisdictional claims in published maps and institutional affiliations.

Increased evidence suggests that the SARS-CoV-2 infection may affect the tissue distribution and effector capabilities of NK cells and that a rapid NK cell response may determine a patient's clinical outcome. However, more research is required to pinpoint the precise role of NK cells in the pathophysiology of COVID-19. Patients who have SARS-CoV-2 infection experience lymphopenia as a symptom. In patients with severe infections, neutrophils and monocytopenia frequently coexist with this lymphopenia [11]. Numerous independent studies revealed that the amount of NK cells in the bloodstream is also influenced by the SARS-CoV-2 infection [12,13] without differences in the location of NK cell subsets. This decrease in circulating NK cells appears to be related to the illness's severity and the acute stage [14,15]. NK cell counts gradually decrease in patients with a fatal course of the illness following the onset of symptoms, contrary to what has been demonstrated for T and NK cell numbers, which are increased in the latter stages of the illness [12,13,16]. According to recent studies, the quantity of NK cells in hospitalized patients and the rate of viral load reduction are directly related. Circulating NK cell counts may be used as a prognostic clinical parameter to predict the course of COVID-19. Patients with "normal" (>40 cells/L) NK cell numbers experience a faster decline in viral load than patients with "low" (40 cells/L) NK cell numbers, regardless of the clinical status. It is tempting to assume that the SARS-CoV-2 vaccination would be successful in restoring NK cells and their function, given the decreased frequency of NK cells seen in COVID-19 patients. Clinical studies have demonstrated that the BNT162b2 mRNA vaccine boosts cellular and humoral immunity, including the expansion of NK cells [17,18].

In this study, we tracked the development of circulating NK cells after Comirnaty (Pfizer Australia Pty Ltd) vaccination, concentrating on the activation of NK cells, given their relevant role in infection control.

2. Materials and Methods

2.1 Study Population

Twenty healthy volunteers were enlisted for the study. The exclusion criteria were the presence of adverse effects following the vaccination, a history of smoking, and heterologous immunization. The inclusion criteria were the absence of prior COVID-19 infection, the absence of adverse effects, and the absence of comorbidities. Following approval by the Area Vasta Emilia Centro della Regione Emilia-Romagna (CE-AVEC) ethics committee (protocol # 122/2021/Oss/AOUFe), samples were obtained with informed consent. Table 1 lists the demographic characteristics.

2.2 Human PBMCs Isolation

Peripheral blood mononuclear cells (PBMCs) collected 9 months after the second vaccination and 1 month

after the booster dose with mRNA vaccines were isolated from the whole blood of healthy donors by centrifugation using Lymphocyte separation medium (LSM; Corning; Merck Life Science S.r.l., Milan, Italy).

Table 1. Demographic and clinical characteristics.

Female, n (%)	50 (10)
Age (years), mean (SD)	36 (10)
Smoker, n (%)	0 (0)
Comorbidities n (%)	0 (0)
mRNA vaccine*	20 (100%)
Blood sample after second immunization (months ± SD)	9.0 ± 0.15
Blood sample after booster dose (months ± SD)	1.0 ± 0.12

*All the subjects received three doses of Comirnaty (Pfizer Australia Pty Ltd).

2.3 Antigen Presenting Cell Preparation and Antigen Loading

LSM (Corning; Merck Life Science S.r.l., Milan, Italy) was used to separate peripheral blood mononuclear cells (PBMCs) from whole blood of healthy donors 9 months after the second vaccination and 1 month after the booster dose with mRNA vaccines. Cells were plated at a density of 1×10^6 cells/mL in a T-25 flask and allowed to adhere for 2 h at 37 °C. Nonadherent cells were removed and used to obtain NK cells.

For five days, adherent cells were grown in specific media (CellGro DC, CellGenix; Freiburg, Germany) with 1000 IU/mL of GM-CSF (granulocyte-macrophage colony-stimulating factor) and 50 ng/mL of IL-4 (interleukin-4) (R&D System). Three spike protein antigens (Wuhan, Alpha B.1.1.7, Delta B.1.617.2, and Omicron B.1.1.529 full-length spike protein, BioServ, Flemington, NJ, USA) were added to the antigen-presenting cells on day 4 at a concentration of 40 µg/mL for 24 h. Tumor necrosis factor-α (20 ng/mL), interleukin-1 (10 ng/mL), and interferon-γ (1000 IU/mL) were used to stimulate the final antigen following cell maturation for two days [19].

2.4 NK Cell Purification and Stimulation

According to product instructions, NK cells were extracted from peripheral blood samples using the positive magnetic cell separation technique (Miltenyi Biotech, Gladbach, Germany). According to flow cytometry results using CD56-PerCp-Cy5.5 and CD16-FITC moAbs from e-Bioscience in Frankfurt, DE, the NK cell concentration was >90% (data not shown). Autologous pure NK cells were added at a rate of 1.5×10^6 /well for 4 h to allow for NK-cell stimulation after plating 1.5×10^5 /well spike-loaded antigen-presenting cells into a 12-well plate. As a positive control, NK cells were treated with 25 ng/mL PMA (Sigma, St. Louis, MO, USA) and 1 µM ionomycin (Sigma, St. Louis, MO, USA).

2.5 Granzyme ELISpot Assay

A total of 10^6 stimulated NK cells were placed into microplates in a humidified 37°C CO_2 incubator for 24 h. Granzyme-B release was quantified by the Human Granzyme B ELISpot assay (R&D Systems, Milan, Italy).

2.6 Flow Cytometry Analysis

Autologous pure NK cells were stimulated with spike-loaded antigen-presenting cells, as reported in Section 2.4. As a positive control, NK cells were treated with 25 ng/mL PMA (Sigma, St. Louis, MO, USA) and 1 μM ionomycin (Sigma, St. Louis, MO, USA). NK cells were stained with the following antibodies (Biolegends): APC mouse anti-human CD3, PerCP-vio700 mouse anti-human CD56, FITC mouse anti-human CD16, PE mouse anti-human NKG2A, NKG2D, NKG2C, CD127, and CD57. The samples were incubated for 30 minutes with the moAbs or anti-isotype controls (Exbio, Praha, CZ) in ice, washed, and analyzed with FACS Aria flow cytometer and FlowJo software (Becton Dickinson, San Jose, CA, USA), acquiring 10,000 events. Lymphocytes were identified according to forward/side scatter profile, and NK cells ($\text{CD}3^-/\text{CD}56^+$) were defined and gated within the lymphocyte gate (Supplementary Fig. 1b). Cell viability was assessed by propidium iodide staining. CD107a degranulation assay was performed after 1 h of incubation at 37°C and 3 h of treatment with Golgi Stop solution (Becton Dickinson, San Jose, CA, USA).

2.7 Anti-Spike RBD IgG Quantification

Plasma samples collected from vaccinated control subjects were evaluated by commercial ELISA assay for anti-RBD (receptor binding domain) IgG levels (ThermoFisher Scientific, Milan, Italy), following assay protocols. Anti-spike RBD IgG was considered specific for SARS-CoV-2 spike protein when a ratio >1.3 compared to the calibrator was obtained.

2.8 Neutralization Rate Evaluation

In vitro testing was done to determine the anti-SARS-CoV-2 infection-specific anti-spike antibodies' neutralizing power [20]. The SARS-CoV-2 inoculum was donated by Prof. Caruso of the University of Brescia in Italy and was isolated from a nasopharyngeal swab taken from a patient with COVID-19 (a Caucasian man of Italian descent, genome sequences available at GenBank (SARS-CoV-2-UNIBS-AP66: ERR4145453). This SARS-CoV-2 isolate belonged to the B1 clade, which also comprises the majority of Italians and sequences from other European and American nations. Plaque assay was used to measure the virus titer in Vero E6 cells, as previously mentioned [12]. Patient plasma samples were used to cultivate Calu-3/SARS-CoV-2-infected cells. The viral load was determined by real-time PCR for the SARS-CoV-2 genome performed on RNA extracted from cell supernatants, compared to infected con-

trols. The neutralization was reported as the decreased viral load percentage.

2.9 Viral RNA Detection

RNA extraction was performed by using the MagMAX Viral/Pathigen Nucleic Acid Isolation kit (ThermoFisher, Italy) according to the manufacturer's instructions, 48 h post-infection (hpi) [21]. SARS-CoV-2 titration was performed by RealTime-PCR with the TaqMan 2019nCoV assay kit v1 (ThermoFisher, Italy).

2.10 Statistical Analysis

Statistical analysis was performed by a parametric approach for the normal distribution, as assessed using the Kolmogorov-Smirnov test. Fisher's exact test was used to compare percentage frequencies, and Student's *t*-test was used to compare variables. Spearman's correlation test was used to evaluate linear regression. A value of $p < 0.05$ was accepted as statistically significant. The statistical analysis was performed by GraphPad software version 9 (Dotmatics, Boston, MA, USA).

3. Results

3.1 Spike-Binding and Neutralizing Antibody Levels

The sera of healthy donors showed significant spike-binding and neutralizing antibody variability following a second immunization (Fig. 1a,b). We observed an increase in the spike-binding and neutralizing antibody levels 1 month after the booster dose (Fig. 1a,b) (Student's *t*-test, Fisher's exact test, $p = 0.001$ respectively), demonstrating the success of the booster dosage in enhancing the humoral response towards SARS-CoV-2.

3.2 NK Cell Activation and Immunophenotype

We examined the immunological profile of NK cells nine months after the second vaccination and 1 month after the booster dose since the innate immune response is an important part of the protective immune response to infections [22,23]. Between 9 months after the second vaccination and 1 month after the booster dose, we detected no variation in the frequency of $\text{CD}3^- \text{CD}16^+ \text{CD}56^{\text{dim}}$ and $\text{CD}3^- \text{CD}16^- \text{CD}56^{\text{bright}}$ cells (data not shown). Fig. 2a shows the enrichment of $\text{CD}16^+ \text{CD}56^{\text{dim}}$ NK cells expressing NKG2A, NKG2C, and NKG2D 1 month after the booster dose (Fig. 2a-c) as compared to 9 months after the second vaccination ($p = 0.001$; Fisher's exact test). At 1 month after the booster dose, CD127, a differentiation marker, was more commonly seen in $\text{CD}16^- \text{CD}56^{\text{bright}}$ NK cells than at nine months following the second immunization (Fig. 2d) ($p = 0.001$; Fisher's exact test). There was no evidence of $\text{CD}127^+$ expression in $\text{CD}16^+ \text{CD}56^{\text{dim}}$ NK cells. Compared to the group that received the booster dose nine months after the first vaccine, highly mature $\text{CD}57^+$ NK cells were especially abundant among $\text{CD}16^+ \text{CD}56^{\text{dim}}$ NK cells (Fig. 2e) ($p = 0.001$; Fisher's exact test). There

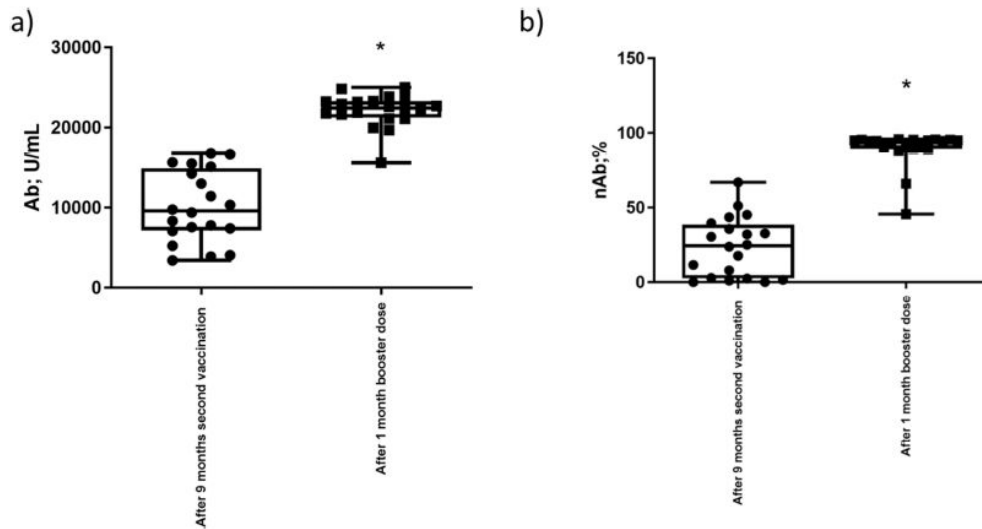


Fig. 1. Anti-Spike IgG evaluation. (a) Anti-spike SARS-CoV-2 RBD IgG (Ab) plasma levels in 20 healthy individuals 9 months after the second vaccination and 1 month after the booster dose. The results are reported as the mean \pm standard deviation. **p* values evaluated by the Students *t*-test. (b) Percentage of inhibition of SARS-CoV-2 infection of Calu3 in co-culture with plasma samples of 20 healthy individuals 9 months after the second vaccination and 1 month after the booster dose. The results are reported as the mean \pm standard deviation. **p* values evaluated by Fisher's exact test.

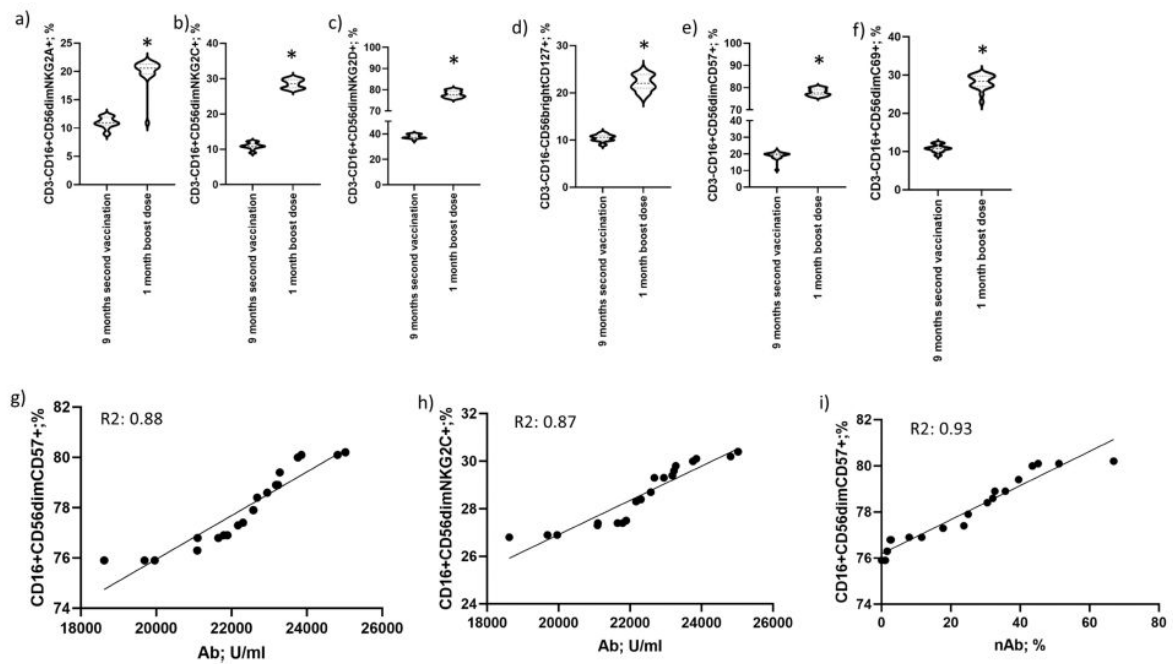


Fig. 2. NK cell immunophenotype. Differential profile of CD56^{dim} and CD56^{bright} NK cells 9 months after the second vaccination and 1 month after boost dose. The frequency of CD56^{dim} NK cells expressing (a) NKG2A, (b) NKG2C, (c) NKG2D, (e) CD57, and (f) CD69, and of CD56^{bright} NK cells expressing (d) CD127 in the peripheral blood of vaccinated subjects was assessed by flow cytometry. The results are reported as the mean \pm standard deviation. * significant *p* values evaluated by Fisher's exact test. The expansion of CD56^{dim} NKG2C⁺ or CD57⁺ NK cells in vaccinated subjects, 1 month after boost dose, according to SARS-CoV-2 seropositivity. Correlation between (g) CD56^{dim}CD57⁺, (h) CD56^{dim}NKG2C⁺ cells and SARS-CoV-2 serology. (i) Correlation between CD56^{dim}CD57⁺ cells and neutralizing SARS-CoV-2 serology. *r*² values were evaluated by Spearman's correlation test.

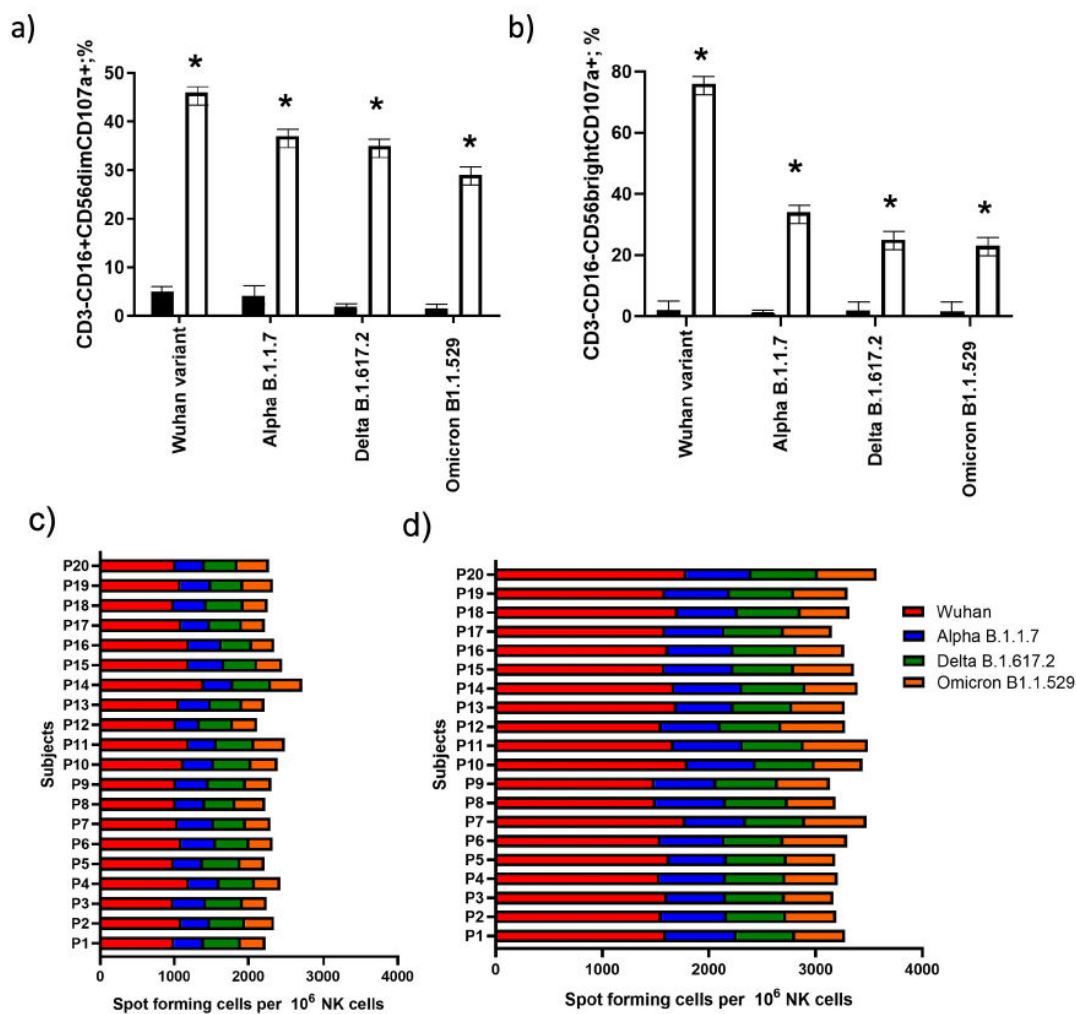


Fig. 3. NK cell activation and subset evaluation. The number of (a) CD56^{dim} and (b) CD56^{bright} NK cells expressing CD107a stimulated with Wuhan, Alpha B.1.1.7, Delta B.1.617.2, Omicron B1.1.529 variants. Black histogram: 9 months after the second vaccination; white histogram: 1 month after the booster dose. The results are reported as the mean \pm standard deviation. **p* values evaluated by Fisher's exact test. Spot forming cell per 10^6 NK cells secreting Granzyme-B after stimulation with Wuhan, Alpha B.1.1.7, Delta B.1.617.2, Omicron B1.1.529 variants. (c) 9 months after the second vaccination. (d) 1 month after the booster dose.

was no evidence of CD57 expression in CD16⁻CD56^{bright} NK cells. Additionally, in the month after the booster dose (Fig. 2d) (*p* = 0.001; Fisher's exact test), the percentage of CD16⁺CD56^{dim}CD69⁺ NK cells increased.

The results revealed considerable differences in NK surface markers expression 1 month after the booster dose, including a high level of NKG2A/C/D⁺ and CD57⁺ in CD56^{dim}CD16⁺ NK subsets and an increase of CD16⁻CD56^{bright}CD127⁺ NK cells.

3.3 Expansion of NKG2C⁺ and CD57⁺ NK Cells, and SARS-CoV-2 Levels of Seropositivity

Since there is evidence that at least some NK-cell subsets, such as the rise in NKG2C⁺CD57⁺ NK cells after viral infection, are involved in the adaptive immune response to particular antigens [19,21], we looked at the relationship between CD16⁺CD56^{dim}NKG2C⁺ or CD57⁺ NK cell numbers and SARS-CoV-2 seropositivity. In the 1-month post-booster dose group, the percentages of CD16⁺CD56^{dim}NKG2C⁺ or CD16⁺CD56^{dim}CD57⁺ cells (Fig. 2h,i) were significantly linked with the SARS-CoV-2 serology (*r*²: 0.88, 0.87, respectively; Spearman's correlation test).

3.4 Activation Markers in NK Subsets

We determined how frequently NK cells with CD16⁺CD56^{bright} and CD16⁺CD56^{dim} phenotypes released Granzyme-B and degranulated (expressed CD107a) after being stimulated by Spike. When compared to 9 months after the second vaccination, the group that received the booster dose showed enrichment of CD16⁺CD56^{dim}CD107a⁺ cells, with the Wuhan variant reaching a frequency of 46%, followed by the Alpha B.1.1.7 (37%), Delta B.1.617.2 (35%), and Omicron B.1.1.529 (29%; Fig. 3a). Following 1 month in the booster group, CD16⁻CD56^{bright}CD107a⁺ cells were most frequently observed (76%), and they were less frequently observed (34%), (25%) and (23%), respectively, 1 month after challenges with the variants Alpha B.1.1.7, Delta B.1.617.2, and Omicron B.1.1.529 in Fig. 3b. In a similar manner, the percentage of Granzyme-B⁺ NK cells increased after the booster dose when challenged with the Wuhan, Alpha B.1.1.7, Delta B.1.617.2, and Omicron B.1.1.529 variants (Fig. 3b; $p = 0.001$, Fisher's exact test), with the Wuhan variant inducing an increased percentage of Granzyme-B⁺ NK cells in both the 9 months following the second vaccination and the booster dose time points (Fig. 3b; $p < 0.001$).

The 1-month post-boost dose group showed enrichment of both CD56^{bright}CD16⁻CD107a⁺ and CD56^{dim}CD16⁺Granzyme-B⁺ NK cells.

4. Discussion

The elimination of viruses such as SARS-CoV-2 is known to be significantly assisted by NK cells [24]. The production of activated NK cells (i.e., expressing CD69 and CD107a) is essential for the success of vaccines. In order to further evaluate NK cell activity, we evaluated CD3⁻CD16⁺CD56^{dim} and CD16⁻CD56^{bright} blood cells, as well as the expression of surface receptors and activation markers in these cells [25].

One month following the booster dose, we identified a unique NK-cell profile that was enriched for maturing NK "memory" CD56^{dim}CD57⁺ cells [26], immature CD127⁺ expression [27,28], and CD107a⁺ and/or Granzyme-B secreting cells. In addition, the patients had CD56^{dim} cells that expressed NKG2A⁺NKG2C⁺NKG2D⁺. These findings showed that after receiving the booster dose for a month, the participants had an unusually activated NK-cell profile, most likely as a result of long-term exposure to SARS-CoV-2.

After one month of a booster dose, CD127 (IL-7 receptor chain) expression on CD56^{bright} NK cells increased. This was a recognizable change to the NK-cell surface marker. The prospect of dynamic replacement in NK cells is increased by the hypothesis that CD127⁺ NK cells are derived from the thymus. A subgroup of NK cells that express CD127 in mice lymph nodes is also thought to originate from the thymus [27]. Studies have documented the accumulation of immature CD127⁺ NK cells in mice

with developing tumors or those with persistent viral infections [28]. More studies are required to evaluate whether CD56^{bright} CD127⁺ NK cells in the peripheral blood of humans may be cells migrating from the thymus and homing to other sites.

NKG2D is an activating receptor essential for the antiviral and anticancer functions of NK cells. NK-cell CD56^{dim} subsets exhibited a significant increase in NKG2D expression one month after the boost dose. This finding may be related to SARS-CoV-2 resistance. SARS-CoV-2 S protein peptides that interact with the NKG2D receptor have been found through the use of in silico analysis. Cov1 and Cov2 were able to bind to NKG2D receptors and NK cells, respectively. These peptides induced NK cytotoxicity against lung cancer cells and promoted interferon-gamma secretion by NK cells by phosphorylating Vav1, a downstream-signaling protein of NK activation genes [29].

Individuals showed increased Granzyme-B synthesis one month after the boost dose, as well as increased CD69 expression, a hallmark of cell activation [30], in CD56^{dim} NK cells, and CD107a degranulation [31] in both CD56^{dim} and CD56^{bright} NK cells. Despite the fact that the CD56^{bright} subset is normally thought to be more secretory, the proportion of CD107a⁺ cells significantly increased. It is important to note that the four different SARS-CoV-2 genotypes that were evaluated increase the production of CD107a and Granzyme-B. These results suggest that different NK-cell subsets may activate to different degrees in the peripheral blood following a booster dosage and subsequent interaction with SARS-CoV-2 variants.

The purpose of NK cells that simultaneously express numerous receptors is unknown; however, it is most likely involved in the activation or inhibition of NK-cell subsets. It has been noted that SARS-CoV-2 causes an increase in HLA-E expression [32], which causes NK cells to perform less effectively for protection against the virus. It's intriguing to observe that 1 month following the booster dose, CD57 and NKG2C were substantially expressed on CD56^{dim} NK cells, and there was a clear correlation between this expression and IgG titers for SARS-CoV-2. We hypothesize that repeated anti-SARS-CoV-2 vaccinations are what led to the establishment of memory-like NK cells following the booster dosage, which has not yet been described.

5. Conclusions

Activating profiles with enhanced NKG2D⁺ expression and an increased percentage of CD107a⁺ and Granzyme B-expressing cells within both the CD56^{dim} and CD56^{bright} NK-cell subsets were detected in patients 1 month after the first dosage. The presence of memory-like CD56^{dim}CD57⁺NKG2C⁺ cells, an activating phenotype, as well as the increase in CD127 expression in NK CD56^{bright} cells, confirm a high frequency of immature and thymic-derived cells. More research is needed to determine

how the immune system reaction to SARS-CoV-2 is influenced by the expression of activating/inhibitory receptors on cytotoxic CD56^{bright} and CD56^{dim} NK cells and regulatory CD56^{bright} NK cells. These findings are encouraging since the majority of vaccine-induced NK cell responses are still able to distinguish between various SARS-CoV-2 variants. Nevertheless, it is crucial to monitor any variations that can lead to a potential decline in NK cell responses.

Availability of Data and Materials

The datasets used and/or analyzed during the current study are available from the corresponding author on reasonable request.

Author Contributions

These should be presented as follows: RR, MC, GZ designed the research study. LM collected data and patients. SR, GS, SB, FC, VG performed the research. VG, DB, AP analyzed the data. GZ, AP, RR, MC wrote the manuscript. All authors contributed to editorial changes in the manuscript. All authors read and approved the final manuscript. All authors have participated sufficiently in the work to take public responsibility for appropriate portions of the content and agreed to be accountable for all aspects of the work in ensuring that questions related to its accuracy or integrity.

Ethics Approval and Consent to Participate

The study was conducted in accordance with the Declaration of Helsinki, and approved by the Institutional Review Board of the Area Vasta Emilia Centro della Regione Emilia-Romagna (CE-AVEC) with the number 122/2021/Oss/AOUFe. Informed consent was obtained from all subjects involved in the study.

Acknowledgment

We thank Iva Pivanti for technical support.

Funding

This research was funded by University of Ferrara grants (5x1000; Crowdfunding 2021; FIR2021).

Conflict of Interest

The authors declare no conflict of interest.

Supplementary Material

Supplementary material associated with this article can be found, in the online version, at <https://doi.org/10.31083/j.fb12807156>.

References

- [1] Olliaro P, Torreale E, Vaillant M. COVID-19 vaccine efficacy and effectiveness-the elephant (not) in the room. *The Lancet Microbe*. 2021; 2: e279–e280.
- [2] Collier ARY, McMahan K, Yu J, Tostanoski LH, Aguayo R, Ansel J, *et al*. Immunogenicity of COVID-19 mRNA Vaccines in Pregnant and Lactating Women. *JAMA*. 2021; 325: 2370–2380.
- [3] Turner JS, O'Halloran JA, Kalaidina E, Kim W, Schmitz AJ, Zhou JQ, *et al*. SARS-CoV-2 mRNA vaccines induce persistent human germinal centre responses. *Nature*. 2021; 596: 109–113.
- [4] Andrews N, Tessier E, Stowe J, Gower C, Kirsebom F, Simmons R, *et al*. Duration of Protection against Mild and Severe Disease by Covid-19 Vaccines. *The New England Journal of Medicine*. 2022; 386: 340–350.
- [5] Lodoen MB, Lanier LL. Natural killer cells as an initial defense against pathogens. *Current Opinion in Immunology*. 2006; 18: 391–398.
- [6] Peter ME, Hadji A, Murmann AE, Brockway S, Putzbach W, Pattanayak A, *et al*. The role of CD95 and CD95 ligand in cancer. *Cell Death and Differentiation*. 2015; 22: 549–559.
- [7] Topham NJ, Hewitt EW. Natural killer cell cytotoxicity: how do they pull the trigger? *Immunology*. 2009; 128: 7–15.
- [8] Gismondi A, Bernardini G, Santoni A. NK cells and chemokines. In *Natural Killer Cells* (pp. 203–213). Elsevier: Amsterdam. 2010.
- [9] Corvino D, Kumar A, Bald T. Plasticity of NK cells in Cancer. *Frontiers in Immunology*. 2022; 13: 888313.
- [10] Poli A, Michel T, Thérèse M, André E, Hentges F, Zimmer J. CD56^{bright} natural killer (NK) cells: an important NK cell subset. *Immunology*. 2009; 126: 458–465.
- [11] García LF. Immune Response, Inflammation, and the Clinical Spectrum of COVID-19. *Frontiers in Immunology*. 2020; 11: 1441.
- [12] Zheng M, Gao Y, Wang G, Song G, Liu S, Sun D, *et al*. Functional exhaustion of antiviral lymphocytes in COVID-19 patients. *Cellular & Molecular Immunology*. 2020; 17: 533–535.
- [13] Giamarellos-Bourboulis EJ, Netea MG, Rovina N, Akinosoglou K, Antoniadou A, Antonakos N, *et al*. Complex Immune Dysregulation in COVID-19 Patients with Severe Respiratory Failure. *Cell Host & Microbe*. 2020; 27: 992–1000 e1003.
- [14] Maucourant C, Filipovic I, Ponzetta A, Aleman S, Cornillet M, Hertwig L, *et al*. Natural killer cell immunotypes related to COVID-19 disease severity. *Science Immunology*. 2020; 5: eabd6832.
- [15] Wilk AJ, Rustagi A, Zhao NQ, Roque J, Martínez-Colón GJ, McKechnie JL, *et al*. A single-cell atlas of the peripheral immune response in patients with severe COVID-19. *Nature Medicine*. 2020; 26: 1070–1076.
- [16] Wang F, Hou H, Yao Y, Wu S, Huang M, Ran X, *et al*. Systemically comparing host immunity between survived and deceased COVID-19 patients. *Cellular & Molecular Immunology*. 2020; 17: 875–877.
- [17] Polack FP, Thomas SJ, Kitchin N, Absalon J, Gurtman A, Lockhart S, *et al*. Safety and Efficacy of the BNT162b2 mRNA Covid-19 Vaccine. *The New England Journal of Medicine*. 2020; 383: 2603–2615.
- [18] La Sala L, Gandini S, Bruno A, Allevi R, Gallazzi M, Senesi P, *et al*. SARS-CoV-2 Immunization Orchestrates the Amplification of IFN γ -Producing T Cell and NK Cell Persistence. *Frontiers in Immunology*. 2022; 13: 798813.
- [19] Zheng Z, Takahashi M, Narita M, Toba K, Liu A, Furukawa T, *et al*. Generation of dendritic cells from adherent cells of cord blood by culture with granulocyte-macrophage colony-stimulating factor, interleukin-4, and tumor necrosis factor- α . *Journal of Hematotherapy & Stem Cell Research*. 2000; 9: 453–464.
- [20] Rizzo R, Bortolotti D, Morandi L, Rizzo S, Schiuma G, Beltrami S, *et al*. Humoral and adaptive immune responses to the

- SARS-CoV-2 vaccine. *International Journal of Infectious Diseases*. 2022; 122: 412–414.
- [21] Bezzeri V, Gentili V, Api M, Finotti A, Papi C, Tamanini A, *et al*. SARS-CoV-2 viral entry and replication is impaired in Cystic Fibrosis airways due to ACE2 downregulation. *Nature Communications*. 2023; 14: 132.
- [22] Tejjaro JR, Farber DL. COVID-19 vaccines: modes of immune activation and future challenges. *Nature Reviews. Immunology*. 2021; 21: 195–197.
- [23] Schiuma G, Beltrami S, Bortolotti D, Rizzo S, Rizzo R. Innate Immune Response in SARS-CoV-2 Infection. *Microorganisms*. 2022; 10: 501.
- [24] Eliassen E, Di Luca D, Rizzo R, Barao I. The Interplay between Natural Killer Cells and Human Herpesvirus-6. *Viruses*. 2017; 9: 367.
- [25] Rizzo S, Schiuma G, Beltrami S, Gentili V, Rizzo R, Bortolotti D. Role of KIR Receptor in NK Regulation during Viral Infections. *Immuno*. 2021; 1: 305–331.
- [26] Lopez-Vergès S, Milush JM, Pandey S, York VA, Arakawa-Hoyt J, Pircher H, *et al*. CD57 defines a functionally distinct population of mature NK cells in the human CD56^{dim}CD16⁺ NK-cell subset. *Blood*. 2010; 116: 3865–3874.
- [27] Gasteiger G, Hemmers S, Bos PD, Sun JC, Rudensky AY. IL-2-dependent adaptive control of NK cell homeostasis. *The Journal of Experimental Medicine*. 2013; 210: 1179–1187.
- [28] Vosshenrich CAJ, García-Ojeda ME, Samson-Villéger SI, Pasqualetto V, Enault L, Richard-Le Goff O, *et al*. A thymic pathway of mouse natural killer cell development characterized by expression of GATA-3 and CD127. *Nature Immunology*. 2006; 7: 1217–1224.
- [29] Kim H, Byun JE, Yoon SR, Koohy H, Jung H, Choi I. SARS-CoV-2 peptides bind to NKG2D and increase NK cell activity. *Cellular Immunology*. 2022; 371: 104454.
- [30] Borrego F, Robertson MJ, Ritz J, Peña J, Solana R. CD69 is a stimulatory receptor for natural killer cell and its cytotoxic effect is blocked by CD94 inhibitory receptor. *Immunology*. 1999; 97: 159–165.
- [31] Alter G, Malenfant JM, Altfeld M. CD107a as a functional marker for the identification of natural killer cell activity. *Journal of Immunological Methods*. 2004; 294: 15–22.
- [32] Bortolotti D, Gentili V, Rizzo S, Rotola A, Rizzo R. SARS-CoV-2 Spike 1 Protein Controls Natural Killer Cell Activation via the HLA-E/NKG2A Pathway. *Cells*. 2020; 9: 1975.

5.2. SARS-CoV-2 atypical infections

5.2.1. SARS-CoV-2 and pregnancy

The human placenta is a highly specialized organ, consisting in a dynamic interface between embryonic and maternal tissues, that supports the normal growth and development of fetus, as well as its nutrition [364].

The structure of placenta is very complex and includes several distinct maternal and fetal tissues. In particular, the decidua represents the maternal interface of placenta, characterized by the presence of specialized structures named chorion villi (Figure 13). In particular, three essential layers could be distinguished in placenta villi: syncytiotrophoblast (ST), an external layer covering the villi, cytotrophoblast (CT), an internal cellular part under the ST, and extra villous trophoblasts (EVT), in contact with both CT and decidua [365] (Figure 13), where is observed the presence of macrophages and decidual NK cells (dNKs). In particular, dNK cells represent the 40% of the total EVT resident leukocyte population, reaching the 75% in early pregnancy [366].

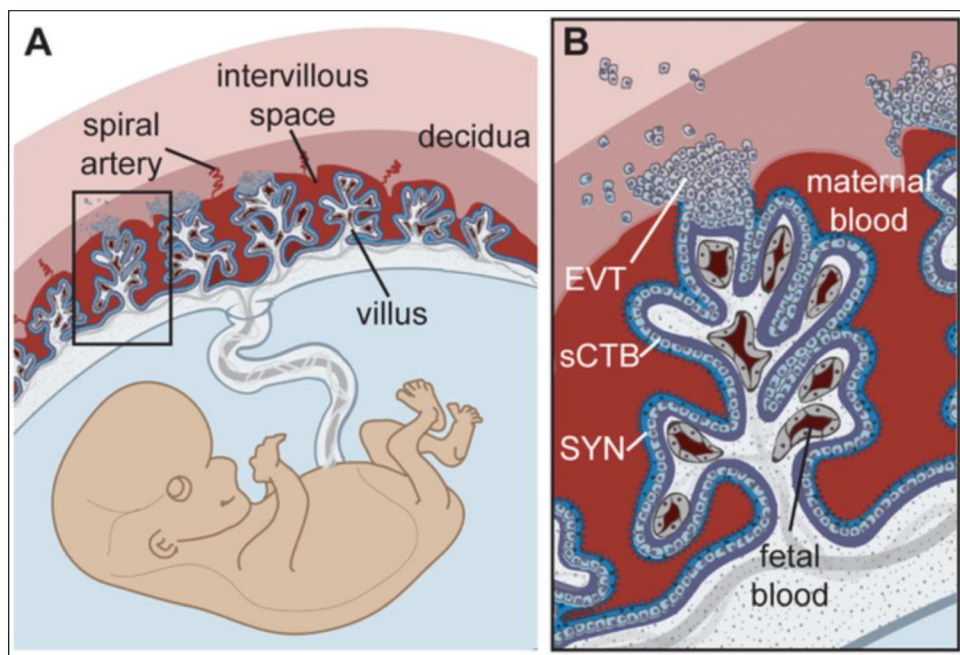


Figure 13. Panoramic of the placental structure (A). Characteristic layers of fetal/maternal interface in placenta: syncytiotrophoblast (ST), cytotrophoblast (CT) and extra villous trophoblasts (EVT) (B) [365].

Together with immune cells, the immunomodulatory molecule HLA-G plays a fundamental role during the early stages of pregnancy, protecting the semi-allogeneic fetus from the

attack of maternal immunity [367] through the interaction with specific inhibitory receptors expressed on immune cells [368].

Furthermore, HLA-G takes part in the placentation process, regulating the neo-angiogenesis [369]. The accurate modulation of placental processes is correlated to the peculiar changes in HLA-G expression during pregnancy: in fact, while the molecule presents high levels in the first trimester, a reduction of its expression is observed till the moment of birth, in order to promote the inflammatory environment that is need to induce the delivery [370].

Alterations in this physiological gestational HLA-G expression are often associated to pregnancy complications, such as increased risk of abortion, implantation failure and preeclampsia [371]. The tolerogenic environment found during pregnancy, in which HLA-G participates, is often exploited by pathogens as an immune-evasion mechanism.

Among these, both DNA and RNA viruses take advantage of the peculiar immunological status of pregnancy to escape the maternal immune system, thus leading to different clinical manifestations. Due to the impact of viral infections during pregnancy and the need to develop most effective diagnosis and therapies against gestational infection, in our review we summarized the most significant infections elicited by RNA (Rubella Virus, Measles Virus, HIV), DNA (Human Parvoviruses, Human Hepatitis Viruses, Human Papillomaviruses, Herpesviruses) and emerging (Dengue Virus, Zika Virus, West Nile Virus and SARS-CoV-2) viruses ([372], paper attached). The consideration concerning this condition, below reported, highlight the importance of viral infection impact on placenta tissues, correlating them to the main pregnancy complications ([372], paper attached).



Review

Gestational Viral Infections: Role of Host Immune System

Silvia Beltrami ^{1,†}, Sabrina Rizzo ^{1,†}, Giovanna Schiuma ¹, Giorgia Speltri ¹, Dario Di Luca ²,
Roberta Rizzo ^{1,*} and Daria Bortolotti ^{1,‡}

¹ Department of Chemical, Pharmaceutical and Agricultural Science, University of Ferrara, 44121 Ferrara, Italy; silvia.beltrami@unife.it (S.B.); sabrina.rizzo@unife.it (S.R.); giovanna.schiuma@unife.it (G.S.); giorgia.speltri@edu.unife.it (G.S.); brtdra@unife.it (D.B.)

² Department of Medical Sciences, University of Ferrara, 44121 Ferrara, Italy; ddl@unife.it

* Correspondence: rbr@unife.it; Tel.: +39-0532-455-382

† These authors contributed equally to this work.

‡ These authors contributed equally to this work.

Abstract: Viral infections in pregnancy are major causes of maternal and fetal morbidity and mortality. Infections can develop in the neonate transplacentally, perinatally, or postnatally (from breast milk or other sources) and lead to different clinical manifestations, depending on the viral agent and the gestational age at exposure. Viewing the peculiar tolerogenic status which characterizes pregnancy, viruses could exploit this peculiar immunological status to spread or affect the maternal immune system, adopting several evasion strategies. In fact, both DNA and RNA virus might have a deep impact on both innate and acquired immune systems. For this reason, investigating the interaction with these pathogens and the host's immune system during pregnancy is crucial not only for the development of most effective therapies and diagnosis but mostly for prevention. In this review, we will analyze some of the most important DNA and RNA viruses related to gestational infections.

Keywords: pregnancy; viruses; immune system; DNA viruses; RNA viruses



Citation: Beltrami, S.; Rizzo, S.; Schiuma, G.; Speltri, G.; Di Luca, D.; Rizzo, R.; Bortolotti, D. Gestational Viral Infections: Role of Host Immune System. *Microorganisms* **2023**, *11*, 1637. <https://doi.org/10.3390/microorganisms11071637>

Academic Editors: Andrea Marzi, Davide Gibellini and José Ramón Blanco

Received: 11 May 2023

Revised: 13 June 2023

Accepted: 19 June 2023

Published: 22 June 2023



Copyright: © 2023 by the authors. Licensee MDPI, Basel, Switzerland. This article is an open access article distributed under the terms and conditions of the Creative Commons Attribution (CC BY) license (<https://creativecommons.org/licenses/by/4.0/>).

1. Introduction

Pregnancy is characterized by a distinct immunological status that is designed to protect the fetus from maternal rejection but also to allow an appropriate fetal development and defense against pathogens [1,2].

The placenta represents the interface through maternal and fetal tissues, in which immunological changes occur that permit rejection avoidance of the semi-allogenic fetus by the maternal immunity and, at the same time, protect the fetus from viral infections until its birth [3].

The placental innate immune response to pathogens is important to protect both the fetus and mother. Thus, impairments of these immune effectors could allow the development of infections that might be associated to several diseases in pregnancy. The potential capacity of pathogen patterns' recognition and other host defense strategies have been described in the innate immune cells at the placental–decidual interface [4].

The protective effect of placenta toward infection is also due to its ability to transmit maternal protective antibodies to the fetus through the chorionic villus of the syncytiotrophoblast (SCT). Maternal Immunoglobulin G (IgG) passage to fetal circulation is mediated by neonatal FcRn receptors (FcγRI, FcγRII and FcγRIII) expressed on placental macrophages [5], and their concentrations in fetal blood increase from the beginning of the second trimester until the end of pregnancy.

The peculiar immunological status observed during pregnancy is characterized by an increase in circulating immune cells, which reaches the peak in the second trimester. During the first trimester, Foxp3⁺ regulatory T (T-reg) cells, essential for healthy gestational development and establishment of the tolerogenic status, are induced by estrogen [6–8]

and found to be abundant in peripheral, deciduous and umbilical cord blood [9]. Here, T-reg participates in the control of CD4+ and CD8+ T lymphocyte activation via Interleukin-10 (IL-10) and Transforming Growth Factor (TGF) release [10]. In fact, hormonal changes represent an important factor which affects immune responses during pregnancy, which might result in a decrease in the number of dendritic cells (DCs) and monocytes as well as a decrease in the activation of macrophages, T cells and B cells [11]. In fact, compared to the postpartum period, CD4+ and CD8+ T cells activation is down-regulated and, particularly during the third trimester, B lymphocytes are reduced [12].

Another notable aspect concerns the natural killer (NK) cells, lymphocytes of the innate immune system that function as the first line of defense against viral infection, which are found increased in maternal blood during the first trimester [13] and can account for up to 70% of the total deciduous leukocytes in early pregnancy [14]. In this contest, NK cells are specifically named decidual NK cells (dNK); they have a significant role in the regulation of cytokine production, particularly IL-10, as well as the generation of angiogenic factors and chemokines, which is crucial to control trophoblast invasion and vascularization at the implantation site [14–16]. Importantly, during the second and third trimesters of pregnancy, cytotoxic CD56 dim NK cells are lower than in the first trimester and postpartum period. In particular, NK cells shift their phenotype toward a more secretory profile, depicted as an increase in CD56 expression (NK CD56 bright), and produce less Interferons (IFNs), Tumor Necrosis Factors (TNFs) and IL-6 [17,18] compared to the postpartum period.

Of course, the activation of dNK toward viral infections reduces the potential risk of vertical transmission to the fetus. dNKs have been proposed to play a protective role against several infection through several mechanisms including the modulation of their cytotoxic effector functions [19] and the interactions between the killer-cell immunoglobulin receptors (KIRs) expressed by dNK and HLA molecules on the surface of the infected cells [20,21].

Hence, this implies that in the decidua, dNKs can eliminate harmful infection depending on the combination of KIR/HLA interactions between dNK and infected cells.

Again, concerning maternal monocytes, despite there being no evident differences in their total number, they exhibit phenotypic modifications, such as an increased expression of adhesion molecules (CD11a, CD54) and a high-affinity to IgG receptor FcR-I (CD64) [22]. In particular, Hofbauer (HB) cells, the fetal macrophages of the human placenta [23], can be detected as early as 3 weeks post-conception and are present throughout pregnancy [24]. Despite their role in villous and trophoblast remodeling [25], it has been postulated that HB cells may have a role in controlling infection during pregnancy, even if whether the HB cells can serve as a reservoir or limit virus replication is still unknown. As a proof of concept, isolated HB cells from healthy term placenta secreted elevated pro-inflammatory cytokines such as IL-6, MCP-1, IP-10, and IFN- α upon *in vitro* infection with Zika Virus (ZIKV) [26], even if HB cells are permissive for ZIKV infection and replication [27–29].

Blood-borne viruses can potentially be transmitted through the SCT barrier, even if SCT expresses only a few viral entry receptors. For example, SCT does not express ZIKV entry receptors (Axl and Tyro3) [30] and the Cytomegalovirus (CMV) entry co-receptor integrin α/β [31]. On the other hand, the STC apical surface expresses neonatal Fc receptor (FcRn) that functions to selectively transport maternal IgG [32], and it could be exploited by certain viruses to enter the placenta including ZIKV, Human Immunodeficiency Virus-1 (HIV-1), and CMV [33,34]. This FcRN-mediated viral entry at the STC, together with local inflammation and tissue damage, might disrupt its effective role as a barrier to most pathogens, giving the opportunity for vertical transmission.

However, humoral maternal response also actively participates, reducing the risk of vertical transmission, as supported by the low-affinity maternal antibodies that correlate with higher viral loads in the decidua, whereas intermediate to high neutralizing antibodies are associated with low viral replication [35].

Finally, also, a role in the development of placenta immune competence against the viral infection of both intra and extracellular-specific antiviral microRNAs has been suggested [36].

Clinical studies have shown that a high percentage of pregnancy complications, such as miscarriage, preterm delivery, growth retardation and preeclampsia, can be caused by intrauterine infections due to viruses, bacteria and other etiological agents [37]. The transmission of pathogens from mother to fetus can occur through several pathways: (a) via the maternal vascular endothelium to extravascular or endovascular trophoblasts (EVTs); (b) via infected macrophages in maternal blood that transmit the infection to placental trophoblasts; (c) via paracellular pathways from maternal blood to fetal capillaries [38,39]; and (d) via vertical transmission or ascending infection on urogenital tract [40]. The possible clinical consequences of maternal infection are explained in Table 1 [41].

Table 1. Summary of the possible outcome of infection during pregnancy, for both mother and fetus.

	Infection of Placenta without Infection of the Fetus	Fetal Infection without Placental Infection	Absence of Fetal and Placental Infection	Infection of Placenta and Fetus
Microorganism interaction	Microorganisms reach the intervillous space of the maternal side on placenta. They do not spread to the fetus.	Microorganisms can cross directly through the chorionic villi, using pinocytosis or diaphysis mechanisms.	Interaction of microorganisms that might reach the fetus with placenta.	Microorganisms pass from the infected placenta to the fetal compartment through the chorionic villi, directly infecting fetal membranes and amniotic fluid.
Effects	The infection does not involve the fetus thanks to fetal defense mechanisms by placental macrophages and the local production of antibodies and cytokines.	Infection of maternal leukocytes and erythrocytes.	The fetus is protected from the attack of microbial agents by the maternal endothelial reticular system and circulating leukocytes.	Transplacental transmission of infection can lead to death, with a subsequent resorption of the embryo, intrauterine fetal death or premature term birth of infected infant.

2. Methods

From this perspective, we have reviewed the main current data referring to pregnancy in correlation with the immune system and infections as well as to signaling functions and the potential impact on clinical conditions. Data were selected following eligibility criteria according to the reviewed topic. We used a set of electronic databases (Medline/PubMed, Scopus, Web of Sciences (WOS), Cochrane Library) for a systematic search until May 2023 using MeSH keywords/terms, such as “pregnancy”, “viruses”, “immune system”, “DNA viruses”, and “RNA viruses”. We applied no date or language restrictions. We followed the Preferred Reporting Items for the Systematic Review and Meta-Analysis (PRISMA) statement [42]. Two independent reviewers performed title–abstract screening on all selected studies; then, the full texts of the selected articles were reviewed. In cases of duplicate information, the data were checked and combined. Studies reporting pregnancy as well as viral infections were selected. Publications were selected using specific keywords (i.e., pregnancy, infection, virus, etc.) also according to the date of publication (not older than 1988) and to guarantee the fulfillment of the topic of this review. Studies that were just case reports and commentaries were excluded. The extraction of the data from included studies was performed by two reviewers separately, considering key characteristics including publication year, author, type of study, country, sample size, and laboratory findings. The funnel plot and Egger’s regression test were used to assess publication bias [43].

Therefore, it is evident that infections could have several repercussions on both the embryo and the fetus. More specifically, in the first weeks of gestation, often before the woman becomes aware of the pregnancy, they can cause the death of the embryo, while after the first 6 to 8 weeks of gestation, the presence of a pathogen can interfere with fetal organogenesis or, in general, cause miscarriage or stillbirth. In many cases, early infections during pregnancy are associated with placental abnormalities, causing

Intrauterine Growth Restriction (IUGR) [44]. On the contrary, infections in the third trimester are often responsible for premature births [45].

In addition, infections in newborns can be the cause of congenital diseases, due to the ability of microorganisms to survive and replicate in the tissues of infected infants, for months or years after infection in utero. In general, the presence of infectious agents and the release of endo- and exotoxins during pregnancy activate an immune response in both mother and fetus, triggering an inflammatory status due to the production of pro-inflammatory cytokines (TNF α , IL1- α , IL1- β , IL-6 and IL-8), which in turn stimulates chemotaxis, infiltration and the activation of other immune system cells [37,46].

Several studies have investigated the special immunological condition reported during physiological pregnancy, evidencing the importance of specific immune-regulatory processes, in which a crucial role belongs to the major histocompatibility complex molecules, in humans HLAs (Human Leukocyte Antigens), which are also involved in the response against viral infections [47,48]. The loss or down-regulation of classical HLA class-Ia antigens, as well as the neo-expression of non-classical HLA class-Ib antigens (HLA-E, -F, and -G), is a frequent strategy used by viruses for evading immune surveillance [49–51]. Among these non-classical HLA-Ib molecules, HLA-G and HLA-E represent the most studied for their tolerogenic role toward the fetus during pregnancy [52] and for their regulating function in neoangiogenesis during placentation [53].

HLA-G is an immunosuppressive molecule working through the interaction with specific inhibitory receptors (ILT2/LILRB1, ILT4/LILRB2 and KIR2DL4) expressed on immune cells, which leads to the inhibition of NK cells, CD8+ cytotoxic T lymphocytes and of macrophage-mediated cytotoxicity, allo-response, and maturation by CD4+ T cells, as well as the DCs functions. HLA-E is another crucial component of the immunological network at the fetal–maternal interaction [54]. HLA-E antigens have been discovered as ligands for a subset of immunoglobulin superfamily NK cell receptors CD94/NKG2, and their interaction may be responsible for the suppression of NK cell killer functions. In particular, peptide-loaded HLA-E binding to the inhibitory NKG2A receptor reduces NK cytokine cytotoxicity and secretion [55].

Again, the maternal HLA-C genotype seems to be crucial in defining uterine NK (uNK) cells function and maturation through interactions between maternal-activating or inhibitory killer immunoglobulin-like receptors (KIRs) expressed on the NK cell surface [56,57], and their peculiar expression has been reported to be associated to pre-eclampsia [58].

Viewing the role of HLA molecules in the antigen presentation process, several viruses are known to exploit classical and non-classical HLA-I regulation to avoid immune system recognition [59], including HHV-6 [60], HIV [61], CMV [62], Hepatitis B Virus (HBV) [63], Hepatitis C Virus (HCV) [64] and Human Papilloma Virus (HPV) [65].

Another important strategy adopted by viruses to evade their recognition by the host immune system consists of the escape from pattern recognition receptors (PRRs), which identified pathogen-associated molecular patterns (PAMPs), inducing inflammatory pathways by effectors of innate immunity [66]. Among the PRRs, Toll-like receptors (TLRs) are typically found on endosomal membranes [67], but this class of receptors is also expressed in the cellular cytoplasm or nucleus, which belongs to retinoic acid-inducible gene-I (RIG I)-like receptors (RLRs) [68]. Despite the activation of the PRRs pathway being enhanced and fundamental in pregnancy for viral infection clearance, the over-induction of the immune response initiated by PRRs might damage the surrounding tissues [69,70]. In fact, PRRs and mainly TLRs are expressed on trophoblasts, and they are also involved in placental damages, such as pre-eclampsia [71], preterm birth [72] and miscarriage [73]. Consequently, the lack of PRRs-mediated response might contribute to the fetal transmission of infection during pregnancy [74].

Therefore, both PRRs and HLA molecules may play protective and detrimental roles at the same time, potentially resulting in disorders linked to acute and chronic inflammation, since both DNA and RNA viruses often exploited the physiological tolerogenic condition

that characterizes pregnancy as an immunological evasion strategy [75], facilitating the onset of complications in the pregnant woman and fetus.

3. DNA Viruses and Gestational Infection

Due to the immune-tolerogenic state characteristic of pregnancy, there are several infections that can occur in pregnant women, showing poor outcome. Among these, some of the most widespread infections are represented by DNA viruses. Similarly, to bacteria or RNA viruses, DNA viruses infections during pregnancy are associated with increased health risks to both mother and fetus. However, although not all DNA viruses are related to an increased risk of complications during pregnancy, several of them can directly infect the fetus and/or cause placental dysfunction. For this reason, it is important to be aware of the potential impact of these viruses on both mother and fetus health, on the maternal immune system and in their effect in pregnancy outcome.

3.1. Human Parvoviruses

Among gestational infections, it is possible to mention Human Parvoviruses, consisting of Parvo B19 Virus (B19V) and less frequently observed Adeno-associated viruses (AAVs) and Human Bocaviruses (HBoVs).

Although in healthy adults most B19V infections result in mild non-specific illness [76], B19V causes the fifth disease during childhood and persistent anemia in immunocompromised patients, such as pregnant women. During pregnancy, in fact, congenital B19V infection can be responsible for fetal anemia, leading to hydrops fetalis, increasing the risk of miscarriage (Figure 1). Nevertheless, even if fetal abnormalities as a result of congenital Parvovirus B19V infection are mostly uncommon [77], this infection could increase the risk of neurodevelopmental impairment [78,79] (Figure 1). Since it has been observed that B19V is capable of inducing hydrops fetalis, many studies focused on analyzing this phenomenon. Garcia et al. [80] described six cases of non-immune hydrops that were fetal B19V-associated, pointing out the presence of a mononuclear cell infiltrate in the villous stroma and intervillous space in the whole cohort [80]. Nevertheless, it has been suggested that B19V infection is not only associated with an active maternal humoral immune response but also with an inflammation-mediated immune response at the maternal–fetal interface of the placenta [81]. However, although the presence of a lymphocyte infiltrate within placentas from women who became infected during pregnancy has been demonstrated, its specificity for B19V has not been evaluated yet [81].

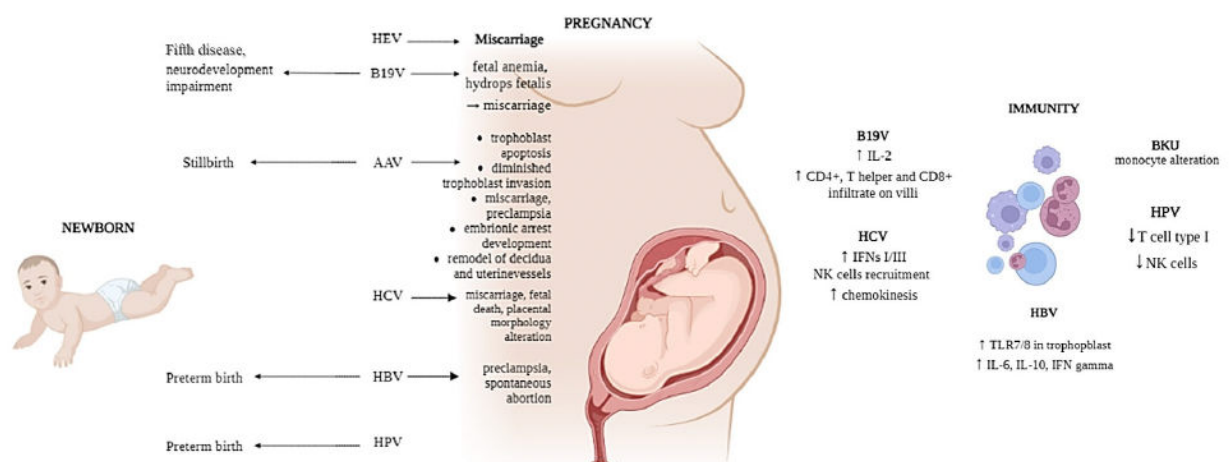


Figure 1. Representation of the main DNA viruses and their infection in newborn, pregnancy and mother immunity.

Even if the cell-mediated immune response to placental Parvovirus infection is not well characterized, a high increase in IL-2 production has been highlighted in placentas from women with parvovirus B19 infections compared to placentas from healthy controls [81], and nearly 90% of the Parvovirus-infected placentas had either a CD4+ T-helper or CD8+ cytolytic infiltrate into the villi [81].

Among human Parvoviruses, it is possible to distinguish AAV as well. Among these, AAV2 and AAV3 are responsible for infecting humans, even if Adeno-associated viruses usually require co-infection with a helper virus (Adenovirus) to cause a productive infection. AAV2 can infect placental trophoblast cells, inducing placental dysfunction when the infection occurs in early pregnancy [82]. AAV2 also induces trophoblast apoptosis and reduces cell invasion [83,84], increasing the risk of spontaneous miscarriage, stillbirth and pre-eclampsia [84–86] (Figure 1). Moreover, *in vitro* studies demonstrated that AAV2 infection inhibits the development of mouse embryos [87], and *in vivo* studies of pregnant mice showed fetal demise after AAV2 infection [84]. All these results suggest the possibility that early embryonic and trophoblastic viral infection could hinder the implantation or placentation process, possibly by inducing an anti-trophoblast cellular immune response [85] (Figure 1).

3.2. Human Hepatitis Viruses

Additional DNA viruses often underestimated during pregnancy are Hepatitis B virus (HBV), Hepatitis C virus (HCV) and Hepatitis E virus (HEV).

HBV is a member of the Hepadnaviridae family that generally infects hepatocytes and causes inflammation of the liver [76] that could progress to chronic infection. Vertical transmission during birth leads to a high percentage of chronicity compared to a later infection, but the chances of mother-to-child transmission can be reduced by antiviral treatment during and after pregnancy [88]. The consequences of HBV infection during pregnancy are still unclear; however, research has shown that maternal HBV infection increases the risk of preterm birth [89]. HBV is one of the many viruses that have also been studied in the context of pattern recognition receptors (PRRs) signaling in trophoblasts. In particular, TLR7 and TLR8 expression in the placenta of HBV non-transmitted neonates was higher than in transmitted neonates [90]. In fact, HBV infection increased TLR7, TLR8, MyD88, IL8, IFN- α and IFN- β mRNA levels in Swan71 cells, supporting the capability of HBV to translocate across the placenta [90]. Therefore, the increase in TLR7/8 observed in trophoblast cells exposed to HBV suggests a role for TLR7/8 signaling in the prevention of maternal–fetal transmission (Figure 1). Moreover, HBV is also able to up-regulate IL-6, IL-10, and IFN- γ through its HBV-X protein in trophoblast cell line [91], consequently stimulating immune responses (Figure 1).

HCV is also a leading cause of hepatitis in the western world, and its vertical transmission shows a rate between 3% and 6% [92]. Since nowadays, there are currently no vaccinations for HCV and no preventive strategies to reduce the risk of vertical transmission, its gestational infection should not be underestimated.

In a cohort made up of 145 HCV-positive pregnant women, 3.4% experienced intrauterine fetal death, which was higher than the miscarriage rate in the general population (0.5%) [93], although little evidence supports the association between HCV and miscarriage (Figure 1). Since HCV receptors are expressed on the surface of trophoblasts and extravillous trophoblast (EVT) cells, these cells are susceptible to HCV infection leading to some gestational complications and have some impacts on the morphology of the placenta as well [94] (Figure 1). HCV vertical transmission seems also to be facilitated by the specific NK cell receptor repertoire. Khakoo et al. [95] found a correlation between KIR2DL3 receptor, an inhibitory receptor expressed on NK cells, and HLA-C1 on decidua in HCV infection resolution, but it is yet unclear if the mother's HLA-C status at the maternal–fetal interface influences the decidual NK (dNK)-cell repertoire in HCV.

Some additional immune pathways that are stimulated by HCV infection and affect NK cells recruitment involve the up-regulation in Type I/III IFNs and other chemokines in

trophoblast cells by HCV-RNA [74] (Figure 1). This causes the enhancement of dNK T cell and $\gamma\delta$ T-cell cytotoxicity, resulting in damaging of the placental barrier (Figure 1). On the contrary, the reduced expression of NK cell activation markers CD69, NKp44 and TRAIL seems to improve HCV vertical transmission [96]. Nowadays, there are currently no vaccinations for HCV and no preventive strategies to reduce the risk of vertical transmission.

Concerning the Hepatitis E virus (HEV), its involvement in pregnancy could be attributed to hormonal and immunological changes that could make pregnant women more susceptible to HEV infection as well as a high viral load [97]. Pregnancy increases the levels of hormones including progesterone, estrogen and human chorionic gonadotropin, affecting the immune system function and in fact, estrogen and progesterone are reported to affect B-cell proliferation, CD8+ T-cell cytotoxicity and NK cells activation, promoting the spread of the infection [97,98]. The mechanisms underlying adverse fetal outcomes associated to HEV infection are largely unknown. However, an *in vivo* study conducted in HEV-infected pregnant mice showed a shift in the immune response from Th2 tolerogenic response, which is essential for maintaining pregnancy, to the pro-inflammatory Th1 profile [97]. This immune response alteration has also been seen in HEV-infected pregnant women who have hepatic failure, which could be considered a biomarker for miscarriage [99] (Figure 1).

3.3. Human Papillomaviruses

Human papillomavirus (HPV) represents another group of important gestational infections. HPV mostly spreads by direct skin contact, but some cases of vertical transmission during pregnancy have also been reported [100]. Trophoblast cells have been shown to be susceptible to several HPV strains, which can consequently alter physiological placental function [101], inducing gestational complications such as preterm birth, pre-eclampsia and spontaneous abortion [102,103] (Figure 1). A higher incidence of cervical neoplasia has been found in immunosuppressed women [104] and therefore, this phenomenon could be observed in pregnancy as well, since it is a state of mild immunosuppression due to the reduction in the Th1 cell-mediated response or decrease in NK cells (Figure 1). Thus, pregnant women are characterized by a physiological state with an enhanced risk of HPV infection, which is followed by the development of neoplasia. Furthermore, since a steroidal hormone receptor binding element on the transcriptional promoter of HPV-16 is responsible for inducing HPV transcription, the involvement of hormonal activation of HPV replication has been suggested [105]. This condition supports that the altered immunity state and the increased steroidal hormonal levels during pregnancy might influence the subsequent progression of the disease development [105].

3.4. Human Polyomaviruses

Among the fourteen different species of Polyomaviruses known to infect humans, the most studied in association to gestational infection are BK virus (BKV) and JC virus (JCV) because of their capability to be vertically transmitted, representing a risk for both mother and fetus [106].

In particular, the detection of BKV is frequent in pregnant women with prevalence between 15% and 65% [107–109]. Recently, an increased BKV reactivation was shown during pregnancy [110,111], which might be due to multiple reasons, including immunological and hormonal changes happening in pregnant women. The development of tolerance toward the fetus, characterized by the physiological depression of cell-mediated immunity, is the main cause of reactivation of latent viruses during pregnancy, such as BKV. Moreover, changes in monocyte function during pregnancy seem to modulate the level of BKV reactivation as well [112] (Figure 1).

4. Human Herpesviruses

Human herpesviruses (HHVs) are highly widespread among humans and therefore are among the pathogens most responsible for gestational infections. HHVs are classified into three subfamilies (alpha-, beta- and gammaherpesvirinae), and they are able to establish

permanent latency within the host in specific cells [113]. The alphaherpesvirinae family includes herpes simplex type-1 (HSV-1 or HHV-1), herpes simplex type-2 (HSV-2 or HHV-2) and varicella zoster virus (VZV or HHV-3). The betaherpesvirinae family includes cytomegalovirus (CMV or HHV-5), HHV-6A/B and HHV-7. The gammaherpesvirinae family consists of Epstein–Barr virus (EBV or HHV-4) and Kaposi’s sarcoma-associated herpesvirus (KSHV or HHV-8) [76].

4.1. HSV-1 and HSV-2

Normally, HSV-1 predominates in orofacial lesions and typically is found in the trigeminal ganglia, while HSV-2 is most found in the lumbosacral ganglia. The greatest risk of disease in the newborn is represented by the late-pregnancy infection of genitals in a previously unexposed woman, while recurrent infections are rarely associated with disseminated neonatal disease in immune-competent women.

However, a primary HSV infection of a pregnant woman leads to greater risks for both mother and child. Although HSV-infected pregnant women have rare or no clinical recurrences, there is still the risk of intrapartum transmission [114].

Women who already has antibodies to both HSV-1 and HSV-2 at the onset of pregnancy, which is the most common condition, have the least risk of perinatal transmission [115]. On the contrary, new-onset HSVs infection occurring late in pregnancy carries a 30% to 50% risk of neonatal infection, while early pregnancy infection carries a risk of less than 1% [116]. The possible explanation could be that when primary HSVs infection occurs during late pregnancy, the time for developing specific antibodies and suppressing viral replication before labor is not enough.

Again, while HSV-1 transmission from mother to newborn seems to be easier in the presence of both primary infection or recurrences [117], primary HSV-2 infection transmission to the fetus is less frequent [118], but it has been associated with a higher incidence of preterm birth [119] (Figure 2). The clinical manifestations of neonatal HSVs infection include encephalitis and disseminated disease, with a mortality rate of more than 50%. Survivors are, however, compromised, usually with significant neurologic deficits, blindness, seizures and learning disabilities (Figure 2). Different studies have also stated that HSVs infection can affect maternal immune responses, resulting in loss of HLA-G [120], cell death and reduced human chorionic gonadotropin (HCG) secretion [121] (Figure 2). These changes in trophoblast function could explain why both HSV-1 and HSV-2 have been associated with spontaneous pregnancy loss [122] and IUGR pregnancies [85,123] (Figure 2).

Moreover, HSV is capable of increasing the expression of TLR3, RIG-I, IFI6 and IFN- β proteins as well as decreasing TNF α production in terms of human placental explant cultures [124] (Figure 2), affecting maternal innate immune system antiviral responses.

4.2. CMV

Among herpesviruses, CMV is one of the most vertically transmitted and it represents the most common cause of congenital infection in high-income countries, causing neurological disability and sensorineural hearing loss in newborns [125] (Figure 2). The intrauterine infection caused by CMV occurs in 0.3% to 2.3% of births [126]. CMV intrauterine transmission is more common after primary infection (30–40%) than after non-primary infection (1%) [127,128]. Nevertheless, it was estimated that non-primary maternal infections are responsible for the majority of congenital CMV infections [129].

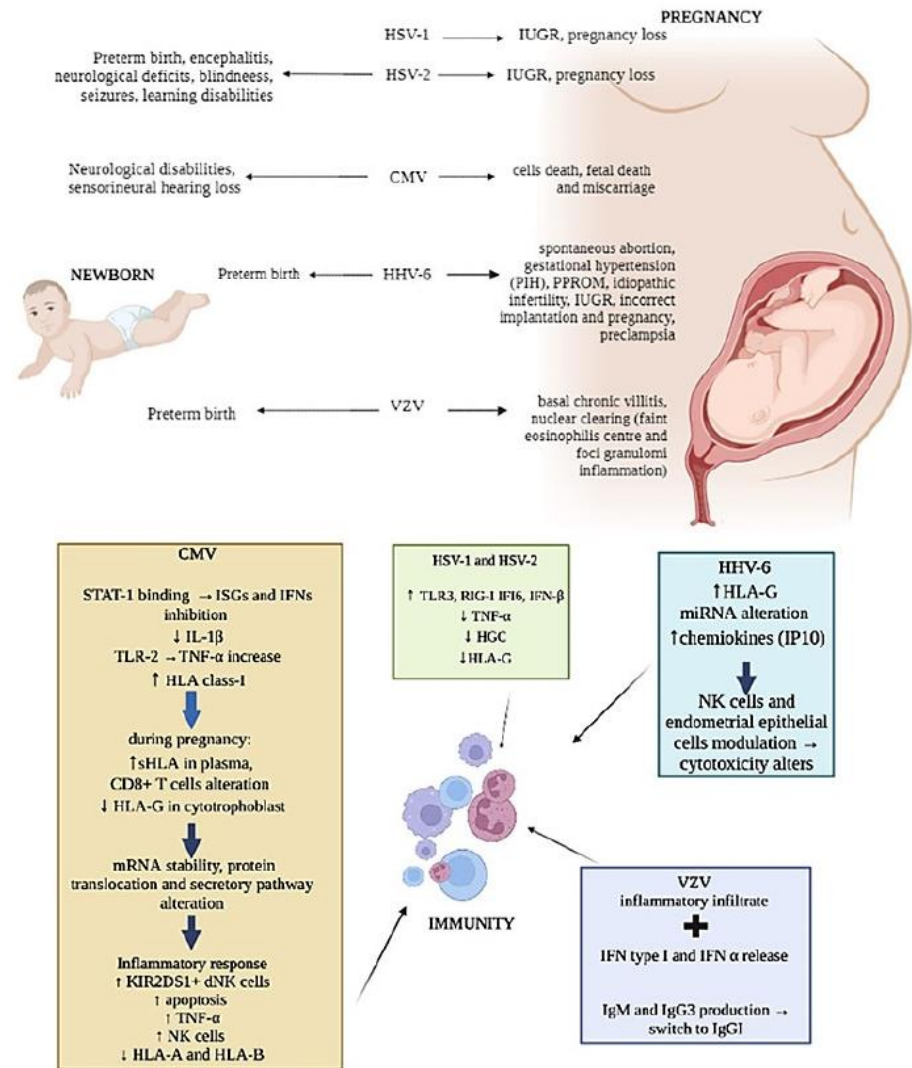


Figure 2. Representation of herpesviruses infection’s main effects on newborn, pregnancy and mother immunity.

CMV, such as many other viruses, employs multiple mechanisms to exploit the vulnerability of the placenta and impair the innate host response in order to spread the infection, including the expression of several viral proteins such as IE1 [130], IE86 [131], UL44, IE2 and UL94 [130,132,133].

The effect of CMV on the placenta has been confirmed by proving that ultraviolet-inactivated human CMV leads to syncytiotrophoblast apoptosis via TLR2, also increasing TNFα production [134,135]. Interestingly, in human villous explants, CMV did not induce the expression of RIG-I and MDA5 proteins and cytokine production [136], suggesting that RLRs could play a central role in the inhibition of vertical transmission of the virus as well as in the selectivity of vertical transmission of viruses across the placenta.

CMV can modulate the expression of HLA molecules by encoding specific viral proteins, mainly decreasing their expression on the cell surface to prevent immune cells recognition. In addition, CMV can selectively up-regulate specific HLA class-I molecules [137] (Figure 2). As aforementioned, HLA-G is physiologically expressed at the maternal–fetal interface on trophoblasts and is one of the major molecules targeted by viruses during pregnancy [138]. The concentrations of sHLA-G normally increases in the plasma of pregnant women during the first trimester of pregnancy [139], but during CMV infection, a

reduction in HLA-G in cytotrophoblasts was observed [140] together with its up-regulation in peripheral blood cells [141] (Figure 2). This effect is due to the interaction of specific CMV proteins with the HLA-G promoter, which affects mRNA stability and protein translation and secretion [142–144] (Figure 2).

Several studies have reported the failure of dNK to control CMV infection. Since NK cells activity is regulated by the expression of activation/inhibitory killer immunoglobulin-like receptors (KIRs), such as KIR2DL4, KIR2DS1/5, etc. as activating, and KIR2DL1/2/3, etc. as inhibiting, the expression of these receptors and of their ligands on target cells can be exploited by viruses as immune-escape mechanisms. Crespo et al. [145] demonstrate that CMV infection of human HLA-C2 + decidual stromal cells drives the cytotoxic activation of dNK and placental NK (pNK) cells in vitro by engaging KIR2DS2, and that KIR2DS1 or KIR2DS5-negative pregnant women have a lower ability to control placental CMV infection, developing complications. Van der Ploeg et al. [21] reported the molecular basis for the increased degranulation response of KIR2DS1 + dNK to CMV infection (Figure 2). Yan et al. [146] show that a KIR2DL4/HLA-G combination induces high NK cytotoxicity, which might be beneficial uterine CMV infection. Other studies described the presence of adaptive NK cell expansion found during different viral infections, concluding that in CMV-infected individuals, adaptive NK cells may be established probably as the result of opportunistic viral reactivation [147].

Moreover, the interaction between CMV and dNK cells can be the cause fetal death or miscarriage due to NK cell cytotoxic activity [148] (Figure 2). However, the CMV infection of EVT did not diminish the ability of EVT to increase FOXP3+ and PD1HI T-regs [149], suggesting that its infection does not alter the capacity of EVT to promote immune tolerance. This finding confirms the observation that dNK fails to degranulate in response to CMV-infected EVT, thus also maintaining immune tolerance in the presence of infection [20].

Moreover, the failure of dNK to respond to CMV-infected EVT during in vitro co-culture [20] may leave decidual CD8+ T cells as the predominant effector cell to clear pathogen-infected EVT.

Seropositive women during late pregnancy demonstrated an accumulation of highly differentiated CMV-specific T cells [150]. In fact, CMV seropositivity was shown to dramatically alter the maternal CD8+ T-cell repertoire during pregnancy [150], and T-cell responses to CMV rely heavily on HLA-C-restricted signals [151] (Figure 2). CMV CD8+ T cells were also found increased particularly in decidual tissue and were found able to produce IFN γ and restricted to recognizing viral peptides presented by HLA-A or HLA-B molecules, limiting the spread of infection to trophoblasts and/or the fetus [152].

4.3. HHV-6

HHV-6 is widely spread during pregnancy as well. HHV-6 DNA has been detected in blood and tissue samples from women with several types of gestational problems, including spontaneous abortions, gestational hypertension and preterm birth, in association with the detection of high anti-HHV-6 IgM and IgG titers [153] (Figure 2). HHV-6 DNA was also found in the amniotic fluid of women with gestational complications [154], as pregnancy induced hypertension (PIH) and the premature preterm rupture of membranes (PPROM) (Figure 2).

To date, despite different congenital herpetic infections having been associated with late IUGR, no direct implication of HHV-6 infection has been reported. In particular, HLA-G expression and HHV-6 infection have been evaluated in placentas from late-onset IUGR newborns compared to placentas from uncomplicated pregnancies [155], since HHV-6 is known to exploit the modulation of HLA-G as an immune-escape mechanism.

HLA-G increased and HHV-6 presence were found to correlate in IUGR placenta samples [155]. These preliminary results underline a direct relationship between HHV-6 infection and HLA-G deregulation that might affect vessel remodeling and prevent the correct pregnancy outcome in the IUGR condition (Figure 2).

However, HHV6 is comprised of two species, HHV-6A and HHV-6B [156,157]. While most of the population is infected by HHV-6B by 2 years of age, HHV-6A infection usually occurs later [158–160]. In particular, HHV-6A clinical manifestations are still unclear, but the presence of HHV-6A in endometrial epithelial cells of a subgroup of idiopathic infertile women [161] supported the role of HHV-6A [162] (Figure 2).

Moreover, it has been observed that HHV-6A infection induces a profound remodulation of miRNA expression in human cells of different origin [163], including human endometrial cells, in which HHV-6A modulates at least 16 miRNAs with potentially critical roles during embryo implantation [164]. These virus-induced alterations in the miRNA expression of endometrial cells might affect trophoblast cell behavior (Figure 2), supporting the hypothesis that HHV-6A might be associated with interference in correct implantation and pregnancy outcome [165].

The abilities of NK and endometrial cells have been described to be changed by HHV-6A infection. In fact, phenotypical and functional modifications of both endometrial NK (eNK) and epithelial cells have been reported in HHV-6A-positive infertile women samples, suggesting an imprint due to HHV-6A infection on both eNK cell immune-phenotype and receptors repertoire (Figure 2). In particular, during HHV-6A infection, eNK cells seem to acquire a cytotoxic profile as an attempt to limit the infection, which involves the NKG2D receptor [162]. The persistence of activated eNK and of subclinical HHV-6A infection could alter endometrial environment and disadvantage embryo implantation and placentation, and it could potentially have serious adverse side effects, such as pre-eclampsia, fetal growth restriction and stillbirth, as demonstrated by the increase in chemokines, mainly IP10 and FasL, in uterine flushing samples from HHV-6A-positive infertile women (Figure 2).

In addition, Rizzo et al. observed a lower percentage of KIR2DL4-positive eNK cells in primary infertile women in correlation to the diminished expression of soluble HLA-G [166]. This evidence supports the potential role of HHV-6 in female diseases, as a consequence of HLA-G modulation, that can in turn induce anergy to eNK cells via the inhibitory KIR2DL4 receptor [166].

4.4. VZV

VZV is the etiological agent for chicken pox at time of primary infection, and it is usually associated to mild clinical course, but in pregnant women, it may occasionally lead to serious maternal and fetal diseases. Maternal VZV can infect the baby by different routes: (a) transplacental viremia, (b) ascending infection during birth or (c) respiratory droplet/direct contact with infectious lesions after birth.

Even if the primary mechanism of VZV transfer across the placenta remains unclear, it is postulated that infected T cells might be present in the decidua basalis [4], where both CD4+ and CD8+ T cells are reprogrammed by the virus, becoming more capable of crossing into the intervillous space [167].

However, reports vary on the histological features of VZV placental infection, suggesting that VZV could be transmitted to the fetus via the placenta without apparent viral replication within the placenta [168] (Figure 2).

Interestingly, nearly 20% of infants with intrauterine-acquired VZV primary infection develop neonatal or infantile zoster, usually with uncomplicated course [169]. The disease is thought to represent reactivation of the virus after primary infection in utero, and the short viral latency may be explained by the immature cell-mediated immune response in young children.

Moreover, recurrent chickenpox has been documented in pregnant women [170], underlining again the key role of the immune system.

In addition to the tests of general antibody reactivity, tests of antibody avidity [171] and IgG isotype [172] can be used to assess the nature of VZV antibody responses. The avidity of antibodies seems to increase thereafter and during shingles, while there is a switch from IgM and IgG3 to IgG1 after primary disease [173] (Figure 2). Therefore, the

clinical manifestation of these pregnant women can be due to the high virus load and low immune responses [174], whether the effect of pregnancy and associated hormones on VZV replication is not known.

VZV infection causes a very early release of IFN type I, which is particularly abundant at the lesion level [175] (Figure 2). NK cells can also be found early after VZV infection [176], suggesting their central role in controlling viral spread. In fact, while both cytotoxic NK and primed CD8+ T cells were nearly absent during the early phase of life-threatening primary VZV infection [177], their responses to VZV seem to be protective and associated to mild symptoms [178]. As an example, the detection of T cells within three days after the appearance of the varicella rash, with rapid host response to primary VZV infection, has been known to be associated with milder rash and a more rapid clearance of viremia in healthy subjects [176].

5. RNA Viruses and Gestational Infection

Viruses with an RNA genome pose a threat to global human health since they can cause severe pandemics and epidemics [179]. Many viral epidemics have occurred recently, putting vulnerable persons, including pregnant women, at risk. In fact, pregnant women who experience RNA virus infection, such as EBOLA virus, often went into worse results than the general population and non-pregnant women, reporting for example increased incidence of preterm labor and unfavorable fetal outcomes [180].

Maternal susceptibility to RNA viral infections is firstly due to an over- or under-activity of the maternal innate immune system. In a normal pregnancy, in contrast to the general inhibition of specialized immune cells, a global up-regulation of innate immune cells and effector mechanisms is observed [181,182]. Compared to the non-pregnant state, complement activity increases, and there is a substantial rise in circulating phagocytes and type I IFN-producing plasmacytoid DCs [17,183]. The innate pathways that drive anti-RNA-viral defense are specifically enhanced during pregnancy, according to longitudinal investigations of serial blood samples from pregnant women. For instance, IFN-induced STAT-1 activation, a crucial response to viral infection, rises in NK cells, monocytes and myeloid DCs throughout gestation [181,184].

Among the most important pregnancy-related RNA virus infections, there are Rubella, HIV and emerging viruses such as Ebola, Zika, Dengue and SARS-CoV-2 infections, which are associated with an increased risk of spontaneous miscarriage, bleeding and death during pregnancy (Figure 3).

5.1. Rubella Virus

Dr. Norman Gregg described for the first time the catastrophic teratogenic consequences induced by rubella virus (RV), consisting of congenital cataracts and other malformations in the newborn following rubella (German measles) infection in the mother during pregnancy [185,186] (Figure 3). Despite the serious teratogenic effects reported, many RV cases are asymptomatic; thus, women of childbearing age are routinely tested for antibodies to RV in order to identify and immunize susceptible women. The vertical transmission of the infection depends on the gestational age at infection, leading to the development of congenital rubella syndrome (CRS), which is a condition that might affect any organ due to fetal non-lytic infections [185] (Figure 3), in which the virus can persist in different biological fluids for several months after infection [187].

First and early second trimesters of pregnancy seem to be the most susceptible times for CRS development. In fact, while there are few problems if the infection is transmitted to the fetus after 17 weeks of gestation, CRS affects nearly all fetuses infected in the first 8 weeks of pregnancy [185]. Deafness is the most prevalent of the several symptoms of CRS, while in the most critical cases, infected tissues from aborted fetuses showed extensive non-inflammatory necrotic damage to the brain (vascular necrotic lesions in cerebral blood vessels), heart (myocardium, endothelial cells in cardiac vessels), ears (epithelium of cochlear duct), and eyes (lens, iris, retina) [188]

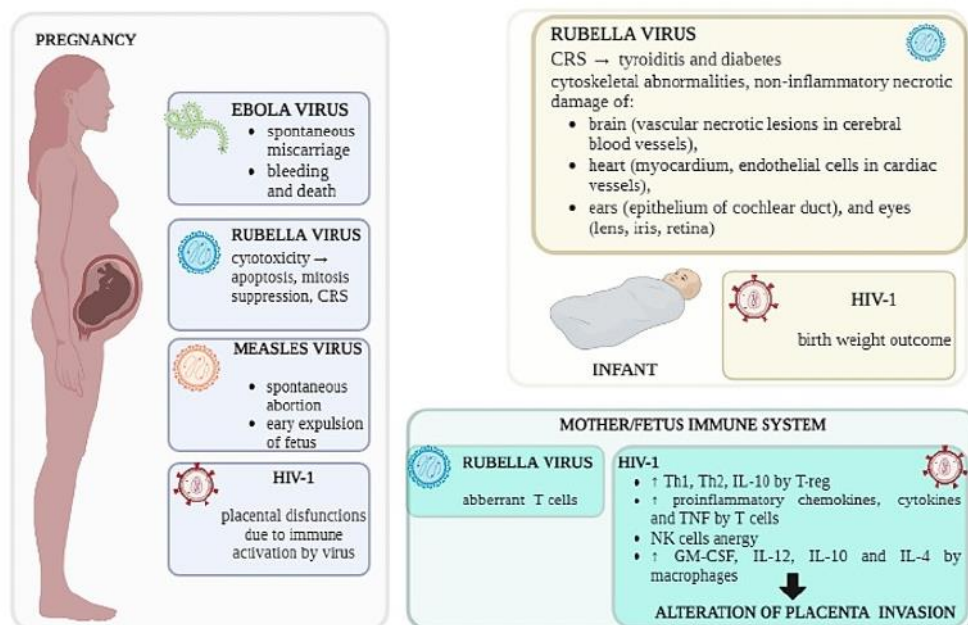


Figure 3. Representation of RNA viral infection and their effect in pregnancy, infants and mother/fetus immunity.

(Figure 3). Additional studies have shown that CRS is linked to autoimmune diseases and increases the risk of thyroiditis and diabetes [189] (Figure 3).

Unfortunately, to date, little is known about the effect of RV on both the maternal and fetal immune system, and the few studies available reported an impaired cell-mediated immunity to rubella virus during pregnancy that could lead to congenital infection if it occurs early in utero, with a profound effect on the developing immune system [190–192].

It seems that rubella reinfection during pregnancy is not associated with a lack of neutralizing antibodies or persistent impairment of rubella-specific T responses. In particular, specific T response was present in almost cases of vertical transmission [191].

The specificity of a prenatal diagnosis, recommended when a maternal infection is diagnosed, is approximately 100% and is based on the detection of virus-specific-IgM in fetal blood or on the detection of the viral genome in amniotic fluid, fetal blood, or chorionic villus biopsies. The detection of RV-IgM by immunocapture ELISA, which has sensitivity and specificity that approach 100% in infected neonates, is the foundation for a postnatal diagnosis of congenital Infection. Regardless of whether a clinical manifestation of CRS is seen, it is crucial to perform a postnatal diagnosis of a congenital infection in order to give a specific follow-up treatment plan (including neurological and hearing monitoring) if an infection is found [187,193].

5.2. Measles Virus

Measles (rubeola) is a highly contagious respiratory disease brought on by a single-stranded, enveloped RNA virus that belongs to the Paramyxoviridae family, genus Morbillivirus [194].

Numerous studies have shown that pregnant women are more likely to suffer and die from measles than non-pregnant ones. In fact, even if measles virus (MV) is not teratogenic as rubella virus, it affects the physiological processes of immunotolerance that are present during pregnancy through alterations mainly on cell-mediated immunity that could result in spontaneous abortion or the early expulsion of the fetus [195] (Figure 3). Despite intensive vaccination campaigns that have been adopted in the most industrialized regions of the world, MV infection remains widespread, and the number of measles cases

reported in the USA are rising, together with the chance of MV infection in pregnant women and the number of infections in women of reproductive age [196]. A study conducted on this outbreak showing the significant impact of the disease on pregnancy outcomes reported that 16% of pregnant women who underwent the infection had adverse outcomes probably correlated to increased CD8+ levels [197].

5.3. HIV

Despite highly active antiretroviral therapy (ART), HIV infection continues to be a concern for international health and for pregnancy as well. Currently, 81% of HIV-positive pregnant women worldwide are receiving ART and globally, the number of new perinatal infections has decreased by 50% because of increased ART use [198]. Even though the introduction of combination antiretroviral medication has significantly improved pregnancy outcomes and the health of children born to HIV-infected mothers, there are still worries about the effects of maternal HIV infection on pregnancy outcome and the health of HIV-exposed uninfected newborns [199].

One of the biggest changes from the immunological point of view that occurs during pregnancy and enables maternal–fetal tolerance is the increase in Th2 lymphocytes at the expense of Th1 [200,201], which is characterized by increased activated T cells and high levels of TNFs (Figure 3). Additionally, pregnant HIV-1-infected women’s placentas exhibit histological indicators of inflammation and an increased production of pro-inflammatory cytokines and chemokines [202] (Figure 3), which could impact the migration of T-cell subtypes to the placenta [203]. Additionally, a down-regulated expression of cytokine receptors, such as CD127 (IL-7 receptor) (Figure 3), highly expressed on tissue-resident T cells, could interfere with proper T-cell function.

NK cells are also necessary for placenta modeling vascularization [204]. This process is controlled by interactions between killer-cell immunoglobulin-like receptors (KIRs) expressed on maternal uterine NK cells and their corresponding HLA-C ligands on invading trophoblasts [205]. According to several studies, HIV-1 infection impairs NK cell function, resulting in the loss of effector functions and an increase in anergic NK cells, affecting the ability of uterine NK cells to support the invasion of maternal spiral arteries in the placenta [206,207] (Figure 3). Additionally, since HIV-1 infection has been linked to changes in chemokine receptors on immune cells, such as CCR5, the homing of NK cells to the placenta may be affected in HIV-1 infection [208]. Placental dendritic cells and macrophages in healthy pregnancy mostly display tolerogenic characteristics, as evidenced by a decreased expression of IL-12 and a high production of IL-10 and IL-4. Meanwhile, macrophages in HIV-1-infected women’s placentas have been seen to produce more GM-CSF and IL-2 while producing less IL-10 and IL-4 [209,210] (Figure 3).

In addition to the RNA viruses mentioned so far, also, emerging RNA viruses have gained attention for their potential in causing complications during pregnancy and will be reviewed below.

6. Emerging Viruses and Pregnancy

6.1. Dengue Virus

Among the emerging viral infections representing a risk factor during the gestational period, Dengue Virus (DENV) infection is gaining more and more importance. Defining the risks associated with DENV infection in pregnancy has proved particularly challenging due to different reasons, such as the high proportion of asymptomatic cases and the difficulties associated with accurately diagnosing acute dengue fever (dengue IgM cross-reacts with other flaviviruses, and co-infections are common) [211]. The first to definitively establish the association between pregnancy and severe DENV infection have been Machado, comparing the outcomes in infected pregnant women to matched non-pregnant women of reproductive age, and they found an increased risk of severe dengue in the pregnant women (odds ratio 3.38) with a trend toward higher mortality (3 vs. 1.1%) [212]. Another

study showed an 8.6-fold increase in the risk of postpartum hemorrhage in the presence of severe infection [213].

However, placental tropism, innate immune adaptations and the physiological increase in vascular permeability occurring in normal pregnancy could be at the base of this increased susceptibility to severe DENV infection in pregnancy [214].

Some of the multiple effects of DENV infection include the depletion of human megakaryocytes that leads to dengue-induced thrombocytopenia (Figure 4). Campbell et al. found that DENV leads to a marked up-regulation of interferon-induced transmembrane protein 3 (IFITM3) on platelets, with a corresponding release of type I IFNs, and that the highest levels of IFITM3 expression correlated with the mildest disease [215,216] (Figure 4). It is conceivable that enhanced DENV-mediated megakaryocyte depletion, or a failure to up-regulate platelet IFITM3, could contribute to the higher rates of hemorrhagic complications during pregnancy.

However, type I IFN production is central to the innate anti-DENV response, although no specific studies have been conducted in pregnancy. In fact, DENV binds various PRRs, including RIG-I, endosomal TLR3 and endosomal TLR7, and the activation of these RNA sensors induces the deposition of Cb4 and C2a complement proteins on the virion surface, promoting the complement-mediated virolysis. Interestingly, emerging evidence states that vitamin D supplementation reduces cultured human DC susceptibility to DENV2 through the down-regulation of TLR3, TLR7 and TLR9 signaling [217], strengthening the importance of these sensors in the control of DENV infection.

Again, it has been suggested that RNA interference is also involved in the activation of apoptosis in infected cells and is an important contributor to DENV defense as well [218].

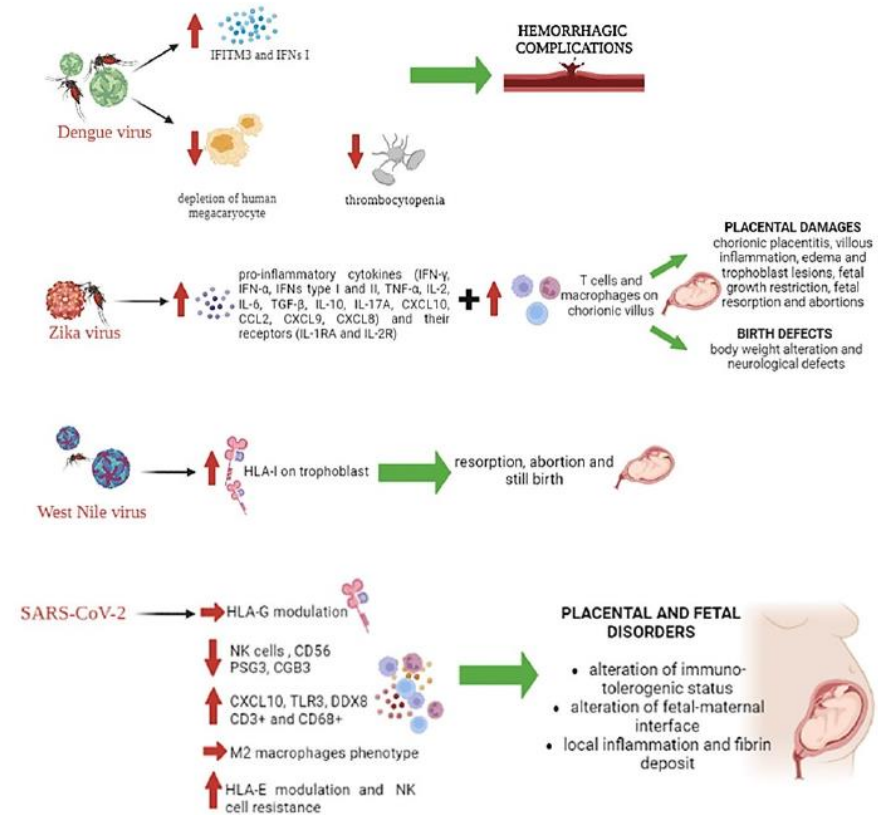


Figure 4. Representation of emerging viruses and their role in immune response alteration as cause of placenta and fetal disorders.

6.2. Zika Virus

As already mentioned before, ZIKV infection during pregnancy has recently been associated with birth defects and abortions, mainly when infection occurs during the first and second trimesters of pregnancy [219–222] (Figure 4).

Unfortunately, there is little information about the immune response to ZIKV infection in pregnant women [223]. During pregnancy, immunoglobulin synthesis is increased, whereas the cell-mediated response is decreased. These systemic changes are associated with an altered Th1/Th2 balance, with a prevailing anti-inflammatory Th2-like profile [224], that shifts toward a Th1/Th17 pro-inflammatory profile by the end of pregnancy [225], which could participate in viral pathogenesis (Figure 4).

The factors involved in ZIKV gestational pathogenesis are still unclear but may include prior exposure to closely related flaviviruses [226], a phenomenon originally described between DENV serotypes, which is known as antibody-dependent enhancement (ADE).

It has been shown that the presence of DENV-specific antibodies in ZIKV-infected pregnant mice significantly increased placental damage, fetal growth restriction and fetal resorption [227] (Figure 4). This was associated with enhanced viral replication in the placenta, leading to an increased frequency of infected trophoblasts.

ZIKV-infected human placental tissues also showed increased viral replication in the presence of DENV antibodies, which was reversed by FcγR blocking antibodies. Furthermore, ZIKV-mediated fetal pathogenesis was enhanced in mice in the presence of DENV-reactive monoclonal antibodies but not in the presence of the L234A and L235A (LALA) variant, indicating a dependence on FcγR engagement [227].

In a vertical-transmission model, ZIKV-immune plasma infused to timed pregnant mice increased fetal demise and decreased the body weight of the newborns [228] (Figure 4). Together, these data show that passive immunization with homotypic ZIKV antibodies, depending on the concentration, could either worsen or limit a subsequent ZIKV infection, suggesting the importance of immunity in the pathogenesis of this infection and underlining the key role exerted by antibodies.

Generally, pregnant women infected by ZIKV present chronic placentitis with chronic villous inflammation, edema, and trophoblastic lesions [229] (Figure 4). There is evidence that ZIKV infection compromises mesenchymal and Hofbauer cells in human villi [230], and further analysis reveals that ZIKV stimulates the proliferation of placental macrophages within the chorionic villous stroma [231] (Figure 4). CD163 or CD68-positive cells are colocalized with ZIKV antigens *in vivo* [30,232], as confirmed by *ex vivo* models showing a higher permissivity of placental macrophages to ZIKV than trophoblasts [233].

Although little is known about the cell-mediated immune response to ZIKV infection during pregnancy, a recent study reported a decreased frequency of granzyme B expressing total of CD8⁺ T cells in pregnant mice compared to non-pregnant mice [234], suggesting that the anti-ZIKV T-cell response quantity or quality may be reduced during pregnancy. It has been demonstrated that CD8⁺ T cells are necessary and sufficient to protect against systemic ZIKV challenge in both naïve and DENV-immune non-pregnant mice [235–237].

A similar requirement for CD8⁺ T cells against ZIKV was observed in the context of pregnancy prior to DENV exposure [235] together with a partially protective role for CD4⁺ T cells, suggesting that CD4⁺ T cell-mediated help may shape an optimal cross-reactive CD8⁺ T-cell response during the ZIKV infection of DENV-immune pregnant females. Alternatively, CD4⁺ T cells may exert their effect by regulating humoral immunity and the production of Th1 cytokines (IFN-γ, TNF-α, and IL-2) or CD4⁺ regulatory T cells could minimize pathology at the maternal–fetal interface [238].

In addition to this pro-inflammatory adaptive immune response, ZIKV infection also induces innate immunity activation as well. The innate immune response is mainly mediated by the induction of types I and III IFN, which induces an early autocrine antiviral stage in infected cells [239,240] (Figure 4).

Again, also, high levels of IFN-γ, TNF-α, IL-6, TGF-β and IL-10 [241] have been observed during acute ZIKV infection in pregnant women [242,243] (Figure 4). The in-

creases in IFN- α and IFN- γ suggest that pregnant women elicit effective antiviral responses [244,245], and the high levels of IL-10 suggest an antiviral response that could favor recovery and favorable evolution [246–248] (Figure 4).

6.3. West Nile Virus

Even though exposure to infected mosquitoes is the most important risk factor for West Nile Virus (WNV) infection, viral transmission includes blood transfusion [249], organ transplantation [250] and breastfeeding [251] as well as transplacental infection during pregnancy [252].

Transplacental WNV infection [253] is rare, since human placenta is a barrier which separates maternal and fetal circulations. However, as already mentioned for other viruses, it is not a perfect barrier, and in case of primary viral infections without a pre-formed maternal adaptive immunity, it can transmit the infection to the fetus.

Even if WNV was found in infants within a month of delivery from WNV-positive mothers, suggesting congenital transmission of the virus [253], little is known about the specific mechanisms exploited by WNV to cross the placenta, and it is unclear whether and how the virus is able to induce clinical manifestation in infants [253].

In vivo studies have reported an extremely high mortality rate in pregnant mice (98%, 60/61) compared with non-pregnant controls (52%, 28/53) independent of the infecting dose or the week of pregnancy [254]. Interestingly, although WNV RNA could be detected in both placentas and fetuses, antibody titers were similar between pregnant and non-pregnant mice and between surviving and non-surviving animals as well as WNV RNA titers in brains. In addition, from these observations in mice, it is possible to point out that pregnancy increases the risk of severe WNV infection and may help to understand the pathogenic mechanisms involved in WNV infection during human pregnancy [254].

Detailed studies of WNV infection of immunosuppressed human hosts, which are characterized by a similar immunotolerant condition as pregnancy, have highlighted important aspects of the disease pathogenesis during the gestational period as well [255]. While usually cleared within a week, severe infections in immunosuppressed patients have shown long-term chronic infection (months) of unknown pathogenesis [255,256].

As well as other viral infections, several innate immune escape strategies are exploited by WNV. These strategies target key signaling IFNs response, which underscores the importance of bypassing this early immune response for effective viral replication [257].

Moreover, as well as being able to regulate HLA-I and/or II expression on many different types of embryonic cells [258–260], WNV infection is also able to induce HLA-I on primary trophoblast giant cells after 16 h of infection in the absence of type I or II IFNs [261] (Figure 4). This demonstrates that the block to HLA expression in the early embryo is not absolute and has effects on the recognition and eradication of viral disease by the maternal cellular immune system during early pregnancy. Thus, the embryo and placenta HLA expression early in gestation, together with concurrent viral antigen expression, could lead to the destruction of the embryo by both virus- and allo-specific maternal cytotoxic T cells. Indeed, there is a high incidence of resorption, abortion and stillbirth of embryos of several mammals due to transplacental infection by flaviviruses such as WNV [262], especially if the virus infects the woman during initial implantation [263] (Figure 4).

6.4. SARS-CoV-2

Several studies have investigated the possible multi-tissue tropism of SARS-CoV-2, basing on the wide expression of ACE2 and the proteases TMPRSS2, two of the most studied cellular receptors involved in viral entry by Spike interaction, in sites other than lungs [264].

A role for SARS-CoV-2 in pathological pregnancy has been firstly suggested by the finding of the co-expression of ACE2 and TMPRSS2 throughout gestation [265,266].

This suggested a possible effect on SARS-CoV-2 infection at both the placental and transplacental level. Moreover, other alternative receptors for SARS-CoV-2 entry into

syncytiotrophoblast cells has been suggested, such as DPP4 (CD26) and CD147 [267]. A differential expression of both ACE2 and CD147 in the placenta of SARS-CoV-2-infected pregnant women compared to non-COVID-19-infected pregnant women has been reported but without any direct evidence of viral transmission to the newborns [268,269].

Placental susceptibility to SARS-CoV-2 infection has been associated with a large debate concerning the occurrence of transplacental transmission. Although no transplacental transmission was initially reported, the first report of detection of SARS-CoV-2 in the placenta evidenced the presence of the virus only at syncytiotrophoblast levels and found local tissue inflammation and fibrin deposition [270] (Figure 4) in association with an inflammatory infiltrate of immune cells composed of CD3+ lymphocytes and CD68+ macrophages (Figure 4). The infiltration of CD68+ placenta macrophages in SARS-CoV-2-infected placenta was next confirmed [271,272], which was associated with an M2 phenotype in a case report of an asymptomatic COVID-19-positive woman [273] (Figure 4). Interestingly, Facchetti et al. reported a strong expression of SARS-CoV-2 Spike protein in areas with dense monocytes–macrophage inflammation, which suggested a local activation of these cells [272]. Thus, to date, although the presence of placental macrophages into placenta lesions was clearly established, their role in SARS-CoV-2 infection of the placenta remains to be elucidated.

However, a recent study reported a case of a 34-year-old woman admitted to the ICU due to severe COVID-19 infection whose newborn died by pulmonary embolism and thrombosis of the superior vena cava, in which immunohistochemical analysis demonstrated a SARS-CoV-2 NP presence in neonatal tissues [274].

As previously mentioned, placental infections might affect HLA-G expression, leading to placental and fetal disorders [155] (Figure 4), and the capability of SARS-CoV-2 to modulate HLA-G in its immune escape process has been confirmed [275–278].

It is established that during pregnancy, NK cells represent the main immune cell type in endometrial tissues (40% of the total leukocyte population, which increases to 60% and up to 75%) and show an increased degranulation response at the end of pregnancy, suggesting their role in inhibiting possible vertical transmission of infection [279]. However, although representing the first line of defense during viral infections is of extreme importance during pregnancy, NK cells have been reported to be anergic in COVID-19 patients [280]. A decrease in CD56-expressing immune cells, most associated with NK cells, has been observed [269] (Figure 4). The decrease in CD56 expression induces a cytotoxic phenotype that might alter the immune tolerogenic status at the fetal–maternal interface. Consequently, deficiencies and phenotypic alterations of CD56-positive NK cells might modify the placental homeostasis during SARS-CoV-2 infection with possible clinical implications on pregnancy [269] (Figure 4). Moreover, the mechanisms exploited by SARS-CoV-2 to modulate NK function have been evaluated [280], showing that the S1 protein is able to up-regulate HLA-E expression that induces cell resistance to NK cell lysis by interacting with the NK cell inhibitory receptor CD94/NKG2A (Figure 4) [281,282].

Interestingly, placenta samples delivered from SARS-CoV-2-positive subjects showed an increased expression of three immune genes: CXCL10, a pro-inflammatory chemokine secreted in response to interferon gamma, TLR3 and DDX58, involved in recognizing double-stranded RNA [268] (Figure 4), supporting the role of SARS-CoV-2 infection in modifying immune gene expression at the placenta level [283].

7. Vaccines and Antiviral Therapy in Pregnancy

A public health policy known as maternal immunization aims to protect pregnant women directly against the infectious disease in question as well as to give newborns and early children the best possible passive immunity. The best time to administer vaccinations is before conception, but there are some circumstances in which it is necessary to administer vaccines throughout pregnancy and postpartum [284].

Pregnant women who receive the vaccine develop vaccine-specific antibodies, which are passed to their unborn children through the placenta or through lactation. Only IgGs,

among the various antibody isotypes, can cross the placenta starting from the 13th weeks of gestation, giving the fetus passive immunity. The fetal IgG levels then start to decline in the late second and early third trimester, showing a drop of up to 50% from the level reported in term children, supporting the timing of immunization in pregnancy to protect preterm infants [285]. The immune response peak resulting from a later vaccination (28–32 weeks) could closely match with the timing of maximal transplacental transfer of IgG and therefore potentially provide greater protection to the infant [285]. In fact, vaccination in the second trimester would provide longer exposure to maternal IgG, increasing the possibility of higher functional IgG in the infant [286]. To increase the proportion of pregnant women who receive vaccinations, future studies using various methodologies may offer a larger window of optimal vaccine scheduling. Pertussis, tetanus, diphtheria, polio, and the seasonal influenza vaccine are the only infections that can currently be vaccinated against while pregnant. However, future vaccines for pregnant women, including those for respiratory syncytial virus (RSV) and group B streptococcus (GBS), are now being developed [284]. There are live, inactivated, and multivalent monovalent and multivalent vaccines available for immunization.

Live vaccines contain attenuated viruses that need to be multiplied for protective immunity to develop. As a result, this type of vaccine is contraindicated during pregnancy because the vaccine virus could theoretically spread to the fetus and endanger it [286]. To prevent this, women should wait one month before becoming pregnant after receiving a live vaccine.

Although it is not recommended during pregnancy, a live attenuated varicella vaccine was launched in 1995, and women who accidentally received it during pregnancy exhibited no issues [287]. However, because VZV vaccinations are contraindicated during pregnancy, it is advised that all women considering pregnancies be screened for varicella immunity and that non-immune women be immunized before becoming pregnant. On the other hand, postpartum vaccinations for non-immune pregnant women are advised [287].

The dengue infection has a similar live attenuated tetravalent vaccination. The live-attenuated flavivirus vaccine (CYD-TDV), which was approved in December 2015 for use in people as young as 9 years old [288,289], expresses the structural antigens of DENV. These antigens serve as the targets of the host immune response by inducing innate immune cells, neutralizing antibodies, and T-cell responses. Considering the potential danger of virus transmission to the fetus, CYD-TDV is contraindicated in pregnant women, just like the other live attenuated vaccines. Preclinical *in vivo* animal investigations have not identified any teratogenic effects in the offspring [290], but no assessments have been carried out in people. Further research is therefore required to determine the safety of dengue vaccine during pregnancy.

In contrast to live attenuated vaccines, mRNA–lipid nanoparticle (LNP) COVID-19 vaccines currently lack safety information for use during pregnancy, albeit in rare circumstances, severely vulnerable pregnant women have been evaluated. However, there are many justifications for vaccination during pregnancy that support the safety of COVID-19 vaccinations. The primary factor contributing to these vaccines' promising safety is that they are made of mRNA encapsulated in a lipid nanoparticle, which prompts the host to produce coronavirus spike proteins, thereby inducing the production of antibodies [291] without containing live viruses or adjuvants that could harm a fetus in development [292].

Additionally, the HPV vaccine is a vaccination that is gaining popularity during pregnancy. The virus-like particles (VLPs) in HPV vaccines are recombinant and augmented by an adjuvant, which stimulates a stronger immune response than a natural infection [293].

Even though giving the vaccine to pregnant women is not advised [294], it commonly happens accidentally because most recipients are fertile young women. The recommended protocol is to postpone the three-dose regimen until after the fetus is fully developed if a woman is discovered to be pregnant while receiving an HPV series. Government regulations, however, do not apply to pregnancy testing before immunization because they

could impede compliance and have a detrimental impact on vaccine uptake by delaying vaccination.

The chances of spontaneous miscarriage, serious birth defects, stillbirth, and preterm birth were not shown to be significantly greater with quadrivalent HPV vaccination during pregnancy in a large, statewide study conducted in Denmark [295]. Although no unfavorable outcomes of the pregnancy have been linked to vaccination, it is nevertheless important to properly demonstrate the safety of vaccination in pregnant women and, in the meantime, avoid its administration.

The emergency vaccination against hepatitis A and B during high-risk pregnancy has been accepted [296] in addition to the administration of influenza, tetanus, diphtheria, and pertussis vaccines [297], since the administration of other vaccines to pregnant women should be based on whether the benefits outweigh the risks [298]. Recombinant HB vaccines are the only type of HBV vaccination that is widely available, safe for newborns [299,300] and adults [301,302] and efficacious compared to plasma-derived vaccines. According to studies [303–307], HBV vaccination during pregnancy is immunogenic and causes a passive transfer of antibodies to the fetus.

However, one study looked at the timing of vaccination and found that babies born to moms who had their vaccinations during pregnancy had lower anti-HBs levels than babies born to mothers who received their vaccinations prior to becoming pregnant [308]. Therefore, based on this observation, it may be advised that women who are planning a pregnancy receive their shots before conception. This will improve the benefits for the unborn child and reduce the possibility of unfavorable pregnancy outcomes caused by vaccine safety.

The clinical trials of various medicines and antiviral medications, however, rarely include pregnant women in their cohorts due to ethical considerations, as has been noted for vaccine safety studies [308]. Therefore, even though the danger in animals is not always a reliable indicator of the same risk in people [309], animal studies are occasionally the only source to evaluate how experimental medical interventions would harm the fetus [310]. Because there are not any clinical trials conducted while pregnant, the safety of a medicine for pregnant women can only be determined after it is sold and used.

Acyclovir and zidovudine are the two first antiviral medications to be introduced because of the significant morbidity of the genital herpes simplex virus and HIV epidemics [311]. Since then, their effectiveness and safety have been established in non-pregnant patients, but use in pregnancy has been prohibited due to several fetus-related issues. Acyclovir and zidovudine have only been used during pregnancy in case reports and pharmacokinetic investigations [312].

Acyclovir reduces viral DNA replication by selectively inhibiting human HSV DNA polymerase, whereas zidovudine inhibits HIV-1 reverse transcriptase, which is an enzyme involved in a crucial stage of the HIV life cycle. ZDV's antiviral effect depends on the drug's intracellular conversion to a triphosphate metabolite, which needs host cell kinases to occur [313]. The data are currently sparse, and there are no prospective controlled studies, even though the body of research on the safety of oral acyclovir and valacyclovir does not show that these two antiviral medications have a deleterious impact on the fetus [313].

However, because of the encouraging data that have already been presented, doctors are permitted to treat pregnant patients with acyclovir or valacyclovir for primary or recurrent HSV infection, treating the mother while also reducing viral transmission without harming the fetus [313]. Moreover, as was the case with HSV and HIV, managing chronic hepatitis B (CHB) during pregnancy while using antiviral medications is a difficulty that could have negative effects on both the mother and fetus. The impact of antiviral medication during pregnancy for maternal liver illness and the prevention of perinatal transmission are important factors to consider and research. However, antiviral therapy can only very rarely be used during pregnancy [314]. Most pregnant women in the immune-tolerance period should be observed without treatment [311,315]. Antiviral medication may be started during pregnancy or continued if it was started before pregnancy, for example, if

pregnant women have an acute hepatitis flare-up or have underlying severe or advanced liver disease, such as cirrhosis [316].

In contrast to the antiviral therapies previously mentioned, the novel perspective suggested for the treatment of hepatitis is that the potential risks of fetal exposure to antiviral medications should not prevent the start of therapy, as it may be lifesaving for both mother and fetus. The preferred medication appears to be tenofovir (TDF), which functions as a nucleotide reverse transcriptase inhibitor, and it should be continued throughout the pregnancy [317].

Additionally, among the various approaches that have been suggested to treat COVID-19 patients, specific antiviral therapies [318] such as nucleoside analogs, which inhibit reverse transcription and are the most effective antiviral agents currently on the market against SARS-CoV-2 infection [319,320], play a crucial role. Remdesivir efficacy and safety, for instance, have been assessed in pregnant women with coronavirus disease 2019 (COVID-19), with the clinical condition improving mostly in those who had a better clinical status at baseline and received remdesivir treatment earlier. Even though most deliveries by cesarean section were urgent cases and no vertical transmissions were reported, transaminitis was a side effect that was noticed [321–325]. Remdesivir's effectiveness and safety profile in treating pregnant women with COVID-19 are therefore still unknown, and more research is required.

The current therapy choices for flavivirus infections are largely supportive care-based (antipyretics, analgesics, and antihistamines). ZIKV and dengue are similar enough that some antiviral treatments that work for both infections can be investigated [326]. Clinical trials in dengue-infected humans have already evaluated a few drugs, including chloroquine, balapiravir, and celtosivir, whose mechanisms of action include immunomodulatory activity, nucleoside inhibition, and host-glucosidase inhibitor, respectively. Unfortunately, there was no proof that the plasma viremia had been effectively reduced [327], and the drug's possible teratogenicity or toxicity should be carefully considered [326].

8. Conclusions

Immunological modifications during pregnancy allow maternal tolerance of the semi-allogeneic fetus while simultaneously increasing maternal vulnerability to infection. The processes that contribute to maternal and fetal harm caused by viral infections are complicated and heavily reliant on pathogenesis variables such as viral susceptibility, tissue and cellular tropism, and host–pathogen interactions in the placenta niche. The placenta is a physical and immunological barrier that protects the fetus from infections in the maternal blood. Nevertheless, certain pathogens, particularly viruses, can enter the fetal compartment via hematogeneous or decidual spread, causing congenital disorder and eventually fetus death. Previous epidemics of numerous new viral infections have resulted in poor pregnancy outcomes, including maternal and fetal morbidity and death, as well as peripartum infections with severe sequelae, even in the absence of maternal-to-fetal transmission. The major change around the subset of immunity cells at the maternal–fetal interface regard natural killer (NK) cells, macrophages, dendritic cells (DCs) and T cells, whose function and secretome can be changed during viral infections, potentially leading to preterm birth, congenital malformations, abortion, or stillbirth. These findings highlight the necessity of understanding the mechanisms through which viruses can reach the placenta or can lead to negative outcomes. Considering the success of tetanus vaccination during pregnancy, recommendations for immunization during gestation against several infectious diseases have increased. Given the advances in targeted drug delivery using nanoparticles (NPs), several research groups are currently focusing on developing virus-like particles (VLP) or NPs meant to be used for gestational active immunization [284]. Since the research and development of VLPs and NP presents an opportunity for effective pregnancy therapy, their translation into healthcare settings must go through a lengthy and challenging toxicity testing process. Virus-like particles (VLPs) or NPs are supramolecular entities that resemble viruses but do not have the potential to infect. VLP/NP may be customized to target

specific immune system cells while simultaneously presenting antigens to the immune system, making them attractive vaccination candidates [285]. For example, wild-type SARS-CoV-2 and group-specific antigen (Gag) VLPs with a diameter of around 145 nm represent very interesting alternatives for the development of novel coronavirus vaccine candidates [286]. Similarly, Garg and colleagues [287] recently published a new VLP-based Zika virus vaccination that was proven to induce neutralizing antibodies postimmunization. The preliminary experiments, however, were performed in nonpregnant mice, and no data on the VLP influence on pregnancy were presented. Differences in the real physiology, anatomy, and uterine environment, as well as the cost of conducting studies on mouse models, limit the utility of such models. Therefore, new promising strategies for studying VLP have been developed, which are based on reproducing the mother–fetus interface on a chip, organ-on-chip (OoC) [288].

Despite all the evidence, essential research on the development of safe antiviral medicines and vaccinations that prompt maternal immune response should be promoted.

Author Contributions: Conceptualization, D.B. and R.R.; methodology, G.S. (Giovanna Schiuma); formal analysis, S.R., S.B. and G.S. (Giovanna Schiuma); data curation, S.R., S.B. and G.S. (Giovanna Schiuma), G.S. (Giorgia Speltri); writing—original draft preparation, S.R. and S.B.; writing—review and editing, D.B., R.R. and D.D.L. All authors have read and agreed to the published version of the manuscript.

Funding: This research received no external funding.

Data Availability Statement: All the data are reported in the manuscript.

Acknowledgments: We kindly thank Iva Pivanti for the technical support.

Conflicts of Interest: The authors declare no conflict of interest.

References

- Mor, G.; Cardenas, I. The immune system in pregnancy: A unique complexity. *Am. J. Reprod. Immunol.* **2010**, *63*, 425–433. [[CrossRef](#)]
- PrabhuDas, M.; Bonney, E.; Caron, K.; Dey, S.; Erlebacher, A.; Fazleabas, A.; Fisher, S.; Golos, T.; Matzuk, M.; McCune, J.M.; et al. Immune mechanisms at the maternal-fetal interface: Perspectives and challenges. *Nat. Immunol.* **2015**, *16*, 328–334. [[CrossRef](#)]
- Ando, T.; Davies, T.F. Self-recognition and the role of fetal microchimerism. *Best. Pract. Res. Clin. Endocrinol. Metab.* **2004**, *18*, 197–211. [[CrossRef](#)]
- Hoo, R.; Nakimuli, A.; Vento-Tormo, R. Innate Immune Mechanisms to Protect Against Infection at the Human Decidual-Placental Interface. *Front. Immunol.* **2020**, *11*, 2070. [[CrossRef](#)]
- Simister, N.E. Placental transport of immunoglobulin G. *Vaccine* **2003**, *21*, 3365–3369. [[CrossRef](#)]
- Polanczyk, M.J.; Carson, B.D.; Subramanian, S.; Afentoulis, M.; Vandembark, A.A.; Ziegler, S.F.; Offner, H. Cutting edge: Estrogen drives expansion of the CD4+CD25+ regulatory T cell compartment. *J. Immunol.* **2004**, *173*, 2227–2230. [[CrossRef](#)]
- Tai, P.; Wang, J.; Jin, H.; Song, X.; Yan, J.; Kang, Y.; Zhao, L.; An, X.; Du, X.; Chen, X.; et al. Induction of regulatory T cells by physiological level estrogen. *J. Cell. Physiol.* **2008**, *214*, 456–464. [[CrossRef](#)]
- Polanczyk, M.J.; Hopke, C.; Huan, J.; Vandembark, A.A.; Offner, H. Enhanced FoxP3 expression and Treg cell function in pregnant and estrogen-treated mice. *J. Neuroimmunol.* **2005**, *170*, 85–92. [[CrossRef](#)]
- Areia, A.; Vale-Pereira, S.; Alves, V.; Rodrigues-Santos, P.; Moura, P.; Mota-Pinto, A. Membrane progesterone receptors in human regulatory T cells: A reality in pregnancy. *BJOG* **2015**, *122*, 1544–1550. [[CrossRef](#)]
- Tsuda, S.; Nakashima, A.; Shima, T.; Saito, S. New Paradigm in the Role of Regulatory T Cells During Pregnancy. *Front. Immunol.* **2019**, *10*, 573. [[CrossRef](#)]
- Schumacher, A.; Costa, S.D.; Zenclussen, A.C. Endocrine factors modulating immune responses in pregnancy. *Front. Immunol.* **2014**, *5*, 196. [[CrossRef](#)]
- Steinhoff, M.C.; Omer, S.B.; Roy, E.; Arifeen, S.E.; Raqib, R.; Altaye, M.; Breiman, R.F.; Zaman, K. Influenza immunization in pregnancy—antibody responses in mothers and infants. *N. Engl. J. Med.* **2010**, *362*, 1644–1646. [[CrossRef](#)]
- Watanabe, M.; Iwatani, Y.; Kaneda, T.; Hidaka, Y.; Mitsuda, N.; Morimoto, Y.; Amino, N. Changes in T, B, and NK lymphocyte subsets during and after normal pregnancy. *Am. J. Reprod. Immunol.* **1997**, *37*, 368–377. [[CrossRef](#)]
- Ander, S.E.; Diamond, M.S.; Coyne, C.B. Immune responses at the maternal-fetal interface. *Sci. Immunol.* **2019**, *4*, eaat6114. [[CrossRef](#)]
- Ferreira, L.M.R.; Meissner, T.B.; Tilburgs, T.; Strominger, J.L. HLA-G: At the Interface of Maternal-Fetal Tolerance. *Trends Immunol.* **2017**, *38*, 272–286. [[CrossRef](#)]

16. Vento-Tormo, R.; Efremova, M.; Botting, R.A.; Turco, M.Y.; Vento-Tormo, M.; Meyer, K.B.; Park, J.E.; Stephenson, E.; Polanski, K.; Goncalves, A.; et al. Single-cell reconstruction of the early maternal-fetal interface in humans. *Nature* **2018**, *563*, 347–353. [[CrossRef](#)]
17. Kraus, T.A.; Engel, S.M.; Sperling, R.S.; Kellerman, L.; Lo, Y.; Wallenstein, S.; Escribese, M.M.; Garrido, J.L.; Singh, T.; Loubeau, M.; et al. Characterizing the pregnancy immune phenotype: Results of the viral immunity and pregnancy (VIP) study. *J. Clin. Immunol.* **2012**, *32*, 300–311. [[CrossRef](#)]
18. Luppi, P. How immune mechanisms are affected by pregnancy. *Vaccine* **2003**, *21*, 3352–3357. [[CrossRef](#)]
19. Siewiera, J.; El Costa, H.; Tabiasco, J.; Berrebi, A.; Cartron, G.; Le Bouteiller, P.; Jabrane-Ferrat, N. Human cytomegalovirus infection elicits new decidual natural killer cell effector functions. *PLoS Pathog.* **2013**, *9*, e1003257. [[CrossRef](#)]
20. Crespo, A.C.; Strominger, J.L.; Tilburgs, T. Expression of KIR2DS1 by decidual natural killer cells increases their ability to control placental HCMV infection. *Proc. Natl. Acad. Sci. USA* **2016**, *113*, 15072–15077. [[CrossRef](#)]
21. van der Ploeg, K.; Chang, C.; Ivarsson, M.A.; Moffett, A.; Wills, M.R.; Trowsdale, J. Modulation of Human Leukocyte Antigen-C by Human Cytomegalovirus Stimulates KIR2DS1 Recognition by Natural Killer Cells. *Front. Immunol.* **2017**, *8*, 298. [[CrossRef](#)]
22. Moore, A.G.; Brown, D.A.; Fairlie, W.D.; Bauskin, A.R.; Brown, P.K.; Munier, M.L.; Russell, P.K.; Salamonsen, L.A.; Wallace, E.M.; Breit, S.N. The transforming growth factor- α superfamily cytokine macrophage inhibitory cytokine-1 is present in high concentrations in the serum of pregnant women. *J. Clin. Endocrinol. Metab.* **2000**, *85*, 4781–4788. [[CrossRef](#)]
23. Enders, A.C.; King, B.F. The cytology of Hofbauer cells. *Anat. Rec.* **1970**, *167*, 231–236. [[CrossRef](#)]
24. Castellucci, M.; Zaccaro, D.; Pescetto, G. A three-dimensional study of the normal human placental villous core. I. The Hofbauer cells. *Cell. Tissue Res.* **1980**, *210*, 235–247. [[CrossRef](#)]
25. Wetzka, B.; Clark, D.E.; Charnock-Jones, D.S.; Zahradnik, H.P.; Smith, S.K. Isolation of macrophages (Hofbauer cells) from human term placenta and their prostaglandin E2 and thromboxane production. *Hum. Reprod.* **1997**, *12*, 847–852. [[CrossRef](#)]
26. Quicke, K.M.; Bowen, J.R.; Johnson, E.L.; McDonald, C.E.; Ma, H.; O’Neal, J.T.; Rajakumar, A.; Wrammert, J.; Rimawi, B.H.; Pulendran, B.; et al. Zika Virus Infects Human Placental Macrophages. *Cell. Host Microbe* **2016**, *20*, 83–90. [[CrossRef](#)]
27. de Noronha, L.; Zanoluca, C.; Burger, M.; Suzukawa, A.A.; Azevedo, M.; Rebutini, P.Z.; Novadzki, I.M.; Tanabe, L.S.; Presibella, M.M.; Duarte Dos Santos, C.N. Zika Virus Infection at Different Pregnancy Stages: Anatomopathological Findings, Target Cells and Viral Persistence in Placental Tissues. *Front. Microbiol.* **2018**, *9*, 2266. [[CrossRef](#)]
28. Bhatnagar, J.; Rabeneck, D.B.; Martines, R.B.; Reagan-Steiner, S.; Ermias, Y.; Estetter, L.B.; Suzuki, T.; Ritter, J.; Keating, M.K.; Hale, G.; et al. Zika Virus RNA Replication and Persistence in Brain and Placental Tissue. *Emerg. Infect. Dis.* **2017**, *23*, 405–414. [[CrossRef](#)]
29. El Costa, H.; Gouilly, J.; Mansuy, J.M.; Chen, Q.; Levy, C.; Cartron, G.; Veas, F.; Al-Daccak, R.; Izopet, J.; Jabrane-Ferrat, N. ZIKA virus reveals broad tissue and cell tropism during the first trimester of pregnancy. *Sci. Rep.* **2016**, *6*, 35296. [[CrossRef](#)]
30. Tabata, T.; Pettitt, M.; Puerta-Guardo, H.; Michlmayr, D.; Wang, C.; Fang-Hoover, J.; Harris, E.; Pereira, L. Zika Virus Targets Different Primary Human Placental Cells, Suggesting Two Routes for Vertical Transmission. *Cell. Host Microbe* **2016**, *20*, 155–166. [[CrossRef](#)]
31. Maidji, E.; Genbacev, O.; Chang, H.T.; Pereira, L. Developmental regulation of human cytomegalovirus receptors in cytotrophoblasts correlates with distinct replication sites in the placenta. *J. Virol.* **2007**, *81*, 4701–4712. [[CrossRef](#)]
32. Simister, N.E.; Story, C.M.; Chen, H.L.; Hunt, J.S. An IgG-transporting Fc receptor expressed in the syncytiotrophoblast of human placenta. *Eur. J. Immunol.* **1996**, *26*, 1527–1531. [[CrossRef](#)]
33. Rathore, A.P.S.; Saron, W.A.A.; Lim, T.; Jahan, N.; St John, A.L. Maternal immunity and antibodies to dengue virus promote infection and Zika virus-induced microcephaly in fetuses. *Sci. Adv.* **2019**, *5*, eaav3208. [[CrossRef](#)]
34. Gupta, S.; Gach, J.S.; Becerra, J.C.; Phan, T.B.; Pudney, J.; Moldoveanu, Z.; Joseph, S.B.; Landucci, G.; Supnet, M.J.; Ping, L.H.; et al. The Neonatal Fc receptor (FcRn) enhances human immunodeficiency virus type 1 (HIV-1) transcytosis across epithelial cells. *PLoS Pathog.* **2013**, *9*, e1003776. [[CrossRef](#)]
35. Pereira, L.; Maidji, E.; McDonagh, S.; Genbacev, O.; Fisher, S. Human cytomegalovirus transmission from the uterus to the placenta correlates with the presence of pathogenic bacteria and maternal immunity. *J. Virol.* **2003**, *77*, 13301–13314. [[CrossRef](#)]
36. Zaga-Clavellina, V.; Diaz, L.; Olmos-Ortiz, A.; Godinez-Rubi, M.; Rojas-Mayorquin, A.E.; Ortuno-Sahagun, D. Central role of the placenta during viral infection: Immuno-competences and miRNA defensive responses. *Biochim. Biophys. Acta Mol. Basis Dis.* **2021**, *1867*, 166182. [[CrossRef](#)]
37. Goncalves, L.F.; Chaiworapongsa, T.; Romero, R. Intrauterine infection and prematurity. *Ment. Retard. Dev. Disabil. Res. Rev.* **2002**, *8*, 3–13. [[CrossRef](#)]
38. Coyne, C.B. The Tree(s) of Life: The Human Placenta and My Journey to Learn More about It. *PLoS Pathog.* **2016**, *12*, e1005515. [[CrossRef](#)]
39. Delorme-Axford, E.; Sadovsky, Y.; Coyne, C.B. The Placenta as a Barrier to Viral Infections. *Annu. Rev. Virol.* **2014**, *1*, 133–146. [[CrossRef](#)]
40. Arora, N.; Sadovsky, Y.; Dermody, T.S.; Coyne, C.B. Microbial Vertical Transmission during Human Pregnancy. *Cell. Host Microbe* **2017**, *21*, 561–567. [[CrossRef](#)]
41. Kourtis, A.P.; Read, J.S.; Jamieson, D.J. Pregnancy and infection. *N. Engl. J. Med.* **2014**, *370*, 2211–2218. [[CrossRef](#)] [[PubMed](#)]

42. Moher, D.; Shamseer, L.; Clarke, M.; Ghersi, D.; Liberati, A.; Petticrew, M.; Shekelle, P.; Stewart, L.A.; Group, P.-P. Preferred reporting items for systematic review and meta-analysis protocols (PRISMA-P) 2015 statement. *Syst. Rev.* **2015**, *4*, 1. [[CrossRef](#)] [[PubMed](#)]
43. Nathan Mantel, W.H. Statistical Aspects of the Analysis of Data From Retrospective Studies of Disease. *JNCI J. Natl. Cancer Inst.* **1959**, *22*, 719–748. [[CrossRef](#)]
44. Adams Waldorf, K.M.; McAdams, R.M. Influence of infection during pregnancy on fetal development. *Reproduction* **2013**, *146*, R151–R162. [[CrossRef](#)]
45. Agrawal, V.; Hirsch, E. Intrauterine infection and preterm labor. *Semin. Fetal Neonatal Med.* **2012**, *17*, 12–19. [[CrossRef](#)]
46. Fahey, J.O. Clinical management of intra-amniotic infection and chorioamnionitis: A review of the literature. *J. Midwifery Womens Health* **2008**, *53*, 227–235. [[CrossRef](#)]
47. Xu, X.; Zhou, Y.; Wei, H. Roles of HLA-G in the Maternal-Fetal Immune Microenvironment. *Front. Immunol.* **2020**, *11*, 592010. [[CrossRef](#)]
48. Jasinski-Bergner, S.; Schmiedel, D.; Mandelboim, O.; Seliger, B. Role of HLA-G in Viral Infections. *Front. Immunol.* **2022**, *13*, 826074. [[CrossRef](#)]
49. Rai, K.R.; Shrestha, P.; Yang, B.; Chen, Y.; Liu, S.; Maarouf, M.; Chen, J.L. Acute Infection of Viral Pathogens and Their Innate Immune Escape. *Front. Microbiol.* **2021**, *12*, 672026. [[CrossRef](#)]
50. Monette, A.; Moulard, A.J. T Lymphocytes as Measurable Targets of Protection and Vaccination Against Viral Disorders. *Int. Rev. Cell. Mol. Biol.* **2019**, *342*, 175–263. [[CrossRef](#)]
51. Finlay, B.B.; McFadden, G. Anti-immunology: Evasion of the host immune system by bacterial and viral pathogens. *Cell* **2006**, *124*, 767–782. [[CrossRef](#)] [[PubMed](#)]
52. Gregori, S.; Amodio, G.; Quattrone, F.; Panina-Bordignon, P. HLA-G Orchestrates the Early Interaction of Human Trophoblasts with the Maternal Niche. *Front. Immunol.* **2015**, *6*, 128. [[CrossRef](#)]
53. Rizzo, R.; D'Accolti, M.; Bortolotti, D.; Caccuri, F.; Caruso, A.; Di Luca, D.; Caselli, E. Human Herpesvirus 6A and 6B inhibit in vitro angiogenesis by induction of Human Leukocyte Antigen, G. *Sci. Rep.* **2018**, *8*, 17683. [[CrossRef](#)] [[PubMed](#)]
54. Tripathi, P.; Naik, S.; Agrawal, S. Role of HLA-G, HLA-E and KIR2DL4 in Pregnancy. *Int. J. Hum. Genet.* **2017**, *7*, 219–233. [[CrossRef](#)]
55. Houchins, J.P.; Lanier, L.L.; Niemi, E.C.; Phillips, J.H.; Ryan, J.C. Natural killer cell cytolytic activity is inhibited by NKG2-A and activated by NKG2-C. *J. Immunol.* **1997**, *158*, 3603–3609. [[CrossRef](#)] [[PubMed](#)]
56. Apps, R.; Gardner, L.; Hiby, S.E.; Sharkey, A.M.; Moffett, A. Conformation of human leucocyte antigen-C molecules at the surface of human trophoblast cells. *Immunology* **2008**, *124*, 322–328. [[CrossRef](#)] [[PubMed](#)]
57. Sharkey, A.M.; Gardner, L.; Hiby, S.; Farrell, L.; Apps, R.; Masters, L.; Goodridge, J.; Lathbury, L.; Stewart, C.A.; Verma, S.; et al. Killer Ig-like receptor expression in uterine NK cells is biased toward recognition of HLA-C and alters with gestational age. *J. Immunol.* **2008**, *181*, 39–46. [[CrossRef](#)]
58. Moffett, A.; Loke, C. Immunology of placentation in eutherian mammals. *Nat. Rev. Immunol.* **2006**, *6*, 584–594. [[CrossRef](#)]
59. Seliger, B.; Ritz, U.; Ferrone, S. Molecular mechanisms of HLA class I antigen abnormalities following viral infection and transformation. *Int. J. Cancer* **2006**, *118*, 129–138. [[CrossRef](#)]
60. Caselli, E.; Campioni, D.; Cavazzini, F.; Gentili, V.; Bortolotti, D.; Cuneo, A.; Di Luca, D.; Rizzo, R. Acute human herpesvirus-6A infection of human mesothelial cells modulates HLA molecules. *Arch. Virol.* **2015**, *160*, 2141–2149. [[CrossRef](#)]
61. Davis, Z.B.; Cogswell, A.; Scott, H.; Mertsching, A.; Boucau, J.; Wambua, D.; Le Gall, S.; Planelles, V.; Campbell, K.S.; Barker, E. A Conserved HIV-1-Derived Peptide Presented by HLA-E Renders Infected T-cells Highly Susceptible to Attack by NKG2A/CD94-Bearing Natural Killer Cells. *PLoS Pathog.* **2016**, *12*, e1005421. [[CrossRef](#)] [[PubMed](#)]
62. Llano, M.; Guma, M.; Ortega, M.; Angulo, A.; Lopez-Botet, M. Differential effects of US2, US6 and US11 human cytomegalovirus proteins on HLA class Ia and HLA-E expression: Impact on target susceptibility to NK cell subsets. *Eur. J. Immunol.* **2003**, *33*, 2744–2754. [[CrossRef](#)]
63. Rizzo, R.; Trentini, A.; Bortolotti, D.; Manfrinato, M.C.; Rotola, A.; Castellazzi, M.; Melchiorri, L.; Di Luca, D.; Dallochio, F.; Fainardi, E.; et al. Matrix metalloproteinase-2 (MMP-2) generates soluble HLA-G1 by cell surface proteolytic shedding. *Mol. Cell. Biochem.* **2013**, *381*, 243–255. [[CrossRef](#)]
64. Nattermann, J.; Feldmann, G.; Ahlenstiel, G.; Langhans, B.; Sauerbruch, T.; Spengler, U. Surface expression and cytolytic function of natural killer cell receptors is altered in chronic hepatitis C. *Gut* **2006**, *55*, 869–877. [[CrossRef](#)]
65. Goncalves, M.A.; Le Discorde, M.; Simoes, R.T.; Rabreau, M.; Soares, E.G.; Donadi, E.A.; Carosella, E.D. Classical and non-classical HLA molecules and p16(INK4a) expression in precursors lesions and invasive cervical cancer. *Eur. J. Obstet. Gynecol. Reprod. Biol.* **2008**, *141*, 70–74. [[CrossRef](#)]
66. Mogensen, T.H. Pathogen recognition and inflammatory signaling in innate immune defenses. *Clin. Microbiol. Rev.* **2009**, *22*, 240–273. [[CrossRef](#)]
67. Chan, Y.K.; Gack, M.U. Viral evasion of intracellular DNA and RNA sensing. *Nat. Rev. Microbiol.* **2016**, *14*, 360–373. [[CrossRef](#)]
68. Wies, E.; Wang, M.K.; Maharaj, N.P.; Chen, K.; Zhou, S.; Finberg, R.W.; Gack, M.U. Dephosphorylation of the RNA sensors RIG-I and MDA5 by the phosphatase PPI is essential for innate immune signaling. *Immunity* **2013**, *38*, 437–449. [[CrossRef](#)] [[PubMed](#)]
69. Takeuchi, O.; Akira, S. Pattern recognition receptors and inflammation. *Cell* **2010**, *140*, 805–820. [[CrossRef](#)] [[PubMed](#)]

70. Tamura, K.; Ishikawa, G.; Yoshie, M.; Ohneda, W.; Nakai, A.; Takeshita, T.; Tachikawa, E. Glibenclamide inhibits NLRP3 inflammasome-mediated IL-1 β secretion in human trophoblasts. *J. Pharmacol. Sci.* **2017**, *135*, 89–95. [\[CrossRef\]](#)
71. Kim, Y.M.; Romero, R.; Oh, S.Y.; Kim, C.J.; Kilburn, B.A.; Armant, D.R.; Nien, J.K.; Gomez, R.; Mazor, M.; Saito, S.; et al. Toll-like receptor 4: A potential link between "danger signals," the innate immune system, and preeclampsia? *Am. J. Obstet. Gynecol.* **2005**, *193*, 921–927. [\[CrossRef\]](#)
72. Koga, K.; Cardenas, I.; Aldo, P.; Abrahams, V.M.; Peng, B.; Fill, S.; Romero, R.; Mor, G. Activation of TLR3 in the trophoblast is associated with preterm delivery. *Am. J. Reprod. Immunol.* **2009**, *61*, 196–212. [\[CrossRef\]](#)
73. Romero, R.; Kusanovic, J.P.; Chaiworapongsa, T.; Hassan, S.S. Placental bed disorders in preterm labor, preterm PROM, spontaneous abortion and abruptio placentae. *Best Pr. Res. Clin. Obstet. Gynaecol.* **2011**, *25*, 313–327. [\[CrossRef\]](#)
74. Motomura, K.; Hara, M.; Ito, I.; Morita, H.; Matsumoto, K. Roles of human trophoblasts' pattern recognition receptors in host defense and pregnancy complications. *J. Reprod. Immunol.* **2023**, *156*, 103811. [\[CrossRef\]](#) [\[PubMed\]](#)
75. Amiot, L.; Vu, N.; Samson, M. Immunomodulatory properties of HLA-G in infectious diseases. *J. Immunol. Res.* **2014**, *2014*, 298569. [\[CrossRef\]](#) [\[PubMed\]](#)
76. Estes, M.K. *Fields Virology*; Lippincott Williams & Wilkins: Philadelphia, PA, USA, 2013; p. 1347.
77. Ormoy, A.; Ergaz, Z. Parvovirus B19 infection during pregnancy and risks to the fetus. *Birth Defects Res.* **2017**, *109*, 311–323. [\[CrossRef\]](#)
78. de Jong, E.P.; Walther, F.J.; Kroes, A.C.; Oepkes, D. Parvovirus B19 infection in pregnancy: New insights and management. *Prenat. Diagn.* **2011**, *31*, 419–425. [\[CrossRef\]](#)
79. De Jong, E.P.; Lindenburg, I.T.; van Klink, J.M.; Oepkes, D.; van Kamp, I.L.; Walther, F.J.; Lopriore, E. Intrauterine transfusion for parvovirus B19 infection: Long-term neurodevelopmental outcome. *Am. J. Obstet. Gynecol.* **2012**, *206*, 204.e1–204.e5. [\[CrossRef\]](#) [\[PubMed\]](#)
80. Garcia, A.G.; Pegado, C.S.; Cubel Rde, C.; Fonseca, M.E.; Sloboda, I.; Nascimento, J.P. Feto-placental pathology in human parvovirus B19 infection. *Rev. Inst. Med. Trop. Sao Paulo* **1998**, *40*, 145–150. [\[CrossRef\]](#)
81. Jordan, J.A.; Huff, D.; DeLoia, J.A. Placental cellular immune response in women infected with human parvovirus B19 during pregnancy. *Clin. Diagn. Lab. Immunol.* **2001**, *8*, 288–292. [\[CrossRef\]](#)
82. Arechavaleta-Velasco, F.; Gomez, L.; Ma, Y.; Zhao, J.; McGrath, C.M.; Sammel, M.D.; Nelson, D.B.; Parry, S. Adverse reproductive outcomes in urban women with adeno-associated virus-2 infections in early pregnancy. *Hum. Reprod.* **2008**, *23*, 29–36. [\[CrossRef\]](#) [\[PubMed\]](#)
83. Koi, H.; Zhang, J.; Makrigiannakis, A.; Getsios, S.; MacCalman, C.D.; Kopf, G.S.; Strauss, J.F., 3rd; Parry, S. Differential expression of the coxsackievirus and adenovirus receptor regulates adenovirus infection of the placenta. *Biol. Reprod.* **2001**, *64*, 1001–1009. [\[CrossRef\]](#) [\[PubMed\]](#)
84. Arechavaleta-Velasco, F.; Ma, Y.; Zhang, J.; McGrath, C.M.; Parry, S. Adeno-associated virus-2 (AAV-2) causes trophoblast dysfunction, and placental AAV-2 infection is associated with preeclampsia. *Am. J. Pathol.* **2006**, *168*, 1951–1959. [\[CrossRef\]](#)
85. Arechavaleta-Velasco, F.; Koi, H.; Strauss, J.F., 3rd; Parry, S. Viral infection of the trophoblast: Time to take a serious look at its role in abnormal implantation and placentation? *J. Reprod. Immunol.* **2002**, *55*, 113–121. [\[CrossRef\]](#)
86. Tobiasch, E.; Rabreau, M.; Geletneky, K.; Larue-Charlus, S.; Severin, F.; Becker, N.; Schlehofer, J.R. Detection of adeno-associated virus DNA in human genital tissue and in material from spontaneous abortion. *J. Med. Virol.* **1994**, *44*, 215–222. [\[CrossRef\]](#)
87. Botquin, V.; Cid-Arregui, A.; Schlehofer, J.R. Adeno-associated virus type 2 interferes with early development of mouse embryos. *J. Gen. Virol.* **1994**, *75 Pt 10*, 2655–2662. [\[CrossRef\]](#) [\[PubMed\]](#)
88. Cheung, K.W.; Lao, T.T. Hepatitis B—Vertical transmission and the prevention of mother-to-child transmission. *Best. Pract. Res. Clin. Obstet. Gynaecol.* **2020**, *68*, 78–88. [\[CrossRef\]](#)
89. Liu, J.; Zhang, S.; Liu, M.; Wang, Q.; Shen, H.; Zhang, Y. Maternal pre-pregnancy infection with hepatitis B virus and the risk of preterm birth: A population-based cohort study. *Lancet Glob. Health* **2017**, *5*, e624–e632. [\[CrossRef\]](#)
90. Tian, T.; Sun, D.; Wang, P.; Wang, H.; Bai, X.; Yang, X.; Wang, Z.; Dong, M. Roles of Toll-like Receptor 7 and 8 in Prevention of Intrauterine Transmission of Hepatitis B Virus. *Cell. Physiol. Biochem.* **2015**, *37*, 445–453. [\[CrossRef\]](#)
91. Cui, H.; Li, Q.L.; Chen, J.; Na, Q.; Liu, C.X. Hepatitis B virus X protein modifies invasion, proliferation and the inflammatory response in an HTR-8/SVneo cell model. *Oncol. Rep.* **2015**, *34*, 2090–2098. [\[CrossRef\]](#)
92. Giugliano, S.; Petroff, M.G.; Warren, B.D.; Jasti, S.; Linscheid, C.; Ward, A.; Kramer, A.; Dobrinskikh, E.; Sheiko, M.A.; Gale, M., Jr.; et al. Hepatitis C Virus Sensing by Human Trophoblasts Induces Innate Immune Responses and Recruitment of Maternal NK Cells: Potential Implications for Limiting Vertical Transmission. *J. Immunol.* **2015**, *195*, 3737–3747. [\[CrossRef\]](#) [\[PubMed\]](#)
93. Kushner, T.; Terrault, N.A. Hepatitis C in Pregnancy: A Unique Opportunity to Improve the Hepatitis C Cascade of Care. *Hepatol. Commun.* **2019**, *3*, 20–28. [\[CrossRef\]](#)
94. Rusyn, I.; Lemon, S.M. Mechanisms of HCV-induced liver cancer: What did we learn from in vitro and animal studies? *Cancer Lett.* **2014**, *345*, 210–215. [\[CrossRef\]](#) [\[PubMed\]](#)
95. Khakoo, S.I.; Thio, C.L.; Martin, M.P.; Brooks, C.R.; Gao, X.; Astemborski, J.; Cheng, J.; Goedert, J.J.; Vlahov, D.; Hilgartner, M.; et al. HLA and NK cell inhibitory receptor genes in resolving hepatitis C virus infection. *Science* **2004**, *305*, 872–874. [\[CrossRef\]](#)
96. Hurtado, C.W.; Golden-Mason, L.; Brocato, M.; Krull, M.; Narkewicz, M.R.; Rosen, H.R. Innate immune function in placenta and cord blood of hepatitis C—seropositive mother-infant dyads. *PLoS ONE* **2010**, *5*, e12232. [\[CrossRef\]](#)

97. Wu, C.; Wu, X.; Xia, J. Hepatitis E virus infection during pregnancy. *Viol. J.* **2020**, *17*, 73. [[CrossRef](#)] [[PubMed](#)]
98. Bose, P.D.; Das, B.C.; Kumar, A.; Gondal, R.; Kumar, D.; Kar, P. High viral load and deregulation of the progesterone receptor signaling pathway: Association with hepatitis E-related poor pregnancy outcome. *J. Hepatol.* **2011**, *54*, 1107–1113. [[CrossRef](#)]
99. Yang, C.; Hao, X.; Li, Y.; Long, F.; He, Q.; Huang, F.; Yu, W. Successful Establishment of Hepatitis E Virus Infection in Pregnant BALB/c Mice. *Viruses* **2019**, *11*, 451. [[CrossRef](#)] [[PubMed](#)]
100. Freitas, A.C.; Mariz, F.C.; Silva, M.A.; Jesus, A.L. Human papillomavirus vertical transmission: Review of current data. *Clin. Infect. Dis.* **2013**, *56*, 1451–1456. [[CrossRef](#)]
101. Racicot, K.; Mor, G. Risks associated with viral infections during pregnancy. *J. Clin. Investig.* **2017**, *127*, 1591–1599. [[CrossRef](#)]
102. Gomez, L.M.; Ma, Y.; Ho, C.; McGrath, C.M.; Nelson, D.B.; Parry, S. Placental infection with human papillomavirus is associated with spontaneous preterm delivery. *Hum. Reprod.* **2008**, *23*, 709–715. [[CrossRef](#)] [[PubMed](#)]
103. Slatter, T.L.; Hung, N.G.; Clow, W.M.; Royds, J.A.; Devenish, C.J.; Hung, N.A. A clinicopathological study of episomal papillomavirus infection of the human placenta and pregnancy complications. *Mod. Pathol.* **2015**, *28*, 1369–1382. [[CrossRef](#)] [[PubMed](#)]
104. Palefsky, J.M.; Gillison, M.L.; Strickler, H.D. Chapter 16: HPV vaccines in immunocompromised women and men. *Vaccine* **2006**, *24* (Suppl. S3), S3/140–146. [[CrossRef](#)]
105. Moodley, M.; Moodley, J.; Chetty, R.; Herrington, C.S. The role of steroid contraceptive hormones in the pathogenesis of invasive cervical cancer: A review. *Int. J. Gynecol. Cancer* **2003**, *13*, 103–110. [[CrossRef](#)] [[PubMed](#)]
106. Linthorst, J.; Welkers, M.R.A.; Siermans, E.A. Clinically relevant DNA viruses in pregnancy. *Prenat. Diagn.* **2023**, *43*, 457–466. [[CrossRef](#)] [[PubMed](#)]
107. Jin, L.; Gibson, P.E.; Booth, J.C.; Clewley, J.P. Genomic typing of BK virus in clinical specimens by direct sequencing of polymerase chain reaction products. *J. Med. Virol.* **1993**, *41*, 11–17. [[CrossRef](#)]
108. Markowitz, R.B.; Eaton, B.A.; Kubik, M.F.; Latorra, D.; McGregor, J.A.; Dynan, W.S. BK virus and JC virus shed during pregnancy have predominantly archetypal regulatory regions. *J. Virol.* **1991**, *65*, 4515–4519. [[CrossRef](#)]
109. Bhattacharjee, S.; Chakraborty, T. High reactivation of BK virus variants in Asian Indians with renal disorders and during pregnancy. *Virus Genes.* **2004**, *28*, 157–168. [[CrossRef](#)]
110. Cheungpasitporn, W.; Thongprayoon, C.; Craici, I.M.; Sharma, K.; Chesdachai, S.; Khoury, N.J.; Ettore, A.S. Reactivation of BK polyomavirus during pregnancy, vertical transmission, and clinical significance: A meta-analysis. *J. Clin. Virol.* **2018**, *102*, 56–62. [[CrossRef](#)]
111. Boldorini, R.; Allegrini, S.; Miglio, U.; Paganotti, A.; Cocca, N.; Zaffaroni, M.; Riboni, F.; Monga, G.; Viscidi, R. Serological evidence of vertical transmission of JC and BK polyomaviruses in humans. *J. Gen. Virol.* **2011**, *92*, 1044–1050. [[CrossRef](#)]
112. Coleman, D.V.; Gardner, S.D.; Mulholland, C.; Fridiksdottir, V.; Porter, A.A.; Lilford, R.; Valdimarsson, H. Human polyomavirus in pregnancy. A model for the study of defence mechanisms to virus reactivation. *Clin. Exp. Immunol.* **1983**, *53*, 289–296. [[PubMed](#)]
113. Cohen, J.I. Herpesvirus latency. *J. Clin. Investig.* **2020**, *130*, 3361–3369. [[CrossRef](#)]
114. Enright, A.M.; Prober, C.G. Neonatal herpes infection: Diagnosis, treatment and prevention. *Semin. Neonatol.* **2002**, *7*, 283–291. [[CrossRef](#)]
115. Kriebs, J.M. Understanding herpes simplex virus: Transmission, diagnosis, and considerations in pregnancy management. *J. Midwifery Womens Health* **2008**, *53*, 202–208. [[CrossRef](#)] [[PubMed](#)]
116. Dinc, B.; Bozdayi, G.; Biri, A.; Kalkanci, A.; Dogan, B.; Bozkurt, N.; Rota, S. Molecular detection of cytomegalovirus, herpes simplex virus 2, human papillomavirus 16-18 in Turkish pregnant. *Braz. J. Infect. Dis.* **2010**, *14*, 569–574. [[CrossRef](#)]
117. Brown, Z.A.; Wald, A.; Morrow, R.A.; Selke, S.; Zeh, J.; Corey, L. Effect of serologic status and cesarean delivery on transmission rates of herpes simplex virus from mother to infant. *JAMA* **2003**, *289*, 203–209. [[CrossRef](#)] [[PubMed](#)]
118. Brown, Z.A.; Gardella, C.; Wald, A.; Morrow, R.; Corey, L. Genital Herpes Complicating Pregnancy. *Obstet. Gynecol.* **2006**, *107*, 426. [[CrossRef](#)]
119. Brown, Z.A.; Benedetti, J.; Selke, S.; Ashley, R.; Watts, D.H.; Corey, L. Asymptomatic maternal shedding of herpes simplex virus at the onset of labor: Relationship to preterm labor. *Obstet. Gynecol.* **1996**, *87*, 483–488. [[CrossRef](#)]
120. Schust, D.J.; Hill, A.B.; Ploegh, H.L. Herpes simplex virus blocks intracellular transport of HLA-G in placentally derived human cells. *J. Immunol.* **1996**, *157*, 3375–3380. [[CrossRef](#)]
121. Nørskov-Lauritsen, N.; Aboagye-Mathisen, G.; Juhl, C.B.; Petersen, P.M.; Zachar, V.; Ebbesen, P. Herpes simplex virus infection of cultured human term trophoblast. *J. Med. Virol.* **1992**, *36*, 162–166. [[CrossRef](#)]
122. Robb, J.A.; Benirschke, K.; Barmeyer, R. Intrauterine latent herpes simplex virus infection: I. Spontaneous abortion. *Hum. Pathol.* **1986**, *17*, 1196–1209. [[CrossRef](#)] [[PubMed](#)]
123. Brown, Z.A.; Vontver, L.A.; Benedetti, J.; Critchlow, C.W.; Sells, C.J.; Berry, S.; Corey, L. Effects on infants of a first episode of genital herpes during pregnancy. *N. Engl. J. Med.* **1987**, *317*, 1246–1251. [[CrossRef](#)]
124. Jabłońska, A.; Studzińska, M.; Suski, P.; Kalinka, J.; Paradowska, E. Enhanced expression of IFI16 and RIG-I in human third-trimester placentas following HSV-1 infection. *Clin. Exp. Immunol.* **2018**, *193*, 255–263. [[CrossRef](#)]
125. Leruez-Ville, M.; Foulon, I.; Pass, R.; Ville, Y. Cytomegalovirus infection during pregnancy: State of the science. *Am. J. Obstet. Gynecol.* **2020**, *223*, 330–349. [[CrossRef](#)]
126. Lycke, E.; Norrby, S.R. HerpesVirus Infections: State of the Art. *Scand. J. Infect. Dis.* **2015**, *23*, 1–118. [[CrossRef](#)]

127. Kenneson, A.; Cannon, M.J. Review and meta-analysis of the epidemiology of congenital cytomegalovirus (CMV) infection. *Rev. Med. Virol.* **2007**, *17*, 253–276. [[CrossRef](#)] [[PubMed](#)]
128. Fowler, K.B.; Stagno, S.; Pass, R.F.; Britt, W.J.; Boll, T.J.; Alford, C.A. The outcome of congenital cytomegalovirus infection in relation to maternal antibody status. *N. Engl. J. Med.* **1992**, *326*, 663–667. [[CrossRef](#)]
129. de Vries, J.J.; van Zwet, E.W.; Dekker, F.W.; Kroes, A.C.; Verkerk, P.H.; Vossen, A.C. The apparent paradox of maternal seropositivity as a risk factor for congenital cytomegalovirus infection: A population-based prediction model. *Rev. Med. Virol.* **2013**, *23*, 241–249. [[CrossRef](#)]
130. Amsler, L.; Verweij, M.; DeFilippis, V.R. The tiers and dimensions of evasion of the type I interferon response by human cytomegalovirus. *J. Mol. Biol.* **2013**, *425*, 4857–4871. [[CrossRef](#)]
131. Botto, S.; Abraham, J.; Mizuno, N.; Pryke, K.; Gall, B.; Landais, I.; Streblow, D.N.; Fruh, K.J.; DeFilippis, V.R. Human Cytomegalovirus Immediate Early 86-kDa Protein Blocks Transcription and Induces Degradation of the Immature Interleukin-1beta Protein during Virion-Mediated Activation of the AIM2 Inflammasome. *mBio* **2019**, *10*, e02510-18. [[CrossRef](#)]
132. Zou, H.M.; Huang, Z.F.; Yang, Y.; Luo, W.W.; Wang, S.Y.; Luo, M.H.; Fu, Y.Z.; Wang, Y.Y. Human Cytomegalovirus Protein UL94 Targets MITA to Evade the Antiviral Immune Response. *J. Virol.* **2020**, *94*, e00022-20. [[CrossRef](#)]
133. Fu, Y.Z.; Su, S.; Zou, H.M.; Guo, Y.; Wang, S.Y.; Li, S.; Luo, M.H.; Wang, Y.Y. Human Cytomegalovirus DNA Polymerase Subunit UL44 Antagonizes Antiviral Immune Responses by Suppressing IRF3- and NF-kappaB-Mediated Transcription. *J. Virol.* **2019**, *93*, e00181-19. [[CrossRef](#)] [[PubMed](#)]
134. Chan, G.; Guilbert, L.J. Ultraviolet-inactivated human cytomegalovirus induces placental syncytiotrophoblast apoptosis in a Toll-like receptor-2 and tumour necrosis factor-alpha dependent manner. *J. Pathol.* **2006**, *210*, 111–120. [[CrossRef](#)] [[PubMed](#)]
135. Chaudhuri, S.; Lowen, B.; Chan, G.; Davey, A.; Riddell, M.; Guilbert, L.J. Human cytomegalovirus interacts with toll-like receptor 2 and CD14 on syncytiotrophoblasts to stimulate expression of TNFalpha mRNA and apoptosis. *Placenta* **2009**, *30*, 994–1001. [[CrossRef](#)] [[PubMed](#)]
136. Jablonska, A.; Swierzko, A.S.; Studzinska, M.; Suski, P.; Kalinka, J.; Lesnikowski, Z.J.; Cedzynski, M.; Paradowska, E. Insight into the expression of RIG-I-like receptors in human third trimester placentas following ex vivo cytomegalovirus or vesicular stomatitis virus infection. *Mol. Immunol.* **2020**, *126*, 143–152. [[CrossRef](#)]
137. Lin, A.; Xu, H.; Yan, W. Modulation of HLA expression in human cytomegalovirus immune evasion. *Cell. Mol. Immunol.* **2007**, *4*, 91–98.
138. Rizzo, R.; Vercammen, M.; van de Velde, H.; Horn, P.A.; Rebmann, V. The importance of HLA-G expression in embryos, trophoblast cells, and embryonic stem cells. *Cell. Mol. Life Sci.* **2011**, *68*, 341–352. [[CrossRef](#)]
139. Rizzo, R.; Andersen, A.S.; Lassen, M.R.; Sorensen, H.C.; Bergholt, T.; Larsen, M.H.; Melchiorri, L.; Stignani, M.; Baricordi, O.R.; Hviid, T.V. Soluble human leukocyte antigen-G isoforms in maternal plasma in early and late pregnancy. *Am. J. Reprod. Immunol.* **2009**, *62*, 320–338. [[CrossRef](#)]
140. Jun, Y.; Kim, E.; Jin, M.; Sung, H.C.; Han, H.; Geraghty, D.E.; Ahn, K. Human cytomegalovirus gene products US3 and US6 down-regulate trophoblast class I MHC molecules. *J. Immunol.* **2000**, *164*, 805–811. [[CrossRef](#)]
141. Onno, M.; Pangault, C.; Le Fric, G.; Guilloux, V.; Andre, P.; Fauchet, R. Modulation of HLA-G antigens expression by human cytomegalovirus: Specific induction in activated macrophages harboring human cytomegalovirus infection. *J. Immunol.* **2000**, *164*, 6426–6434. [[CrossRef](#)]
142. Park, B.; Spooner, E.; Houser, B.L.; Strominger, J.L.; Ploegh, H.L. The HCMV membrane glycoprotein US10 selectively targets HLA-G for degradation. *J. Exp. Med.* **2010**, *207*, 2033–2041. [[CrossRef](#)]
143. Barel, M.T.; Rensing, M.; Pizzato, N.; van Leeuwen, D.; Le Bouteiller, P.; Lenfant, F.; Wiertz, E.J. Human cytomegalovirus-encoded US2 differentially affects surface expression of MHC class I locus products and targets membrane-bound, but not soluble HLA-G1 for degradation. *J. Immunol.* **2003**, *171*, 6757–6765. [[CrossRef](#)]
144. Schust, D.J.; Tortorella, D.; Seebach, J.; Phan, C.; Ploegh, H.L. Trophoblast class I major histocompatibility complex (MHC) products are resistant to rapid degradation imposed by the human cytomegalovirus (HCMV) gene products US2 and US11. *J. Exp. Med.* **1998**, *188*, 497–503. [[CrossRef](#)]
145. Crespo, A.C.; van der Zwan, A.; Ramalho-Santos, J.; Strominger, J.L.; Tilburgs, T. Cytotoxic potential of decidual NK cells and CD8+ T cells awakened by infections. *J. Reprod. Immunol.* **2017**, *119*, 85–90. [[CrossRef](#)]
146. Yan, W.H.; Lin, A.; Chen, B.G.; Zhou, M.Y.; Dai, M.Z.; Chen, X.J.; Gan, L.H.; Zhu, M.; Shi, W.W.; Li, B.L. Possible roles of KIR2DL4 expression on uNK cells in human pregnancy. *Am. J. Reprod. Immunol.* **2007**, *57*, 233–242. [[CrossRef](#)]
147. Beziat, V.; Hilton, H.G.; Norman, P.J.; Traherne, J.A. Deciphering the killer-cell immunoglobulin-like receptor system at super-resolution for natural killer and T-cell biology. *Immunology* **2017**, *150*, 248–264. [[CrossRef](#)]
148. Tanaka, K.; Yamada, H.; Minami, M.; Kataoka, S.; Numazaki, K.; Minakami, H.; Tsutsumi, H. Screening for vaginal shedding of cytomegalovirus in healthy pregnant women using real-time PCR: Correlation of CMV in the vagina and adverse outcome of pregnancy. *J. Med. Virol.* **2006**, *78*, 757–759. [[CrossRef](#)]
149. Salvany-Celades, M.; van der Zwan, A.; Benner, M.; Setrajic-Dragos, V.; Bougleux Gomes, H.A.; Iyer, V.; Norwitz, E.R.; Strominger, J.L.; Tilburgs, T. Three Types of Functional Regulatory T Cells Control T Cell Responses at the Human Maternal-Fetal Interface. *Cell. Rep.* **2019**, *27*, 2537–2547 e2535. [[CrossRef](#)]

150. Lissauer, D.; Choudhary, M.; Pachnio, A.; Goodyear, O.; Moss, P.A.; Kilby, M.D. Cytomegalovirus sero positivity dramatically alters the maternal CD8+ T cell repertoire and leads to the accumulation of highly differentiated memory cells during human pregnancy. *Hum. Reprod.* **2011**, *26*, 3355–3365. [[CrossRef](#)]
151. Ameres, S.; Mautner, J.; Schlott, F.; Neuenhahn, M.; Busch, D.H.; Plachter, B.; Moosmann, A. Presentation of an immunodominant immediate-early CD8+ T cell epitope resists human cytomegalovirus immunoevasion. *PLoS Pathog.* **2013**, *9*, e1003383. [[CrossRef](#)]
152. van Egmond, A.; van der Keur, C.; Swings, G.M.; Scherjon, S.A.; Claas, F.H. The possible role of virus-specific CD8(+) memory T cells in decidual tissue. *J. Reprod. Immunol.* **2016**, *113*, 1–8. [[CrossRef](#)]
153. Liu, W.; Niu, Z.; Li, Q.; Pang, R.T.; Chiu, P.C.; Yeung, W.S. MicroRNA and Embryo Implantation. *Am. J. Reprod. Immunol.* **2016**, *75*, 263–271. [[CrossRef](#)]
154. Cai, M.; Kolluru, G.K.; Ahmed, A. Small Molecule, Big Prospects: MicroRNA in Pregnancy and Its Complications. *J. Pregnancy* **2017**, *2017*, 6972732. [[CrossRef](#)]
155. Bortolotti, D.; Gentili, V.; Santi, E.; Taliento, C.; Vitagliano, A.; Schiuma, G.; Beltrami, S.; Rizzo, S.; Lanza, G.; Rizzo, R.; et al. Late-onset intrauterine growth restriction and HHV-6 infection: A pilot study. *J. Med. Virol.* **2021**, *93*, 6317–6322. [[CrossRef](#)] [[PubMed](#)]
156. Ablashi, D.; Agut, H.; Alvarez-Lafuente, R.; Clark, D.A.; Dewhurst, S.; DiLuca, D.; Flamand, L.; Frenkel, N.; Gallo, R.; Gompels, U.A.; et al. Classification of HHV-6A and HHV-6B as distinct viruses. *Arch. Virol.* **2014**, *159*, 863–870. [[CrossRef](#)] [[PubMed](#)]
157. Eliassen, E.; Marci, R.; Di Luca, D.; Rizzo, R. The use of heparin in infertility and recurrent pregnancy loss: Are its antiviral properties at play? *Med. Hypotheses* **2017**, *102*, 41–47. [[CrossRef](#)]
158. De Bolle, L.; Naesens, L.; De Clercq, E. Update on human herpesvirus 6 biology, clinical features, and therapy. *Clin. Microbiol. Rev.* **2005**, *18*, 217–245. [[CrossRef](#)] [[PubMed](#)]
159. Di Luca, D.; Dolcetti, R.; Mirandola, P.; De Re, V.; Secchiero, P.; Carbone, A.; Boiocchi, M.; Cassai, E. Human herpesvirus 6: A survey of presence and variant distribution in normal peripheral lymphocytes and lymphoproliferative disorders. *J. Infect. Dis.* **1994**, *170*, 211–215. [[CrossRef](#)] [[PubMed](#)]
160. Kondo, K.; Kondo, T.; Okuno, T.; Takahashi, M.; Yamanishi, K. Latent human herpesvirus 6 infection of human monocytes/macrophages. *J. Gen. Virol.* **1991**, *72 Pt 6*, 1401–1408. [[CrossRef](#)]
161. Marci, R.; Gentili, V.; Bortolotti, D.; Lo Monte, G.; Caselli, E.; Bolzani, S.; Rotola, A.; Di Luca, D.; Rizzo, R. Presence of HHV-6A in Endometrial Epithelial Cells from Women with Primary Unexplained Infertility. *PLoS ONE* **2016**, *11*, e0158304. [[CrossRef](#)]
162. Caselli, E.; Bortolotti, D.; Marci, R.; Rotola, A.; Gentili, V.; Soffritti, I.; D'Accolti, M.; Lo Monte, G.; Siculo, M.; Barao, I.; et al. HHV-6A Infection of Endometrial Epithelial Cells Induces Increased Endometrial NK Cell-Mediated Cytotoxicity. *Front. Microbiol.* **2017**, *8*, 2525. [[CrossRef](#)]
163. Rizzo, R.; Soffritti, I.; D'Accolti, M.; Bortolotti, D.; Di Luca, D.; Caselli, E. HHV-6A/6B Infection of NK Cells Modulates the Expression of miRNAs and Transcription Factors Potentially Associated to Impaired NK Activity. *Front. Microbiol.* **2017**, *8*, 2143. [[CrossRef](#)] [[PubMed](#)]
164. Ma, H.L.; Gong, F.; Tang, Y.; Li, X.; Li, X.; Yang, X.; Lu, G. Inhibition of Endometrial Tiam1/Rac1 Signals Induced by miR-22 Up-Regulation Leads to the Failure of Embryo Implantation During the Implantation Window in Pregnant Mice. *Biol. Reprod.* **2015**, *92*, 152. [[CrossRef](#)] [[PubMed](#)]
165. Bortolotti, D.; Soffritti, I.; D'Accolti, M.; Gentili, V.; Di Luca, D.; Rizzo, R.; Caselli, E. HHV-6A Infection of Endometrial Epithelial Cells Affects miRNA Expression and Trophoblast Cell Attachment. *Reprod. Sci.* **2020**, *27*, 779–786. [[CrossRef](#)] [[PubMed](#)]
166. Rizzo, R.; Lo Monte, G.; Bortolotti, D.; Graziano, A.; Gentili, V.; Di Luca, D.; Marci, R. Impact of soluble HLA-G levels and endometrial NK cells in uterine flushing samples from primary and secondary unexplained infertile women. *Int. J. Mol. Sci.* **2015**, *16*, 5510–5516. [[CrossRef](#)]
167. Sen, N.; Mukherjee, G.; Sen, A.; Bendall, S.C.; Sung, P.; Nolan, G.P.; Arvin, A.M. Single-cell mass cytometry analysis of human tonsil T cell remodeling by varicella zoster virus. *Cell. Rep.* **2014**, *8*, 633–645. [[CrossRef](#)]
168. Kawana, K.; Yoshikawa, H.; Sata, T. Post-partum detection of varicella-zoster virus DNA in the placenta. *Int. J. Gynaecol. Obstet.* **1996**, *55*, 165–166. [[CrossRef](#)]
169. Sauerbrei, A.; Wutzler, P. Herpes simplex and varicella-zoster virus infections during pregnancy: Current concepts of prevention, diagnosis and therapy. Part 2: Varicella-zoster virus infections. *Med. Microbiol. Immunol.* **2007**, *196*, 95–102. [[CrossRef](#)]
170. McGregor, J.A.; Mark, S.; Crawford, G.P.; Levin, M.J. Varicella zoster antibody testing in the care of pregnant women exposed to varicella. *Am. J. Obstet. Gynecol.* **1987**, *157*, 281–284. [[CrossRef](#)]
171. Kangro, H.O.; Manzoor, S.; Harper, D.R. Antibody avidity following varicella-zoster virus infections. *J. Med. Virol.* **1991**, *33*, 100–105. [[CrossRef](#)]
172. Asano, Y.; Hiroishi, Y.; Itakura, N.; Hirose, S.; Kajita, Y.; Nagai, T.; Yazaki, T.; Takahashi, M. Immunoglobulin Subclass Antibodies to Varicella-Zoster Virus. *Pediatrics* **1987**, *80*, 933–936. [[CrossRef](#)]
173. Junker, A.K.; Tilley, P. Varicella-zoster virus antibody avidity and IgG-subclass patterns in children with recurrent chickenpox. *J. Med. Virol.* **1994**, *43*, 119–124. [[CrossRef](#)] [[PubMed](#)]
174. Asano, Y.; Itakura, N.; Kajita, Y.; Suga, S.; Yoshikawa, T.; Yazaki, T.; Ozaki, T.; Yamanishi, K.; Takahashi, M. Severity of viremia and clinical findings in children with varicella. *J. Infect. Dis.* **1990**, *161*, 1095–1098. [[CrossRef](#)]

175. Gerlini, G.; Mariotti, G.; Bianchi, B.; Pimpinelli, N. Massive recruitment of type I interferon producing plasmacytoid dendritic cells in varicella skin lesions. *J. Investig. Dermatol.* **2006**, *126*, 507–509. [[CrossRef](#)]
176. Arvin, A.M.; Koropchak, C.M.; Williams, B.R.; Grumet, F.C.; Fount, S.K. Early immune response in healthy and immunocompromised subjects with primary varicella-zoster virus infection. *J. Infect. Dis.* **1986**, *154*, 422–429. [[CrossRef](#)] [[PubMed](#)]
177. Banovic, T.; Yanilla, M.; Simmons, R.; Robertson, L.; Schroder, W.A.; Raffelt, N.C.; Wilson, Y.A.; Hill, G.R.; Hogan, P.; Nourse, C.B. Disseminated varicella infection caused by varicella vaccine strain in a child with low invariant natural killer T cells and diminished CD1d expression. *J. Infect. Dis.* **2011**, *204*, 1893–1901. [[CrossRef](#)]
178. Duncan, C.J.; Hambleton, S. Varicella zoster virus immunity: A primer. *J. Infect.* **2015**, *71* (Suppl. S1), S47–S53. [[CrossRef](#)] [[PubMed](#)]
179. Dhanya, C.R.; Shailaja, A.; Mary, A.S.; Kandiyil, S.P.; Savithri, A.; Lathakumari, V.S.; Veetil, J.T.; Vandanamthadathil, J.J.; Madhavan, M. RNA Viruses, Pregnancy and Vaccination: Emerging Lessons from COVID-19 and Ebola Virus Disease. *Pathogens* **2022**, *11*, 800. [[CrossRef](#)] [[PubMed](#)]
180. Bebell, L.M.; Oduyebo, T.; Riley, L.E. Ebola virus disease and pregnancy: A review of the current knowledge of Ebola virus pathogenesis, maternal, and neonatal outcomes. *Birth Defects Res.* **2017**, *109*, 353–362. [[CrossRef](#)]
181. Aghaeepour, N.; Ganio, E.A.; McIlwain, D.; Tsai, A.S.; Tingle, M.; Van Gassen, S.; Gaudilliere, D.K.; Baca, Q.; McNeil, L.; Okada, R.; et al. An immune clock of human pregnancy. *Sci. Immunol.* **2017**, *2*, eaan2946. [[CrossRef](#)]
182. Kay, A.W.; Fukuyama, J.; Aziz, N.; Dekker, C.L.; Mackey, S.; Swan, G.E.; Davis, M.M.; Holmes, S.; Blish, C.A. Enhanced natural killer-cell and T-cell responses to influenza A virus during pregnancy. *Proc. Natl. Acad. Sci. USA* **2014**, *111*, 14506–14511. [[CrossRef](#)] [[PubMed](#)]
183. Lurie, S.; Rahamim, E.; Piper, I.; Golan, A.; Sadan, O. Total and differential leukocyte counts percentiles in normal pregnancy. *Eur. J. Obstet. Gynecol. Reprod. Biol.* **2008**, *136*, 16–19. [[CrossRef](#)] [[PubMed](#)]
184. Chen, K.; Liu, J.; Liu, S.; Xia, M.; Zhang, X.; Han, D.; Jiang, Y.; Wang, C.; Cao, X. Methyltransferase SETD2-Mediated Methylation of STAT1 Is Critical for Interferon Antiviral Activity. *Cell* **2017**, *170*, 492–506 e414. [[CrossRef](#)] [[PubMed](#)]
185. Lee, J.Y.; Bowden, D.S. Rubella virus replication and links to teratogenicity. *Clin. Microbiol. Rev.* **2000**, *13*, 571–587. [[CrossRef](#)] [[PubMed](#)]
186. Gregg, N.M. Congenital Cataract Following German Measles in the Mother. In *Problems of Birth Defects*; Springer: Berlin/Heidelberg, Germany, 1941; pp. 170–180.
187. Best, J.M.; Enders, G. Chapter 3 Laboratory Diagnosis of Rubella and Congenital Rubella. *Perspect. Med. Virol.* **2006**, *15*, 39–77.
188. Breeze, A.C. Infectious diseases of the fetus and newborn infant, 6th edn. *Arch. Dis. Child.-Fetal Neonatal Ed.* **2007**, *92*, F156. [[CrossRef](#)]
189. Ramondetti, F.; Sacco, S.; Comelli, M.; Bruno, G.; Falorni, A.; Iannilli, A.; d’Annunzio, G.; Iafusco, D.; Songini, M.; Toni, S.; et al. Type 1 diabetes and measles, mumps and rubella childhood infections within the Italian Insulin-dependent Diabetes Registry. *Diabet. Med.* **2012**, *29*, 761–766. [[CrossRef](#)]
190. Thong, Y.H.; Steele, R.W.; Vincent, M.M.; Hensen, S.A.; Bellanti, J.A. Impaired in vitro cell-mediated immunity to rubella virus during pregnancy. *N. Engl. J. Med.* **1973**, *289*, 604–606. [[CrossRef](#)]
191. O’Shea, S.; Corbett, K.M.; Barrow, S.M.; Banatvala, J.E.; Best, J.M. Rubella reinfection; role of neutralising antibodies and cell-mediated immunity. *Clin. Diagn. Virol.* **1994**, *2*, 349–358. [[CrossRef](#)]
192. South, M.A.; Montgomery, J.R.; Rawls, W.E. Immune deficiency in congenital rubella and other viral infections. *Birth Defects Orig. Artic. Ser.* **1975**, *11*, 234–238.
193. Mace, M.; Cointe, D.; Six, C.; Levy-Bruhl, D.; Parent du Chatelet, I.; Ingrand, D.; Grangeot-Keros, L. Diagnostic value of reverse transcription-PCR of amniotic fluid for prenatal diagnosis of congenital rubella infection in pregnant women with confirmed primary rubella infection. *J. Clin. Microbiol.* **2004**, *42*, 4818–4820. [[CrossRef](#)] [[PubMed](#)]
194. McLean, H.Q.; Fiebelkorn, A.P.; Temte, J.L.; Wallace, G.S.; Centers for Disease, C. Prevention of measles, rubella, congenital rubella syndrome, and mumps, 2013: Summary recommendations of the Advisory Committee on Immunization Practices (ACIP). *MMWR Recomm. Rep.* **2013**, *62*, 1–34. [[PubMed](#)]
195. Ragusa, R.; Platania, A.; Cuccia, M.; Zappala, G.; Giorgianni, G.; D’Agati, P.; Bellia, M.A.; Marranzano, M. Measles and Pregnancy: Immunity and Immunization-What Can Be Learned from Observing Complications during an Epidemic Year. *J. Pregnancy* **2020**, *2020*, 6532868. [[CrossRef](#)]
196. Strebel, P.M.; Orenstein, W.A. Measles. *N. Engl. J. Med.* **2019**, *381*, 349–357. [[CrossRef](#)] [[PubMed](#)]
197. Raghupathy, R. Th1-type immunity is incompatible with successful pregnancy. *Immunol. Today* **1997**, *18*, 478–482. [[CrossRef](#)]
198. Eke, A.C.; Lockman, S.; Mofenson, L.M. Antiretroviral Treatment of HIV/AIDS During Pregnancy. *JAMA* **2023**, *329*, 1308–1309. [[CrossRef](#)]
199. Pfeifer, C.; Bunders, M.J. Maternal HIV infection alters the immune balance in the mother and fetus; implications for pregnancy outcome and infant health. *Curr. Opin. HIV AIDS* **2016**, *11*, 138–145. [[CrossRef](#)]
200. Mellor, A.L.; Munn, D.H. Immunology at the maternal-fetal interface: Lessons for T cell tolerance and suppression. *Annu. Rev. Immunol.* **2000**, *18*, 367–391. [[CrossRef](#)] [[PubMed](#)]
201. Uchida, N.; Ohyama, K.; Bessho, T.; Takeichi, M.; Toyoda, H. Possible roles of proinflammatory and chemoattractive cytokines produced by human fetal membrane cells in the pathology of adverse pregnancy outcomes associated with influenza virus infection. *Mediators Inflamm.* **2012**, *2012*, 270670. [[CrossRef](#)]

202. Mwanjumba, F.; Gaillard, P.; Inion, I.; Verhofstede, C.; Claeys, P.; Chohan, V.; Vansteelandt, S.; Mandaliya, K.; Praet, M.; Temmerman, M. Placental inflammation and perinatal transmission of HIV-1. *J. Acquir. Immune Defic. Syndr.* **2002**, *29*, 262–269. [[CrossRef](#)]
203. Shive, C.L.; Clagett, B.; McCausland, M.R.; Mudd, J.C.; Funderburg, N.T.; Freeman, M.L.; Younes, S.A.; Ferrari, B.M.; Rodriguez, B.; McComsey, G.A.; et al. Inflammation Perturbs the IL-7 Axis, Promoting Senescence and Exhaustion that Broadly Characterize Immune Failure in Treated HIV Infection. *J. Acquir. Immune Defic. Syndr.* **2016**, *71*, 483–492. [[CrossRef](#)]
204. Moffett, A.; Hiby, S.E.; Sharkey, A.M. The role of the maternal immune system in the regulation of human birthweight. *Philos. Trans. R. Soc. Lond. B. Biol. Sci.* **2015**, *370*, 20140071. [[CrossRef](#)] [[PubMed](#)]
205. Hiby, S.E.; Apps, R.; Sharkey, A.M.; Farrell, L.E.; Gardner, L.; Mulder, A.; Claas, F.H.; Walker, J.J.; Redman, C.W.; Morgan, L.; et al. Maternal activating KIRs protect against human reproductive failure mediated by fetal HLA-C2. *J. Clin. Investig.* **2010**, *120*, 4102–4110. [[CrossRef](#)]
206. Alter, G.; Malenfant, J.M.; Delabre, R.M.; Burgett, N.C.; Yu, X.G.; Lichterfeld, M.; Zaunders, J.; Altfeld, M. Increased natural killer cell activity in viremic HIV-1 infection. *J. Immunol.* **2004**, *173*, 5305–5311. [[CrossRef](#)] [[PubMed](#)]
207. Alter, G.; Teigen, N.; Davis, B.T.; Addo, M.M.; Suscovich, T.J.; Waring, M.T.; Streeck, H.; Johnston, M.N.; Staller, K.D.; Zaman, M.T.; et al. Sequential deregulation of NK cell subset distribution and function starting in acute HIV-1 infection. *Blood* **2005**, *106*, 3366–3369. [[CrossRef](#)] [[PubMed](#)]
208. Behbahani, H.; Popek, E.; Garcia, P.; Andersson, J.; Spetz, A.L.; Landay, A.; Flener, Z.; Patterson, B.K. Up-regulation of CCR5 expression in the placenta is associated with human immunodeficiency virus-1 vertical transmission. *Am. J. Pathol.* **2000**, *157*, 1811–1818. [[CrossRef](#)]
209. Blois, S.M.; Illarregui, J.M.; Tometten, M.; Garcia, M.; Orsal, A.S.; Cordo-Russo, R.; Toscano, M.A.; Bianco, G.A.; Kobelt, P.; Handjiski, B.; et al. A pivotal role for galectin-1 in fetomaternal tolerance. *Nat. Med.* **2007**, *13*, 1450–1457. [[CrossRef](#)]
210. Kammerer, U.; Eggert, A.O.; Kapp, M.; McLellan, A.D.; Geijtenbeek, T.B.; Dietl, J.; van Kooyk, Y.; Kampgen, E. Unique appearance of proliferating antigen-presenting cells expressing DC-SIGN (CD209) in the decidua of early human pregnancy. *Am. J. Pathol.* **2003**, *162*, 887–896. [[CrossRef](#)]
211. Carles, G. What are the true consequences of dengue during pregnancy? *Lancet Infect. Dis.* **2016**, *16*, 765–766. [[CrossRef](#)]
212. Machado, C.R.; Machado, E.S.; Rohloff, R.D.; Azevedo, M.; Campos, D.P.; de Oliveira, R.B.; Brasil, P. Is pregnancy associated with severe dengue? A review of data from the Rio de Janeiro surveillance information system. *PLoS Negl. Trop. Dis.* **2013**, *7*, e2217. [[CrossRef](#)]
213. Basurko, C.; Everhard, S.; Matheus, S.; Restrepo, M.; Hilderal, H.; Lambert, V.; Boukhari, R.; Duvernois, J.P.; Favre, A.; Valmy, L.; et al. A prospective matched study on symptomatic dengue in pregnancy. *PLoS ONE* **2018**, *13*, e0202005. [[CrossRef](#)]
214. Charlier, C.; Beaudoin, M.C.; Couderc, T.; Lortholary, O.; Lecuit, M. Arboviruses and pregnancy: Maternal, fetal, and neonatal effects. *Lancet Child. Adolesc. Health* **2017**, *1*, 134–146. [[CrossRef](#)] [[PubMed](#)]
215. Vogt, M.B.; Lahon, A.; Arya, R.P.; Spencer Clinton, J.L.; Rico-Hesse, R. Dengue viruses infect human megakaryocytes, with probable clinical consequences. *PLoS Negl. Trop. Dis.* **2019**, *13*, e0007837. [[CrossRef](#)] [[PubMed](#)]
216. Campbell, R.A.; Schwertz, H.; Hottz, E.D.; Rowley, J.W.; Manne, B.K.; Washington, A.V.; Hunter-Mellado, R.; Tolley, N.D.; Christensen, M.; Eustes, A.S.; et al. Human megakaryocytes possess intrinsic antiviral immunity through regulated induction of IFITM3. *Blood* **2019**, *133*, 2013–2026. [[CrossRef](#)] [[PubMed](#)]
217. Martinez-Moreno, J.; Hernandez, J.C.; Urcuqui-Inchima, S. Effect of high doses of vitamin D supplementation on dengue virus replication, Toll-like receptor expression, and cytokine profiles on dendritic cells. *Mol. Cell. Biochem.* **2020**, *464*, 169–180. [[CrossRef](#)] [[PubMed](#)]
218. Uno, N.; Ross, T.M. Dengue virus and the host innate immune response. *Emerg. Microbes Infect.* **2018**, *7*, 167. [[CrossRef](#)]
219. Brasil, P.; Pereira, J.P., Jr.; Moreira, M.E.; Ribeiro Nogueira, R.M.; Damasceno, L.; Wakimoto, M.; Rabello, R.S.; Valderramos, S.G.; Halai, U.A.; Salles, T.S.; et al. Zika Virus Infection in Pregnant Women in Rio de Janeiro. *N. Engl. J. Med.* **2016**, *375*, 2321–2334. [[CrossRef](#)]
220. Coyne, C.B.; Lazear, H.M. Zika virus—reigniting the TORCH. *Nat. Rev. Microbiol.* **2016**, *14*, 707–715. [[CrossRef](#)]
221. Honein, M.A.; Dawson, A.L.; Petersen, E.E.; Jones, A.M.; Lee, E.H.; Yazdy, M.M.; Ahmad, N.; Macdonald, J.; Evert, N.; Bingham, A.; et al. Birth Defects Among Fetuses and Infants of US Women With Evidence of Possible Zika Virus Infection During Pregnancy. *JAMA* **2017**, *317*, 59–68. [[CrossRef](#)]
222. Reynolds, M.R.; Jones, A.M.; Petersen, E.E.; Lee, E.H.; Rice, M.E.; Bingham, A.; Ellington, S.R.; Evert, N.; Reagan-Steiner, S.; Oduyebo, T.; et al. Vital Signs: Update on Zika Virus-Associated Birth Defects and Evaluation of All U.S. Infants with Congenital Zika Virus Exposure—U.S. Zika Pregnancy Registry, 2016. *MMWR Morb. Mortal. Wkly. Rep.* **2017**, *66*, 366–373. [[CrossRef](#)]
223. Cumming, H.E.; Bourke, N.M. Type I IFNs in the female reproductive tract: The first line of defense in an ever-changing battleground. *J. Leukoc. Biol.* **2019**, *105*, 353–361. [[CrossRef](#)] [[PubMed](#)]
224. Racicot, K.; Kwon, J.Y.; Aldo, P.; Silasi, M.; Mor, G. Understanding the complexity of the immune system during pregnancy. *Am. J. Reprod. Immunol.* **2014**, *72*, 107–116. [[CrossRef](#)]
225. Ruiz, R.J.; Fullerton, J.; Dudley, D.J. The interrelationship of maternal stress, endocrine factors and inflammation on gestational length. *Obstet. Gynecol. Surv.* **2003**, *58*, 415–428. [[CrossRef](#)] [[PubMed](#)]

226. Bardina, S.V.; Bunduc, P.; Tripathi, S.; Duehr, J.; Frere, J.J.; Brown, J.A.; Nachbagauer, R.; Foster, G.A.; Krysztof, D.; Tortorella, D.; et al. Enhancement of Zika virus pathogenesis by preexisting antinflavivirus immunity. *Science* **2017**, *356*, 175–180. [[CrossRef](#)] [[PubMed](#)]
227. Brown, J.A.; Singh, G.; Acklin, J.A.; Lee, S.; Duehr, J.E.; Chokola, A.N.; Frere, J.J.; Hoffman, K.W.; Foster, G.A.; Krysztof, D.; et al. Dengue Virus Immunity Increases Zika Virus-Induced Damage during Pregnancy. *Immunity* **2019**, *50*, 751–762 e755. [[CrossRef](#)] [[PubMed](#)]
228. Shim, B.S.; Kwon, Y.C.; Ricciardi, M.J.; Stone, M.; Otsuka, Y.; Berri, F.; Kwal, J.M.; Magnani, D.M.; Jackson, C.B.; Richard, A.S.; et al. Zika Virus-Immune Plasmas from Symptomatic and Asymptomatic Individuals Enhance Zika Pathogenesis in Adult and Pregnant Mice. *mBio* **2019**, *10*, e00758-19. [[CrossRef](#)]
229. Simoni, M.K.; Jurado, K.A.; Abrahams, V.M.; Fikrig, E.; Guller, S. Zika virus infection of Hofbauer cells. *Am. J. Reprod. Immunol.* **2017**, *77*, e12613. [[CrossRef](#)]
230. Bayer, A.; Lennemann, N.J.; Ouyang, Y.; Bramley, J.C.; Morosky, S.; Marques, E.T., Jr.; Cherry, S.; Sadovskiy, Y.; Coyne, C.B. Type III Interferons Produced by Human Placental Trophoblasts Confer Protection against Zika Virus Infection. *Cell. Host Microbe* **2016**, *19*, 705–712. [[CrossRef](#)]
231. Noronha, L.; Zanluca, C.; Azevedo, M.L.; Luz, K.G.; Santos, C.N. Zika virus damages the human placental barrier and presents marked fetal neurotropism. *Mem. Inst. Oswaldo Cruz* **2016**, *111*, 287–293. [[CrossRef](#)]
232. Jurado, K.A.; Simoni, M.K.; Tang, Z.; Uraki, R.; Hwang, J.; Householder, S.; Wu, M.; Lindenbach, B.D.; Abrahams, V.M.; Guller, S.; et al. Zika virus productively infects primary human placenta-specific macrophages. *JCI Insight* **2016**, *1*. [[CrossRef](#)]
233. Adibi, J.J.; Zhao, Y.; Cartus, A.R.; Gupta, P.; Davidson, L.A. Placental Mechanics in the Zika-Microcephaly Relationship. *Cell. Host Microbe* **2016**, *20*, 9–11. [[CrossRef](#)] [[PubMed](#)]
234. Winkler, C.W.; Myers, L.M.; Woods, T.A.; Messer, R.J.; Carmody, A.B.; McNally, K.L.; Scott, D.P.; Hasenkrug, K.J.; Best, S.M.; Peterson, K.E. Adaptive Immune Responses to Zika Virus Are Important for Controlling Virus Infection and Preventing Infection in Brain and Testes. *J. Immunol.* **2017**, *198*, 3526–3535. [[CrossRef](#)] [[PubMed](#)]
235. Regla-Nava, J.A.; Elong Ngono, A.; Viramontes, K.M.; Huynh, A.T.; Wang, Y.T.; Nguyen, A.T.; Salgado, R.; Mamidi, A.; Kim, K.; Diamond, M.S.; et al. Cross-reactive Dengue virus-specific CD8(+) T cells protect against Zika virus during pregnancy. *Nat. Commun.* **2018**, *9*, 3042. [[CrossRef](#)] [[PubMed](#)]
236. Elong Ngono, A.; Vizcarra, E.A.; Tang, W.W.; Sheets, N.; Joo, Y.; Kim, K.; Gorman, M.J.; Diamond, M.S.; Shresta, S. Mapping and Role of the CD8(+) T Cell Response During Primary Zika Virus Infection in Mice. *Cell. Host Microbe* **2017**, *21*, 35–46. [[CrossRef](#)] [[PubMed](#)]
237. Wen, J.; Tang, W.W.; Sheets, N.; Ellison, J.; Sette, A.; Kim, K.; Shresta, S. Identification of Zika virus epitopes reveals immunodominant and protective roles for dengue virus cross-reactive CD8(+) T cells. *Nat. Microbiol.* **2017**, *2*, 17036. [[CrossRef](#)]
238. Wen, J.; Shresta, S. T Cell Immunity to Zika and Dengue Viral Infections. *J. Interferon Cytokine Res.* **2017**, *37*, 475–479. [[CrossRef](#)]
239. Ngono, A.E.; Shresta, S. Immune Response to Dengue and Zika. *Annu. Rev. Immunol.* **2018**, *36*, 279–308. [[CrossRef](#)]
240. Seong, R.K.; Lee, J.K.; Shin, O.S. Zika Virus-Induction of the Suppressor of Cytokine Signaling 1/3 Contributes to the Modulation of Viral Replication. *Pathogens* **2020**, *9*, 163. [[CrossRef](#)]
241. Kumar, A.; Devi, S.G.; Kar, P.; Agarwal, S.; Husain, S.A.; Gupta, R.K.; Sharma, S. Association of cytokines in hepatitis E with pregnancy outcome. *Cytokine* **2014**, *65*, 95–104. [[CrossRef](#)]
242. Foo, S.S.; Chen, W.; Chan, Y.; Lee, W.S.; Lee, S.A.; Cheng, G.; Nielsen-Saines, K.; Brasil, P.; Jung, J.U. Biomarkers and immunoprofiles associated with fetal abnormalities of ZIKV-positive pregnancies. *JCI Insight* **2018**, *3*, e124152. [[CrossRef](#)]
243. Camacho-Zavala, E.; Santacruz-Tinoco, C.; Munoz, E.; Chacon-Salinas, R.; Salazar-Sanchez, M.I.; Grajales, C.; Gonzalez-Ibarra, J.; Borja-Aburto, V.H.; Jaenisch, T.; Gonzalez-Bonilla, C.R. Pregnant Women Infected with Zika Virus Show Higher Viral Load and Immunoregulatory Cytokines Profile with CXCL10 Increase. *Viruses* **2021**, *13*, 80. [[CrossRef](#)] [[PubMed](#)]
244. Barros, J.B.S.; da Silva, P.A.N.; Koga, R.C.R.; Gonzalez-Dias, P.; Carmo Filho, J.R.; Nagib, P.R.A.; Coelho, V.; Nakaya, H.I.; Fonseca, S.G.; Pfrimer, I.A.H. Acute Zika Virus Infection in an Endemic Area Shows Modest Proinflammatory Systemic Immunoactivation and Cytokine-Symptom Associations. *Front. Immunol.* **2018**, *9*, 821. [[CrossRef](#)] [[PubMed](#)]
245. Yockey, L.J.; Iwasaki, A. Interferons and Proinflammatory Cytokines in Pregnancy and Fetal Development. *Immunity* **2018**, *49*, 397–412. [[CrossRef](#)] [[PubMed](#)]
246. Naveca, F.G.; Pontes, G.S.; Chang, A.Y.; Silva, G.; Nascimento, V.A.D.; Monteiro, D.; Silva, M.S.D.; Abdalla, L.F.; Santos, J.H.A.; Almeida, T.A.P.; et al. Analysis of the immunological biomarker profile during acute Zika virus infection reveals the over-expression of CXCL10, a chemokine linked to neuronal damage. *Mem. Inst. Oswaldo Cruz* **2018**, *113*, e170542. [[CrossRef](#)] [[PubMed](#)]
247. Lum, F.M.; Lye, D.C.B.; Tan, J.J.L.; Lee, B.; Chia, P.Y.; Chua, T.K.; Amrun, S.N.; Kam, Y.W.; Yee, W.X.; Ling, W.P.; et al. Longitudinal Study of Cellular and Systemic Cytokine Signatures to Define the Dynamics of a Balanced Immune Environment During Disease Manifestation in Zika Virus-Infected Patients. *J. Infect. Dis.* **2018**, *218*, 814–824. [[CrossRef](#)] [[PubMed](#)]
248. O'Garra, A.; Vieira, P.L.; Vieira, P.; Goldfeld, A.E. IL-10-producing and naturally occurring CD4+ Tregs: Limiting collateral damage. *J. Clin. Invest.* **2004**, *114*, 1372–1378. [[CrossRef](#)]
249. Pealer, L.N.; Marfin, A.A.; Petersen, L.R.; Lanciotti, R.S.; Page, P.L.; Stramer, S.L.; Stobierski, M.G.; Signs, K.; Newman, B.; Kapoor, H.; et al. Transmission of West Nile virus through blood transfusion in the United States in 2002. *N. Engl. J. Med.* **2003**, *349*, 1236–1245. [[CrossRef](#)]

250. Iwamoto, M.; Jernigan, D.B.; Guasch, A.; Trepka, M.J.; Blackmore, C.G.; Hellinger, W.C.; Pham, S.M.; Zaki, S.; Lanciotti, R.S.; Lance-Parker, S.E.; et al. Transmission of West Nile virus from an organ donor to four transplant recipients. *N. Engl. J. Med.* **2003**, *348*, 2196–2203. [\[CrossRef\]](#)
251. From the Centers for Disease Control and Prevention. Possible West Nile virus transmission to an infant through breast-feeding—Michigan, 2002. *JAMA* **2002**, *288*, 1976–1977.
252. Hayes, E.B.; O’Leary, D.R. West Nile virus infection: A pediatric perspective. *Pediatrics* **2004**, *113*, 1375–1381. [\[CrossRef\]](#)
253. O’Leary, D.R.; Kuhn, S.; Kniss, K.L.; Hinckley, A.F.; Rasmussen, S.A.; Pape, W.J.; Kightlinger, L.K.; Beecham, B.D.; Miller, T.K.; Neitzel, D.F.; et al. Birth outcomes following West Nile Virus infection of pregnant women in the United States: 2003–2004. *Pediatrics* **2006**, *117*, e537–e545. [\[CrossRef\]](#) [\[PubMed\]](#)
254. Cordoba, L.; Escribano-Romero, E.; Garmendia, A.; Saiz, J.C. Pregnancy increases the risk of mortality in West Nile virus-infected mice. *J. Gen. Virol.* **2007**, *88*, 476–480. [\[CrossRef\]](#) [\[PubMed\]](#)
255. Armah, H.B.; Wang, G.; Omalu, B.I.; Tesh, R.B.; Gyure, K.A.; Chute, D.J.; Smith, R.D.; Dulai, P.; Vinters, H.V.; Kleinschmidt-DeMasters, B.K.; et al. Systemic distribution of West Nile virus infection: Postmortem immunohistochemical study of six cases. *Brain Pathol.* **2007**, *17*, 354–362. [\[CrossRef\]](#)
256. Garcia, M.N.; Hasbun, R.; Murray, K.O. Persistence of West Nile virus. *Microbes Infect.* **2015**, *17*, 163–168. [\[CrossRef\]](#)
257. Gack, M.U.; Diamond, M.S. Innate immune escape by Dengue and West Nile viruses. *Curr. Opin. Virol.* **2016**, *20*, 119–128. [\[CrossRef\]](#) [\[PubMed\]](#)
258. King, N.J.; Kesson, A.M. Interferon-independent increases in class I major histocompatibility complex antigen expression follow flavivirus infection. *J. Gen. Virol.* **1988**, *69 Pt 10*, 2535–2543. [\[CrossRef\]](#)
259. Liu, Y.; King, N.; Kesson, A.; Blanden, R.V.; Mullbacher, A. Flavivirus infection up-regulates the expression of class I and class II major histocompatibility antigens on and enhances T cell recognition of astrocytes in vitro. *J. Neuroimmunol.* **1989**, *21*, 157–168. [\[CrossRef\]](#)
260. Bao, S.; King, N.J.; Dos Remedios, C.G. Flavivirus induces MHC antigen on human myoblasts: A model of autoimmune myositis? *Muscle Nerve* **1992**, *15*, 1271–1277. [\[CrossRef\]](#)
261. King, N.J.; Maxwell, L.E.; Kesson, A.M. Induction of class I major histocompatibility complex antigen expression by West Nile virus on gamma interferon-refractory early murine trophoblast cells. *Proc. Natl. Acad. Sci. USA* **1989**, *86*, 911–915. [\[CrossRef\]](#)
262. Monath, T. Pathobiology of the Flaviviruses. In *The Togaviridae and Flaviviridae Edited by: Schlesinger SSMJ*; Springer: Berlin/Heidelberg, Germany, 1986.
263. Sugamata, M.; Miura, T. Japanese encephalitis virus infection in fetal mice at different stages of pregnancy I. Stillbirth. *Acta virologica* **1982**, *26*, 279–282.
264. Senapati, S.; Banerjee, P.; Bhagavatula, S.; Kushwaha, P.P.; Kumar, S. Contributions of human ACE2 and TMPRSS2 in determining host-pathogen interaction of COVID-19. *J. Genet.* **2021**, *100*, 1–16. [\[CrossRef\]](#)
265. Pique-Regi, R.; Romero, R.; Tarca, A.L.; Sandler, E.D.; Xu, Y.; Garcia-Flores, V.; Leng, Y.; Luca, F.; Hassan, S.S.; Gomez-Lopez, N. Single cell transcriptional signatures of the human placenta in term and preterm parturition. *Elife* **2019**, *8*, e52004. [\[CrossRef\]](#) [\[PubMed\]](#)
266. Pique-Regi, R.; Romero, R.; Tarca, A.L.; Luca, F.; Xu, Y.; Alazizi, A.; Leng, Y.; Hsu, C.D.; Gomez-Lopez, N. Does the human placenta express the canonical cell entry mediators for SARS-CoV-2? *Elife* **2020**, *9*, e58716. [\[CrossRef\]](#) [\[PubMed\]](#)
267. Li, Y.; Zhang, Z.; Yang, L.; Lian, X.; Xie, Y.; Li, S.; Xin, S.; Cao, P.; Lu, J. The MERS-CoV Receptor DPP4 as a Candidate Binding Target of the SARS-CoV-2 Spike. *iScience* **2020**, *23*, 101160. [\[CrossRef\]](#)
268. Dong, L.; Pei, S.; Ren, Q.; Fu, S.; Yu, L.; Chen, H.; Chen, X.; Yin, M. Evaluation of vertical transmission of SARS-CoV-2 in utero: Nine pregnant women and their newborns. *Placenta* **2021**, *111*, 91–96. [\[CrossRef\]](#)
269. Schiuma, G.; Beltrami, S.; Santi, E.; Scutiero, G.; Sanz, J.M.; Semprini, C.M.; Rizzo, S.; Fernandez, M.; Zidi, I.; Gafa, R.; et al. Effect of SARS-CoV-2 infection in pregnancy on CD147, ACE2 and HLA-G expression. *Placenta* **2023**, *132*, 38–43. [\[CrossRef\]](#)
270. Hosier, H.; Farhadian, S.F.; Morotti, R.A.; Deshmukh, U.; Lu-Culligan, A.; Campbell, K.H.; Yasumoto, Y.; Vogels, C.B.; Casanovas-Massana, A.; Vijayakumar, P.; et al. SARS-CoV-2 infection of the placenta. *J. Clin. Investig.* **2020**, *130*, 4947–4953. [\[CrossRef\]](#) [\[PubMed\]](#)
271. Vivanti, A.J.; Vauloup-Fellous, C.; Prevot, S.; Zupan, V.; Suffee, C.; Do Cao, J.; Benachi, A.; De Luca, D. Transplacental transmission of SARS-CoV-2 infection. *Nat. Commun.* **2020**, *11*, 3572. [\[CrossRef\]](#)
272. Facchetti, F.; Bugatti, M.; Drera, E.; Tripodo, C.; Sartori, E.; Cancila, V.; Papaccio, M.; Castellani, R.; Casola, S.; Boniotti, M.B.; et al. SARS-CoV2 vertical transmission with adverse effects on the newborn revealed through integrated immunohistochemical, electron microscopy and molecular analyses of Placenta. *EBioMedicine* **2020**, *59*, 102951. [\[CrossRef\]](#)
273. Schoenmakers, S.; Snijder, P.; Verdijk, R.M.; Kuiken, T.; Kamphuis, S.S.M.; Koopman, L.P.; Krasemann, T.B.; Rousian, M.; Broekhuizen, M.; Steegers, E.A.P.; et al. SARS-CoV-2 placental infection and inflammation leading to fetal distress and neonatal multi-organ failure in an asymptomatic woman. *MedRxiv* **2020**. [\[CrossRef\]](#)
274. Greco, S.; Sanz, J.M.; Bortolotti, D.; Semprini, C.M.; Gafa, R.; Santi, E.; Maestri, I.; Rizzo, R.; Greco, P.; Passaro, A.J.F.i.M. Case report: Tissue positivity for SARS-CoV-2 in a preterm born infant death of thrombosis. A possible intrauterine transmission. *Front. Med.* **2023**, *10*, 1127529. [\[CrossRef\]](#)

275. Rizzo, R.; Neri, L.M.; Simioni, C.; Bortolotti, D.; Occhionorelli, S.; Zauli, G.; Secchiero, P.; Semprini, C.M.; Laface, I.; Sanz, J.M.; et al. SARS-CoV-2 nucleocapsid protein and ultrastructural modifications in small bowel of a 4-week-negative COVID-19 patient. *Clin. Microbiol. Infect.* **2021**, *27*, 936–937. [[CrossRef](#)]
276. Bortolotti, D.; Simioni, C.; Neri, L.M.; Rizzo, R.; Semprini, C.M.; Occhionorelli, S.; Laface, I.; Sanz, J.M.; Schiuma, G.; Rizzo, S.; et al. Relevance of VEGF and CD147 in different SARS-CoV-2 positive digestive tracts characterized by thrombotic damage. *FASEB J.* **2021**, *35*, e21969. [[CrossRef](#)] [[PubMed](#)]
277. Traina, L.; Mucignat, M.; Rizzo, R.; Gafa, R.; Bortolotti, D.; Passaro, A.; Zamboni, P. COVID-19 induced aorto duodenal fistula following evar in the so called "negative" patient. *Vascular* **2023**, *31*, 189–195. [[CrossRef](#)] [[PubMed](#)]
278. Bortolotti, D.; Gentili, V.; Rizzo, S.; Schiuma, G.; Beltrami, S.; Spadaro, S.; Strazzabosco, G.; Campo, G.; Carosella, E.D.; Papi, A.; et al. Increased sHLA-G Is Associated with Improved COVID-19 Outcome and Reduced Neutrophil Adhesion. *Viruses* **2021**, *13*, 1855. [[CrossRef](#)] [[PubMed](#)]
279. de Mendonca Vieira, R.; Meagher, A.; Crespo, A.C.; Kshirsagar, S.K.; Iyer, V.; Norwitz, E.R.; Strominger, J.L.; Tilburgs, T. Human Term Pregnancy Decidual NK Cells Generate Distinct Cytotoxic Responses. *J. Immunol.* **2020**, *204*, 3149–3159. [[CrossRef](#)]
280. Bortolotti, D.; Gentili, V.; Rizzo, S.; Rotola, A.; Rizzo, R. SARS-CoV-2 Spike 1 Protein Controls Natural Killer Cell Activation via the HLA-E/NKG2A Pathway. *Cells* **2020**, *9*, 1975. [[CrossRef](#)]
281. Braud, V.; Jones, E.Y.; McMichael, A. The human major histocompatibility complex class Ib molecule HLA-E binds signal sequence-derived peptides with primary anchor residues at positions 2 and 9. *Eur. J. Immunol.* **1997**, *27*, 1164–1169. [[CrossRef](#)]
282. Anfossi, N.; Andre, P.; Guia, S.; Falk, C.S.; Roetynck, S.; Stewart, C.A.; Bresó, V.; Frassati, C.; Reviron, D.; Middleton, D.; et al. Human NK cell education by inhibitory receptors for MHC class I. *Immunity* **2006**, *25*, 331–342. [[CrossRef](#)]
283. Lesseur, C.; Jessel, R.H.; Ohrn, S.; Ma, Y.; Li, Q.; Dekio, F.; Brody, R.I.; Wetmur, J.G.; Gigase, F.A.J.; Lieber, M.; et al. Gestational SARS-CoV-2 infection is associated with placental expression of immune and trophoblast genes. *Placenta* **2022**, *126*, 125–132. [[CrossRef](#)]
284. Chauhan, G.; Madou, M.J.; Kalra, S.; Chopra, V.; Ghosh, D.; Martinez-Chapa, S.O. Nanotechnology for COVID-19: Therapeutics and Vaccine Research. *ACS Nano* **2020**, *14*, 7760–7782. [[CrossRef](#)] [[PubMed](#)]
285. Chandrasekar, V.; Singh, A.V.; Maharjan, R.S.; Dakua, S.P.; Balakrishnan, S.; Dash, S.; Laux, P.; Luch, A.; Singh, S.; Pradhan, M. Perspectives on the Technological Aspects and Biomedical Applications of Virus-Like Particles/Nanoparticles in Reproductive Biology: Insights on the Medicinal and Toxicological Outlook. *Adv. NanoBiomed Res.* **2022**, *2*, 2200010. [[CrossRef](#)]
286. Boix-Besora, A.; Lorenzo, E.; Lavado-Garcia, J.; Godia, F.; Cervera, L. Optimization, Production, Purification and Characterization of HIV-1 GAG-Based Virus-like Particles Functionalized with SARS-CoV-2. *Vaccines* **2022**, *10*, 250. [[CrossRef](#)]
287. Garg, H.; Mehmetoglu-Gurbuz, T.; Ruddy, G.M.; Joshi, A. Capsid containing virus like particle vaccine against Zika virus made from a stable cell line. *Vaccine* **2019**, *37*, 7123–7131. [[CrossRef](#)] [[PubMed](#)]
288. Shojaei, S.; Ali, M.S.; Suresh, M.; Upreti, T.; Mogourian, V.; Helewa, M.; Labouta, H.I. Dynamic placenta-on-a-chip model for fetal risk assessment of nanoparticles intended to treat pregnancy-associated diseases. *Biochim. Biophys. Acta Mol. Basis Dis.* **2021**, *1867*, 166131. [[CrossRef](#)] [[PubMed](#)]
289. Villar, L.; Dayan, G.H.; Arredondo-Garcia, J.L.; Rivera, D.M.; Cunha, R.; Deseda, C.; Reynales, H.; Costa, M.S.; Morales-Ramirez, J.O.; Carrasquilla, G.; et al. Efficacy of a tetravalent dengue vaccine in children in Latin America. *N. Engl. J. Med.* **2015**, *372*, 113–123. [[CrossRef](#)] [[PubMed](#)]
290. Ravel, G.; Rogue, A.; Spézia, F.; Mantel, N.; Gould, S.; Forster, R. Transfer of tetravalent dengue vaccine during gestation and lactation in mice. *Toxicology Letters* **2015**, *238*. [[CrossRef](#)]
291. Riley, L.E.; Jamieson, D.J. Inclusion of Pregnant and Lactating Persons in COVID-19 Vaccination Efforts. *Ann. Intern. Med.* **2021**, *174*, 701–702. [[CrossRef](#)]
292. Januszek, S.M.; Faryniak-Zuzak, A.; Barnas, E.; Lozinski, T.; Gora, T.; Siwiec, N.; Szczerba, P.; Januszek, R.; Kluz, T. The Approach of Pregnant Women to Vaccination Based on a COVID-19 Systematic Review. *Medicina (Kaunas)* **2021**, *57*. [[CrossRef](#)]
293. Poland, G.A.; Jacobson, R.M.; Koutsky, L.A.; Tamms, G.M.; Railkar, R.; Smith, J.F.; Bryan, J.T.; Cavanaugh, P.F., Jr.; Jansen, K.U.; Barr, E. Immunogenicity and reactogenicity of a novel vaccine for human papillomavirus 16: A 2-year randomized controlled clinical trial. *Mayo. Clin. Proc.* **2005**, *80*, 601–610. [[CrossRef](#)]
294. Bonde, U.; Joergensen, J.S.; Lamont, R.F.; Mogensen, O. Is HPV vaccination in pregnancy safe? *Hum. Vaccin Immunother* **2016**, *12*, 1960–1964. [[CrossRef](#)] [[PubMed](#)]
295. Scheller, N.M.; Pasternak, B.; Molgaard-Nielsen, D.; Svanstrom, H.; Hviid, A. Quadrivalent HPV Vaccination and the Risk of Adverse Pregnancy Outcomes. *N. Engl. J. Med.* **2017**, *376*, 1223–1233. [[CrossRef](#)] [[PubMed](#)]
296. Celikel, A.; Ustunsoz, A.; Guvenc, G. Determination of vaccination status of pregnant women during pregnancy and the affecting factors. *J. Clin. Nurs.* **2014**, *23*, 2142–2150. [[CrossRef](#)] [[PubMed](#)]
297. Swamy, G.K.; Garcia-Putnam, R. Vaccine-preventable diseases in pregnancy. *Am. J. Perinatol.* **2013**, *30*, 89–97. [[CrossRef](#)]
298. Makris, M.C.; Polyzos, K.A.; Mavros, M.N.; Athanasiou, S.; Rafailidis, P.I.; Falagas, M.E. Safety of hepatitis B, pneumococcal polysaccharide and meningococcal polysaccharide vaccines in pregnancy: A systematic review. *Drug. Saf.* **2012**, *35*, 1–14. [[CrossRef](#)]
299. Hieu, N.T.; Kim, K.H.; Janowicz, Z.; Timmermans, I. Comparative efficacy, safety and immunogenicity of Hepavax-Gene and Engerix-B, recombinant hepatitis B vaccines, in infants born to HBsAg and HBeAg positive mothers in Vietnam: An assessment at 2 years. *Vaccine* **2002**, *20*, 1803–1808. [[CrossRef](#)]

300. Shivananda; Somani, V.; Srikanth, B.S.; Mohan, M.; Kulkarni, P.S. Comparison of two hepatitis B vaccines (GeneVac-B and Engerix-B) in healthy infants in India. *Clin. Vaccin. Immunol.* **2006**, *13*, 661–664. [[CrossRef](#)]
301. Hernandez-Bernal, F.; Aguilar-Betancourt, A.; Aljovin, V.; Arias, G.; Valenzuela, C.; de Alejo, K.P.; Hernandez, K.; Oquendo, O.; Figueredo, N.; Figueroa, N.; et al. Comparison of four recombinant hepatitis B vaccines applied on an accelerated schedule in healthy adults. *Hum. Vaccin.* **2011**, *7*, 1026–1036. [[CrossRef](#)]
302. Van Damme, P.; Minervini, G.; Liss, C.L.; McCarson, B.; Vesikari, T.; Boslego, J.W.; Bhuyan, P.K. Safety, tolerability and immunogenicity of a recombinant hepatitis B vaccine manufactured by a modified process in healthy young adults. *Hum. Vaccin.* **2009**, *5*, 92–97. [[CrossRef](#)]
303. Ayoola, E.A.; Johnson, A.O. Hepatitis B vaccine in pregnancy: Immunogenicity, safety and transfer of antibodies to infants. *Int. J. Gynaecol. Obstet.* **1987**, *25*, 297–301. [[CrossRef](#)]
304. Ingardia, C.J.; Kelley, L.; Steinfeld, J.D.; Wax, J.R. Hepatitis B vaccination in pregnancy: Factors influencing efficacy. *Obstet. Gynecol.* **1999**, *93*, 983–986. [[CrossRef](#)]
305. Ingardia, C.J.; Kelley, L.; Lerer, T.; Wax, J.R.; Steinfeld, J.D. Correlation of maternal and fetal hepatitis B antibody titers following maternal vaccination in pregnancy. *Am. J. Perinatol.* **1999**, *16*, 129–132. [[CrossRef](#)]
306. Sheffield, J.S.; Hickman, A.; Tang, J.; Moss, K.; Kourosh, A.; Crawford, N.M.; Wendel, G.D., Jr. Efficacy of an accelerated hepatitis B vaccination program during pregnancy. *Obstet. Gynecol.* **2011**, *117*, 1130–1135. [[CrossRef](#)] [[PubMed](#)]
307. Grosheide, P.M.; Schalm, S.W.; van Os, H.C.; Fetter, W.P.; Heijtkink, R.A. Immune response to hepatitis B vaccine in pregnant women receiving post-exposure prophylaxis. *Eur. J. Obstet. Gynecol. Reprod. Biol.* **1993**, *50*, 53–58. [[CrossRef](#)] [[PubMed](#)]
308. Charlton, R.A.; Cunnington, M.C.; de Vries, C.S.; Weil, J.G. Data resources for investigating drug exposure during pregnancy and associated outcomes: The General Practice Research Database (GPRD) as an alternative to pregnancy registries. *Drug. Saf.* **2008**, *31*, 39–51. [[CrossRef](#)] [[PubMed](#)]
309. Hoar, R.M. Developmental Toxicity: Extrapolation Across Species. *J. Am. Coll. Toxicol.* **2016**, *14*, 11–20. [[CrossRef](#)]
310. Koren, G.; Pastuszak, A.; Ito, S. Drugs in pregnancy. *N. Engl. J. Med.* **1998**, *338*, 1128–1137. [[CrossRef](#)]
311. Lok, A.S.; McMahon, B.J. Chronic hepatitis B: Update 2009. *Hepatology* **2009**, *50*, 661–662. [[CrossRef](#)]
312. Brown, Z.A.; Watts, D.H. Antiviral therapy in pregnancy. *Clin. Obstet. Gynecol.* **1990**, *33*, 276–289. [[CrossRef](#)]
313. Kang, S.H.; Chua-Gocheo, A.; Bozzo, P.; Einarson, A. Safety of antiviral medication for the treatment of herpes during pregnancy. *Can. Fam. Physician.* **2011**, *57*, 427–428.
314. Pan, C.Q.; Duan, Z.P.; Bhamidimarri, K.R.; Zou, H.B.; Liang, X.F.; Li, J.; Tong, M.J. An algorithm for risk assessment and intervention of mother to child transmission of hepatitis B virus. *Clin. Gastroenterol. Hepatol.* **2012**, *10*, 452–459. [[CrossRef](#)]
315. European Association For The Study Of The, L. EASL clinical practice guidelines: Management of chronic hepatitis B virus infection. *J. Hepatol.* **2012**, *57*, 167–185. [[CrossRef](#)] [[PubMed](#)]
316. Keeffe, E.B.; Dieterich, D.T.; Han, S.H.; Jacobson, I.M.; Martin, P.; Schiff, E.R.; Tobias, H. A treatment algorithm for the management of chronic hepatitis B virus infection in the United States: 2008 update. *Clin. Gastroenterol. Hepatol.* **2008**, *6*, 1315–1341, quiz 1286. [[CrossRef](#)] [[PubMed](#)]
317. Pan, C.Q.; Lee, H.M. Antiviral therapy for chronic hepatitis B in pregnancy. *Semin. Liver. Dis.* **2013**, *33*, 138–146. [[CrossRef](#)] [[PubMed](#)]
318. Simsek Yavuz, S.; Unal, S. Antiviral treatment of COVID-19. *Turk. J. Med. Sci.* **2020**, *50*, 611–619. [[CrossRef](#)]
319. Grein, J.; Ohmagari, N.; Shin, D.; Diaz, G.; Asperges, E.; Castagna, A.; Feldt, T.; Green, G.; Green, M.L.; Lescure, F.X.; et al. Compassionate Use of Remdesivir for Patients with Severe Covid-19. *N. Engl. J. Med.* **2020**, *382*, 2327–2336. [[CrossRef](#)]
320. Amirian, E.S.; Levy, J.K. Current knowledge about the antivirals remdesivir (GS-5734) and GS-441524 as therapeutic options for coronaviruses. *One Health* **2020**, *9*, 100128. [[CrossRef](#)]
321. Nasrallah, S.; Nguyen, A.Q.; Hitchings, L.; Wang, J.Q.; Hamade, S.; Maxwell, G.L.; Khoury, A.; Gomez, L.M. Pharmacological treatment in pregnant women with moderate symptoms of coronavirus disease 2019 (COVID-19) pneumonia. *J. Matern. Fetal. Neonatal. Med.* **2022**, *35*, 5970–5977. [[CrossRef](#)]
322. Maldarelli, G.A.; Savage, M.; Mazur, S.; Oxford-Horrey, C.; Salvatore, M.; Marks, K.M. Remdesivir Treatment for Severe COVID-19 in Third-Trimester Pregnancy: Case Report and Management Discussion. *Open. Forum. Infect. Dis.* **2020**, *7*, ofaa345. [[CrossRef](#)]
323. Anderson, J.; Schauer, J.; Bryant, S.; Graves, C.R. The use of convalescent plasma therapy and remdesivir in the successful management of a critically ill obstetric patient with novel coronavirus 2019 infection: A case report. *Case Rep. Womens Health* **2020**, *27*, e00221. [[CrossRef](#)]
324. McCoy, J.A.; Short, W.R.; Srinivas, S.K.; Levine, L.D.; Hirshberg, A. Compassionate use of remdesivir for treatment of severe coronavirus disease 2019 in pregnant women at a United States academic center. *Am. J. Obstet. Gynecol. MFM* **2020**, *2*, 100164. [[CrossRef](#)] [[PubMed](#)]
325. Singh, V.; Choudhary, A. Treatment With Remdesivir in Two Pregnant Patients With COVID-19 Pneumonia. *Cureus* **2021**, *13*, e14986. [[CrossRef](#)] [[PubMed](#)]

326. Schuler-Faccini, L.; Sanseverino, M.; Vianna, E.; da Silva, A.A.; Larrandaburu, M.; Marcolongo-Pereira, C.; Abeche, A.M. Zika virus: A new human teratogen? Implications for women of reproductive age. *Clin. Pharmacol. Ther.* **2016**, *100*, 28–30. [[CrossRef](#)] [[PubMed](#)]
327. Simmons, C.P.; McPherson, K.; Van Vinh Chau, N.; Hoai Tam, D.T.; Young, P.; Mackenzie, J.; Wills, B. Recent advances in dengue pathogenesis and clinical management. *Vaccine* **2015**, *33*, 7061–7068. [[CrossRef](#)] [[PubMed](#)]

Disclaimer/Publisher's Note: The statements, opinions and data contained in all publications are solely those of the individual author(s) and contributor(s) and not of MDPI and/or the editor(s). MDPI and/or the editor(s) disclaim responsibility for any injury to people or property resulting from any ideas, methods, instructions or products referred to in the content.

Several reports had highlighted the ability of viruses to exploit or affect HLA-G expression during pregnancy to avoid immune recognition and increase their spread, including HHVs [373–375], HIV [376, 377] and HPV [325].

During pregnancy, HLA-G strictly collaborates with dNK cells, which not only prevent the rejection of fetus, but also promote fetus protection against possible infections that can occur through vertical transmission [337]. View the role of both tolerogenic HLA-G and dNK cells, it might be deduced that their impairment could be crucial in the onset of placental infections.

Concerning SARS-CoV-2, recent studies reported its ability to infect placental annexes [238], suggesting a potential mother-fetus transmission. This hypothesis was supported by several evidences, including the presence of SARS-CoV-2 mRNA or virions in ST, together with the finding of the presence of congenital infection during the first trimester of pregnancy in fetal organs, such as lung and kidney [378]. The study conducted by Greco et al on a newborn from severe COVID-19-positive mother dead after thrombosis, demonstrated the consistent presence of SARS-CoV-2 NP and Spike protein in several fetal tissues, supporting viral ability to reach fetus during infection [379]. Again, the concomitance of maternal COVID-19 infection with thrombosis in fetal circulation [380], but also placental insufficiency, miscarriage, as well as preeclampsia [381], was reported in association with SARS CoV-2 infection in pregnancy.

Interesting, it seems that the different expression levels of both ACE2 [382] and CD147 [383] on placenta could determine various clinical outcomes of SARS-CoV-2 gestational infection, that ranges from severe to asymptomatic disease, also depending to maternal immunological response to the virus [384].

The aforementioned pathological conditions found in pregnant COVID-19 women can be correlated to peculiar immune-escape strategies exploited by SARS-CoV-2, such as the induction of the immunotolerogenic HLA-G molecule [385]. Given the importance of viral receptors and HLA-G expression in gestational COVID-19, we investigated the presence of placental SARS-CoV-2 infection in association with ACE2, CD147, HLA-G and CD56, as a marker for dNK cells ([386], paper attached).

The analysis of placenta specimens obtained by COVID-19 women reported the presence of SARS-CoV-2 in placenta tissues, as confirmed by the presence of viral NP expression in both ST and in EVT by IHC analysis ([386], paper attached). Simultaneously, placental samples from COVID-19 mothers positive for *in situ* placental SARS-CoV-2 infection, presented a high expression of CD147 and HLA-G, mainly at ST levels, while on the contrary, CD56 expression in the decidua was found decreased, compared to control group ([386], paper attached).

Thus, our results suggest that SARS-CoV-2 can easily infect placenta tissues where it can modulate HLA-G to enact viral immune-escape. Furthermore, the reported low CD56 expression in dNK cells is in line with NK cell anergy observed in COVID-19, typically described in of SARS-CoV-2 infection.



Contents lists available at ScienceDirect

Placenta

journal homepage: www.elsevier.com/locate/placenta

Effect of SARS-CoV-2 infection in pregnancy on CD147, ACE2 and HLA-G expression

Giovanna Schiuma^{a,1}, Silvia Beltrami^{a,1}, Erica Santi^b, Gennaro Scutiero^b, Juana Maria Sanz^a, Chiara Marina Semprini^c, Sabrina Rizzo^a, Mercedes Fernandez^a, Ines Zidi^e, Roberta Gafà^d, Angelina Passaro^{c,d}, Pantaleo Greco^b, Daria Bortolotti^{a,1}, Roberta Rizzo^{a,f,*}

^a Department of Chemical, Pharmaceutical and Agricultural Sciences, University of Ferrara, Via Luigi Borsari, 46, 44121, Ferrara, Italy

^b Department of Medical Sciences, Obstetric and Gynecological Clinic, University of Ferrara, Via Luigi Borsari, 46, 44121, Ferrara, Italy

^c Medical Department, University Hospital of Ferrara Arcispedale Sant'Anna, Via Aldo Moro, 8 Cona, 44124, Ferrara, Italy

^d Department of Translational Medicine, University of Ferrara, Via Luigi Borsari, 46, 44121, Ferrara, Italy

^e Laboratory Microorganismes and Active Biomolecules, Sciences Faculty of Tunis, University Tunis El Manar, Tunis, Tunisia

^f LTTA—Clinical Research Center, University of Ferrara, Via Luigi Borsari, 46 - 44100, 44121, Ferrara, Italy

ARTICLE INFO

Keywords:

SARS-CoV-2
Placental infection
ACE2
CD147
HLA-G

ABSTRACT

Introduction: Recent studies reported a differential expression of both ACE2 and CD147 in pregnant women associated to SARS-CoV-2 placental infection. The aim of this study is to further investigate the placental SARS-CoV-2 infection and the potential effect on protein expression (ACE2, CD147, HLA-G and CD56).

Methods: The study was on three subgroups: i) 18 subjects positive for SARS-CoV-2 swab at delivery; ii) 9 subjects that had a positive SARS-CoV-2 swab during pregnancy but resulted negative at delivery; iii) 11 control subjects with physiological pregnancy and with no previous or concomitant SARS-CoV-2 swab positivity. None of the subjects were vaccinated for SARS-CoV-2 infection. The placenta samples were analyzed for SARS-CoV-2 NP (Nucleocapsid protein) positivity and the expression of ACE2, CD147, HLA-G and CD56.

Results: We observed a higher percentage of SARS-CoV-2 NP positive placenta samples in the group of SARS-CoV-2 PCR positive at delivery in comparison with SARS-CoV-2 PCR negative at delivery. The localization of SARS-CoV-2 NP positivity in placenta samples was mainly in syncytiotrophoblast (ST) of SARS-CoV-2 PCR positive at delivery group and in extra-villous trophoblast (EVT) of SARS-CoV-2 PCR negative at delivery group. CD147, HLA-G positivity was higher in ST of SARS-CoV-2 PCR positive at delivery group, while CD56-expressing immune cells were decreased in comparison with control subjects.

Discussion: We confirmed the ability of SARS-CoV-2 to infect placenta tissues. The simultaneous SARS-CoV-2 swab positivity at delivery and the positivity of the placenta tissue for SARS-CoV-2 NP seems to create an environment that modifies the expression of specific molecules, as CD147 and HLA-G. These data suggest a possible impact of SARS-CoV-2 infection during pregnancy, that might be worthy to be monitored also in vaccinated subjects.

1. Introduction

After severe acute respiratory syndrome coronavirus 2 (SARS-CoV-2) pandemic outbreak in December 2019, most of studies concerning SARS-CoV-2 infection have been focused on coronavirus disease 2019

(COVID-19) severe respiratory disease, highlighting as main cellular receptor for viral entry the Angiotensin Converting Enzyme (ACE) 2 [1].

Then, several studies also investigated the possible multi-tissue tropism of SARS-CoV-2, basing on the wide expression of ACE2 in sites other than lungs [2]. It is known that SARS-CoV-2 cell entry via

Abbreviations: SARS-CoV-2, severe acute respiratory syndrome coronavirus 2; ACE-2, Angiotensin Converting Enzyme 2; TMPRSS2, Transmembrane serine protease 2; COVID-19, Coronavirus disease 2019; HLA, Human Leukocyte Antigen; NK, Natural killer; KIR, Killer-cell immunoglobulin-like receptor; ILT, Ig-like transcript.

* Corresponding author. Department of Chemical, Pharmaceutical and Agricultural Sciences, University of Ferrara, Via Luigi Borsari, 46, 44121, Ferrara, Italy.
E-mail address: rbr@unife.it (R. Rizzo).

¹ Equally contributed to the research.

<https://doi.org/10.1016/j.placenta.2023.01.004>

Received 14 June 2022; Received in revised form 20 December 2022; Accepted 4 January 2023

Available online 5 January 2023

0143-4004/© 2023 Elsevier Ltd. All rights reserved.

ACE2 engagement by the viral Spike protein also involved the proteases TMPRSS2 [3]. Placenta tissues are characterized by a lower TMPRSS2 expression compared to other tissues, like lungs, with a preferential expression at trophoblasts [4]. A few placental cells and chorioamniotic membranes co-express ACE2 and TMPRSS2 throughout gestation [5,6], suggesting a possible effect on SARS-CoV-2 placental and transplacental infection, as the co-presence of both these receptors, facilitating SARS-CoV-2 cell entry. For this reason, the presence of alternative receptors for SARS-CoV-2 entry into syncytiotrophoblast cells has been suggested [7] such as DPP4 (CD26) and CD147 [8,9]. CD147 is characterized by a diffuse tissue expression [10], in concomitance with the emerging data reporting SARS-CoV-2 infection in different body sites [11]. A recent work of Dong et al. reported a differential expression of both ACE2 and CD147 in a small cohort of pregnant women associated to SARS-CoV-2 placental infection compared to non-COVID19 infected pregnant women, with no direct evidence of viral transmission to the newborns [12].

Moreover, SARS-CoV-2 infection is associated to different clinical outcomes, that ranges from severe to asymptomatic disease [8]. This clinical heterogeneity may be correlated to a differential expression of susceptibility factors, as ACE2 and CD147, but also to peculiar escape mechanisms that the virus could exploit in some individuals, as for example the induction of the immunotolerogenic molecule Human Leukocyte Antigen (HLA)-G [13–15].

HLA-G is a non-classical HLA class I molecule firstly described in pregnancy, where it allows the protection of the semi-allogenic fetus from the maternal immune system through the interaction with specific inhibitory receptors [16].

HLA-G placenta expression during pregnancy is characterized by peculiar changes, with high levels of the molecules in the first trimester, which are reducing as they approach the birth, in order to promote the typical inflammatory environment needed to induce the delivery [17]. The presence of placental infections might affect HLA-G expression, leading to placental and fetal disorders, as recently reported for HHV-6 infection in association with IUGR condition [18].

Recently, the ability of SARS-CoV-2 to induce HLA-G has been described in bowel tissues [19–21], supporting the involvement of this molecule in its immune escape process. In particular, Natural Killer (NK) cells, that represent the first line of defense during viral infections, have been reported to be anergic in COVID-19 patients [22]. NK cells are also key players during pregnancy, representing the main immune cell type in endometrial tissues where they act to allow a correct decidualization and placentation process [23] and to kill target infected cells. Decidual natural killer cells (dNK) are the predominant leukocyte population in normal human endometrium [24]. Their content varies throughout the normal menstrual cycle, likely due to recruitment of peripheral NK cells (pNK) and/or in utero proliferation/differentiation of stem uNK cells. They represent 40% of the total leukocyte population during the proliferative phase which increases to 60% by mid-secretory phase and up to 75% in early pregnancy. At the end of pregnancy, dNKs show a different protein and gene expression profile which is associated to an increase degranulation response, suggesting their key role in counteract possible vertical transmission of infection to the fetus [25]. NK cell activity is controlled by the interaction between specific receptors (KIR (Killer immunoglobulin like receptor), ILT (Ig-like transcript)) with surface proteins. HLA-G molecules interact with ILT2 and ILT4 receptors, inducing an inhibitory signal in NK cells [26].

The evaluation of the effect of SARS-CoV-2 infection during pregnancy has raised interest. Even if virus vertical transmission is still controversial [27], several researches have evaluated the possible different susceptibility to SARS-CoV-2 infection, analyzing the placenta tissues. It has been demonstrated that SARS-CoV-2 can infect the placenta [28], documenting congenital SARS-CoV-2 infection during the first trimester of pregnancy with fetal organs, such as lung and kidney, as targets for coronavirus [29].

The aim of this study is to further investigate the placental SARS-

CoV-2 infection and the potential effect on protein expression as ACE2, CD147, HLA-G and CD56, as a marker of CD56 positive immune cells (NK cells, T cells), in placental tissues from subjects positive or negative for SARS-CoV-2 infection at delivery.

2. Materials and methods

2.1. Study population

The study was conducted on one prospective cohort of 38 patients enrolled at the time of childbirth at the Gynecology and Obstetrics Department of the Sant'Anna University Hospital in Ferrara, during the period from March to December 2020. Three subgroups were identified, namely, a cohort made up of 18 subjects positive for SARS-CoV-2 infection at delivery and 9 subjects that were positive for SARS-CoV-2 infection during pregnancy but resulted negative for SARS-CoV-2 infection at delivery and a control group made up of 11 subjects with physiological pregnancy and with no previous or concomitant SARS-CoV-2 infection, that will be referred as control group. None of the subjects were vaccinated for SARS-CoV-2 infection. SARS-CoV-2 infection was tested with a molecular swab (RT-PCR) test for the presence of SARS-CoV-2 RNA and identified to be sustained by wild type Wuhan Hu-1 isolates. Clinical data were collected for the cohort. All subjects gave their informed consent for inclusion in the study. The study was conducted in accordance with the Declaration of Helsinki, and the protocol was approved by the local Ethics Committee (Comitato Etico di Area Vasta Emilia Centro della Regione Emilia-Romagna, CE-AVEC). All the data were anonymized and no connection with the patient identity was possible.

2.2. Placenta sample collection

The placenta samples were collected after delivery and sent to the Pathology Lab for examination as previously described [18]. They were initially examined in the unfixed state then the membranes were removed by trimming them along the placental margin and the umbilical cord was removed after recording the length and site of insertion. The placental disk weights and three-dimensional measures were recorded, and the parenchyma was sectioned at 1–2 cm intervals on the maternal surface; after formalin fixation, a full-thickness section from the central portion of the placenta was sampled for histology.

2.3. Immunohistochemical analysis

Placenta slides were deparaffined by using Toluene, rehydrated in decreasing ethanol concentration [19–21]. Heat antigen retrieval in Citrate Buffer pH6.1 with 0,05% Tween20 was performed. Slides were stained using the Ultratek kit (Histoline) with the following antibody: SARS-CoV-2 NP (Nucleocapsid protein) (NB100-56576, Novus Biologicals, Centennial, 1:250 dilution), Human Leukocyte Antigen-G (HLA-G) antibody (MEM-G2, Exbio, dilution 1:400), CD147 (clone MEM-M6/1, dilution 1:100, Novus Biologicals), CD56 (clone 123C3.D5, dilution 1:100, Novus Biologicals), ACE2 (clone EPR4435-2, 1:250 dilution, Abcam).

After immunohistochemical staining, the slides were scanned using the Philips Ultra Fast Scanner version 1.6, digitalized slides were converted in BigTIFF format and were then imported into QuPath software for further image analysis. First, the Simple tissue detection tool was used to create annotation of the tissue region to be analyzed. The Cell detection tool was used to detect every cell in the tissue by using a built-in cell segmentation algorithm. To enable distinction between positively and negatively stained cells, the Intensity feature in the Detection classifier was used. The tissues were scored based on number of positively stained cells/mm². An H-score between 0 and 300 was obtained where 300 was equal to 100% of cells strongly stained (3+) [19–21].

2.4. Statistical analysis

Frequencies were analyzed by Fisher’s exact test, biological variables and H-Score comparisons were evaluated by Mann-Whitney U test. The statistical analysis was performed by GraphPad Software version 6.

3. Results

3.1. SARS-CoV-2 gestational infection is associated to clinical alterations

The prospective cohort was subdivided into three groups, characterized by a positive swab test for SARS-CoV-2 infection at the delivery (SARS-CoV-2 PCR positive at delivery) by a positive swab test for SARS-CoV-2 infection during pregnancy but negativized at the delivery (SARS-CoV-2 PCR negative at delivery) or without any positive swab test for SARS-CoV-2 during pregnancy and at delivery (controls). The subjects were matched for age, BMI and gestational period at delivery, to avoid confounding variables (Table 1). No subjects presented comorbidities, both pregnancy related, such as preeclampsia and gestational diabetes mellitus, and preexisting, such as chronic hypertension, pregestational diabetes, and heart disease (Table 1). The SARS-CoV-2 PCR positive at delivery group were all affected by the SARS-CoV-2 wild type Wuhan Hu-1 isolate, which includes most of the Italian sequences during the enrollment period. The SARS-CoV-2 PCR positive at delivery group presented hyperpyrexia (body temperature above 38°Celsius) and/or dyspnea (subjective difficulty in breathing) that needed oxygen therapy ($p = 2.1 \times 10^{-7}$; Fisher exact test). Two subjects with a positive SARS-CoV-2 swab at delivery needed to be transferred to intensive care units for supportive cares. None of the newborns from the SARS-CoV-2 PCR positive at delivery groups resulted positive for SARS-CoV-2 swab

Table 1 Demographic and clinical characteristics.

Clinical data	SARS-CoV-2 PCR positive at delivery ^a (N = 18)	SARS-CoV-2 PCR negative at delivery ^a (N = 9)	Control (N = 11)	p-value
Age; years (mean ± SD)	29.9 ± 6.9	31.8 ± 2.8	34.9 ± 5.5	
BMI (mean ± SD)	23.4 ± 3.5	27.2 ± 7.3	21.7 ± 2.1	
Comorbidities (N)	0	0	0	
Gestational period of infection; weeks (mean ± SD)	39.2 ± 1.6	22.2 ± 3.5	–	0.012 ^e
Severity of infection (N)	Severe ^b : 2 Mild: 16	Severe ^b : 0 Mild: 9	–	0.54 ^d
Gestational period of delivery; weeks (mean ± SD)	39.2 ± 1.8	38.9 ± 2.1	39.5 ± 2.7	
Hyperpyrexia and/or dyspnea (N)	18	0	–	2.1 × 10 ⁻⁷ ^d
Weight of fetus at birth; g (mean ± SD)	3353.6 ± 445.3	3192.2 ± 423.8	3343.6 ± 230.4	¹ vs ² 0.35 ^c ¹ vs ³ 0.56 ^c ² vs ³ 0.36 ^c
Apgar 5 min (mean ± SD)	9.9 ± 0.2	10.0 ± 0.0	9.9 ± 1.3	¹ vs ² 0.95 ^c ¹ vs ³ 0.98 ^c ² vs ³ 0.96 ^c
Newborn gender (Male; Female)	Male:6 ¹ Female:12	Male:2 ² Female:7	Male:5 ³ Female:6	¹ vs ² 0.68 ^d ¹ vs ³ 0.69 ^d ² vs ³ 0.37 ^d
Newborn swab result (N)	Positive: 0 Negative: 18	Positive: 0 Negative: 9	–	1 ^d

^a Swab results at delivery.
^b intensive care units for supportive cares.
^c Mann-Whitney U test.
^d Fisher exact test.

testing at childbirth. The SARS-CoV-2 PCR positive and negative at delivery groups differed for the gestational period of infection, that was 39.2 ± 1.6 weeks for SARS-CoV-2 PCR positive at delivery group and 22.2 ± 3.5 weeks for SARS-CoV-2 PCR negative at delivery group ($p = 0.012$; Mann-Whitney U test).

3.2. SARS-CoV-2 PCR positive at delivery group showed a ST positivity for SARS-CoV-2 NP

Placenta samples obtained from the three groups were analyzed for SARS-CoV-2 NP presence by IHC. The 78% of the placenta samples from the SARS-CoV-2 PCR positive at delivery group were positive for SARS-CoV-2 NP expression in comparison with the 39% of the SARS-CoV-2 PCR negative at delivery group ($p < 0.0001$, Fisher’s exact test). The control group placenta samples were all negative for SARS-CoV-2 NP staining.

SARS-CoV-2 NP positivity showed a different localization between syncytiotrophoblast (ST) and extra-villous trophoblast (EVT). SARS-CoV-2 NP positivity was preferentially found in the ST of SARS-CoV-2 PCR positive at delivery group samples (100% vs 57%, $p < 0.01$, Fisher exact test), while the infection was at EVT level in SARS-CoV-2 PCR negative at delivery group (86% vs 71%, $p < 0.01$, Fisher exact test) (Fig. 1a). The analysis of the staining for SARS-CoV-2 NP revealed a higher intensity in the ST of SARS-CoV-2 PCR positive at delivery group compared to the SARS-CoV-2 PCR negative at delivery group (Fig. 1b, $p = 0.0316$, Mann-Whitney U test).

3.3. ACE2, CD147 and HLA-G are differentially expressed in placental samples

We investigated the expression and localization of these three molecules to identify a possible implication in placental SARS-CoV-2 infection susceptibility.

Both receptors were expressed in all the placental samples. CD147 diffuse expression and higher H score were found in the ST (Fig. 2a and b) of all the placenta samples, with the strongest staining (H score) in SARS-CoV-2 PCR positive at delivery group, independently to placental SARS-CoV-2 NP positivity ($p < 0.001$; Mann-Whitney U test). CD147 membrane staining was present in EVT, with no significant differences between the placenta samples (Fig. 2a and b).

ACE2 is expressed by EVT of all the placental samples, but with a different cellular distribution (Fig. 2a, c). SARS-CoV-2 NP negative placenta presented a diffused expression of ACE2, while SARS-CoV-2 NP positive placenta, independently from the SARS-CoV-2 positivity or negativity of swab at delivery, showed a membrane-associated staining (Fig. 2a, c). Control placenta samples showed a slight intracellular ACE2 staining in comparison with SARS-CoV-2 PCR positive or negative at delivery groups (Fig. 2a, c; $p < 0.001$; Mann-Whitney U test).

Since we have previously shown that HLA-G molecules are modulated during SARS-CoV-2 infection in the intestinal villi during thromboembolic events [19–21], we evaluated HLA-G expression in placenta samples taking into consideration the implication of HLA-G molecules during viral infection in pregnancy [18].

HLA-G expression was evident in ST and EVT of all the placental samples, with a significant increase in ST of SARS-CoV-2 PCR positive at delivery group with SARS-CoV-2 NP positive placenta samples (Fig. 2a, d). HLA-G expression was also evident in EVT, with an induced expression in SARS-CoV-2 PCR positive at delivery group with SARS-CoV-2 NP positive placenta samples and in SARS-CoV-2 PCR negative at delivery group with SARS-CoV-2 NP positive placenta samples (Fig. 2d; $p < 0.01$; Mann Whitney U test).

3.4. SARS-CoV-2 placental infection influences CD56 positive immune cell presence

We analyzed placental tissues for the presence of CD56 positive

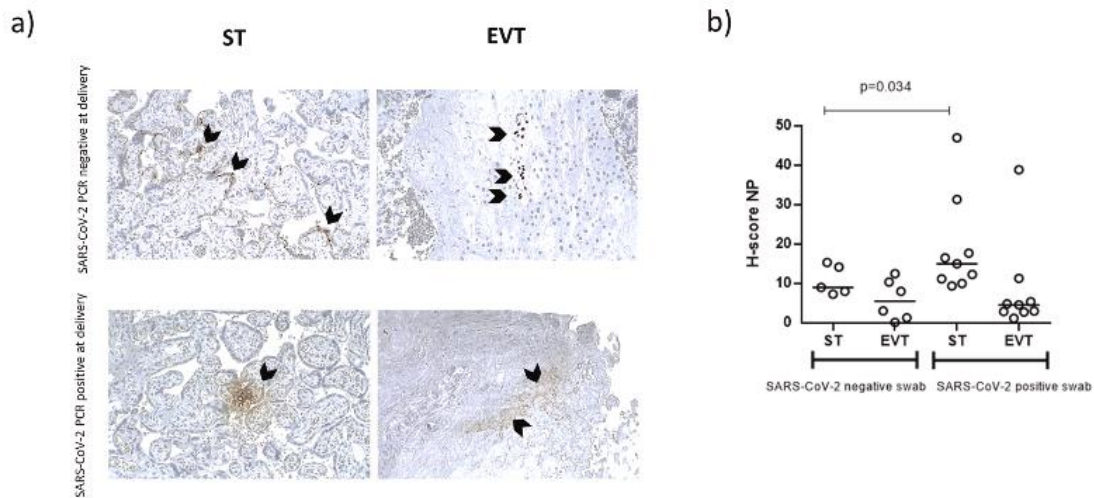


Fig. 1. a) Immunohistochemical staining for SARS-CoV-2 Nucleocapsid protein (NP) of the placenta tissues from SARS-CoV-2 PCR positive at delivery group (SARS-CoV-2 positive swab) or SARS-CoV-2 PCR negative at delivery group (SARS-CoV-2 negative swab). Magnifications are 10×. ST: syncytiotrophoblast; EVT: extra-villous trophoblast. b) H-score values. p values were obtained by Mann-Whitney test.

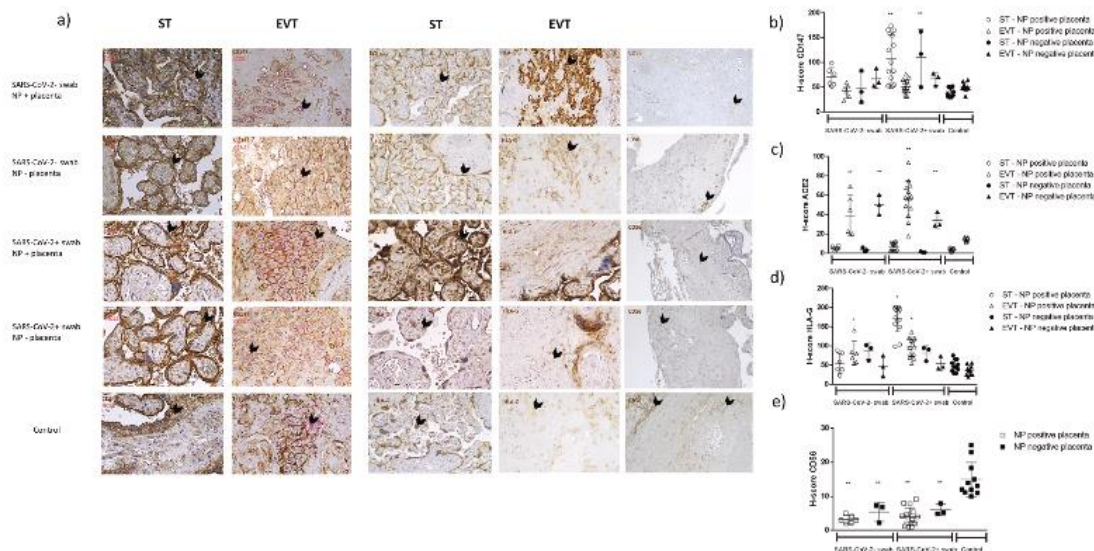


Fig. 2. a) Immunohistochemical staining for CD147, ACE2, HLA-G and CD56 of the placenta tissues from SARS-CoV-2 PCR positive at delivery group (SARS-CoV-2+ swab) or SARS-CoV-2 PCR negative at delivery group (SARS-CoV-2- swab), both with (NP + placenta) or without (NP - placenta) positive staining for SARS-CoV-2 Nucleocapsid protein (NP) in placenta tissues, and SARS-CoV-2 negative swab during pregnancy and at delivery group (control). Magnifications are 10×. ST: syncytiotrophoblast; EVT: extra-villous trophoblast. b) H-score values. p values were obtained by Mann-Whitney test.

immune cells, that account mainly to decidual NK (dNK) cells. We observed the presence of CD56 positive immune cells in the endometrial tissues (Fig. 2a; e). All the placenta samples of SARS-CoV-2 PCR positive and negative at delivery groups showed a significant decrease in CD56 positive cells compared to controls (Fig. 2e; $p < 0.001$; Mann Whitney *U* test).

4. Discussion

The immune system is modified during pregnancy to protect the growth of a semi-allogeneic fetus in the body of the pregnant woman, resulting in a peculiar immune response to microbial infections during pregnancy [24]. SARS-CoV-2 infection modifies the immune response of the host, mainly in those subjects affected by a severe disease [22,30].

The immune deregulation involves an increase in blood leukocytes (leukocytosis), decrease in lymphocytes (lymphopenia) and an increase in neutrophil-to-lymphocyte ratio (NLR).

Recent studies reported the presence of SARS-CoV-2 mRNA or virions in ST [29]. Whilst the possibility of vertical transmission of SARS-CoV-2 from pregnant woman to fetus during pregnancy is suggested, the role of the placenta in infection with the virus has not yet been fully understood. We evaluated the placental SARS-CoV-2 infection and the potential effect on protein expression as ACE2, CD147, HLA-G and CD56, as a marker of CD56 expressing immune cells (mainly NK cells, but also alpha beta T cells, gamma delta T cells, dendritic cells, and monocytes) [31], in placental tissues from pregnant women, positive or negative for SARS-CoV-2 infection at delivery.

We observed a higher percentage of SARS-CoV-2 positive placenta

samples in SARS-CoV-2 PCR positive at delivery group in comparison with SARS-CoV-2 PCR negative at delivery group. The localization of SARS-CoV-2 positivity in placenta samples was mainly in ST of SARS-CoV-2 PCR positive at delivery group and in EVT of SARS-CoV-2 PCR negative at delivery group. CD147 and HLA-G positivity was higher in SARS-CoV-2 PCR positive at delivery group and mainly localized in ST. These results support previous observations on the presence of CD147 as protein complexes on the plasma membrane of primary human ST, suggesting a role of CD147 in trophoblast function [32], and a role for HLA-G molecules as immune escape mechanism of the virus. HLA-G expression is normally reduced during delivery. The increase in SARS-CoV-2 infected tissues sustains a possible induction by SARS-CoV-2 infection, as reported in other tissues [19–21].

ACE2 staining was evidenced in EVT of all the placental samples, with a diffused expression in SARS-CoV-2 negative placenta, and a membrane-associated staining in SARS-CoV-2 positive placenta. These results agree with previous data on the prevalent localization of ACE2 in the physiologic interface between pregnant woman and fetus, rather than in other placental villous cells [33]. The increased ACE2 membrane expression suggests a possible re-localization of ACE2 at the cell membrane after the internalization during SARS-CoV-2 infections via a clathrin-mediated endocytosis [34], in which ACE2 is recycled back to the cell surface and the virus is further replicated in the cell. However, this study has several limitations: i) the cohort was enrolled two years ago; ii) all the subjects were infected with wild type SARS-CoV-2 strain; iii) no subjects were vaccinated. It would be important to analyze a larger cohort, infected with different SARS-CoV-2 strains and with or without a protocol of vaccination. The confirmation of our results would clarify the effect of SARS-CoV-2 infection in placenta tissues. Interestingly, placenta samples delivered from SARS-CoV-2 positive subjects showed a decreased expression of two trophoblast genes (PSG3, with immunoregulatory and angiogenic functions and CGB3, essential for pregnancy maintenance) and increased expression of three immune genes (CXCL10, pro-inflammatory chemokine secreted in response to interferon gamma, TLR3 and DDX58, involved in recognizing double-stranded RNA) [35]. These data support our data and the role of SARS-CoV-2 infection in modifying immune and trophoblast gene expression [35].

We observed a decrease in CD56 expressing immune cells. The expression of CD56 is most stringently associated with, but certainly not limited to, NK cells, where upon activation, CD56dim NK cells can adopt a CD56bright-like immunophenotype or upregulate their CD56 expression in general [36]. Endometrial NK cells are CD56bright NK cells, that act as cytokine producing cells, that control embryo implantation and placentation. Numerical and functional deficiencies and phenotypic alterations of CD56 positive immune cells might modify the placental homeostasis during SARS-CoV-2 infection, with possible clinical implications.

In conclusion, these results confirm the ability of SARS-CoV-2 to infect placenta tissues, as previously reported [37,38]. The simultaneous swab SARS-CoV-2 positivity at delivery and the NP positivity of the placenta tissue seems to create a peculiar environment that modifies the expression of specific molecules, as SARS-CoV-2 infection related molecules (ACE2, CD147), immune regulators (HLA-G) and immune cells (CD56). There is a clear modification in the immune environment, with an increase in the immune-tolerogenic molecule HLA-G, that can act as immune-escape mechanism for SARS-CoV-2, and a decrease in CD56 expressing immune cells, suggesting that SARS-CoV-2 infection might influence the expression of CD56 and consequently cell behavior. The decrease in CD56 expression induces a cytotoxic phenotype, that might alter the immune tolerogenic status at the fetal-maternal interface.

These results sustain the need of further studies to determine whether such changes in the immune system result in higher susceptibility or are protective against SARS-CoV-2 infection during pregnancy.

Funding

This work was supported by Crowdfunding grant of the University of Ferrara.

Author contributions

Giovanna Schiuma, Daria Bortolotti, Pantaleo Greco, Angelina Passaro, Roberta Rizzo: conceived and designed the analysis; Giovanna Schiuma, Silvia Beltrami, Daria Bortolotti, Roberta Rizzo: wrote the paper; Erica Santi, Gennaro Scutiero, Juana Maria Sanz, Chiara Marina Semprini: collected the samples and data; Ines Zidi: contributed data or analysis tools; Mercedes Fernandez, Sabrina Rizzo, Silvia Beltrami, Roberta Gafà: performed the analysis.

Declaration of competing interest

None of the authors declared any conflict of interest.

Acknowledgements

We thank Iva Pivanti for the technical support.

References

- [1] M. Galan, F. Jimenez-Altayo, Small resistance artery disease and ACE2 in hypertension: a new paradigm in the context of COVID-19, *Front Cardiovasc Med* 7 (2020), 588692, <https://doi.org/10.3389/fcvm.2020.588692>.
- [2] L. Meng-Yuan, L. Lin, Y. Zhang, W. Xiao-Sheng, Expression of the SARS-CoV-2 cell receptor gene ACE2 in a wide variety of human tissues, *Infect Dis Poverty* 28 (1) (2020) 45, <https://doi.org/10.1186/s40249-020-00662-x.3>, 9.
- [3] S. Senapati, P. Banerjee, S. Bhagavatlou, P.P. Kushwaha, S. Kumar, Contributions of human ACE2 and TMPRSS2 in determining host-pathogen interaction of COVID-19, *J. Genet.* 100 (2021) 12, <https://doi.org/10.1007/s12041-021-01262-w>.
- [4] Y. Ouyang, T. Bagalkot, W. Fitzgerald, E. Sadovsky, T. Chu, A. Martínez-Marchal, M. Brieno-Enriquez, E.J. Su, L. Margolis, A. Sorkin, Y. Sadovsky, Term human placental trophoblasts express SARS-CoV-2 entry factors ACE2, TMPRSS2, and furin, *mSphere* 6 (2021), <https://doi.org/10.1128/mSphere.00250-21> e00250-21.
- [5] R. Pique-Regi, R. Romero, A.L. Tarca, E.D. Sandler, Y. Xu, V. Garcia-Flores, Y. Leng, F. Luca, S.S. Hassan, N. Gomez-Lopez, Single cell transcriptional signatures of the human placenta in term and preterm parturition, *Elife* 8 (2019), <https://doi.org/10.7554/eLife.52004>.
- [6] R. Pique-Regi, R. Romero, A.L. Tarca, F. Luca, Y. Xu, A. Alazizi, Y. Leng, C.D. Hsu, N. Gomez-Lopez, Does the human placenta express the canonical cell entry mediators for SARS-CoV-2? *Elife* 9 (2020), e58716 <https://doi.org/10.7554/eLife.58716>.
- [7] D.E. Gordon, G.M. Jang, M. Bouhaddou, J. Xu, K. Obernier, K.M. White, M. J. O'Meara, V.V. Rezelj, J.Z. Guo, D.L. Swaney, et al., A SARS-CoV-2-human protein-protein interaction map reveals drug targets and potential drug-repurposing, *bioRxiv* 583 (2020) 459–568.
- [8] L.M. Portela, S.A. Santos, F.B. Constantino, A.C. Camargo, K.T. Colombelli, M. N. Fioretto, C.N. Barquilha, L.L. Périco, C.A. Hiruma-Lima, W.R. Scarano, et al., Increased oxidative stress and cancer biomarkers in the ventral prostate of older rats submitted to maternal malnutrition, *Mol. Cell. Endocrinol.* 523 (2021), 111148, <https://doi.org/10.1016/j.mce.2020.111148>.
- [9] Y. Li, Z. Zhang, L. Yang, X. Lian, Y. Xie, S. Li, S. Xin, P. Cao, J. Lu, The MERS-CoV receptor DPP4 as a candidate binding target of the SARS-CoV-2 spike, *iScience* 23 (2020) 6 101160, <https://doi.org/10.1016/j.isci.2020.101160>.
- [10] V. Yurchenko, S. Constant, M. Bukrinsky, Dealing with the family: CD147 interactions with cyclophilins, *Immunology* 117 (2006) 301–309, <https://doi.org/10.1111/j.1365-2567.2005.02316.x>.
- [11] L. Jia, L. Yufeng, L. Qian, Y. Qun, W. Xi, Z. Huanyu, C. Rong, R. Liang, M. Juan, D. Fei, Y. Bing, L. Liang, H. Zhihong, W. Manli, Z. Yiwu, SARS-CoV-2 cell tropism and multiorgan infection, *Cell Discovery* 7 (2021) 17, <https://doi.org/10.1038/s41421-021-00249-2>.
- [12] L. Dong, S. Pei, Q. Ren, S. Fu, L. Yu, H. Chen, X. Chen, M. Yin, Evaluation of vertical transmission of SARS-CoV-2 in utero: nine pregnant women and their newborns, *Placenta* 111 (2021) 91–96, <https://doi.org/10.1016/j.placenta.2021.06.007>.
- [13] D. Bortolotti, J. LeMaout, C. Trapella, D. Di Luca, E.D. Carosella, R. Rizzo, Pseudomonas aeruginosa quorum sensing molecule N-(3-Oxododecanoyl)-L-Homoserine-Lactone induces HLA-G expression in human immune cells, *Infect. Immun.* 83 (2015) 3918–3925, <https://doi.org/10.1128/IAI.00803-15>.
- [14] J. LeMaout, K. Zafaranloo, C. Le Danffand, E.D. Carosella, HLA-G up-regulates ILT2, ILT3, ILT4, and KIR2DL4 in antigen presenting cells, NK cells, and T cells, *Faseb. J.* 19 (2005) 662–664, <https://doi.org/10.1096/fj.04-1617fje>.
- [15] E. Eliassen, D. Di Luca, R. Rizzo, I. Barao, The interplay between natural killer cells and human herpesvirus-6, *Viruses* 9 12 (2017) 367, <https://doi.org/10.3390/v9120367>.

- [16] R. Rizzo, D. Bortolotti, S. Bolzani, E. Fainardi, HLA-G molecules in autoimmune diseases and infections, *Front. Immunol.* 5 (2014) 592, <https://doi.org/10.3389/fimmu.2014.00592.eCollection2014>.
- [17] R. Rizzo, M. Stignani, P. Amoudruz, C. Nilsson, L. Melchiorri, O. Baricordi, E. Sverremark-Ekström, Allergic women have reduced sHLA-G plasma levels at delivery, *Am. J. Reprod. Immunol.* 61 (5) (2009) 368–376, <https://doi.org/10.1111/j.1600-0897.2009.00703.x>.
- [18] D. Bortolotti, V. Gentili, E. Santi, C. Taliento, A. Vitagliano, G. Schiuma, S. Beltrami, S. Rizzo, G. Lanza, R. Rizzo, R. Gafà, P. Greco, Late-onset intrauterine growth restriction and HHV-6 infection: a pilot study, *J. Med. Virol.* 93 (11) (2021) 6317–6322, <https://doi.org/10.1002/jmv.27138>.
- [19] R. Rizzo, L.M. Neri, C. Simioni, D. Bortolotti, S. Occhionorelli, G. Zauli, P. Secchiero, C.M. Semprini, I. Laface, J.M. Sanz, G. Lanza, R. Gafà, A. Passaro, SARS-CoV-2 nucleocapsid protein and ultrastructural modifications in small bowel of a 4-week-negative COVID-19 patient, *Clin. Microbiol. Infect.* 27 (6) (2021) 936–937, <https://doi.org/10.1016/j.cmi.2021.01.012>.
- [20] D. Bortolotti, C. Simioni, L.M. Neri, R. Rizzo, C.M. Semprini, S. Occhionorelli, I. Laface, J.M. Sanz, G. Schiuma, S. Rizzo, G. Varano, S. Beltrami, V. Gentili, R. Gafà, A. Passaro, Relevance of VEGF and CD147 in different SARS-CoV-2 positive digestive tracts characterized by thrombotic damage, *FASEB J* 35 12 (2021), e21969, <https://doi.org/10.1096/fj.202100821RRR>.
- [21] L. Traina, M. Mucignat, R. Rizzo, R. Gafà, D. Bortolotti, A. Passaro, P. Zamboni, COVID-19 induced aorto duodenal fistula following evar in the so called "negative" patient, *Vascular* 17 (2021), 17085381211053695, <https://doi.org/10.1177/17085381211053695>.
- [22] D. Bortolotti, V. Gentili, S. Rizzo, A. Rotola, R. Rizzo, SARS-CoV-2 spike 1 protein controls natural killer cell activation via the HLA-E/NG2A pathway, *Cells* 9 (2020), <https://doi.org/10.3390/cells9091975>, 1975.
- [23] E. Caselli, D. Bortolotti, R. Marci, A. Rotola, V. Gentili, I. Soffritti, M. D'Accolti, G. Lo Monte, M. Sicolo, I. Barao, D. Di Luca, R. Rizzo, HHV-6A infection of endometrial epithelial cells induces increased endometrial NK cell-mediated cytotoxicity, *Front. Microbiol.* 8 (2017) 2525, <https://doi.org/10.3389/fmicb.2017.02525.eCollection2017>.
- [24] R. Marci, V. Gentili, D. Bortolotti, G. Lo Monte, E. Caselli, S. Bolzani, A. Rotola, D. Di Luca, R. Rizzo, Presence of HHV-6A in endometrial epithelial cells from women with primary unexplained infertility, *PLoS One* 11 (7) (2016), e0158304, <https://doi.org/10.1371/journal.pone.0158304>.
- [25] R. de Mendonça Vieira, A. Meagher, Á.C. Crespo, S.K. Kshirsagar, V. Iyer, E. R. Norwitz, J.L. Strominger, T. Tilburgs, Human term pregnancy decidual NK cells generate distinct cytotoxic responses, *J. Immunol.* 204 (12) (2020) 3149–3159, <https://doi.org/10.4049/jimmunol.1901435>.
- [26] B. Favier, J. Lemaoult, E. Lesport, E.D. Carosella, ILT2/HLA-G interaction impairs NK-cell functions through the inhibition of the late but not the early events of the NK-cell activating synapse, *Faseb. J.* 3 (2010) 689–699, <https://doi.org/10.1096/fj.09-135194>.
- [27] M. Mirbeyk, A. Saghazadeh, N. Rezaei, A systematic review of pregnant women with COVID-19 and their neonates, *Arch. Gynecol. Obstet.* 1 (2021) 5–38, <https://doi.org/10.1007/s00404-021-06049-z>.
- [28] M.Y. Valdespino-Vázquez, C.A. Helguera-Repetto, M. León-Juárez, O. Villavicencio-Carrisoza, A. Flores-Pliego, E.R. Moreno-Verduzco, D.L. Díaz-Pérez, I. Villegas-Mota, et al., Fetal and placental infection with SARS-CoV-2 in early pregnancy, *J. Med. Virol.* 93 (7) (2021) 4480–4487, <https://doi.org/10.1002/jmv.26965>.
- [29] L.B. Argueta, L.A. Lacko, Y. Bram, T. Tada, L. Carrau, A. Figueiredo Rendeiro, T. Zhang, et al., Inflammatory responses in the placenta upon SARS-CoV-2 infection late in pregnancy, *iScience* 25 (5) (2022), 104223, <https://doi.org/10.1016/j.isci.2022.104223>.
- [30] F. Caccuri, S. Messali, D. Bortolotti, D. Di Silvestre, A. De Palma, C. Cattaneo, A. Bertelli, A. Zani, M. Milanese, M. Giovanetti, G. Campisi, V. Gentili, A. Bugatti, F. Filippini, E. Scaltriti, S. Pongolini, A. Tucci, S. Fiorentini, P. d'Ursi, M. Ciccozzi, P. Mauri, R. Rizzo, A. Caruso, Competition for dominance within replicating quasispecies during prolonged SARS-CoV-2 infection in an immunocompromised host, *Virus Evolution* (2022) veac042, <https://doi.org/10.1093/ve/veac04226>.
- [31] H.H. Van Acker, A. Capsomidis, E.L. Smits, V.F. Van Tendeloo, CD56 in the immune system: more than a marker for cytotoxicity? *Front. Immunol.* 8 (2017) 892, <https://doi.org/10.3389/fimmu.2017.00892.eCollection2017>.
- [32] L. Cheuk-Lun, M.P.Y. Lam, K.K.W. Lam, C.O.N. Leung, R.T.K. Pang, I.K. Chu, T.H. L. Wan, J. Chai, W.S.B. Yeung, P.C.N. Chiu, Identification of CD147 (basigin) as a mediator of trophoblast functions, *Hum. Reprod.* 28 (11) (2013) 2920–2929, <https://doi.org/10.1093/humrep/det355>.
- [33] E. Taglaiera, Y. Benarroch, K. Ropd, E. Barnett, V. Sabharwal, C. Yarrington, E. M. Wachman, Consistent localization of SARS-CoV-2 spike glycoprotein and ACE2 over TMPRSS2 predominance in placental villi of 15 COVID-19 positive maternal-fetal dyads, *Placenta* 100 (2020) 69–74, [10.1016/j.placenta.2020.08.015](https://doi.org/10.1016/j.placenta.2020.08.015).
- [34] A. Bayati, R. Kumar, V. Francis, P.S. McPherson, SARS-CoV-2 infects cells after viral entry via clathrin-mediated endocytosis, *J. Biol. Chem.* 296 (2021), 100306, <https://doi.org/10.1016/j.jbc.2021.100306>.
- [35] C. Lesseur, R.H. Jessel, S. Ohrn, Y. Ma, Q. Li, F. Dekio, et al., Gestational SARS-CoV-2 infection is associated with placental expression of immune and trophoblast genes, *Placenta* 126 (2022) 125–132, <https://doi.org/10.1016/j.placenta.2022.06.017>.
- [36] A. Poli, T. Michel, M. Thérésine, E. Andrès, F. Hentges, J. Zimmer, CD56bright natural killer (NK) cells: an important NK cell subset, *Immunology* 126 (4) (2009) 458–465, <https://doi.org/10.1111/j.1365-2567.2008.03027.x>.
- [37] L. Patané, D. Morotti, M.R. Giunta, C. Sigismondi, M.G. Piccoli, L. Frigerio, et al., Vertical transmission of COVID-19: SARS-CoV-2 RNA on the fetal side of the placenta in pregnancies with COVID-19 positive mothers and neonates at birth, *Am. J. Obstet. Gynecol.* 2 (3) (2020), 100145, <https://doi.org/10.1016/j.ajogmf.2020.100145>.
- [38] G. Algarroba, P. Rekawek, S.A. Vahanian, Visualization of SARS-CoV-2 virus invading the human placenta using electron microscopy, *Am. J. Obstet. Gynecol.* 223 (2) (2020) 275–278, <https://doi.org/10.1016/j.ajog.2020.05.0>.

5.2.2. SARS-CoV-2 and bowel diseases

Nowadays, even more evidences strengthen the correlation of COVID-19 sequelae not only at lung level, but also in presence of SARS-CoV-2 infection in different extrapulmonary sites, such as gastrointestinal tract [110]. SARS-CoV-2 gut infection has been linked to long-COVID status, in which was described the prolonged presence of gastroenteric symptoms in patients who experienced severe COVID-19 [106]. Thus, the enteric system was identified as a putative reservoir of infection, which participates in the viral spread and might play a role in the persistence of SARS-CoV-2 infection, after the resolution of the primary respiratory infection [387].

Basing on numerous evidence on the effect of HLA-G and CD147 expression in SARS-CoV-2 infection, a role for these molecules in SARS-CoV-2-associated bowel disease was speculated [388]. In fact, HLA-G involvement in COVID-19 bowel symptomatology was supported by the finding of its up-regulation in gut samples from severe COVID-19 patients [386], possibly exploiting its immunomodulatory function to improve virus persistence and spread to other body sites.


Interestingly, HLA-G shows also a correlation with CD147 expression at gut level, which involves matrix metalloproteinases-9 (MMP9) and Vascular Endothelial Growth Factor (VEGF) expression [166, 389].

Thus, view the role of both HLA-G and CD147 in vascular homeostasis, a potential implication of these molecules in bowel vascular damages and thrombotic events associated to SARS-CoV-2 infection was suggested.

Basing on these data, we further investigated the mechanisms responsible of bowel vascular injury and thrombotic damages observed in COVID-19 patients ([390], paper attached). Our study confirmed that SARS-CoV-2 gut infection induced a detrimental effect at vascular level, as demonstrated by the elevated VEGF levels found in COVID-19 biopsies [391]. This condition seems to involve the engagement of CD147 by the virus, which correlates with high viral tissue extent and leads to vascular damage and thrombosis, modulating HLA-G shedding via MMP-9 ([390], paper attached).

RESEARCH ARTICLE

Relevance of VEGF and CD147 in different SARS-CoV-2 positive digestive tracts characterized by thrombotic damage

Daria Bortolotti¹ | Carolina Simioni^{2,3} | Luca Maria Neri^{3,4} | Roberta Rizzo¹ | Chiara Marina Semprini^{4,5} | Savino Occhionorelli^{4,6} | Iliara Laface⁴ | Juana Maria Sanz¹ | Giovanna Schiuma¹ | Sabrina Rizzo¹ | Gabriele Varano⁴ | Silvia Beltrami¹ | Valentina Gentili¹ | Roberta Gafà^{4,7} | Angelina Passaro^{4,5} 

¹Department of Chemical and Pharmaceutical Sciences, University of Ferrara, Ferrara, Italy

²Department of Life Sciences and Biotechnology, University of Ferrara, Ferrara, Italy

³Laboratory for Technologies of Advanced Therapies (LTTA)-Electron Microscopy Center, University of Ferrara, Ferrara, Italy

⁴Department of Translational Medicine, University of Ferrara, Ferrara, Italy

⁵Medical Department, University Hospital of Ferrara Arcispedale Sant'Anna, Ferrara, Italy

⁶Surgery Department, University Hospital of Ferrara Arcispedale Sant'Anna, Ferrara, Italy

⁷Oncological and Medical Department, University Hospital of Ferrara Arcispedale Sant'Anna, Ferrara, Italy

Correspondence

Angelina Passaro, Department of Translational Medicine, University of Ferrara, Via Luigi Borsari, 46 - 44121 Ferrara, Italy.
Email: angelina.passaro@unife.it

Roberta Rizzo, Department of Chemical and Pharmaceutical Sciences, University of Ferrara, Via Luigi Borsari, 46 - 44121, Ferrara, Italy.
Email: roberta.rizzo@unife.it

Funding information

This study was supported by COVID-19 grant from the University of Ferrara (PI: Roberta Rizzo and Angelina Passaro) and by crowdfunding campaign from University of Ferrara (PI Daria Bortolotti).

Abstract

Several evidence suggests that, in addition to the respiratory tract, also the gastrointestinal tract is a main site of severe acute respiratory syndrome CoronaVirus 2 (SARS-CoV-2) infection, as an example of a multi-organ vascular damage, likely associated with poor prognosis. To assess mechanisms SARS-CoV-2 responsible of tissue infection and vascular injury, correlating with thrombotic damage, specimens of the digestive tract positive for SARS-CoV-2 nucleocapsid protein were analyzed deriving from three patients, negative to naso-oro-pharyngeal swab for SARS-CoV-2. These COVID-19-negative patients came to clinical observation due to urgent abdominal surgery that removed different sections of the digestive tract after thrombotic events. Immunohistochemical for the expression of SARS-CoV-2 combined with a panel of SARS-CoV-2 related proteins

Abbreviations: ac, adsorption cells; ACE2, angiotensin-converting enzyme 2; acm, apical cell membrane; CD147, cluster of differentiation 147; COVID-19, coronavirus disease 2019; csg, cytoplasmic secretory granules; e, erythrocytes; gc, glycocalyx; GCs, goblet cells; HLA-E, human leukocyte antigen-E; HLA-G, human leukocyte antigen-G; HLA-I, human leukocyte antigen class-I; IHC, immunohistochemical; MMP-9, matrix metalloproteinase-9; NP, nucleocapsid protein; SARS-CoV-2, severe acute respiratory syndrome CoronaVirus 2; SP, spike protein; TEM, transmission electron microscopy; VEGF, vascular endothelial growth factor.

Daria Bortolotti and Carolina Simioni contributed equally to this article and both should be considered first author.

Luca Maria Neri and Roberta Rizzo contributed equally to this article and both should be considered second author.

Roberta Gafà and Angelina Passaro contributed equally to this article and both should be considered senior author.

This is an open access article under the terms of the Creative Commons Attribution-NonCommercial License, which permits use, distribution and reproduction in any medium, provided the original work is properly cited and is not used for commercial purposes.

© 2021 The Authors. *The FASEB Journal* published by Wiley Periodicals LLC on behalf of Federation of American Societies for Experimental Biology.

angiotensin-converting enzyme 2 receptor, cluster of differentiation 147 (CD147), human leukocyte antigen-G (HLA-G), vascular endothelial growth factor (VEGF) and matrix metalloproteinase-9 was performed. Tissue samples were also evaluated by electron microscopy for ultrastructural virus localization and cell characterization. The damage of the tissue was assessed by ultrastructural analysis. It has been observed that CD147 expression levels correlate with SARS-CoV-2 infection extent, vascular damage and an increased expression of VEGF and thrombosis. The confirmation of CD147 co-localization with SARS-CoV-2 Spike protein binding on gastrointestinal tissues and the reduction of the infection level in intestinal epithelial cells after CD147 neutralization, suggest CD147 as a possible key factor for viral susceptibility of gastrointestinal tissue. The presence of SARS-CoV-2 infection of gastrointestinal tissue might be consequently implicated in abdominal thrombosis, where VEGF might mediate the vascular damage.

KEYWORDS

CD147, digestive tract, inflammation, SARS-CoV-2, thrombosis

1 | INTRODUCTION

Symptomatic coronavirus disease 2019 (COVID-19) patients have been commonly identified as individuals who developed signs and symptoms suggestive of COVID-19. Even if epidemiology and virological studies suggest that virus transmission from an infected person mainly occur from respiratory tract through direct droplet and aerosol transmission,¹ also respiratory asymptomatic infections play an important role in infection spread and clinical outcome.²

As already reported,³ evidences suggest that severe acute respiratory syndrome CoronaVirus 2 (SARS-CoV-2) may replicate inside various cell types and tissues besides the lung, including the gastrointestinal tract, suggesting intestine as a main site of SARS-CoV-2 infection.³

The ability of SARS-CoV-2 to infect a broad spectrum of tissues could be imputed to the diffuse tissue expression of SARS-CoV-2 cellular receptor angiotensin-converting enzyme 2 (ACE2),⁴ which regulates blood pressure, fluids, electrolyte balance and systemic vascular resistance.^{4,5}

ACE2 was established as the functional host receptor for SARS-CoV-2,⁶ and its presence could confer susceptibility to host cell entry of the virus.

Besides ACE2, other molecules seem to participate in SARS-CoV-2 infection,⁷ including several molecules that might be involved in SARS-CoV-2 cell susceptibility, such as Neuropilin 1 and cluster of differentiation 147 (CD147), cyclophilin A, reported to be associated with enhanced viral infection.⁸⁻¹²

CD147 is expressed in a wide range of tissues, including lungs and intestinal vascular endothelium,¹³ where it plays a role in the control of intestinal inflammation.¹⁴ CD147 expression is increased during pathological conditions in the lung,

bowel tissues,¹³ and during stroke.¹⁵ Recent studies described a possible interaction between CD147 binding site and SARS-CoV-2 spike protein (SP) receptor-binding domain by electrostatic interactions involving the residues Arg403, Asn481, and Gly502.¹⁶ The treatment with Meplazumab, an anti-CD147 humanized antibody, is able to inhibit SARS-CoV-2 infection.⁸ Again, Fenizia et al., have reported that CD147 binding to cyclophilin A does not play a role in SARS-CoV-2 entry, but CD147 regulates ACE2 levels and both receptors are affected by virus infection, supporting a possible CD147 involvement in SARS-CoV-2 infection.¹⁷ Anyway, controversial results were reported with no evidence for a direct SARS-CoV-2 spike binding for CD147.¹⁸ This is suggestive of a possible role of CD147 as a susceptibility factor for SARS-CoV-2 infection that might cooperate with SARS-CoV-2 specific receptors. In particular, CD147 expression has been reported on vascular endothelium in the absence of ACE2, underlying the potential implication of this molecules in vascular damages due to SARS-CoV-2 infection, independently from ACE2 presence.¹⁹

In this view, the engagement of both ACE2 and CD147 by SARS-CoV-2 may explain the vascular damage and thrombosis associated to excessive inflammation observed in COVID-19 patients.²⁰ The detrimental effect of SARS-CoV-2 infection at vascular level is also confirmed by the elevated vascular endothelial growth factor (VEGF) levels found in COVID-19 patients.²¹

Despite SARS-CoV-2 infection triggers to cytokine-storm process in COVID-19 patients,²² the host immune system could not efficiently counteract the infection.²³ It is known that viruses may induce the expression of immunomodulatory non-classical human leukocyte antigen class-I molecules,²⁴ such as human leukocyte antigen-E²⁵ and human leukocyte antigen-G (HLA-G).²⁶ HLA-G controls the immune

system activation by interacting with specific inhibitory receptors expressed on immune cells.²⁷ HLA-G immunomodulatory function is exploited by viruses as an immune-escape mechanism,^{28,29} and has recently reported in SARS-CoV-2 gastroenteric infection,³ suggesting a role of HLA-G in gastrointestinal pathogenetic mechanisms in COVID-19.

Another regulator of the COVID-19 inflammatory process is represented by matrix metalloproteinases-9 (MMP-9), which is considered an early indicator of respiratory failure³⁰ and has been also reported as involved in the modulation of inflammation in intestinal pathological conditions.³¹ Moreover, MMPs are known to be involved in HLA-G cleavage³² and, in particular, MMP-9 is known to be upregulated in lung macrophages via CD147,^{15,33,34} together with VEGF increase in bowel disease.

In this study, the presence of SARS-CoV-2 infection was investigated in digestive tract tissues specimens obtained from three SARS-CoV-2 tested negative patients that underwent abdominal surgery for acute abdominal symptoms and that presented a clinical history very suspicious for COVID-19 infection. Tissues were evaluated for the expression of SARS-CoV-2 nucleocapsid protein (NP), ACE2, CD147, HLA-G, VEGF, and MMP-9. Moreover, transmission electron microscopy (TEM) analyses were performed in order to characterize morpho-functional alterations.

2 | MATERIAL AND METHODS

The study adheres to the ethical principles for medical research involving human subjects as required by the 2013 revision of the Declaration of Helsinki—WMA Declaration of Helsinki—Ethical Principles for Medical Research Involving Human Subjects.

The study was structured in accordance with the STROBE guidelines for observational studies and STROME-ID for reporting of molecular epidemiology for infectious diseases. It was evaluated by the Ethics Committee of the Area Vasta Emilia Centro della Regione Emilia-Romagna (CE-AVEC) with the number 122/2021/Oss/AOUFe.

2.1 | Patients

Three patients (1 female and 2 male) aged 64–76 presenting with acute abdominal symptoms were respectively submitted to ileum and gallbladder surgical resection (patient 1), sigmoidectomy (patient 2), and duodenal-jejunum tract resection (patient 3) at the Department of Surgical Emergencies at the University Hospital of Ferrara (Italy). On admission, patients did not show any usual clinical signs of COVID-19. Patient clinical characteristics are reported in Table 1.

During hospitalization, patients performed multiple times oro/naso-pharyngeal swabs resulting always negative for SARS-CoV-2. All the surgical specimens were collected and routinely processed at the Pathology Lab.

2.2 | Immunohistochemical analysis

Immunohistochemical (IHC) analysis was performed on the collected samples for detection of SARS-CoV-2 NP (NB100-56576, Novus Biologicals, Centennial, 1:250 dilution), HLA-G antibody (MEM-G2, Exbio, dilution 1:400), CD147 (clone MEM-M6/1, dilution 1:100, Novus Biologicals), ACE2 (clone EPR4435-2, 1:250 dilution, Abcam), VEGF-A (VG-1, 5 µg/ml concentration, Abcam), MMP9 (clone EP1254, 1:1000 dilution, Abcam). Slides were counterstained with H-E. Specificity for SARS-CoV-2 staining was investigated performing SARS-CoV-2 NP IHC analysis on samples obtained from a non COVID-19 patient, as described previously³ (Figure S1).

2.3 | Evaluation of SARS-CoV-2 SP binding and CD147 expression on bowel tissues

SARS-CoV-2 SP binding and CD147 expression was evaluated on bowel samples from non-COVID-19 patients by IHC analysis.^{35,36} Briefly, tissue slides were incubated with trimeric full-length SARS-CoV-2 SP (1 µg/ml, AcroBiosystems) for 1 h at RT, in order to allow protein-receptor binding, and then incubated with SARS-CoV-2 SP antibody (dilution 1:400, SinoBiological) for detection. The same experiment was performed also adding CD147 antibody (clone MEM-M6/1, dilution 1:100, Novus Biologicals), following the ImmPRESS Duet Double Staining Polymer Kit (Vector Laboratories) protocol to visualize SARS-CoV-2 SP and CD147 co-localization.

2.4 | Cell lines

Human colorectal adenocarcinoma Caco-2 cell line (ATCC HTB-37) was grown in EMEM medium with 1% L-glutamine, 1% Penicillin/Streptomycin and 20% FBS. Vero E6 cells (ATCC CRL-1586) were grown in EMEM medium with 1% L-glutamine, 1% Penicillin/Streptomycin, and 10% FBS.

2.5 | SARS-CoV-2 infection and viral RNA detection

SARS-CoV-2, a kind gift of Professor Arnaldo Caruso from University of Brescia, was isolated from a nasopharyngeal

TABLE 1 Patient's clinical characterization

Patients	Sex, age	Relevant clinical features	Symptoms ad admission	Biological parameters
Patient 1	F, 76	Hypercholesterolemia, heavy smoker, mastectomy for breast cancer 30 years previously No chronic therapy	Abdominal pain and vomiting Abdominal CT showed on an atherosclerotic plaque in proximity of the celiac trunk, abdominal fluid accumulation and distended, radiologically heterogeneous, gallbladder (no gallstones), surrounded by fluid She died at home 4 months later	White blood cells $15.76 \times 10^3/\mu\text{l}$, lactate dehydrogenase 293 U/L
Patient 2	F, 64	None No chronic therapy	Severe abdominal pain	Hemoglobin 8.6 g/dl, white blood cells $1.20 \times 10^3/\mu\text{l}$, D-dimer 4.4 $\mu\text{g/ml}$, C-reactive protein 32 mg/dl, Troponin I 448 ng/L, B-type natriuretic peptide 230 pg/ml
Patient 3	M, 79	Coronary heart disease and dilated ventricular apex Treated with warfarin	Abdominal pain and high fever	Hemoglobin 8.6 g/dl, White blood cells $1.40 \times 10^3/\mu\text{l}$, Procalcitonin 79 ng/ml, C-reactive protein 25 mg/dl, Prothrombin time 4.16 s, D-dimer 3.38 $\mu\text{g/ml}$

swab retrieved from a patient with COVID-19 (Caucasian man of Italian origin, genome sequences available at GenBank - SARS-CoV-2-UNIBS-AP66: ERR4145453).³⁷ This SARS-CoV-2 isolate clustered in the B1 clade which includes most of the Italian sequences, together with sequences derived from other European countries and United States. The identity of the strain was verified in Vero E6 cells using real-time polymerase chain reaction (PCR) and metagenomic sequencing, from which the reads were mapped to nCoV-2019 (genomic data are available at EBI under study accession no. PRJEB38101). We propagated the clinical isolate in Vero E6 cells and determined the viral titer using a standard plaque assay. Caco-2 cells were infected with a multiplicity of infection (MOI) of 0.05 for 1 h at 37°C. RNA extraction was performed 24 h post infection (hpi) as described previously²⁵ by using MagMAX Viral/Pathigen Nuclei Acid Isolation kit (ThermoFisher, Italy) according to the manufacturer's instructions. SARS-CoV-2 titration by RealTime-PCR was performed with the TaqMan 2019nCoV assay kit v1 (ThermoFisher, Italy).

2.6 | ACE2 and CD147 blocking assay

ACE2 and CD147 blocking was performed in Caco-2 cells using the specific neutralizing antibodies Anti-ACE2 (human) mAb blocking (AC384) (AdipoGen; USA) and

the CD147 Monoclonal Antibody (RL73), Functional Grade (eBioscience; USA). Briefly, Caco-2 cells were incubated with the neutralizing antibodies (alone or in combination) at the concentration of 0.5 $\mu\text{g/ml}$ for 1 h, before SARS-CoV-2 infection. Then, cells were infected with SARS-CoV-2 inoculum at a MOI of 0.05 and RNA was collected for viral titration, as described above.

2.7 | Transmission electron microscopy

For TEM analysis, samples were fixed in 2.5% glutaraldehyde in 0.1 M phosphate buffer pH 7.4 and post-fixed in 2% osmium tetroxide, dehydrated in acetone solutions and included in Araldite Durcupan ACM (Fluka). Samples were then counterstained with uranyl acetate in saturated solution and lead citrate and observed under transmission electron microscope Zeiss EM910 at 100 kv. Duodenal and colon samples obtained from non-COVID-19 patients were also analyzed to compare the results.

2.8 | Statistical analysis

IHC slide images were analyzed using QuPath software for evaluation of cell percentage positivity and H-Score for each antigen investigated.

An H-score between 0 and 300 was obtained where 300 was equal to 100% of cells strongly stained (3+). Frequencies were analyzed by Chi-square test and H-Score comparisons were evaluated by Student t-test. The statistical analysis was performed by GraphPad Software.

3 | RESULTS

3.1 | Digestive tract showed a differential susceptibility to SARS-CoV-2 infection

The analysis of specimens from gallbladder, ileum, duodenal-jejunum tract, and colon resections evidenced a different distribution of SARS-CoV-2 infection (Figure 1). As showed in Figure 1A–D, the highest presence of SARS-CoV-2 infection was found in gallbladder from patient 1 (Figure 1B) and in colon from patient 2 (Figure 1C). Considering the percentage of positive cells for SARS-CoV-2 NP, there was a significant difference among the four tissues analyzed (Figure 2A), with the highest frequency of positive cells in the gallbladder from patient 1 ($p < .0001$). This trend was confirmed also in terms of the amount of viral presence expressed as H-Score (Figure 2B, $p < .01$ and $p < .001$). Interestingly, considering patients 1, a different distribution between gallbladder and ileum was observed, supporting the evidence of a different susceptibility to SARS-CoV-2 infection of the two tissues (Figures 1A,B and 2A,B).

3.2 | CD147 expression and SARS-CoV-2 gastrointestinal infection

The four specimens were then investigated for the expression of ACE2 and CD147 surface molecules. The IHC analyses (Figure 1E–H) revealed that ACE2 is expressed in all the tissues, except for the colon sample from patient 2 (Figure 1G), as confirmed also by evaluation of positive cell percentage (Figure 2A, $p < .0001$ Chi-square test) and by H-Score (Figure 2C; $p < .05$ and $p < .001$). This result was very controversial, since a consistent presence of infection in the colon sample from patient 2 was reported (Figure 1C). The IHC analysis for CD147 (Figure 1I–L) showed the highest expression in patient 1 gallbladder (Figure 1J), while mild expression in the colon of patient 2 (Figure 1K) and a low expression in ileum of patient 1 and in duodenum of patient 3 (Figure 1I,L) was found respectively, as confirmed by positive cell percentage (Figure 2A, $p < .0001$) and H-Score (Figure 2D; $p < .01$) analysis. The increased expression of CD147 observed in gallbladder from patient 1 (Figure 1J) and in colon from patient 2 (Figure 1K) correlates with the amount of SARS-CoV-2 infection detected in these two samples, suggesting CD147 as crucial in SARS-CoV-2 cell entry at the digestive tract level, despite ACE2 expression. This observation is strengthened by the different expression of CD147 found in ileum and gallbladder samples from patient 1 (Figure 1I,J), in contrast with the comparable expression of ACE2 in the two samples (Figure 1E,F), where a correlation between high

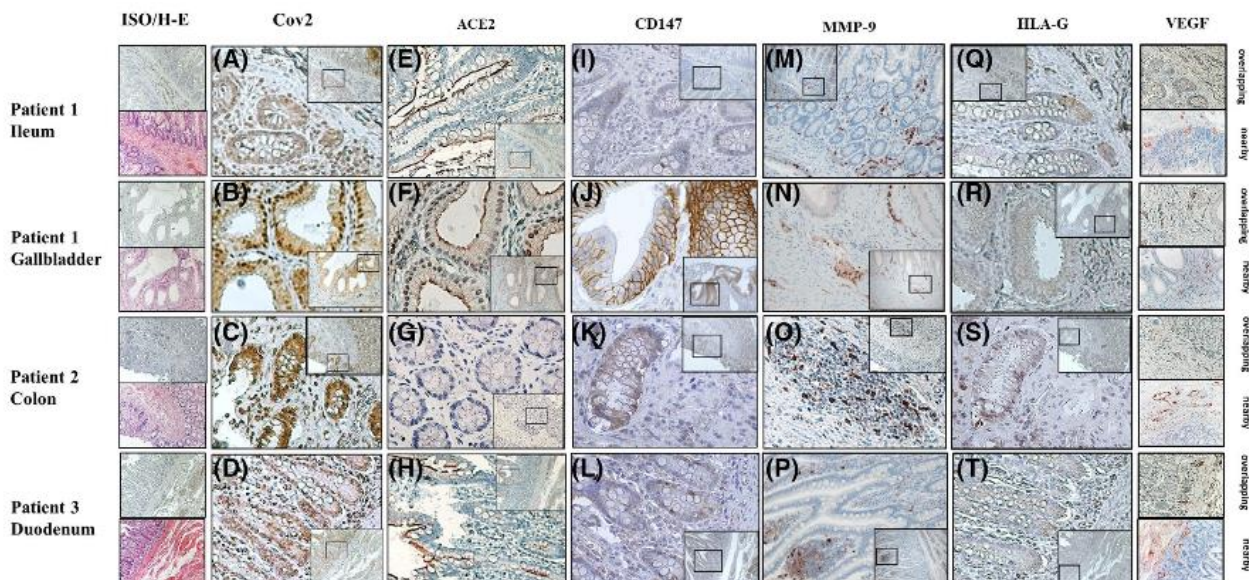


FIGURE 1 Biopsies immunohistochemical analysis. Patient 1 ileum (upper line panels) and gallbladder (second line panels), Patient 2 colon (third line panels) and Patient 3 ileum (bottom panels) were stained for SARS-CoV-2 NP (Cov-2, A–D); ACE2 (E–H), CD147 (I–L), MMP-9 (M–P), HLA-G (Q–T), and for VEGF (right column panels) at site of infection (overlapping) or in an adjacent area (nearby). Samples were also stained with control isotype and with Hematoxylin-Eosin staining (left column panels). Images magnification is 20× or 40×

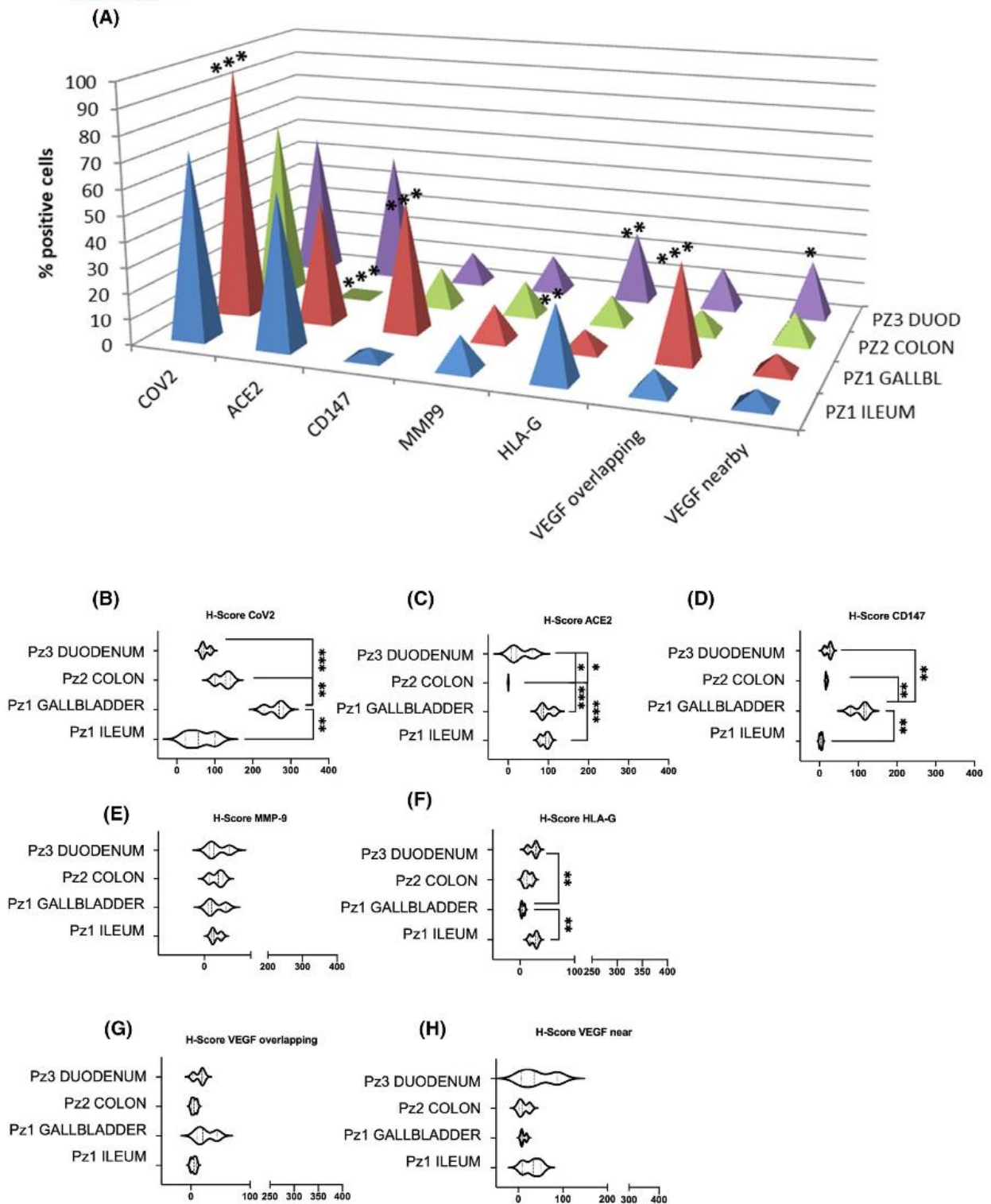


FIGURE 2 Evaluation of sample staining by QuPath software. All the antigens investigated by IHC analysis in tissue biopsies were evaluated by QuPath software for positive cell percentage (A) and for H-Score (B–H) for each antigen (SARS-CoV-2 NP (B), ACE2 (C) CD147 (D), MMP-9 (E), HLA-G (F) VEGF overlapping (G), and nearby (H) the site of infection)

CD147 expression and presence of SARS-CoV-2 has been found in the gallbladder, but not in the ileum.

3.3 | MMP-9 expression during SARS-CoV-2 infection is independent from viral entry

Tissue samples were then stained for MMP-9, which has been described associated to lung function reduction in COVID-19 patients.³⁰ MMP-9 expression was found in all the samples analyzed (Figures 1M–P and 2A,E), with no significant differences. This result suggests that, contrary to what has been observed in the lungs, MMP-9 expression in the digestive tract is not involved in the pathogenic process associated to the virus.

3.4 | SARS-CoV-2 digestive tract infection modulates HLA-G expression and shedding via CD147

HLA-G expression at gut level has been reported to be modulated by SARS-CoV-2 as a mechanism of immune-escape.³

The analysis for the presence of HLA-G in the four tissue samples reported a low-mild expression in patient 1 ileum, patient 2 colon and patient 3 duodenum (Figure 1Q,S,T), while a significant lower HLA-G expression was found in the gallbladder from patient 1 (Figure 1R) in terms of both cell percentage (Figure 2A, $p < .001$) and H-Score (Figure 2F, $p < .01$). Since HLA-G is not normally expressed at the digestive tract level, the reported presence of the molecule seems to confirm its role in SARS-CoV-2 immune-escape. Furthermore, HLA-G expression inversely correlate with CD147, suggesting that the ability of CD147 to also modulate other MMPs than MMP-9³⁸ may contribute to HLA-G membrane shedding.³² Possibly, the high expression of CD147 (Figure 1J) reported in gallbladder, but not in the ileum, from patient 1, could be responsible for the loss of HLA-G observed via CD147/MMPs induction on the gallbladder sample.

3.5 | SARS-CoV-2 digestive tract infection leads to venous thrombotic event via VEGF

In order to evaluate the possible correlation between SARS-CoV-2 infection and abdominal damage associated to thrombosis, all samples were evaluated for VEGF expression in the same areas which SARS-CoV-2 IHC reactivity was demonstrated (Figure 1 overlapping) and also in the adjacent area (Figure 1 nearby). An increased VEGF

expression was found in areas with SARS-CoV-2 presence in patient 1 gallbladder (Figure 1 overlapping), showing statistical significance considering the percentage of positive cells (Figure 2A, $p < .00001$), but not in terms of H-Score (Figure 2G), even if patients 2 gallbladder showed higher score compared with the other samples.

Concerning VEGF expression in the infection adjacent area (Figure 1 nearby), patient 3 duodenum showed the highest percentage of VEGF positive cells (Figures 1 and 2, $p = .0014$) and the highest H-Score (Figure 2H), without reaching significance.

These data suggested a role of the virus in inducing VEGF expression, possibly facilitating the onset of the venous thrombotic event. This is even more evident concerning patient 1 gallbladder, where the expression of VEGF is associated to a notable SARS-CoV-2 presence (Figure 1B).

3.6 | SARS-CoV-2 SP binding-site co-localizes with CD147 expression in gastrointestinal tissues

We evaluated the possible co-localization of SARS-CoV-2 SP binding-site and CD147 expression in bowel tissues of SARS-CoV-2-negative samples.

As shown in Figure 3, SARS-CoV-2 SP is able to bind bowel tissues as gallbladder and ileum in the proximity of sites where CD147 is expressed. The double staining assay showed a co-localization of CD147 and SP proteins, that supports a possible CD147 involvement in viral infection in gastrointestinal tissues.^{16,17}

As a proof of concept, we analyzed the role of CD147 in SARS-CoV-2 infection of epithelial intestinal cells. Caco-2 cell line was infected with SARS-CoV-2, and the viral load was evaluated by quantitative reverse-transcription PCR. We confirmed that Caco-2 cell line is permissive to SARS-CoV-2 infection (Figure 4A). Since Caco-2 cells express both ACE2 and CD147 receptors¹⁴ we blocked both of them to evaluate their role in SARS-CoV-2 infection of epithelial intestinal cells. The blocking of the ACE-2 receptor reduced the viral load (Figure 4B). Interestingly, the blocking of CD147 reduced drastically SARS-CoV-2 infection of Caco-2 cells, similarly to ACE-2/CD147 blocked cells (Figure 4B). These results, in an in vitro setting, suggest a role of CD147 in SARS-CoV-2 infection of epithelial intestinal cells.

3.7 | SARS-CoV-2 infection induces morphological changes in the digestive tract

TEM analysis was performed in order to characterize morpho-functional alterations and differences of the

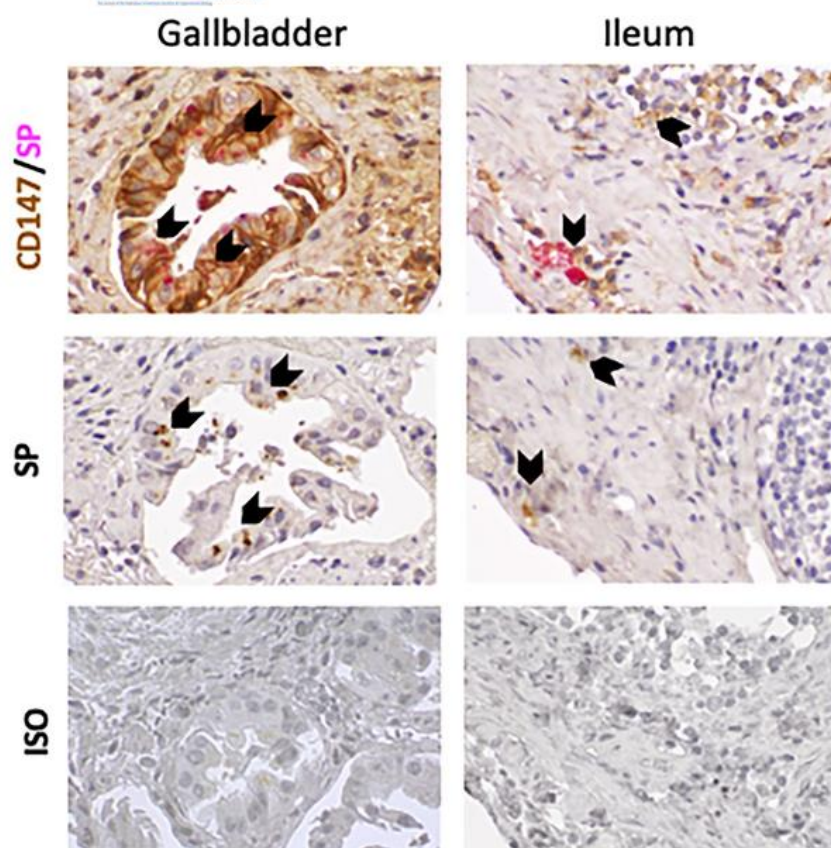


FIGURE 3 Evaluation of SARS-CoV-2 Spike Protein (SP) binding-site and to CD147 co-localization in non-COVID19 bowel samples by IHC analysis. The upper panel reports the double IHC staining for SP (magenta) and CD147 (brown); the middle panel shows the SP (brown) binding to the tissues (ileum and gallbladder); the lower panel represents tissue staining for Isotype control. Black arrows indicate SARS-CoV-2 SP-CD147 co-localization. Magnification 60x

three patient tissues. A significantly different morphological gut microvilli profile was revealed. A colon sample and a duodenal sample from non-COVID-19 patients showed the well organized and aligned microvilli, with a regular distribution protruding from the apical cell membrane (acm) and a homogeneous glycocalyx (gc) (Figure 5A–D). In the colon of patient 2 and in the duodenum of patient 3 microvilli displayed a shorter length than the normal condition, they were severely damaged and, in the colon, a section appears detached from the epithelium (Figure 5E–H). It was not possible to evaluate the morphological state of the ileum of patient 1 as the tissue appeared completely haemorrhagic (data not shown).

Subsequently, for the three patients, the apical region and the lamina propria were also analyzed. Patient 1 ileum presented a high inflammation status and it was not possible to appreciate the morphology of the components of the intestinal epithelium. In particular, in both acquisitions a significant number of erythrocytes (e) can be seen (Figure S2A,B). In patients 2 and 3 samples, cytoplasmic rarefaction accompanied by an overall disintegration of the various cellular components, can generally be observed. In patient 2 colon sample goblet cells can be appreciated, as well as cytoplasmic secretory granules,

adsorption cells, and mucus granules are shown in the duodenum of patient 3 (Figure S2C–F).

4 | DISCUSSION

Concerning COVID-19, the presence of a peculiar intestinal pathological condition has not been reported previously, although the intestinal infarct represents an interstitial pneumonia complication in positive COVID-19 patients.^{39,40}

In this work, digestive tract specimens obtained from three persistently SARS-CoV-2-negative patients that underwent abdominal surgery for acute abdominal symptoms and that presented a clinical history suspicious for COVID-19 infection, were characterized for SARS-CoV-2 presence, specific antigens expression and morphology, with the aim to investigate the possible direct effect of the virus in the onset of intra-abdominal venous thrombotic events.

Our results reported the presence of SARS-CoV-2 infection in all the samples analyzed (Figure 1A–D), with the highest levels found in patient 1 gallbladder and patient 2 colon in term of H-Score (Figure 2B). Interestingly, the comparison between patient 1 ileum and gallbladder

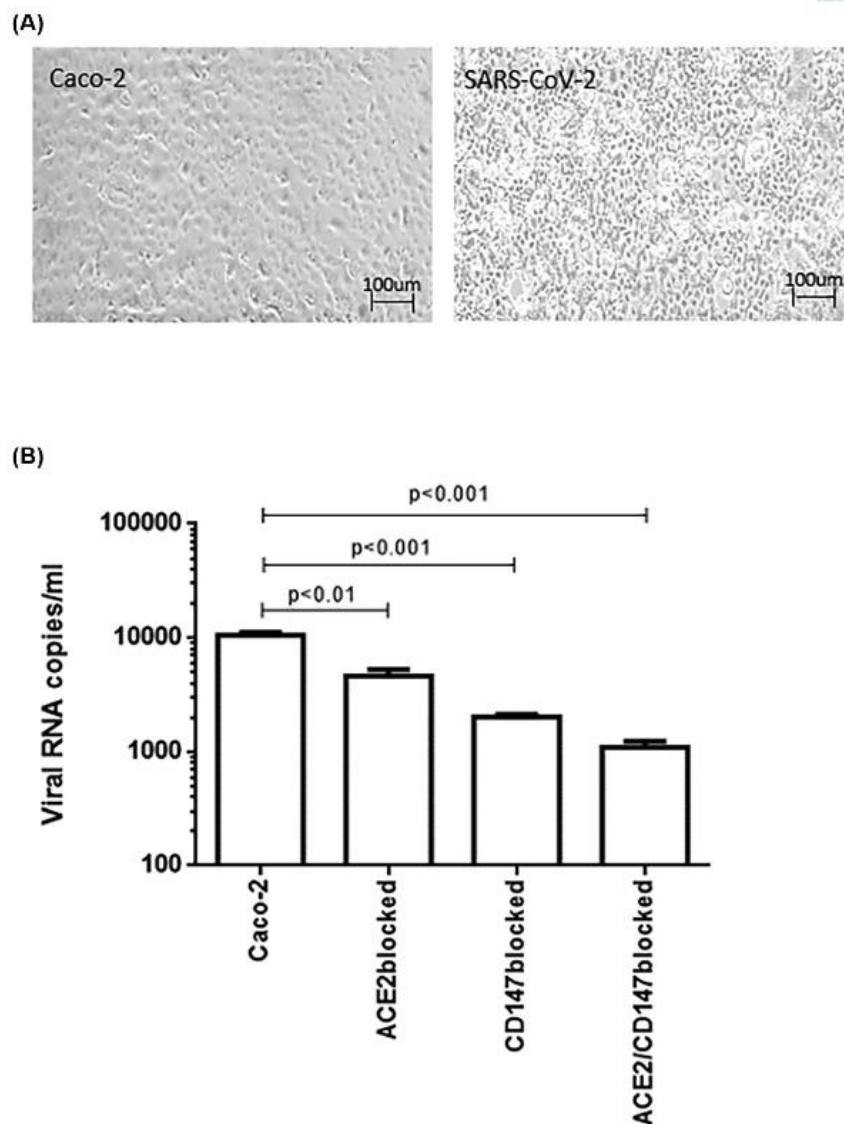


FIGURE 4 In vitro evaluation of SARS-CoV-2 infection of epithelial intestinal cells. (A) Caco-2 cell line was infected with SARS-CoV-2 at a multiplicity of infection (MOI) of 0.05 for 1 h at 37°C. Images of cells were captured with an optical microscope to detect the typical SARS-CoV-2-induced cytopathic effects. (B) Caco-2 cells were pre-treated with anti-ACE2 (ACE2 blocked) or anti-CD147 (CD147 blocked) moAbs and infected with SARS-CoV-2. Viral yield was quantified in the cell supernatant using quantitative reverse-transcription PCR (qRT-PCR). Data are representative of three independent experiments

revealed a different amount of viral infection (Figure 1B), which was significantly higher in gallbladder sample (Figure 2A,B), suggesting a different susceptibility of the two tissues. We evaluated the expression of ACE2 and CD147 surface molecules. ACE2 is the main SARS-CoV-2 receptor, while CD147 is considered a possible susceptibility factor for SARS-CoV-2 infection,¹⁶ expressed during pathological conditions in the lung, bowel tissues¹³ and during stroke.¹⁵

We observed a comparable expression of ACE2 receptor in all tissues (Figure 1E–H), except for patient 2 colon (Figure 1G). On the contrary, there is a differential

expression of the CD147 (Figure 1I–N). CD147 appeared to be highly expressed in patient 1 gallbladder (Figures 1L and 2A,D), where we also observed ACE2 expression. Patient 2 colon sample, despite the absence of ACE2 expression, presented a reliable expression of CD147 (Figure 1M) in the presence of a significant SARS-CoV-2 infection. These data suggest a possible involvement of CD147 in gastrointestinal SARS-CoV-2 infection, that might act in the presence of low levels of ACE2 expression. No significant difference was observed in MMP-9 expression (Figures 1O–R and 2A,E). In fact, despite CD147 induce MMP-9 expression⁴¹ and increased MMP-9 has

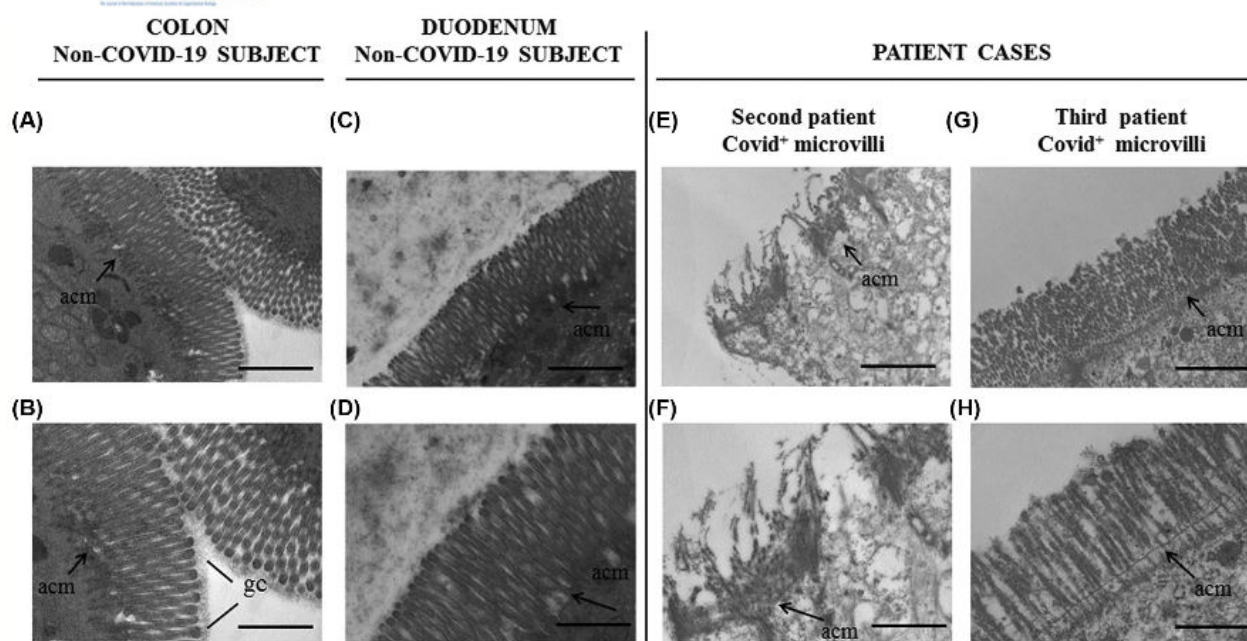


FIGURE 5 Morphology evaluation by TEM analysis. Representative TEM images of the epithelial cell apical surface microvilli of: (A and B): a colon of non-COVID-19 subject; (C and D): a duodenum of non-COVID-19 subject; (E and F): the colon of the second Covid+ patient; (G and H): the duodenum of the third Covid+ patient. Acm, apical cell membrane; gc, glycocalyx. Scale bars correspond to 2 μ m (A,C,E,G) and 1 μ m (B,D,F,H)

been associated to lung failure in COVID-19 patients,³⁰ MMP-9 was not found increased even in the presence of high CD147 expression.

Again, the expression of HLA-G in the presence of SARS-CoV-2 was reported in all the intestinal tissue samples, but not in patient 1 gallbladder sample (Figures 1S–V and 2A,F), where its lack was associated to a high CD147 expression. The modulation of HLA-G by SARS-CoV-2 in the gut as an immunoevasion mechanism has already been described previously³ and is in line with our results.

It could be hypothesized that the absence of HLA-G found in patient 1 gallbladder (Figure 1T) could derive by the shedding of HLA-G due to other MMPs induced by CD147,^{33,34} supporting once again a differential behaviour of viral infection in different tissues, mediated by a peculiar CD147 expression.

Moreover, the analysis of VEGF revealed an increased expression in the areas in which relevant SARS-CoV-2 presence was demonstrated, particularly considering patient 1 gallbladder (Figure 1 overlapping, Figure 2A,G), in association to consistent CD147 expression (Figure 1L). This data suggested that the onset of the thrombotic event during SARS-CoV-2 infection may involve VEGF via CD147, in line with previous data reporting CD147 involvement in VEGF modulation in pathological bowel conditions.¹⁴ Moreover, CD147 expression has been reported on vascular endothelium in the absence of ACE2, underlying the potential implication of this molecules in

the presence of vascular damages due to SARS-CoV-2 infection, independently from ACE2 presence.¹⁹

Our finding on SARS-CoV-2 SP binding-site on bowel tissue that co-localized with CD147 expression (Figure 3) is in line with previous results concerning CD147 engagement during viral infection^{16,17} and supported its role as a susceptibility factor in SARS-CoV-2 bowel infection and ischemia. As a proof of concept, the blocking of CD147 receptor decreased drastically SARS-CoV-2 infection in intestinal epithelial cells (Figure 4B).

Finally, the morphological profile analysis of tissues samples by TEM revealed the presence of microvilli with a significant shorter length, partially deepened beyond the acm and with an irregular gc distribution in patients 2 and 3 COVID-19 tissues, compared to the controls.

In conclusion, this work supported the existence of a peculiar pathogenic process for SARS-CoV-2 infection in the digestive tract of patients without any symptom attributable to typical COVID-19 disease but characterized by abdominal thrombosis. The hypothesis is that, since CD147 can regulate ACE2 levels and both molecules are affected by virus infection,¹⁷ the differential expression of CD147 observed along the digestive tract might determine a different tissue susceptibility to SARS-CoV-2 infection.

In fact, the highest extent of infection was reported in the presence of high CD147 expression, which was in turn associated with high VEGF levels, suggesting a possible role in thrombosis onset in this patient subset. Anyway,

due to the small number of subjects evaluated in this study, these data need to be confirmed in a larger group of samples.

ACKNOWLEDGMENTS

The authors thank Paola Boldrini (LTTA–Electron Microscopy Center, University of Ferrara, Italy), Cristina Bosi (Department of Translational Medicine, University of Ferrara, Italy) and Alessandro Sofia (University of Ferrara) for helpful collaboration.

DISCLOSURES

The authors declare that they have no conflicts of interest.

AUTHOR CONTRIBUTIONS

Daria Bortolotti and Carolina Simioni contributed equally to this article and both should be considered first author. Luca Maria Neri and Roberta Rizzo contributed equally to this article and both should be considered second author. Roberta Gafà and Angelina Passaro contributed equally to this article and both should be considered second author. Daria Bortolotti and Carolina Simioni wrote the first version of the paper. Angelina Passaro, Roberta Rizzo, and Luca Maria Neri also contributed to conception and design of the work. Roberta Rizzo, Luca Maria Neri and Angelina Passaro interpretation of the data and shared the first version of the paper. Carolina Simioni, Ilaria Laface and Gabriele Varano acquired images of biological samples in Transmission Electron Microscopy (TEM) and analyzed these data. Daria Bortolotti and Giovanna Schiuma, Sabrina Rizzo, Silvia Beltrami performed Immunohistochemical (IHC) analysis. Valentina Gentili performed SARS-CoV-2 infection of Caco-2 cell line and viral load quantitation. Savino Occhionorelli performed surgical intervention and specimen collection. Chiara Marina Semprini and Juana Maria Sanz collected biological samples and clinical data. Roberta Gafà performed the histopathological analysis and critically analyzed the images of IHC and TEM. Roberta Rizzo, Luca Maria Neri, Carolina Simioni, Daria Bortolotti, Chiara Marina Semprini, and Roberta Gafà acquired the images for the construction of the figures. Roberta Gafà performed the anatomo-histo-cytopathological diagnosis. All Authors contributed to literature search and revised the manuscript. Angelina Passaro is the corresponding author. She designed the study, coordinated the work of individual researchers or groups, made its own research funds available, assessed the quality of the data, and reviewed the manuscript. All authors approve the final version to be published. They are responsible for all aspects of the work and ensure its accuracy and integrity.

ORCID

Angelina Passaro  <https://orcid.org/0000-0001-8462-7000>

REFERENCES

- Burke RM, Midgley CM, Dratch A, et al. Active monitoring of persons exposed to patients with confirmed COVID-19 - United States, January-February 2020. *MMWR Morb Mortal Wkly Rep.* 2020;69:245-246.
- Loconsole D, Passerini F, Palmieri VO, et al. Recurrence of COVID-19 after recovery: a case report from Italy. *Infection.* 2020;48:965-967.
- Rizzo R, Neri LM, Simioni C, et al. SARS-CoV-2 nucleocapsid protein and ultrastructural modifications in small bowel of a 4-week-negative COVID-19 patient. *Clin Microbiol Infect.* 2021;27:936-937.
- Galan M, Jimenez-Altayo F. Small resistance artery disease and ACE2 in hypertension: a new paradigm in the context of COVID-19. *Front Cardiovasc Med.* 2020;7:588692.
- Yan T, Xiao R, Lin G. Angiotensin-converting enzyme 2 in severe acute respiratory syndrome coronavirus and SARS-CoV-2: a double-edged sword? *FASEB J.* 2020;34:6017-6026.
- Fu J, Zhou B, Zhang L, et al. Expressions and significances of the angiotensin-converting enzyme 2 gene, the receptor of SARS-CoV-2 for COVID-19. *Mol Biol Rep.* 2020;47:4383-4392.
- Evans JP, Liu S-L. Role of host factors in SARS-CoV-2 entry. *J Biol Chem.* 2021;297:100847.
- Wang K, Chen W, Zhang Z, et al. CD147-spike protein is a novel route for SARS-CoV-2 infection to host cells. *Signal Transduct Target Ther.* 2020;5:283.
- Chekol Abebe E, Mengie Ayele T, Tilahun Muche Z, Asmamaw Dejenie T. Neuropilin 1: a novel entry factor for SARS-CoV-2 infection and a potential therapeutic target. *Biol Targets Ther.* 2021;15:143-152.
- Ji K-Y, Kim S-M, Yee S-M, et al. Cyclophilin A is an endogenous ligand for the triggering receptor expressed on myeloid cells-2 (TREM2). *FASEB J.* 2021;35(4):e21479.
- Yurchenko V, Constant S, Eisenmesser E, Bukrinsky M. Cyclophilin-CD147 interactions: a new target for anti-inflammatory therapeutics. *Clin Exp Immunol.* 2010;160:305-317.
- Liu C, von Brunn A, Zhu D. Cyclophilin A and CD147: novel therapeutic targets for the treatment of COVID-19. *Med Drug Discov.* 2020;7:100056.
- Yurchenko V, Constant S, Bukrinsky M. Dealing with the family: CD147 interactions with cyclophilins. *Immunology.* 2006;117:301-309.
- Wang H, Ye J, Liu R, et al. Clinical significance of CD147 in children with inflammatory bowel disease. *Biomed Res Int.* 2020;2020:1-7.
- Jin R, Liu S, Wang M, Zhong W, Li G. Inhibition of CD147 attenuates stroke-associated pneumonia through modulating lung immune response in mice. *Front Neurol.* 2019;10:853.
- Helal MA, Shouman S, Abdelwaly A, et al. Molecular basis of the potential interaction of SARS-CoV-2 spike protein to CD147 in COVID-19 associated-lymphopenia. *J Biomol Struct Dyn.* 2020;26:1-11.
- Fenzia C, Galbiati S, Vanetti C, et al. SARS-CoV-2 entry: at the crossroads of CD147 and ACE2. *Cells.* 2021;10:1434.
- Shilts J, Crozier TWM, Greenwood EJD, Lehner PJ, Wright GJ. No evidence for basigin/CD147 as a direct SARS-CoV-2 spike binding receptor. *Sci Rep.* 2021;11:413.
- Zong J, Li Y, Du D, Liu Y, Yin Y. CD147 induces up-regulation of vascular endothelial growth factor in U937-derived foam

- cells through PI3K/AKT pathway. *Arch Biochem Biophys*. 2016;609:31-38.
20. Pamukçu B. Inflammation and thrombosis in patients with COVID-19: a prothrombotic and inflammatory disease caused by SARS coronavirus-2. *Anatol J Cardiol*. 2020;24:224-234.
 21. Meini S, Giani T, Tascini C. Intussusceptive angiogenesis in Covid-19: hypothesis on the significance and focus on the possible role of FGF2. *Mol Biol Rep*. 2020;47:8301-8304.
 22. Song P, Li W, Xie J, Hou Y, You C. Cytokine storm induced by SARS-CoV-2. *Clin Chim Acta*. 2020;509:280-287.
 23. Song CY, Xu J, He JQ, Lu YQ. Immune dysfunction following COVID-19, especially in severe patients. *Sci Rep*. 2020;10:15838.
 24. Saulle I, Vicentini C, Clerici M, Biasin M. Antigen presentation in SARS-CoV-2 infection: the role of class I HLA and ERAP polymorphisms. *Hum Immunol*. 2021;82:551-560.
 25. Bortolotti D, Gentili V, Rizzo S, Rotola A, Rizzo R. SARS-CoV-2 spike 1 protein controls natural killer cell activation via the HLA-E/NKG2A pathway. *Cells*. 2020;9:1975.
 26. Rizzo R, Bortolotti D, Bolzani S, Fainardi E. HLA-G molecules in autoimmune diseases and infections. *Front Immunol*. 2014;5:592.
 27. LeMaout J, Zafaranloo K, Le Danff C, Carosella ED. HLA-G up-regulates ILT2, ILT3, ILT4, and KIR2DL4 in antigen presenting cells, NK cells, and T cells. *FASEB J*. 2005;19:662-664.
 28. Rizzo R, Di Luca D. Human herpesvirus 6A and 6B and NK cells. *Acta Microbiol Immunol Hung*. 2018;65:119-125.
 29. Bortolotti D, LeMaout J, Trapella C, Di Luca D, Carosella ED, Rizzo R. *Pseudomonas aeruginosa* quorum sensing molecule N-(3-oxododecanoyl)-L-homoserine-lactone induces HLA-G expression in human immune cells. *Infect Immun*. 2015;83:3918-3925.
 30. Ueland T, Holter JC, Holten AR, et al. Distinct and early increase in circulating MMP-9 in COVID-19 patients with respiratory failure. *J Infect*. 2020;81:e41-e43.
 31. Nighot P, Al-Sadi R, Rawat M, Guo S, Watterson DM, Ma T. Matrix metalloproteinase 9-induced increase in intestinal epithelial tight junction permeability contributes to the severity of experimental DSS colitis. *Am J Physiol Liver Physiol*. 2015;309:G988-G997.
 32. Rizzo R, Trentini A, Bortolotti D, et al. Matrix metalloproteinase-2 (MMP-2) generates soluble HLA-G1 by cell surface proteolytic shedding. *Mol Cell Biochem*. 2013;381:243-255.
 33. Jouneau S, Khorasani N, De Souza P, et al. EMMPRIN (CD147) regulation of MMP-9 in bronchial epithelial cells in COPD. *Respirology*. 2011;16:705-712.
 34. Zeng H, Qiu Y, Qu Y, et al. Expression of CD147 in advanced non-small cell lung cancer correlated with cisplatin-based chemotherapy resistance. *Neoplasma*. 2011;58(5):449-454.
 35. Hasegawa K, Kudoh S, Ito T. Somatostatin receptor staining in FFPE sections using a ligand derivative dye as an alternative to immunostaining. *PLoS ONE*. 2017;12:e0172030.
 36. Montet X, Yuan H, Weissleder R, Josephson L. Enzyme-based visualization of receptor-ligand binding in tissues. *Lab Invest*. 2006;86:517-525.
 37. Rizzo S, Savastano MC, Bortolotti D, et al. COVID-19 ocular prophylaxis: the potential role of ozonated-oils in liposome eyedrop gel. *TVST J*. 2021;10(9):7.
 38. Sun J, Hemler MEE. Regulation of MMP-1 and MMP-2 production through CD147/extracellular matrix metalloproteinase inducer interactions. *Cancer Res*. 2001;61:2276-2281.
 39. Keshavarz P, Rafiee F, Kavandi H, Goudarzi S, Heidari F, Gholamrezaezhad A. Ischemic gastrointestinal complications of COVID-19: a systematic review on imaging presentation. *Clin Imaging*. 2020;73:86-95.
 40. Besutti G, Bonacini R, Iotti V, et al. Abdominal visceral infarction in 3 patients with COVID-19. *Emerg Infect Dis*. 2020;26:1926-1928.
 41. Suzuki S, Toyoma S, Kawasaki Y, Nanjo H, Yamada T. CD147 promotes invasion and MMP-9 expression through MEK signaling and predicts poor prognosis in hypopharyngeal squamous cell carcinoma. *Adv Clin Exp Med*. 2021;30:41-48.

SUPPORTING INFORMATION

Additional supporting information may be found in the online version of the article at the publisher's website.

How to cite this article: Bortolotti D, Simioni C, Neri LM, et al. Relevance of VEGF and CD147 in different SARS-CoV-2 positive digestive tracts characterized by thrombotic damage. *FASEB J*. 2021;35:e21969. doi:[10.1096/fj.202100821RRR](https://doi.org/10.1096/fj.202100821RRR)

6. SARS-CoV-2 treatment

The occurrence of atypical COVID-19 involving several body sites required the administration of different therapies, mainly to reduce the gastrointestinal and vascular symptomatology, and to control the correlated long-COVID sequelae.

Despite the large use of the common antiviral therapies in the treatment of SARS-CoV-2 infection, a variety of other potential antimicrobial agents are currently utilized [392]. In particular, polymers of biocide class showed an inhibitory effect against SARS-CoV-2 survival, becoming a relevant alternative antiviral approach for COVID-19 treatment [393]. Along these classic polymers, photoactive polymers and oligomers have recently shown to be significantly effective in the light-induced inactivation of SARS-CoV-2 [394]. Moreover, an interesting alternative for infection resolution is constituted by water-insoluble polymeric compounds, that present an active principle electrostatically bound to the backbone of a water-soluble anionic polymer. The advantage of this type of polymeric compounds consists in their solubilization in a volatile organic solvent that allows their use in spray-coating for surfaces, diminishing surfaces transmission.

Basing on this evidence, we assessed the potential employment of a synthetic polymeric formulations positively charged (polystyrene sulfonate, silver and benzalkonium, or simply a polystyrene sulfonate and benzalkonium) against bacterial and viral infections ([395], paper attached). We evaluated the antimicrobial properties of these formulations against Gram-positive, Gram-negative bacteria and *Candida albicans*, also their antiviral activity toward 229E alpha-coronavirus and SARS-CoV-2 ([395], paper attached).

The study revealed that polymeric formulations were able to control SARS-CoV-2 infection already after 5 min of contact with the treated surfaces. Our results supported the potential of this formulation as a candidate for the realization of transparent surface coatings, which can maintain the remarkable antibacterial activity together with SARS-CoV-2 antiviral properties, useful to control virus transmission trough contact with contaminated surfaces ([395], paper attached).



Transparent Polymeric Formulations Effective against SARS-CoV-2 Infection

Valentina Gentili, Daniele Pazzi, Sabrina Rizzo, Giovanna Schiuma, Edoardo Marchini, Stefania Papadia, Andrea Sartorel, Dario Di Luca, Francesca Caccuri, Carlo Alberto Bignozzi,* and Roberta Rizzo*



Cite This: *ACS Appl. Mater. Interfaces* 2021, 13, 54648–54655



Read Online

ACCESS

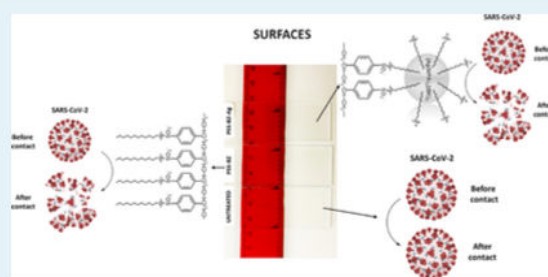
Metrics & More

Article Recommendations

Supporting Information

ABSTRACT: The main route of the transmission of the SARS-CoV-2 virus is through airborne small aerosol particles containing viable virus as well as through droplets transmitted between people within close proximity. Transmission via contaminated surfaces has also been recognized as an important route for the spread of SARS-CoV-2 coronavirus. Among a variety of antimicrobial agents currently in use, polymers represent a class of biocides that have become increasingly important as an alternative to existing biocidal approaches. Two transparent polymeric compounds, containing silver and benzalkonium ions electrostatically bound to a polystyrene sulfonate backbone, were synthesized, through simple procedures, and evaluated for their antimicrobial properties against Gram-positive and Gram-negative bacteria and *Candida albicans* (ISO EN 1276) and for their antiviral activity toward 229E and SARS-CoV-2 coronaviruses (ISO UNI EN 14476:2019). The results showed that the two tested formulations are able to inhibit the growth of $(1.5\text{--}5.5) \times 10^{11}$ CFU of Gram-positive bacteria, Gram-negative bacteria, and of the fungal species *Candida albicans*. Both compounds were able to control the 229E and SARS-CoV-2 infection of a target cell in a time contact of 5 min, with a virucidal effect from 24 to 72 h postinfection, according to the European Medicines Agency (EMA) guidelines, where a product is considered virucidal upon achieving a reduction of 4 logarithms. This study observed a decrease of more than 5 logarithms, which implies that these formulations are likely ideal candidates for the realization of transparent surface coatings that are capable of maintaining remarkable antibacterial activity and SARS-CoV-2 antiviral properties over time.

KEYWORDS: benzalkonium, silver, SARS-CoV-2, antiviral, antibacterial



1. INTRODUCTION

The global COVID-19 pandemic highlighted the need for innovative methods and technologies to mitigate the spread of viruses. The main route of the transmission of the SARS-CoV-2 virus occurs through small, airborne aerosol particles containing viable virus as well as through larger droplets that are transmitted between people within close proximity.¹ Transmission via contaminated surfaces has also been recognized as an important route for the spread of SARS-CoV-2 coronavirus, and several approaches to produce antimicrobial surfaces have been recently explored.^{2,3}

Notable results have been obtained with nanostructured surfaces,^{4,5} surfaces coated with copper oxide,^{6,7} and surface coated with cuprous oxide particles bound with polyurethane.⁸

Among a variety of available antimicrobial agents, polymers represent a class of biocides that have become increasingly important as an alternative to existing biocides. Conventional disinfectants are based on low-molecular-weight liquids or gases, so their use and duration are restricted by their volatility. Antimicrobial polymers can be tethered to surfaces enabling the killing of microbes without releasing biocides. Many of the

previously reported antimicrobial polymers have focused on antibacterial capabilities; however, there has been much less focus on antiviral properties. Antimicrobial polymers have been known since 1965, when Cornell and Donaruma described polymers and copolymers that kill bacteria.⁹ Since then, a number of reports appeared in the literature describing bactericidal coatings incorporating bound⁸ or unbound biocidal agents, such as metal-oxide particles,¹⁰ chlorine dioxide,¹¹ iodine compounds,^{12,13} silver nanoparticles,¹⁴ benzophenone,¹⁵ or quaternary ammonium (QA) compounds^{16,17} mixed with a polymeric binder. Among these coatings, QA compounds are probably the most widely used antibacterial agents for medical and public health applications because they have been shown to

Received: June 4, 2021

Accepted: October 21, 2021

Published: November 9, 2021



be effective against both Gram-negative and Gram-positive bacteria.¹⁸

According to the literature,¹⁹ there are three general types of antimicrobial polymer: (1) polymeric biocides, where the repeating unit is a biocide; (2) biocidal polymers, where the active unit is randomly embedded within a macromolecule, and (3) biocide-releasing polymers where the polymeric backbone acts as a carrier support for the biocides that can be transferred to the cell. In addition to these classic polymers, photoactive polymers and oligomers have recently demonstrated highly effective light-induced inactivation of SARS-CoV-2, which may cause a 5-log reduction in pfu/mL within 10 min of irradiation.²⁰

Our work has focused on simple polymeric compounds where an active principle can be electrostatically bound to the backbone of a water-soluble anionic polymer, resulting in the formation of water-insoluble polymeric materials, which can be then solubilized in alcoholic solvents. In this first study, we have considered silver-containing species and benzalkonium ions electrostatically bound to polystyrene sulfonate. The alcoholic solutions of these polymeric materials are ideal for realizing antimicrobial coatings on everyday items handled by people such as doorknobs, keyboards, handles, as well as on any type of filtration system where the polymeric backbone adheres to the solid substrate because of significant van der Waals interactions. The resulting films are transparent and are expected to exhibit a long-lasting antimicrobial effect.

The observation that the coated materials are highly effective against Gram-positive and Gram-negative bacteria and *Candida albicans* prompted us to investigate the antiviral activity of the solid polymeric film because viruses can also survive for a period of hours to several days once established on inanimate surfaces. We report here strong evidence of the activity of polymeric films against 229E and SARS-CoV-2 coronaviruses.

2. MATERIALS AND METHODS

2.1. Materials. All chemical products were purchased from Sigma-Aldrich. Elemental analysis C,H,N was performed with a LECO CHN analyzer. Silver was determined through plasma atomic absorption spectrometry with a Perkin Elmer Optima 3100 XL. Fourier transform infrared (FT-IR) spectra were recorded on a Bruker Vertex 70 FT-IR in diffuse reflectance mode dispersing the chemical powder in KBr (potassium bromide). Dimensional analysis and zeta potential were obtained with a Z-sizer Malvern instrument.

2.2. Preparation. The preparation of the silver complex, complex salts, and micellar derivatives was first described in the patent application PCT/EP2020/060686.

$\text{Na}_3[\text{Ag}(\text{MPA})_2]$ (MPA = 2-Mercapto-4-methyl-5-thiazolacetate). To a 1.135 g amount of the protonated MPA (2-mercapto-4-methyl-5-thiazolacetic acid, Aldrich), 12.36 g of 1 M NaOH solution in water was added. Distilled water (186.5 g) was then added, and the solution was kept stirring for 5 min. An aqueous solution (100 g) containing 0.51 g of di AgNO_3 was finally added, and the yellow solution was kept under stirring for an additional 30 min. The $\text{Na}_3[\text{Ag}(\text{MPA})_2]$ complex salt was precipitated by the addition of an excess of acetone, filtered, and air-dried; Ag^+ % = 0.108%. Elemental analysis: calculated for $\text{Na}_3\text{AgC}_{12}\text{N}_2\text{S}_4\text{O}_4\text{H}_{10}$; C 26.14; N, 5.08; H, 1.83; Ag, 19.57. Found: C, 25.87; N 5.0; H 1.88; Ag 19.46.

$[\text{Ag}(\text{MPA})_2](\text{Bz})_3$ (Bz = Benzalkonium) Micellar Derivatives. Benzalkonium (Bz) CAS. n 63,449–41-2 is a mixture of alkylbenzyl-dimethylammonium chlorides, in which the alkyl group has various even-numbered alkyl chains from 8 to 18. The average molecular weight of the chloride salt is 370 g. Uncharged $[\text{Ag}(\text{MPA})_2](\text{Bz})_3$ salt can be easily precipitated by the addition of a slight excess of benzalkonium chloride to an aqueous solution of the silver complex $\text{Na}_3[\text{Ag}(\text{MPA})_2]$. The addition of an excess of benzalkonium chloride results, instead, in the dissolution of $[\text{Ag}(\text{MPA})_2](\text{Bz})_3$, because of the formation of

positively charged micellar derivatives with a size distribution in the range 10–500 nm (see the next section).

Polymeric salts PSS-Bz-Ag and PSS-Bz. Polymeric salts of the positively charged micellar derivatives of $[\text{Ag}(\text{MPA})_2](\text{Bz})_3$ or Bz ions were obtained in distilled water by the addition of sodium polystyrene sulfonate (PSS). The precipitated neutral polymers containing PSS, $\text{Ag}(\text{MPA})_2$, and Bz moieties (PSS-Bz-Ag) or PSS and Bz ions (PSS-Bz) were separated from the aqueous solutions by filtration, washed with water, and dried at 50 °C. The polymeric solid was then dissolved in isopropanol or ethanol to obtain a solution of PSS-Bz-Ag containing Bz 1.25%, PSS 0.62%, and Ag 0.0025% and a solution of PSS-Bz containing Bz 1.25% and PSS 0.62%.

2.3. Bacterial Strains. The antimicrobial activity of the liquid products PSS-Bz-Ag (composition: Bz 1.25%, Ag^+ 0.0025%, PSS 0.62%, ethanol) and PSS-Bz (composition: Bz 1.25%, PSS 0.62%, ethanol) was tested against the following strains of microorganisms (purchased from Diagnostic International Distribution S.p.A.): *Pseudomonas aeruginosa* ATCC 15442, *Staphylococcus aureus* ATCC 6538, *Escherichia coli* ATCC 10536, *Enterococcus hirae* ATCC 10541, *Candida albicans* ATCC 10231, in accordance with ISO EN 1276. Microbial suspensions were prepared according to EN1276 from lyophilized pellets resuspended in the LB (Luria Broth) medium. The concentration was determined by spectrophotometry, horizontal method, and biochemical test. Microbial suspensions of the different strains were prepared with concentrations expressed as colony-forming units (CFU) comprised between 1.5×10^{12} and 5.5×10^{12} for each species. Samples (100 μL) of the two products were deposited in the center of Petri dishes and dried for 2 h in an oven at 37 °C. The microbial pool (100 μL) was then added and left in contact with PSS-Bz-Ag or PSS-Bz for 5 min. TSA (tryptone soya agar) was added after cooling at 40 °C and incubated at 37 °C for 24 h. Microbial titration was determined using the horizontal method. The experiments were performed in triplicate.

2.4. Cells and Viruses. MRC5 human fibroblast cells (ATCC CCL171) and African green monkey epithelial kidney cells, VeroE6 (ATCC CRL1586), were grown in monolayers in Eagle's minimal essential medium (MEM) with nonessential amino acids (Lonza Biosciences; Italy) supplemented with 10% heat-inactivated fetal calf serum (FCS, Gibco-Life Technologies; Italy), penicillin (100 units/mL; Sigma-Aldrich), streptomycin (100 $\mu\text{g}/\text{mL}$; Sigma-Aldrich; Italy), and L-glutamine (2 mM; Sigma-Aldrich; Italy).

Human coronavirus 229E (ATCC VR-740) and the clinical isolate of SARS-CoV-2, kindly provided by Prof. A. Caruso and Prof. F. Caccuri, University of Brescia, Italy, were propagated and titrated by qPCR assay on MRC5 or VeroE6 cells, respectively.^{21,22} All procedures were carried out in a biosafety level-3 (BSL-3) laboratory.

2.5. Cytotoxicity Control. Cytotoxicity control was performed on MRC5 and VeroE6 cells. The culture medium was mixed with PSS-Bz-Ag, PSS-Bz, or PBS (phosphate-buffered saline, 1X control solution) (Gibco, USA). The resulting solutions were added to cell cultures and incubated for 5, 10, 15 min, 24, 48, and 72 h. Cell viability was examined by the MTT (3-(4,5-dimethylthiazol-2-yl)-2,5-diphenyl tetrazolium bromide) colorimetric assay (Roche Diagnostics Corporation, Indianapolis, IN) and trypan blue dye (Sigma-Aldrich; Italy) exclusion. 2% DMSO (dimethyl sulfoxide; Sigma-Aldrich; USA) was used as the positive control of cell cytotoxicity. The experiments were performed in triplicate.

2.6. Antiviral Assays. The antiviral effect on the 229E and SARS-CoV-2 infection was evaluated by quantitative assays (plaque assay), in accordance with ISO UNI EN 14476:2019.

The 229E and human coronavirus SARS-Cov-2 suspensions were prepared by infecting the monolayers of MRC5 and VeroE6 cells, respectively. The infections were performed at 1.0 multiplicity of infections (MOIs).²⁰

On the day of testing, sterile Petri dishes (35 mm diameter) were prepared, as previously reported (Section 2.3). The viral suspension was added to the PSS-Bz-Ag, PSS-Bz, or PBS (control)-treated Petri dishes and incubated for 5 min at room temperature. The viral suspension was then harvested and incubated with susceptible cells for 1 h at 37 °C to let the viral particle infect the cells. The virus inoculum

was then removed, the cells were washed, and 1 mL of EMEM 2% FCS was added. The ability of the viral particles to infect susceptible cells was assessed on cell culture supernatants 24, 48, and 72 h postinfection (p.i.). Viral titration was performed by plaque assay and quantitative reverse transcription (qRT)-PCR.

2.6.1. Plaque Assay. Cell culture supernatants were harvested and placed in an ice bath immediately. The samples were inoculated in cell cultures immediately, within 10 s. Five days after infection, cells were methanol-fixed, and plaques were stained with crystal violet (0.1%) and counted. The experiments were performed in triplicate.

2.6.2. Quantitative Reverse Transcription-PCR. RNA was extracted from clarified cell culture supernatants (16,000 g \times 10 min) using PureLink Viral RNA/DNA Mini Kit (Invitrogen) according to the manufacturer's instructions. RNA was eluted in 15 μ L of RNase-free water and stored at -80 $^{\circ}$ C until use. Briefly, RNA was reverse-transcribed with SuperScript IV VIL0 (Invitrogen). 229E quantification was performed by real-time PCR with an HCoV-229E-specific qPCR gene assay (Vi06439671_s1, Catalog number: 4,331,182, ThermoFisher).¹⁹ SARS-CoV-2 quantification and amplification of the S gene were performed using the PowerUp SYBR Green Master Mix (Applied Biosystems) as follows: primers: RBD-qF1: 5'-CAATGGTT-TAACAGGCACAGG-3' and RBD-qR1: 5'-CTCAAGTGTCTGTG-GATCACG-3'.²⁰ A standard curve was generated by the determination of copy numbers derived from serial dilutions (10^2 – 10^8 copies) of the corresponding gene block (IDT Technologies). Each quantification was run in triplicates.

2.6.3. After-Effect Control. After-effect controls were conducted by mixing cell suspension with PSS-Bz-Ag, PSS-Bz, or PBS (10 s, see Section 2.6.1). The cells were then harvested and infected with viral inoculum for 1 h at 37 $^{\circ}$ C. The viral suspension was then incubated with susceptible cells for 1 h at 37 $^{\circ}$ C to allow for the viral particles to infect the cells. The virus inoculum was then removed, the cells were washed, and 1 mL of EMEM 2% FCS was added. The ability of the viral particles to infect susceptible cells was assessed on cell culture supernatants 24, 48, and 72 h postinfection (p.i.) by plaque assay. The experiments were performed in triplicate.

2.6.4. Interference Control. On the day of testing, sterile Petri dishes (35 mm diameter) were prepared, as previously reported (Section 2.3). Cell suspensions were added to the treated Petri dishes (PSS-Bz-Ag, PSS-Bz, or PBS (control)) for 1 h at room temperature, corresponding to the time period of the viral inoculum contact. The cells were then harvested and infected with a viral suspension (1.0 m.o.i.) for 1 h. The ability of the viral particles to infect susceptible cells was assessed on cell culture supernatants 24, 48, and 72 h postinfection (p.i.) by plaque assay. The experiments were performed in triplicate.

2.7. Statistical Analysis. Statistical comparisons of the data of the control and treatment groups were performed using Student's t-test as the data displayed a normal distribution based on the Kolmogorov–Smirnov test. Differences were considered significant at $p < 0.05$. Statistical analyses were performed using GraphPad Prism version 9.

3. RESULTS AND DISCUSSION

3.1. PSS-Bz-Ag and PSS-Bz Characterization. Elemental analysis and spectroscopic data for the silver complex were consistent with the presence of two MPA anionic ligands coordinated to Ag⁺ ions. The FT-IR spectrum of MPA showed the strong CO-stretching band of the carboxylic function at 1704 ± 2 cm^{-1} and an S-H stretching band at 2555 ± 2 cm^{-1} ; this band disappeared in the anionic silver complex, consistent with the coordination of sulfur to Ag⁺. Intense bands due to asymmetric and symmetric stretching modes of carboxylate appeared at 1580 ± 2 and 1386 ± 2 cm^{-1} , respectively.

The addition of benzalkonium chloride to the anionic silver complex Ag(MPA)₂³⁻, in water, resulted in the neutralization of the negative charge with the formation of a precipitate consistent with the stoichiometry (Bz)₃[Ag(MPA)₂]. The salt could be solubilized in water by the addition of an excess of benzalkonium chloride to form micelles with diameters of the order of 2–3 nm

and a zeta potential of ca. +9 mV. Subsequent addition of PSS to the micellar product allowed to obtain a polymeric material, PSS-Bz-Ag, insoluble in water, but exceedingly soluble in alcoholic solvents. Analogous polymers, PSS-Bz, were obtained by the addition of an excess of benzalkonium chloride to aqueous solutions of PSS. The two polymers did not show any appreciable water solubility, as shown by the analysis of the electronic absorption spectra of filtered suspensions and by the lack of the antimicrobial activity of the LB or Eagle MEM culture media left in contact for 20 h with the solid polymers (see solubility of the polymeric PSS-Bz-Ag and PSS-Bz components and Figure S1 and S2 in the Supporting Information).

The IR spectra of solid PSS-Bz-Ag and PSS-Bz (Figure S3) were similar, with vibrational bands matching the superposition of the intense bands of benzalkonium and PSS.

Solutions of PSS-Bz-Ag in alcohol were composed of micellar aggregates with diameters of the order of 10 nm and zeta potential of -3.9 mV (Figure S4a). Minority aggregates with higher diameters could be observed in the size distribution by intensity spectra (Figure S4b).

Films of PSS-Bz-Ag and PSS-Bz polymers can be produced on any type of surface by spray coating or wiping the alcoholic solutions that evaporate quickly, leaving a very transparent layer, as shown in Figure 1.

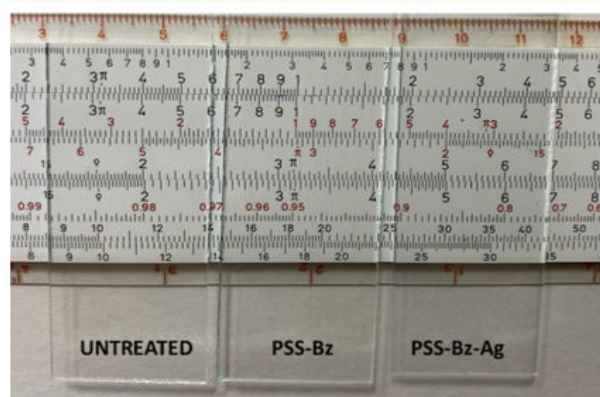


Figure 1. Glass slides untreated and treated with PSS-Bz-Ag and PSS-Bz.

3.2. Antimicrobial Activity of PSS-Bz-Ag and PSS-Bz Compounds.

To assess the antimicrobial activity of PSS-Bz-Ag and PSS-Bz, 100 μ L of the two products was deposited on a plastic substrate and allowed to dry. The microbial pool (100 μ L) was then added and left to be in contact with PSS-Bz-Ag or PSS-Bz for 5 min. We used different dilutions of the microbial suspension, with a range of 1.5×10^{12} and 5.5×10^{12} CFU for each species. As shown in Figure 2, while in the control dish, there is a continuum of colonies (Figure 2a), we observed no colonies in the Petri dishes of PSS-Bz-Ag- or PSS-Bz-treated microbial suspensions (Figure 2b,c), indicating a complete antimicrobial activity of both PSS-Bz-Ag and PSS-Bz that is comparable to isopropanol 80%, used as the positive control (Figure 2d). The analytical result obtained indicates that the two formulations are able to inhibit the growth of $(1.5\text{--}5.5) \times 10^{11}$ CFU of Gram-positive bacteria, Gram-negative bacteria, and the fungal species *Candida albicans* (Figure 2e). At higher concentrations, we observed the appearance of some colonies in isopropanol 80% (1×10^7 CFU) and, to a lesser extent, in

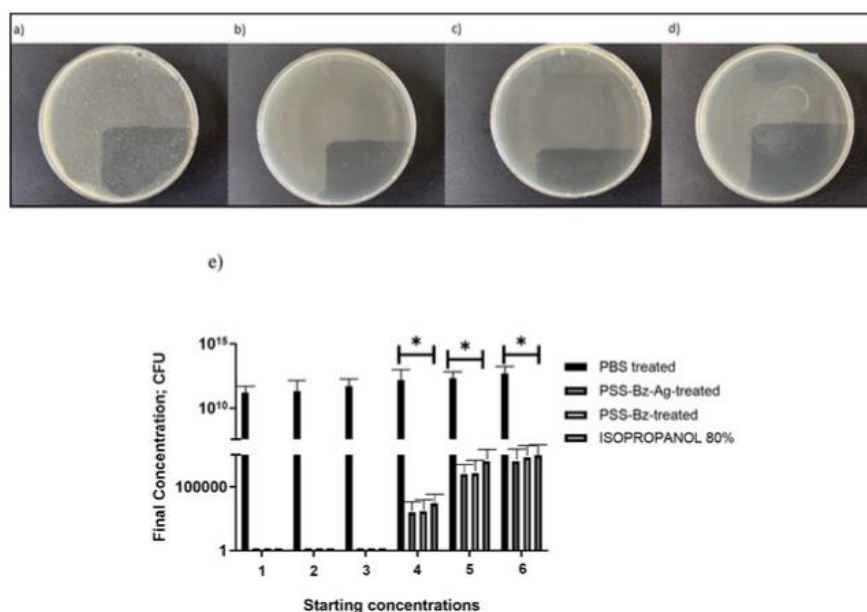


Figure 2. Antimicrobial activity of PSS-Bz-Ag and PSS-Bz. Representative cultures of microbial suspensions: (a) PBS (control), (b) PSS-Bz-Ag, (c) PSS-Bz, or (d) isopropanol 80% treated. (e) Analytical results on different microbial suspensions, containing *Pseudomonas aeruginosa*, *Staphylococcus aureus*, *Escherichia coli*, *Enterococcus hirae*, and *Candida albicans* (concentrations 1: 1.5×10^{11} ; 2: 2.0×10^{11} ; 3: 5.0×10^{11} ; 4: 1.5×10^{12} ; 5: 2.0×10^{12} ; and 6: 5.5×10^{12} for each species). Data are reported as mean \pm standard deviation of three replicates. * p value < 0.001; Student's t-test.

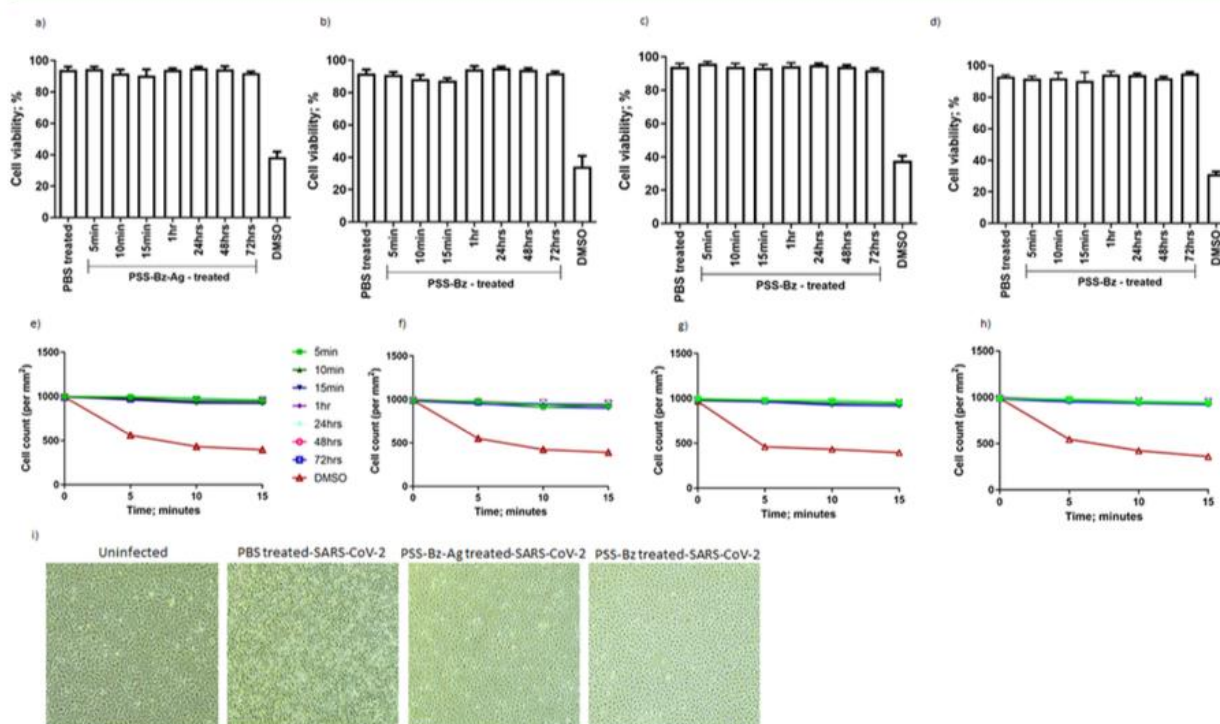


Figure 3. Cytotoxicity effect of the PSS-Bz-Ag compound on (a, b) MRC5 and (c, d) VeroE6 cell lines and PSS-Bz compounds on (e, f) MRC5 and (g, h) VeroE6 cell lines. (i) SARS-CoV-2 replication in VeroE6 cells after treatment with PSS-Bz-Ag and PSS-Bz compounds, 48 h postinfection. Data are reported as mean \pm standard deviation of three replicates.

PSS-Bz-Ag- (1×10^6 CFU) and PSS-Bz (1.2×10^6 CFU)-treated samples.

3.3. Cytotoxicity and Interference Tests for PSS-Bz-Ag and PSS-Bz Compounds. First, we assessed the cytotoxic effect of PSS-Bz-Ag or PSS-Bz toward human cells. We mixed

the culture medium with PSS-Bz-Ag or PSS-Bz, and we used MRC5 and VeroE6 cell lines to perform the cytotoxic assay (MTT). We sprayed a plastic surface with PSS-Bz-Ag, PSS-Bz, or PBS and added the resulting solutions to MRC5 or VeroE6 cells for 5, 10, 15 min and 1, 24, 48, and 72 h. We observed that both PSS-Bz-Ag and PSS-Bz were not cytotoxic for human cells. In fact, the MTT assay (Figure 3a–d) and the viable cell count (Figure 3e–h) did not show any significant difference in comparison with PBS-treated cells (p : NS; Student's t -test).

The interference control was performed by adding to cell cultures with PSS-Bz-Ag, PSS-Bz, or PBS for 1 h. PSS-Bz-Ag, PSS-Bz, or PBS solutions were removed, and the cells were infected with viral inoculum (1.0 m.o.i.) for 1 h. Viral titration showed no interference effect; in fact, viral plaques in PBS-treated samples did not differ from PSS-Bz-Ag- or PSS-Bz-treated samples (p : NS; Student's t -test) (Table 1).

Table 1. Interference Test^a

time postinfection (h)	logarithmic reduction (LR) (pfu/mL)	
	PSS-Bz-Ag	PSS-Bz
229E		
24	0.3 ± 0.1	0.3 ± 0.1
48	0.3 ± 0.1	0.2 ± 0.1
72	0.2 ± 0.2	0.1 ± 0.2
SARS-CoV-2		
24	0.3 ± 0.1	0.3 ± 0.1
48	0.2 ± 0.2	0.2 ± 0.1
72	0.2 ± 0.1	0.1 ± 0.2

^aLR of 229E and SARS-CoV-2 viral plaques after PSS-Bz-Ag, PSS-Bz, or Ag treatment in comparison with PBS-treated control. Data are reported as mean ± standard deviation of three replicates.

3.4. Antiviral Test for PSS-Bz-Ag and PSS-Bz Compounds. We tested the anti-229E and anti-SARS-CoV-2 effect of both PSS-Bz-Ag and PSS-Bz. The viral inoculum was exposed to a treated surface with PSS-Bz-Ag, PSS-Bz, or PBS. The time of contact of the viral inoculum was 5 min at room temperature, and then, the viral inoculum was recovered and used to infect MRC5 and VeroE6 cells and the target cells for 229E and SARS-CoV-2 in vitro assays. The viral inoculum was recovered after 1 h, and the cells were analyzed for viral titer 24, 48, and 72 h postinfection. These time points were selected as they allowed the detection of viral progeny formation, suggestive of viral infectivity. The viral load was determined by plaque assay. We observed a decreased viral plaque count after the treatment with both compounds in both cell lines, as reported in Table 2. At all time points, we observed a > 5 logarithmic reduction (LR) of plaque formation in 229E-infected samples treated with PSS-Bz-Ag or PSS-Bz ($p < 0.001$; Student's t -test). SARS-CoV-2-infected samples showed a > 5 LR of plaque formation in the PSS-Bz-treated samples ($p < 0.001$; Student's t -test). The PSS-Bz-Ag treatment was less effective at 24 h postinfection ($p = 0.02$; Student's t -test) and reached a > 5 LR of plaque formation after 48–72 h postinfection ($p < 0.001$; Student's t -test).

To obtain a further confirmation of the results obtained using the plaque formation test, we evaluated viral RNA by RT-qPCR in the culture medium collected from infected MRC5 and VeroE6 cells. We observed a decreased viral load after the treatment with both compounds in both cell lines (Table 3).

The results showed that PSS-Bz-Ag led to a 6.1 ± 0.6 LR for 229E RNA copies and a 3.7 ± 0.2 LR for SARS-CoV-2 RNA copies at 24 h postinfection (Table 3) ($p < 0.001$; $p = 0.012$,

Table 2. LR of 229E and SARS-CoV-2 Viral Plaques after PSS-Bz-Ag, PSS-Bz, or Ag Treatment in Comparison with the PBS-Treated Control^a

time post-infection (h)	LR (pfu/mL)			
	PSS-Bz-Ag	PSS-Bz	Ag 0.0025%	Ag 0.125%
229E				
24	5.9 ± 0.3	6.1 ± 0.5	0.2 ± 0.3	0.4 ± 0.3
48	5.9 ± 0.8	5.9 ± 0.6	0.3 ± 0.4	0.4 ± 0.4
72 h	5.2 ± 0.6	5.9 ± 0.4	0.2 ± 0.3	0.3 ± 0.3
SARS-CoV-2				
24	3.8 ± 0.6	5.3 ± 0.5	0.9 ± 0.5	0.9 ± 0.4
48	5.0 ± 0.3	5.5 ± 0.5	0.8 ± 0.6	0.8 ± 0.5
72	>7 ± 0.5	5.4 ± 0.4	0.8 ± 0.5	0.8 ± 0.5

^aData are reported as mean ± standard deviation of three replicates.

Table 3. LR of 229E and SARS-CoV-2 Viral RNA after PSS-Bz-Ag, PSS-Bz, or Ag Treatment^a

time postinfection (h)	LR genome copies/mL			
	PSS-Bz-Ag	PSS-Bz	Ag 0.0025%	Ag 0.108%
229E				
24	6.1 ± 0.6	6.5 ± 0.4	0.5 ± 0.3	0.6 ± 0.4
48	6.0 ± 0.3	6.4 ± 0.2	0.5 ± 0.2	0.6 ± 0.3
72	5.9 ± 0.4	6.3 ± 0.5	0.5 ± 0.2	0.6 ± 0.2
SARS-CoV-2				
24	3.7 ± 0.2	5.2 ± 0.4	0.8 ± 0.2	0.9 ± 0.3
48	4.9 ± 0.5	5.3 ± 0.2	0.7 ± 0.2	0.8 ± 0.2
72	6.8 ± 0.3	5.2 ± 0.1	0.6 ± 0.3	0.8 ± 0.3

^aData are reported as mean ± standard deviation of three replicates.

respectively; Student's t -test). We observed a similar reduction of 229E RNA copies at different time points, while SARS-CoV-2 RNA copies were significantly reduced over time (24 vs 48 h $p < 0.021$; 24 vs 72 h $p < 0.001$; 48 vs 72 h $p = 0.019$; Student's t -test). PSS-Bz led to a 6.5 ± 0.4 LR for 229E RNA copies and a 5.2 ± 0.4 LR for SARS-CoV-2 RNA copies at 24 h postinfection (Table 3). We observed a similar reduction of 229E and SARS-CoV-2 RNA copies over time (Table 3). These results confirm that both PSS-Bz and PSS-Bz-Ag are able to control 229E and SARS-CoV-2 infection of a target cell with a virucidal effect 24 h postinfection, according to the EMA guidelines,²³ where a product is considered virucidal as soon as it has achieved a reduction of ≥ 4 logarithm.

To evaluate the possible after-effect of PSS-Bz and PSS-Bz-Ag, cell suspensions were added to the treated Petri dishes (PSS-Bz-Ag, PSS-Bz, or PBS (control)) for 1 h at room temperature, corresponding to the time period of the viral inoculum contact. The cells were then harvested and infected with a viral suspension (1.0 m.o.i.) for 1 h. The ability of the viral particles to infect susceptible cells was comparable to that of control samples (PBS-treated) at all time points (Table 4), demonstrating that both PSS-Bz and PSS-Bz-Ag are effective on viral particles and not on human cells.

Because both the main difference between PSS-Bz-Ag and PSS-Bz compounds is the presence of Ag in PSS-Bz-Ag, we evaluated the effect of the Ag complex alone at two concentrations, one corresponding to the concentration in PSS-Bz-Ag (0.0025% w/w and a 50 times higher concentration (0.125% w/w) on 229E and SARS-CoV-2 infection. The Ag treatment had a slight effect on viral plaque formation, with both

Table 4. After-Effect Test^a

time postinfection (h)	LR (pfu/mL)	
	PSS-Bz-Ag	PSS-Bz
229E		
24	0.2 ± 0.1	0.1 ± 0.1
48	0.1 ± 0.2	0.1 ± 0.1
72	0.1 ± 0.2	0.1 ± 0.1
SARS-CoV-2		
24	0.2 ± 0.1	0.1 ± 0.1
48	0.1 ± 0.2	0.1 ± 0.1
72	0.1 ± 0.1	0.1 ± 0.1

^aLogarithmic reduction of 229E and SARS-CoV-2 viral plaques after PSS-Bz-Ag, PSS-Bz, or Ag treatment in comparison with the PBS-treated control. Data are reported as mean ± standard deviation of three replicates.

Ag concentrations (Table 2). Interestingly, the effect is not concentration- and time-dependent (Table 2). RNA copy analysis confirmed the plaque assay results (Table 3), showing a slight LR of RNA copies with both Ag concentrations. These results support the hypothesis that the main virucidal component is benzalkonium chloride. Literature data support this efficacy based on the cationic “headgroup” of benzalkonium chloride that is progressively adsorbed to the negatively charged phosphate heads of phospholipids in the lipid bilayer. This might be effective mainly on enveloped viruses as SARS-CoV-2, together with the alkyl chain “tail” component of benzalkonium chloride, that perturbs the membrane bilayer by permeating the barrier and disrupting its physical and biochemical properties. Protein function is subsequently disturbed, and the combination of these effects results in the solubilization of the bilayer constituents into benzalkonium chloride/phospholipid micelles.

Multiple studies have reported on the virucidal effect of Benzalkonium chloride against coronaviruses. Rabenau et al. found that, as a surface disinfectant in a concentration of 0.5%, benzalkonium chloride demonstrated a reduction factor of >4 against SARS-CoV.²⁴ Meanwhile, by evaluating the virucidal activity of different oral rinses against three strains of SARS-CoV-2, Meister et al. reported log reductions of >3.1, >2.8, and >2.6, respectively, for a rinse containing 0.035% benzalkonium chloride.²⁵

Interestingly, PSS-Bz-Ag and PSS-Bz showed a different efficacy toward the two viral strains. In particular, both PSS-Bz-Ag and PSS-Bz affected 229E infectivity with a similar efficacy during culture time points (~6 LR). PSS-Bz strongly affected SARS-CoV-2 infectivity at all culture time points (>6 LR). On the contrary, the PSS-Bz-Ag effect is time-dependent, increasing from about 4 to 7 LR at 24 and 72 h culture, respectively. This different behavior is unclear at present, and it might be due to the differences in the PSS-Bz-Ag and PSS-Bz structures, which are illustrated in Figure 4a,b.

In PSS-Bz-Ag, the synthetic design obliges positively charged Bz micellar assemblies, trapping the neutral [Ag(MPA)₂](Bz)₃ complex salt, to interact electrostatically with the sulfonic groups of PSS (Figure 4a). The electrostatic interaction is strong because the polymer does not dissolve in the polar water solvent, but the alkyl chain of Bz is mainly engaged in the solubilization of the neutral complex salt. In PSS-Bz, on the contrary, the direct electrostatic interaction of the quaternary nitrogen with negative sulfonates leaves the alkyl chain completely free from interacting with the microbial membrane, as shown in Figure 4b. Surface coatings with PSS-Bz should cause a higher damage to the virus

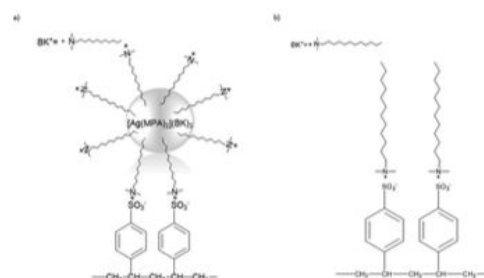


Figure 4. (a) PSS-Bz-Ag and (b) PSS-Bz schematic structures of the polymeric assemblies.

most probably for this reason, in fact, it is generally accepted that the mechanism of the microbicidal action of QA compounds is due to the dissociation of cellular membrane lipid bilayers, which compromises cellular permeability controls and induces the leakage of cellular contents. We might hypothesize that PSS-Bz is able to interfere with the SARS-CoV-2-cell contact, reducing infectivity at all time points, while PSS-Bz-Ag might interfere with SARS-CoV-2 replication, with a time-dependent effect. The strong efficacy of both compounds on 229E infection supports the different resistances of these two coronaviruses.²⁶ The results obtained with interference and after-effect tests confirm that both compounds are effective during the 5 min of contact, and they are not removed within the viral inoculum. The water insolubility of these products should allow and help maintain their effectiveness over time.

4. CONCLUSIONS

We have examined the antibacterial and antiviral properties of polymeric compounds that can be easily synthesized by coupling positively charged antimicrobial agents (either as a cationic molecule or metal complex) with a negatively charged polymer such as sulfonated polystyrene. Our general approach has been to produce a water-insoluble material, which could be solubilized in a volatile organic solvent for spray-coating surfaces. Specifically, we have analyzed the properties of the transparent polymeric formulations consisting of polystyrene sulfonate, silver, and benzalkonium or simply by polystyrene sulfonate and benzalkonium. These studies support a very high antibacterial and antiviral effect toward 229E and SARS-CoV-2, as evidenced by a > 5 LR in the infectious agent after 5 min of contact with the treated surface. The reported examples can be useful for the production of new polymeric materials containing different cationic antimicrobial species.

■ ASSOCIATED CONTENT

Supporting Information

The Supporting Information is available free of charge at <https://pubs.acs.org/doi/10.1021/acsami.1c10404>.

Solubility of the polymeric PSS-Bz-Ag and PSS-Bz components, FT-IR spectra, and the size distribution of PSS-Bz-Ag (PDF)

■ AUTHOR INFORMATION

Corresponding Authors

Carlo Alberto Bignozzi – Department of Chemical, Pharmaceutical and Agricultural Sciences, University of Ferrara, Ferrara 44100, Italy; Phone: 00390532455130; Email: g4s@unife.it

Roberta Rizzo – Department of Chemical, Pharmaceutical and Agricultural Sciences, University of Ferrara, Ferrara 44100, Italy; Phone: 00390532455382; Email: rbr@unife.it; Fax: 00390532974470

Authors

Valentina Gentili – Department of Chemical, Pharmaceutical and Agricultural Sciences, University of Ferrara, Ferrara 44100, Italy

Daniele Pazzi – Department of Chemical, Pharmaceutical and Agricultural Sciences, University of Ferrara, Ferrara 44100, Italy

Sabrina Rizzo – Department of Chemical, Pharmaceutical and Agricultural Sciences, University of Ferrara, Ferrara 44100, Italy

Giovanna Schiuma – Department of Chemical, Pharmaceutical and Agricultural Sciences, University of Ferrara, Ferrara 44100, Italy

Edoardo Marchini – Department of Chemical, Pharmaceutical and Agricultural Sciences, University of Ferrara, Ferrara 44100, Italy; orcid.org/0000-0002-8092-1349

Stefania Papadia – Department of Chemical, Pharmaceutical and Agricultural Sciences, University of Ferrara, Ferrara 44100, Italy

Andrea Sartorel – Department of Chemical Sciences, University of Padova, Padova 35131, Italy; orcid.org/0000-0002-4310-3507

Dario Di Luca – Department of Medical Sciences, University of Ferrara, Ferrara 44100, Italy

Francesca Caccuri – Department of Microbiology and Virology, Spedali Civili, Brescia 25125, Italy

Complete contact information is available at:
<https://pubs.acs.org/10.1021/acsami.1c10404>

Author Contributions

R.R., C.B.: conceptualization; data curation; funding acquisition; V.G.: investigation; methodology; project administration; D.P.: antibacterial analysis; E.M., S.P.: chemical compound synthesis; A.S.: dimensional analysis and Z potential quantification; S.R., G.S., F.C., D.D.L.: antiviral analysis.

Funding

We acknowledge the financial support from the University of Ferrara crowdfunding (R.R.; V.G.); FAR 2019, 2020 (R.R.; V.G.) and from DEBx Medical B.V. (The Netherlands).

Notes

The authors declare no competing financial interest.

ACKNOWLEDGMENTS

We thank Iva Pivanti and Dr. Mercedes Fernandez for providing technical support and Linda Sartor for English revision. We thank also Prof. Cliff Timpson of the Roger William University for English language corrections.

ABBREVIATIONS

LR, logarithmic reduction
QA, quaternary ammonium
KBr, potassium bromide
Bz, benzalkonium
CFU, colony-forming units
TSA, tryptone soya agar
MTT, (3-(4,5-dimethylthiazol-2-yl)-2,5-diphenyl tetrazolium bromide

FTIR, Fourier transform infrared
HEPA, high-efficiency particulate air filter

REFERENCES

- (1) Mousavi, E. S.; Kananizadeh, N.; Martinello, R. A.; Sherman, J. D. COVID-19 Outbreak and Hospital Air Quality: A Systematic Review of Evidence on Air Filtration and Recirculation. *Environ. Sci. Technol.* **2021**, *55*, 4134–4147.
- (2) Kampf, G.; Todt, D.; Pfaender, S.; Steinmann, E. Persistence of coronaviruses on inanimate surfaces and their inactivation with biocidal agents. *J. Hosp. Infect.* **2020**, *104*, 246–251.
- (3) Sia, S. F.; Yan, L. M.; Chin, A. W. H.; Fung, K.; Choy, K. T.; Wong, A. Y. L.; Kaewpreedee, P.; Perera, R.; Poon, L. L. M.; Nicholls, J. M.; Peiris, M.; Yen, H. L. Pathogenesis and transmission of SARS-CoV-2 in golden hamsters. *Nature* **2020**, *583*, 834–838.
- (4) Hasan, J.; Crawford, R. J.; Ivanova, E. P. Antibacterial surfaces: the quest for a new generation of biomaterials. *Trends Biotechnol.* **2013**, *31*, 295–304.
- (5) Hasan, J.; Pyke, A.; Nair, N.; Yarlagadda, T.; Will, G.; Spann, K.; Yarlagadda, P. Antiviral Nanostructured Surfaces Reduce the Viability of SARS-CoV-2. *ACS Biomater. Sci. Eng.* **2020**, *6*, 4858–4861.
- (6) Sousa, B. C.; Cote, D. L. Antimicrobial Copper Cold Spray Coatings and SARS-CoV-2 Surface Inactivation. *MRS Adv.* **2020**, *5*, 2873–2880.
- (7) Hosseini, M.; Chin, A. W. H.; Behzadinasab, S.; Poon, L. L. M.; Ducker, W. A. Cupric Oxide Coating That Rapidly Reduces Infection by SARS-CoV-2 via Solids. *ACS Appl. Mater. Interfaces* **2021**, *13*, 5919–5928.
- (8) Behzadinasab, S.; Chin, A.; Hosseini, M.; Poon, L.; Ducker, W. A. A Surface Coating that Rapidly Inactivates SARS-CoV-2. *ACS Appl. Mater. Interfaces* **2020**, *12*, 34723–34727.
- (9) Cornell, R. J.; Donaruma, L. G. 2-Methacryloxytropones. Intermediates for the Synthesis of Biologically Active Polymers. *J. Med. Chem.* **1965**, *8*, 388–390.
- (10) Ramakrishna, S.; Subramanian, S. Fibers for Decontamination of Chemical and Biological agents. World Patent WO2008127200, 2008 April 11.
- (11) Leung, W. K.; Lau, A. P.; Yeung, K. L. Bactericidal and sporicidal performance of a polymer-encapsulated chlorine dioxide-coated surface. *J. Appl. Microbiol.* **2009**, *106*, 1463–1472.
- (12) Ahmad, S. I.; Hasan, N.; Zainul Abid, C. K. V.; Mazumdar, N. Preparation and characterization of films based on crosslinked blends of gum acacia, polyvinylalcohol, and polyvinylpyrrolidone-iodine complex. *J. Appl. Polym. Sci.* **2008**, *109*, 775–781.
- (13) Punyani, S.; Narayanan, P.; Vasudevan, P.; Singh, H. Sustained release of iodine from a polymeric hydrogel device for water disinfection. *J. Appl. Polym. Sci.* **2007**, *103*, 3334–3340.
- (14) Lee, S. B.; Trofin, L.; Rae, A.; Blakel, K. Treated articles and methods of treating articles. World Patent: WO2008063680, 2008.
- (15) Hong, K. H.; Sun, G. Photoinduced antimicrobial polymer blends with benzophenone as a functional additive. *J. Appl. Polym. Sci.* **2009**, *112*, 2019–2026.
- (16) Vachon, D. J.; Nordali, S. F.; Walter, D. C. Antimicrobial And Biological Active Polymer Composites And Related Methods, Materials and Devices. U.S. Patent 15/509.834, 2017.
- (17) Wong, S. Y.; Li, Q.; Veselinovic, J.; Kim, B. S.; Klibanov, A. M.; Hammond, P. T. Bactericidal and virucidal ultrathin films assembled layer by layer from polycationic N-alkylated polyethylenimines and polyanions. *Biomaterials* **2010**, *31*, 4079–4087.
- (18) Tashiro, T. Antibacterial and Bacterium Adsorbing Macromolecules. *Macromol. Mater. Eng.* **2001**, *286*, 63–87.
- (19) Siedenbiedel, F.; Tiller, J. C. Antimicrobial Polymers in Solution and on Surfaces: Overview and Functional Principles. *Polymer* **2012**, *4*, 46–71.
- (20) Monge, F. A.; Jagadesan, P.; Bondu, V.; Donabedian, P. L.; Ista, L.; Chi, E. Y.; Schanze, K. S.; Whitten, D. G.; Kell, A. M. Highly Effective Inactivation of SARS-CoV-2 by Conjugated Polymers and Oligomers. *ACS Appl. Mater. Interfaces* **2020**, *12*, 55688–55695.

(21) Ionescu, A. C.; Brambilla, E.; Manzoli, L.; Orsini, G.; Gentili, V.; Rizzo, R. Efficacy of personal protective equipment and H₂O₂-based spray against coronavirus in dental setting. *Oral Dis.* **2020**, DOI: 10.1111/odi.13736.

(22) Rizzo, S.; Savastano, M. C.; Bortolotti, D.; Savastano, A.; Gambini, G.; Caccuri, F.; Gentili, V.; Rizzo, R. COVID-19 Ocular Prophylaxis: The Potential Role of Ozonated-Oils in Liposome Eyedrop Gel. *Transl. Vis. Sci. Technol.* **2021**, *10*, 7.

(23) EMEA/CPMP/BWP/268/95/3AB8A Note for guidance on virus validation studies: The design, contribution and interpretation of studies validating the inactivation and removal of viruses, 1996.

(24) Rabenau, H. F.; Kampf, G.; Cinatl, J.; Doerr, H. W. Efficacy of various disinfectants against SARS coronavirus. *J. Hosp. Infect.* **2005**, *61*, 107–111.

(25) Meister, T. L.; Brüggemann, Y.; Todt, D.; Conzelmann, C.; Müller, J. A.; Groß, R.; Münch, J.; Krawczyk, A.; Steinmann, J.; Steinmann, J.; Pfaender, S.; Steinmann, E. Virucidal Efficacy of Different Oral Rinses Against Severe Acute Respiratory Syndrome Coronavirus 2. *J. Infect. Dis.* **2020**, *222*, 1289–1292.

(26) Aboubakr, H. A.; Sharafeldin, T. A.; Goyal, S. M. Stability of SARS-CoV-2 and other coronaviruses in the environment and on common touch surfaces and the influence of climatic conditions: A review. *Transbound Emerg. Dis.* **2021**, *68*, 296–312.

7. Novelty of the thesis

The thesis presents a series of findings aimed at enhancing our understanding of how SARS-CoV-2 affects the immune system and leads to disease. While traditionally focused on respiratory infection, the research delves into the virus's impact on tissues beyond the lungs, notably the placenta and gastrointestinal system, which is a novel and significant aspect of study. Understanding these broader effects is crucial, especially given the lingering consequences of COVID-19, known as long COVID.

One key focus of the thesis is on the mechanisms underlying the exhaustion of NK cells observed in COVID-19 patients. It highlights the role of specific molecules like HLA-G and HLA-E, which modulate the immune response, and explores how the virus manipulates these molecules to evade the immune system. Additionally, the research investigates the differential effects of SARS-CoV-2 Variants Of Concern (VOCs) on the efficacy of vaccination strategies, analyzing both antibody and cell-mediated immune responses. These insights aim to improve therapeutic approaches and provide a deeper understanding of how viral infections impact human health.

Importantly, this research extends beyond SARS-CoV-2 to contribute to our understanding of other viral infections, particularly given the rising threat of emergent and re-emergent viral diseases. By shedding light on the complex interplay between viruses and the immune system, the thesis offers valuable insights that could inform future research and the development of effective strategies for combating viral diseases.

8. Conclusions and perspective

The data herein summarized, discussed some important aspects concerning the role of host immune system during SARS-CoV-2 infection and the possible correlation of the virus in associated diseases. SARS-CoV-2 is a *Betacoronavirus*, known to be the etiological agent of COVID-19, which caused global pandemic in 2020. The higher impact of SARS-CoV-2, respect to MERS and SARS-CoV, was associated to 658 million of confirmed cases from March 2021 [5].

The transmission of SARS-CoV-2 via respiratory droplets represents the main way of transmission, associated to the onset of the typical pulmonary sequelae in COVID-19 [164], that can possibly evolve in extra-pulmonary diseases and long-COVID-19 condition. SARS-CoV-2 ability to infect several tissues is due to the wide distribution of ACE2 and CD147, the main viral entry receptors.

This thesis aims to investigate SARS-CoV-2 infection from different points of view, firstly focusing on SARS-CoV-2 modulation of host immune system.

In fact, both typical and atypical COVID-19 seem to depend on SARS-CoV-2 modulation of both innate [315] and adaptive host immune systems [355]. In particular, host innate immunity is the first involved in the protection against SARS-CoV-2, exploiting mechanism such as TLRs [315] and HLA-I molecules [323], to control the infection and stimulate an efficient acquired immune response, consequently triggering the virus to develop peculiar immune-escape strategies ([396], paper attached).



Perspective

Innate Immune Response in SARS-CoV-2 Infection

Giovanna Schiuma [†] , Silvia Beltrami [†] , Daria Bortolotti ^{*†} , Sabrina Rizzo [‡] and Roberta Rizzo [‡]

Department of Chemical, Pharmaceutical and Agricultural Sciences, University of Ferrara, 44121 Ferrara, Italy; giovanna.schiuma@unife.it (G.S.); silvia.beltrami@unife.it (S.B.); sabrina.rizzo@unife.it (S.R.); rbr@unife.it (R.R.)

* Correspondence: daria.bortolotti@unife.it

† These authors contribute equally to this work.

‡ These authors contribute equally to this work.

Abstract: An efficient host immune response is crucial in controlling viral infections. Despite most studies focused on the implication of T and B cell response in COVID-19 (Corona Virus Disease-19) patients or in their activation after vaccination against SARS-CoV-2, host innate immune response has raised even more interest as well. In fact, innate immunity, including Natural Killer (NK) cells, monocytes/macrophages and neutrophils, represent the first line of defense against the virus and it is essential to determine the correct activation of an efficient and specific acquired immune response. In this perspective, we will report an overview on the main findings concerning SARS-CoV-2 interaction with innate host immune system, in correlation with pathogenesis and viral immune escape mechanisms.

Keywords: SARS-CoV-2; immunity; innate immune cells; immune-evasion; natural killer cells



Citation: Schiuma, G.; Beltrami, S.; Bortolotti, D.; Rizzo, S.; Rizzo, R. Innate Immune Response in SARS-CoV-2 Infection. *Microorganisms* **2022**, *10*, 501. <https://doi.org/10.3390/microorganisms10030501>

Received: 10 December 2021

Accepted: 22 February 2022

Published: 23 February 2022

Publisher's Note: MDPI stays neutral with regard to jurisdictional claims in published maps and institutional affiliations.



Copyright: © 2022 by the authors. Licensee MDPI, Basel, Switzerland. This article is an open access article distributed under the terms and conditions of the Creative Commons Attribution (CC BY) license (<https://creativecommons.org/licenses/by/4.0/>).

1. Introduction

SARS-CoV-2 is a positive-sense single-stranded RNA (ssRNA) virus that has emerged around the end of December 2019, in Wuhan, Hubei-China, associated with a severe respiratory syndrome named COVID-19 (Corona Virus Disease-19) and declared pandemic in March 2020.

SARS-CoV-2 can infect target cells through the interaction between its structural glycoprotein Spike (S) protein [1] and ACE-2 (Angiotensin Converting Enzyme-2) receptor. The wide tissue expression of ACE-2 determines SARS-CoV-2 tropism for several organs and explains the variety of symptoms associated to the infection [1]. In addition to ACE-2, other molecules, such as CD147 and neuropilin 1 (NRP1), have been identified as possible co-receptors able to enhance the ability of SARS-CoV-2 to enter human cells [2,3]. Both CD147 and NRP1 are widely distributed in body tissues and play diverse physiological as well as pathological and therapeutic roles in different clinical conditions, including COVID-19 [4,5], involving host immune system activation [6,7].

Different findings have reported SARS-CoV-2 ability, and particularly of its Spike protein, to interfere with host immune activation [8].

During SARS-CoV-2 infection, both innate and adaptive immune system are engaged [9]. The innate immune system, referred to Natural Killer (NK) cells, monocytes/macrophages and dendritic (DC) cells, is the first to be recruited, followed by T and B lymphocytes responses, responsible for the specific pathogen recognition and for the establishment of the immunological memory.

SARS-CoV-2 infection has been described as associated to peculiar effects involving both immune components, strongly related to COVID-19 symptoms such as the “cytokine storm” condition [10]. Even if most studies focused on T and B cells response to SARS-CoV-2 infection, and the engagement of immunological memory raised after natural infection or vaccination, innate immunity plays a crucial role in COVID-19 onset, as the first line of defense against SARS-CoV-2 infection [11].

In this perspective, we will review the main current data referred to SARS-CoV-2 interaction with innate host immune system, in correlation with pathogenesis and viral immune escape mechanisms. Data were selected following eligibility criteria accordingly to the reviewed topic, as reported in Section 2 (Figure 1).

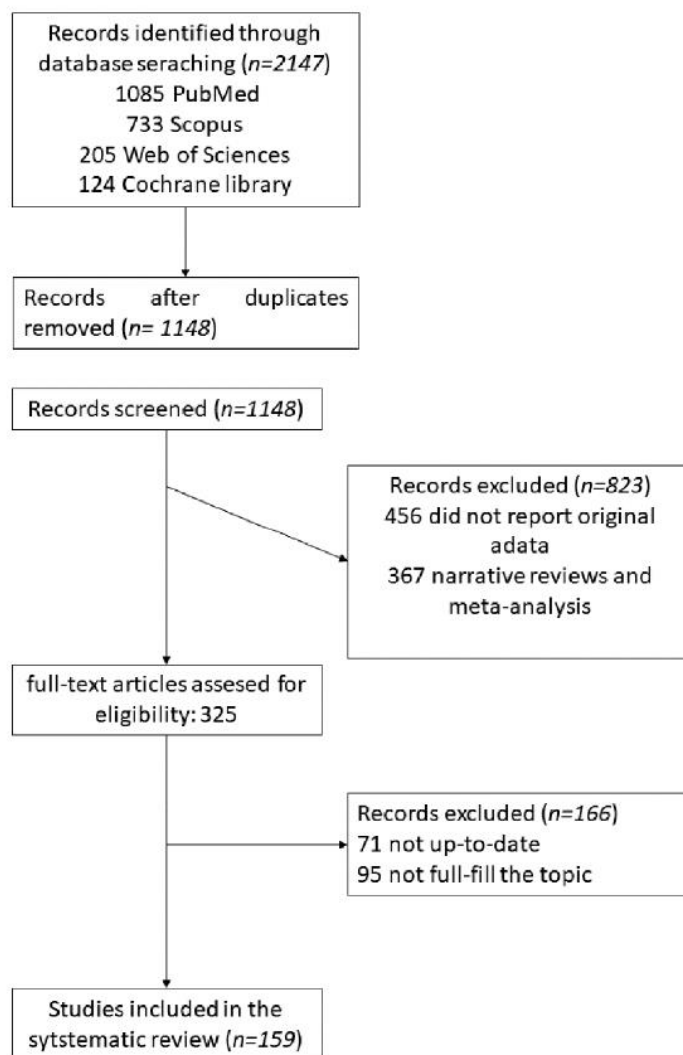


Figure 1. Data selection following eligibility criteria accordingly to the reviewed topic.

2. Materials and Methods

2.1. Search Strategy

We used a set of electronic databases (Medline/PubMed, Scopus, Web of Sciences (WOS), Cochrane library) for a systematic search until January 2022 using MeSH keywords/terms: “COVID-19,” “2019 novel coronavirus,” “RNA sensors” “inflammasome”, “interferon”, immune cells”, “innate immunity”, “Natural killer cells”, “NETs”, “monocytes”, “macrophages”, “neutrophils”, “cytokine storm”, “immune cross-talk”, “immune-escape”, “antiviral effect”. We applied no date or language restriction. We followed the Preferred Reporting Items for the Systematic Review and Meta-Analysis (PRISMA) statement [12].

2.2. Study Selection

We selected two independent reviewers to performed title-abstract screening on all selected studies, then the full-text of the selected articles were reviewed. In cases of duplicate information from the same patient, the data were checked and combined, but only considered as a single case.

2.3. Inclusion Criteria

Studies reporting innate immune response, as well as COVID-19 were selected. Publications were selected using specific keywords (“COVID-19,” “2019 novel coronavirus,” “RNA sensors” “inflammasome”, “interferon”, immune cells”, “innate immunity”, “Natural killer cells”, “NETs”, “monocytes”, “macrophages”, “neutrophils”, “cytokine storm”, “immune cross-talk”, “immune-escape”, “anti-viral effect”) and MeSH Advanced Search Builder. Articles were filtered also according to the date of publication (not older than late 2020–2021) and to fulfill the topic of this perspective.

2.4. Exclusion Criteria

Studies which were just case reports, and commentaries were excluded. Moreover, publication without DOI (e.g., conference abstracts and clinical trials) were excluded.

2.5. Data Extraction

The extraction of the data from included studies was performed by two reviewers separately, considering key characteristics including publication year, author, type of study, country, sample size, laboratory findings. In case of opposite reviewer’s selection, we report both of them or, in view of other publications, we reported those most accredited.

2.6. The Assessment of Methodological Quality and Risk of Bias

The funnel-plot and Egger’s regression test were used to assess publication bias [13].

3. SARS-CoV-2 Innate Immune System Response

Innate immune system functions protect the host from potential dangerous non-self antigens. For this reason, innate immunity includes different strategy for infection detection and elimination.

In the case of SARS-CoV-2, viral recognition by tissue-resident immune cells within the lung provides a local immune response resulting in the recruitment of further innate immune cells from the blood. This activation is triggered by different SARS-CoV-2 structural components and involves different kinds of immune cells and specific intracellular pathways.

3.1. RNA-Sensing of SARS-CoV-2

After host infection, SARS-CoV-2 virus could be recognized through a complex system of sensors, named Pattern Recognition Receptors (PRRs), expressed by epithelial cells as well as by local cells of the innate immune response, such as alveolar macrophages [14]. PRRs recognize specific pathogen portions, called “pathogen-associated molecular patterns” (PAMPs), such as pathogen genome.

The PRRs family includes different components that are involved in the sensing of RNA virus infections. Among these, the most studied referred to SARS-CoV-2 infection sensing, are Toll-Like Receptors (TLRs), and RIG-I-like receptors (RLRs). TLRs consist in a large family of 9 membrane-associated receptors able to recognize different PAMPs [15,16], localized on cell surface (TLR1, TLR2, TLR4, TLR5 and TLR6) or on intracellular membrane (TLR3, TLR7, TLR8 and TLR9). TLRs expressed on cell surface are involved in the recognition of extracellular pathogens, while intracellular TLRs expressed on endosomes and endoplasmic reticulum are engaged during intracellular infection. RLRs intracellular pattern recognition receptors which play a key role in the activation of innate immune system during viral infection. In fact, RLRs are cytoplasmatic RNA helicases involved in the sensing of non-self RNA [17], which include melanoma differentiation-associated

protein 5 (MDA-5), retinoic acid-inducible gene I (RIG-I) and the Probable ATP-dependent RNA helicase DHX58 known as LGP2. RLRs are normally inactive in uninfected cells and become active in presence of viral RNA, leading to interferons production to control the infection.

ssRNA genome of SARS-CoV-2 has been reported to be recognized by specific TLRs (TLR3, TLR7, and TLR8), all localized on the endosomal membrane [18,19], and also by MDA-5 and RIG-I, which are able to sense intracellular double-stranded RNA (dsRNA) produced during the infection [17].

After viral RNA binding, both TLRs and RLRs engage adaptor proteins TIR-domain-containing adapter-inducing interferon- β (TRIF) and myeloid differentiation factor 88 (MyD88) are recruited by TLRs, while RIG-1 and MDA5 activate mitochondrial antiviral-signaling protein (MAVS) and consequently recruit specific kinases, such as TANK-binding kinase 1 (TBK1). Then, phosphorylated interferon regulatory factors (IRFs), including IRF3 and IRF7 and transcriptional factors nuclear factor kappa light-chain-enhancer of activated B cells (NF- κ B) translocate in the nucleus, inducing the transcriptional activation of genes coding inflammatory cytokines and interferons (IFNs) [9,20,21]. These molecules attract more innate immune cells, such as polymorphonuclear leukocytes, monocytes, NK cells, DC cells, which in turn produce other factors, such as Monokine Induced by Gamma interferon [22], Interferon gamma-induced Protein 10 (IP-10) and Monocyte Chemoattractant Protein 1 (MCP-1), attracting lymphocytes at the site of infection (Figure 2) [9,23,24]. Importantly, TLRs are involved in both innate responses against SARS-CoV-2 infection and in the arise of COVID-19 hyperinflammatory phenotype [17]. Rizzo et al. have recently showed that the activation of TLR3 and TLR7 by SARS-CoV-2 genome differentially involves IRF3 and IRF7, leading to a peculiar production of pro-inflammatory cytokines, such as IL-1 α , IL-1 β , IL-4, and IL-6, as well as interferons [25]. Furthermore, TLR7 deficient genetic variants has been reported to be associated with a less efficient control of SARS-CoV-2 infection [19].

This role of TLR7 in the antiviral response towards SARS-CoV-2 might represents a potential target for therapy, e.g., with imiquimod, in order to increase TLR7 activation and, consequently, its antiviral effect [26]. Again, alterations of other TLRs, such as TLR2, TLR4 and TLR6, are described associated to excessive inflammation in COVID-19 patients, suggesting the modulation of TLRs as prophylaxis for SARS-CoV-2 infection [19].

Both genomic and subgenomic SARS-CoV-2 RNAs are replicated via double-stranded intermediates in the cytoplasm [27]. In this case, RIG-I and MDA5 play a crucial role in the SARS-CoV-2 dsRNA sensing. Taisho et al., reported a peculiar recognition of the 3' untranslated region of the SARS-CoV-2 RNA genome by RIG-I helicase domains which inhibits the activation of the conventional MAVS-dependent pathways, avoiding cytokine induction. Nevertheless, the interaction of RIG-I with the viral genome directly abrogates viral RNA-dependent RNA polymerase mediation of the first step of replication. These findings suggest the distinctive role of RIG-I as a restraining factor in the early phase of SARS-CoV-2 infection in human lung cells [28]. The crucial role of RLRs in SARS-CoV-2 infection management is also demonstrated by Yang et al., that showed that a deficiency in MDA5, RIG-I or MAVS enhanced viral replication [29].

Since the virus could take over by dampening IFNs antiviral effect, the proinflammatory response increases due to the high infiltration of monocytes/macrophages, neutrophils, and several other adaptive immune cells from the bloodstream, resulting in the typical COVID-19 associated "cytokine storms" (Figure 3).

In addition, the formation of aggregates composed by extracellular DNA fibers, histones, microbicidal proteins, and proteases released from the recruited neutrophils, named also extracellular traps (NETs), causes an hyperinflammatory environment that amplifies the innate immune response, prolonging the recruitments of monocyte/macrophages, neutrophils, NK cells and eosinophils, leading to intensified tissue damage associated with acute respiratory distress syndrome (ARDS) (Figure 3) [30].

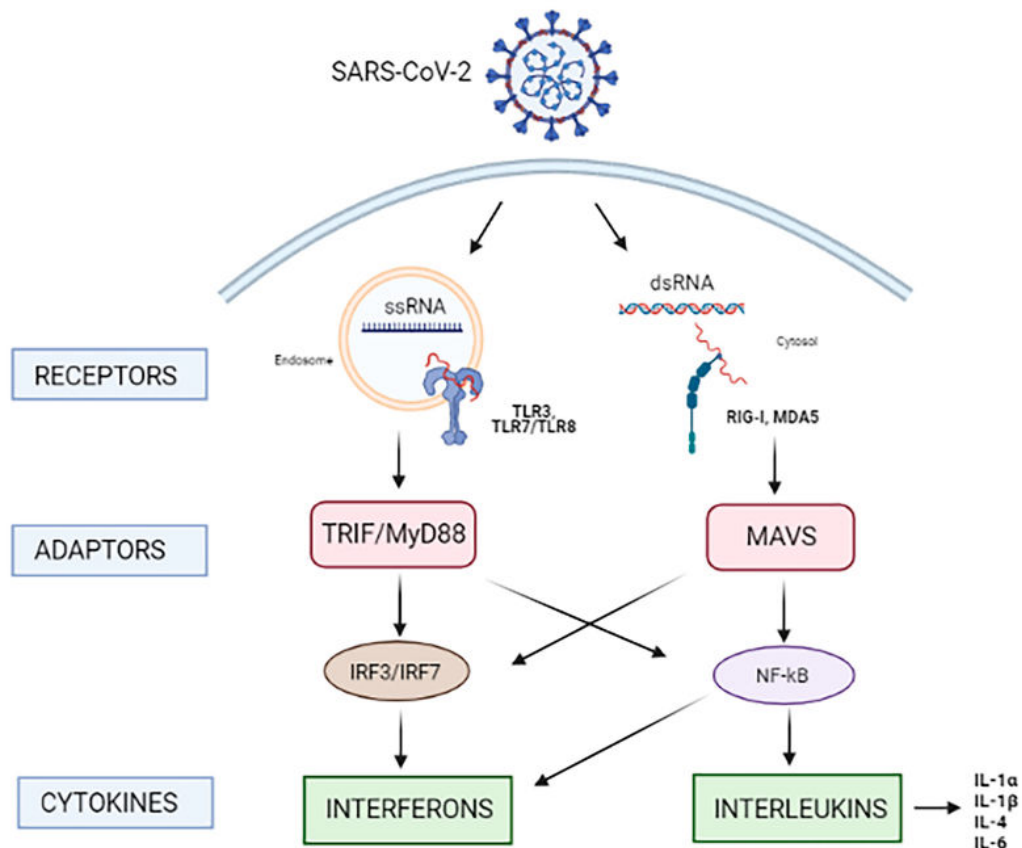


Figure 2. SARS-CoV-2 RNA sensing. After host cells viral infection, SARS-CoV-2 genome is sensed by endosomal Toll-like receptors (TLRs) TLR3, TLR7 and TLR8. TLRs recruit adaptor proteins TIR-domain-containing adapter-inducing interferon- β (TRIF) and myeloid differentiation factor 88 (MyD88). The sensing of replicating virus also occurs by cytosolic RIG-I-like receptors (RLRs) retinoic acid inducible gene I (RIG-I) and melanoma differentiation associated protein (MDA5), that recognize the subgenomic dsRNA of SARS-CoV-2. RIG-I and MDA5 recruit the mitochondrial antiviral signaling protein (MAVS). TLRs and RLRs signaling activate downstream transcription factors, including interferon regulatory factor 3 and 7 (IRF3 and IRF7) and nuclear factor kappa light-chain-enhancer of activated B cells (NF- κ B), resulting in production of antiviral interferons and different chemokines (IL-1 α , IL-1 β , IL-4 e IL-6), which in turn leads to the IRF-3 and IRF-7 phosphorylation required for the expression of IFNs.

As previously discussed, in a significant proportion of infected patients, SARS-CoV-2 induces severe symptoms that are often caused by high levels of pro-inflammatory cytokines which are in part released because of NETs generation, found in more than 80% of neutrophils from COVID-19 patients.

NETs formation follows a multistep process called NETosis, which includes at least three mechanisms: (i) the classical or suicidal NETosis, (ii) the noncanonical pathway, and (iii) the vital NETosis. Although these processes share key components, the required stimuli, the timing and the ultimate result are different [31].

In particular, the suicidal NETosis is triggered by the activation of toll-like receptors (TLRs) and complement receptors (CRs) by various ligands [31,32], the noncanonical pathway is stimulated by the lipopolysaccharide (LPS) of gram-negative bacteria, while vital NETosis can be activated by LPS via TLR4, activated platelets, complement proteins, and TLR2 ligands [33].

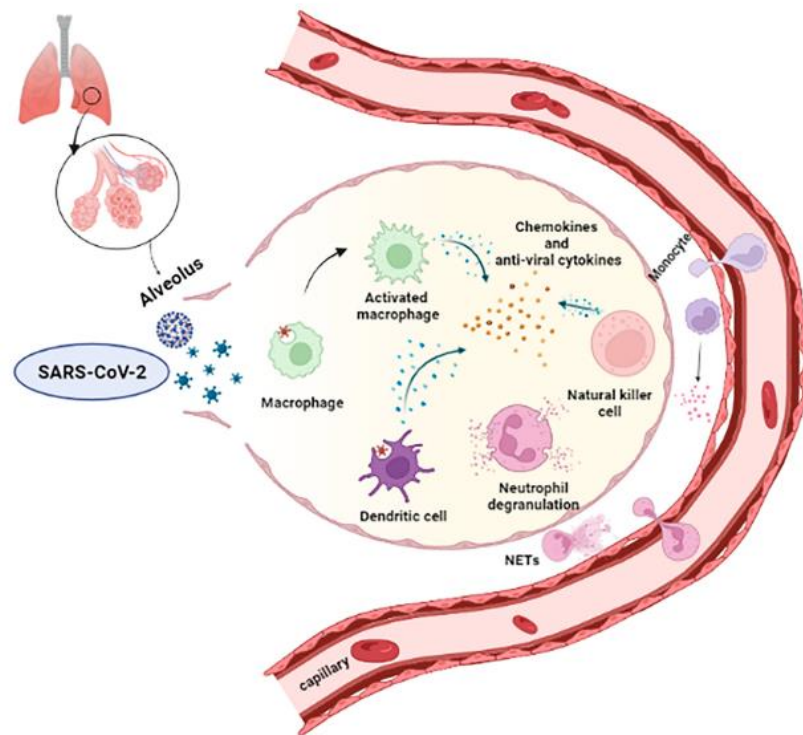


Figure 3. Innate immune response and cytokines storm in SARS-CoV-2 infected lung. The initial viral recognition by tissue-resident immune cells triggers a local innate response. The release of soluble factors, including proinflammatory cytokines and chemokines, from resident immune cells and infected epithelial cells attracts and activates neutrophils, monocytes, macrophages, dendritic cells (DC), natural killers (NK), and innate lymphoid cells into the site of infection, where they contribute to the elimination of the infected cells before virus spreading. This inflammatory environment increased immune cell infiltration from the bloodstream, triggering the “cytokine storm” condition. The hyperinflammation is also sustained by aggregates composed by extracellular DNA fibers, histones, microbicidal proteins, and proteases released from the recruited neutrophils, named also extracellular traps (NETs).

One of the major regulators of NETs formation is the peptidyl arginine deiminase type 4 (PAD4), an important intracellular mechanism of NETosis [34]. PAD4 participates in NETs formation by altering the chromatin status through the cooperation with the neutrophil elastase (NE) and myeloperoxidase [35]. The resulting decondensed chromatin discharged into the extracellular space and leads to neutrophil death, in a process also called NOX-dependent NETosis [36].

Since NETs release by neutrophil is mediated by PAD4 activation, these results suggest that in COVID-19 patients circulating neutrophils might be more susceptible to the release of PAD4-dependent NETs, which might cause the systemic increase of soluble NETs observed [37].

In addition, in studies performed on murine models of infection and inflammation, the inhibition of PAD4 resulted in reduced NET-associated lung injury [38,39], suggesting the systemic or pulmonary administration of PAD4 inhibitors as a potential treatment for severe COVID-19 [40]. Whilst the idea of blocking NET formation is gaining attraction as a potential therapy for the treatment of severe COVID-19 [40–42], this approach could also result in reduced anti-microbial immunity. In fact, although deleterious when generated in excess, NETs play an important role in the entrapment, neutralization and eradication of

bacterial and fungal pathogens [43,44] and consequently the use of PAD4 inhibitors could increase the susceptibility of severe COVID-19 patients to secondary infections.

3.2. SARS-CoV-2 Inflammasome and Interferon Response

In addition to NETs generation, several studies investigated other possible causes of the characteristic hyperinflammatory environment associated to COVID-19, evidencing that another crucial condition is represented by the ability of SARS-CoV-2 to directly or indirectly activate inflammasomes.

In severe manifestations of COVID-19, a massive inflammatory response appears to occur through stimulation of the pyrin domain-containing 3 (NLRP3) inflammasome, that consists in the sensor NLRP3, a NOD-like receptor that interacts with the N-terminus of the adapter protein ASC (also known as PYCARD) via PYD–PYD interactions and an the effector caspase 1, recruited by the caspase recruitment domain (CARD) present in the C-terminus of ASC [45]. The involvement of NLRP3-inflammasome in COVID-19 is confirmed by SARS-CoV-2 N protein possibility to directly interact with NLRP3, thus promoting the inflammasome activation (Figure 4) [46,47].

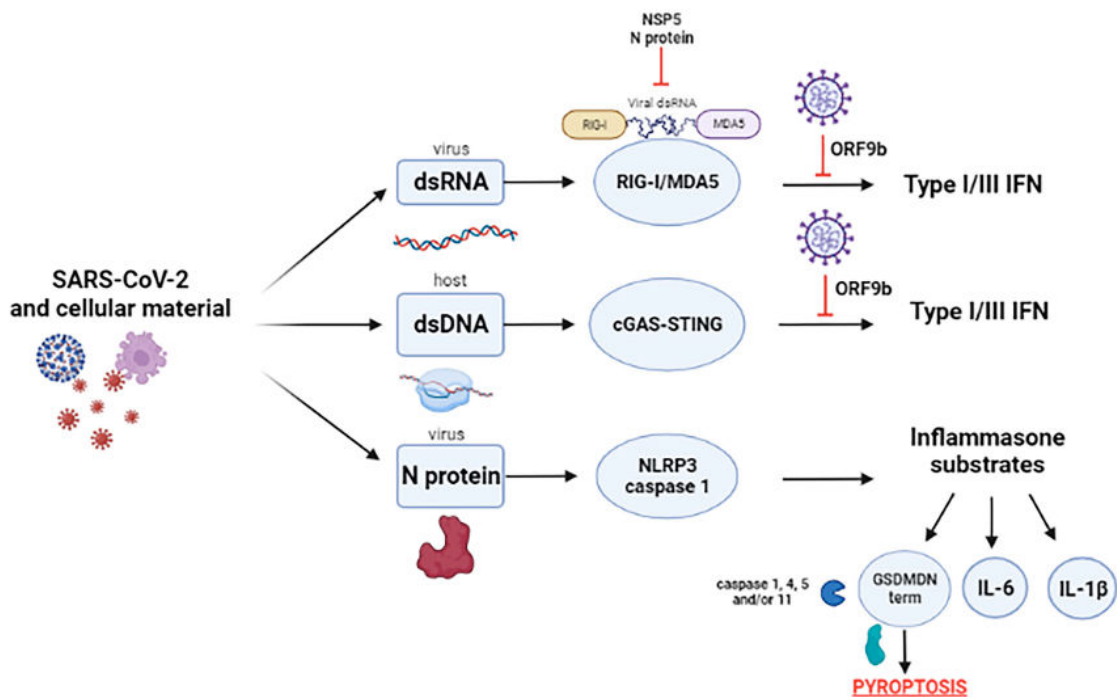


Figure 4. Virus- and host-derived molecules are sensed by several PRRs (Pathogen Recognition Receptors) to induce antiviral and inflammatory responses. SARS-CoV-2 ORF9b and NPS5/N proteins inhibit the activation of type I/III IFNs induced by retinoic acid-inducible gene I (RIG-I)/melanoma differentiation associated protein (MDA5)—mitochondrial antiviral-signaling protein (MAVS) and Cyclic GMP-AMP synthase (cGAS)—Stimulator of Interferon Genes (STING) signaling. SARS-CoV-2 N protein is also able to activate pyrin domain-containing 3 (NLRP3) inflammasome, whose main activation marker is caspase 1, that can lead to the production of IL1B and IL-6 and to pyroptosis, through gastermin D (GSDMD) Nterm cleavage by caspase 1, 4, 5, and/or 11.

Once activated, NLRP3 inflammasome causes the release of several proinflammatory cytokines, including IL-6 and IL-1β (Figure 4) [48], which have been reported to have a key role in the pathogenesis of acute lung injury, included COVID-19, affecting type II alveolar epithelial cells ACE2 expression [49,50].

Moreover, NLRP3 activation can lead to pyroptosis, an inflammatory programmed cell death pathway activated through Gasdermin D (GSDMD) cleavage by caspase 1, 4, 5, and/or 11 (Figure 4) that takes place in T lymphocytes and is crucial in the pathogenetic process associated to viral infections [51]. GSDMD triggers pyroptosis by exposing its amino-terminal cell death domain (GSDMDN_{term}) after caspase cleavage and, in this cleaved form, GSDMD can insert into the cell membrane by binding phosphatidylinositol phosphates and phosphatidylserines, forming pores that kill the cell from within [52,53].

Interestingly, even if SARS-CoV-2 infection promotes activation of the NLRP3 inflammasome involving caspase-1, it has been reported that its nucleocapsid proteins are able to inhibit host pyroptosis by blocking GSDMD cleavage [54]. The nucleocapsid binds GSDMD and hinders GSDMD processing by caspase-1, therefore these insights into how SARS-CoV-2 antagonizes cellular inflammatory responses may open new perspectives for COVID-19 treatment.

Although SARS-CoV-2 provokes a pro-inflammatory state, antiviral responses, such as IFNs release, result decreased.

Regarding the pathways driving IFN responses to SARS-CoV-2 infection, it is well known that the virus is a poor type I IFN inducer *in vitro* [55] and IFN-I analysis on a cohort of 50 COVID-19 patients with various disease severity revealed a highly impaired IFN-I response (characterized by no IFN- β and low IFN- α production and activity), which was associated with a persistent viremia and an exacerbated inflammatory state [56]. However, other findings have shown the presence of neutralizing IFN-I antibodies in critical COVID-19 patients [57] and account for up to 20% of cases of COVID-19 death [58].

Among the pathways involved in the altered IFN-I response, RIG-/MDA-5-MAVS and cGAS-STING signaling seem to be particularly involved.

As said above, during SARS-CoV-2 infection, it was expected that the viral ssRNA would be detected by RIG-I and MDA5 RNA sensors, in analogy to other coronaviruses [59]. Despite this evidence, there are numerous findings reporting low amounts and delayed kinetics of these cytosolic RNA sensors, which affect the expression of type I and III IFN in SARS-CoV-2-infected cell lines [60,61]. In particular, SARS-CoV-2 accessory genes ORF9b, an alternative open reading frame within the nucleocapsid (N) gene, has been found to inhibit the activation of types I and III IFNs at mitochondria level [62] by interfering with RIG-I/MDA5-MAVS signaling [63] (Figure 4). SARS-CoV-2 ORF9b also suppressed the induction of types I and III IFNs interfering with TRIF and Stimulator of Interferon Genes (STING) function (Figure 4), which are the adaptor protein for the endosome RNA-sensing pathway triggered by TLR3-TRIF and for the cytosolic DNA-sensing pathway involving the Cyclic GMP-AMP synthase (cGAS)-STING signaling, respectively. In particular, SARS-CoV-2 ORF9b inhibits TBK1 phosphorylation induced by both RIG-/MDA-5-MAVS and cGAS-STING signaling and consequently inhibits the phosphorylation and nuclear translocation of IRF3 and types I and III IFN transcription [63].

In addition, both NSP5 and N viral protein disrupted RIG-I-MAVS complex to attenuate the RIG-I-mediated antiviral immunity to affect the IFNs response, while the N protein also affected the recognition of dsDNA by RIG-I (Figure 4) [64].

Concerning cGAS-STING signaling, in both infected cell cultures and COVID-19 patient samples, a specific activation of NF- κ B mediated by cGAS-STING recruitment was described (Figure 4) and supported by its attenuation after treatment with several STING-targeting drugs [65]. Moreover, cGAS-STING activity was detected in lung samples of COVID-19 patients with prominent tissue destruction and associated with type I IFN responses. Indeed, a lung-on-chip model revealed that SARS-CoV-2 activates cGAS-STING signaling in endothelial cells through mitochondrial DNA release, leading to cell death and type I IFN production [66].

3.3. SARS-CoV-2 Effect on Monocytes and Macrophages

Monocytes and macrophages are antigen presenting cells (APCs) crucial in leucocytes recruitment and inflammation regulation [67] which ensure early responses to pathogens during acute infections.

Alterations of monocyte subset frequency has been reported in inflammatory diseases and infections [68], such as SARS-CoV-2 infection, characterized by low monocyte levels, that gradually increase following recovery [69].

Macrophages consist in a heterogeneous family of phagocytic cells tissue-resident [70].

Among these there are lung alveolar macrophages, distinguished into alveolar and interstitial macrophages, which include M1 and M2 macrophages [71]. During SARS-CoV-2 infection, TLR-4, 5, 3, 7 and 9 expressed by macrophages actively sense SARS-CoV-2 N and S proteins and promote M1 polarization of these cells [72].

It has been recently suggested that monocytes/macrophages participate in the onset of cytokine storms observed in COVID-19 patients, and their function seems to be associated to ARDS [73] and poor prognosis [74–77] in presence of high CCL2 and CCL7 levels [78]. On the other hand, this high percentages of monocyte/macrophages is co-present with lymphopenia.

Moreover, the expression of viral receptor ACE-2, furin and TMPRSS2 (transmembrane protease serine 2), has been demonstrated in an alveolar mice model [79], suggesting that these cells can be targeted by SARS-CoV-2. Again, monocytes and macrophages culturing in the presence of SARS-CoV-2 S and N proteins resulted in high levels of IL-6 [80] (Figure 5).

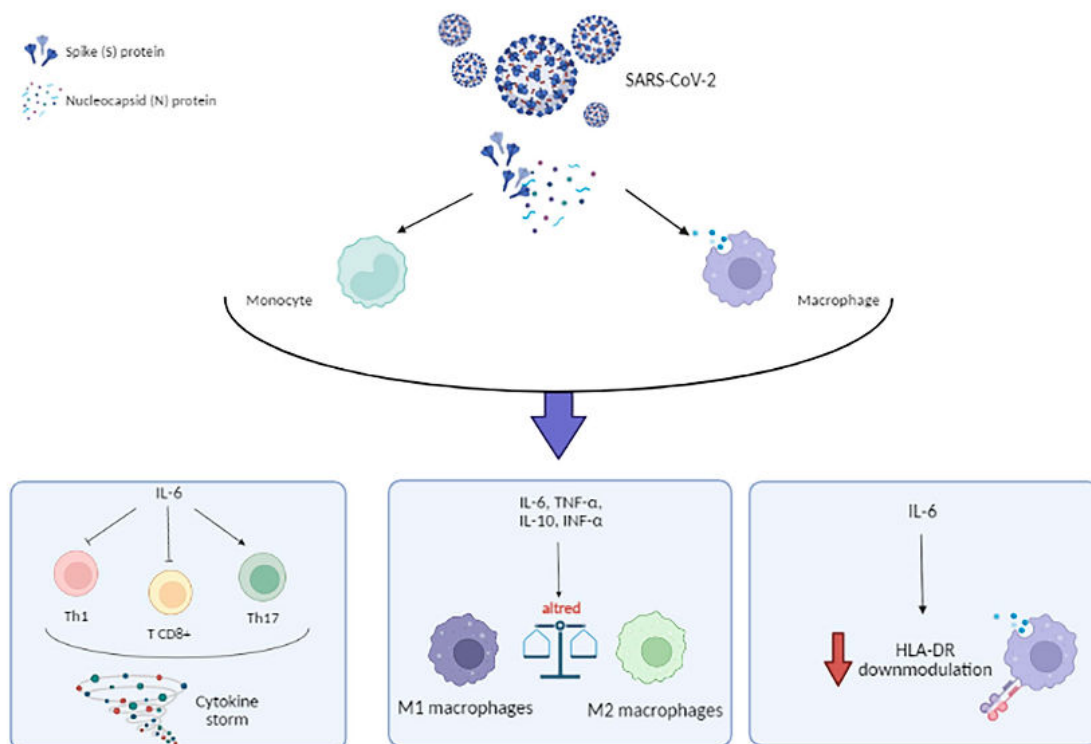


Figure 5. Schematic representation of monocytes/macrophages activation by SARS-CoV-2 Spike (S) and Nucleocapsid (N) proteins and their effect on cytokine profile and Human Leukocyte Antigen-DR (HLA-DR) down-modulation.

In fact, IL-6 plays a central role in SARS-CoV-2-induced cytokine storms associated to ARDS condition [81,82] through Th1 [83,84] and CD8+ T cell inhibition [85] and promotion of Th17 differentiation [86] (Figure 5).

Typically, SARS-CoV-2 infection firstly stimulates the production of immunoregulatory cytokines by both monocytes and macrophages, and then the virus elicits a transient program dominated by the upregulation of IFN α gene [87]. The most interested cells in the phenotypic change are macrophages, because during viral infection their phenotype has been shown to shifted to an anti-inflammatory of M2 type (Figure 5).

During SARS-CoV-2 infection, monocytes/macrophages undergo different morphological and phenotypical changes. In particular, a shift from an anti-inflammatory M2 type to an excessive monocyte-macrophage activation is associated to respiratory failure in severe COVID-19 patients [88] (Figure 5), characterized by subsets of mixed M1/M2 macrophage, higher expression of CD80 and CD206 and secretion of IL-6, IL-10, TNF- α , compared to controls [88].

As APCs, also SARS-CoV-2 effect on Human Leukocyte Antigen [89] expression on monocyte and macrophage is crucial in the control of the infection. In particular, alteration of specific HLA class II, named HLA-DR, often occurs in response of viral infections [90]. It has been observed that severe COVID-19 present low expression of HLA-DR on monocytes [91] in correlation with ICU (Intensive Care Unit) need (Figure 5) [92,93], probably due to the antagonizing action of IL-6 (Figure 5) [94]. Consequently, HLA-DR decreased expression might be a marker of immune suppression during SARS-CoV-2 infection [91,94].

3.4. Role of Neutrophils in COVID-19

Neutrophils are the drivers of hyperinflammation, through degranulation of primary granules and pro-inflammatory cytokines release [95], known to be implicated in COVID-19 pathology [41,96]. Despite their functional protective role, neutrophils extensive and prolonged activation that may occur during SARS-CoV-2 infection, might lead to detrimental effects in the lungs, resulting in cellular infiltrations, ARDS and increased mortality [97]. In fact, high neutrophil count correlate with COVID-19 severity and has been reported to be prognostic marker of ARDS and death [98,99].

Chemokines produced during COVID-19-ARDS recruit neutrophils in the site of infection, supported by transcriptional analysis of bronchoalveolar lavage fluid from patients with high levels of CXCL-2 and CXCL-8 [100,101]. Once recruited in the site of infection, neutrophils release different proinflammatory mediators, including cytokines (interferon- α , interferon- β , tumor necrosis factor, and interleukins 1 β , 6, and 10) and chemokine (e.g., CXCL10) that participate in COVID-19 pathogenesis [102].

In particular, lung autopsies from patients with ARDS revealed occlusion of pulmonary vessels by NETs, generated by neutrophils-recruitment into alveolar spaces mainly by IL-1b [103] that participate to cytokine overproduction and ARDS [104].

Indeed, high levels NETs DNA complexes have been found in serum samples from hospitalized COVID-19 patients, compared to patients with mild/moderate disease and healthy controls [105,106], confirming that the increased infiltration of neutrophil in severe cases contributes to the imbalance of lung's immune response [95].

During neutrophils recruitment to the inflammatory site, endothelial cell-surface molecules have a crucial role, in particular E-selectin and Intercellular Adhesion Molecule-I (ICAM-I). Bortolotti et al. reported that during COVID-19 the expression of these molecules might be modified by HLA-G [35], an immunomodulatory non classical HLA class-I molecule already described associated to COVID-19 condition [107].

3.5. SARS-CoV-2 Effect on Natural Killer Cells Activity

NK cells belong to the innate immune system and can recognize pathogens since the early phases of infection. NK cell activation toward infected cells is mainly based on the detection of HLA-I molecule expressed on target cells, that leads to NK cell cytotoxicity when HLA-I is absent. This recognition depends on the engagement of inhibitory and activating NK cell receptors (NKR) [108], including CD94/NKG2A, CD94/NKG2C, CD94/NKG2E,

NKG2D, leukocyte immunoglobulin-like receptors (LILR) and Killer Immunoglobulin-like Receptors (KIR) [109].

It has already been discussed that COVID-19 patients develop an uncontrolled immune response associated with lymphopenia [110,111], showing the reduction of T cell and CD8+ T cell count [112,113], as well as NK cells. Moreover, COVID-19 NK cells have shown a functional exhaustion that, together with their reduced number, have been correlated with the severity of clinical presentation and outcome of the disease [114]. Furthermore, to confirm the key role of NK cells in the outcome of COVID-19, there are some individuals which physiologically have lower expansion and functions of these cells (older patients and immunosuppressed), that exhibited a higher susceptibility to severe and fatal form of COVID-19 [115,116].

The NK cell decrease observed after SARS-CoV-2 infection can be the consequence of both cell death and cell redistribution in infected sites. Xiong et al. showed that several upregulated genes in PBMCs from COVID-19 patients are involved in the apoptosis pathways, suggesting that the peripheral decreased NK cell number may be due to cell-death [100]. By contrast, in favor to the lungs target-site sequestration mechanism, analysis of bronchoalveolar lavage fluid (BALF) samples allowed the detection of higher amounts of NK cells in COVID-19 patients as compared to controls [117]. These data suggest that, upon SARS-CoV-2 infection, NK cells exit the peripheral blood and moves into the lung where they potentially contribute to local inflammation and injury. By contrast, circulating NK cells display an exhausted phenotype that facilitate virus spread to other organs.

This reduction of NK cells functions is firstly related to local and systemic inflammation. Specifically, elevated IL-6 and IL-10 levels observed in COVID-19, can inhibit NK cytotoxicity, mediated by Granzyme-B production, Fas/FasL (Fas ligand) interaction and CD16 binding with the Fc (constant fraction) of antibodies. Moreover, IL-6 may further impair NK activity by reducing the expression of the activating NKG2D receptor (Figure 6) [118].

The reduced peripheral NK cell count and impaired cytotoxic activity observed in severe SARS-CoV-2-infected subjects, together with the increase of circulating IL-6 levels, suggests that the functional impairment of NK activity leads to enhanced innate immune cell activation with massive proinflammatory cytokine production [119,120].

Another very interesting mechanism of NK cell exhaustion during COVID-19 involving the inhibitory NKG2A receptor has been hypothesized. Zheng et al. observed a significant overexpression of NKG2A receptor (Figure 6) that was decreased simultaneously with the increase in the number of NK cells when the patients were rescued after the infection [112].

The involvement of NKG2A receptor in the mechanisms exploited by SARS-CoV-2 to affect NK cells activation have been investigated by Bortolotti et al. [121]. In this work, authors evaluated the possible effect of SARS-CoV-2 spike proteins (SP) expression by lung epithelial cells on NK cell recruitment and activation [122], reporting that the intracellular expression of SP1 by lung cells reduces the activation of NK cells and their ability to degranulate, identifying SP1 as a causative agent of NK cell function inactivation.

To better understand the molecular mechanisms exploited by this viral protein in controlling NK cells activation, Bortolotti et al. [121] have enlarged the study to the possible involvement of NK cell receptors and ligands.

As mentioned above, HLA molecules partly control NK cells via the interaction with their specific NKRs [123] and it has been demonstrated that SP1 is able to specifically up-regulate HLA-E on lung epithelial cells (Figure 6), which is stabilized by SP1-derived HLA-E binding peptide, and at the same time provoked the overexpression of CD94/NKG2A inhibitory receptor levels on NK cells (Figure 6) [121]. These data are in agreement with the recognized crosstalk between HLA-E and CD94/NKG2A, that induces a higher surface level of HLA-E molecules concurrently with a prevalent expression of NKG2A receptor on the surface of NK cells [124].

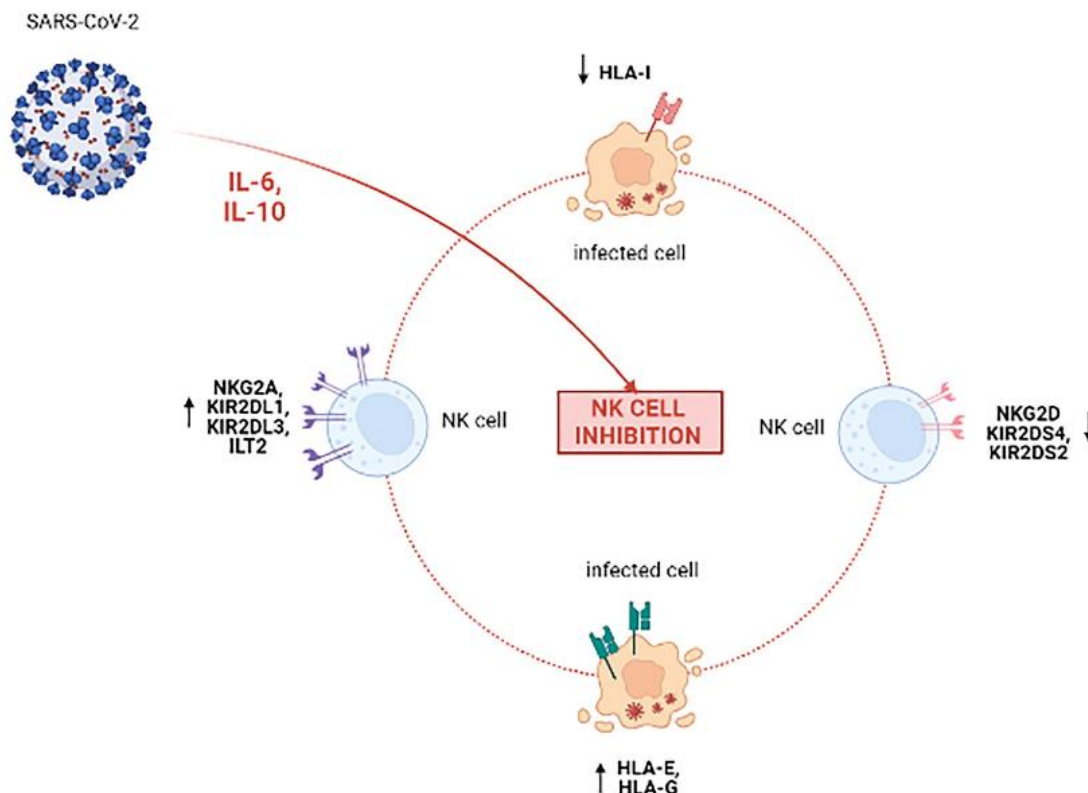


Figure 6. Impairment of NK cells' functions during SARS-CoV-2 infection. The release of cytokines such as interleukin (IL)-6 and IL-10 affects NK cell activation through changes in NK receptor and HLA molecules expression.

In addition, individual genetic asset could also contribute to explain the variability in the response of NK cells to SARS-CoV-2. In fact, it has been found out that severe COVID-19 patients showed non-functional or reduced activating receptors (e.g., KIR2DS2) and the prevalence of inhibitory KIRs, in particular of KIR2DL1 and KIR2DL3 (Figure 6) [125–128], and patients recovering from mild or moderate infection showed the increase of ILT2 inhibitory receptors (Figure 6).

Taken together, these data confirm that patients with severe COVID-19 have a severely compromised innate immune response likely due to a functional exhaustion of peripheral NK cells. Thus, this innate immunity compromise caused by NK cells function exhaustion, is likely to be the direct effect of SARS-CoV-2 infection [129,130].

4. SARS-CoV-2 Innate Response and Acquired Immunity Cross-Talk

Activation of innate immune system during SARS-CoV-2 infection is crucial in determining the induction of an efficient T and B cell response to obtain specific antibodies secretion and cell-mediated killing of infected cells [131].

During SARS-CoV-2 infection, peptides synthesized during viral replication are loaded on HLA class I proteins and presented on the surface of infected cells. The viral peptide-HLA-I complexes recognition by CD8+ cytotoxic T cells induces their activation and expansion [132], leading to the development of virus-specific effector and memory T cells. Moreover, also CD4+ helper T cell, mostly T helper 1 lymphocytes (Th1) and T helper 17 lymphocytes (Th17) [133] recognize SARS-CoV-2 antigens bound by HLA class II (MHLA-II) on professional Antigen presenting cells (APCs) and in turn Follicular helper (FH) T contribute to B cell activation into plasma cells (PC), that release specific anti-SARS-CoV-2

antibodies. At first, IgM are released during the acute phase of infection [134], followed by IgG or secretory IgA, that will also persist as part of immunological memory [135] (Figure 7).

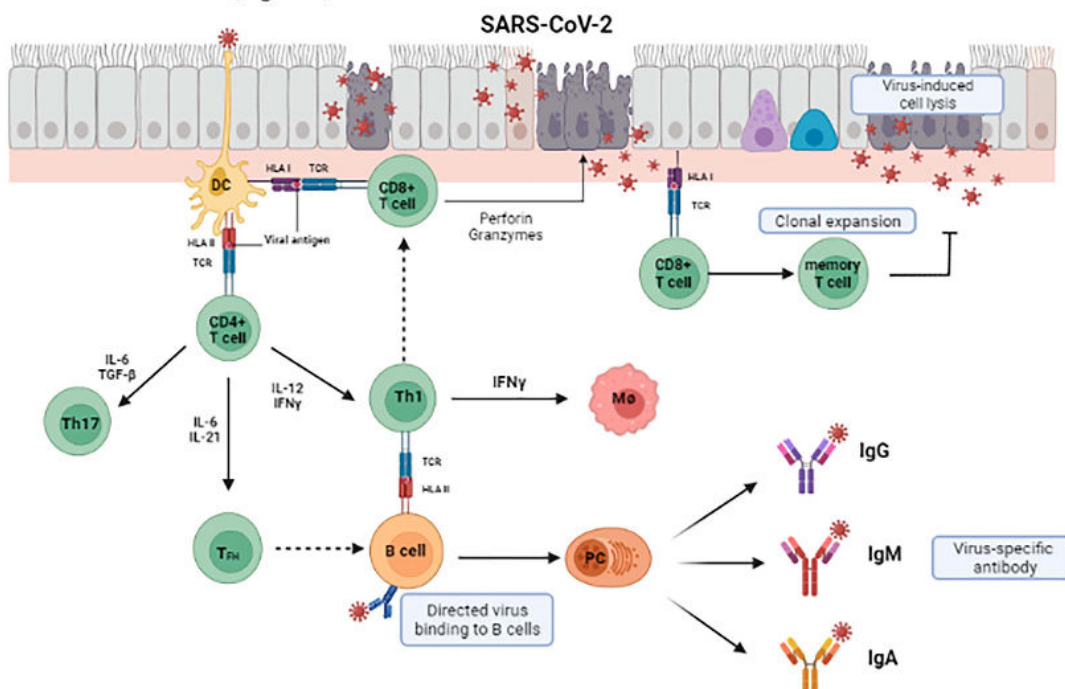


Figure 7. Adaptive immune response during SARS-CoV-2 infection. CD8+ T lymphocytes cytotoxicity is induced by recognition of viral antigens expressed on infected epithelial cells. Subepithelial dendritic cells (DC) recognize and present SARS-CoV-2 antigens to CD4+ T lymphocytes, inducing IFN- γ secretion and their differentiation toward memory T helper 1 lymphocytes (Th1), T helper 17 lymphocytes (Th17), and T follicular helper (TFH). TFH helps B cells to develop into plasmacells (PC) and promote the production of IgM, IgA, and IgG isotype SARS-CoV-2-specific antibodies, while Th1, once activated by B cell antigen presentation, activates naïve monocyte (M ϕ), through IFN- γ secretion.

Among APCs, dendritic cells (DCs) represent an important point of junction between innate and adaptive immunity during viral infections. In fact, DCs correct procession and presentation of viral epitopes is fundamental to guarantee a successful B and T cell priming [136].

The antigenic anatomy of APC/T cell interactions, mediated by HLA-II molecules, is critical to the initiation of productive immune events. In fact, different HLA haplotypes are related to a different susceptibility for distinct diseases, including COVID-19. Nguyen et al. [137] sampled the SARS-CoV-2 proteome for interactions with HLA antigens and found that patients characterized by HLA-B*46:01 had the least predicted binding sites for SARS-CoV-2 peptides. However, they also found that the individuals who were HLA-B*15:03 positive showed the highest capacity to bind SARS-CoV-2 peptides. They conclude that individual genetic variations may be critical to the generation of sterilizing immunity to SARS-CoV-2 as well as generation of responses to vaccines. In addition, HLA class I phenotypical variations are important in directing CD8+ T cell responses that mediate cytotoxicity. Poulton et al. [138] found a significant association between HLA-DQB1*06 and SARS-CoV-2 infection risk in transplant patients. A further study in an Italian transplant population, found that HLA-DRB1*08 showed no peptide binding to SARS-CoV-2 peptides, in association with increased mortality from SARS-CoV-2 [139]. This finding suggests that HLA antigen typing can identify individuals at higher risk for SARS-CoV-2 infection,

which could also be ‘super-spreaders’ and at higher risk to develop a severe COVID-19 and poor responses to vaccines [140].

The severe complications associated with SARS-CoV-2 infection encouraged the development of different vaccination strategies. All the vaccine designs, as inactivated and protein subunit vaccines, viral vector vaccines and mRNA vaccines, strongly induce both humoral and cellular specific immunity [141]. For example, SARS-CoV-2 Spike protein encoded by mRNA-based vaccines, once translated and presented by host cells, stimulates Th1, CD8+ T and B cells activation, inducing the production of specific neutralizing antibodies against the virus and normally trigger immune memory, preserving the individual from the developing of the disease. Of course, the production of immunostimulatory epitopes and their efficient presentation by APC are at the basis of a successful immunization.

The mRNA-based SARS-CoV-2 vaccines elicit antibody responses against the Receptor Binding Domain (RBD) of the spike protein, targeting the same epitopes as occur in natural infection, leading to the production of neutralizing antibodies that target the same epitopes as those produced by natural infection. A study conducted on patients infected by SARS-CoV-2 and subjects vaccinated with Pfizer and Moderna mRNA-based vaccines showed the presence of high titers of IgM and IgG anti-SARS-CoV-2 Spike protein RBD eight weeks after the second injection of vaccine. Moreover, the plasma neutralizing activity and relative numbers of RBD-specific memory B cells of vaccinated volunteers were equivalent to those of individuals who had recovered from natural infection [142,143] and potently neutralize SARS-CoV-2 by targeting a number of different RBD epitopes in common with monoclonal antibodies isolated from infected donors [144–146].

5. SARS-CoV-2 Immuno-Escaping Mechanisms

As already discussed, innate immune system activation during viral infection leads mainly to IFNs and cytokines production in order to eliminate invading viruses. As other viruses, also SARS-CoV-2 is able to exploit different escape strategies to avoid immune system recognition.

For example, Min et al. [147] have showed how IFN pathway can be a prime target for immune evasion, which could be inhibited by suppressing IFN induction (through decreasing potential PAMPs or disrupting the signaling cascades of IFN induction), function or production. In addition, Kasuga et al. [148] have showed that SARS-CoV-2 proteins, such as nucleocapsid (N) and membrane (M) proteins, are involved in interfering and suppressing IFN signaling [119,149].

The recent concern about virus mutations and their effects is further justified by the fact that RNA viruses are characterized by higher mutation rates [150] and SARS-CoV-2 genome alterations are estimated to be 1–2 mutations every month [151]. The genetic diversity of SARS-CoV-2 is the result of errors generated by its RNA-dependent RNA polymerase (RdRp) and recombination [152]. The capacity of coronaviruses to recombine plays a significant role in their evolution and is associated with the strand switching ability of RdRp. As long as a significant number of the world population is infected with SARS-CoV-2, mutations will continue to occur because of the huge number of genome replications and error-prone replication. Therefore, new variants will continue to emerge, and some of them may pose a greater risk for immune escape, being the result of mutations derived by selection based on fitness advantage.

Notably, the main evasive strategy adopted by SARS-CoV-2 is represented by Spike protein mutation acquisition.

SARS-CoV-2 has different spike protein variants categorized based on their spreading ability, disease severity, immunity, and treatment response. As of 21 October 2021, the European Centre for Disease Prevention and Control (ECDC) classified variants of concern (VOC), including Beta or B.1.351 (K417N, E484K, N501Y, D614G, A701V), Gamma or P.1 (K417T, E484K, N501Y, D614G, H655Y), and Delta or B.1.617.2 (L452R, T478K, D614G, P681R); variants of interest (VOI), involving Mu or B.1.621 (R346K, E484K, N501Y, D614G, and P681H) and Lambda or C.37 (L452Q, F490S, and D614G); whereas variants under

monitoring include various spike protein mutations circulating in different parts of the world [153]. In addition to these, on 26 November 2021 another variant has been designed as VOC [154], which is known as Omicron or B.1.1.529.

In particular, most mutations on SARS-CoV-2 spike protein occur within RBD fragment, especially in the—RBM (S438 to Q506 and K417)—residues involved in ACE2 binding [155,156], suggesting that RBD is the substantial immune-dominance region of SARS-CoV-2 spike protein.

Since all the available vaccination strategies are based on SARS-CoV-2 Spike protein immunization and aim to induce a strong acquired immune response [139], alterations on this protein not only might increase viral tropism and spreading by enhancing its interaction with cellular receptors, but also decreasing vaccines efficiency [89].

Furthermore, SARS-CoV-2 evasion of lymphocytes responses has been investigated in vitro, showing that mutations on SARS-CoV-2 Spike and other viral proteins (HLA-I-restricted epitopes) are able to evade in vitro CD8+ T cell responses through abolishing HLA-I binding [157].

In addition, in order to reduce HLA-I presentation, SARS-CoV-2 open reading frame 8 (ORF8) is responsible for mediating HLA-I down-modulation by directly interacting with these molecules [158]. The result is that SARS-CoV-2-infected cells by expressing ORF8 are much less sensitive to lysis by cytotoxic T lymphocytes and evade immune surveillance, due to the antigen presentation system impairment caused by this viral protein.

Moreover, SARS-CoV-2 can also infect regulatory T (Treg) cells through the binding of NRP1 [159], another coreceptor of SARS-CoV-2, thereby reducing Treg population and leading to uncontrolled host proinflammatory responses.

Again, SARS-CoV-2 has developed several strategies to escape innate immune system, based on TLRs and RLRs sensing interference by several viral proteins, thus affecting cytokine and interferon production (Figure 3) [9,147,148].

6. Conclusions/Perspectives

The central role of host innate immune system during SARS-CoV-2 infection is under investigation. Since innate immunity is involved in the earliest stages of SARS-CoV-2 infection, its correct activation is necessary to guarantee an efficient control of viral spread. The primary antiviral effect exerted by innate immune system, based mainly on interferons production and direct killing of infected cells by NK cells, cytokines secretion and a correct antigens presentation, is strictly connected to the activation of T and B lymphocytes. In view of this, the identification of the strategies able to improve the innate immune response towards SARS-CoV-2 infection might represent an advantage not only to control the natural infection, but also to increase the active immunization by vaccination. There are several courses of action that can be undertaken to effectively subdue the pandemic. At first, it would be necessary to closely monitor the emergence of novel SARS-CoV2 variants globally. Secondly, vaccination protocols should be adjusted to current variants. Finally, an effort should be made to develop therapeutic protocols involving monoclonal antibodies in order to offer reliable protection against emerging variants.

Author Contributions: D.B. and R.R.; conceptualization, D.B. and R.R.; writing—original draft preparation, G.S., S.B. and S.R.; writing—review and editing, D.B., R.R. and S.R.; supervision. All authors have read and agreed to the published version of the manuscript.

Funding: This research received no external funding.

Acknowledgments: We thank Mercedes Fernandez for literature analysis and Alessandro Sofia for informatic technical support.

Conflicts of Interest: The authors declare no conflict of interest.

References

- Shah, M.; Ahmad, B.; Choi, S.; Woo, H.G. Mutations in the SARS-CoV-2 spike RBD are responsible for stronger ACE2 binding and poor anti-SARS-CoV mAbs cross-neutralization. *Comput. Struct. Biotechnol. J.* **2020**, *18*, 3402–3414. [[CrossRef](#)]
- Wang, K.; Chen, W.; Zhou, Y.-S.; Lian, J.-Q.; Zhang, Z.; Du, P.; Gong, L.; Zhang, Y.; Cui, H.-Y.; Geng, J.-J.; et al. SARS-CoV-2 invades host cells via a novel route: CD147-spike protein. *Signal Transduct. Target. Ther.* **2020**, *5*, 1–10. [[CrossRef](#)]
- Cantuti-Castelvetri, L.; Ojha, R.; Pedro, L.D.; Djannatian, M.; Franz, J.; Kuivanen, S.; van der Meer, F.; Kallio, K.; Kaya, T.; Anastasina, M.; et al. Neuropilin-1 facilitates SARS-CoV-2 cell entry and infectivity. *Science* **2020**, *370*, 856–860. [[CrossRef](#)]
- Chekol Abebe, E.; Mengie Ayele, T.; Tilahun Muche, Z.; Asmamaw Dejenie, T. Neuropilin 1: A Novel Entry Factor for SARS-CoV-2 Infection and a Potential Therapeutic Target. *Biologics* **2021**, *15*, 143–152. [[CrossRef](#)]
- Bortolotti, D.; Simioni, C.; Neri, L.M.; Rizzo, R.; Semprini, C.M.; Occhionorelli, S.; Laface, I.; Sanz, J.M.; Schiuma, G.; Rizzo, S.; et al. Relevance of VEGF and CD147 in different SARS-CoV-2 positive digestive tracts characterized by thrombotic damage. *FASEB J.* **2021**, *35*, e21969. [[CrossRef](#)]
- Mayi, B.S.; Leibowitz, J.A.; Woods, A.T.; Ammon, K.A.; Liu, A.E.; Raja, A. The role of Neuropilin-1 in COVID-19. *PLoS Pathog.* **2021**, *17*, e1009153. [[CrossRef](#)]
- Geng, J.; Chen, L.; Yuan, Y.; Wang, K.; Wang, Y.; Qin, C.; Wu, G.; Chen, R.; Zhang, Z.; Wei, D.; et al. CD147 antibody specifically and effectively inhibits infection and cytokine storm of SARS-CoV-2 and its variants delta, alpha, beta, and gamma. *Signal Transduct. Target. Ther.* **2021**, *6*, 347. [[CrossRef](#)]
- Weisblum, Y.; Schmidt, F.; Zhang, F.; DaSilva, J.; Poston, D.; Lorenzi, J.C.; Muecksch, F.; Rutkowska, M.; Hoffmann, H.H.; Michailidis, E.; et al. Escape from neutralizing antibodies by SARS-CoV-2 spike protein variants. *eLife* **2020**, *9*, e61312. [[CrossRef](#)]
- Garcia, L.F. Immune Response, Inflammation, and the Clinical Spectrum of COVID-19. *Front. Immunol.* **2020**, *11*, 1441. [[CrossRef](#)]
- Song, P.; Li, W.; Xie, J.; Hou, Y.; You, C. Cytokine storm induced by SARS-CoV-2. *Clin. Chim. Acta* **2020**, *509*, 280–287. [[CrossRef](#)]
- Schultze, J.L.; Aschenbrenner, A.C. COVID-19 and the human innate immune system. *Cell* **2021**, *184*, 1671–1692. [[CrossRef](#)]
- Moher, D.; Shamseer, L.; Clarke, M.; Ghersi, D.; Liberati, A.; Petticrew, M.; Shekelle, P.; Stewart, L.A.; Group, P.-P. Preferred reporting items for systematic review and meta-analysis protocols (PRISMA-P) 2015 statement. *Syst. Rev.* **2015**, *4*, 1. [[CrossRef](#)]
- Mantel, N.; Haenszel, W. Statistical Aspects of the Analysis of Data from Retrospective Studies of Disease. *JNCI J. Natl. Cancer Inst.* **1959**, *22*, 719–748. [[CrossRef](#)]
- Fung, T.S.; Liu, D.X. Human Coronavirus: Host-Pathogen Interaction. *Annu. Rev. Microbiol.* **2019**, *73*, 529–557. [[CrossRef](#)]
- Lee, B.L.; Barton, G.M. Trafficking of endosomal Toll-like receptors. *Trends Cell Biol.* **2014**, *24*, 360–369. [[CrossRef](#)]
- Kawasaki, T.; Kawai, T. Toll-like receptor signaling pathways. *Front. Immunol.* **2014**, *5*, 461. [[CrossRef](#)]
- Jung, H.E.; Lee, H.K. Current Understanding of the Innate Control of Toll-like Receptors in Response to SARS-CoV-2 Infection. *Viruses* **2021**, *13*, 2132. [[CrossRef](#)]
- Cervantes-Barragan, L.; Zust, R.; Weber, F.; Spiegel, M.; Lang, K.S.; Akira, S.; Thiel, V.; Ludewig, B. Control of coronavirus infection through plasmacytoid dendritic-cell-derived type I interferon. *Blood* **2007**, *109*, 1131–1137. [[CrossRef](#)]
- Khanmohammadi, S.; Rezaei, N. Role of Toll-like receptors in the pathogenesis of COVID-19. *J. Med. Virol.* **2021**, *93*, 2735–2739. [[CrossRef](#)]
- Hur, S. Double-Stranded RNA Sensors and Modulators in Innate Immunity. *Annu. Rev. Immunol.* **2019**, *37*, 349–375. [[CrossRef](#)]
- Lowery, S.A.; Sariol, A.; Perlman, S. Innate immune and inflammatory responses to SARS-CoV-2: Implications for COVID-19. *Cell Host Microbe* **2021**, *29*, 1052–1062. [[CrossRef](#)]
- Amodio, G.; Mugione, A.; Sanchez, A.M.; Vigano, P.; Candiani, M.; Somigliana, E.; Roncarolo, M.G.; Panina-Bordignon, P.; Gregori, S. HLA-G expressing DC-10 and CD4(+) T cells accumulate in human decidua during pregnancy. *Hum. Immunol.* **2013**, *74*, 406–411. [[CrossRef](#)]
- Perlman, S.; Dandekar, A.A. Immunopathogenesis of coronavirus infections: Implications for SARS. *Nat. Rev. Immunol.* **2005**, *5*, 917–927. [[CrossRef](#)]
- Chen, J.; Subbarao, K. The Immunobiology of SARS*. *Annu. Rev. Immunol.* **2007**, *25*, 443–472. [[CrossRef](#)]
- Bortolotti, D.; Gentili, V.; Rizzo, S.; Schiuma, G.; Beltrami, S.; Strazzabosco, G.; Fernandez, M.; Caccuri, F.; Caruso, A.; Rizzo, R. TLR3 and TLR7 RNA Sensor Activation during SARS-CoV-2 Infection. *Microorganisms* **2021**, *9*, 1820. [[CrossRef](#)]
- Poulas, K.; Farsalinos, K.; Zanidis, C. Activation of TLR7 and Innate Immunity as an Efficient Method against COVID-19 Pandemic: Imiquimod as a Potential Therapy. *Front. Immunol.* **2020**, *11*, 1373. [[CrossRef](#)]
- Li, Y.; Renner, D.M.; Comar, C.E.; Whelan, J.N.; Reyes, H.M.; Cardenas-Diaz, F.L.; Truitt, R.; Tan, L.H.; Dong, B.; Alysandratos, K.D.; et al. SARS-CoV-2 induces double-stranded RNA-mediated innate immune responses in respiratory epithelial-derived cells and cardiomyocytes. *Proc. Natl. Acad. Sci. USA* **2021**, *118*. [[CrossRef](#)]
- Yamada, T.; Sato, S.; Sotoyama, Y.; Orba, Y.; Sawa, H.; Yamauchi, H.; Sasaki, M.; Takaoka, A. RIG-I triggers a signaling-abortive anti-SARS-CoV-2 defense in human lung cells. *Nat. Immunol.* **2021**, *22*, 820–828. [[CrossRef](#)]
- Yang, D.M.; Geng, T.T.; Harrison, A.G.; Wang, P.H. Differential roles of RIG-I like receptors in SARS-CoV-2 infection. *Mil. Med. Res.* **2021**, *8*, 49. [[CrossRef](#)]
- Beacon, T.H.; Su, R.C.; Lakowski, T.M.; Delcuve, G.P.; Davie, J.R. SARS-CoV-2 multifaceted interaction with the human host. Part II: Innate immunity response, immunopathology, and epigenetics. *IUBMB Life* **2020**, *72*, 2331–2354. [[CrossRef](#)]
- Jorch, S.K.; Kubes, P. An emerging role for neutrophil extracellular traps in noninfectious disease. *Nat. Med.* **2017**, *23*, 279–287. [[CrossRef](#)]

32. Yang, H.; Biermann, M.H.; Brauner, J.M.; Liu, Y.; Zhao, Y.; Herrmann, M. New Insights into Neutrophil Extracellular Traps: Mechanisms of Formation and Role in Inflammation. *Front. Immunol.* **2016**, *7*, 302. [\[CrossRef\]](#)
33. Tabrizi, Z.A.; Khosrojerdi, A.; Aslani, S.; Hemmatzadeh, M.; Babaie, F.; Bairami, A.; Shomali, N.; Hosseinzadeh, R.; Safari, R.; Mohammadi, H. Multi-facets of neutrophil extracellular trap in infectious diseases: Moving beyond immunity. *Microb. Pathog.* **2021**, *158*, 105066. [\[CrossRef\]](#)
34. Wang, Y.; Li, M.; Stadler, S.; Correll, S.; Li, P.; Wang, D.; Hayama, R.; Leonelli, L.; Han, H.; Grigoryev, S.A.; et al. Histone hypercitullination mediates chromatin decondensation and neutrophil extracellular trap formation. *J. Cell Biol.* **2009**, *184*, 205–213. [\[CrossRef\]](#)
35. Bortolotti, D.; Gentili, V.; Rizzo, S.; Schiuma, G.; Beltrami, S.; Spadaro, S.; Strazzabosco, G.; Campo, G.; Carosella, E.D.; Papi, A.; et al. Increased sHLA-G Is Associated with Improved COVID-19 Outcome and Reduced Neutrophil Adhesion. *Viruses* **2021**, *13*, 1855. [\[CrossRef\]](#)
36. Chen, T.; Li, Y.; Sun, R.; Hu, H.; Liu, Y.; Herrmann, M.; Zhao, Y.; Munoz, L.E. Receptor-Mediated NETosis on Neutrophils. *Front. Immunol.* **2021**, *12*, 775267. [\[CrossRef\]](#)
37. Veras, F.P.; Pontelli, M.C.; Silva, C.M.; Toller-Kawahisa, J.E.; de Lima, M.; Nascimento, D.C.; Schneider, A.H.; Caetite, D.; Tavares, L.A.; Paiva, I.M.; et al. SARS-CoV-2-triggered neutrophil extracellular traps mediate COVID-19 pathology. *J. Exp. Med.* **2020**, *217*. [\[CrossRef\]](#)
38. Lefrancais, E.; Mallavia, B.; Zhuo, H.; Calfee, C.S.; Looney, M.R. Maladaptive role of neutrophil extracellular traps in pathogen-induced lung injury. *JCI Insight* **2018**, *3*. [\[CrossRef\]](#)
39. Du, M.; Yang, L.; Gu, J.; Wu, J.; Ma, Y.; Wang, T. Inhibition of Peptidyl Arginine Deiminase-4 Prevents Renal Ischemia-Reperfusion-Induced Remote Lung Injury. *Mediat. Inflamm.* **2020**, *2020*, 1724206. [\[CrossRef\]](#)
40. Narasaraju, T.; Tang, B.M.; Herrmann, M.; Muller, S.; Chow, V.T.K.; Radic, M. Neutrophilia and NETopathy as Key Pathologic Drivers of Progressive Lung Impairment in Patients with COVID-19. *Front. Pharmacol.* **2020**, *11*, 870. [\[CrossRef\]](#)
41. Barnes, B.J.; Adrover, J.M.; Baxter-Stoltzfus, A.; Borczuk, A.; Cools-Lartigue, J.; Crawford, J.M.; Dassler-Plenker, J.; Guerci, P.; Huynh, C.; Knight, J.S.; et al. Targeting potential drivers of COVID-19: Neutrophil extracellular traps. *J. Exp. Med.* **2020**, *217*. [\[CrossRef\]](#)
42. Strich, J.R.; Ramos-Benitez, M.J.; Randazzo, D.; Stein, S.R.; Babyak, A.; Davey, R.T.; Suffredini, A.F.; Childs, R.W.; Chertow, D.S. Fostamatinib Inhibits Neutrophils Extracellular Traps Induced by COVID-19 Patient Plasma: A Potential Therapeutic. *J. Infect. Dis.* **2021**, *223*, 981–984. [\[CrossRef\]](#)
43. Brinkmann, V.; Reichard, U.; Goosmann, C.; Fauler, B.; Uhlemann, Y.; Weiss, D.S.; Weinrauch, Y.; Zychlinsky, A. Neutrophil extracellular traps kill bacteria. *Science* **2004**, *303*, 1532–1535. [\[CrossRef\]](#)
44. Urban, C.F.; Nett, J.E. Neutrophil extracellular traps in fungal infection. *Semin. Cell Dev. Biol.* **2019**, *89*, 47–57. [\[CrossRef\]](#)
45. Swanson, K.V.; Deng, M.; Ting, J.P. The NLRP3 inflammasome: Molecular activation and regulation to therapeutics. *Nat. Rev. Immunol.* **2019**, *19*, 477–489. [\[CrossRef\]](#)
46. Pan, P.; Shen, M.; Yu, Z.; Ge, W.; Chen, K.; Tian, M.; Xiao, F.; Wang, Z.; Wang, J.; Jia, Y.; et al. SARS-CoV-2 N protein promotes NLRP3 inflammasome activation to induce hyperinflammation. *Nat. Commun.* **2021**, *12*, 4664. [\[CrossRef\]](#)
47. Paludan, S.R.; Mogensen, T.H. Innate immunological pathways in COVID-19 pathogenesis. *Sci. Immunol.* **2022**, *7*, eabm5505. [\[CrossRef\]](#)
48. Freeman, T.L.; Swartz, T.H. Targeting the NLRP3 Inflammasome in Severe COVID-19. *Front. Immunol.* **2020**, *11*, 1518. [\[CrossRef\]](#)
49. Zhao, C.; Zhao, W. NLRP3 Inflammasome—A Key Player in Antiviral Responses. *Front. Immunol.* **2020**, *11*, 211. [\[CrossRef\]](#)
50. Xu, H.; Zhong, L.; Deng, J.; Peng, J.; Dan, H.; Zeng, X.; Li, T.; Chen, Q. High expression of ACE2 receptor of 2019-nCoV on the epithelial cells of oral mucosa. *Int. J. Oral Sci.* **2020**, *12*, 8. [\[CrossRef\]](#)
51. de Gassart, A.; Martinon, F. Pyroptosis: Caspase-11 Unlocks the Gates of Death. *Immunity* **2015**, *43*, 835–837. [\[CrossRef\]](#)
52. Shi, J.; Zhao, Y.; Wang, K.; Shi, X.; Wang, Y.; Huang, H.; Zhuang, Y.; Cai, T.; Wang, F.; Shao, F. Cleavage of GSDMD by inflammatory caspases determines pyroptotic cell death. *Nature* **2015**, *526*, 660–665. [\[CrossRef\]](#)
53. He, W.T.; Wan, H.; Hu, L.; Chen, P.; Wang, X.; Huang, Z.; Yang, Z.H.; Zhong, C.Q.; Han, J. Gasdermin D is an executor of pyroptosis and required for interleukin-1 β secretion. *Cell Res.* **2015**, *25*, 1285–1298. [\[CrossRef\]](#)
54. Ma, J.; Zhu, F.; Zhao, M.; Shao, F.; Yu, D.; Ma, J.; Zhang, X.; Li, W.; Qian, Y.; Zhang, Y.; et al. SARS-CoV-2 nucleocapsid suppresses host pyroptosis by blocking Gasdermin D cleavage. *EMBO J.* **2021**, *40*, e108249. [\[CrossRef\]](#)
55. Lei, X.; Dong, X.; Ma, R.; Wang, W.; Xiao, X.; Tian, Z.; Wang, C.; Wang, Y.; Li, L.; Ren, L.; et al. Activation and evasion of type I interferon responses by SARS-CoV-2. *Nat. Commun.* **2020**, *11*, 3810. [\[CrossRef\]](#)
56. Hadjadj, J.; Yatim, N.; Barnabei, L.; Corneau, A.; Boussier, J.; Smith, N.; Pere, H.; Charbit, B.; Bondet, V.; Chenevier-Gobeaux, C.; et al. Impaired type I interferon activity and inflammatory responses in severe COVID-19 patients. *Science* **2020**, *369*, 718–724. [\[CrossRef\]](#)
57. Bastard, P.; Rosen, L.B.; Zhang, Q.; Michailidis, E.; Hoffmann, H.H.; Zhang, Y.; Dorgham, K.; Philippot, Q.; Rosain, J.; Beziat, V.; et al. Autoantibodies against type I IFNs in patients with life-threatening COVID-19. *Science* **2020**, *370*, eabd4585. [\[CrossRef\]](#)
58. Bastard, P.; Gervais, A.; Le Voyer, T.; Rosain, J.; Philippot, Q.; Manry, J.; Michailidis, E.; Hoffmann, H.H.; Eto, S.; Garcia-Prat, M.; et al. Autoantibodies neutralizing type I IFNs are present in ~4% of uninfected individuals over 70 years old and account for ~20% of COVID-19 deaths. *Sci. Immunol.* **2021**, *6*, eabl4340. [\[CrossRef\]](#)

59. Zalinger, Z.B.; Elliott, R.; Rose, K.M.; Weiss, S.R. MDA5 Is Critical to Host Defense during Infection with Murine Coronavirus. *J. Virol.* **2015**, *89*, 12330–12340. [[CrossRef](#)]
60. Wu, J.; Shi, Y.; Pan, X.; Wu, S.; Hou, R.; Zhang, Y.; Zhong, T.; Tang, H.; Du, W.; Wang, L.; et al. SARS-CoV-2 ORF9b inhibits RIG-I-MAVS antiviral signaling by interrupting K63-linked ubiquitination of NEMO. *Cell Rep.* **2021**, *34*, 108761. [[CrossRef](#)]
61. Liu, G.; Lee, J.H.; Parker, Z.M.; Acharya, D.; Chiang, J.J.; van Gent, M.; Riedl, W.; Davis-Gardner, M.E.; Wies, E.; Chiang, C.; et al. ISG15-dependent activation of the sensor MDA5 is antagonized by the SARS-CoV-2 papain-like protease to evade host innate immunity. *Nat. Microbiol.* **2021**, *6*, 467–478. [[CrossRef](#)]
62. Jiang, H.W.; Zhang, H.N.; Meng, Q.F.; Xie, J.; Li, Y.; Chen, H.; Zheng, Y.X.; Wang, X.N.; Qi, H.; Zhang, J.; et al. SARS-CoV-2 Orf9b suppresses type I interferon responses by targeting TOM70. *Cell. Mol. Immunol.* **2020**, *17*, 998–1000. [[CrossRef](#)]
63. Han, L.; Zhuang, M.W.; Deng, J.; Zheng, Y.; Zhang, J.; Nan, M.L.; Zhang, X.J.; Gao, C.; Wang, P.H. SARS-CoV-2 ORF9b antagonizes type I and III interferons by targeting multiple components of the RIG-I/MDA-5-MAVS, TLR3-TRIF, and cGAS-STING signaling pathways. *J. Med. Virol.* **2021**, *93*, 5376–5389. [[CrossRef](#)]
64. Zheng, Y.; Deng, J.; Han, L.; Zhuang, M.W.; Xu, Y.; Zhang, J.; Nan, M.L.; Xiao, Y.; Zhan, P.; Liu, X.; et al. SARS-CoV-2 NSP5 and N protein counteract the RIG-I signaling pathway by suppressing the formation of stress granules. *Signal Transduct. Target. Ther.* **2022**, *7*, 22. [[CrossRef](#)]
65. Neufeldt, C.J.; Cerikan, B.; Cortese, M.; Frankish, J.; Lee, J.Y.; Plociennikowska, A.; Heigwer, F.; Prasad, V.; Joecks, S.; Burkart, S.S.; et al. SARS-CoV-2 infection induces a pro-inflammatory cytokine response through cGAS-STING and NF-kappaB. *Commun. Biol.* **2022**, *5*, 45. [[CrossRef](#)]
66. Di Domizio, J.; Gulen, M.F.; Saidoune, F.; Thacker, V.V.; Yatim, A.; Sharma, K.; Nass, T.; Guenova, E.; Schaller, M.; Conrad, C.; et al. The cGAS-STING pathway drives type I IFN immunopathology in COVID-19. *Nature* **2022**, 1–9. [[CrossRef](#)]
67. Van Furth, R.; Cohn, Z.A. The origin and kinetics of mononuclear phagocytes. *J. Exp. Med.* **1968**, *128*, 415–435. [[CrossRef](#)]
68. Narasimhan, P.B.; Marcovecchio, P.; Hamers, A.A.J.; Hedrick, C.C. Nonclassical Monocytes in Health and Disease. *Annu. Rev. Immunol.* **2019**, *37*, 439–456. [[CrossRef](#)] [[PubMed](#)]
69. Rajamanickam, A.; Kumar, N.P.; Pandiarajan, A.N.; Selvaraj, N.; Munisankar, S.; Renji, R.M.; Venkatramani, V.; Murhekar, M.; Thangaraj, J.W.V.; Kumar, M.S.; et al. Dynamic alterations in monocyte numbers, subset frequencies and activation markers in acute and convalescent COVID-19 individuals. *Sci. Rep.* **2021**, *11*, 20254. [[CrossRef](#)]
70. Bassler, K.; Schulte-Schrepping, J.; Wernat-Herresthal, S.; Aschenbrenner, A.C.; Schultze, J.L. The Myeloid Cell Compartment-Cell by Cell. *Annu. Rev. Immunol.* **2019**, *37*, 269–293. [[CrossRef](#)]
71. Hu, G.; Christman, J.W. Editorial: Alveolar Macrophages in Lung Inflammation and Resolution. *Front. Immunol.* **2019**, *10*, 2275. [[CrossRef](#)]
72. Choudhury, A.; Das, N.C.; Patra, R.; Mukherjee, S. In silico analyses on the comparative sensing of SARS-CoV-2 mRNA by the intracellular TLRs of humans. *J. Med. Virol.* **2021**, *93*, 2476–2486. [[CrossRef](#)]
73. Roy, R.K.; Sharma, U.; Wasson, M.K.; Jain, A.; Hassan, M.I.; Prakash, H. Macrophage Activation Syndrome and COVID 19: Impact of MAPK Driven Immune-Epigenetic Programming by SARS-Cov-2. *Front. Immunol.* **2021**, *12*, 763313. [[CrossRef](#)] [[PubMed](#)]
74. Yang, Y.; Shen, C.; Li, J.; Yuan, J.; Yang, M.; Wang, F.; Li, G.; Li, Y.; Xing, L.; Peng, L.; et al. Exuberant elevation of IP-10, MCP-3 and IL-1ra during SARS-CoV-2 infection is associated with disease severity and fatal outcome. *medRxiv* **2020**. [[CrossRef](#)]
75. Naninov, N. In the eye of the COVID-19 cytokine storm. *Nat. Rev. Immunol.* **2020**, *20*, 277. [[CrossRef](#)] [[PubMed](#)]
76. Gomez-Rial, J.; Rivero-Calle, I.; Salas, A.; Martinon-Torres, F. Role of Monocytes/Macrophages in Covid-19 Pathogenesis: Implications for Therapy. *Infect. Drug Resist.* **2020**, *13*, 2485–2493. [[CrossRef](#)]
77. Nicholls, J.; Dong, X.P.; Jiang, G.; Peiris, M. SARS: Clinical virology and pathogenesis. *Respirology* **2003**, *8*, S6–S8. [[CrossRef](#)]
78. Zhou, Z.; Ren, L.; Zhang, L.; Zhong, J.; Xiao, Y.; Jia, Z.; Guo, L.; Yang, J.; Wang, C.; Jiang, S.; et al. Heightened Innate Immune Responses in the Respiratory Tract of COVID-19 Patients. *Cell Host Microbe* **2020**, *27*, 883–890.e882. [[CrossRef](#)]
79. Bao, L.; Deng, W.; Huang, B.; Gao, H.; Liu, J.; Ren, L.; Wei, Q.; Yu, P.; Xu, Y.; Qi, F.; et al. The pathogenicity of SARS-CoV-2 in hACE2 transgenic mice. *Nature* **2020**, *583*, 830–833. [[CrossRef](#)]
80. Karwaciak, I.; Salkowska, A.; Karas, K.; Dastyk, J.; Ratajewski, M. Nucleocapsid and Spike Proteins of the Coronavirus SARS-CoV-2 Induce IL6 in Monocytes and Macrophages-Potential Implications for Cytokine Storm Syndrome. *Vaccines* **2021**, *9*, 54. [[CrossRef](#)]
81. Liu, Y.; Chen, D.; Hou, J.; Li, H.; Cao, D.; Guo, M.; Ling, Y.; Gao, M.; Zhou, Y.; Wan, Y.; et al. An inter-correlated cytokine network identified at the center of cytokine storm predicted COVID-19 prognosis. *Cytokine* **2021**, *138*, 155365. [[CrossRef](#)]
82. Fajnzylber, J.; Regan, J.; Coxen, K.; Corry, H.; Wong, C.; Rosenthal, A.; Worrall, D.; Giguel, F.; Piechocka-Trocha, A.; Atyeo, C.; et al. SARS-CoV-2 viral load is associated with increased disease severity and mortality. *Nat. Commun.* **2020**, *11*, 5493. [[CrossRef](#)]
83. Diehl, S.; Anguita, J.; Hoffmeyer, A.; Zapton, T.; Ihle, J.N.; Fikrig, E.; Rincón, M. Inhibition of Th1 Differentiation by IL-6 Is Mediated by SOCS1. *Immunity* **2000**, *13*, 805–815. [[CrossRef](#)]
84. Ni, L.; Cheng, M.L.; Feng, Y.; Zhao, H.; Liu, J.; Ye, F.; Ye, Q.; Zhu, G.; Li, X.; Wang, P.; et al. Impaired Cellular Immunity to SARS-CoV-2 in Severe COVID-19 Patients. *Front. Immunol.* **2021**, *12*, 603563. [[CrossRef](#)]
85. Tsukamoto, H.; Senju, S.; Matsumura, K.; Swain, S.L.; Nishimura, Y. IL-6-mediated environmental conditioning of defective Th1 differentiation dampens antitumour immune responses in old age. *Nat. Commun.* **2015**, *6*, 6702. [[CrossRef](#)]
86. Hou, W.; Kang, H.S.; Kim, B.S. Th17 cells enhance viral persistence and inhibit T cell cytotoxicity in a model of chronic virus infection. *J. Exp. Med.* **2009**, *206*, 313–328. [[CrossRef](#)]

87. Boumaza, A.; Gay, L.; Mezouar, S.; Diallo, A.B.; Michel, M.; Desnues, B.; Raoult, D.; Scola, B.L.; Halfon, P.; Vitte, J.; et al. Monocytes and macrophages, targets of SARS-CoV-2: The clue for Covid-19 immunoparalysis. *bioRxiv* **2020**. [[CrossRef](#)]
88. Zhang, D.; Guo, R.; Lei, L.; Liu, H.; Wang, Y.; Wang, Y.; Qian, H.; Dai, T.; Zhang, T.; Lai, Y.; et al. Frontline Science: COVID-19 infection induces readily detectable morphologic and inflammation-related phenotypic changes in peripheral blood monocytes. *J. Leukoc. Biol.* **2021**, *109*, 13–22. [[CrossRef](#)]
89. Liu, Z.; VanBlargan, L.A.; Bloyet, L.M.; Rothlauf, P.W.; Chen, R.E.; Stumpf, S.; Zhao, H.; Errico, J.M.; Theel, E.S.; Liebeskind, M.J.; et al. Identification of SARS-CoV-2 spike mutations that attenuate monoclonal and serum antibody neutralization. *Cell Host Microbe* **2021**, *29*, 477–488.e474. [[CrossRef](#)]
90. Benlyamani, I.; Venet, F.; Coudereau, R.; Gossez, M.; Monneret, G. Monocyte HLA-DR Measurement by Flow Cytometry in COVID-19 Patients: An Interim Review. *Cytom. A* **2020**, *97*, 1217–1221. [[CrossRef](#)]
91. Gatti, A.; Radrizzani, D.; Vigano, P.; Mazzone, A.; Brando, B. Decrease of Non-Classical and Intermediate Monocyte Subsets in Severe Acute SARS-CoV-2 Infection. *Cytom. A* **2020**, *97*, 887–890. [[CrossRef](#)]
92. Spinetti, T.; Hirzel, C.; Fux, M.; Walti, L.N.; Schober, P.; Stueber, F.; Luedi, M.M.; Schefold, J.C. Reduced Monocytic Human Leukocyte Antigen-DR Expression Indicates Immunosuppression in Critically Ill COVID-19 Patients. *Anesth. Analg.* **2020**, *131*, 993–999. [[CrossRef](#)] [[PubMed](#)]
93. Wilk, A.J.; Rustagi, A.; Zhao, N.Q.; Roque, J.; Martinez-Colon, G.J.; McKechnie, J.L.; Ivison, G.T.; Ranganath, T.; Vergara, R.; Hollis, T.; et al. A single-cell atlas of the peripheral immune response to severe COVID-19. *medRxiv* **2020**. [[CrossRef](#)] [[PubMed](#)]
94. Giamarellos-Bourboulis, E.J.; Netea, M.G.; Rovina, N.; Akinosoglou, K.; Antoniadou, A.; Antonakos, N.; Damoraki, G.; Gkavogianni, T.; Adami, M.E.; Katsaounou, P.; et al. Complex Immune Dysregulation in COVID-19 Patients with Severe Respiratory Failure. *Cell Host Microbe* **2020**, *27*, 992–1000.e1003. [[CrossRef](#)] [[PubMed](#)]
95. Parackova, Z.; Zentsova, I.; Bloomfield, M.; Vrabcova, P.; Smetanova, J.; Kloperk, A.; Meseznikov, G.; Casas Mendez, L.F.; Vymazal, T.; Sediva, A. Disharmonic Inflammatory Signatures in COVID-19: Augmented Neutrophils' but Impaired Monocytes' and Dendritic Cells' Responsiveness. *Cells* **2020**, *9*, 2206. [[CrossRef](#)] [[PubMed](#)]
96. Pelaia, C.; Tinello, C.; Vatrella, A.; De Sarro, G.; Pelaia, G. Lung under attack by COVID-19-induced cytokine storm: Pathogenic mechanisms and therapeutic implications. *Ther. Adv. Respir. Dis.* **2020**, *14*, 1753466620933508. [[CrossRef](#)] [[PubMed](#)]
97. Meizlish, M.L.; Pine, A.B.; Bishai, J.D.; Goshua, G.; Nadelmann, E.R.; Simonov, M.; Chang, C.H.; Zhang, H.; Shallow, M.; Bahel, P.; et al. A neutrophil activation signature predicts critical illness and mortality in COVID-19. *medRxiv* **2020**. [[CrossRef](#)]
98. Huang, C.; Wang, Y.; Li, X.; Ren, L.; Zhao, J.; Hu, Y.; Zhang, L.; Fan, G.; Xu, J.; Gu, X.; et al. Clinical features of patients infected with 2019 novel coronavirus in Wuhan, China. *Lancet* **2020**, *395*, 497–506. [[CrossRef](#)]
99. Wu, C.; Chen, X.; Cai, Y.; Xia, J.; Zhou, X.; Xu, S.; Huang, H.; Zhang, L.; Zhou, X.; Du, C.; et al. Risk Factors Associated With Acute Respiratory Distress Syndrome and Death in Patients with Coronavirus Disease 2019 Pneumonia in Wuhan, China. *JAMA Intern. Med.* **2020**, *180*, 934–943. [[CrossRef](#)]
100. Xiong, Y.; Liu, Y.; Cao, L.; Wang, D.; Guo, M.; Jiang, A.; Guo, D.; Hu, W.; Yang, J.; Tang, Z.; et al. Transcriptomic characteristics of bronchoalveolar lavage fluid and peripheral blood mononuclear cells in COVID-19 patients. *Emerg. Microbes Infect.* **2020**, *9*, 761–770. [[CrossRef](#)]
101. Li, X.; Liu, Y.; Li, J.; Sun, L.; Yang, J.; Xu, F.; Zhou, J.; Wan, L.; Xu, X.; Le, A.; et al. Immune characteristics distinguish patients with severe disease associated with SARS-CoV-2. *Immunol. Res.* **2020**, *68*, 398–404. [[CrossRef](#)] [[PubMed](#)]
102. Zheng, J.; Wang, Y.; Li, K.; Meyerholz, D.K.; Allamargot, C.; Perlman, S. Severe Acute Respiratory Syndrome Coronavirus 2-Induced Immune Activation and Death of Monocyte-Derived Human Macrophages and Dendritic Cells. *J. Infect. Dis.* **2021**, *223*, 785–795. [[CrossRef](#)] [[PubMed](#)]
103. Eda, H.; Burnette, B.L.; Shimada, H.; Hope, H.R.; Monahan, J.B. Interleukin-1beta-induced interleukin-6 production in A549 cells is mediated by both phosphatidylinositol 3-kinase and interleukin-1 receptor-associated kinase-4. *Cell Biol. Int.* **2011**, *35*, 355–358. [[CrossRef](#)] [[PubMed](#)]
104. Cavalcante-Silva, L.H.A.; Carvalho, D.C.M.; Lima, E.A.; Galvao, J.; da Silva, J.S.F.; Sales-Neto, J.M.; Rodrigues-Mascarenhas, S. Neutrophils and COVID-19: The road so far. *Int. Immunopharmacol.* **2021**, *90*, 107233. [[CrossRef](#)]
105. Middleton, E.A.; He, X.-Y.; Denorme, F.; Campbell, R.A.; Ng, D.; Salvatore, S.P.; Mostyka, M.; Baxter-Stoltzfus, A.; Borczuk, A.C.; Loda, M.; et al. Neutrophil extracellular traps contribute to immunothrombosis in COVID-19 acute respiratory distress syndrome. *Blood* **2020**, *136*, 1169–1179. [[CrossRef](#)]
106. Zuo, Y.; Yalavarthi, S.; Shi, H.; Gockman, K.; Zuo, M.; Madison, J.A.; Blair, C.; Weber, A.; Barnes, B.J.; Egeblad, M.; et al. Neutrophil extracellular traps in COVID-19. *JCI Insight* **2020**, *5*. [[CrossRef](#)]
107. Rizzo, R.; Bortolotti, D.; Bolzani, S.; Fainardi, E. HLA-G Molecules in Autoimmune Diseases and Infections. *Front. Immunol.* **2014**, *5*, 592. [[CrossRef](#)]
108. Moretta, A.; Bottino, C.; Vitale, M.; Pende, D.; Cantoni, C.; Mingari, M.C.; Biassoni, R.; Moretta, L. Activating receptors and coreceptors involved in human natural killer cell-mediated cytotoxicity. *Annu. Rev. Immunol.* **2001**, *19*, 197–223. [[CrossRef](#)]
109. Rizzo, S.; Schiuma, G.; Beltrami, S.; Gentili, V.; Rizzo, R.; Bortolotti, D. Role of KIR Receptor in NK Regulation during Viral Infections. *Immuno* **2021**, *1*, 305–331. [[CrossRef](#)]
110. Qin, C.; Zhou, L.; Hu, Z.; Zhang, S.; Yang, S.; Tao, Y.; Xie, C.; Ma, K.; Shang, K.; Wang, W.; et al. Dysregulation of Immune Response in Patients with Coronavirus 2019 (COVID-19) in Wuhan, China. *Clin. Infect. Dis.* **2020**, *71*, 762–768. [[CrossRef](#)]

111. Tan, L.; Wang, Q.; Zhang, D.; Ding, J.; Huang, Q.; Tang, Y.Q.; Wang, Q.; Miao, H. Lymphopenia predicts disease severity of COVID-19: A descriptive and predictive study. *Signal Transduct. Target. Ther.* **2020**, *5*, 33. [[CrossRef](#)] [[PubMed](#)]
112. Zheng, M.; Gao, Y.; Wang, G.; Song, G.; Liu, S.; Sun, D.; Xu, Y.; Tian, Z. Functional exhaustion of antiviral lymphocytes in COVID-19 patients. *Cell. Mol. Immunol.* **2020**, *17*, 533–535. [[CrossRef](#)] [[PubMed](#)]
113. Chen, G.; Wu, D.; Guo, W.; Cao, Y.; Huang, D.; Wang, H.; Wang, T.; Zhang, X.; Chen, H.; Yu, H.; et al. Clinical and immunological features of severe and moderate coronavirus disease 2019. *J. Clin. Investig.* **2020**, *130*, 2620–2629. [[CrossRef](#)] [[PubMed](#)]
114. Wen, W.; Su, W.; Tang, H.; Le, W.; Zhang, X.; Zheng, Y.; Liu, X.; Xie, L.; Li, J.; Ye, J.; et al. Immune cell profiling of COVID-19 patients in the recovery stage by single-cell sequencing. *Cell Discov.* **2020**, *6*, 1–18. [[CrossRef](#)]
115. Hazeldine, J.; Lord, J.M. The impact of ageing on natural killer cell function and potential consequences for health in older adults. *Ageing Res. Rev.* **2013**, *12*, 1069–1078. [[CrossRef](#)] [[PubMed](#)]
116. Gounder, S.S.; Abdullah, B.J.J.; Radzuanb, N.; Zain, F.; Sait, N.B.M.; Chua, C.; Subramani, B. Effect of Aging on NK Cell Population and Their Proliferation at Ex Vivo Culture Condition. *Anal. Cell. Pathol.* **2018**, *2018*, 7871814. [[CrossRef](#)]
117. Liao, M.; Liu, Y.; Yuan, J.; Wen, Y.; Xu, G.; Zhao, J.; Cheng, L.; Li, J.; Wang, X.; Wang, F.; et al. Single-cell landscape of bronchoalveolar immune cells in patients with COVID-19. *Nat. Med.* **2020**, *26*, 842–844. [[CrossRef](#)]
118. Osman, M.S.; van Eeden, C.; Cohen Tervaert, J.W. Fatal COVID-19 infections: Is NK cell dysfunction a link with autoimmune HLH? *Autoimmun. Rev.* **2020**, *19*, 102561. [[CrossRef](#)]
119. Mu, J.; Fang, Y.; Yang, Q.; Shu, T.; Wang, A.; Huang, M.; Jin, L.; Deng, F.; Qiu, Y.; Zhou, X. SARS-CoV-2 N protein antagonizes type I interferon signaling by suppressing phosphorylation and nuclear translocation of STAT1 and STAT2. *Cell Discov.* **2020**, *6*, 1–4. [[CrossRef](#)]
120. Mazzoni, A.; Salvati, L.; Maggi, L.; Capone, M.; Vanni, A.; Spinicci, M.; Mencarini, J.; Caporale, R.; Peruzzi, B.; Antonelli, A.; et al. Impaired immune cell cytotoxicity in severe COVID-19 is IL-6 dependent. *J. Clin. Investig.* **2020**, *130*, 4694–4703. [[CrossRef](#)]
121. Bortolotti, D.; Gentili, V.; Rizzo, S.; Rotola, A.; Rizzo, R. SARS-CoV-2 Spike 1 Protein Controls Natural Killer Cell Activation via the HLA-E/NKG2A Pathway. *Cells* **2020**, *9*, 1975. [[CrossRef](#)] [[PubMed](#)]
122. Guan, W.J.; Ni, Z.Y.; Hu, Y.; Liang, W.H.; Ou, C.Q.; He, J.X.; Liu, L.; Shan, H.; Lei, C.L.; Hui, D.S.C.; et al. Clinical Characteristics of Coronavirus Disease 2019 in China. *N. Engl. J. Med.* **2020**, *382*, 1708–1720. [[CrossRef](#)] [[PubMed](#)]
123. Anfossi, N.; Andre, P.; Guia, S.; Falk, C.S.; Roetyncck, S.; Stewart, C.A.; Bresco, V.; Frassati, C.; Reviron, D.; Middleton, D.; et al. Human NK cell education by inhibitory receptors for MHC class I. *Immunity* **2006**, *25*, 331–342. [[CrossRef](#)] [[PubMed](#)]
124. Lee, N.; Llano, M.; Carretero, M.; Ishitani, A.; Navarro, F.; Lopez-Botet, M.; Geraghty, D.E. HLA-E is a major ligand for the natural killer inhibitory receptor CD94/NKG2A. *Proc. Natl. Acad. Sci. USA* **1998**, *95*, 5199–5204. [[CrossRef](#)]
125. Littera, R.; Chessa, L.; Deidda, S.; Angioni, G.; Campagna, M.; Lai, S.; Melis, M.; Cipri, S.; Firinu, D.; Santus, S.; et al. Natural killer-cell immunoglobulin-like receptors trigger differences in immune response to SARS-CoV-2 infection. *PLoS ONE* **2021**, *16*, e0255608. [[CrossRef](#)]
126. Hsu, K.C.; Liu, X.R.; Selvakumar, A.; Mickelson, E.; O'Reilly, R.J.; Dupont, B. Killer Ig-like receptor haplotype analysis by gene content: Evidence for genomic diversity with a minimum of six basic framework haplotypes, each with multiple subsets. *J. Immunol.* **2002**, *169*, 5118–5129. [[CrossRef](#)]
127. Middleton, D.; Gonzalez, A.; Gilmore, P.M. Studies on the expression of the deleted KIR2DS4*003 gene product and distribution of KIR2DS4 deleted and nondeleted versions in different populations. *Hum. Immunol.* **2007**, *68*, 128–134. [[CrossRef](#)]
128. Saresella, M.; Trabattoni, D.; Marventano, I.; Piancone, F.; La Rosa, F.; Caronni, A.; Lax, A.; Bianchi, L.; Banfi, P.; Navarro, J.; et al. NK Cell Subpopulations and Receptor Expression in Recovering SARS-CoV-2 Infection. *Mol. Neurobiol.* **2021**, *58*, 6111–6120. [[CrossRef](#)]
129. Jewett, A. The Potential Effect of Novel Coronavirus SARS-CoV-2 on NK Cells; A Perspective on Potential Therapeutic Interventions. *Front. Immunol.* **2020**, *11*, 1692. [[CrossRef](#)]
130. Market, M.; Angka, L.; Martel, A.B.; Bastin, D.; Olanubi, O.; Tennakoon, G.; Boucher, D.M.; Ng, J.; Ardolino, M.; Auer, R.C. Flattening the COVID-19 Curve With Natural Killer Cell Based Immunotherapies. *Front. Immunol.* **2020**, *11*, 1512. [[CrossRef](#)]
131. Kumar, S.; Nyodu, R.; Maurya, V.K.; Saxena, S.K. Host Immune Response and Immunobiology of Human SARS-CoV-2 Infection. In *Coronavirus Disease 2019 (COVID-19); Medical Virology: From Pathogenesis to Disease Control*; Springer: Berlin/Heidelberg, Germany, 2020; pp. 43–53.
132. Jansen, J.M.; Gerlach, T.; Elbahesh, H.; Rimmelzwaan, G.F.; Saletti, G. Influenza virus-specific CD4+ and CD8+ T cell-mediated immunity induced by infection and vaccination. *J. Clin. Virol.* **2019**, *119*, 44–52. [[CrossRef](#)] [[PubMed](#)]
133. Rahman Nurdianto, A.; Rohmah, M.K. Perspective of molecular immune response of SARS-COV-2 infection. *J. Teknol. Lab.* **2020**, *9*, 58–66. [[CrossRef](#)]
134. Long, Q.X.; Liu, B.Z.; Deng, H.J.; Wu, G.C.; Deng, K.; Chen, Y.K.; Liao, P.; Qiu, J.F.; Lin, Y.; Cai, X.F.; et al. Antibody responses to SARS-CoV-2 in patients with COVID-19. *Nat. Med.* **2020**, *26*, 845–848. [[CrossRef](#)] [[PubMed](#)]
135. Azkur, A.K.; Akdis, M.; Azkur, D.; Sokolowska, M.; van de Veen, W.; Bruggen, M.C.; O'Mahony, L.; Gao, Y.; Nadeau, K.; Akdis, C.A. Immune response to SARS-CoV-2 and mechanisms of immunopathological changes in COVID-19. *Allergy* **2020**, *75*, 1564–1581. [[CrossRef](#)]
136. Bose, P.; Sunita, P.; Pattanayak, S.P. Molecular Insights into the Crosstalk between Immune Inflammation Nexus and SARS-CoV-2 Virus. *Curr. Microbiol.* **2021**, *78*, 3813–3828. [[CrossRef](#)]

137. Nguyen, A.; David, J.K.; Maden, S.K.; Wood, M.A.; Weeder, B.R.; Nellore, A.; Thompson, R.F. Human Leukocyte Antigen Susceptibility Map for Severe Acute Respiratory Syndrome Coronavirus 2. *J. Virol.* **2020**, *94*, e00510-20. [[CrossRef](#)]
138. Poulton, K.; Wright, P.; Hughes, P.; Savic, S.; Welberry Smith, M.; Guiver, M.; Morton, M.; van Dellen, D.; Tholouli, E.; Wynn, R.; et al. A role for human leucocyte antigens in the susceptibility to SARS-Cov-2 infection observed in transplant patients. *Int. J. Immunogenet.* **2020**, *47*, 324–328. [[CrossRef](#)]
139. Amoroso, A.; Magistrini, P.; Vespasiano, F.; Bella, A.; Bellino, S.; Puoti, F.; Alizzi, S.; Vaisitti, T.; Boros, S.; Grossi, P.A.; et al. HLA and AB0 Polymorphisms May Influence SARS-CoV-2 Infection and COVID-19 Severity. *Transplantation* **2021**, *105*, 193–200. [[CrossRef](#)]
140. Jordan, S.C. Innate and adaptive immune responses to SARS-CoV-2 in humans: Relevance to acquired immunity and vaccine responses. *Clin. Exp. Immunol.* **2021**, *204*, 310–320. [[CrossRef](#)]
141. Creech, C.B.; Walker, S.C.; Samuels, R.J. SARS-CoV-2 Vaccines. *JAMA* **2021**, *325*, 1318–1320. [[CrossRef](#)]
142. Gaebler, C.; Wang, Z.; Lorenzi, J.C.C.; Muecksch, F.; Finkin, S.; Tokuyama, M.; Cho, A.; Jankovic, M.; Schaefer-Babajew, D.; Oliveira, T.Y.; et al. Evolution of antibody immunity to SARS-CoV-2. *Nature* **2021**, *591*, 639–644. [[CrossRef](#)] [[PubMed](#)]
143. Robbiani, D.F.; Gaebler, C.; Muecksch, F.; Lorenzi, J.C.C.; Wang, Z.; Cho, A.; Agudelo, M.; Barnes, C.O.; Gazumyan, A.; Finkin, S.; et al. Convergent antibody responses to SARS-CoV-2 in convalescent individuals. *Nature* **2020**, *584*, 437–442. [[CrossRef](#)] [[PubMed](#)]
144. Barnes, C.O.; Jette, C.A.; Abernathy, M.E.; Dam, K.A.; Esswein, S.R.; Gristick, H.B.; Maljutin, A.G.; Sharaf, N.G.; Huey-Tubman, K.E.; Lee, Y.E.; et al. SARS-CoV-2 neutralizing antibody structures inform therapeutic strategies. *Nature* **2020**, *588*, 682–687. [[CrossRef](#)] [[PubMed](#)]
145. Barnes, C.O.; West, A.P., Jr.; Huey-Tubman, K.E.; Hoffmann, M.A.G.; Sharaf, N.G.; Hoffman, P.R.; Koranda, N.; Gristick, H.B.; Gaebler, C.; Muecksch, F.; et al. Structures of Human Antibodies Bound to SARS-CoV-2 Spike Reveal Common Epitopes and Recurrent Features of Antibodies. *Cell* **2020**, *182*, 828–842 e816. [[CrossRef](#)]
146. Wang, Z.; Schmidt, F.; Weisblum, Y.; Muecksch, F.; Barnes, C.O.; Finkin, S.; Schaefer-Babajew, D.; Cipolla, M.; Gaebler, C.; Lieberman, J.A.; et al. mRNA vaccine-elicited antibodies to SARS-CoV-2 and circulating variants. *Nature* **2021**, *592*, 616–622. [[CrossRef](#)]
147. Min, Y.Q.; Huang, M.; Sun, X.; Deng, F.; Wang, H.; Ning, Y.J. Immune evasion of SARS-CoV-2 from interferon antiviral system. *Comput. Struct. Biotechnol. J.* **2021**, *19*, 4217–4225. [[CrossRef](#)]
148. Kasuga, Y.; Zhu, B.; Jang, K.J.; Yoo, J.S. Innate immune sensing of coronavirus and viral evasion strategies. *Exp. Mol. Med.* **2021**, *53*, 723–736. [[CrossRef](#)]
149. Zheng, Y.; Zhuang, M.W.; Han, L.; Zhang, J.; Nan, M.L.; Zhan, P.; Kang, D.; Liu, X.; Gao, C.; Wang, P.H. Severe acute respiratory syndrome coronavirus 2 (SARS-CoV-2) membrane (M) protein inhibits type I and III interferon production by targeting RIG-I/MDA-5 signaling. *Signal Transduct. Target. Ther.* **2020**, *5*, 299. [[CrossRef](#)]
150. Duffy, S. Why are RNA virus mutation rates so damn high? *PLoS Biol.* **2018**, *16*, e3000003. [[CrossRef](#)]
151. Duchene, S.; Featherstone, L.; Haritopoulou-Sinanidou, M.; Rambaut, A.; Lemey, P.; Baele, G. Temporal signal and the phylogenetic threshold of SARS-CoV-2. *Virus Evol.* **2020**, *6*, veaa061. [[CrossRef](#)]
152. Parczewski, M.; Ciechanowicz, A. Molecular epidemiology of SARS-CoV-2: A review of current data on genetic variability of the virus. *Pol. Arch. Intern. Med.* **2020**, *131*, 63–69. [[CrossRef](#)] [[PubMed](#)]
153. Mengist, H.M.; Kombe Kombe, A.J.; Mekonnen, D.; Abebaw, A.; Getachew, M.; Jin, T. Mutations of SARS-CoV-2 spike protein: Implications on immune evasion and vaccine-induced immunity. *Semin. Immunol.* **2021**, *55*, 101533. [[CrossRef](#)] [[PubMed](#)]
154. Gao, S.J.; Guo, H.; Luo, G. Omicron variant (B.1.1.529) of SARS-CoV-2, a global urgent public health alert! *J. Med. Virol.* **2021**, *94*, 1255–1256. [[CrossRef](#)] [[PubMed](#)]
155. Cao, Y.; Su, B.; Guo, X.; Sun, W.; Deng, Y.; Bao, L.; Zhu, Q.; Zhang, X.; Zheng, Y.; Geng, C.; et al. Potent Neutralizing Antibodies against SARS-CoV-2 Identified by High-Throughput Single-Cell Sequencing of Convalescent Patients' B Cells. *Cell* **2020**, *182*, 73–84.e16. [[CrossRef](#)] [[PubMed](#)]
156. Lv, Z.; Deng, Y.Q.; Ye, Q.; Cao, L.; Sun, C.Y.; Fan, C.; Huang, W.; Sun, S.; Sun, Y.; Zhu, L.; et al. Structural basis for neutralization of SARS-CoV-2 and SARS-CoV by a potent therapeutic antibody. *Science* **2020**, *369*, 1505–1509. [[CrossRef](#)] [[PubMed](#)]
157. Agerer, B.; Koblichke, M.; Gudipati, V.; Montano-Gutierrez, L.F.; Smyth, M.; Popa, A.; Genger, J.W.; Endler, L.; Florian, D.M.; Muhlgrabner, V.; et al. SARS-CoV-2 mutations in MHC-I-restricted epitopes evade CD8(+) T cell responses. *Sci. Immunol.* **2021**, *6*, eabg6461. [[CrossRef](#)] [[PubMed](#)]
158. Zhang, Y.; Chen, Y.; Li, Y.; Huang, F.; Luo, B.; Yuan, Y.; Xia, B.; Ma, X.; Yang, T.; Yu, F.; et al. The ORF8 protein of SARS-CoV-2 mediates immune evasion through down-regulating MHC-Iota. *Proc. Natl. Acad. Sci. USA* **2021**, *118*. [[CrossRef](#)]
159. Overacre-Delgoffe, A.E.; Chikina, M.; Dadey, R.E.; Yano, H.; Brunazzi, E.A.; Shayan, G.; Horne, W.; Moskovitz, J.M.; Kolls, J.K.; Sander, C.; et al. Interferon-gamma Drives Treg Fragility to Promote Anti-tumor Immunity. *Cell* **2017**, *169*, 1130–1141.e11. [[CrossRef](#)]

In conclusion, this PhD thesis summarized all the studies, already published, in which I have investigated the pathogenetic mechanism associated to SARS-CoV-2 infection, with the purpose to make an extensive overview on the main aspects connected to SARS-CoV-2 typical and atypical infection. The results herein reported might contribute to enhance the knowledge of SARS-CoV-2 pathogenesis, clarifying its infection end evasion mechanisms, to improve both diagnostic and therapy tools.

9. Other works

During my PhD course, I also participated to other studies concerning to the impact of Herpesviruses infections in human diseases. I investigated the role of herpetic infections in neurodegenerative processes, pregnancy and oncogenesis.

As showed in the following attached papers, I focused my studies on Alzheimer Disease (AD) and Multiple Sclerosis (MS), already reported to be associated to HHVs infections [397].

My research particularly investigated HHV-6 role in the neurodegenerative process, paying attention to NK cell function modulation due to specific KIRs genotypes (*Paper 1*, paper attached) and to the role of the U24 viral protein in trigger MS autoimmunity (*Paper 2*, paper attached).

Moreover, HHV-6 is known to be involved in pregnancy-associated diseases, included primary idiopathic infertility [398], where the modulation of HLA-G by the virus seems to be a determinant condition.

Intra-Uterine Growth Restriction (IUGR) condition is due to an altered placental irroration, but no evidence was reported on the association of this condition with HHV-6 placental infection. Thus, we assessed the possible association between HHV-6 placental infection and HLA-G expression alteration in IUGR placental samples (*Paper 3*, paper attached), confirming the involvement of the infection evasion mechanism based on HLA-G modulation as a possible factor triggering IUGR onset (*Paper 3*, paper attached). Specifically, the IHC results obtained in this work, as also in the other, previously described in this thesis, were improved during my period abroad to the Zurich University.

Concerning HHV-6, thanks to the collaboration with the Organic Chemistry group of the University of Ferrara, I also analyzed the possible use of new antiviral strategies based on the use of rhodaminic inhibitors as potential fusion intermediate inhibitors (*Paper 4*, paper attached), which resulted promising as an alternative therapy to classical antiviral drugs on both HHV-6A and HHV-6B infections.

Finally, I also analyzed the role of the inhibitory KIR2DL2 receptor in the predisposition to Kaposi Sarcoma, in presence of HHV-8 infection (*Paper 5*, paper attached), already identified as major the etiological agent of Kaposi sarcoma (KS) [399].



Article

Herpesvirus Infections in KIR2DL2-Positive Multiple Sclerosis Patients: Mechanisms Triggering Autoimmunity

Daria Bortolotti ¹ , Valentina Gentili ¹ , Alessandra Bortoluzzi ², Marcello Govoni ² , Giovanna Schiuma ¹ , Silvia Beltrami ¹ , Sabrina Rizzo ¹, Eleonora Baldi ³, Elisabetta Caselli ¹ , Maura Pugliatti ^{4,5} , Massimiliano Castellazzi ^{4,5} , Mercedes Fernández ¹ , Enrico Fainardi ⁶ and Roberta Rizzo ^{1,*}

¹ Department of Chemical, Pharmaceutical and Agricultural Science, University of Ferrara, 44121 Ferrara, Italy; daria.bortolotti@unife.it (D.B.); valentina.gentili@unife.it (V.G.); giovanna.schiuma@unife.it (G.S.); silvia.beltrami@unife.it (S.B.); sabrina.rizzo@unife.it (S.R.); elisabetta.caselli@unife.it (E.C.); mercedes.fernandez@unife.it (M.F.)

² Rheumatology Unit, Department of Medical Sciences, University of Ferrara and Azienda Ospedaliero-Universitaria S. Anna, 44124 Ferrara, Italy; alessandra.bortoluzzi@unife.it (A.B.); marcello.govoni@unife.it (M.G.)

³ Division of Neurology, Department of Neuroscience and Rehabilitation, "Sant'Anna" University-Hospital, 44124 Ferrara, Italy; eleonora.baldi@gmail.com

⁴ Department of Biomedical and Specialist Surgical Sciences, University of Ferrara, 44121 Ferrara, Italy; maura.pugliatti@unife.it (M.P.); massimiliano.castellazzi@unife.it (M.C.)

⁵ Interdepartmental Research Center for the Study of Multiple Sclerosis and Inflammatory and Degenerative Diseases of the Nervous System, University of Ferrara, 44124 Ferrara, Italy

⁶ Department of Experimental and Clinical Biomedical Sciences, University of Florence, 50121 Florence, Italy; enrico.fainardi@unifi.it

* Correspondence: rbr@unife.it



Citation: Bortolotti, D.; Gentili, V.; Bortoluzzi, A.; Govoni, M.; Schiuma, G.; Beltrami, S.; Rizzo, S.; Baldi, E.; Caselli, E.; Pugliatti, M.; et al. Herpesvirus Infections in KIR2DL2-Positive Multiple Sclerosis Patients: Mechanisms Triggering Autoimmunity. *Microorganisms* **2022**, *10*, 494. <https://doi.org/10.3390/microorganisms10030494>

Academic Editor: Alain Doglio

Received: 23 December 2021

Accepted: 21 February 2022

Published: 23 February 2022

Publisher's Note: MDPI stays neutral with regard to jurisdictional claims in published maps and institutional affiliations.



Copyright: © 2022 by the authors. Licensee MDPI, Basel, Switzerland. This article is an open access article distributed under the terms and conditions of the Creative Commons Attribution (CC BY) license (<https://creativecommons.org/licenses/by/4.0/>).

Abstract: In multiple sclerosis (MS), there is a possible relationship with viral infection, evidenced by clinical evidence of an implication of infectious events with disease onset and/or relapse. The aim of this research is to study how human herpesvirus (HHVs) infections might dysregulate the innate immune system and impact autoimmune responses in MS. We analyzed 100 MS relapsing remitting patients, in the remission phase, 100 healthy controls and 100 subjects with other inflammatory neurological diseases (OIND) (neuro-lupus) for their immune response to HHV infection. We evaluated NK cell response, levels of HHVs DNA, IgG and pro- and anti-inflammatory cytokines. The results demonstrated that the presence of KIR2DL2 expression on NK cells increased the susceptibility of MS patients to HHV infections. We showed an increased susceptibility mainly to EBV and HHV-6 infections in MS patients carrying the KIR2DL2 receptor and HLA-C1 ligand. The highest HHV-6 viral load was observed in MS patients, with an increased percentage of subjects positive for IgG against HHV-6 in KIR2DL2-positive MS and OIND subjects compared to controls. MS and OIND patients showed the highest levels of IL-8, IL-12p70, IL-10 and TNF-alpha in comparison with control subjects. Interestingly, MS and OIND patients showed similar levels of IL-8, while MS patients presented higher IL-12p70, TNF-alpha and IL-10 levels in comparison with OIND patients. We can hypothesize that HHVs' reactivation, by inducing immune activation via also molecular mimicry, may have the ability to induce autoimmunity and cause tissue damage and consequent MS lesion development.

Keywords: herpesvirus; multiple sclerosis; NK cell; KIR

1. Introduction

In multiple sclerosis (MS), there is a possible relationship with viral infection, evidenced by clinical evidence of an implication of infectious events with disease onset and/or relapse. The viral infection can directly infect the central nervous system (CNS) and induce an inflammatory response that might result in brain damage. Neurotrophic herpesviruses can enter the CNS evading the host protective immune response, inducing acute cell

dysfunction. Subsequently, the latent infection typical of herpesviruses might reactivate resulting in disease relapse. The reactivation of viral infection can induce lymphocyte activation and the secretion of pro-inflammatory cytokines that affect cell-specific functions and enhance neurodegeneration [1]. Disease-associated genetic variants can exacerbate the disease onset [2]. Herpesviridae have shown a possible association with MS, resulting as valuable biomarker candidates of disease progression and therapy outcome. Their preferential tropism for CNS and their latent persisting infections that enable their immune-escape, account for their potential pathogenic role in neuroinflammation, resulting in the persistence of chronic inflammation and the accumulation of neurological deficits. Epstein-Barr virus (EBV) and human herpesvirus 6 (HHV-6) have been identified in pathological and sero-epidemiological studies. EBV reactivation has been linked to disease activity in early MS suggesting a possible implication in MS immunopathology [3]. HHV-6 active infection seems to be involved in MS exacerbations [4], and reactivation may have a role in triggering autoimmune response and tissue damage associated with MS lesion development [5,6]. Our group showed that HHV-6 supports a productive, low level of replication in the CNS of patients at the early stages of the disease [7].

Recent observations suggest that innate immunity, and in particular natural killer (NK) cells, might be involved in the etiology of MS [8]. NK cells' regulation is controlled by NK membrane receptors: leukocyte immunoglobulin-like receptors (LILR), C-type lectin, killer immunoglobulin-like receptors (KIR), natural cytotoxicity receptors (NCRs) and CD2. KIRs are transmembrane glycoproteins encoded by 15 highly polymorphic genes, with structural domains that characterize their functions [9]. The KIRs have different numbers of the extracellular domains (2D and 3D), and a cytoplasmic tail with a different length (L (long) or S (short)) that determines protein function (inhibitory or activating, respectively) [10], with KIR2DL4 as the unique long-tailed activating KIR. The association of KIR gene polymorphisms has already been demonstrated in several autoimmune disorders such as rheumatoid arthritis, ankylosing spondylitis and inflammatory bowel disease [11–13]. In particular, KIR receptors might have a protective or detrimental role in autoimmune diseases due to their inhibitory or activating control of NK cells, the functions of which can be suppressed or enhanced in predisposed subjects.

We have recently showed that MS patients characterized by the expression of KIR2DL2 on NK cell surface are more susceptible to HHV infection [14–16]. In particular, NK cells from MS patients expressing KIR2DL2 are less activated towards HHV infection. On the contrary, control KIR2DL2-positive and negative subjects presented no statistical differences in the activation status. Interestingly, other authors have observed a correlation between KIR2DL2 and the HHV infection reactivation in healthy subjects [17]. The authors recognized receptor/ligand pair KIR2DL2/HLA-C1 as a predisposing factor for HSV-1 infection and reactivation. These results suggest a possible role of KIR2DL2 in HHV infection susceptibility in the human population, that affects NK cell activation only in MS patients. We can hypothesize that HHVs' reactivation, by inducing immune activation via molecular mimicry, may have the ability to induce autoimmunity and cause tissue damage and consequent MS lesion development.

The aim of this research is to study how such dysregulation of the innate immune system could impact autoimmune responses in MS.

2. Materials and Methods

2.1. Subjects

In total, 100 MS relapsing remitting patients, in remission phase (mean age: 39 ± 10 years), recruited at the MS Centre of the Department of Neurology, University of Ferrara, Italy, from 2015 to 2018 (Supplementary Table S1a), 100 healthy controls (mean age: 38 ± 11 years) and 100 subjects with other inflammatory neurological diseases (OIND) (mean age: 37 ± 12 years) (NLES: neuro-lupus) (Supplementary Table S1b) were recruited. The samples were collected after informed consent, following the acceptance by the Area Vasta Emilia Centro (N: 01052016). MS was defined on the basis of McDonald's classification [18]. The patients had relapsing

remitting MS according to Lublin [19]. Disease classification was assessed during sample collection using Kurtzke's Expanded Disability Status Scale (EDSS) [20] (mean value at entry: 2.0 ± 1.0 , range from 0.0 to 5.6) (Supplementary Table S1a). At entry, the patients had no signs of acute infections, fever or other symptoms. The patients were not receiving potential disease-modifying therapies (e.g., methylprednisolone or azathioprine, glatiramer acetate or interferon-beta) during the 6 months preceding the study. OIND patients satisfying the 1997 revised American College of Rheumatology Criteria regularly attending the Lupus Clinic of the Rheumatology Unit, Department of Medical Sciences, Sant'Anna Hospital, University of Ferrara, Italy were recruited during the same period [21]. Neuropsychiatric manifestations were assessed in accordance with the 1999 ACR nomenclature and case definitions and diagnoses followed the EULAR recommendations [22]. The attribution of NP events was based on physician judgement and considering ACR 'association' and 'exclusion' factors (i.e., their absence favors attribution to SLE), and as 'SLE-favoring factors' of the Italian Study Group on the NPSLE validated attribution model were also evaluated (Supplementary Table S1b) [23]. None of the female MS patients, OIND and control subjects was pregnant before and during the study.

2.2. Quantification of Peripheral Blood Antibodies

Anti-HHV antibodies were evaluated in plasma samples from MS and control subjects with diagnostic ELISA kits (EBV, HHV-6, VZV; HSV-1; HSV-2) (Bethyl Laboratories, Montgomery, TX, USA). The endpoint Ig titers were evaluated with serial dilutions (1:10; 1:40; 1:60; 1:110; 1:240; 1:360) of the samples.

2.3. Genotyping of KIR and HLA

Genomic DNA was extracted from whole blood (QIAamp DNA Blood Mini kit, Hilden, Germany). The Olerup Typing kit (West Chester, PA, USA) was used to genotype KIR and HLA alleles and to quantify HHVs genomes by real-time PCR (Supplementary Table S2) following the manufacturer's procedures.

2.4. Quantification of Cytokine Levels

The levels of 9 different cytokines (Interferon-gamma (IFN-gamma), Interleukin-1alpha (IL-1alpha), IL-1beta, IL-4, IL-6, IL-8, IL-10, IL12p70, Tumor-necrosis factor alpha (TGF-alpha)) implicated in inflammation control (Aushon, Billerica, MA, USA) were analyzed on serum samples via a Multiplex ELISA kit (Cytokine 2 Array; Chemokine 2 Array). Serum samples were collected in a serum separator tube (SST), spun at 1000 G at room temperature centrifuge for 10–15 min, recovered and stored at -80°C .

2.5. Peripheral Blood Mononuclear Cell (PBMC) Culture

A clinical hematologic analysis showed no differences in cell counts between the three groups (Supplementary Table S1c). PBMCs were extracted from whole blood by Ficoll gradient (Cederlane, Hornby, ON, Canada). After extraction, PBMCs were resuspended in 2 mL of RPMI-1640 (Euroclone, Pavia, Italy) supplemented with 100 U/mL Penicillin G, 2 mM L-Glutamine, 20% FCS and 100 $\mu\text{g}/\text{mL}$ Streptomycin (Euro-clone, Pavia, Italy).

Natural killer cells were obtained from peripheral blood samples using the negative magnetic cell separation system (Miltenyi Biotec, Gladbach, Germany) [24]. The NK cell content was $>90\%$ as assessed by flow cytometry with CD3-PerCp-Cy5.5, CD56-FITC mAbs staining (e-Bioscience, Frankfurt, DE) (data not shown). NK cells were resuspended at 2×10^6 cells/mL in 20 mL of RPMI 1640 (BioWhittaker) containing 1 mM non-essential amino acids, 10% human AB serum (Mediatech, Herndon, VA, USA), 1 mM pyruvate, 2 mM glutamine, 20 mM HEPES, 100 $\mu\text{g}/\text{mL}$ Strep-tomycin and 100 U/mL Penicillin (Gibco BRL Life Technologies). Cells were stimulated with 100 U/mL of IL-2 (Hoffmann-LaRoche) on day 0 and cultured for 5 to 6 days at 37°C , 5% CO_2 .

2.6. Peripheral Blood Monocyte-Derived Microglia

Monocytes (adherent PBMC) were obtained from PBMCs cultured in T25 tissue culture flasks (2×10^6 to 5×10^6 cells/mL) using RPMI-1640 Glutamax medium (Invitrogen, Milan, Italy) supplemented with 1% antibiotics/antimycotic (10,000 g/mL streptomycin sulfate, 10,000 units/mL penicillin G sodium and 25 g/mL Amphotericin B, Invitrogen). After overnight incubation, adherent cells, which are mainly monocytes (>90%), as confirmed by a flow cytometry analysis, using anti-CD14-FITC and anti-CD16-PE moAbs (BD Biosciences, Milan, Italy), FACSCantoII flow cytometer (BD, Milan, Italy) and FlowJo LLC analysis software (Ashland, Catlettsburg, OR, USA) (Supplementary Figure S1), were used for the generation of microglia (M-MG). The differentiation of PBM-microglia was obtained in 6-well tissue culture plates (Sarstedt, Nümbrecht, Germany) using RPMI-1640 Glutamax supplemented with 1% antibiotic/antimycotic (serum-free condition) and a mixture of human recombinant cytokines, including GM-CSF (10 ng/mL; PeproTech, London, UK), M-CSF (10 ng/mL; PeproTech, London, UK), beta-nerve growth factor (NGF-beta 10 ng/mL; PeproTech, London, UK) and CCL2 (100 ng/mL) for up to 14 days. The generation of M-microglia was confirmed by morphology evaluation and immune-phenotype characterization for the expression of Iba1 by anti-Iba-1 PE moAb and of substance P with anti-substance P FITC mouse monoclonal antibody (moAb) [25,26].

2.7. HHV Infection

Cell-free virus inocula were obtained as previously described: EBV from lymphoblastoid cell line LCL-B95.8 (kind gift of Professor R. Dolcetti) activated using 20 ng/mL TPA (12-O-tetradecanoylphorbol-13-acetate) (Sigma-Aldrich, St. Louis, MO, USA) [26]; HHV-6A (strain U1102) grown in the J-Jhan cell line (ATCC TIB-153) [27]; HHV-6B (strain Z29) [24] grown in the Sup T1 cell line (ATCC CRL-1942); HSV-1 (strain F) grown on Vero cells (ATCC CCL81); VZV (ATCC VR-1433) grown on MRC5 cells (ATCC CCL171). The infection of M-MG was performed at a multiplicity of infection (m.o.i.) of 0.1 plaque forming unit/cell. A UV-inactivated virus was used as a negative control.

2.8. Viral Load Quantification

Overall, 1, 3, 7 and 14 days post-infection, the cells were harvested and DNA was extracted with the GeneAll Exgene™ Cell SV kit (GeneAll Biotechnology, Seoul, Korea). Real-time PCR for HHVs was performed (as reported in Supplementary Table S2) following the manufacturer's procedures.

2.9. Cytometric Analysis and CD107a Degranulation Assay

NK cells were characterized as CD3 negative cells with a specific CD panel (CD56-FITC, CD16-PerCp-Cy5.5, CD107a-PE) (e-Bioscience, Frankfurt, Germany), anti-KIR2DL2-2DS2-2DL3/CD158b-PE (ThermoScientific, Erembodegem, BE) monoclonal antibodies. Samples were incubated with the moAbs for 30 min in ice and washed. The analysis was performed with FACS CantoII flow cytometer and FlowJo software (Becton Dickinson, San Jose, CA, USA), acquiring 10,000 events. Lymphocytes were identified according to the forward/side scatter profile and NK cells (CD3⁻/CD56⁺) were defined and gated within the lymphocyte gate. For the CD107a degranulation assay, after 1 h of incubation at 37 °C and 3 h of treatment with Golgi Stop solution (Becton Dickinson, San Jose, CA, USA), PBMCs were stained. CD158b levels were evaluated in the CD3⁻/CD56⁺/CD16⁺ gated cells. Cell viability was assessed by propidium iodide staining. Anti-isotype controls (Exbio, Praha, Czech Republic) were performed. Ten thousand events were acquired.

2.10. Statistical Analyses

The Hardy–Weinberg equilibrium was assessed by the extended version of Fisher's exact test implemented in Arlequin 3.01. Biological variables were evaluated by Student's *t* test, Fisher's exact test and a logistic regression analysis by Graph pad software. Significant

p values were defined as <0.05. *p* values were corrected (pc) for multiple comparisons, using the Bonferroni correction.

3. Results

3.1. KIR/HLA Typing

The patients were evaluated for the frequency of KIRs' receptors and HLA ligands. The results are reported in Table 1. We enrolled 100 MS RR patients, in remission phase (Supplementary Table S1a), 100 healthy controls and 100 subjects with other inflammatory neurological diseases (OIND: neuro-lupus, NLES) (Supplementary Table S1b).

Table 1. KIR/HLA frequency.

KIR and HLA	MS (<i>n</i> = 100)	OIND (<i>n</i> = 100)	CNTR (<i>n</i> = 100)	<i>P</i>	pc
Activating KIR					
KIR2DS1	50	36	37	0.09	
KIR2DS2	62	34	37	7.0×10^{-4}	4.2×10^{-3}
KIR2DS3	36	29	28	0.28	
KIR2DS4	87	84	83	0	
KIR2DS5	45	31	30	0.04	
KIR3DS1	12	32	33	7.0×10^{-4}	4.2×10^{-3}
Inhibitory KIR					
KIR2DL1	89	87	86	0.67	
KIR2DL2	62	38	36	4.0×10^{-4}	3.2×10^{-3}
KIR2DL3	72	76	77	0.52	
KIR2DL4	98	99	100	0	
KIR2DL5	60	44	46	0.06	
KIR3DL1	94	81	83	0.025	
KIR3DL2	98	99	100	0	
KIR3DL3	98	99	100	0	
KIR genotype					
AA	28	33	35	0.36	
Bx	72	66	65		
HLA genotype					
C1/C1	26	21	20	0.40	
C1/C2	46	25	23	9.9×10^{-4}	5.0×10^{-3}
C2/C2	29	44	43	0.055	
HLA-Bw4	78	73	71	0	
HLA-Bw6	92	82	84	0.13	
KIR and their ligands					
KIR2DS1/KIR2DL1 present/HLA-C2 present	40	27	28	0.1	
KIR2DS1/KIR2DL1 present/HLA-C2 absent	10	7	8	0.81	
KIR2DS1/KIR2DL1 absent/HLA-C2 present	2	1	1	0	
KIR2DS2/KIR2DL2 present/HLA-C1 present	48	27	28	0.00561	0.037
KIR2DS2/KIR2DL2 present/HLA-C1 absent	14	14	14	0	
KIR2DS2/KIR2DL2 absent/HLA-C1 present	6	32	31	6.4×10^{-6}	5.8×10^{-5}
KIR3DS1/KI3DL1 present/HLA-Bw4 present	30	24	25	0.53	
KIR3DS1/KI3DL1 present/HLA-Bw4 absent	9	6	7	0.80	
KIR3DS1/KI3DL1 absent/HLA-Bw4 present	1	2	3	0.62	

The KIR and HLA allelic distribution was in the Hardy–Weinberg equilibrium. Patients with MS showed a significantly increased frequency of the activating receptor KIR2DS2 (62% vs. 37%; pc: 4.2×10^{-3}) and a reduced frequency of the activating receptor KIR3DS1 (12% vs. 33%; pc: 4.2×10^{-3}) in comparison with controls. MS patients had an increased frequency of the inhibitory receptor KIR2DL2 (62% vs. 36%; pc: 3.2×10^{-3}). No significant

differences were found in the distribution of KIR genotypes (AA or Bx) but there was an increase in the HLA-C1/C2 genotype in MS patients (46% vs. 23%; $p < 5 \times 10^{-3}$). The combination KIR2DS2/KIR2DL2 present/C1 present was significantly increased in MS patients in comparison with controls (48% vs. 28%; $p < 0.037$) while the combination KIR2DS2/KIR2DL2 absent/C1 present was significantly decreased in MS patients (6% vs. 31%; $p < 5.8 \times 10^{-5}$). The logistic regression analysis showed the combination KIR2DS2/KIR2DL2 present/C1 present strictly correlated with the MS condition ($p = 0.03$; $p = 0.016$, respectively). No significant differences were observed between KIR/HLA frequencies in OIND patients in comparison with controls (Table 1).

3.2. Microglial Cells-NK Cells Co-Culture during HHVs' Infection

We standardized the protocol to obtain human microglial cells from peripheral blood monocytes. We obtained a sufficient quantity of cells from each sample to carry out the analyses (Figure 1a). The generation of M-MG was confirmed by a morphology evaluation and immune-phenotype characterization for the expression of calcium binding protein Iba1 and substance P, typical characteristics of microglia (Figure 1a). We performed viral infection on microglial cells, obtaining a good viral load after 14 days after infection for HHV-6A, HHV-6B and EBV, while a lower viral replication was observed for HSV-1 and VZV (Figure 1b).

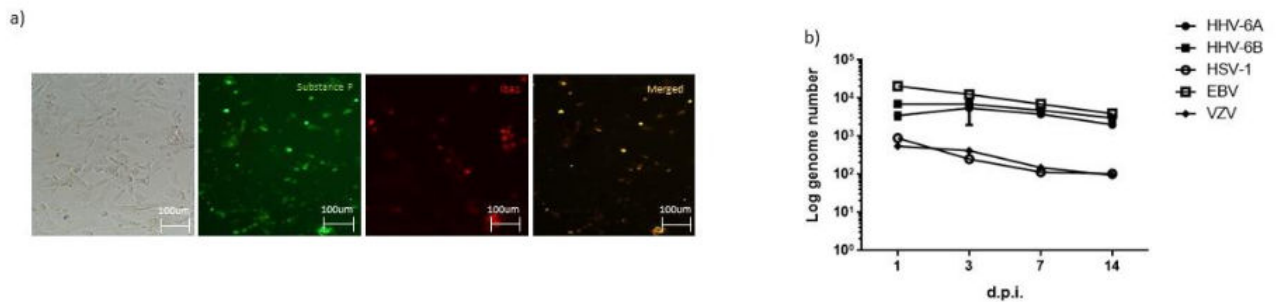


Figure 1. (a) Microglial cell obtained from peripheral blood monocytes, stained for substance P and Iba1. (b) Viral load in control microglial cells infected with HHVs.

Positive and negative KIR2DL2 natural killer (NK) cells from MS and OIND patients were co-cultured with HSV-1, HHV-6A, HHV-6B, VZV and EBV microglial-infected cells. The activation of NK cells was evaluated as a percentage of NK cells expressing the CD107a degranulation marker. We showed an increase in activated KIR2DL2-negative NK cells from all the three populations in the presence of HSV-1, HHV-6A, HHV-6B, VZV and EBV-infected cells (Figure 2a–c) ($p < 0.001$; t-Student's test). KIR2DL2-positive NK cells from the control population in the presence of HSV-1, HHV-6A, HHV-6B, VZV and EBV-infected cells showed an increase in CD107a expression (Figure 2d). In contrast, KIR2DL2-positive NK cells from MS patients were not activated in the presence of cells infected with HHV-6A, HHV-6B and EBV (Figure 2e). KIR2DL2-positive NK cells from OIND patients were not activated in the presence of cells infected with EBV (Figure 2f).

On the basis of the results obtained with NK cell activation, we evaluated the viral load in MS patients' microglial cells. We observed that KIR2DL2-negative subjects from the MS population were able to control viral infections, in agreement with the results obtained from the NK cell activation assay (Figure 3a–d). In particular, KIR2DL2-negative NK cells were able to control EBV, HHV-6A and HHV-6B more efficiently than NK cells from control subjects. KIR2DL2-positive MS patients controlled only VZV and HSV-1 infections similar to control subjects (Figure 3h,i). Interestingly, KIR2DL2-positive OIND patients controlled all the infections apart from EBV infection, similarly to what was observed for NK cell activation (Figure 3j).

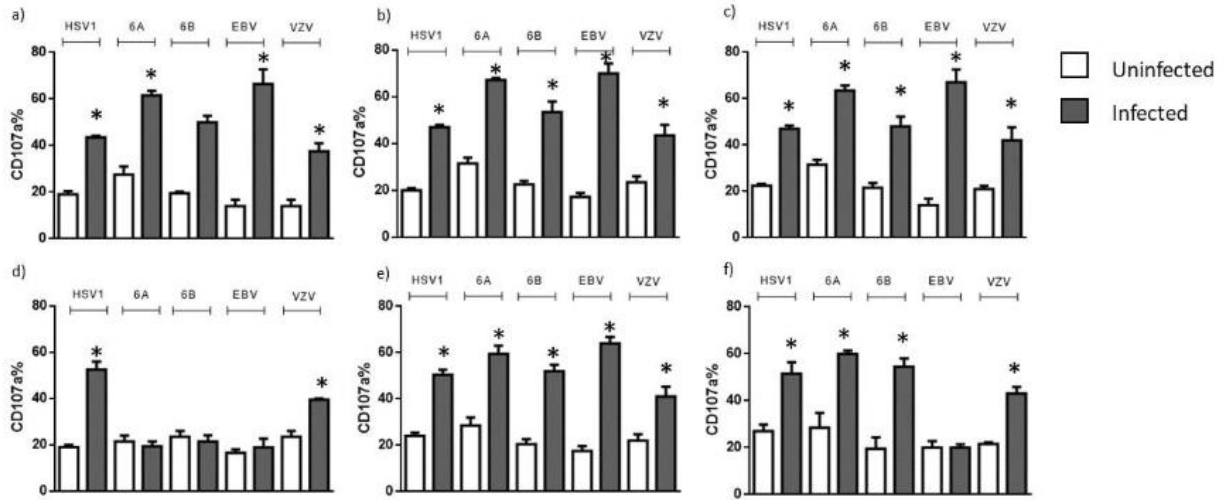


Figure 2. Frequencies of CD107a-positive NK cells after the co-culture with microglia cells infected with HHVs in KIR2DL2-negative (a) control, (b) MS and (c) OIND populations and in KIR2DL2-positive (d) control, (e) MS and (f) OIND populations. * significant *p* value, Student’s *t* test. The data are presented as mean ± SE.

When we evaluated the NK cell phenotype from MS patients after the co-culture with microglial-infected cells, we observed a significant increase in KIR2DL2 expression (Figure 4a). The augmented KIR2DL2 expression was more evident in the co-culture with HHV-6A, HHV-6B and EBV-infected microglia cells (Figure 4a). These data are in accordance with the results obtained with viral load quantification and NK cell activation status, supporting the role of KIR2DL2 in controlling NK cell activation in the presence of HHV infections. We evaluated the possible impact of KIR2DL2 expression on clinical status in MS patients. We observed that the subjects that respond with a greater increase of KIR2DL2 expression in the presence of an HHV infection were characterized by a higher EDSS (Figure 4b), supporting an involvement also in disease status. Similarly, the subjects that respond with a greater increase of KIR2DL2 expression in the presence of an HHV infection were characterized by a higher frequency of MRI disease activity (Figure 4c).

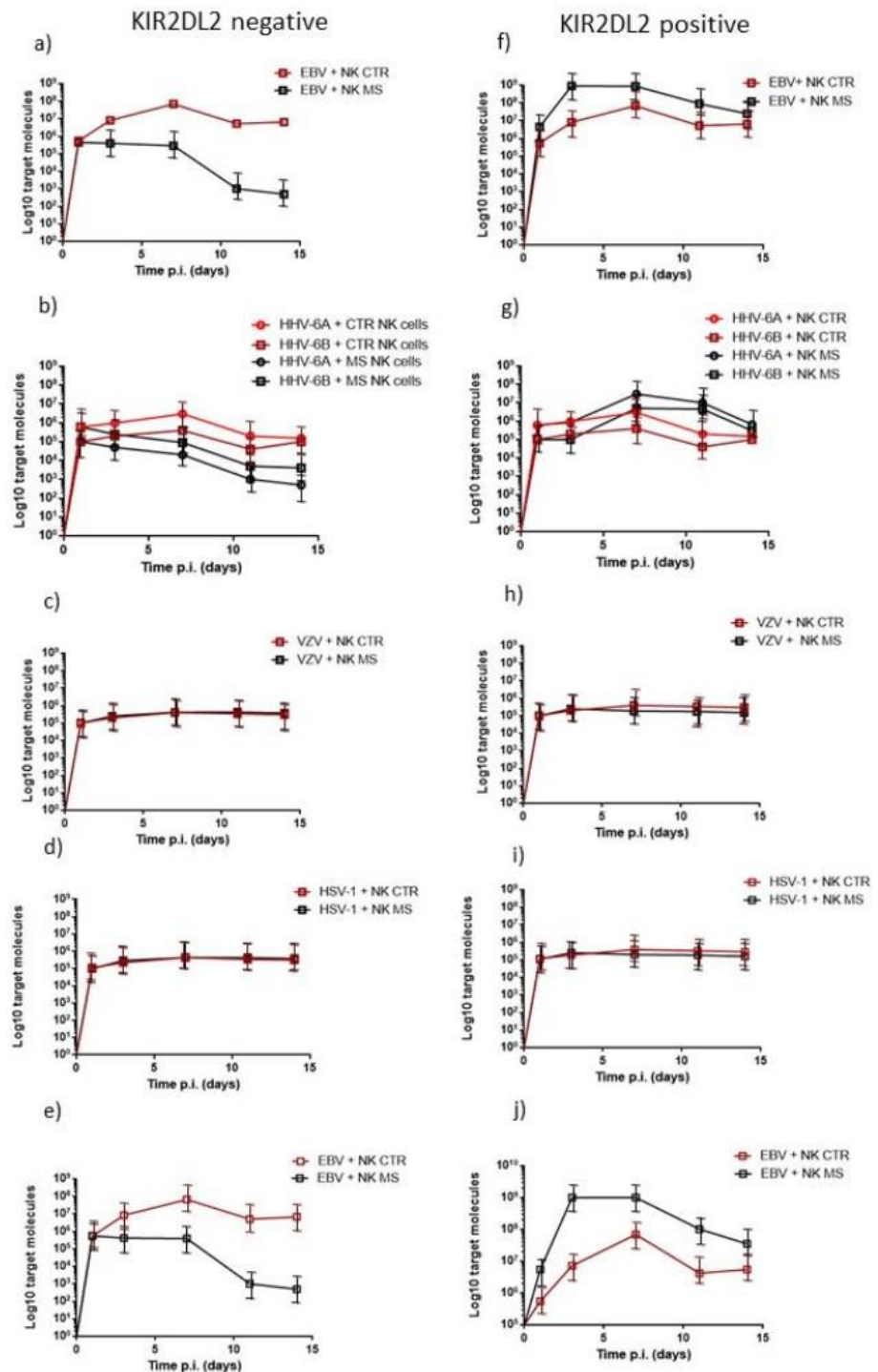


Figure 3. Microglial cells were infected and co-cultured with control or MS NK cells. Viral load was reported in KIR2DL2-negative subjects for (a) EBV, (b) HHV-6, (c) VZV and (d) HSV-1. Viral load was reported in KIR2DL2-positive subjects for (f) EBV, (g) HHV-6, (h) VZV and (i) HSV-1. Viral load in KIR2DL2-negative OIND patients for (e) EBV. Viral load in KIR2DL2-positive OIND patients for (j) EBV. NK CTR: NK cells from control subjects; NK MS: NK cells from MS patients. The data are presented as mean ± SE.

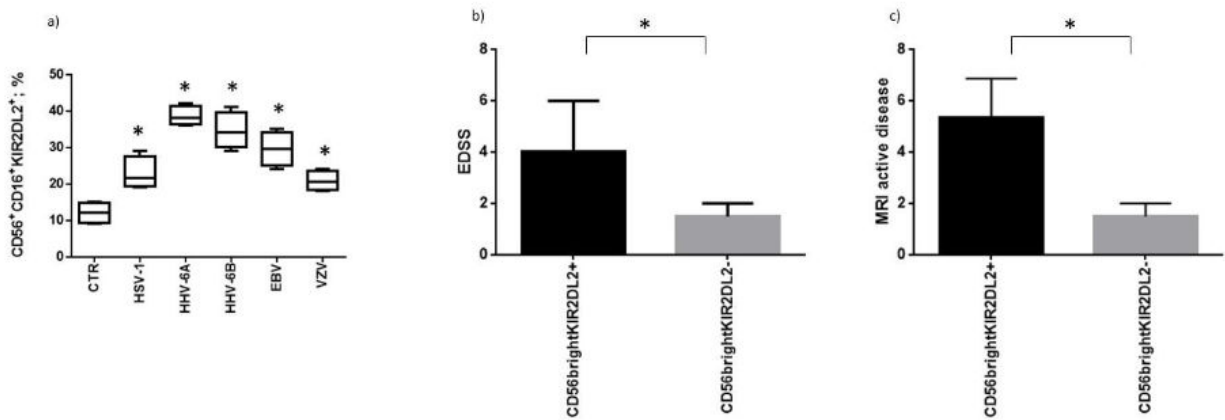


Figure 4. (a) Frequency of MS subjects with KIR2DL2 expressing NK cells after the co-culture with microglia cells infected with HHVs. Distribution of MS subjects with KIR2DL2-positive or negative NK cells on the basis of (b) EDS and (c) MRI disease activity. * significant *p* value, Student’s *t* test. The data are presented as mean ± SE.

3.3. Levels of HHVs’ DNA in Peripheral Blood

The three populations were analyzed for the presence of viral DNA (HSV-1, VZV, EBV, HHV-6) in peripheral blood. The presence of the EBV genome was observed in 10% of healthy controls, 16% of subjects with MS and in 39% of OIND subjects, with a significant difference between MS patients and OIND patients (*p* = 0.0004; Fisher exact test) and OIND patients and controls (*p* < 0.0001; Fisher exact test). Similarly, analyzing the viral load, OIND patients had a higher number of viral genome copies/mL of blood than MS patients (*p* < 0.0001; Student’s *t* test) and controls (*p* = 0.0007; Student’s *t* test) (Figure 5a).

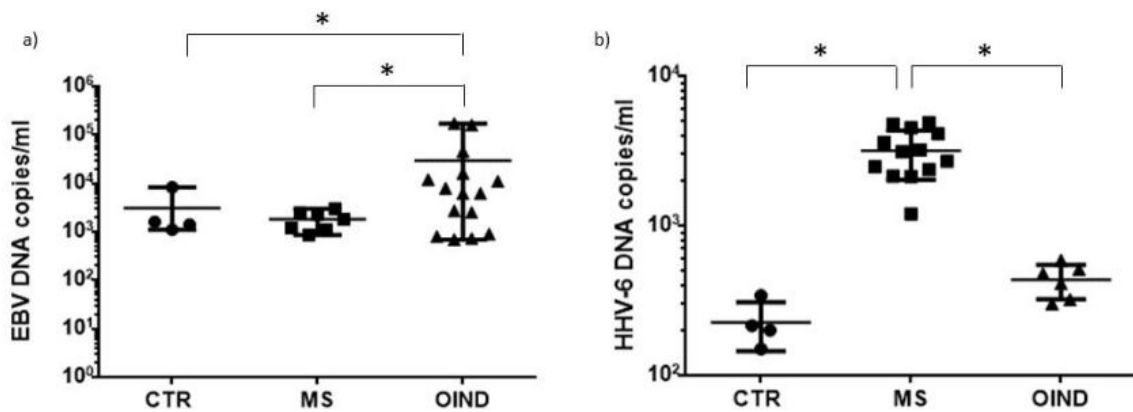


Figure 5. Viral load of (a) EBV and (b) HHV-6 in control, MS and OIND populations. * significant *p* value, Student’s *t* test. The data are presented as mean ± SE.

Overall, 10% of controls, 31% of MS patients and 14.6% of OIND patients were positive for the presence of the HHV-6 genome (Figure 5b), with the highest viral load in MS patients in comparison with controls (*p* = 0.001; Student’s *t* test) and OIND patients (*p* < 0.0001; Student’s *t* test). Subjects who tested positive for the presence of the HHV-6 genome in Q-PCR were then characterized for the type of virus, HHV-6A or HHV-6B. The subjects positive for the HHV-6A genome were 60% of MS patients and 30% of OIND patients (*p* < 0.0001; Student’s *t* test), while no control subject was positive for the HHV-6A genome. The subjects positive for the HHV-6B genome were 20% of MS patients, 45% of OIND patients (*p* = 0.0002; Student’s *t* test) and 100% of control subjects (vs. MS and OIND

$p < 0.0001$; Student's t test). The subjects positive for HHV-6A/-6B genomes were 20% of MS patients, 25% of OIND patients ($p = 0.5$; Student's t test), while no control subject was positive for HHV-6A/-6B genomes. No samples tested positive for the presence of HSV-1 or VZV DNA as was expected as the site of latency of both these viruses was not the peripheral blood but in ganglion cells. No differences were observed subdividing the samples on the basis of KIR2DL2 positivity (data not shown).

3.4. Levels of Antibodies towards HHVs

We evaluated the levels of antibodies (IgM and IgG) towards HHVs (HSV-1, HSV-2; EBV; HHV-6; VZV) in the plasma samples of the three cohorts.

The results obtained by the analysis of EBV EBNA1 IgG evidenced that 75% of MS patients were positive, in comparison with 40% of OIND patients ($p < 0.0001$; Fisher exact test) and 30% of control subjects ($p < 0.0001$; Fisher exact test). By dividing the samples on the presence of the KIR2DL2 receptor, 90% of MS patients were positive for EBV EBNA1 IgG in comparison with 49% of OIND patients ($p < 0.0001$; Fisher exact test) and the 50% of control subjects ($p < 0.0001$; Fisher exact test). The results obtained with EBV VCA IgG were comparable to EBNA1 IgG results.

The results obtained from the VZV IgG analysis showed that 90% of MS and OIND patients and 80% of control subjects were positive for VZV IgG. By dividing the samples according to the presence of the KIR2DL2 receptor, a slight increase in the subjects positive for VZV IgG was observed in OIND subjects (50%) compared to control subjects (35%) ($p = 0.05$; Fisher exact test).

The results obtained from the IgG analysis for HHV-6 showed that 100% of MS patients, 95% of OIND patients and 100% of control subjects were positive for HHV-6 IgG. By dividing the samples on the basis of the presence of the KIR2DL2 receptor, a higher percentage of MS (60%) and OIND (60%) patients tested positive for HHV-6 IgG in comparison with control subjects (40%) ($p = 0.007$, Fisher exact test).

The results obtained from the IgG analysis for HSV-1 showed that 60% of MS patients and 70% of control subjects were positive in comparison with 35% of OIND patients ($p = 0.007$; Fisher exact test). By dividing the samples on the basis of the presence of the KIR2DL2 receptor, a higher percentage of the subjects positive for IgG against HSV-1 was observed in MS patients (60%) and control subjects (65%) in comparison with OIND patients ($p = 0.0007$; Fisher exact test).

These results showed that the expression of the KIR2DL2 receptor seems to correlate with the increased positivity for anti-EBV, anti-HHV-6 and anti-HSV-1 IgG; we assessed the levels of positivity for EBV, HHV-6 and HSV-1 IgG in the three populations. We performed serial two-fold dilutions of controls and test samples (initial dilution 1:20 v/v) in dilution buffer (PBS containing 1% skimmed milk). We observed that OIND patients showed the highest titers for EBNA-1 IgG (Figure 6a), while MS patients presented the highest levels for anti-HHV-6 IgG (Figure 6b). The control subjects presented the highest levels for anti-HSV-1 IgG (Figure 6c).

3.5. Levels of Inflammatory Cytokines in Plasma Samples

In order to assess the inflammatory state of the subjects, the plasma levels of nine pro or anti-inflammatory cytokines (IL-1alpha, IL-1beta, INF-gamma, IL-10, IL-4, IL-6, IL-8, IL-12 and TNF-alpha) were evaluated. They were selected as representative of a different immune response and previously implicated in both MS and neuro-lupus diseases [28,29].

MS and OIND patients showed the highest levels of IL-8, IL-12p70, IL-10 and TNF-alpha in comparison with control subjects (Figure 7; $p < 0.0001$; Student's t test). Interestingly, MS and OIND patients showed similar levels of IL-8 ($p = 0.36$; Student's t test), while MS patients presented higher IL-12p70, TNF-alpha and IL-10 levels in comparison with OIND patients ($p < 0.0001$; Student's t test). No differences were observed when subdividing the samples on the basis of KIR2DL2 positivity (data not shown).

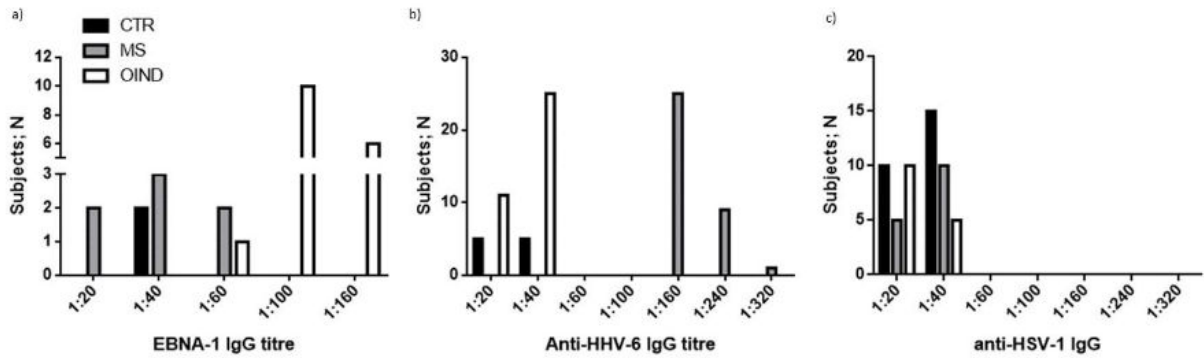


Figure 6. Levels for (a) anti-EBNA-1 IgG, (b) anti HHV-6 IgG and (c) anti HSV-1 IgG in control, MS and OIND populations.

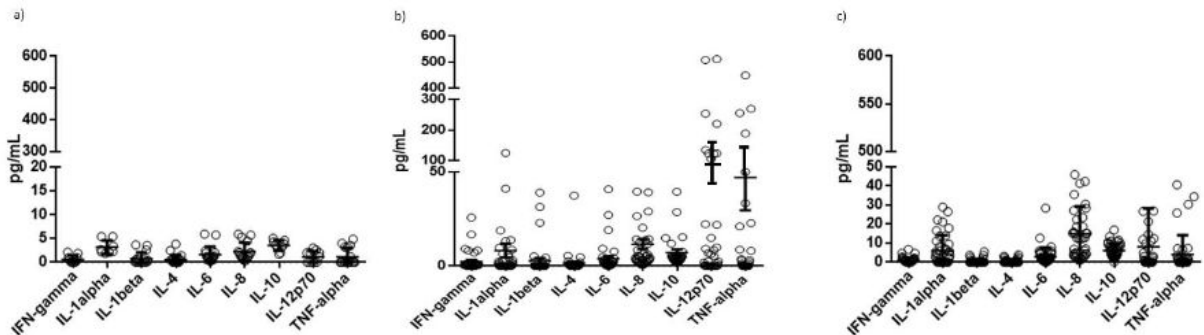


Figure 7. Cytokine serum levels in (a) control, (b) MS and (c) OIND populations. The data are presented as mean ± SE.

4. Discussion

The results of this study demonstrated that KIR2DL2 expression on NK cells gives MS patients a higher susceptibility to HHV infection, confirming our previous results on HSV-1 [14–16]. In particular, KIR2DL2 expression on NK cells reduced NK cell activation and consequently HHVs’ clearance in microglia cells from MS patients. Interestingly, the co-culture of NK cells with HHV-infected microglia cells induced a significant increase in KIR2DL2 expression on CD16+CD56+ NK cells. When we evaluated the control subjects we observed no statistical differences in the activation status of NK cells between KIR2DL2-positive and negative subjects. Interestingly, previous results showed a correlation between KIR2DL2 and the recurrence of HHV infection in healthy subjects [17]. The authors recognized receptor/ligand pair KIR2DL2/HLA-C1 as a predisposing factor for HSV-1 infection and reactivation. These results suggest the implication of KIR2DL2 in HHV infection susceptibility in the human population, that has a deep effect on NK cell activation in MS patients. In particular, we observed that the subjects that respond with a greater increase in KIR2DL2 expression in the presence of an HHV infection were characterized by a higher EDSS, supporting an involvement also in disease status. Similarly, the subjects that responded with a greater increase in KIR2DL2 expression in the presence of an HHV infection were characterized by a higher frequency of MRI disease activity.

We showed an increased susceptibility mainly to EBV and HHV-6 infections in MS patients carrying the KIR2DL2 receptor and HLA-C1 ligand. We can hypothesize that HHV-6 and EBV reactivation, by inducing immune activation via molecular mimicry, may have the ability to induce autoimmunity and cause tissue damage and consequent MS lesion development. HHV-6 and EBV infections are common and have a worldwide distribution, and like most herpesviruses they are a ubiquitous infectious agent, infecting

greater than 90% of the world's population [30,31]. The association between MS and HHV-6 is supported by its ability to productively infect glial cells [32–34]; the persistence of HHV-6 DNA for months in the brain [34]; and the high neuropathogenicity of HHV-6 in a marmoset model [35].

As a proof of concept of the increased susceptibility, we evaluated the levels of HHVs' DNAs. In total, 31% of MS patients, 14.6% of OIND patients and 10% of controls were positive for the presence of the HHV-6 genome, with the highest viral load in MS patients. MS patients presented mainly HHV-6A infection or HHV-6A/-6B co-infection, while OIND patients and controls presented mainly HHV-6B infection. The three cohorts were also evaluated for anti-HHV-6 IgG. The results obtained by the analysis of EBV EBNA1 IgG evidenced that MS patients presented a higher percentage of positive subjects, mainly in the KIR2DL2-positive group. The results obtained from the IgG analysis for HHV-6 showed a higher percentage of subjects positive for IgG against HHV-6 in KIR2DL2-positive MS and OIND subjects compared to controls. The VZV IgG and HSV-1 IgG analysis showed that MS and OIND patients had the highest percentage of positive subjects, mainly in the KIR2DL2-positive subjects. The increase in only HHV-6 viral load, with the high levels of both EBV and HHV-6 IgG levels in MS patients, sustained a possible increased reactivation of these two viruses in MS patients with low levels of replication but the ability to induce humoral response. This reactivation might result without evident clinical sequelae, but it is able to modify the immune cell status. To evaluate this point, we analyzed the levels of pro- and anti-inflammatory cytokines in serum samples. We observed the highest levels of pro-inflammatory cytokines in MS and OIND [28,29]. In particular, TNF-alpha, IL-8 and IL-12p70 were higher in both MS and OIND patients in comparison with control subjects. These results confirm the enhanced inflammatory status in MS and OIND patients, characterized by an increased cytokine production. Interestingly, there was also an increase in IL-10 levels in MS and OIND patients in comparison with controls, suggesting a role in counteracting the inflammatory environment in MS and OIND patients.

In fact, EBV reactivation appears to be linked to disease activity in early MS and it has been reported that EBV reactivation in the CNS may play an important role in MS immunopathology [36]. EBNA2 variants have been identified as biomarkers of MS disease course and therapy response [37]. The evaluation of EBV-infected B cells in post-mortem brains of MS cases still provides controversial results [38,39]. However, the efficacy of B cell depleting therapies in relapsing remitting and progressive MS and the pilot trial with in vitro expanded autologous EBV-specific T cell therapy could be considered an indirect evidence of EBV implication in MS, since memory B cells are the target of latent EBV infection [40,41]. Concerning HHV-6, a higher frequency of active infection seems to be related to MS onset [42,43]. In addition, MS plaques showed an increased frequency of HHV-6 DNA and proteins when compared with control tissues [44] and the serum of MS patients presented higher anti-HHV-6 antibody titers than in healthy controls [45]. The possibility to give a complete characterization of NK cell response in each MS patient might help in increasing the safety of therapies with biological and immune-suppressive drugs (e.g., Fingolimod, Natalizumab), that could reactivate HHV infection [46]. Further analyses are needed to confirm these results in a multicentric study, increasing the number of subjects to be enrolled.

5. Conclusions

Our results demonstrated that the presence of KIR2DL2 expression on NK cells increased the susceptibility of MS patients to HHV infections. We showed an increased susceptibility mainly to EBV and HHV-6 infections in MS patients carrying the KIR2DL2 receptor and HLA-C1 ligand. The highest HHV-6 viral load was observed in MS patients, with an increased percentage of the subjects positive for IgG against HHV-6 in KIR2DL2-positive MS and OIND subjects compared to controls. MS and OIND patients showed the highest levels of IL-8, IL-12p70, IL-10 and TNF-alpha in comparison with control subjects. Interestingly, MS and OIND patients showed similar levels of IL-8, while MS patients

presented higher IL-12p70, TNF-alpha and IL-10 levels in comparison with OIND patients. We can hypothesize that HHVs' reactivation, by inducing immune activation via molecular mimicry, may have the ability to induce autoimmunity and cause tissue damage and consequent MS lesion development.

The availability of Lirilumab (IPH2102/BMS-986015) [47], a human monoclonal antibody that blocks the interaction of the KIR2DL2 receptor and its ligands, with an ongoing randomized Phase II trial in tumors, could allow a therapeutic approach to promote NK cell activation towards HHV infection in MS patients with a possible rebound in disease outcome. Nevertheless, further studies are needed to confirm whether these approaches may help in MS clinical management.

Supplementary Materials: The following supporting information can be downloaded at <https://www.mdpi.com/article/10.3390/microorganisms10030494/s1>: Table S1a: Demographic and clinical characteristics of MS patients; Table S1b: Demographic and clinical characteristics of SLE patients with neuropsychiatric involvement; Table S1c: Clinical hematology results; Table S2: Real-time PCR primers for HHVs' genome quantitation. Figure S1: Representative staining of monocyte cells obtained from peripheral blood to produce microglia cells. (a) FSC/SSC gating; (b) Monocytes were stained as CD14+CD16− cells.

Author Contributions: Conceptualization, R.R., D.B.; methodology, V.G.; formal analysis, G.S., S.B., S.R., M.F.; samples collection, E.B., M.P., M.C., A.B., M.G.; writing—original draft preparation, R.R., D.B.; writing—review and editing, R.R., E.F., E.C.; supervision, R.R., E.F., M.P., M.G.; funding acquisition, R.R. All authors have read and agreed to the published version of the manuscript.

Funding: This research was funded by FISM—Fondazione Italiana Sclerosi Multipla onlus grant n° Cod 2019/R-Single/004.

Institutional Review Board Statement: The study was conducted in accordance with the Declaration of Helsinki, and approved by the Ethics Committee Area Vasta Emilia Centro with the number: 01052016).

Informed Consent Statement: Informed consent was obtained from all subjects involved in the study.

Data Availability Statement: The data presented in this study are all available upon request.

Acknowledgments: We thank Iva Pivanti and Alessandro Sofia for the technical support.

Conflicts of Interest: The authors declare no conflict of interest.

References






- Chen, W.W.; Zhang, X.; Huang, W.J. Role of neuroinflammation in neurodegenerative diseases. *Mol. Med. Rep.* **2016**, *13*, 3391–3396. [[CrossRef](#)] [[PubMed](#)]
- Hamza, T.H.; Zabetian, C.P.; Tenesa, A.; Laederach, A.; Montimurro, J.; Yearout, D.; Kay, D.M.; Doheny, K.F.; Paschall, J.; Pugh, E.; et al. Common genetic variation in the HLA region is associated with late-onset sporadic Parkinson's disease. *Nat. Genet.* **2010**, *42*, 781–785. [[CrossRef](#)] [[PubMed](#)]
- Bar-Or, A.; Pender, M.P.; Khanna, R.; Steinman, L.; Hartung, H.P.; Maniar, T.; Croze, E.; Aftab, B.T.; Giovannoni, G.; Joshi, M.A.; et al. Epstein–Barr Virus in Multiple Sclerosis: Theory and Emerging Immunotherapies. *Trends Mol. Med.* **2020**, *26*, 296–310. [[CrossRef](#)] [[PubMed](#)]
- Alvarez-Lafuente, R.; De Las Heras, V.; Bartolomé, M.; García-Montojo, M.; Arroyo, R. Human herpesvirus 6 and multiple sclerosis: A one-year follow-up study. *Brain Pathol.* **2006**, *16*, 20–27. [[CrossRef](#)] [[PubMed](#)]
- Opsahl, M.L.; Kennedy, P.G.E. Early and late HHV-6 gene transcripts in multiple sclerosis lesions and normal appearing white matter. *Brain* **2005**, *128*, 516–527. [[CrossRef](#)] [[PubMed](#)]
- Komaroff, A.L.; Pellett, P.E.; Jacobson, S. Human herpesviruses 6A and 6B in brain diseases: Association versus causation. *Clin. Microbiol. Rev.* **2020**, *34*, 34. [[CrossRef](#)]
- Caselli, E.; Boni, M.; Bracci, A.; Rotola, A.; Cermelli, C.; Castellazzi, M.; Di Luca, D.; Cassai, E. Detection of antibodies directed against human herpesvirus 6 U94/REP in sera of patients affected by multiple sclerosis. *J. Clin. Microbiol.* **2002**, *40*, 4131–4137. [[CrossRef](#)]
- Gross, C.C.; Schulte-Mecklenbeck, A.; Wiendl, H.; Marcenaro, E.; Kerlero de Rosbo, N.; Uccelli, A.; Laroni, A. Regulatory Functions of Natural Killer Cells in Multiple Sclerosis. *Front Immunol.* **2016**, *7*, 606. [[CrossRef](#)]
- Campbell, K.S.; Purdy, A.K. Structure/Function of Human Killer Cell Immunoglobulin-Like Receptors: Lessons from Polymorphisms, Evolution, Crystal Structures and Mutations. *Immunology* **2011**, *132*, 315–325. [[CrossRef](#)]

10. Pende, D.; Falco, M.; Vitale, M.; Cantoni, C.; Vitale, C.; Munari, E.; Bertaina, A.; Moretta, F.; Del Zotto, G.; Pietra, G.; et al. Killer Ig-Like Receptors (KIRs): Their Role in Nk Cell Modulation and Developments Leading to Their Clinical Exploitation. *Front Immunol.* **2019**, *10*, 1179. [[CrossRef](#)]
11. Rezaei, R.; Mostafaei, S.; Aslani, S.; Jamshidi, A.; Mahmoudi, M. Association study between killer immunoglobulin-like receptor polymorphisms and ankylosing spondylitis disease: An updated meta-analysis. *Int. J. Rheum. Dis.* **2018**, *21*, 1746–1755. [[CrossRef](#)] [[PubMed](#)]
12. Fathollahi, A.; Aslani, S.; Mostafaei, S.; Rezaei, N.; Mahmoudi, M.J.I.R. The role of killer-cell immunoglobulin-like receptor (KIR) genes in susceptibility to inflammatory bowel disease: Systematic review and meta-analysis. *BMC Med. Genet* **2019**, *20*, 24. [[CrossRef](#)] [[PubMed](#)]
13. Aghaei, H.; Mostafaei, S.; Aslani, S.; Jamshidi, A.; Mahmoudi, M. Association study between KIR polymorphisms and rheumatoid arthritis disease: An updated meta-analysis. *BMC Med. Genet* **2019**, *20*, 24. [[CrossRef](#)] [[PubMed](#)]
14. Rizzo, R.; Gentili, V.; Casetta, I.; Caselli, E.; De Gennaro, R.; Granieri, E.; Cassai, E.; Di Luca, D.; Rotola, A. Altered natural killer cells' response to herpes virus infection in multiple sclerosis involves KIR2DL2 expression. *J. Neuroimmunol.* **2012**, *251*, 55–64. [[CrossRef](#)]
15. Rizzo, R.; Bortolotti, D.; Fainardi, E.; Gentili, V.; Bolzani, S.; Baldi, E.; Casetta, I.; Granieri, E.; Rotola, A.; Furlan, R.; et al. KIR2DL2 inhibitory pathway enhances Th17 cytokine secretion by NK cells in response to herpesvirus infection in multiple sclerosis patients. *J. Neuroimmunol.* **2016**, *294*, 1–5. [[CrossRef](#)]
16. Ben Fredj, N.; Rizzo, R.; Bortolotti, D.; Nefzi, F.; Chebel, S.; Rotola, A.; Frih-Ayed, M.; Di Luca, D.; Aouni, M. Evaluation of the implication of KIR2DL2 receptor in multiple sclerosis and herpesvirus susceptibility. *J. Neuroimmunol.* **2014**, *271*, 30–35. [[CrossRef](#)]
17. Estefanía, E.; Gómez-Lozano, N.; Portero, F.; de Pablo, R.; Solís, R.; Sepúlveda, S.; Vaquero, M.; González, M.A.; Suárez, E.; Roustán, G.; et al. Influence of KIR gene diversity on the course of HSV-1 infection: Resistance to the disease is associated with the absence of KIR2DL2 and KIR2DS2. *Tissue Antigens* **2007**, *70*, 34–41. [[CrossRef](#)]
18. McDonald, W.I.; Compston, A.; Edan, G.; Goodkin, D.; Hartung, H.-P.; Lublin, F.D.; McFarland, H.F.; Paty, D.W.; Polman, C.H.; Reingold, S.C.; et al. Recommended diagnostic criteria for multiple sclerosis: Guidelines from the International Panel on the Diagnosis of Multiple Sclerosis. *Ann. Neurol.* **2001**, *50*, 121–127. [[CrossRef](#)]
19. Kurtzke, J.F. Rating neurological impairment in multiple sclerosis: An expanded disability scale (EDSS). *Neurology* **1983**, *33*, 1444–1452. [[CrossRef](#)]
20. Lublin, D.F.; Reingold, S.C. Defining the clinical course of multiple sclerosis: Results of an international survey. *Neurology* **1996**, *46*, 907–911. [[CrossRef](#)]
21. Hochberg, M.C. Updating the American College of Rheumatology revised criteria for the classification of systemic lupus erythematosus. *Arthritis Care Res.* **1997**, *40*, 1725. [[CrossRef](#)] [[PubMed](#)]
22. Alunno, A.; Najm, A.; Machado, P.M.; Bertheussen, H.; Burmester, G.-R.R.; Carubbi, F.; De Marco, G.; Giacomelli, R.; Hermine, O.; Isaacs, J.D.; et al. 2021 update of the EULAR points to consider on the use of immunomodulatory therapies in COVID-19. *Ann. Rheum. Dis.* **2021**, *81*, 34–40. [[CrossRef](#)] [[PubMed](#)]
23. Bortoluzzi, A.; Fanouriakis, A.; Appenzeller, S.; Costallat, L.; Scirè, C.A.; Murphy, E.; Bertias, G.; Hanly, J.; Govoni, M. Validity of the Italian algorithm for the attribution of neuropsychiatric events in systemic lupus erythematosus: A retrospective multicentre international diagnostic cohort study. *BMJ Open* **2017**, *7*, e015546. [[CrossRef](#)] [[PubMed](#)]
24. Bortolotti, D.; Gentili, V.; Caselli, E.; Siculo, M.; Soffritti, I.; D'Accolti, M.; Barao, L.; Rotola, A.; Di Luca, D.; Rizzo, R. DNA Sensors' Signaling in NK Cells During HHV-6A, HHV-6B and HHV-7 Infection. *Front Microbiol.* **2020**, *11*, 226. [[CrossRef](#)]
25. Leone, C.; Le Pavec, G.; Mème, W.; Porcheray, F.; Samah, B.; Dormont, D.; Gras, G. Characterization of human monocyte-derived microglia-like cells. *Glia* **2006**, *54*, 183. [[CrossRef](#)]
26. Bortolotti, D.; Gentili, V.; Rotola, A.; Caselli, E.; Rizzo, R. HHV-6A infection induces amyloid-beta expression and activation of microglial cells. *Alzheimers Res. Ther.* **2019**, *11*, 104. [[CrossRef](#)]
27. Bortolotti, D.; Gentili, V.; Rotola, A.; Cultrera, R.; Marci, R.; Di Luca, D.; Rizzo, R. HHV-6A infection of endometrial epithelial cells affects immune profile and trophoblast invasion. *Am. J. Reprod. Immunol.* **2019**, *82*, e13174. [[CrossRef](#)]
28. Wang, K.; Song, F.; Fernandez-Escobar, A.; Luo, G.; Wang, J.; Sun, Y. The Properties of Cytokines in Multiple Sclerosis: Pros and Cons. *Am. J. Med. Sci.* **2018**, *356*, 552–560. [[CrossRef](#)]
29. Trysberg, E.; Carlsten, H.; Tarkowski, A. Intrathecal cytokines in systemic lupus erythematosus with central nervous system involvement. *Lupus* **2000**, *9*, 498–503. [[CrossRef](#)]
30. Caselli, E.; Di Luca, D. Molecular biology and clinical associations of Roseoloviruses human herpesvirus 6 and human herpesvirus 7. *New Microbiol.* **2007**, *30*, 173–187.
31. Henle, W.; Henle, G. Seroepidemiology of the virus. In *The Epstein-Barr Virus*; Epstein, M.A., Achong, B.G., Eds.; Springer: Berlin/Heidelberg, Germany, 1979; pp. 61–78.
32. Donati, D.; Akhyani, N.; Fogdell-Hahn, A.; Cermelli, C.; Cassiani-Ingoni, R.; Vortmeyer, A.; Heiss, J.D.; Cogen, P.; Gaillard, W.D.; Sato, S.; et al. Detection of human herpesvirus-6 in mesial temporal lobe epilepsy surgical brain resections. *Neurology* **2003**, *61*, 1405–1411. [[CrossRef](#)] [[PubMed](#)]
33. Harberts, E.; Yao, K.; Wohler, J.E.; Maric, D.; Ohayon, J.; Henkin, R.; Jacobson, S. Human herpesvirus-6 entry into the central nervous system through the olfactory pathway. *Proc. Natl. Acad. Sci. USA* **2011**, *108*, 13734–13739. [[CrossRef](#)] [[PubMed](#)]

34. Reynaud, J.M.; Jégou, J.; Welsch, J.C.; Horvat, B. Human Herpesvirus 6A Infection in CD46 Transgenic Mice: Viral Persistence in the Brain and Increased Production of Proinflammatory Chemokines via Toll-Like Receptor 9. *J. Virol.* **2014**, *88*, 5421–5436. [[CrossRef](#)]
35. Leibovitch, E.; Wohler, J.E.; Macri, S.M.C.; Motanic, K.; Harberts, E.; Gaitán, M.I.; Maggi, P.; Ellis, M.; Westmoreland, S.; Silva, A.; et al. Novel marmoset (*Callithrix jacchus*) model of human Herpesvirus 6A and 6B infections: Immunologic, virologic and radiologic characterization. *PLoS Pathog.* **2013**, *9*, e1003138. [[CrossRef](#)] [[PubMed](#)]
36. Castellazzi, M.; Delbue, S.; Elia, F.; Gastaldi, M.; Franciotta, D.; Rizzo, R.; Bellini, T.; Bergamaschi, R.; Granieri, E.; Fainardi, E. Epstein-Barr Virus Specific Antibody Response in Multiple Sclerosis Patients during 21 Months of Natalizumab Treatment. *Dis. Markers* **2015**, *2015*, 901312. [[CrossRef](#)]
37. Mechelli, R.; Manzari, C.; Policano, C.; Annese, A.; Picardi, E.; Umeton, R.; Fornasiero, A.; D'Erchia, A.M.; Buscarinu, M.C.; Agliardi, C.; et al. Epstein-Barr virus genetic variants are associated with multiple sclerosis. *Neurology* **2015**, *84*, 1362–1368. [[CrossRef](#)]
38. Serafini, B.; Rosicarelli, B.; Franciotta, D.; Magliozzi, R.; Reynolds, R.; Cinque, P.; Andreoni, L.; Trivedi, P.; Salvetti, M.; Faggioni, A.; et al. Dysregulated Epstein-Barr virus infection in the multiple sclerosis brain. *J. Exp. Med.* **2007**, *204*, 2899–2912. [[CrossRef](#)]
39. Willis, S.N.; Stadelmann, C.; Rodig, S.J.; Caron, T.; Gattenloehner, S.; Mallozzi, S.S.; Roughan, J.E.; Almendinger, S.E.; Blewett, M.M.; Brück, W.; et al. Epstein-Barr virus infection is not a characteristic feature of multiple sclerosis brain. *Brain* **2009**, *132*, 3318–3328. [[CrossRef](#)]
40. Lindner, J.M.; Cornacchione, V.; Sathe, A.; Be, C.; Srinivas, H.; Riquet, E.; Leber, X.-C.; Hein, A.; Wrobel, M.B.; Scharenberg, M.; et al. Human Memory B Cells Harbor Diverse Cross-Neutralizing Antibodies against BK and JC Polyomaviruses. *Immunity* **2019**, *50*, 668–676.e5. [[CrossRef](#)]
41. Gelfand, J.M.; Cree, B.A.C.; Hauser, S.L. Ocrelizumab and Other CD20 + B-Cell-Depleting Therapies in Multiple Sclerosis. *Neurotherapeutics* **2017**, *4*, 835–841. [[CrossRef](#)]
42. Thacker, E.L.; Mirzaei, F.; Ascherio, A. Infectious mononucleosis and risk for multiple sclerosis: A meta-analysis. *Ann. Neurol.* **2006**, *59*, 499–503. [[CrossRef](#)] [[PubMed](#)]
43. Nielsen, T.R.; Rostgaard, K.; Nielsen, N.M.; Koch-Henriksen, N.; Haahr, S.; Sørensen, P.S.; Hjalgrim, H. Multiple sclerosis after infectious mononucleosis. *Arch. Neurol.* **2007**, *64*, 72–75. [[CrossRef](#)] [[PubMed](#)]
44. Challoner, P.B.; Smith, K.T.; Parker, J.D.; MacLeod, D.L.; Coulter, S.N.; Rose, T.M.; Schultz, E.R.; Bennett, J.L.; Garber, R.L.; Chang, M.; et al. Plaque-associated expression of human herpesvirus 6 in multiple sclerosis. *Proc. Natl. Acad. Sci. USA* **1995**, *92*, 7440–7444. [[CrossRef](#)] [[PubMed](#)]
45. Engdahl, E.; Gustafsson, R.; Huang, J.; Biström, M.; Lima Bomfim, I.; Stridh, P.; Khademi, M.; Brenner, N.; Butt, J.; Michel, A.; et al. Increased Serological Response Against Human Herpesvirus 6A Is Associated With Risk for Multiple Sclerosis. *Front Immunol.* **2019**, *10*, 2715. [[CrossRef](#)]
46. Epstein, D.J.; Dunn, J.; Deresinski, S. Infectious Complications of Multiple Sclerosis Therapies: Implications for Screening, Prophylaxis, and Management. *Open Forum Infect. Dis.* **2018**, *5*, 174. [[CrossRef](#)]
47. Vey, N.; Karlin, L.; Sadot-Lebouvier, S.; Broussais, F.; Berton-Rigaud, D.; Rey, J.; Charbonnier, A.; Marie, D.; André, P.; Paturel, C.; et al. A phase 1 study of lirilumab (antibody against killer immunoglobulin-like receptor antibody KIR2D; IPH2102) in patients with solid tumors and hematologic malignancies. *Oncotarget* **2018**, *9*, 17675–17688. [[CrossRef](#)]

Article

Studying the Interactions of U24 from HHV-6 in Order to Further Elucidate Its Potential Role in MS

Keng-Shuo Pi ¹, Daria Bortolotti ², Yurou Sang ^{1,3}, Giovanna Schiuma ², Silvia Beltrami ², Sabrina Rizzo ², Alessandra Bortoluzzi ⁴, Eleonora Baldi ⁵, A. Louise Creagh ⁶, Charles A. Haynes ⁶, Roberta Rizzo ^{2,*} and Suzana K. Straus ^{1,*}

¹ Department of Chemistry, University of British Columbia, 2036 Main Mall, Vancouver, BC V6T 1Z1, Canada

² Department of Chemical, Pharmaceutical and Agricultural Sciences, University of Ferrara, 44121 Ferrara, Italy

³ Faculty of Health Sciences, Simon Fraser University, 8888 University Drive, Burnaby, BC V5A 1S6, Canada

⁴ Rheumatology Unit, Department of Medical Sciences, University of Ferrara and Azienda Ospedaliero-Universitaria S. Anna, 44121 Ferrara, Italy

⁵ Department of Neuroscience and Rehabilitation, Division of Neurology, “Sant’Anna” University-Hospital, 44121 Ferrara, Italy

⁶ Michael Smith Laboratories and Department of Chemical and Biological Engineering, University of British Columbia, 2185 East Mall, Vancouver, BC V6T 1Z4, Canada

* Correspondence: rbr@unife.it (R.R.); sstraus@chem.ubc.ca (S.K.S.);
Tel.: +39-0532-455382 (R.R.); +1-604-822-2537 (S.K.S.)



Citation: Pi, K.-S.; Bortolotti, D.; Sang, Y.; Schiuma, G.; Beltrami, S.; Rizzo, S.; Bortoluzzi, A.; Baldi, E.; Creagh, A.L.; Haynes, C.A.; et al. Studying the Interactions of U24 from HHV-6 in Order to Further Elucidate Its Potential Role in MS. *Viruses* **2022**, *14*, 2384. <https://doi.org/10.3390/v14112384>

Academic Editor: Anthony V. Nicola

Received: 20 September 2022

Accepted: 27 October 2022

Published: 28 October 2022

Publisher’s Note: MDPI stays neutral with regard to jurisdictional claims in published maps and institutional affiliations.



Copyright: © 2022 by the authors. Licensee MDPI, Basel, Switzerland. This article is an open access article distributed under the terms and conditions of the Creative Commons Attribution (CC BY) license (<https://creativecommons.org/licenses/by/4.0/>).

Abstract: A number of studies have suggested that human herpesvirus 6A (HHV-6A) may play a role in multiple sclerosis (MS). Three possible hypotheses have been investigated: (1) U24 from HHV-6A (U24-6A) mimics myelin basic protein (MBP) through analogous phosphorylation and interaction with Fyn-SH3; (2) U24-6A affects endocytic recycling by binding human neural precursor cell (NPC) expressed developmentally down-regulated protein 4-like WW3* domain (hNedd4L-WW3*); and (3) MS patients who express Killer Cell Immunoglobulin Like Receptor 2DL2 (KIR2DL2) on natural killer (NK) cells are more susceptible to HHV-6 infection. In this contribution, we examined the validity of these propositions by investigating the interactions of U24 from HHV-6B (U24-6B), a variant less commonly linked to MS, with Fyn-SH3 and hNedd4L-WW3* using heteronuclear single quantum coherence (HSQC) nuclear magnetic resonance (NMR) titrations and isothermal titration calorimetry (ITC). In addition, the importance of phosphorylation and the specific role of U24 in NK cell activation in MS patients were examined. Overall, the findings allowed us to shed light into the models linking HHV-6 to MS and the involvement of U24.

Keywords: human herpes virus; *Roseolovirus*; Fyn-SH3; Nedd4L; multiple sclerosis; phosphorylation; natural killer cells; Killer Cell Immunoglobulin Like Receptor 2DL2

1. Introduction

Human herpesviruses HHV-6A, -6B and -7 are *Roseoloviruses* that have been hypothesized to be implicated in several neurological diseases, including encephalitis, epilepsy, Alzheimer’s and multiple sclerosis (MS) [1–7]. Although the exact cause of MS is still currently unknown, it has been suggested that one or more viruses may be possible triggers [8–12]. Specifically, it has been proposed that potential triggering agents, such as Epstein–Barr virus, HHV-6 (the collective name for HHV-6A and HHV-6B), varicella–zoster virus, cytomegalovirus, C virus and human endogenous retroviruses, play a role [11,13,14]. A number of these viruses are ubiquitous and highly prevalent in adult populations worldwide [15]. To date, only a limited number of potential viral proteins that could be explicitly involved in this triggering have been identified [16–23].

U24 (see Supplemental for nomenclature), a putative tail-anchored membrane protein that is unique to *Roseoloviruses* [24], is one such protein that may be implicated in MS. It is expressed during the early stages of viral infection [25]. Although the exact function

of U24 has not been fully elucidated, a number of studies have suggested a potential link between U24 and MS [15,26–31]. In HHV-6A, the N-terminal segment of U24 consists of a PxxP motif, as well as a PY motif (Table 1). These same two motifs can be found in U24 from HHV-6B, which is not surprising given that HHV-6A and -6B genomes share an overall identity of 90%. Finally, in HHV-7, U24 only possesses the PY motif (Table 1). The proline-rich segment of U24 has been suggested as being important for its function, as such segments are typically involved in protein–protein interactions because of the distinct structure of the polyproline helix they form [13]. A number of important protein–protein interactions involving prolines and linked to MS will be described below.

Table 1. Sequence alignment of myelin basic protein (MBP) and U24 from HHV-6A (U24-6A), -6B, and -7. The PxxP motif is indicated in dark gray, whereas the PY motif is shown in light gray. The subscript in the name of the peptide represents the residue numbers, with the numbering of MBP based on the human 18.5 kDa classic isoform. Negatively charged side-chains are shown in blue, while positively charged residues are in red. The phosphorylated peptides (pU24-6A and pU24-6B) are also included, with pT representing phospho-threonine. 15 residue peptides, with the sequences given here, were used in this study.

Name	Sequence															
	I	V	T	P	R	T	P	P	P	S	Q	G	K	G	R	
MBP ₉₃₋₁₀₇	M	D	P	P	R	T	P	P	P	S	Y	S	E	V	L	
U24-6A ₁₋₁₅	M	D	P	P	R	T	P	P	P	S	Y	S	E	V	L	
pU24-6A ₁₋₁₅	M	D	P	P	R	pT	P	P	P	S	Y	S	E	V	L	
U24-6B ₁₋₁₅	M	D	R	P	R	T	P	P	P	S	Y	S	E	V	L	
pU24-6B ₁₋₁₅	M	D	R	P	R	pT	P	P	P	S	Y	S	E	V	L	
U24-7 ₁₋₁₅	M	-	T	H	E	T	P	P	P	S	Y	N	D	V	M	L

Both U24-6A and -6B share a proline rich segment with myelin basic protein (MBP, Table 1), a key component of the myelin sheath protecting axons in the central nervous system (CNS). In MS, MBP becomes an autoantigen, i.e., a normal constituent of neuronal cells that becomes the target of an immune response from auto-reactive T-cells [9,10,32]. The seven amino acid sequence identity between U24 from HHV-6 and MBP has led to the suggestion that U24 may function by mimicking MBP. Indeed the polyproline region in MBP is essential for it to participate in Fyn-mediated signaling pathways via a direct but non-canonical association between the Fyn-SH3 domain and the PxxP motif [33]. Oligodendrocyte differentiation and maturation, which are processes that are perturbed in MS patients, are impacted by the disruption of these signaling pathways. In addition, MBP has two threonine residues (T95 and T98) within and just before the PxxP motif (Table 1), which can be phosphorylated. Phosphorylation has been shown to affect the local structure of MBP and its disposition on the membrane surface [34]. In addition, MS patients have a degree of phosphorylation at T98 that is lower than that of normal individuals [35]. Phosphorylation was found to decrease the ability of MBP to polymerize actin and to bundle actin filaments, without however affecting the dissociation constant of the MBP-actin complex [36]. Additionally, phosphorylation of MBP leads to a reduced interaction with Fyn-SH3 [37]. Finally, MBP phosphorylation decreases the interaction between MBP and lipids, making it difficult to organize lipids into the multilayers found in the myelin sheath [38]. U24 from HHV-6A has been shown to associate with Fyn-SH3, albeit ca. 1000-fold less than MBP ($K_d = 5$ mM for U24-6A [29] versus 4–8 μ M for MBP [39]). In addition, U24-6A can be phosphorylated by MAPK, but less effectively than MBP [28]. Overall, these findings suggested that although U24-6A may mimic MBP, it most likely does not interfere directly with MBP function.

U24 has been shown to mediate the downregulation of the T-cell receptor complex and also the transferrin receptor (TfR) through its PY motif [40,41], suggesting a general block in early endosomal recycling. These results strongly suggest that U24 expression can influence the activation state of the immune system of infected individuals, supporting the potential link between U24 and MS immune dysregulation [15,26–31]. Endosomal recycling is a process controlled by E3 ubiquitin ligases. Recently, U24-6A and the phosphorylated pU24-

6A have been found to preferentially interact with neural precursor cell (NPC) expressed developmentally down-regulated protein 4 (Nedd4) E3 ubiquitin ligase, via its WW3 domains [30,31]. In the CNS, Nedd4 and Nedd4-like proteins (Nedd4L) play a crucial role in promoting dendrite outgrowth [42,43] and maintaining neuronal survival [44,45]. So hypothetically, U24 could function by affecting Nedd4 or Nedd4L, which may cause defective neural development, resulting in damage of axons or myelin.

On the other hand, U24 may play a role in HHV-6 infectivity. Studies have demonstrated that MS patients who express Killer Cell Immunoglobulin Like Receptor 2DL2 (KIR2DL2) on natural killer (NK) cells are more susceptible to HHV-6 infection [46–48]. In particular, Rizzo et al. have shown reduced NK cell activation and consequently a low HHV-6 clearance in MS patients with a KIR2DL2 allele. KIRs are MHC class I-specific regulatory receptors utilized by human NK cells and CD8 T cells. Several lines of evidence link differences in KIR expression to differential responses to invading pathogens and autoimmune disorders [49–52]. To date, no studies have demonstrated whether U24 plays a direct role in NK cell activation in MS patients.

Given previous findings on U24-6A and U24-7 [29–31] and in order to better understand the potential role of U24 in MS and the features of U24 that are important for the protein–protein interactions discussed above, we have examined here the interaction of U24 from HHV-6B and its phosphorylated form with hNedd4L-WW3* (3rd WW domain in human Nedd4L, where the star was adopted in literature describing sequence comparisons of the human vs. rat/mouse analogues) and Fyn-SH3. Since HHV-6A is more commonly linked with MS than HHV-6B [27,53–55], it is hypothesized that U24-6B binding to hNedd4L-WW3* might be weaker than for U24-6A. In addition, a number of studies have shown that the interaction between proline-rich segments and Fyn-SH3 is highly dependent on the presence of arginine residues that flank the PxxP motif [56–60]. Hence, it is anticipated that U24-6B, with an Arg at position 3 (Table 1) and an Asp at position 2, might bind more tightly to Fyn-SH3 than U24-6A. Finally, since NK cell recognition and specific killing of HHV-infected cells are tightly regulated by KIRs and their MHC-ligands, it would be important to establish the role of KIRs in MS with a particular attention to demonstrating preferential natural killer (NK) cell activation in MS patients upon exposure to U24-6A and -6B and their respective phosphorylated versions.

2. Materials and Methods

2.1. Ethics Statement

The part of this study involving human subjects was conducted following ethics approval by the Area Vasta Emilia Centro (N:01052016), who also approved the experimental protocols used. The study adheres to the ethical principles for medical research involving human subjects as required by the 2013 revision of the Declaration of Helsinki–WMA Declaration of Helsinki–Ethical Principles for Medical Research Involving Human Subjects. Furthermore, none of the female MS patients, Neurolupus (NLES) and control subjects were pregnant before entering the study.

2.2. Synthesis and Purification of 15-Residue Peptides Representing the Polyproline-Rich N-Terminal Region of U24 from HHV-6A and HHV-6B

Two 15-mer peptides representing the N-terminal region of U24-6A and U24-6B (Table 1) were synthesized using N-9-fluorenylmethyloxycarbonyl (N-Fmoc) protected α -amino acids on an automated peptide synthesizer (CS Bio, Menlo Park, CA, USA). Preloaded Fmoc-Leu-Wang resin (Advanced ChemTech, Louisville, KY, USA) and O-(benzotriazol-1-yl)-N,N,N',N'-tetramethyluronium hexafluorophosphate (HBTU, Advanced ChemTech) were used as the coupling reagents. Double coupling was required for the last nine residues of U24-6A (MDPPRTPPP) and U24-6B (MDRPRTPPP). The crude peptide was deprotected and cleaved from the resin in 90% trifluoroacetic acid (TFA) with trace ddH₂O, 1,2-ethanedithiol (EDT) and triethylsilane (TES) as scavengers for at least 5 h. The excess organic solvents were removed under reduced pressure, and the peptide was precipitated

through careful addition of 100 mL of cold diethyl ether into the peptide mixture. The filtered crude peptide powder was then dried under vacuum in a desiccator overnight, redissolved and frozen in de-ionized water and lyophilized to remove all residual solvents. Then, the presence of the desired peptide was determined by MALDI-TOF MS.

Both U24-6A and U24-6B peptides were purified using a C18 reverse-phase high-performance liquid chromatography (HPLC) column (Phenomenex, Torrance, CA, USA, Jupiter, 10 μm 300 \AA , 250 \times 21.2 mm) on a Waters 600 system, monitored by UV absorption at 228 nm and 278 nm using a photodiode array detector. U24-6A peptide was eluted with a gradient from 0 to 15% of acetonitrile for over 28 min at a flow rate of 10 mL/min. In contrast, U24-6B peptide was eluted with a gradient from 0 to 30% of acetonitrile for over 50 min at a flow rate of 10 mL/min. The purified peptides were lyophilized and HPLC purification procedure was repeated a total of four times to ensure high purity ($\geq 95\%$, Figure S1).

Phosphorylated peptides (with a phospho-threonine 6, Table 1) were purchased from Genscript (Piscataway, NJ, USA) and used without further purification.

2.3. Expression and Purification of *hNedd4L-WW3**

The pGEX-4T2 vector plasmid used here was previously described by Sang et al. [30]. The plasmid was transformed into *E. coli* BL21(DE3) for expression according to standard protocols. In preparation for large-scale expression, 5 mL of starting Luria Bertani-carbenicillin (LB-CBC) culture was firstly grown (37 $^{\circ}\text{C}$; 5 to 6 h; 225 rpm). Then, 1 mL of the starting culture was used to inoculate 800 mL of fresh LB-ampicillin (amp). The large culture was then grown (37 $^{\circ}\text{C}$; 5 to 6 h; 225 rpm) till OD_{600} reached 0.5, and cooled down in the cold room for 5 min before induction (16 h; 25 $^{\circ}\text{C}$; 225 rpm) with 400 μM IPTG. 500 μL samples from before and after induction were pelleted via centrifugation for SDS-PAGE analysis to confirm protein expression. The cells were harvested via centrifugation (5000 rpm; 20 min; 4 $^{\circ}\text{C}$) and the remaining cell paste from each 800 mL culture was washed once in 30 mL PBS buffer, centrifuged (3900 rpm; 10 min; 4 $^{\circ}\text{C}$) and stored in -80°C .

The cell paste was thawed on ice and resuspended initially in 5 mL of PBS/Triton buffer (PBS buffer supplemented with 1% Triton X-100). 10 mg of lysozyme, 20 μL protease inhibitor and 20 μL of DNase were added to the mixture. The mixture was incubated on ice for 30 min, after which 5 mL of PBS/Triton buffer was added for a total volume of 10 mL. The mixture was then sonicated (2-s on-pulses; 5 s off-pulses; 37% amplitude power) in an ice bath for 3 min. After centrifugation (9000 rpm; 1 h; 4 $^{\circ}\text{C}$), the supernatant was filtered using a 0.45 μm filter and then applied to 2 mL of PBS buffer washed Glutathione Sepharose 4B resin (GE Healthcare, Burnaby, BC, Canada, GST 4B resin), loaded into a 15 mL centrifuge tube. An end-over-end rotator (SARSTEDT) was used to mix the resin for 2 h at room temperature. Then, the 4B resin was washed with PBS/Triton buffer three times each, followed by sedimentation via centrifugation (3900 rpm; 5 min; 4 $^{\circ}\text{C}$). Subsequently, the resin mixture was washed with Wash4 buffer once (0.5 mM Glutathione reduced in PBS buffer) and PBS buffer three times before adding 3 mL of 50 U/mL thrombin in PBS buffer to the 4B resin for an incubation period of 16 h at room temperature.

The supernatant containing cleaved WW3* domain (sequence in Table S1) was collected via centrifugation (3900 rpm; 10 min; 4 $^{\circ}\text{C}$). The resin was washed with 4 mL of PBS buffer 2 more times before adding the cleaved solution into 200 μL of p-Amino benzamide-agarose (Sigma-Aldrich, St.-Louis, MO, USA), washed with PBS buffer. The resin mixture was incubated at 4 $^{\circ}\text{C}$ for 2 h and pelleted by centrifugation (3900 rpm; 10 min; 4 $^{\circ}\text{C}$). Then, the supernatant was washed with 100 μL of PBS washed fresh GST 4B resin to remove any residual GST protein in the cleaved WW3* domain fractions. 10 μL of the homogenate, supernatant, cell pellet, flow-through, thrombin cleavage product, thrombin wash product, and GST-wash product were collected and analyzed by Tris-Tricine SDS-PAGE with their concentrations adjusted accordingly. MALDI-MS was also used to confirm that the sequence listed in Table S1 was obtained.

2.4. Expression and Purification of ^{15}N -Fyn-SH3

The plasmid used for the expression of GST-Fyn-SH3 protein was a kind gift from C. Pallen (Child & Family Research Institute, Vancouver, BC, Canada). The vector is pGEX kg with the SH3 domain of human Fyn (from residues TGVTLF to YVAPVD; Table S1) cloned into the HindIII–XbaI site [29]. The plasmid was transformed into *E. coli* BL21(DE3) for expression according to standard protocols.

In preparation for large-scale protein expression, 5 mL of starting LB-CBC culture was firstly grown (37 °C; 5 to 6 h; 225 rpm). A cell pellet was obtained via centrifugation (4 °C; 10 min; 3900 rpm) and removal of supernatant. The resultant cell pellet was dissolved and inoculated in 100 mL of ^{15}N -M9-amp media supplemented with 1 g/L ^{15}N - NH_4Cl for a period of ca. 36 h (27 °C; 225 rpm). The 100 mL starting culture was then inoculated into 800 mL of ^{15}N -M9-amp media for about 2 h, 37 °C and 225 rpm until OD_{600} reached 0.5–0.8 and cooled down in the cold room for 5 min before induction (4 h; 37 °C; 225 rpm), using 500 μM IPTG. 500 μL samples from before and after induction were pelleted via centrifugation for electrophoresis analysis to confirm protein expression. The cells were harvested via centrifugation (9000 rpm; 20 min; 4 °C) and the cell paste from each 800 mL culture was harvested as described in the preceding section.

Cleavage and purification were carried out using the identical protocols as described above for the purification of the WW domain, with the exception of one modification in the sonication procedure in which 5 s on-pulses and 10 sec off-pulses for 3 min were used instead. The purity of the obtained protein was verified using SDS-PAGE and MALDI-MS.

2.5. Subjects

40 MS Relapsing Remitting patients, in remission phase (mean age: 38 ± 10 years), 40 healthy controls (mean age: 37 ± 11 years) and 40 subjects with other inflammatory neurological diseases such as NLES (mean age: 36 ± 13 years) were recruited. MS was defined according to the classification of McDonald [61] and the patients were followed at the MS Centre of the Department of Neurology, University of Ferrara, Italy, during the period from 2015 to 2018. Disease disability was assessed in all MS patients at the time of sample collection using Kurtzke's Expanded Disability Status Scale (EDSS) [62] (mean at entry: 2 ± 1 , range from 0 to 5.5). All patients had Relapsing-Remitting course in agreement with the criteria of Lublin [63]. At the time of enrolment in the study, all the MS patients were clinically stable. At entry none of the patients had fever or other symptoms or signs of acute infections. Moreover, none of the patients had received any potential disease-modifying therapies (e.g., azathioprine or methylprednisolone, interferon-beta or glatiramer acetate) during the 6 months preceding the study. NLES patients satisfying the 1997 revised American College of Rheumatology criteria regularly attending the Lupus Clinic of the Rheumatology Unit, Department of Medical Sciences, Sant'Anna Hospital, University of Ferrara, Italy were recruited during the same period [64]. We recorded clinical, demographic, and serological data, as well as data regarding therapy, including corticosteroids (measured as prednisone equivalent), antimalarials, and immunosuppressants. Neuropsychiatric (NP) manifestations were defined according to the 1999 ACR nomenclature and case definitions and diagnostic work-up was performed according to the EULAR recommendations [65]. Attribution of NP events was based on physician judgment and considering ACR 'exclusion' and 'association' factors (i.e., their absence favors attribution to SLE), as well as 'SLE-favoring factors' of the Italian Study Group on NPSLE validated attribution model were also considered [66]. Clinical assessment and blood sampling were performed during routine clinic visits. The samples were collected after informed consent, following the ethics guidelines outlined in Section 2.1.

2.6. Peripheral Blood Mononuclear Cell (PBMC) Culture

PBMCs were purified from whole blood by Ficoll gradient (Cederlane, Hornby, ON, Canada), resuspended in 2 mL of RPMI-1640 (Euroclone, Pavia, Italy) supplemented

with 2 mM L-Glutamine, 100 U/mL Penicillin G, 100 µg/mL Streptomycin and 20% FCS (Euroclone, Pavia, Italy) (RPMI-20%FCS) and counted.

Natural killer cells were separated from peripheral blood samples using the negative magnetic cell separation (MACS) system (Miltenyi Biotech, Gladbach, Germany) [67]. The analysis of purified cell fraction by flow cytometry with CD3-PerCp-Cy5.5, CD56-FITC moAbs (e-Bioscience, Frankfurt, Germany), demonstrated that the NK cell content was >90% (data not shown). NK cells were resuspended at 2×10^6 cells/mL in 20 mL of RPMI 1640 (BioWhittaker, Verviers, Belgium) containing 10% human AB serum (Mediatech, Herndon, VA, USA), 1 mM non-essential amino acids, 2 mM glutamine, 1 mM pyruvate, 20 mM HEPES, 100 U/mL Penicillin and 100 µg/mL Streptomycin (Gibco BRL Life Technologies, Gaithersburg, MD, USA). Cell suspensions were stimulated with 100 U/mL of IL-2 (Hoffmann-LaRoche) on day 0 and cultured for 5 to 6 days at 37 °C, 5% CO₂. NK cells were separated into KIR2DL2 expressing and non-expressing KIR2DL2 cells using CELLection™ Dynabeads (ThermoFisher; Milan, Italy) coated with anti-KIR2DL2 biotinylated antibody (BPS-Bioscience, San Diego, CA, USA). The efficiency of the separation was assessed using flow cytometry.

T cells were separated from peripheral blood samples using the positive magnetic cell separation (MACS) system Pan T Cell Isolation Kit (Miltenyi Biotech, Gladbach, Germany). The analysis of purified cell fraction by flow cytometry with CD2-PE and CD3-FITC (e-Bioscience, Frankfurt, Germany) demonstrated that the T cell content was >90% (data not shown). T cells were resuspended at 2×10^6 cells/mL in 20 mL of Gibco CTS Optmizer Pro SFM (ThermoFisher; Milan, Italy) and cultured for 5 to 6 days at 37 °C, 5% CO₂. T cells were activated with plate bound 0.25 µg/mL antiCD3ε plus soluble antiCD28 in the presence or absence of 100 pM TGF-β1 (R&D Systems, Minneapolis, MN, USA) typically for 24 h.

2.7. T Cell Protein Transfection

T cells were transfected using the Pierce Protein Transfection Kit (ThermoFisher; Milan, Italy) following product instructions. A total of 4×10^5 cells were transfected with 1 µg of peptide (U24, MBP). Transfection was performed for 3–4 h at 37 °C in 1 mL medium without fetal bovine serum (FBS). After transfection, a volume of complete medium with 20% FBS was added to each well. T cells treated with transfection reagent alone or transfected with 0.5 µg control fluorescent antibody (provided in the kit) were used as negative and efficiency control, respectively. A mean transfection efficiency of 95% for all the peptides was obtained (data not shown).

2.8. Lactate Dehydrogenase (LDH) Assay

LDH assay was performed to evaluate the effect of the transfection with U24 or MBP peptides in T cells. Transfected T cells were suspended at 5×10^4 cells/mL and cultured for 4 h on a 96-well microplate at 37 °C with 5% CO₂. A colorimetric-based lactate dehydrogenase (LDH) assay (Cytotoxicity Detection KitPLUS; Basel, Switzerland) was used, according to the manufacturer's instructions. The percentage of viable cells was evaluated using the following equation: $100 - [(Culture Media LDH (OD) of treated cells - Culture Media LDH (OD) of control cells) \times 100]$.

2.9. Proliferation Analysis

EdU assay (Abcam; Cambridge, UK) was performed to evaluate the proliferation of T cells. T cells were treated with fixative solution and incubated for 15 min, then with permeabilization buffer and incubated for 15–20 min. The reaction mixture was added to fluorescently label EdU and incubated for 30 min. The cells were analyzed with flow cytometer (FACS CantoII flow cytometer) and FlowJo software (Becton Dickinson, San Jose, CA, USA), acquiring 10,000 events.

2.10. Smad2 and TGF- β 1 Analysis

Total and phosphorylated human Smad2 and TGF- β 1 levels were evaluated with Human Smad2 ELISA Kit (Abcam; Cambridge, UK), Human Smad2 [pSpS465/467] (ThermoFisher; Milan, Italy) and Human TGF-beta 1 (R&D System; Minneapolis, MN, USA), following the manufacturer's procedures.

2.11. Nedd4L

cDNA was reverse-transcribed from 8.0 μ g total RNA using M-MLT RT (Invitrogen Corp., Carlsbad, CA, USA). Real-time monitoring of PCR was performed using the Light-Cycler System (Roche Applied Science, Indianapolis, IN, USA) and SYBR-Green I dye (Roche Diagnostics) as described previously [68]. Primer sequences and PCR conditions are listed in Table S2, Supplementary Information. The relative expression levels of these genes were obtained by normalizing mRNA expression to glyceraldehyde-3-phosphate dehydrogenase (GAPDH) mRNA expression as an endogenous control in each sample.

RNAi-mediated knockdown of Nedd4L was obtained with Assay ID 136860 (ThermoFisher; Milan, Italy) following manufacturer procedures.

2.12. Stable Cell Lines

To produce 721.221-ICP47-C1 and A2 cells, human HLA-C1 or HLA-A2 cDNAs were cloned into the pQCXIP retroviral vector (Clontech, Mountain View, CA, USA). This vector was cotransfected with pVSV-G (Clontech) into GP2-293 cells and supernatant was harvested two days post-transfection. The supernatant was centrifuged in Ultracel 50k filter centrifuge tubes (Millipore) to yield concentrated VSV-G pseudotyped MLV-based particles. 721.221-ICP47 cells, a derivative of the MHC class I-deficient 721.221 cell line [69] that expresses HSV-1 ICP47 to inhibit the transporter associated with antigen processing (TAP) complex, were transduced by incubation with concentrated virus for 3 h at 37 °C. Three days later, cells were placed under selection with 0.4 μ g/mL puromycin (Invitrogen, Waltham, MA, USA).

2.13. Granzyme B ELISPOT Assay

Granzyme B secretion was measured using the GrB ELISPOT assay. Briefly, MultiScreen-IP plates (PVDF membrane, Millipore, Bedford, MA, USA) were coated overnight at 4 °C with 100 μ L/well of anti-human GrB antibody (7.5 μ g/mL in PBS, clone GB-10, PeliCluster, Cell Sciences, Norwood, MA, USA). Effector cells (100 μ L/well) were added to triplicate wells at specified concentrations followed by 5×10^4 target cells per well (100 μ L). After the specified effector-target cell incubation, the plates were washed and 100 μ L/well of biotinylated anti-human GrB detecting antibody (0.25 μ g/mL in PBS/1% BSA/0.05% Tween 20, clone GB-11, PeliCluster, Cell Sciences) was added. Plates were incubated for 3 h and 50 μ L of Streptavidin-Alkaline Phosphatase (1:1500 in PBS/1% BSA, Gibco BRL Life Technologies, Gaithersburg, MD, USA) was added for 1 h. Spots were visualized with 100 μ L/well of BCIP-NBT phosphatase substrate (KPL, Gaithersburg, MD, USA) and subjected to automated evaluation using the ImmunoSpot Imaging Analyzer system (Cellular Technology Ltd., Cleveland, OH, USA).

2.14. Calcein Acetoxymethyl Ester (CAM) Cytotoxicity Assay

721.221-ICP47-A2 and 721.221-ICP47-C1 cells were incubated overnight at 26 °C with peptides in Hybridoma-Serum Free Medium (Invitrogen) to stabilize cell surface A2/C1-peptide complexes. An aliquot of 2×10^5 peptide-pulsed cells were then stained with a PE-conjugated pan-MHC class I specific antibody (clone W6/32; Dako, Agilent, Santa Clara, CA, USA) to verify the surface stabilization of MHC class I molecules. The remaining peptide-pulsed cells were stained with CAM (Invitrogen) at a 1:100 dilution for 1 h at 26 °C. CAM-stained cells were washed and then incubated with KIR2DL2 positive or negative NK cells for 4 h at different E:T ratios at 26 °C. The release of CAM into the supernatant was measured using

a fluorescent plate reader (excitation 485 nm, absorption 530 nm). Percent specific lysis was calculated as (test release – spontaneous release)/(maximum release – spontaneous release).

2.15. Cytometric Analysis and CD107a Degranulation Assay

NK cells obtained in the different culture conditions from 20 controls and 12 MS patients were characterized with a specific anti-CD panel (CD3-PerCp-Cy5.5, CD56-FITC, CD107a-PE) (e-Bioscience, Frankfurt, Germany), anti-KIR2DL2-2DS2-2DL3/CD158b-PE (ThermoScientific, Erembodegem, Belgium) monoclonal antibodies. Samples, incubated with the moAbs for 30 min in ice and washed, were analysed with FACS CantoII flow cytometer and FlowJo software (Becton Dickinson, San Jose, CA, USA), acquiring 10,000 events. Lymphocytes were identified according to forward/side scatter profile and NK cells (CD3-/CD56+) were defined and gated within the lymphocyte gate. CD158b levels were measured in the CD3-/CD56+ gated cells. Cell viability was assessed by propidium iodide staining. Anti-isotype controls (Exbio, Praha, Czech Republic) were performed. For the CD107a degranulation assay, after 1 h of incubation at 37 °C and 3 h of treatment with Golgi Stop solution (Becton Dickinson, San Jose, CA, USA), PBMCs were stained with anti-CD3 and anti-CD56 moAbs. Ten thousand events were acquired.

2.16. Isothermal Titration Calorimetry Analysis

After dialysis (48 h), the cleaved hNedd4L-WW3* domain in 10 mM sodium phosphate buffer, pH 7.45, was used for ITC experiments. The dialysis buffer alone was utilized to measure heats of dilution and to dissolve the U24 peptides. The sample was then concentrated to 40 to 150 µM, depending on the estimated K_d value, using Microsep centrifugal devices with a MWCO of 1 kDa. The concentration of the sample was determined by the absorbance at 280 nm in the dialysis buffer on a Nanodrop UV-Vis spectrophotometer, and calculated using the theoretical extinction coefficient obtained from the ProtParam tool. A 15× to 30× concentrated peptide stock solution was made by dissolving the purified peptides, U24-6A, U24-6B and pU24-6B, in the same buffer as the protein and its pH was adjusted to match the buffer and hNedd4L-WW3* protein within ±0.02. The peptide amounts were determined gravimetrically and concentrations adjusted according to the absorbance at 280 nm in the dialysis buffer. Both protein and peptide stock solutions were filtered and degassed for 10 min before loading into the sample cell and injection syringe, respectively.

ITC experiments were performed on a MicroCal iTC200 (GE Healthcare) at 25 °C. The titration protocol consisted of a preliminary injection of 0.2 µL of the peptide solution, followed by 19 consecutive 2 µL injections into the sample cell (200 µL) containing the hNedd4L-WW3* domain studied. The time between each injection was 300 s for U24-6A and U24-6B peptides and 180 s for pU24-6B peptide. Control titrations of the peptide solution into protein-free dialysis buffer were completed. The heats of dilution for the peptide were subtracted from the original heats prior to data fitting to a one-to-one bimolecular interaction model to obtain K_d and ΔH° , at a binding stoichiometry n of 1.0 (adjustable parameter). The ITC experiments were independently repeated three times, with mean values and standard deviations reported.

2.17. ^1H - ^{15}N HSQC NMR Titrations and K_d Calculations for the Fyn-SH3 Protein and U24 Peptide Interaction

Solutions of ^{15}N -Fyn-SH3 were prepared by three successive rounds of concentration and dilution with NMR buffer [10 mM sodium phosphate, 10% D_2O , 0.5 mM benzamide, and 0.1% sodium azide (pH 6.0)] using a 15 mL regenerated cellulose centrifugal filter device with a MWCO of 3000 Da (Millipore). The final protein concentration was determined using an extinction coefficient (ϵ_{280}) of $16,960 \text{ cm}^{-1}\text{M}^{-1}$ (ProtParam; <http://www.expasy.ch>, accessed 15 August 2020). The protein solutions (final concentrations = 0.2–0.6 mM) were then transferred to a 5 mm NMR tube, and a ^1H - ^{15}N HSQC spectrum was recorded at 25 °C using a Bruker Avance III 600 MHz NMR spectrometer (Milton, ON, Canada) equipped with a TCI cryoprobe. Small volumes of unlabeled

U24-6B and pU24-6B peptide stock solutions, with concentrations of 12 mM and 16 mM, respectively. HSQC spectra were recorded after each subsequent addition. A total of 14–15 different protein:peptide ratios between 1:0 and 1:16 for pU24-6B peptide and 1:31 for U24-6B were examined. The pH of the solution was measured to be 6.0 at the start of the titration and found to be identical after the last addition of peptide. The amide chemical shifts of Fyn-SH3 were assigned based on previously published assignments by Mal et al. [70], as described by Sang et al. [29]. The dissociation constant (K_d) was calculated according to the method described by Williamson et al. [71].

2.18. ELISA Assay for U24, pU24 and MBP IgG Titration

U24, pU24 and MBP specific IgG titration was performed on plasma samples using 96-wells plates coated with 5 $\mu\text{g}/\text{mL}$ of U24, pU24 or MBP peptide in bicarbonate buffer pH 9.6. Briefly, after peptides coating overnight at 4 $^{\circ}\text{C}$, the plate was washed three times with PBS-Tween-20 0.05% and saturated with PBS with 3% BSA for 1 h and 30 min at 37 $^{\circ}\text{C}$. Plasma samples were serially diluted (1:20, 1:40, 1:60, 1:100, 1:160, 1:240, 1:320) in PBS with 3% BSA and the 50 μL were added to each well for 1 h and 30 min at 37 $^{\circ}\text{C}$. The detection was performed by adding 100 μL of anti IgG-HRP (Bethyl, Montgomery, TX, USA) diluted 1:10,000 for 1 h and 30 min at 37 $^{\circ}\text{C}$, followed by 50 μL of TMB. The plate was read at 450 nm. Titer was defined as the last dilution showing an optical density greater than average negative control plus 3 standard deviations.

2.19. Statistics

Statistical analysis was performed with Stat View (SAS Institute Inc., Cary, NC, USA). Biological data presented a parametric distribution (Kolmogorov-Smirnoff test) and were analyzed by One way ANOVA for multiple comparison and the p values corrected for multiple comparisons, by Bonferroni's correction. Percentages were compared by Fisher exact test. Statistical significance was assumed for $p < 0.05$ (two tailed).

3. Results

3.1. Endocytic Recycling Model: Interactions with hNedd4L-WW3*

3.1.1. U24-6A and -6B Bind hNedd4L-WW3* with Micromolar Affinity

In order to investigate whether the increased positive charge in U24-6B (Table 1) changes the interaction with hNedd4L-WW3*, ITC experiments were conducted using peptides representing the first fifteen residues of U24-6B and U24-6A. The peptides were synthesized and hNedd4L-WW3* was expressed and purified in house. Resulting representative ITC binding isotherms are shown in Figure 1a,b, along with heat of dilution data. In total, three independently performed ITC experiments were conducted for each peptide. The resulting average thermodynamic parameters obtained are summarized in Table 2. Overall, the data showed that the binding affinity for both U24-6A and -6B is nearly identical. Previously, Sang et al. [30] had found K_d to be $6.3 \pm 0.3 \mu\text{M}$, which is not statistically significantly different to that found here. Here, a slightly lower value for ΔH° for the U24-6B/hNedd4L-WW3* interaction was recorded, suggesting that the positive charge arising from Arg3 (Table 1) contributes to a more exothermic interaction, most likely through increased electrostatic interactions. The decrease in the ΔS° value, on the other hand, indicates a more ordered state, possibly reflecting an ordering of solvating water around the charged Arg side-chain. Overall, however, the ΔG° is the same for both U24-6A and -6B, indicating an enthalpy-entropy compensation.

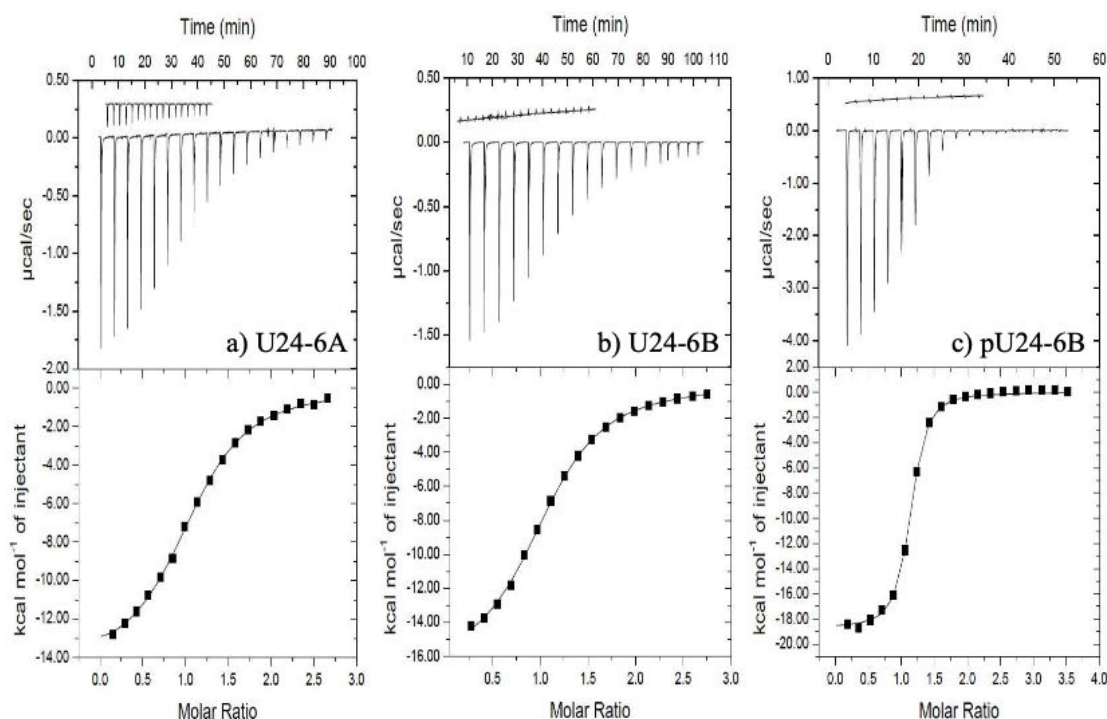


Figure 1. ITC data for (a) U24-6A peptide, (b) U24-6B peptide, and (c) pU24-6B peptide binding to hNedd4L-WW3* at 25 °C. In each case, at least two additional runs were performed and looked nearly identical to the ones shown here. (a) (Upper) Raw titration data for nineteen 2 μ L injections of 0.95 mM U24-6A peptide into the ITC cell containing 0.07 mM hNedd4L-WW3* in 10 mM sodium phosphate pH 7.45. (b) (Upper) Raw titration data for nineteen 2 μ L injections of 0.51 mM U24-6B peptide into the ITC cell containing 0.034 mM hNedd4L-WW3* in 10 mM sodium phosphate pH 7.45. (c) (Upper) Raw titration data for nineteen 2 μ L injections of 1.15 mM pU24-6B peptide into the ITC cell containing 0.068 mM hNedd4L-WW3* in 10 mM sodium phosphate pH 7.45. (a–c) (Upper) Insets show heat of dilution data. (Lower) Integrated heat data (points) and best fit (line) to a “one set of sites” model ($n = 1$; adjustable parameter).

Table 2. Parameters obtained from fitting the ITC data for binding of U24-6A, U24-6B and pU24-6B to hNedd4L-WW3* domains at 25 °C. Calculated values for ΔG° are also included. The parameters were obtained from fitting the data from three separate runs and averaging them. The errors represent \pm one standard deviation. WW3* domain concentrations used in these experiments are in the caption of Figure 1.

Ligand	K_d (μ M)	Target: hNedd4L-WW3*		
		ΔH° (kJ/mol)	ΔS° (J/mol K)	ΔG° (kJ/mol)
U24-6A	8.5 ± 0.7	-59.5 ± 0.9	-103 ± 2	$(-2.9 \pm 0.1) \times 10^1$
U24-6B	8.9 ± 0.9	-71 ± 4	-141.6 ± 0.9	$(-2.9 \pm 0.4) \times 10^1$
pU24-6B	0.88 ± 0.01	-78.4 ± 0.6	-147 ± 2	$(-3.46 \pm 0.08) \times 10^1$

3.1.2. Phosphorylation at Thr6 of U24-6B Enhances the Affinity with hNedd4L-WW3*

Like most viral proteins, U24 is extensively post-translationally modified (PTM) when expressed in eukaryotes. The size of U24 expressed in T-cells and observed on SDS-PAGE gels [41] was found to be two times larger than the expected molecular weight of 10 kDa (based on amino acid sequence). The exact modifications were, however, not identified, but phosphorylation is certainly a possible PTM. Indeed, it has been shown that recombinantly expressed U24 from HHV-6A can be phosphorylated at Thr6 [28]. In addition, previous work by Sang et al. [30] had shown that phosphorylated U24-6A binds very

strongly ($K_d = 0.76 \pm 0.03 \mu\text{M}$; $\Delta H^\circ = -58.7 \pm 0.4 \text{ kJ}\cdot\text{mol}^{-1}$; $\Delta S^\circ = -79.8 \pm 0.9 \text{ J}\cdot\text{mol}^{-1}\cdot\text{K}^{-1}$; $\Delta G^\circ = (-3.49 \pm 0.05) \times 10^1 \text{ kJ}\cdot\text{mol}^{-1}$) to hNedd4L-WW3* domain. This fact, as well as the finding that U24-7 also displayed a high binding affinity to WW3*, with a $K_d = 1.22 \pm 0.01 \mu\text{M}$, suggested that the presence of a positive and negative charge in close proximity helped to favour binding, i.e., the Arg5/pThr6 in pU24-6A might present similar features as the His3/Glu4 pair found in U24-7. In order to examine the effect of adding a positive charge at position Arg3, ITC experiments were conducted to quantify the interaction between pU24-6B and hNedd4L-WW3. A peptide representing the first fifteen residues (Table 1) was used in the study and purchased as a trifluoroacetic acid free compound. The WW3* domain was prepared as previously described.

A resulting representative ITC binding isotherm is shown in Figure 1c. As before, three independently performed experiments were conducted. The resulting average thermodynamic parameters obtained are summarized in Table 2 and showed an order of magnitude lower K_d for pU24-6B, as compared to U24-6B. Similarly to what was observed for the unphosphorylated peptides, the data showed that the binding affinity for both pU24-6A and -6B is not statistically significantly different. The slightly lower values found for ΔH° for the pU24-6B/hNedd4L-WW3* interaction again suggests that the positive charge arising from Arg3 results in more exothermic interactions, most likely due to the increased electrostatic interactions. Additionally, the decrease in the ΔS° value again indicates a more ordered state. The ΔG° is the same for both pU24-6A and p-U24-6B, indicating that enthalpic and entropic effects compensate each other.

3.1.3. Phosphorylated U24-6A and -6B Affect T-Cell Proliferation via Nedd4L Knockdown

To assess the possible effect of U24 on Nedd4L expression in MS, we transfected T cells from 12 MS patients with U24 or MBP peptides, to mimic the expression these proteins inside HHV-6 infected T cells. T-cell viability, evaluated using a lactate dehydrogenase (LDH) assay, was not affected by peptide transfection (Figure 2a). We assessed T-cell proliferation status after protein transfection. The transfection with U24-6A, U24-6B, U24-7 and MBP induced T-cell proliferation, while pU24-6A (p: 0.003; p_c: 0.021; One way ANOVA) and pU24-6B (p: 0.007; p_c: 0.049) significantly decreased T-cell proliferation (Figure 2b). To pinpoint the possible implication of Nedd4L in the inhibition of T-cell proliferation via U24, the levels of Nedd4L mRNA expression were assessed in T cells. The transfection with U24-6A, U24-6B, U24-7 and MBP did not modify Nedd4L mRNA expression, while pU24-6A (p: 0.0025; p_c: 0.018) and pU24-6B (p: 0.004; p_c: 0.028) significantly decreased Nedd4L mRNA expression (Figure 2c), comparable to the effect of a Nedd4L RNAi-mediated knockdown (p: 0.0015; p_c: 0.011) (Figure 2c). Since the effect of the Nedd4L RNAi-mediated knockdown on T-cell proliferation is like the inhibition observed after pU24-6A and pU24-6B transfection, this might suggest that pU24-6A/pU24-6B reduce Nedd4L expression with a consequent reduction of T-cell proliferation. Nedd4L controls the activity of TGF-β1 (Tumour growth factor-beta1), which in turn supports T-cell development, homeostasis, tolerance, and differentiation [72]. Nedd4L inhibits TGF-β1 signaling by triggering Smad2 and TGFBR1 ubiquitination and proteasome-dependent degradation. As a proof of concept, we evaluated the levels of total and phosphorylated Smad2 protein and TGF-β1, under the same culture conditions. An increased expression of total and phosphorylated Smad2 protein and TGF-β1 secretion were observed in Nedd4L RNAi ((total Smad2 = p: 0.004; p_c: 0.028), (phosphorylated Smad2 = p: 0.0026; p_c: 0.018), (TGF-β1 = p: 0.0019; p_c: 0.013)), pU24-6A ((total Smad2 = p: 0.0027; p_c: 0.019), (phosphorylated Smad2 = p: 0.0015; p_c: 0.011), (TGF-β1 = p: 0.0023; p_c: 0.016)), and pU24-6B ((total Smad2 = p: 0.0034; p_c: 0.024), (phosphorylated Smad2 = p: 0.0039; p_c: 0.027), (TGF-β1 = p: 0.0026; p_c: 0.018)) conditions (Figure 2d–f). These data suggest that pU24-6A and pU24-6B act like Nedd4L RNAi in reducing Nedd4L mRNA expression and enhancing TGF-β1 secretion via Smad2 phosphorylation.

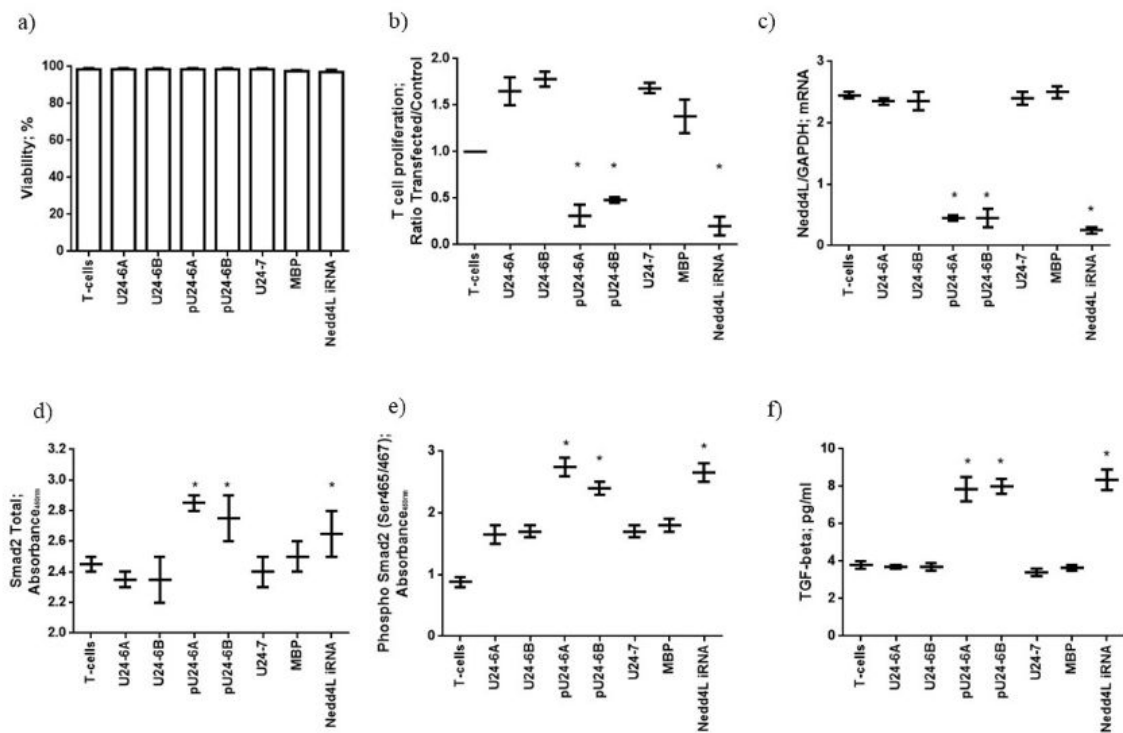


Figure 2. (a) T cells from 12 MS patients were purified and transfected with the transfection reagent alone (T cells) the peptides U24-6A, U24-6B, pU24-6A, pU24-6B, MBP or U24-7 or Ned44L iRNA. T-cell viability was evaluated using a lactate dehydrogenase (LDH) assay. (b) T-cell proliferation was evaluated using an EdU assay. (c) Levels of Ned44L mRNA in comparison with GAPDH mRNA levels. Levels of (d) total Smad2 and (e) phosphorylated Smad2 and (f) TGF- β 1, performed by ELISA assay. The values are reported as mean \pm SD. * significant p value < 0.05 , one way ANOVA for multiple comparison corrected for multiple comparisons, by Bonferroni's correction. iRNA: RNA-mediated knockdown of Ned44L.

3.2. Mimicry Model: Interactions with Fyn-SH3

3.2.1. U24-6B Has a Higher Binding Affinity for Fyn-SH3 Than U24-6A

To further understand the role of U24 in MS, binding interactions with Fyn-SH3 were investigated in order to determine the validity of the MBP mimicry hypothesis. As detailed in the introduction, MBP is an important component of the myelin sheath and it has many additional functions such as cytoskeletal turnover at leading edges of membrane ruffles [73], as well as being involved in Fyn-SH3-mediated signaling pathways during myelin formation. The specific interaction between MBP and Fyn-SH3 has been found to be important in myelination and to be dependent on the phosphorylation state of MBP [33,74].

Sang et al. previously investigated the interaction between a peptide representing the first fifteen residues of U24-6A with Fyn-SH3, using both NMR and ITC [29]. The dissociation equilibrium constant was found to be $K_d = 5.1 \pm 0.3$ mM, i.e., the interaction between both partners is quite weak. Interestingly, removal of the first two residues in the U24-6A sequence, i.e., Met1 and Asp2 (Table 1), resulted in a K_d of 1.9 ± 0.1 mM [75] (Figure S2). To date, no studies have examined binding between U24-6B and Fyn-SH3, nor what effect phosphorylation at Thr6, which is located in the PxxP motif, might have on this interaction.

NMR titration experiments of U24-6B peptide added to ^{15}N -labelled Fyn-SH3 were conducted. As the overlay of ^1H - ^{15}N NMR HSQC spectra shows (Figure 3a), a number of residues were perturbed. The chemical shift changes of these residues were tab-

ulated and the fraction bound was calculated, according the method used by Zarrine-Afsar et al. [76] (Figure 3b), using the K_d values obtained according to the method described by Williamson et al. [71]. Interestingly, the average K_d obtained from 12 shifts was 0.5 ± 0.2 mM. In addition, chemical shift perturbations were mapped onto the Fyn-SH3 structure deposited in the Protein Databank under 1A0N.pdb (Figure 3c) and indicated that while both U24-6A and U24-6B consistently perturbed residues in the RT loop of Fyn-SH3, i.e., R96 and T97, the peripheral residues affected were different for the two ligands. Noticeably, the large region located around residues 114–118 in Fyn-SH3 is highly perturbed by U24-6A, but not at all by U24-6B. In contrast, Y137 is affected by U24-6B but not U24-6A. Overall, the data obtained from NMR suggests that the addition of the positive side-chain at position 3 in the U24 sequence strengthens the binding affinity between U24-6B and Fyn-SH3. The chemical shift perturbations observed also suggest that the mode of binding may be different between U24-6A and U24-6B.

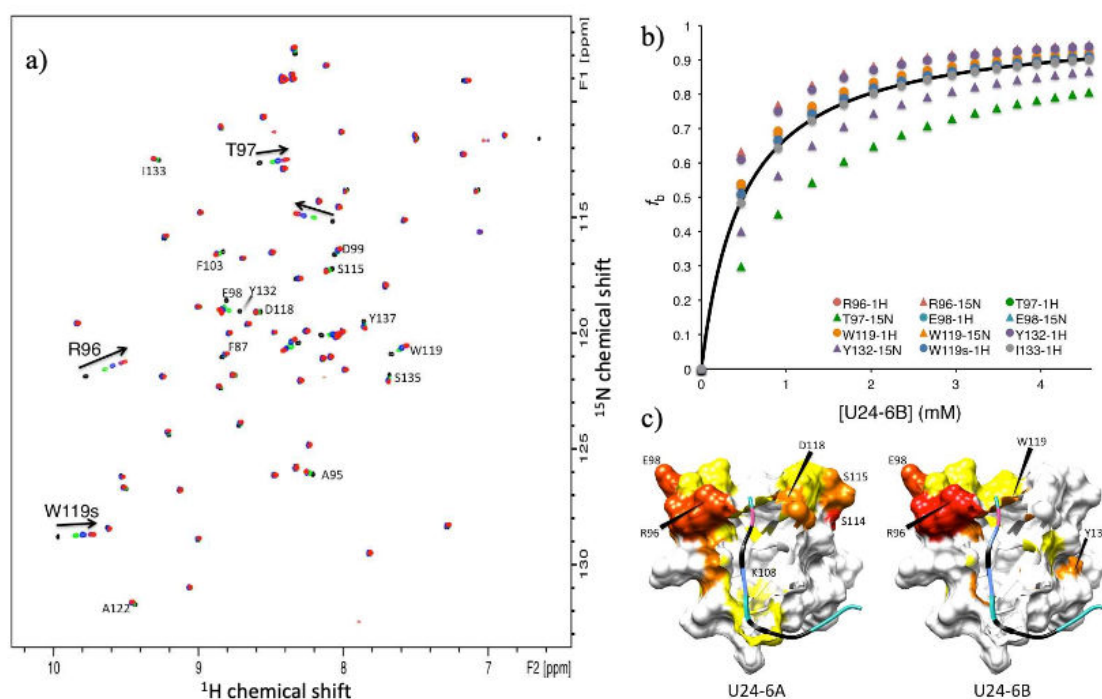


Figure 3. (a) Overlay of 2D ^1H - ^{15}N HSQC spectra of 0.2 mM ^{15}N -labelled Fyn-SH3 in 10 mM sodium phosphate, 10% D_2O , 0.5 mM benzamidine, and 0.1% sodium azide (pH 6.0), recorded at 25 °C using a Bruker Avance III 600 MHz NMR, as a function of increasing U24-6B peptide concentration: (black) 1:0, (green) 1:2, (blue) 1:4, (purple) 1:8 and (red) 1:13 Fyn-SH3/U24-6B molar ratio. Most perturbed resonances (with the exception of four) could be assigned, as designated by the labels indicating residue type and number found next to the peaks ("s" indicates side-chain). (b) Fraction bound as a function of U24-6B peptide concentration (symbols, as indicated in the legend). The curve represents the calculated values of fraction bound for a $K_d = 0.5 \pm 0.2$ mM. (c) Chemical shift perturbations mapped onto model 4 of 1A0N.pdb, i.e., Fyn-SH3 bound to PI3-kinase peptide 2. For U24 ligands, Pro is in black, Arg in light blue, Asp in pink and the PxxP motif is represented as an edged ribbon. The color codes for the chemical shift perturbations are: $\Delta\delta_{norm} = 0.80 - 1.00$ in red, $\Delta\delta_{norm} = 0.60 - 0.79$ in orange red, $\Delta\delta_{norm} = 0.40 - 0.59$ in orange, $\Delta\delta_{norm} = 0.20 - 0.39$ in yellow and values < 0.20 in white, where $\Delta\delta_{norm} = \Delta\delta / \Delta\delta_{max}$, with $\Delta\delta = \sqrt{(\delta_{bound,H} - \delta_{apo,H})^2 + 0.1(\delta_{bound,N} - \delta_{apo,N})^2}$ and $\Delta\delta_{max}$ being the largest value found for a given residue i .

3.2.2. Phosphorylation of U24 Lowers Binding Affinity to Fyn-SH3

What effect phosphorylation at Thr6 might have on binding affinity was examined using NMR titrations with peptides representing the first fifteen amino acids of U24 with a phospho-threonine at position 6, i.e., pU24-6A and pU24-6B (Table 1), and ^{15}N -labelled Fyn-SH3. Saturation was not achieved for both pU24-6A and -6B, in part due to the limited amount of sample available, but also because the K_d for the interaction with Fyn-SH3 is much larger. As seen in Figure 4a, the plateau values were not observed for pU24-6B and pU24-6A, making a precise determination of K_d difficult. Nevertheless, values for the binding affinity could be estimated, based on a number of resonance shifts: $K_d \geq 5$ mM for pU24-6B, whereas $K_d \geq 12$ mM for pU24-6A. Figure 4a illustrates the data for the ^1H resonance of the Trp side-chain, W119s. For both phosphorylated peptides, the trends clearly indicate that, as with MBP, phosphorylation weakens the interaction between U24 and Fyn-SH3.

In order to further characterize where phosphorylated peptides bind to Fyn-SH3, the chemical shift changes, $\Delta\delta_{norm}$, as described in the caption of Figure 3, were plotted as a function of residue number for U24-6A (based on values reported in Sang's thesis [75]) and pU24-6B. As Figure 4b clearly shows, the amino acids that are most perturbed in Fyn-SH3 are different, depending on whether the ligand is U24-6A or pU24-6B. While in both cases shifts in the RT loop binding site are observed, perturbations around residue 114 upon titrations with U24-6A were shifted to residue 108 when the ligand is pU24-6B.

Mapping the observed chemical shift changes onto model 4 of 1A0N.pdb helped clarify why different residues are perturbed upon binding of U24-6A versus pU24-6B. As illustrated in Figure 4c, the perturbation of K108 in Fyn-SH3 upon binding of pU24-6B is consistent with the close proximity of the phosphorylated Thr6, shown in pink in the model on the right. On the other hand, the lack of perturbations for residues 114-118 in Fyn-SH3 upon binding of pU24-6B as compared to U24-6A is not easily accounted for with this model.

Overall, the data presented in this section shows that phosphorylation does not lead to a stronger interaction between proline-rich segments and Fyn-SH3. Although the contact to K108 is strengthened for pU24-6B (i.e., orange versus yellow, Figure 4c), there are very few residues around this amino acid that interact with the ligand, thereby possibly accounting for the weakened interaction with Fyn-SH3 upon phosphorylation of Thr. The model presented in Figure 4c (right) could serve as a first structural model to explain why phosphorylation of MBP leads to a weakened interaction with Fyn-SH3 at a molecular level.

3.3. Immune Control Model: Interaction with KIR Receptors

3.3.1. pU24-6A Controls NK Cell Activation

Previous work had shown that NK cells from MS patients have an increased susceptibility to HHV-6 infection, in particular in the presence of KIR2DL2 receptor [78]. Phosphorylated U24 has an amino acid sequence motif with an elevated half time of dissociation (HTD: 24) from HLA-C1 molecules (estimated by www.bimas.cit.nih.gov/cgi-bin/molbio/ken_parker_comboform, accessed on 20 September 2022), which are ligands for KIR2DL2 [47]. These data suggest a possible interaction of pU24 peptide with NK cells via KIR2DL2/pU24/HLA-C1. To evaluate the possible interaction of U24 with NK cells, we tested for the ability of the peptides to modify NK cell cytotoxicity and degranulation. We enrolled 12 MS Relapsing Remitting patients and primary NK cells from these patients were purified, expanded by IL-2 and IL-15 stimulation [47] and sorted into KIR2DL2 positive and KIR2DL2 negative NK cell subsets using anti-KIR2DL2 coated beads. These NK cells were then tested in cytotoxicity assays for recognition of an HLA-C1 or HLA-A2 expressing transporter associated with antigen processing (TAP)-deficient 721.221 cell line (721.221-ICP47-C1; 721.221-ICP47-A2) incubated with the peptides of interest. Because TAP is necessary for the translocation of peptides from the cytoplasm into the endoplasmic reticulum, MHC class I molecules expressed in these cells cannot load peptides derived from endogenously synthesized proteins, and are rapidly internalized from the plasma

membrane [79]. Thus, most of the HLA-C1 and HLA-A2 molecules expressed by these cells are empty and can be loaded with exogenous peptides. Moreover, peptide binding to HLA-C1 or HLA-A2 can be assessed by staining for an increase in steady-state levels of MHC class I expression on the cell surface. An increased expression of HLA-C1 in the presence of pU24-6A (Figure 5a) (p : 0.0012; p_c : 0.004; One way ANOVA) was observed, while pU24-6B, MBP and U24-7 presented a lower binding affinity for HLA-C1, resulting in a lower stability of HLA-C1 expression at the cell surface, suggesting a lower ability to stabilize HLA-C1 expression (Figure 5a). HLA-A2 expression was not modified by all the peptides tested (Figure 5b).

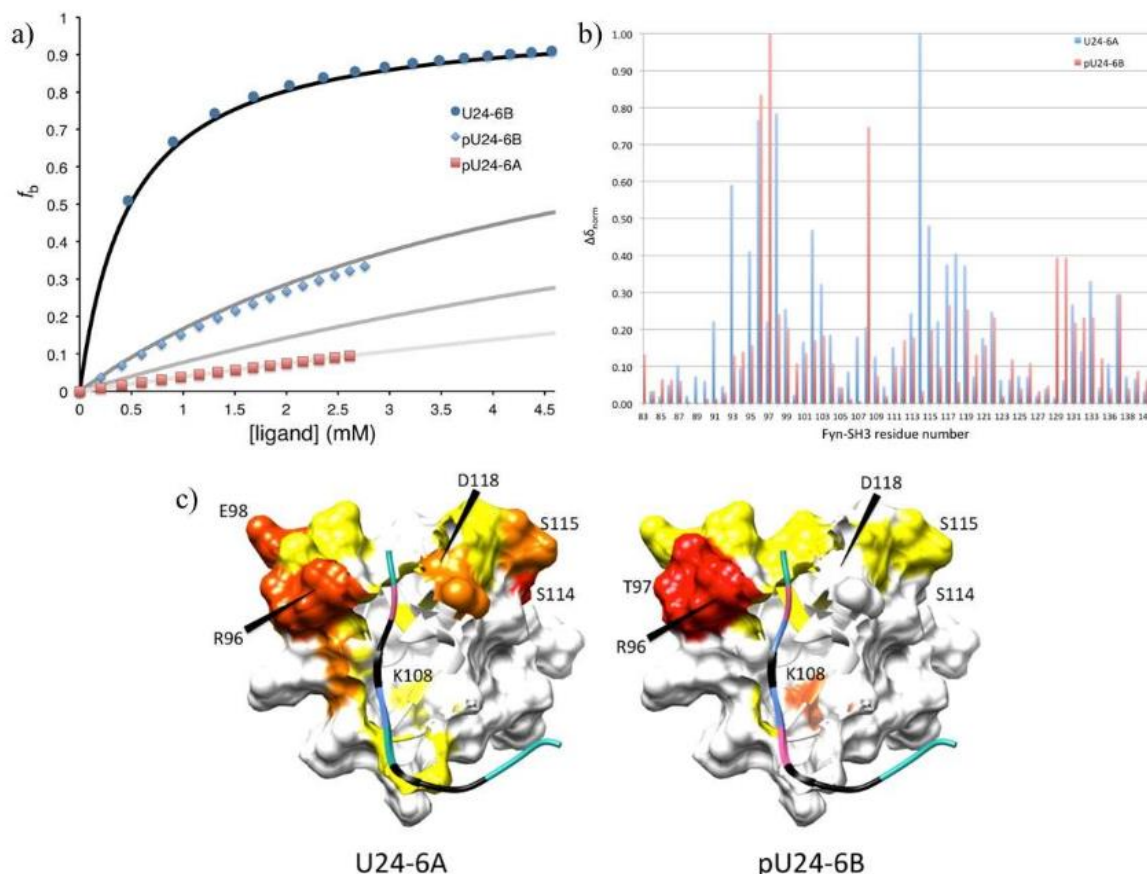


Figure 4. (a) Comparison of the fraction bound as a function of ligand concentration for peptide ligands U24-6B, pU24-6B and pU24-6A (as indicated in the legend), based on the ^1H chemical shift of W119s. The curves in black to light grey represent calculated f_b values for K_d 's of 0.5 mM (black), 5 mM (dark grey), 12 mM (grey), and 25 mM (light grey). In the case of pU24-6A where binding is weakest, the data fit equally well to a K_d of 12 mM (red squares) and 25 mM (fit to data not shown here), which is why both grey and light grey lines are illustrated here. (b) Normalized chemical shift perturbations for residues in Fyn-SH3 for U24-6A (blue bars) and pU24-6B (red bars). The values for $\Delta\delta_{norm}$ are calculated as described in Figure 3. Both ligands interact with R96 and T97 in the RT loop of Fyn-SH3. Interactions with subsequent residues are different between U24-6A and pU24-6B. (c) Chemical shift perturbations mapped onto model 4 of 1A0N.pdb. For the U24 ligands, the prolines are shown in black, arginines in light blue, negatively charged amino acids (i.e., Asp and phospho-Thr6) in pink and the PxxP motif is represented as an edged ribbon. The color codes for the chemical shift perturbations are described in Figure 3. Figure generated using CHIMERA [77].

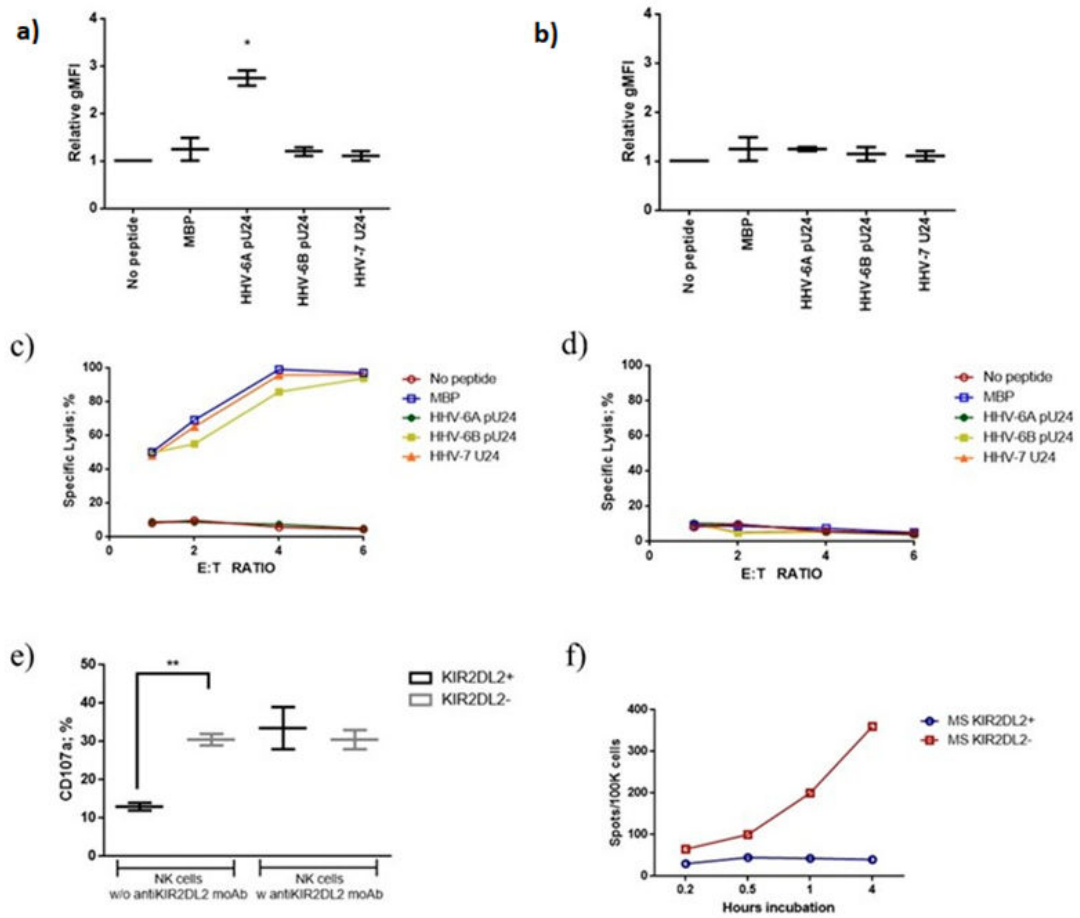


Figure 5. Expression of (a) HLA-C1 in 721.221-ICP47-C1 and (b) HLA-A2 in 721.221-ICP47-A2 after MBP, pU24-6A, pU24-6B or U24-7 treatment. gMFI: The data are presented as mean ± SD. * significant *p* value, Student *t* test. (c) 721.221-ICP47-C1 or (d) 721.221-ICP47-A2 cells were incubated with the different peptides and co-cultured with KIR2DL2 positive NK cells from MS patients. The cytolytic activity of KIR2DL2 positive NK cells was tested by calcein acetoxyethyl ester (CAM) cytotoxicity assay. The data are presented as mean. (e) NK cells from MS patients were co-cultured with 721.221-ICP47-C1 cells incubated with pU24-6A. The expression of CD107a, marker of NK cell activation, was evaluated in the absence (w/o) or presence (w) anti-KIR2DL2 antibody. The data are presented as mean ± SD. * significant *p* value, one way ANOVA for multiple comparison corrected for multiple comparisons, by Bonferroni’s correction. ** significant *p* value, Fisher exact test. (f) Granzyme B Fluorospot assay on KIR2DL2 positive and negative NK cells from MS patients co-cultured with 721.221-ICP47-C1 cells incubated with pU24-6A as a function of an increasing incubation time (0.2, 0.5, 1, or 4 h at 37 °C).

Given these results, the ability of pU24-6A, pU24-6B, MBP and U24-7 to modify the cytolytic activity of KIR2DL2 positive NK cells was tested. 721.221-ICP47-C1 or 721.221-ICP47-A2 cells were incubated with the different peptides and co-cultured with NK cells from MS patients. MBP, pU24-6B and U24-7 pre-incubation induced 721.221-ICP47-C1 cell killing (Figure 5c) (*p* < 0.001; Fisher exact test), while pU24-6A pre-incubation maintained KIR2DL2 positive NK cells unresponsive towards 721.221-ICP47-C1 cells (Figure 5c) (*p*: NS; Fisher exact test). In contrast, no killing was observed with 721.221-ICP47-A2 pre-incubation with the tested peptides and the co-culture with KIR2DL2 positive NK cells (Figure 5d).

To further elucidate the possible role of the KIR2DL2/pU24/HLA-C1 interaction in controlling NK cell activation, KIR2DL2 positive and negative NK cells from MS patients were pre-treated with anti-KIR2DL2 antibody and then co-cultured with 721.221-ICP47-C1 cells incubated with pU24-6A. The expression of CD107a, marker of NK cell activation, was lower in KIR2DL2 positive NK cells in comparison with KIR2DL2 negative NK cells ($p < 0.01$; Fisher exact test) and was reported to levels comparable to KIR2DL2 negative NK cells by anti-KIR2DL2 antibody treatment (p : NS; Fisher exact test) (Figure 5e).

To evaluate the role of pU24-6A in modifying NK cell secretion of Granzyme B (GrB), 721.221-ICP47-C1 cells were incubated with pU24-6A and co-cultured with KIR2DL2 positive NK cells from MS patients. GrB Fluorospot assays were then performed as a function of increasing incubation time (0.2, 0.5, 1, or 4 h at 37 °C). As the time of incubation increased, the resulting number of GrB spots increased linearly in MS patients negative for KIR2DL2 receptor (Figure 5f). On the contrary, MS patients positive for KIR2DL2 receptor presented a lower degranulation cell frequency, which was independent of incubation time (Figure 5f).

Overall, the data presented in this section showed for the first time a clear involvement of pU24-6A in NK cell activation.

3.3.2. MS Patients Showed Increased Levels of U24 Derived Peptide IgG

Based on the findings described above, it could be hypothesized that the presence of high levels of pU24-6A and pU24-6B in MS patients might affect T and NK cell immune response. As a proof of concept of the presence of higher levels of pU24-6A and pU24-6B in MS patients, we evaluated the titration of plasma IgG towards MBP and U24 peptides listed in Table 1, in 40 MS patients, 40 control subjects (CTR) and 40 neurolupus (NLES) patients. The plasma samples were serially diluted (1:20, 1:40, 1:60, 1:100, 1:160, 1:240, 1:320) and titers were defined as the last dilution showing an optical density greater than average negative control plus 3 standard deviations. MS patients showed the highest titers of IgG towards MBP and U24-6A in comparison with healthy patients and neurolupus patients (Figure 6a,b, respectively) (MBP p :0.001; U24-6A p : 0.021). Interestingly, high titers of IgG specific for the phosphorylated form of HHV-6A U24 (pU24-6A) peptide were also observed in MS patients in comparison with controls (Figure 6c) (pU24-6A p : 0.0019). Moreover, we observed a trend to have a higher number of MS patients with high titers of IgG towards U24-6B, pU24-6B and U24-7 in comparison with controls and neurolupus patients (Figure 6d–f). These data suggest a higher immune response towards U24 and its phosphorylated form in MS patients, supporting a biological role of U24 during MS.

4. Discussion

Multiple sclerosis is a complex multifactorial disease. A number of key cells and proteins have been implicated as potentially playing a role [11,13]: from T cells, with their TCR/CD3 receptors on the cell surface, to KIR2DL2 and U24 from HHV-6A. In this contribution, we attempted to shed further light into the function of U24 by examining its interaction with a Nedd4L WW domain, Fyn-SH3 and KIR2DL2. The study focused in large part on U24 from HHV-6B, which shares an almost identical proline rich segment to U24-6A, save for one residue at position 3 (Table 1). Because many studies in the literature suggest that HHV-6A is more frequently associated with MS [8,36,38,41,54,80–94] than HHV-6B [27], directly comparing the interactions of U24-6B to U24-6A is informative.

The ITC results presented in Figure 1 showed surprisingly little difference in the interaction between U24-6A and hNedd4L-WW3* domain and its U24-6B counterpart. This was particularly striking in the case of the phosphorylated peptides, as it might have been anticipated that the introduction of an additional positive charge at residue 3 would perturb the balance of the positive/negative charge pair found to be important in the interaction of pU24-6A and U24-7 with hNedd4L-WW3*. However, upon examination of the predominant structural model found from molecular dynamics simulations reported by Sang et al. [30], the data observed here can be rationalized. As seen in Figure S3a,

binding between U24-6A and hNedd4L-WW3* occurs predominantly between the PY motif and subsequent residues. The PxxP motif at the N-terminal end, which is preceded by Pro3 (indicated by the arrow) in U24-6A, points away from the binding groove in hNedd4L-WW3*. Given that the proline rich segment is known to adopt a PPII helix and that this structure is extended [95], changing Pro3 to Arg3 would not result in stronger interactions, as this part is positioned too far to reach the hNedd4L-WW3* domain. For the phosphorylated peptides, the structural model shown in Figure S3b again shows how a change from Pro3 to Arg3 would have little impact on the binding affinity. Interestingly, the phosphorylation of Thr6 adds a negative charge that comes into close proximity with R492 in hNedd4L-WW3*, thereby stabilizing the interaction and explaining the higher binding affinities observed. Indeed, R492 was found to be perturbed in NMR titrations for pU24-6A and hNedd4L-WW3* [75]. Overall, the reported findings suggest that there is little difference in the interaction between U24-6A or U24-6B and hNedd4L-WW3* domain, both in the unphosphorylated and phosphorylated forms. This would thus suggest that the PY motif of U24 functions similarly in both HHV-6A and -6B.

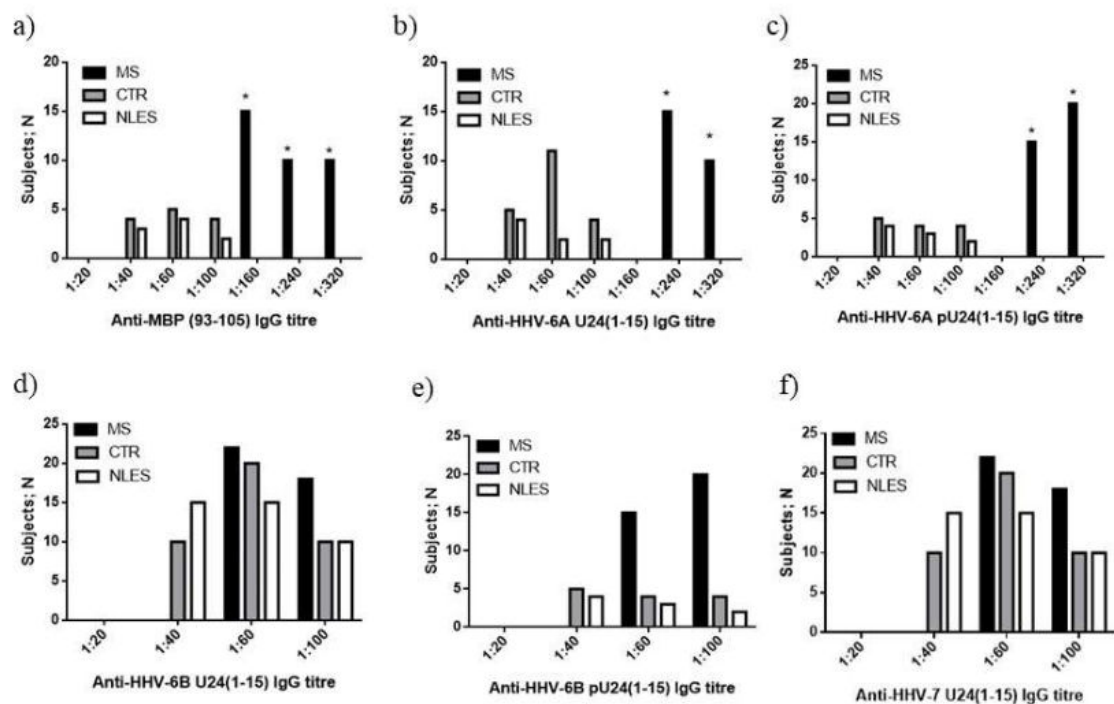


Figure 6. IgG titers, measured in the plasma samples of 40 MS—RRMS patients; 40 CTR—healthy subjects; 40 NLES—neurolupus patients, specific for (a) MBP₉₃₋₁₀₅, (b) U24-6A₁₋₁₅, (c) pU24-6A₁₋₁₅, (d) U24-6B₁₋₁₅, (e) pU24-6B₁₋₁₅, and (f) U24-7₁₋₁₅ (cf. Table 1 for sequences). * significant *p* value, Fisher exact test.

To assess the possible effect of U24 on Nedd4L expression in MS, we transfected T cells from MS patients with U24 or MBP peptides, to mimic the expression these proteins inside HHV-6 infected T cells. The transfection with U24-6A, U24-6B, U24-7 and MBP did not modify Nedd4L mRNA expression, while pU24-6A and pU24-6B significantly decreased Nedd4L mRNA expression, comparable to the effect of a Nedd4L RNAi-mediated knock-down. Since the effect of the Nedd4L RNAi-mediated knockdown on T-cell proliferation is like the inhibition observed after pU24-6A and pU24-6B transfection, this might suggest that pU24-6A/pU24-6B reduce Nedd4L expression with a consequent reduction of T-cell proliferation. Nedd4L controls the activity of TGF- β 1, by triggering Smad2 and TGFBR1 ubiquitination, which in turn supports T-cell development, homeostasis, tolerance, and

differentiation [72]. As a proof of concept, Smad2 phosphorylation and TGF- β 1 secretion consequent to Nedd4L inhibition were significantly augmented in the cases of Nedd4L RNAi and pU24-6A and -6B treatment. These data suggest that pU24-6A and pU24-6B act like Nedd4L RNAi in reducing Nedd4L mRNA expression and enhancing TGF- β 1 secretion via Smad2 phosphorylation.

Fyn tyrosine kinase is mainly localized in the oligodendrocyte plasma membrane [85]. It plays an important role in a range of signaling pathways during CNS development. Many studies have demonstrated that interactions between MBP and SH3-domain-containing proteins play a physiological role in oligodendrocytes and myelin formation, compaction, and overall stability [33,96]. A disruption in this MBP/Fyn-SH3 interaction can lead to myelin dysfunction and consequently MS. The data reported here suggest that U24-6B interactions with Fyn-SH3 are more like the interaction between MBP and Fyn-SH3 (i.e., both, broadly speaking, with μ M affinities) than the interaction between U24-6A and Fyn-SH3 (which is in the mM range). Moreover, it was demonstrated that phosphorylation weakens the interaction, as is also the case between phospho-MBP and Fyn-SH3. The stronger interaction of U24-6B and Fyn-SH3 (relative to U24-6A) suggests that the introduction of a positive charge at Arg3 helps to stabilize binding. Indeed, some of the tightest binding ligands to Fyn, e.g., NS5A [97] and PI3-kinase peptide 2 (1A0N.pdb) [56,57], all have positive charges that flank the PxxP motif.

We previously observed that NK cells from MS patients have an increased susceptibility to HHV-6 infection, in particular in the presence of KIR2DL2 receptor [78]. For the first time, the interaction between KIR2DL2 and U24 was evaluated, as a possible trigger in NK cell activation control. We observed that KIR2DL2 positive NK cells were selectively inhibited by pU24-6A towards 721.221-ICP47-C1 cells, while MBP, pU24-6B and U24-7 did not affect the killing of these cells. In contrast, no killing was observed in 721.221-ICP47-A2 co-cultures with KIR2DL2 positive NK cells. These data showed a clear involvement of pU24-6A in NK cell activation, further supporting that HHV-6A may play a larger role in MS than HHV-6B.

Establishing a link between the viral protein U24 from HHV-6 and multiple sclerosis and more specifically, differentiating between association and causation, is complex, with many different hypotheses having been suggested. As discussed in [15], there is quite a bit of evidence associating HHV-6 to MS, but there is to date no proof indicating any clear causation. In addition, only a few proteins from HHV-6, besides U24, have been identified as possibly being implicated [15,21,55]. The data presented here, while not providing any definitive answers on association/causation, possibly provides some additional clues. For one, if U24's role in MS was to mimic MBP because of their common PxxP motif, the data shown here would suggest that MS would have to be much more prevalent because the causative virus would have to be HHV-6B, which is present in ca. 95% of the population [15,98]. Alternatively, the data could suggest that a single PxxP motif may not be sufficient to mimic MBP well; indeed, LMP2A from Epstein-Barr virus (EBV), which has 4 PxxP motifs [13], has been associated with MS [99–101] and EBV is generally considered a more likely candidate as a viral risk factor for MS [11]. The findings that both pU24-6A and pU24-6B control T cell proliferation via Nedd4L inhibition and that pU24-6A's most important role appears to be NK cell inhibition point to a possible importance of phosphorylation in the function of U24. Reduced proliferation of T cells has been identified as leading to susceptibility to multiple sclerosis [102]. Perhaps exposure to phosphorylated U24 from HHV-6A/6B increases this risk. Likewise, a number of studies have established a link between NK cells and MS, as reviewed extensively in [103]. The fact that pU24-6A specifically affects KIR2DL2 positive NK cells provides the first evidence that it might be this molecule that plays a role in the mechanisms triggering auto-immunity [78]. Finally, the data presented here provides additional support to previous reports in the literature for a biological role for U24 during MS: the ex vivo evaluation of the levels of U24 derived peptide IgGs showed the highest levels of IgG towards U24-6A and pU24-6A. Surprisingly, a higher number of subjects with high levels of IgG towards U24-6B, pU24-6B and U24-7

was found in MS patients in comparison with controls and neurolupus patients, confirming a higher immune response towards U24 and its phosphorylated form in MS patients.

Supplementary Materials: The following supporting information can be downloaded at: <https://www.mdpi.com/article/10.3390/v14112384/s1>, Figure S1: Sample HPLC trace for the purified U24-6B peptide. Figure S2: ITC and NMR titration results for U24-6A_{ΔMD} (U24-6A, residues 3 to 15, Table 1) and Fyn-SH3 domain. Figure S3: Structural models for the binding interaction between (a) U24 and (b) pU24 and hNedd4L-WW3. Table S1: Sequences and molecular weights (MW) of human Fyn-SH3 (Uniprot P06241; residue 82-142 underlined) and hNedd4L-WW3* (Uniprot Q96PU5; residues 497-530 underlined) used in this study. Table S2: Primer sequences and PCR conditions used to generate Nedd4L and the GAPDH control.

Author Contributions: K.-S.P., A.L.C., C.A.H. and S.K.S. designed the biophysical aspects of this project and analyzed data, with K.-S.P. performing the majority of the experimental work. Y.S. provided useful guidance to K.-S.P. for the experiments. D.B., G.S., S.B., S.R., A.B., E.B. and R.R. designed and conducted all the biological experiments, involving patient studies. K.-S.P. and S.K.S. wrote the draft manuscript, and all co-authors contributed to manuscript writing and editing. All authors have read and agreed to the published version of the manuscript.

Funding: Funding to S.K.S. from the Natural Sciences and Engineering Research Council of Canada (RGPIN-2017-03831) and from the University of British Columbia Faculty of Science (STAIR) are gratefully acknowledged. Funding to R.R. is from the FISM-Fondazione Italiana Sclerosi Multipla onlus grant no° Cod 2019/R-Single/004 and is gratefully acknowledged.

Institutional Review Board Statement: See Section 2.1.

Informed Consent Statement: Informed consent was obtained from all subjects involved in the study.

Data Availability Statement: Data is available upon request to the corresponding author.

Acknowledgments: We thank Mark Okon, Iva Pivanti and Mercedes Fernandez for their technical support.

Conflicts of Interest: The authors declare no conflict of interest.

References

- Sola, P.; Merelli, E.; Marasca, R.; Poggi, M.; Luppi, M.; Montorsi, M.; Torelli, G. Human herpesvirus 6 and multiple sclerosis: Survey of anti-HHV-6 antibodies by immunofluorescence analysis and of viral sequences by polymerase chain reaction. *J. Neurol. Neurosurg. Psychiatry* **1993**, *56*, 917–919. [[CrossRef](#)] [[PubMed](#)]
- Salahuddin, S.Z.; Ablashi, D.V.; Markham, P.D.; Josephs, S.F.; Sturzenegger, S.; Kaplan, M.; Halligan, G.; Biberfeld, P.; Wong-Staal, F.; Kramarsky, B.; et al. Isolation of a new virus, HBLV, in patients with lymphoproliferative disorders. *Science* **1986**, *234*, 596–601. [[CrossRef](#)] [[PubMed](#)]
- Leibovitch, E.C.; Jacobson, S. Human Herpesvirus 6 as a Viral Trigger in Mesial Temporal Lobe Epilepsy. *J. Infect. Dis.* **2015**, *212*, 1011–1013. [[CrossRef](#)]
- Theodore, W.H.; Leibovitch, E.; Billioux, B.J.; Inati, S.K.; Zaghloul, K.; Heiss, J.; Gaillard, W.D.; Jacobson, S. Human herpesvirus 6 and epilepsy. *Epilepsia Open* **2021**, *6*, 777–780. [[CrossRef](#)] [[PubMed](#)]
- Rizzo, R.; Bortolotti, D.; Gentili, V.; Rotola, A.; Bolzani, S.; Caselli, E.; Tola, M.R.; Di Luca, D. KIR2DS2/KIR2DL2/HLA-C1 Haplotype Is Associated with Alzheimer's Disease: Implication for the Role of Herpesvirus Infections. *J. Alzheimer's Dis.* **2019**, *67*, 1379–1389. [[CrossRef](#)] [[PubMed](#)]
- Allnutt, M.A.; Johnson, K.; Bennett, D.A.; Connor, S.M.; Troncoso, J.C.; Pletnikova, O.; Albert, M.S.; Resnick, S.M.; Scholz, S.W.; De Jager, P.L.; et al. Human Herpesvirus 6 Detection in Alzheimer's Disease Cases and Controls across Multiple Cohorts. *Neuron* **2020**, *105*, 1027–1035. [[CrossRef](#)] [[PubMed](#)]
- Caserta, M.T.; Hall, C.B.; Schnabel, K.; Mc Intyre, K.; Long, C.; Costanzo, M.; Dewhurst, S.; Insel, R.; Epstein, L.G. Neuroinvasion and persistence of human herpesvirus 6 in children. *J. Infect. Dis.* **1994**, *170*, 1586–1589. [[CrossRef](#)] [[PubMed](#)]
- Schwartz, K.L.; Richardson, S.E.; Ward, K.N.; Donaldson, C.; MacGregor, D.; Banwell, B.; Mahant, S.; Bitnun, A. Delayed Primary HHV-7 Infection and Neurologic Disease. *Pediatrics* **2014**, *133*, e1541–e1547. [[CrossRef](#)]
- Wucherpfennig, K.W.; Strominger, J.L. Molecular mimicry in T cell-mediated autoimmunity: Viral peptides activate human T cell clones specific for myelin basic protein. *Cell* **1995**, *80*, 695–705. [[CrossRef](#)]
- Leibovitch, E.C.; Jacobson, S. Evidence linking HHV-6 with multiple sclerosis: An update. *Curr. Opin. Virol.* **2014**, *9*, 127–133. [[CrossRef](#)]

11. Tarlinton, R.E.; Martynova, E.; Rizvanov, A.A.; Khaiboullina, S.; Verma, S. Role of viruses in the pathogenesis of multiple sclerosis. *Viruses* **2020**, *12*, 643. [[CrossRef](#)] [[PubMed](#)]
12. Leibovitch, E.C.; Jacobson, S. Viruses in chronic progressive neurologic disease. *Mult. Scler.* **2018**, *24*, 48–52. [[CrossRef](#)] [[PubMed](#)]
13. Pi, K.S.; Sang, Y.; Straus, S.K. Viral Proteins with PxxP and PY Motifs May Play a Role in Multiple Sclerosis. *Viruses* **2022**, *14*, 281. [[CrossRef](#)] [[PubMed](#)]
14. Bjornevik, K.; Cortese, M.; Healy, B.C.; Kuhle, J.; Mina, M.J.; Leng, Y.; Elledge, S.J.; Niebuhr, D.W.; Scher, A.I.; Munger, K.L.; et al. Longitudinal analysis reveals high prevalence of Epstein-Barr virus associated with multiple sclerosis. *Science* **2022**, *375*, 296–301. [[CrossRef](#)] [[PubMed](#)]
15. Komaroff, A.L.; Pellett, P.E.; Jacobson, S. Human herpesviruses 6a and 6b in brain diseases: Association versus causation. *Clin. Microbiol. Rev.* **2021**, *34*, e00143-20. [[CrossRef](#)] [[PubMed](#)]
16. Caselli, E.; D'Accolti, M.; Caccuri, F.; Soffritti, I.; Gentili, V.; Bortolotti, D.; Rotola, A.; Cassai, E.; Fiorentini, S.; Zani, A.; et al. The U94 Gene of Human Herpesvirus 6: A Narrative Review of Its Role and Potential Functions. *Cells* **2020**, *9*, 2608. [[CrossRef](#)] [[PubMed](#)]
17. Kearns, P.K.A.; Casey, H.A.; Leach, J.P. Hypothesis: Multiple sclerosis is caused by three-hits, strictly in order, in genetically susceptible persons. *Mult. Scler. Relat. Disord.* **2018**, *24*, 157–174. [[CrossRef](#)]
18. Longnecker, R.; Merchant, M.; Brown, M.E.; Fruehling, S.; Bickford, J.O.; Ikeda, M.; Harty, R.N. WW- and SH3-domain interactions with epstein-barr virus LMP2A. *Exp. Cell Res.* **2000**, *257*, 332–340. [[CrossRef](#)]
19. Winberg, G.; Matskova, L.; Chen, F.; Plant, P.; Rotin, D.; Gish, G.; Ingham, R.; Ernberg, I.; Pawson, T. Latent Membrane Protein 2A of Epstein-Barr Virus Binds WW Domain E3 Protein-Ubiquitin Ligases That Ubiquitinate B-Cell Tyrosine Kinases. *Mol. Cell. Biol.* **2000**, *20*, 8526–8535. [[CrossRef](#)]
20. Panousis, C.G.; Rowe, D.T. Epstein-Barr virus latent membrane protein 2 associates with and is a substrate for mitogen-activated protein kinase. *J. Virol.* **1997**, *71*, 4752–4760. [[CrossRef](#)]
21. Ben-Fredj, N.; Ben-Selma, W.; Rotola, A.; Nefzi, F.; Benedetti, S.; Frih-Ayed, M.; Di Luca, D.; Aouni, M.; Caselli, E. Prevalence of human herpesvirus U94/REP antibodies and DNA in Tunisian multiple sclerosis patients. *J. Neurovirol.* **2013**, *19*, 42–47. [[CrossRef](#)] [[PubMed](#)]
22. Koshizuka, T.; Kobayashi, T.; Ishioka, K.; Suzutani, T. Herpesviruses possess conserved proteins for interaction with Nedd4 family ubiquitin E3 ligases. *Sci. Rep.* **2018**, *8*, 4447. [[CrossRef](#)] [[PubMed](#)]
23. Nobre, L.; Nightingale, K.; Ravenhill, B.J.; Antrobus, R.; Soday, L.; Nichols, J.; Davies, J.; Seirafian, S.; Wang, E.C.Y.; Davison, A.J.; et al. Human cytomegalovirus interactome analysis identifies degradation hubs, domain associations and viral protein functions. *Elife* **2019**, *8*, e49894. [[CrossRef](#)] [[PubMed](#)]
24. Caselli, E.; Di Luca, D. Molecular biology and clinical associations of Roseoloviruses human herpesvirus 6 and human herpesvirus 7. *New Microbiol.* **2007**, *30*, 173–187.
25. Yao, K.; Mandel, M.; Akyani, N.; Maynard, K.; Sengamalay, N.; Fotheringham, J.; Ghedin, E.; Kashanchi, F.; Jacobson, S. Differential HHV-6A Gene Expression in T Cells and Primary Human Astrocytes Based on Multi-Virus Array Analysis. *Glia* **2006**, *53*, 789–798. [[CrossRef](#)]
26. Tejada-Simon, M.V.; Zang, Y.C.Q.; Hong, J.; Rivera, V.M.; Zhang, J.Z. Cross-reactivity with myelin basic protein and human herpesvirus-6 in multiple sclerosis. *Ann. Neurol.* **2003**, *53*, 189–197. [[CrossRef](#)]
27. Leibovitch, E.; Wohler, J.E.; Cummings Macri, S.M.; Motanic, K.; Harberts, E.; Gaitán, M.I.; Maggi, P.; Ellis, M.; Westmoreland, S.; Silva, A.; et al. Novel Marmoset (*Callithrix jacchus*) Model of Human Herpesvirus 6A and 6B Infections: Immunologic, Virologic and Radiologic Characterization. *PLoS Pathog.* **2013**, *9*, e1003138. [[CrossRef](#)]
28. Tait, A.R.; Straus, S.K. Phosphorylation of U24 from Human Herpes Virus type 6 (HHV-6) and its potential role in mimicking myelin basic protein (MBP) in multiple sclerosis. *FEBS Lett.* **2008**, *582*, 2685–2688. [[CrossRef](#)]
29. Sang, Y.; Tait, A.R.; Scott, W.R.P.; Creagh, A.L.; Kumar, P.; Haynes, C.A.; Straus, S.K. Probing the interaction between U24 and the SH3 domain of Fyn tyrosine kinase. *Biochemistry* **2014**, *53*, 6092–6102. [[CrossRef](#)]
30. Sang, Y.; Zhang, R.; Scott, W.R.P.; Creagh, A.L.; Haynes, C.A.; Straus, S.K. U24 from Roseolovirus interacts strongly with Nedd4 WW Domains. *Sci. Rep.* **2017**, *7*, 39776. [[CrossRef](#)]
31. Sang, Y.; Zhang, R.; Creagh, A.L.; Haynes, C.A.; Straus, S.K. Interactions of U24 from Roseolovirus with WW domains: Canonical vs. noncanonical. *Biochem. Cell Biol.* **2017**, *95*, 350–358. [[CrossRef](#)] [[PubMed](#)]
32. Compston, A.; Coles, A. Multiple sclerosis. *Lancet* **2008**, *372*, 1502–1517. [[CrossRef](#)]
33. Vassall, K.A.; Bamm, V.V.; Harauz, G. MyelStones: The executive roles of myelin basic protein in myelin assembly and destabilization in multiple sclerosis. *Biochem. J.* **2015**, *472*, 17–32. [[CrossRef](#)] [[PubMed](#)]
34. Vassall, K.A.; Bamm, V.V.; Jenkins, A.D.; Velte, C.J.; Kattnig, D.R.; Boggs, J.M.; Hinderberger, D.; Harauz, G. Substitutions mimicking deimination and phosphorylation of 18.5-kDa myelin basic protein exert local structural effects that subtly influence its global folding. *Biochim. Biophys. Acta Biomembr.* **2016**, *1858*, 1262–1277. [[CrossRef](#)]
35. Harauz, G.; Musse, A.A. A tale of two citrullines—Structural and functional aspects of myelin basic protein deimination in health and disease. *Neurochem. Res.* **2007**, *32*, 137–158. [[CrossRef](#)]
36. Boggs, J.M.; Rangaraj, G.; Gao, W.; Heng, Y.M. Effect of phosphorylation of myelin basic protein by MAPK on its interactions with actin and actin binding to a lipid membrane in vitro. *Biochemistry* **2006**, *45*, 391–401. [[CrossRef](#)]

37. Smith, G.S.T.; De Avila, M.; Paez, P.M.; Spreuer, V.; Wills, M.K.B.; Jones, N.; Boggs, J.M.; Harauz, G. Proline substitutions and threonine pseudophosphorylation of the SH3 ligand of 18.5-kDa myelin basic protein decrease its affinity for the Fyn-SH3 domain and alter process development and protein localization in oligodendrocytes. *J. Neurosci. Res.* **2012**, *90*, 28–47. [[CrossRef](#)]
38. Atkins, C.M.; Yon, M.; Groome, N.P.; Sweatt, J.D. Regulation of myelin basic protein phosphorylation by mitogen-activated protein kinase during increased action potential firing in the hippocampus. *J. Neurochem.* **1999**, *73*, 1090–1097. [[CrossRef](#)]
39. De Avila, M.; Vassall, K.A.; Smith, G.S.T.; Bamm, V.V.; Harauz, G. The proline-rich region of 18.5 kDa myelin basic protein binds to the SH3-domain of Fyn tyrosine kinase with the aid of an upstream segment to form a dynamic complex in vitro. *Biosci. Rep.* **2014**, *34*, 775–788. [[CrossRef](#)]
40. Sullivan, B.M.; Coscoy, L. Downregulation of the T-cell receptor complex and impairment of T-cell activation by human herpesvirus 6 u24 protein. *J. Virol.* **2008**, *82*, 602–608. [[CrossRef](#)]
41. Sullivan, B.M.; Coscoy, L. The U24 protein from human herpesvirus 6 and 7 affects endocytic recycling. *J. Virol.* **2010**, *84*, 1265–1275. [[CrossRef](#)] [[PubMed](#)]
42. Kawabe, H.; Neeb, A.; Dimova, K.; Young, S.M.; Takeda, M.; Katsurabayashi, S.; Mitkovski, M.; Malakhova, O.A.; Zhang, D.E.; Umikawa, M.; et al. Regulation of Rap2A by the Ubiquitin Ligase Neddd4-1 Controls Neurite Development. *Neuron* **2010**, *65*, 358–372. [[CrossRef](#)] [[PubMed](#)]
43. Liu, K.; Lu, Y.; Lee, J.K.; Samara, R.; Willenberg, R.; Sears-Kraxberger, I.; Tedeschi, A.; Park, K.K.; Jin, D.; Cai, B.; et al. PTEN deletion enhances the regenerative ability of adult corticospinal neurons. *Nat. Neurosci.* **2010**, *13*, 1075–1081. [[CrossRef](#)] [[PubMed](#)]
44. Georgieva, M.V.; de Pablo, Y.; Sanchis, D.; Comella, J.X.; Llovera, M. Ubiquitination of TrkA by Neddd4-2 regulates receptor lysosomal targeting and mediates receptor signaling. *J. Neurochem.* **2011**, *117*, 479–493. [[CrossRef](#)] [[PubMed](#)]
45. Arévalo, J.C.; Waite, J.; Rajagopal, R.; Beyna, M.; Chen, Z.Y.; Lee, F.S.; Chao, M.V. Cell Survival through Trk Neurotrophin Receptors Is Differentially Regulated by Ubiquitination. *Neuron* **2006**, *50*, 549–559. [[CrossRef](#)] [[PubMed](#)]
46. Ben Fredj, N.; Rizzo, R.; Bortolotti, D.; Nefzi, F.; Chebel, S.; Rotola, A.; Frih-Ayed, M.; Di Luca, D.; Aouni, M. Evaluation of the implication of KIR2DL2 receptor in multiple sclerosis and herpesvirus susceptibility. *J. Neuroimmunol.* **2014**, *271*, 30–35. [[CrossRef](#)]
47. Rizzo, R.; Gentili, V.; Casetta, I.; Caselli, E.; De Gennaro, R.; Granieri, E.; Cassai, E.; Di Luca, D.; Rotola, A. Altered natural killer cells' response to herpes virus infection in multiple sclerosis involves KIR2DL2 expression. *J. Neuroimmunol.* **2012**, *251*, 55–64. [[CrossRef](#)]
48. Rizzo, R.; Bortolotti, D.; Fainardi, E.; Gentili, V.; Bolzani, S.; Baldi, E.; Casetta, I.; Granieri, E.; Rotola, A.; Furlan, R.; et al. KIR2DL2 inhibitory pathway enhances Th17 cytokine secretion by NK cells in response to herpesvirus infection in multiple sclerosis patients. *J. Neuroimmunol.* **2016**, *294*, 1–5. [[CrossRef](#)]
49. Velarde-de la Cruz, E.E.; Sánchez-Hernández, P.E.; Muñoz-Valle, J.F.; Palafox-Sánchez, C.A.; Ramírez-de los Santos, S.; Graciano-Machuca, O.; García-Iglesias, T.; Montoya-Buelna, M.; Ramírez-Dueñas, M.G. KIR2DL2 and KIR2DS2 as genetic markers to the methotrexate response in rheumatoid arthritis patients. *Immunopharmacol. Immunotoxicol.* **2016**, *38*, 303–309. [[CrossRef](#)]
50. Littera, R.; Chessa, L.; Deidda, S.; Angioni, G.; Campagna, M.; Lai, S.; Melis, M.; Cipri, S.; Firinu, D.; Santus, S.; et al. Natural killer-cell immunoglobulin-like receptors trigger differences in immune response to SARS-CoV-2 infection. *PLoS ONE* **2021**, *16*, e0255608. [[CrossRef](#)]
51. Giancchetti, E.; Delfino, D.V.; Fierabracci, A. Natural Killer Cells: Potential Biomarkers and Therapeutic Target in Autoimmune Diseases? *Front. Immunol.* **2021**, *12*, 616853. [[PubMed](#)]
52. Dizaji Asl, K.; Velaei, K.; Rafat, A.; Tayefi Nasrabadi, H.; Movassaghpour, A.A.; Mahdavi, M.; Nozad Charoudeh, H. The role of KIR positive NK cells in diseases and its importance in clinical intervention. *Int. Immunopharmacol.* **2021**, *92*, 107361. [[PubMed](#)]
53. Alenda, R.; Álvarez-Lafuente, R.; Costa-Frossard, L.; Arroyo, R.; Mirete, S.; Álvarez-Cermeño, J.C.; Villar, L.M. Identification of the major HHV-6 antigen recognized by cerebrospinal fluid IgG in multiple sclerosis. *Eur. J. Neurol.* **2014**, *21*, 1096–1101. [[CrossRef](#)] [[PubMed](#)]
54. Domínguez-Mozo, M.I.; Nieto-Guerrero, A.; Pérez-Pérez, S.; García-Martínez, M.A.; Arroyo, R.; Alvarez-Lafuente, R. MicroRNAs of Human Herpesvirus 6A and 6B in Serum and Cerebrospinal Fluid of Multiple Sclerosis Patients. *Front. Immunol.* **2020**, *11*, 2142. [[CrossRef](#)] [[PubMed](#)]
55. Engdahl, E.; Gustafsson, R.; Huang, J.; Biström, M.; Lima Bomfim, I.; Stridh, P.; Khademi, M.; Brenner, N.; Butt, J.; Michel, A.; et al. Increased Serological Response Against Human Herpesvirus 6A Is Associated with Risk for Multiple Sclerosis. *Front. Immunol.* **2019**, *10*, 2715. [[CrossRef](#)]
56. Renzoni, D.A.; Pugh, D.J.R.; Siligardi, G.; Das, P.; Morton, C.J.; Rossi, C.; Waterfield, M.D.; Campbell, I.D.; Ladbury, J.E. Structural and thermodynamic characterization of the interaction of the SH3 domain from Fyn with the proline-rich binding site on the p85 subunit of PI3-kinase. *Biochemistry* **1996**, *35*, 15646–15653. [[CrossRef](#)]
57. Morton, C.J.; Pugh, D.J.R.; Brown, E.L.J.; Kahmann, J.D.; Renzoni, D.A.C.; Campbell, I.D. Solution structure and peptide binding of the SH3 domain from human Fyn. *Structure* **1996**, *4*, 705–714. [[CrossRef](#)]
58. Demers, J.P.; Mittermaier, A. Binding mechanism of an SH3 domain studied by NMR and ITC. *J. Am. Chem. Soc.* **2009**, *131*, 4355–4367. [[CrossRef](#)]
59. Meneses, E.; Mittermaier, A. Electrostatic interactions in the binding pathway of a transient protein complex studied by NMR and isothermal titration calorimetry. *J. Biol. Chem.* **2014**, *289*, 27911–27923. [[CrossRef](#)]

60. Jia, C.Y.H.; Nie, J.; Wu, C.; Li, C.; Li, S.S.C. Novel Src homology 3 domain-binding motifs identified from proteomic screen of a pro-rich region. *Mol. Cell. Proteomics* **2005**, *4*, 1155–1166. [[CrossRef](#)]
61. McDonald, W.I.; Compston, A.; Edan, G.; Goodkin, D.; Hartung, H.P.; Lublin, F.D.; McFarland, H.F.; Paty, D.W.; Polman, C.H.; Reingold, S.C.; et al. Recommended diagnostic criteria for multiple sclerosis: Guidelines from the International Panel on the Diagnosis of Multiple Sclerosis. *Ann. Neurol.* **2001**, *50*, 121–127. [[CrossRef](#)] [[PubMed](#)]
62. Kurtzke, J.F. Rating neurologic impairment in multiple sclerosis: An expanded disability status scale (EDSS). *Neurology* **1983**, *33*, 1444–1452. [[CrossRef](#)] [[PubMed](#)]
63. Lublin, F.D.; Reingold, S.C. Defining the clinical course of multiple sclerosis: Results of an international survey. *Neurology* **1996**, *46*, 907–911. [[CrossRef](#)]
64. Hochberg, M.C. Updating the American College of Rheumatology revised criteria for the classification of systemic lupus erythematosus. *Arthritis Rheum.* **1997**, *40*, 1725. [[CrossRef](#)] [[PubMed](#)]
65. Alunno, A.; Najm, A.; Machado, P.M.; Bertheussen, H.; Burmester, G.R.R.; Carubbi, F.; De Marco, G.; Giacomelli, R.; Hermine, O.; Isaacs, J.D.; et al. 2021 update of the EULAR points to consider on the use of immunomodulatory therapies in COVID-19. *Ann. Rheum. Dis.* **2022**, *81*, 34–40. [[CrossRef](#)]
66. Bortoluzzi, A.; Fanouriakos, A.; Appenzeller, S.; Costallat, L.; Scirè, C.A.; Murphy, E.; Bertias, G.; Hanly, J.; Govoni, M. Validity of the Italian algorithm for the attribution of neuropsychiatric events in systemic lupus erythematosus: A retrospective multicentre international diagnostic cohort study. *BMJ Open* **2017**, *7*, 15546. [[CrossRef](#)]
67. Bortolotti, D.; Gentili, V.; Rotola, A.; Cultrera, R.; Marci, R.; Di Luca, D.; Rizzo, R. HHV-6A infection of endometrial epithelial cells affects immune profile and trophoblast invasion. *Am. J. Reprod. Immunol.* **2019**, *82*, e13174. [[CrossRef](#)]
68. Ogawa, K.; Utsunomiya, T.; Mimori, K.; Tanaka, F.; Inoue, H.; Nagahara, H.; Murayama, S.; Mori, M. Clinical significance of human kallikrein gene 6 messenger RNA expression in colorectal cancer. *Clin. Cancer Res.* **2005**, *11*, 2889–2893. [[CrossRef](#)]
69. Gatfield, J.; Lammert, E.; Nickolaus, P.; Münz, C.; Rothenfusser, S.; Fisch, P.; Stevanović, S.; Schild, H.; Rammensee, H.G.; Arnold, D. Cell lines transfected with the TAP inhibitor ICP47 allow testing peptide binding to a variety of HLA class I molecules. *Int. Immunol.* **1998**, *10*, 1665–1672. [[CrossRef](#)]
70. Mal, T.K.; Matthews, S.J.; Kovacs, H.; Campbell, I.D.; Boyd, J. Some NMR experiments and a structure determination employing a [¹⁵N,²H] enriched protein. *J. Biomol. NMR* **1998**, *12*, 259–276. [[CrossRef](#)]
71. Williamson, M.P. Using chemical shift perturbation to characterise ligand binding. *Prog. Nucl. Magn. Reson. Spectrosc.* **2013**, *73*, 1–16. [[CrossRef](#)] [[PubMed](#)]
72. Oh, S.A.; Li, M.O. TGF- β : Guardian of T Cell Function. *J. Immunol.* **2013**, *191*, 3973–3979. [[CrossRef](#)] [[PubMed](#)]
73. Boggs, J.M.; Homchaudhuri, L.; Ranagaraj, G.; Liu, Y.; Smith, G.S.; Harauz, G. Interaction of myelin basic protein with cytoskeletal and signaling proteins in cultured primary oligodendrocytes and N19 oligodendroglial cells. *BMC Res. Notes* **2014**, *7*, 387. [[CrossRef](#)]
74. Kim, J.K.; Mastronardi, F.G.; Wood, D.D.; Lubman, D.M.; Zand, R.; Moscarello, M.A. Multiple sclerosis: An important role for post-translational modifications of myelin basic protein in pathogenesis. *Mol. Cell. Proteomics* **2003**, *2*, 453–462. [[CrossRef](#)] [[PubMed](#)]
75. Sang, Y. Protein Interactions of Membrane Protein U24 from Roseolovirus and Implications for Its Function. Ph.D. Thesis, University of British Columbia, Vancouver, BC, Canada, 2016.
76. Zarrine-Afsar, A.; Mittermaier, A.; Kay, L.E.; Davidson, A.R. Protein stabilization by specific binding of guanidinium to a functional arginine-binding surface on an SH3 domain. *Protein Sci.* **2006**, *15*, 162–170. [[CrossRef](#)] [[PubMed](#)]
77. Pettersen, E.F.; Goddard, T.D.; Huang, C.C.; Couch, G.S.; Greenblatt, D.M.; Meng, E.C.; Ferrin, T.E. UCSF Chimera-A visualization system for exploratory research and analysis. *J. Comput. Chem.* **2004**, *25*, 1605–1612. [[CrossRef](#)]
78. Bortolotti, D.; Gentili, V.; Bortoluzzi, A.; Govoni, M.; Schiuma, G.; Beltrami, S.; Rizzo, S.; Baldi, E.; Caselli, E.; Pugliatti, M.; et al. Herpesvirus Infections in KIR2DL2-Positive Multiple Sclerosis Patients: Mechanisms Triggering Autoimmunity. *Microorganisms* **2022**, *10*, 494. [[CrossRef](#)]
79. Schafer, J.L.; Ries, M.; Guha, N.; Connole, M.; Colantonio, A.D.; Wiertz, E.J.; Wilson, N.A.; Kaur, A.; Evans, D.T. Suppression of a Natural Killer Cell Response by Simian Immunodeficiency Virus Peptides. *PLoS Pathog.* **2015**, *11*, e1005145. [[CrossRef](#)]
80. Tai, A.K.; Luka, J.; Ablashi, D.; Huber, B.T. HHV-6A infection induces expression of HERV-K18-encoded superantigen. *J. Clin. Virol.* **2009**, *46*, 47–48. [[CrossRef](#)]
81. Grut, V.; Biström, M.; Salzer, J.; Stridh, P.; Jons, D.; Gustafsson, R.; Fogdell-Hahn, A.; Huang, J.; Brenner, N.; Butt, J.; et al. Cytomegalovirus seropositivity is associated with reduced risk of multiple sclerosis—A presymptomatic case-control study. *Eur. J. Neurol.* **2021**, *28*, 3072–3079. [[CrossRef](#)]
82. Fleming, J.; Hernandez, G.; Hartman, L.; Maksimovic, J.; Nace, S.; Lawler, B.; Risa, T.; Cook, T.; Agni, R.; Reichelderfer, M.; et al. Safety and efficacy of helminth treatment in relapsing-remitting multiple sclerosis: Results of the HINT 2 clinical trial. *Mult. Scler. J.* **2019**, *25*, 81–91. [[CrossRef](#)] [[PubMed](#)]
83. Zuchero, J.B.; Fu, M.M.; Sloan, S.A.; Ibrahim, A.; Olson, A.; Zaremba, A.; Dugas, J.C.; Wienbar, S.; Caprariello, A.V.; Kantor, C.; et al. CNS Myelin Wrapping Is Driven by Actin Disassembly. *Dev. Cell* **2015**, *34*, 152–167. [[CrossRef](#)] [[PubMed](#)]
84. Chang, K.J.; Redmond, S.A.; Chan, J.R. Remodeling myelination: Implications for mechanisms of neural plasticity. *Nat. Neurosci.* **2016**, *19*, 190–197. [[CrossRef](#)]

85. Krämer-Albers, E.M.; White, R. From axon-glia signalling to myelination: The integrating role of oligodendroglial Fyn kinase. *Cell. Mol. Life Sci.* **2011**, *68*, 2003–2012. [[CrossRef](#)] [[PubMed](#)]
86. Yon, M.; Ackerley, C.A.; Mastronardi, F.G.; Groome, N.; Moscarello, M.A. Identification of a mitogen-activated protein kinase site in human myelin basic protein in situ. *J. Neuroimmunol.* **1996**, *65*, 55–59. [[CrossRef](#)]
87. White, R.; Krämer-Albers, E.M. Axon-glia interaction and membrane traffic in myelin formation. *Front. Cell. Neurosci.* **2014**, *7*, 284. [[CrossRef](#)]
88. Ding, X.; Jo, J.; Wang, C.Y.; Cristobal, C.D.; Zuo, Z.; Ye, Q.; Wirianto, M.; Lindeke-Myers, A.; Choi, J.M.; Mohila, C.A.; et al. The Daam2-VHL-Nedd4 axis governs developmental and regenerative oligodendrocyte differentiation. *Genes Dev.* **2020**, *34*, 1177–1189. [[CrossRef](#)]
89. Schmiedel, D.; Tai, J.; Levi-Schaffer, F.; Dovrat, S.; Mandelboim, O. Human Herpesvirus 6B Downregulates Expression of Activating Ligands during Lytic Infection To Escape Elimination by Natural Killer Cells. *J. Virol.* **2016**, *90*, 9608–9617. [[CrossRef](#)]
90. Sharon, E.; Frenkel, N. Human Herpesvirus 6A Exhibits Restrictive Propagation with Limited Activation of the Protein Kinase R-eIF2 α Stress Pathway. *J. Virol.* **2017**, *91*, 9. [[CrossRef](#)]
91. Reynaud, J.M.; Jegou, J.-F.; Welsch, J.C.; Horvat, B. Human Herpesvirus 6A Infection in CD46 Transgenic Mice: Viral Persistence in the Brain and Increased Production of Proinflammatory Chemokines via Toll-Like Receptor 9. *J. Virol.* **2014**, *88*, 5421–5436. [[CrossRef](#)]
92. Biström, M.; Jons, D.; Engdahl, E.; Gustafsson, R.; Huang, J.; Brenner, N.; Butt, J.; Alonso-Magdalena, L.; Gunnarsson, M.; Vrethem, M.; et al. Epstein-Barr virus infection after adolescence and human herpesvirus 6A as risk factors for multiple sclerosis. *Eur. J. Neurol.* **2021**, *28*, 579–586. [[CrossRef](#)] [[PubMed](#)]
93. Gustafsson, R.K.L.; Engdahl, E.E.; Hammarfjord, O.; Adikari, S.B.; Lourda, M.; Klingström, J.; Svensson, M.; Fogdell-Hahn, A. Human Herpesvirus 6A Partially Suppresses Functional Properties of DC without Viral Replication. *PLoS ONE* **2013**, *8*, e58122. [[CrossRef](#)] [[PubMed](#)]
94. Wu, J.; Engdahl, E.; Gustafsson, R.; Fogdell-Hahn, A.; Waterboer, T.; Hillert, J.; Olsson, T.; Alfredsson, L.; Hedström, A.K. High antibody levels against human herpesvirus-6A interact with lifestyle factors in multiple sclerosis development. *Mult. Scler. J.* **2021**, *28*, 383–392. [[CrossRef](#)] [[PubMed](#)]
95. Shi, L.; Holliday, A.E.; Shi, H.; Zhu, F.; Ewing, M.A.; Russell, D.H.; Clemmer, D.E. Characterizing intermediates along the transition from polyproline I to polyproline II using ion mobility spectrometry-mass spectrometry. *J. Am. Chem. Soc.* **2014**, *136*, 12702–12711. [[CrossRef](#)]
96. Polverini, E.; Rangaraj, G.; Libich, D.S.; Boggs, J.M.; Harauz, G. Binding of the proline-rich segment of myelin basic protein to SH3 domains: Spectroscopic, microarray, and modeling studies of ligand conformation and effects of posttranslational modifications. *Biochemistry* **2008**, *47*, 267–282. [[CrossRef](#)]
97. Macdonald, A.; Mazaleyrat, S.; McCormick, C.; Street, A.; Burgoyne, N.J.; Jackson, R.M.; Cazeaux, V.; Shelton, H.; Saksela, K.; Harris, M. Further studies on hepatitis C virus NS5A-SH3 domain interactions: Identification of residues critical for binding and implications for viral RNA replication and modulation of cell signalling. *J. Gen. Virol.* **2005**, *86*, 1035–1044. [[CrossRef](#)]
98. Akhyani, N.; Berti, R.; Brennan, M.B.; Soldan, S.S.; Eaton, J.M.; McFarland, H.F.; Jacobson, S. Tissue distribution and variant characterization of human herpesvirus (HHV)-6: Increased prevalence of HHV-6A in patients with multiple sclerosis. *J. Infect. Dis.* **2000**, *182*, 1321–1325. [[CrossRef](#)]
99. Aloisi, F.; Serafini, B.; Magliozzi, R.; Howell, O.W.; Reynolds, R. Detection of Epstein-Barr virus and B-cell follicles in the multiple sclerosis brain: What you find depends on how and where you look. *Brain* **2010**, *133*, e157. [[CrossRef](#)]
100. Veroni, C.; Aloisi, F. The CD8 T Cell-Epstein-Barr Virus-B Cell Dialogue: A Central Issue in Multiple Sclerosis Pathogenesis. *Front. Immunol.* **2021**, *12*, 665718. [[CrossRef](#)]
101. Serafini, B.; Rosicarelli, B.; Veroni, C.; Mazzola, G.A.; Aloisi, F. Epstein-Barr Virus-Specific CD8 T Cells Selectively Infiltrate the Brain in Multiple Sclerosis and Interact Locally with Virus-Infected Cells: Clue for a Virus-Driven Immunopathological Mechanism. *J. Virol.* **2019**, *93*, 00980-19. [[CrossRef](#)]
102. Kofler, D.M.; Severson, C.A.; Mousissian, N.; De Jager, P.L.; Hafler, D.A. The CD6 Multiple Sclerosis Susceptibility Allele Is Associated with Alterations in CD4+ T Cell Proliferation. *J. Immunol.* **2011**, *187*, 3286–3291. [[CrossRef](#)] [[PubMed](#)]
103. Mimpen, M.; Smolders, J.; Hupperts, R.; Damoiseaux, J. Natural killer cells in multiple sclerosis: A review. *Immunol. Lett.* **2020**, *222*, 1–11. [[CrossRef](#)] [[PubMed](#)]


Received: 28 May 2021 | Accepted: 7 June 2021

DOI: 10.1002/jmv.27138

RESEARCH ARTICLE

JOURNAL OF
MEDICAL VIROLOGY WILEY

Late-onset intrauterine growth restriction and HHV-6 infection: A pilot study

Daria Bortolotti¹ | Valentina Gentili¹ | Erica Santi² | Cristina Taliento² |
Amerigo Vitagliano² | Giovanna Schiuma¹ | Silvia Beltrami¹ | Sabrina Rizzo¹ |
Giovanni Lanza³ | Roberta Rizzo¹  | Roberta Gafà³ | Pantaleo Greco²

¹Department of Chemical, Pharmaceutical and Agricultural Sciences, University of Ferrara, Ferrara, Italy

²Department of Medical Sciences, Obstetric and Gynecological Clinic, University of Ferrara, Ferrara, Italy

³Department of Translational and for Romagna Medicine, University of Ferrara, Ferrara, Italy

Correspondence

Roberta Rizzo, Department of Chemical, Pharmaceutical and Agricultural Sciences, University of Ferrara, via L.Borsari 46, 44121, Ferrara, Italy.
Email: rbr@unife.it

Funding information

Università degli Studi di Ferrara - FAR2019, FAR2020; HHV-6 Foundation- HHV-6 Grant

Abstract

Late-onset Intrauterine growth restriction (IUGR) refers to impaired growth and development of the fetus, characterized by placental morphological abnormalities that affect the fetus's supply of nutrients. Human leukocyte antigen-G (HLA-G) is physiologically expressed during pregnancy, but decreased in normal placenta during the last weeks of gestation possibly inducing childbirth. Several viruses involved in congenital infection, such as herpesviruses, exploit HLA-G expression as an immune-escape mechanism. To date, despite different congenital herpetic infections having been associated with late IUGR, no direct implication of Human herpesvirus 6 (HHV-6) infection has been reported. We evaluated HLA-G expression and HHV-6 infection in 11 placentas from late-onset IUGR newborns and 11 placentas from uncomplicated pregnancies by histopathological and immunohistochemistry analysis. We found higher levels of HLA-G expression and HHV-6 presence in IUGR placenta samples compared with control placenta samples. We report HHV-6 staining in IUGR placenta samples, characterized by high HLA-G expression. These preliminary data suggest a possible involvement of HHV-6 infection in HLA-G deregulation that might affect vessel remodeling and prevent the correct pregnancy outcome in the IUGR condition.

KEYWORDS

HHV-6, HLA-G, IUGR, placenta

1 | INTRODUCTION

The term intrauterine growth restriction (IUGR) defines the inability of the fetus to reach its prenatal growth potential, and this condition manifests itself as a deviation of fetal growth from the anthropometric reference values for a specific gestational period.¹

The causes of IUGR can be fetal, maternal, placental, genetic, or a combination of these factors.² In particular, IUGR originates mainly

from placental morphological abnormalities, which generates a discrepancy between the supply of nutrients by the placenta and the fetus' demand.³ Infections, particularly those of viral origin, that occur after the first 6–8 weeks of gestation are known to be associated with placental abnormalities that can cause IUGR.⁴

Regarding viral infections of the placenta, several herpetic infections have been reported to be associated with the disease, including cytomegalovirus (CMV), herpes simplex virus 1 (HSV-1),

Roberta Gafà and Pantaleo Greco contributed equally to this study.

varicella-zoster virus (VZV), human herpesvirus 8 (HHV-8).^{5–8} Conversely, associations with human herpesvirus 6 (HHV-6) are not yet known.

HHV-6 is a ubiquitous virus belonging to the Betaherpesvirinae subfamily of Herpesviridae, the presence of which has been described in vaginal secretions,⁹ in the uterine cervix,¹⁰ in placental tissues¹¹ and in endometrial epithelial cells.¹² The presence of HHV-6 infection in endometrial cells was reported as associated with primary idiopathic infertility,^{12,13} in which the presence of the infection leads to the alteration of the immune profile of the endometrium, which involves, in particular, the tolerogenic molecule human leukocyte antigen G (HLA-G), capable of compromising the embryo implantation.^{14,15}

During the various stages of pregnancy, the maternal immune system is finely regulated to protect the semi-allogeneic fetus from the attack of the maternal immune system during the early stages,^{16,17} and then gradually foster a more inflammatory environment near birth.^{18,19} This particular immunological condition is allowed by the action of immune-modulating molecules, among which the HLA-G molecule is one of the most important.

HLA-G is a nonclassical class I major histocompatibility complex (MHC-I) molecule, which during pregnancy plays a key role both in the regulation of the maternal immune system^{16,20} and in the placental process by regulating the neo-angiogenic process.^{21,22} HLA-G is an immunosuppressive molecule, inhibiting NK cells, T lymphocytes, and antigen-presenting cells via inhibitory receptors (ILT2, ILT4, and KIR2DL4). These immune-inhibitory functions are often exploited by micro-organisms, including HHV-6,²³ as an immune evasion mechanism.²⁴

In particular, HHV-6 is able to alter the expression of the HLA-G molecules at the endometrial level and to induce its expression in endothelial cells by means of the viral protein U94, modifying the angiogenic process.²¹ Since the condition of IUGR originates mainly from placental insufficiency due to anomalies in the maternal blood supply, we hypothesize a possible role of placental HHV-6 infection and the consequent modulation of HLA-G expression in IUGR onset.

We investigated the possible correlation between the presence of placental HHV-6 infection the IUGR clinical condition, evaluating the possible implication of the HLA-G molecule in the viral immunological evasion process and, consequently, in the onset of the pathology.

2 | MATERIAL AND METHODS

2.1 | Study population

The study was conducted on 22 patients enrolled at the time of childbirth at the Gynecology and Obstetrics Department of the Sant'Anna University Hospital in Ferrara. In particular, two cohorts were identified, namely, a cohort made up of 11 women with late-onset IUGR, and a control cohort made up of 11 women with physiological pregnancy. IUGR was defined based on the Delphi

consensus criteria, which includes either a very small fetus with abdominal circumference (AC) or estimated fetal weight (EFW) < 3rd percentile or a small fetus (with AC or EFW < 10th percentile) with additional abnormal Doppler velocimetry or a decrease in AC or EFW by two quartiles or more.²⁵ Late-onset IUGR was defined as diagnosed after 32 weeks of pregnancy, according to International Society of Ultrasound in Obstetrics and Gynecology (ISUOG) Guidelines.²⁶ Clinical data were collected for both cohorts, as reported in Table S1. The newborns were characterized by birth weight and 5 min Apgar index score, as reported in Table S1. Finally, the placentas were characterized by weight, umbilical artery pH as reported in Table S1. The study was approved by our hospital's ethics committee. All the data were anonymized and no connection with the patient identity was possible.

2.2 | Examination of placenta samples

The placentas were collected after delivery and sent to the Pathology Lab for examination. They were initially examined in the unfixed state then the membranes were removed by trimming them along the placental margin and the umbilical cord was removed after recording the length and site of insertion. The placental disk weight and three-dimensional measurement were recorded and the parenchyma was sectioned at 1–2 cm intervals on the maternal surface; after formalin fixation, a full-thickness section from the central portion of the placenta was sampled for histology. At least four sections were obtained from each placenta sample: three sections for the different staining (HHV-6, HLA-G, and isotype control); one section as a backup section, if needed.

Subsequently, the samples were processed for histological slide preparation. The study was authorized by the Local Ethical Committee.

2.3 | Immunohistochemistry

The presence of HHV-6 and the expression of HLA-G in placental tissue samples were detected through the use of indirect immunohistochemistry. In particular, tissue slides were deparaffined by using Toluene, rehydrated in decreasing ethanol concentration. Heat antigen retrieval in Citrate Buffer pH 6.1 with 0.05% Tween20 was performed. Slides were stained using the Ultratek kit (Histoline) and the following primary antibody: anti-gp116 (1:200; Santa Cruz) or anti-gp41 (1:200; Santa Cruz) for HHV-6 detection, and MEM/G2 (1:400; Exbio) for HLA-G staining. Anti IgG isotype (normal mouse IgGsc-3877; Santa-Cruz) was used as anti-isotype control.

After immunohistochemical staining, the slides were scanned using the Philips Ultra Fast Scanner version 1.6, digitalized slides were converted into BigTIFF format and were then imported into QuPath software for further image analysis. First, the Simple tissue detection tool was used to create annotation of the tissue region to be analyzed. The Cell detection tool was used to detect every cell in

the tissue by using a built-in cell segmentation algorithm. To enable a distinction between positively and negatively stained cells, the Intensity feature in the Detection classifier was used. The tissues were scored on the basis of the number of positively stained cells/mm².

2.4 | Statistical analysis

The results on HHV-6 frequency and positivity for HLA-G were analyzed by Fisher exact test. Biological variables reported as mean \pm SD were compared between the two study groups by *t* Student test. Levels of positivity in Immunohistochemistry (IHC) reported as median and interquartile value are compared between study groups using the Mann–Whitney test (*U* test). The statistical analysis was performed by GraphPad Software.

3 | RESULTS

3.1 | Characterization of the study population

Both groups of patients (11 IUGR and 11 control women) were characterized for different clinical parameters, shown in Table S1. Clinical data were compared between the two study groups to identify those significantly distinctive of the IUGR disease condition.

In particular, we found that the IUGR group has a higher frequency of induction of delivery than the control group ($p < 0.0001$; Fisher exact test) and a prevalence of cesarean sections in comparison with the control group ($p = 0.001$; Fisher exact test).

Compared with the data referring to the newborns, in the IUGR group, we found a significant reduction in both the infant's birth weight ($p < 0.0001$; *t* test) and placental weight ($p < 0.0001$; *t* test) compared with the control group.

3.2 | Analysis of the presence of HHV-6 in placental samples

Placental biopsies collected from both the IUGR and control groups were analyzed by immunohistochemistry for the presence of HHV-6 infection and HLA-G molecules (Figure 1).

We found a higher percentage of placenta tissues that presented HHV-6 positivity in the IUGR population (9/11; 81.8%) in comparison with the control group (1/11; 9%) ($p < 0.0001$; Fisher exact test). Furthermore, we evaluated the localization of HHV-6 positive staining. We observed that the HHV-6 positive IUGR placenta samples presented HHV-6 staining in 40% of the invasive extravillous trophoblast (EVT), while the HHV-6 positive control placenta sample showed no HHV-6 staining in EVT (40% vs. 0%; $p < 0.0001$ Fisher exact test; Figures 1 and 2A). We observed HHV-6 staining in 63% of the syncytiotrophoblast (ST) cells from HHV-6 positive IUGR placenta samples while the HHV-6 positive control placenta sample showed only the 9% of HHV-6-stained ST (63.6% vs. 9%; $p < 0.0001$

Fisher exact test; Figures 1 and 2B). The level of HHV-6 staining was also evaluated in terms of the number of positively stained cells/mm². As reported in Figure 2C, we observed a higher density of HHV-6 staining in the IUGR placenta samples compared with the control placenta sample ($p < 0.01$, Mann–Whitney *U* test).

3.3 | Analysis of the expression of HLA-G in placental samples

The placenta samples were subsequently analyzed for the expression of the HLA-G molecule by IHC (Figure 1). All the analyzed IUGR placentas presented areas with positive staining for HLA-G. In contrast, there are only low amounts of HLA-G in control term placentas. Interestingly, we showed a high density of HLA-G expression in IUGR placenta samples compared with the control placentas ($p < 0.0001$, Fisher exact test; Figure 2D). When we subdivided the IUGR placenta samples on the basis of the presence of HHV-6 staining, we observed that the samples positive for HHV-6 staining were also characterized by a higher HLA-G expression ($p < 0.05$, Mann–Whitney *U* test; Figure 2E). In the control group, we found only one HHV-6 positive placenta, so the correlation with HLA-G expression was not possible to be evaluated.

4 | DISCUSSION

The causes of IUGR can be fetal, maternal, placental, genetic or a combination of these factors.² In particular, it is known that infections occurring after the first 6–8 weeks of gestation can be associated with placental abnormalities that can cause IUGR.⁴ Previously, we have demonstrated that the coculture of endometrial epithelial cells with spheroids generated from the EVT-derived cell line JEG3 showed a twofold expansion of spheroids on endometrial epithelial-stromal cells (ESC) culture surface from HHV-6A negative endometrium while no expansion was observed on the surface of ESC from HHV-6A positive endometrium.¹⁴ These data suggest that HHV-6 infection might influence trophoblast invasion and consequently placenta formation.

For this purpose, we focused on the possible presence of the HHV-6 virus in IUGR placenta samples.

The clinical data support the role of placental abnormalities in the enrolled IUGR women, with a disproportionate placenta weight and fetus weight at birth.²⁷

We observed HHV-6 staining in 81% of the IUGR placenta samples, mainly in the EVT, while HHV-6 was evidenced only in one control placenta sample.

As HHV-6 is able to alter the expression of HLA-G at the endometrial level and to induce its expression in endothelial cells by means of the viral protein U94,^{23,24} modifying the angiogenic process,^{21,22} we evaluated the HLA-G expression in placenta samples. Interestingly, we showed a high density of HLA-G expression in IUGR placenta samples compared with the control placentas.

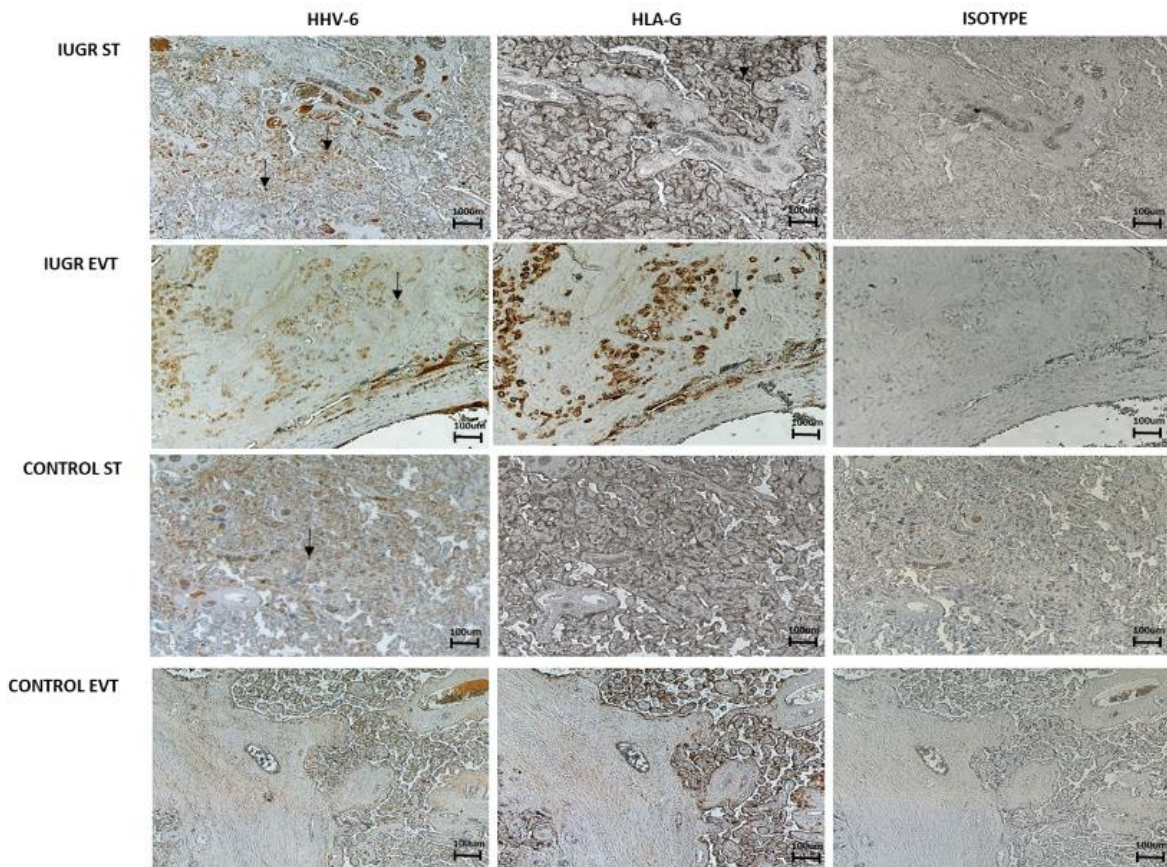


FIGURE 1 Representative immunohistochemical results on IUGR and control placentas, evaluated for gp41 HHV-6 and HLA-G expression. Both syncytiotrophoblasts (ST) and invasive extravillous trophoblast (EVT) were evaluated. Isotype control is reported. Black arrows indicate positive cell staining. HHV-6, human herpesvirus 8; HLA-G, human leukocyte antigen-G; IUGR, intrauterine growth restriction

When we subdivided the IUGR placenta samples on the basis of the presence of HHV-6 staining, we observed that the samples positive for HHV-6 staining were also characterized by a higher HLA-G expression. It is known that HLA-G is a molecule that is highly expressed by the fetal annex, in particular, cytotrophoblasts during the first and second trimester.²⁸ In contrast, there are only trace amounts of HLA-G in term placentas. Our results are consistent with a dysregulation of HLA-G molecules in the IUGR placenta, where the molecule is highly expressed. The correlation between HHV-6 positivity and high levels of HLA-G expression suggests a non-negligible causal connection. In fact, HHV-6 is known to be able to modulate the expression of HLA-G molecules,¹⁴ mainly by the U94 viral protein.²¹ U94 is an early protein expressed by HHV-6 during the latency phase.^{21,23} U94 induces the loss of angiogenic properties of endothelial cells,²¹ as shown by the inability to form capillary-like structures. Moreover, U94 induces the expression of HLA-G molecules via transcription factor ATF3, which stimulates HLA-G activation by recognizing a consensus sequence on its promoter.²¹ The ability of U94 to stimulate HLA-G expression is at the basis of the antiangiogenic effect of U94, as proved by the restoration of the

angiogenic properties in HHV6-infected endothelial cells after the addition of anti-HLA-G antibody.²¹ In fact, HLA-G molecules are highly expressed by the fetal annex, in particular, cytotrophoblasts during the first and second trimester.²⁸ HLA-G is a molecule that in addition to immune-inhibitory functions, is involved in the control of endothelial cell activity.^{29–32} A defect in placental HLA-G expression during pre-eclampsia, a potentially dangerous disorder of human pregnancy associated with placental vascular defects, was constantly observed,^{28,33–35} further suggesting a link between HLA-G and vascular events. In vitro assays demonstrated that HLA-G inhibits endothelial cell proliferation, migration, and capillary tube formation,³⁶ inducing apoptosis of endothelial cells. HLA-G inhibitory effects on endothelial cells are mediated through specific interaction with the CD160 receptor that is expressed by activated endothelial cells.³⁶ CD160 is a glycosylphosphatidylinositol-anchored, MHC Class I-dependent, immunoglobulin-like receptor expressed by the CD56dim peripheral blood major NK cell subset as well as by $\gamma\delta$ T cells, intestinal intraepithelial cells, and some CD8⁺ T cells.³⁷ The ability of HLA-G to induce apoptosis of activated endothelial cells is relevant in the uteroplacental environment as effacement of

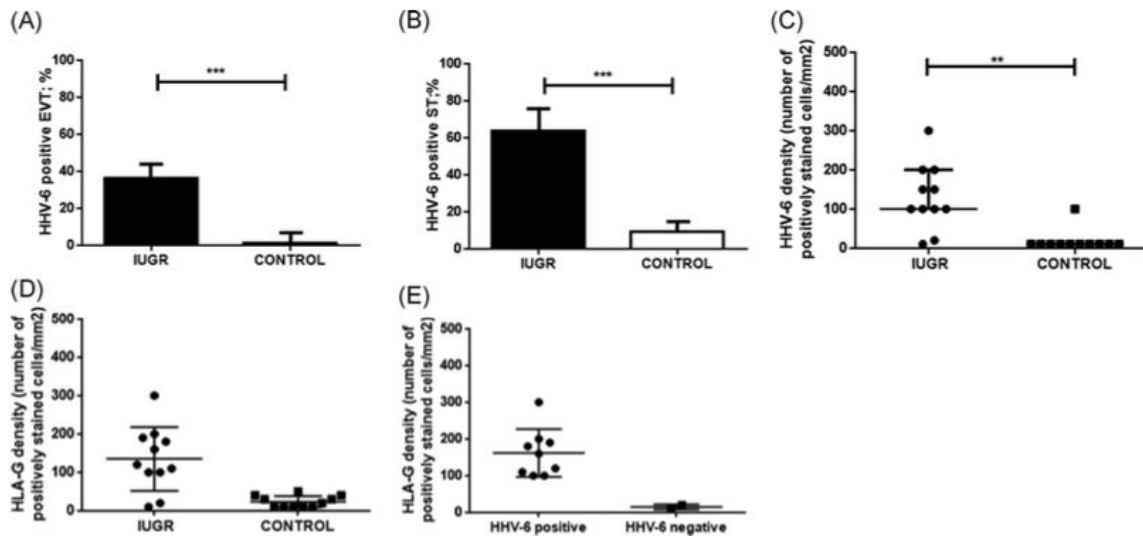


FIGURE 2 (A) Percentage of HHV-6 positive samples in invasive extravillous trophoblast cells (EVT) of IUGR and control placentas. (B) Percentage of HHV-6 positive samples in syncytiotrophoblast (ST) of IUGR and control placentas. The data are reported as mean \pm standard deviation. The statistical analysis was performed by Fisher's exact test. (C) Level of HHV-6 staining evaluated in terms of the number of positively stained cells/mm² in IUGR and control placentas; (D) Level of HLA-G staining evaluated in terms of the number of positively stained cells/mm² in IUGR and control placentas; (E) Level of HLA-G staining evaluated in terms of the number of positively stained cells/mm² in IUGR and control placentas subdivided according to HHV-6 positivity. The data are reported as median \pm standard deviation. The statistical analysis was performed by the Mann-Whitney *U* test. HHV-6, human herpesvirus 8; HLA-G, human leukocyte antigen-G; IUGR, intrauterine growth restriction

pre-existing maternal endothelial cells in the spiral arteries occurs,³⁸ and possibly inhibition of arteriole angiogenesis in the *decidua basalis*.

The main limitation of this study is the limited number of samples analyzed. We are aware that a larger number of samples should be evaluated to confirm our results. However, the literature data support a mechanistic correlation between HHV-6 infection and HLA-G molecule expression.

In conclusion, these preliminary results showed the presence of the HHV-6 virus in a high percentage of IUGR placenta samples corresponding to high HLA-G expression. These data might support the hypothesis that the presence of this virus represents a favorable factor for the onset of placental abnormalities as the high expression of HLA-G molecule during the term period when low levels of HLA-G are commonly present. In fact, the results obtained are in line with the known ability of HHV-6 to modulate HLA-G expression.^{14,21} Consequently, the altered vascular structure of IUGR placental tissue might be caused by the increased expression of the HLA-G molecules.

ACKNOWLEDGMENTS

The authors thank Linda Sartor for writing assistance, Alessandro Sofia for informatics assistance, Cristina Bosi for sample preparation, Grazia Murgiano, and Iva Pivanti for technical assistance. This study was supported by the University of Ferrara FAR 2019 (Roberta Rizzo, Pantaleo Greco) and the HHV-6 foundation grant (Roberta

Rizzo). The funders had no role in the study design, data collection, and analysis, decision to publish, or preparation of the manuscript.

CONFLICT OF INTERESTS

The authors declare that there are no conflict of interests.

AUTHOR CONTRIBUTIONS

Conceptualization; data curation; funding acquisition: Daria Bortolotti, Roberta Rizzo, Pantaleo Greco. *Article revision:* Roberta Gafà. *Investigation:* Valentina Gentili, Giovanna Schiuma, Silvia Beltrami, Sabrina Rizzo. *Clinical data collection:* Erica Santi, Cristina Taliento, Amerigo Vitagliano. *Clinical samples' collection:* Roberta Gafà and Giovanni Lanza.

ORCID

Roberta Rizzo  <http://orcid.org/0000-0001-9507-9126>

REFERENCES

- Gupta M, Saunders WB, Brodsky D, Ouellette MA, eds. *Intrauterine Growth Restriction, in Primary Care of the Premature Infant*. Philadelphia: W.B. Saunders; 2008:77-83.
- Sharma D, Shastri S, Sharma P. Intrauterine growth restriction: antenatal and postnatal aspects. *Clin Med Insights Pediatr*. 2016;10:67-83.
- Aviram R, Shental TB, Kidron D. Placental aetiologies of foetal growth restriction: clinical and pathological differences. *Early Hum Dev*. 2010;86:59-63.
- Adams Waldorf KM, McAdams RM. Influence of infection during pregnancy on fetal development. *Reproduction*. 2013;146:R151-R162.

5. Cordier AG, Nedellec S, Benachi A, Frydman R, Picone O. Arguments for an infectious cause of IUGR. *J Gynecol Obstet Biol Reprod (Paris)*. 2011;40:109-115.
6. Muehlenbachs A, De la Rosa Vázquez O, Bausch DG, et al. Ebola virus disease in pregnancy: clinical, histopathologic, and immunohistochemical findings. *J Infect Dis*. 2017;215:64-69.
7. Lan K, Luo MH. Herpesviruses: epidemiology, pathogenesis, and interventions. *Virol Sin*. 2017;32:347-348.
8. Nikkels AF, Delbecq K, Pierard GE, Wienkotter B, Schalasta G, Enders M. Distribution of varicella-zoster virus DNA and gene products in tissues of a first-trimester varicella-infected fetus. *J Infect Dis*. 2005;191:540-545.
9. Caseta MT, Breese Hall C, Schnabel K, Lofthus G, McDermott MP. Human herpesvirus (HHV)-6 and HHV-7 infections in pregnant women. *J Infect Dis*. 2007;196:1296-1303.
10. Leach CT, Newton ER, McParlin S, Jenson HB. Human herpesvirus 6 infection of the female genital tract. *J Infect Dis*. 1994;169:1281-1283.
11. Finger-Jardim F, Teixeira LO, De Oliveira GR, et al. Herpes simplex virus: prevalence in placental tissue and incidence in neonatal cord blood samples. *J Med Virol*. 2014;86(3):519-524.
12. Marci R, Gentili V, Bortolotti D, et al. Presence of HHV-6A in endometrial epithelial cells from women with primary unexplained infertility. *PLOS One*. 2016;11:e0158304.
13. Caselli E, Bortolotti D, Marci R, et al. HHV-6A infection of endometrial epithelial cells induces increased endometrial NK cell-mediated cytotoxicity. *Front Microbiol*. 2017;8:2525.
14. Bortolotti D, Gentili V, Rotola A, et al. HHV-6A infection of endometrial epithelial cells affects immune profile and trophoblast invasion. *Am J Reprod Immunol*. 2019;82:e13174.
15. Pegoraro A, Bortolotti D, Marci R, et al. The P2X7 receptor 489C>T gain of function polymorphism favors HHV-6A infection and associates with female idiopathic infertility. *Front Pharmacol*. 2020;11:96.
16. Von Rango U. Fetal tolerance in human pregnancy—a crucial balance between acceptance and limitation of trophoblast invasion. *Immunol Lett*. 2008;115:21-32.
17. Steinborn A, Varkonyi T, Scharf A, Bahlmann F, Klee A, Sohn C. Early detection of decreased soluble HLA-G levels in the maternal circulation predicts the occurrence of preeclampsia and intrauterine growth retardation during further course of pregnancy. *Am J Reprod Immunol*. 2007;57:277-286.
18. Osmers RG, Bläser J, Kuhn W, Tschesche H. Interleukin-8 synthesis and the onset of labor. *Obstet Gynecol*. 1995;86:223-229.
19. Gomez-Lopez N, StLouis D, Lehr MA, Sanchez-Rodriguez EN, Arenas-Hernandez M. Immune cells in term and preterm labor. *Cell Mol Immunol*. 2014;11:571-581.
20. Djuricic S, Skibsted L, Hviid TV. A Phenotypic analysis of regulatory T cells and uterine NK cells from first trimester pregnancies and associations with HLA-G. *Am J Reprod Immunol*. 2015;74:427-444.
21. Rizzo R, D'accolti M, Bortolotti D, et al. Human herpesvirus 6A and 6B inhibit in vitro angiogenesis by induction of human leukocyte antigen G. *Sci Rep*. 2018;8:17683.
22. Rajagopalan S, Bryceson YT, Kuppusamy SP, et al. Activation of NK cells by an endocytosed receptor for soluble HLA-G. *PLOS Biol*. 2006;4:e9.
23. Caselli E, Campioni D, Cavazzini F, et al. Acute human herpesvirus-6A infection of human mesothelial cells modulates HLA molecules. *Arch Virol*. 2015;160:2141-2149.
24. Amiot L, Vu N, Samson M. Immunomodulatory properties of HLA-G in infectious diseases. *J Immunol Res*. 2014;2014:298569.
25. Gordijn SJ, Beune IM, Thilaganathan B, et al. Consensus definition of fetal growth restriction: a Delphi procedure. *Ultrasound Obstet Gynecol*. 2016;48:333-339.
26. Leesees CC, Stampalija T, Baschat A, et al. ISUOG practice guidelines: diagnosis and management of small-for-gestational-age fetus and fetal growth restriction. *Ultrasound Obstet Gynecol*. 2020;56:298-312.
27. Bukowski R, Hansen NI, Pinar H, et al. Eunice Kennedy Shriver National Institute of Child Health and Human Development (NICHD) Stillbirth Collaborative Research Network (SCRN). Altered fetal growth, placental abnormalities, and stillbirth. *PLOS One*. 2017;12(8):e0182874.
28. Goldman-Wohl DS, Ariel I, Greenfield C, et al. Lack of human leukocyte antigen-G expression in extravillous trophoblasts is associated with pre-eclampsia. *Mol Hum Reprod*. 2000;6:88-95.
29. Dorling A, Monk NJ, Lechler RI. HLA-G inhibits the transendothelial migration of human NK cells. *Eur J Immunol*. 2000;30(2):586-593.
30. Le Bouteiller P, Pizzato N, Barakonyi A, Solier C. HLA-G, preeclampsia, immunity and vascular events. *J Reprod Immunol*. 2003;59(2):219-234.
31. Menier C, Rabreau M, Challier JC, Le Discorde M, Carosella ED, Rouas-Freiss N. Erythroblasts secrete the nonclassical HLA-G molecule from primitive to definitive hematopoiesis. *Blood*. 2004;104(10):3153-3160.
32. Zeng MH, Fang CY, Wang SS, et al. A study of soluble HLA-G1 protecting porcine endothelial cells against human natural killer cell-mediated cytotoxicity. *Transplant Proc*. 2006;38(10):3312-3314.
33. Colbern GT, Chiang MH, Main EK. Expression of the nonclassical histocompatibility antigen HLA-G by preeclamptic placenta. *Am J Obstet Gynecol*. 1994;170(5 Pt 1):1244-1250.
34. Hara N, Fujii T, Yamashita T, Kozuma S, Okai T, Taketani Y. Altered expression of human leukocyte antigen G (HLA-G) on extravillous trophoblasts in preeclampsia: immunohistological demonstration with anti-HLA-G specific antibody "87G" and anti-cytokeratin antibody "CAM5.2". *Am J Reprod Immunol*. 1996;36(6):349-358.
35. Yie SM, Taylor RN, Librach C. Low plasma HLA-G protein concentrations in early gestation indicate the development of preeclampsia later in pregnancy. *Am J Obstet Gynecol*. 2005;193(1):204-208.
36. Yie SM, Taylor RN, Librach C. Soluble HLA-G1 inhibits angiogenesis through an apoptotic pathway and by direct binding to CD160 receptor expressed by endothelial cells. *Blood*. 2006;108(8):2608-2615.
37. Fons P, Chabot S, Cartwright JE, et al. Cutting edge: MHC class I triggering by a novel cell surface ligand costimulates proliferation of activated human T cells. *J Immunol*. 1999;162(3):1223-1226.
38. Pijnenborg R, Vercruyse L, Hanssens M. The uterine spiral arteries in human pregnancy: facts and controversies. *Placenta*. 2006;27(9-10):939-958.

SUPPORTING INFORMATION

Additional Supporting Information may be found online in the supporting information tab for this article.

How to cite this article: Bortolotti D, Gentili V, Santi E, et al. Late-onset intrauterine growth restriction and HHV-6 infection: A pilot study. *J Med Virol*. 2021;93:6317-6322. <https://doi.org/10.1002/jmv.27138>



Contents lists available at ScienceDirect

Bioorganic Chemistry

journal homepage: www.elsevier.com/locate/bioorg

Synthesis and biological evaluation of novel rhodanine-based structures with antiviral activity towards HHV-6 virus

Valentina Gentili¹, Giulia Turrin¹, Paolo Marchetti, Sabrina Rizzo, Giovanna Schiuma, Silvia Beltrami, Virginia Cristofori, Davide Illuminati, Greta Compagnin, Claudio Trapella*, Roberta Rizzo*, Daria Bortolotti¹, Anna Fantinati¹

University of Ferrara, Department of Chemical, Pharmaceutical and Agricultural Sciences, Via Fossato di Mortara, 17, 44121 Ferrara, Italy

ABSTRACT

An increased awareness of diseases associated with Human herpesvirus 6 (HHV-6) infection or reactivation has resulted in a growing interest in the evaluation of the best treatment options available for the clinical management of HHV-6 disease. However, no compound has yet been approved exclusively for HHV-6 infection treatment. For this reason, the identification of anti-HHV6 compounds provides a valuable opportunity for developing efficient antiviral therapies. A possible target for antiviral drugs is the virus-cell fusion step. In this study, we synthesized potential fusion intermediates inhibitors based on the rhodanine structure. The obtained derivatives were tested for cytotoxicity and for antiviral activity in human cells infected with HHV6. Level of infection was monitored by viral DNA quantification at different time points up to 7 days post infection. Among the synthesized derivatives, **9e** showed a significant inhibitory effect on viral replication that lasted over 7 days, probably attributable to the particular combination of hydrophilic and hydrophobic substituents to the rhodanine moiety. Our results support the use of these amphipathic fusion inhibitors for the treatment of HHV-6 infections.

1. Introduction

Most of available antiviral drugs are design to target specific viral proteins [1,2]. However, this therapeutic approach determines a selection for resistance [3], and also display a limited spectrum of action. In view of this, novel antivirals are therefore needed.

In the last years, several studies were focused on the identification of new antiviral targets based on the interference with viral fusion on cell membrane [4]. In fact, fusion of enveloped virus with the host cell is crucial in viral infectivity. Viral fusion is a process driven by specialized protein expressed on viral envelope that, after conformational modifications due to their binding to specific cellular receptors, leads to envelope-cell membrane fusion and the consequent release of the nucleocapsid into the cytoplasm.

The steps of the viral fusion process evidenced two possible moments on which fusion inhibitors could be effective: *i.* pre-fusion step, which involved the engagement of the cellular receptor during the viral adsorption and *ii.* fusion intermediates step, in which a physical fusion occurs between the lipid bilayers of both envelope and cytoplasmic membrane [5].

Various molecules are proposed in literature as membrane fusion

inhibitors that affect the viral attachment through cell receptor, disturbing the viral adsorption phase [5]. Essentially, these molecules exert their function by blocking the cognate virus-receptor interaction via competition for the entry receptors, representing the classical inhibitors of virus entry [5]. The use of this strategy is exemplified by Maraviroc (Selzentry; Pfizer), a competitive molecule for the virus co-receptor CC-chemokine receptor 5 (CCR5) that inhibits HIV-1 entry [6]. However, despite the potential efficacy of these competitors as antivirals, the development of receptor-specific entry inhibitors for the great majority of viral pathogens is limited by the identification of the actual receptors. In this view, the design of new antivirals, capable of inhibiting cell entry of enveloped viruses by blocking the formation of fusion intermediates seems to represent the most convenient approach. In fact, these molecules could act independently from the cellular receptor involved during viral entry, thus no specific receptor structure is required.

Fusion intermediates inhibitors work mainly by modifying the lipidic structure of both virus and host cell membrane, in order to avoid the release of the nucleocapsid inside the cells. Among antiviral mechanisms of action against the entry of enveloped viruses, the most studied include the induction of cholesterol depletion [7] and the alteration of membrane components that modify membrane fluidity [8] or cause virolysis.

* Corresponding authors at: University of Ferrara, Department of Chemical, Pharmaceutical and Agricultural Sciences, Via Luigi Borsari 46, 44121 Ferrara, Italy (R. Rizzo). University of Ferrara, Department of Chemical, Pharmaceutical and Agricultural Sciences, Via Fossato di Mortara, 17 44121 Ferrara, Italy (C. Trapella).

E-mail addresses: trap@unife.it (C. Trapella), rbr@unife.it (R. Rizzo).

¹ These authors contributed equally to the research.

<https://doi.org/10.1016/j.bioorg.2021.105518>

Received 3 June 2021; Received in revised form 4 October 2021; Accepted 23 November 2021

Available online 26 November 2021

0045-2068/© 2021 Elsevier Inc. All rights reserved.

This, for instance, is observed in treatment with rigid amphipathic fusion inhibitors (RAFI) [9-12].

Other molecules displaying a broad-spectrum of antiviral activity through a selective action on enveloped viruses are rhodanine and thioarbituric derivatives. Their activity is due to lipid oxidation ability, which affects the fluidity of the lipid bilayer and interferes with virus-cell fusion. Recently, polyrhodanine nanostructure has been reported as antiviral, anticancer and bacteriostatic [13].

Fusion intermediate inhibitors are promising antiviral drugs since they exert their function in the early phase of infection, namely before damages have occurred to cells [14,15]. The advantage of using this kind of antivirals includes the broad spectrum of enveloped viruses that could be inhibited without the risk of developing resistance. Some of these antivirals have been described to be effective on different human viruses, such as the respiratory syncytial virus (RSV) [16], Hepatitis B (HBV) [17] and C (HCV) viruses [18,19].

Considering enveloped viruses associated to different human pathological conditions, herpesviruses are among the most studied. In particular, these viruses are characterized by the ability to develop a latency phase after the primary infection, causing as a consequence the onset of symptoms throughout the life span.

The Herpesviridae family includes nine components that infect humans and can be divided into three subfamilies: alpha-, beta- and gamma-herpesvirus according to their different cell tropism and symptomatology.

Human Herpes Virus-6 (HHV-6) is a beta-herpesvirus with a worldwide distribution that exists in two different species characterized by peculiar biological differences [20]: HHV-6A and HHV-6B. HHV-6B is the etiologic agent of roseola (*exanthema subitum*), while the disease associated with HHV-6A infection is still not clearly identified. These differences could be attributed to a different engagement of cell receptors by the two viruses. In fact, while HHV-6B recognizes CD134, expressed on T-cells, HHV-6A uses CD46, expressed on all nucleated cells [21], subtending its ability to infect a wide range of tissues, as confirmed by the recent association of HHV-6A infection with several diseases, including Multiple Sclerosis (MS) [22], Alzheimer's Disease (AD) [23,24] and infertility [25,26]. Importantly, to date, the treatment for HHV-6 infection consists only in antivirals that are already used to treat other herpetic infections and that target specific viral protein in order to inhibit viral replication and gene expression [27,28]. Moreover, HHV-6 establishes a latent infection in the target tissues and it could be reactivated several times during life, thus it requires several treatments with antivirals which can increase the risk of resistances [29,30]. In light of this, the use of fusion intermediates inhibitors to threat HHV-6 infection may represent an efficient strategy to improve infection control and decrease resistance onset.

The data available in literature on the use of fusion inhibitors to control herpetic infections report mainly the effect of some compounds in affecting the pre-fusion phase, by interfering with glycoprotein B interaction and cellular-membrane lipid rafts formation [31-33]. On the other hand, concerning the inhibition of the fusion intermediate formation, Cagno et al. described the antiviral activity of rhodanine derivatives on enveloped viruses including HSV-2 acyclovir resistant strain [34] and Boresstein et al. recently reported the effect of ginkgolic acid on several herpes viruses, including EBV, HSV-1 and HCMV [35].

Conversely, no data are available on the use of fusion intermediates inhibitors for this particular type of infection.

In this study, we have synthesized ten potential fusion intermediates inhibitors based on rhodanine structure, potentially active on HHV-6 infection. We tested the compounds on human cell lines, to determine their toxicity and effectiveness in controlling the HHV-6 infection, in order to identify the most safe and active compound.

2. Results and discussion

2.1. Chemistry

Recently different works has been published on the synthesis of antiviral molecule based on rhodanine heterocycle [34], acting as disrupting molecules for the enveloped viruses such as HSV-2, Influenza A virus, Zika.

Referring to the work of Cagno et al. [34] we chose the rhodanine-based compound **1** as reference compound to develop a SAR study focused on the modification of its hydrophilic head and lipophilic chain (Fig. 1). Different specific modifications have been made, considering RAFIs and their mechanism of action as starting point for this study [36].

The synthesis of the rhodanine scaffold was focused on the introduction of several aromatic rings, starting from different primary chiral and achiral amines, in order to build a small library of compounds bearing a series of substituents attached to the nitrogen atom (Scheme 1).

The synthesis of rhodanine derivatives has been achieved in a one-pot reaction between bromo-acetyl bromide (**2**) and the corresponding primary amine **3a-f** in carbon disulfide, to obtain in moderate to good yield the rhodanine core **4a-f**. Then, as shown in Scheme 2, to insert structural modifications of the polar head of the compound **1** (Fig. 1), we used a palladium catalyzed Suzuki reaction as a key step for the formation of the carbon-carbon bond between the iodo derivatives **5a-e** and the five-membered heterocycles, **6a-b** (furan or thiophene). Due to the instability of the rhodanine scaffold in basic conditions [37], we decided to work with the corresponding methyl ester derivatives **5a-e** to obtain the aldehydic compounds **7a-e** with higher yields. Then, we removed the ester function in the next step through lithium hydroxide hydrolysis, to afford compounds **8a-d**.

Once obtained the derivatives **8a-d**, we could bind them with the rhodanine scaffold through a Knoevenagel condensation [38], to obtain the desired products **9a**. Starting from **9a** we conceptualized new compounds with different lipophilic tails (**9b-f**) or different hydrophilic heads (**10a-d**) as depicted in Scheme 3.

2.2. Biological evaluation

2.2.1. Evaluation of cytotoxicity of **9a** and derivate compounds with different lipophilic tails

9a-f cytotoxicity was assayed in human lymphocytic cell lines by MTT assay, after 24 h treatment at 100 μ M, 10 μ M and 1 μ M. As shown in Fig. 2, all the compounds did not affect cell viability at the concentrations of 1 μ M and 10 μ M, while the concentration of 100 μ M showed a high cytotoxic effect ($p < 0.0001$, Student T test). The anti-viral efficacy was evaluated for the concentrations of 1 and 10 μ M, that are hundred-times lower than the cytotoxic concentration and ensure a safe use as

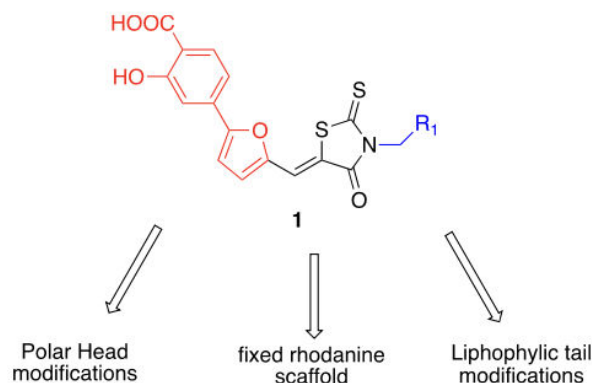
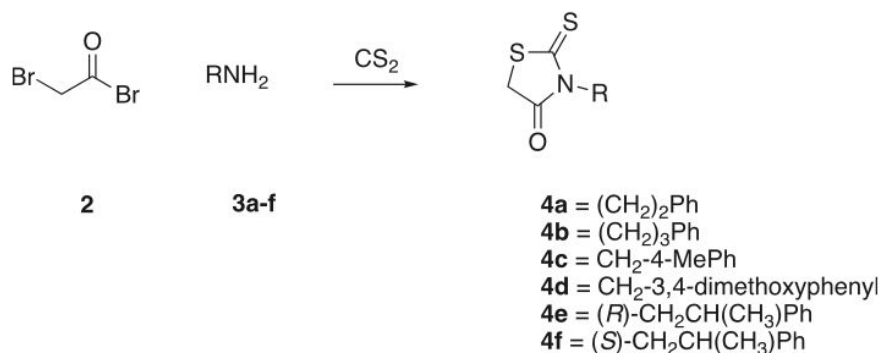
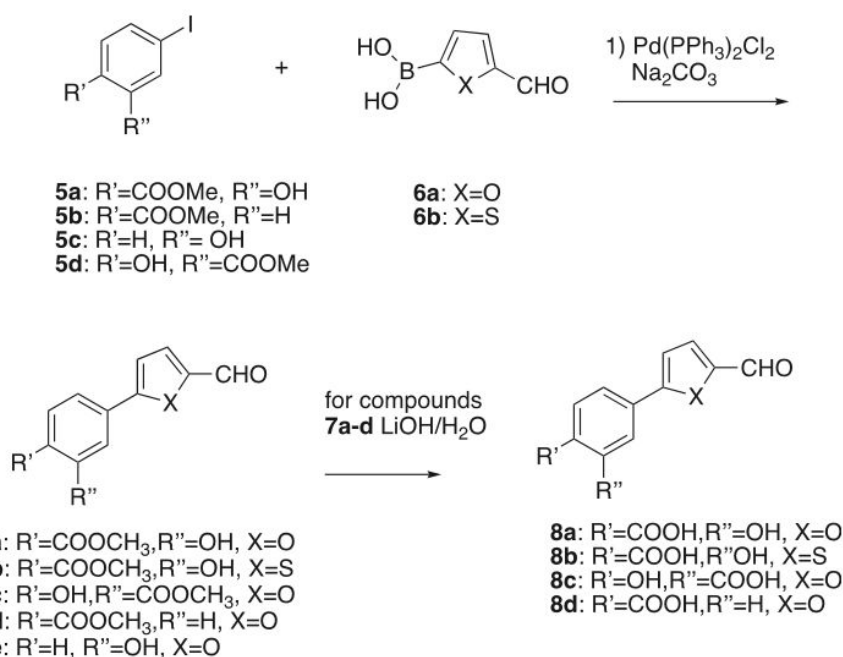


Fig. 1. Structure of the rhodanine-based reference compound.



Scheme 1. Synthesis of rhodanine derivatives with modifications at lipophilic tail.



Scheme 2. Synthesis of polar head bearing the aldehyde moiety.

a drug. The absence of cytotoxicity in the 1 and 10 μM range of concentration could be explained by the fact that cellular membranes are metabolically active and are characterized by a regenerative activity, that is absent in viromes.

2.2.2. Anti-HHV-6 activity of **9a** and derivate compounds with different lipophilic tails

The antiviral activity of **9a-f** compounds was tested on HHV-6A infected J-Jhan cells and HHV-6B SupT1 infected cells. The compounds were added to infected cell cultures at the concentration of 1 and 10 μM and pellet cell samples were collected at 24, 48, 72 h (hpi) and 7 days post infection (dpi) for HHV-6 DNA quantification by real time PCR. Results are reported as percentage compared to untreated infected control.

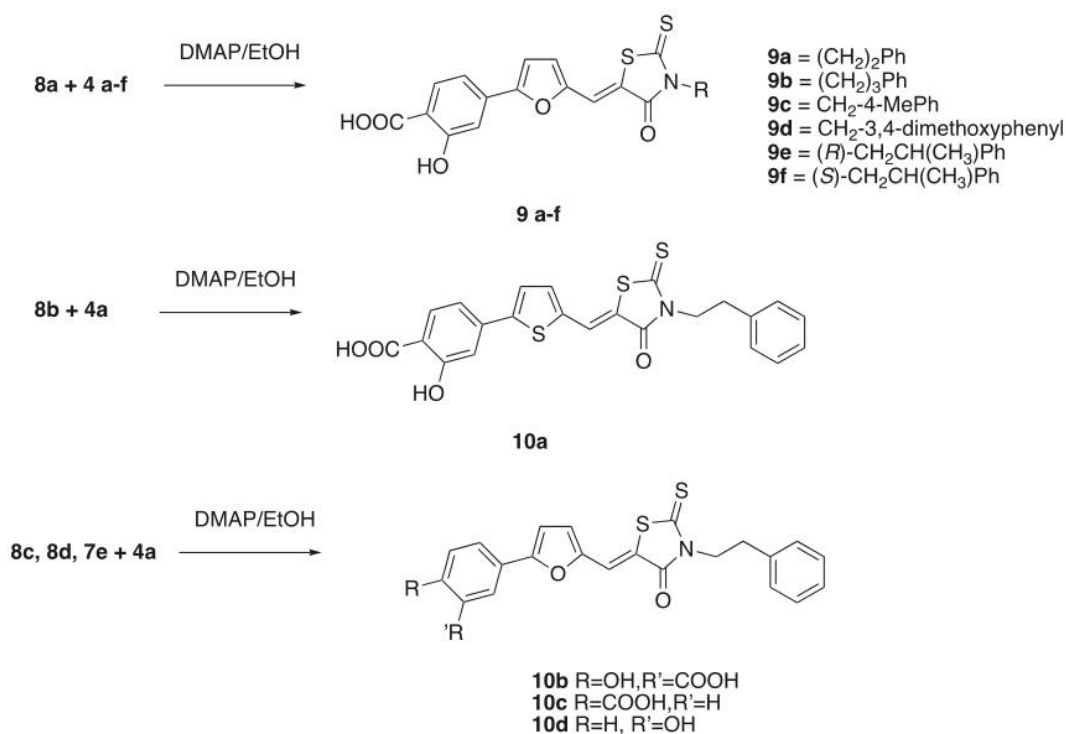
9a-9d molecules did not affect viral replication when used at the concentration of 1 μM (Fig. 3a, b), while **9e** and **9f** molecules were able to decrease viral replication in a significant level ($p < 0.0001$, Student T test) (Fig. 3a, b).

The treatment at 10 μM was more effective in reducing HHV-6A and HHV-6B replication (Fig. 3c, d). In particular, the highest antiviral effect

was observed in presence of **9a**, **9e** and **9f** treatment, which significantly decreased viral replication at all the time points considered, showing a decrease of 90–75% of viral load already after 24 hpi compared to untreated control ($p < 0.01$, Student T test), followed by a complete drop of the viral infection till 7 dpi for **9a** and **9e** ($p < 0.0001$, Student T test) (Fig. 3c, d). On the contrary, in presence of **9b**, **9c** and **9d** treatment we observed no effect on viral load at 24 hpi, while there was a drop in both HHV-6A and HHV-6B replication at 48 hpi that is maintained until 7dpi ($p < 0.0001$, Student T test) (Fig. 3c, d).

2.2.3. Evaluation of cytotoxicity and antiviral activity of **9a** derivatives with modified hydrophilic head

MTT assay was performed to assess the **10a**, **10b** and **10c** derivatives cytotoxicity on human lymphocyte cell lines after treatment for 24 h at the concentration of 1 and 10 μM . The results showed that **10a**, **10b** and **10d** did not affect cell viability, while **10c** resulted in a significant cytotoxic effect (Fig. 4, $p < 0.05$ Student T test). We hypothesize that the toxicity of compound **10c** might be due to the lack of the phenol OH that is involved in the hydrogen bond with the carboxylic moiety. In fact, both **10b** and **10d** are not toxic, where the OH group of **10b** makes a



Scheme 3. Synthesis of the final rhodanine scaffold bearing different polar heads and lipophylic tails.

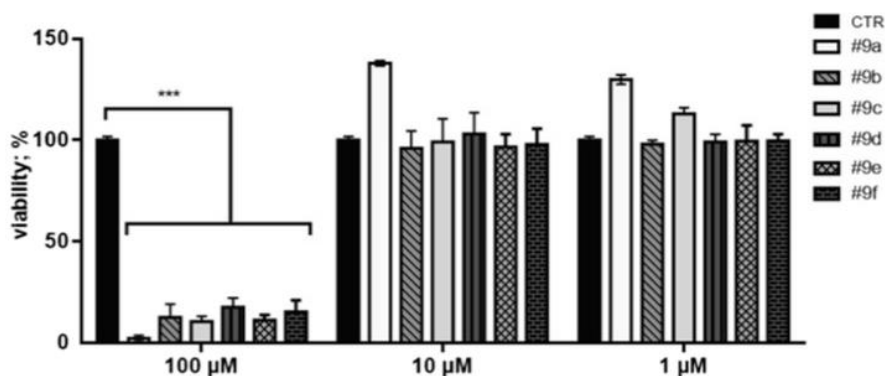


Fig. 2. Cell viability analysis by MTT assay in human lymphocyte cell lines after 24 h treatment with #9a-9f at the concentrations of 1, 10 and 100 μM. Values are reported as mean ± SD of 3 independent experiments.

hydrogen bond with the carboxylic moiety, 10d lacks the COOH function, supporting that the toxicity of 10c might be related to this acidic function when it's not involved in the hydrogen bond due to the lack of hydroxyl group. Basing on this result, 10c was not considered for further analysis.

Antiviral activity of 10a, 10b and 10d compounds was evaluated. As shown in Fig. 5, the HHV-6A and HHV-6B viral load was reduced of 52 and 54% ($p = 0.0016$, Student T test) and 90 and 89% ($p = 0.0002$, Student T test), respectively, after 72hpi and 7dpi after treatment with 10b. 10a treatment reduced the viral load of 52% ($p = 0.0046$, Student T test) and 49% ($p = 0.0044$, Student T test), at 48hpi and 72hpi, respectively, but the anti-HHV-6A and HHV-6B effect was lost after 7dpi (Fig. 5). 10d treatment reduced the viral load of 90% ($p < 0.0001$, Student T test) at 24hpi and 48hpi, but the anti-HHV-6A and HHV-6B effect was lost after 72hpi (Fig. 5).

This data confirmed that the modification of 9a polarity obtained in

these derivatives does not improve its inhibition of the viral replication, suggesting that this moiety participates only partially at the antiviral effect.

3. Conclusion

Despite the increasing evidence reporting HHV-6A and HHV-6B association with different diseases [22-26], there are no specific antiviral drugs available acting against this specific virus. The present study explores the antiviral effects of rhodanine-based fusion intermediate inhibitors on HHV-6 infection in human cells. Since HHV-6 is an enveloped virus, we synthesized potential fusion intermediate inhibitors [14,15], characterized by the presence of a rhodanine scaffold, with the aim of blocking the virion-cell fusion. We obtained different derivatives by substitution and bioisosteric replacements of hydrophilic head and lipophilic tail of the molecules tested for their cytotoxicity and antiviral

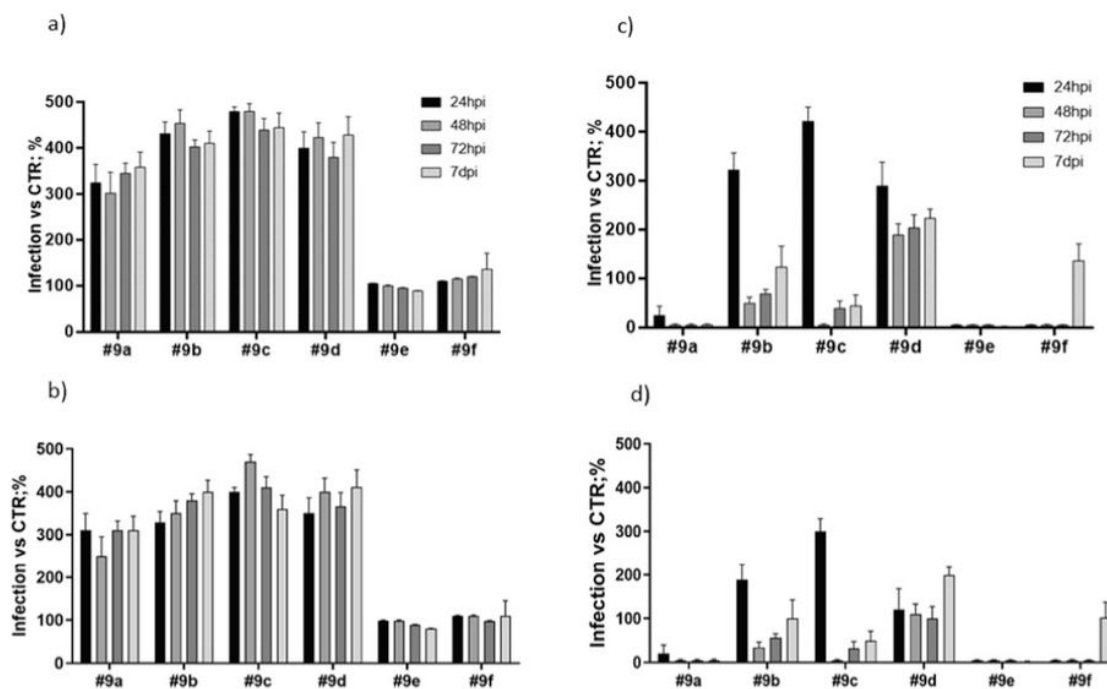


Fig. 3. Infection percentage compared to the untreated infected control (CTR) after treatment at 1 μM (a, b) and 10 μM (c, d) with #9a-9f compounds 24, 48 and 72 h and 7 days post infection with HHV-6A (a, c) and HHV-6B (b, d). HHV-6 genomes were quantified by real time-PCR and normalized for housekeeping RNaseP gene. Data were reported as mean percentage \pm SD obtained from 3 independent experiments compared to untreated infected cells.

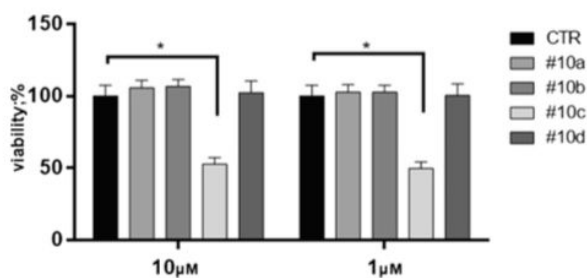


Fig. 4. Cell viability analysis by MTT assay in human lymphocyte cell lines after 24 h treatment with #10a, #10b, #10c and #10d at the concentration of 1 and 10 μM , compared to untreated control (CTR). Values are reported as mean \pm SD of 3 independent experiments. * $p < 0.05$ Student T test.

effect on HHV-6A and HHV-6B replication. Experimental results identified the 9a derivative as the lead compound, showing a complete reduction of HHV-6 viral load 48 h after infection, when used at 10 μM , without showing any cytotoxicity. In order to improve the antiviral effect of the lead compound 9a, we worked on the modification of the hydrophilic head or the lipophilic tail to increase the amphipathy of the molecule, obtaining different derivatives. Among these, compound 9e at the concentration of 10 μM , showed the highest antiviral activity, with a complete abatement of the viral load after 24 h and no cytotoxicity. The improved efficacy of compound 9e could be attributed to its peculiar combination of hydrophilic and hydrophobic substituents to the rhodanine moiety, that possibly allowed a better interaction with the viral envelope. The insertion into the viral envelop might induce envelope structure destabilization and virolysis that inhibit virion fusion and infection of the target cell. These results support the use of amphipathic fusion intermediate inhibitors based on rhodanine structure to treat HHV-6A and HHV-6B infection. Despite the two viruses engage different cellular receptors, we observed a comparable inhibitory effect by

treating with inhibitors based on rhodanine structure. This could be ascribable to the amphipathic nature of the compounds, which disorganize the viral envelope structure, avoiding the viral fusion with the host cell membranes, without engaging specific viral structures. In fact, enveloped viruses as HHV-6, gain their external membrane during virolysis release directly from cell surface. Anyway, while cell membranes are metabolically active, viral envelopes are not. In this way, rhodanine derivatives could induce virolysis and interfere with envelope-cell fusion process by intercalating in the viral outer phospholipidic bilayer without inducing critical cell membrane alteration, as proved by the absence of cytotoxicity observed after treating cells with antiviral concentrations.

This characteristic might avoid the onset of resistance in the new viral progeny, that usually observed with repeated treatments with common antiviral drugs.

4. Experimental section

4.1. Chemistry

Reagents were purchased from commercial suppliers and used without further purification. ^1H and ^{13}C NMR spectra were recorded, in deuterated DMSO or CDCl_3 solution, respectively, at 400 and 100 MHz on a Varian Mercury Plus 400, and peak positions are given in parts per million and were referenced to residual ^1H signals of the deuterated solvents respectively ($\delta^1\text{H}$ 7.26 for CDCl_3 , $\delta^1\text{H}$ 2.50 for $\text{DMSO}-d_6$). J values are expressed in Hertz. Positive-ion electrospray ionization (ESI) mass spectra were recorded on ESI Micromass ZQ 2000 instrument. Thin layer chromatography (TLC) was carried out using Merck precoated silica gel F-254 plates. Flash chromatography was done using Merck silica gel 60 (0.063–0.200 mm). Solvents were dried according to standard procedures, and reactions requiring anhydrous conditions were performed under argon. Solutions containing the final products were dried with Na_2SO_4 , filtered, and concentrated under reduced

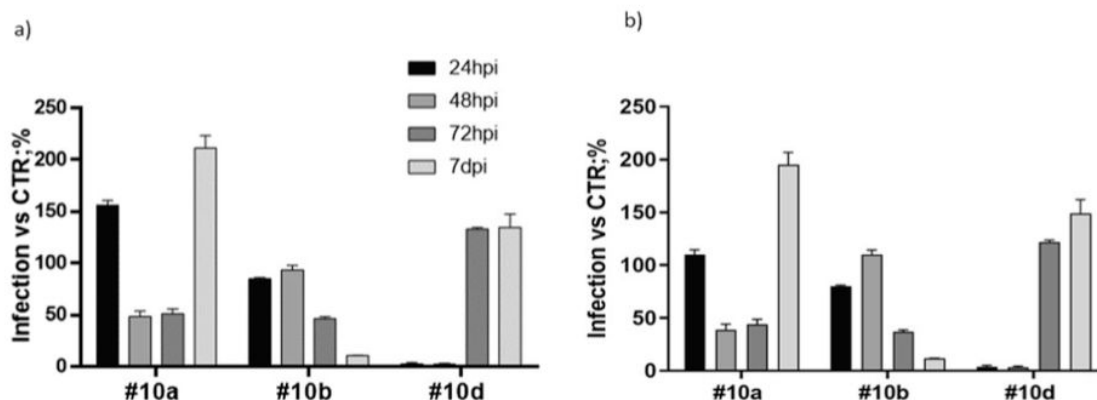


Fig. 5. Infection percentage compared to the untreated infected control after treatment with 10 μ M 10a, 10b and 10d compounds 24, 48 and 72 h and 7 days post infection with HHV-6A (a) and HHV-6B (b). HHV-6 genomes were quantified by real time-PCR and normalized for housekeeping RNaseP gene. Data were reported as mean percentage \pm SD obtained from 3 independent experiments compared to untreated infected cells.

pressure using a rotatory evaporator. The purity of the tested compounds was determined by combustion elemental analyses conducted by the Microanalytical Laboratory of the Chemistry Department of the University of Ferrara, Italy, with a Yanagimoto MT-5 CHN recorder elemental analyzer. All tested compounds yielded data consistent with a purity of at least 95% compared with the theoretical values. Melting points were determined on a Reichert-Kofler apparatus and are uncorrected.

4.1.1. General procedure for the synthesis of rhodanines 4a-f

Bromoacetyl bromide (1 mmol) was added, drop by drop, to a mixture of the pertinent amine (1 mmol) in CS_2 (5 mL) at 0–2 °C. The reaction mixture was allowed to warm up to room temperature and then heated at 100 °C for 3 h. After this time, AcOEt (25 mL) was added and the mixture was washed with H_2O (3 \times 7 mL). After evaporation of the solvent the resulting crude product (brown–red oil) was purified by column chromatography using as eluent mixtures of solvents in the proportions indicated for each compound.

4.1.2. General procedure for the synthesis of compounds 7a-e

Methyl-4-iodosalicylate 5a-e (1.00 mmol) and 5-formyl-2-furan boronic acid 6a, b (1.30 mmol) were dissolved in EtOH (10 mL) and DMF (5 mL) mL. The reaction mixture was stirred for 10 min under Argon at room temperature, then $\text{Pd}(\text{PPh}_3)_2\text{Cl}_2$ (0.1 mmol) and a 2 M solution of Na_2CO_3 (4 mL) were added. After 1 h, to the resultant orange suspension was added H_2O (20 mL) and 2 N HCl till pH = 4–5 and then extracted with EtOAc (3 \times 20 mL). When necessary, the mixture was stirred until organic and aqueous layers become clear. The combined organic layers were washed with brine (2 \times 10 mL), dried over Na_2SO_4 , filtered, and evaporated to give a crude product that was purified by flash chromatography with the opportune eluent to yield the desired product 7a-e as brown-orange solids.

4.1.3. General procedure for the synthesis of compounds 8a-d

LiOH (10 mmol) was added to a solution of compounds 7a-e (1 mmol) in CH_3OH (10 mL) and H_2O (5 mL). The reaction mixture was refluxed till ester disappeared in TLC (~1h), acidified with HCl 2 N till pH 4–5 and extracted with AcOEt (3 \times 25 mL). The combined organic layers were washed with a NaHCO_3 saturated solution (2 \times 20 mL) and brine (2 \times 20 mL). The desired products 8a-e were obtained as brown–red solid after evaporation of the solvent.

4.1.4. General procedure for the synthesis of final compounds 9a-f, 10 and 10a-c

A solution of compounds 8a-8d (1 mmol), 4a-f (1 mmol) and DMAP

(0.2 mmol) in EtOH (10 mL) was refluxed overnight. The resulting suspension was filtered and the filtrate washed with cooled isopropanol to give the product as an orange-red solid that was purified by column chromatography using as eluent mixtures of solvents in the proportions indicated for each compound.

4.1.5. (4a) 3-(2-phenylethyl)-2-thioxo-1,3-thiazolidin-4-one

Oil, Yield 59%. ^1H NMR (CDCl_3) d: 2.92–2.96 (m, 2H), 3.92 (s, 2H), 4.18–4.22 (m, 2H), 7.25–7.31 (m, 5H). ^{13}C NMR (CDCl_3) d: 35.7, 35.3, 45.7, 126.8, 128.6, 128.9, 137.4, 173.5, 200.9. M.p.: 106–8 °C. R_f AcOEt/P 1/4: 0.51.

4.1.6. (4b) 3-(3-phenylpropyl)-2-thioxo-1,3-thiazolidin-4-one

Oil, Yield 55%. ^1H NMR (CDCl_3) d: 1.98–2.04 (m, 2H), 2.69 (t, 2H, J = 10.2), 3.74 (s, 2H), 4.01–4.06 (m, 2H), 7.18–7.27 (m, 5H) 126.4, 128.5, 128.7, 141.0, 174.1, 200.6. ^{13}C NMR (CDCl_3) d: R_f AcOEt/P 1/6: 0.46.

4.1.7. (4c) 3-(4'-methylphenylmethyl)-2-thioxo-1,3-thiazolidin-4-one

Solid, Yield 65%. ^1H NMR (CDCl_3) d: 2.33 (s, 3H), 3.98 (s, 2H), 5.16 (s, 2H), 7.13 (d, 2H, J = 8), 7.35 (d, 2H, J = 8). ^{13}C NMR (CDCl_3) d: 21.4, 35.5, 47.5, 129.2, 129.3, 131.8, 138.1, 173.9, 201.1. M.p.: 71–2 °C. R_f AcOEt/P 1/10: 0.25.

4.1.8. (4d) 3-(3',4'-dimethoxyphenylmethyl)-2-thioxo-1,3-thiazolidin-4-one

Oil, Yield 53%. ^1H NMR (DMSO) d: 3.71 (s, 3H), 3.72 (s, 3H), 4.33 (s, 2H), 5.00 (s, 2H), 6.80–6.86 (m, 1H), 6.87 (d, 1H, J = 8), 6.95 (d, 1H, J = 2). ^{13}C NMR (DMSO) d: 35.8, 46.6, 55.3, 55.4, 111.5, 112.0, 120.2, 127.3, 148.2, 148.4, 174.4, 203.1. R_f AcOEt/P 1/1: 0.523.

4.1.9. [(R)-4e] (R)-3-(2-phenylpropyl)-2-thioxo-1,3-thiazolidin-4-one

Oil, Yield 62%. ^1H NMR (CDCl_3) d: 1.31 (d, 3H, J = 7.2), 3.47–3.57 (m, 1H), 3.79 (d, 1H, J = 22), 3.88 (d, 1H, J = 22), 4.10–4.17 (m, 2H) 7.24–7.33 (m, 5H). ^{13}C NMR (CDCl_3) d: 17.6, 34.5, 36.1, 50.4, 126.4, 126.8, 127.9, 142.0, 173.1, 200.8. R_f AcOEt/P 1/6: 0.3.

4.1.10. [(S)-4f] (S)-3-(2-phenylpropyl)-2-thioxo-1,3-thiazolidin-4-one

Oil, Yield 56%. ^1H NMR (CDCl_3) d: 1.31 (d, 3H, J = 7.2), 3.47–3.57 (m, 1H), 3.79 (d, 1H, J = 22), 3.88 (d, 1H, J = 22), 4.10–4.17 (m, 2H) 7.24–7.33 (m, 5H). ^{13}C NMR (CDCl_3) d: 17.6, 34.5, 36.1, 50.4, 126.4, 126.8, 127.9, 142.0, 173.1, 200.8. R_f AcOEt/P 1/6: 0.3.

4.1.11. (7a) 4-(5-formylfuran-2-yl)-2-hydroxybenzoate methyl ester

Solid, Yield: 65% ^1H NMR (DMSO) d 3.90 (s, 3H), 7.45–7.47 (m, 3H),

7.67 (d, 1H, J = 3.6), 7.88 (d, 1H, J = 8), 9.65 (s, 1H), 10.6 (s, 1H). ¹³C NMR (CDMSO) d: 52.4, 111.1, 113.0, 113.8, 115.7, 124.7, 131.0, 134.4, 152.1, 156.1, 159.9, 168.3, 178.2. [M + H]⁺: 247.4. M.p.: 155–7 °C. R_f AcOEt/Pet 1/2: 0.43.

4.1.12. (7b) 4-(5-formylthiophen-2-yl)-2-hydroxybenzoate methyl ester

Solid, Yield: 70 %. ¹H NMR (CDCl₃) d: 3.98 (s, 3H), 7.17–7.19 (m, 1H), 7.29 (d, 1H, J = 2), 7.48 (d, 1H, J = 4), 7.75 (d, 1H, J = 4), 7.87–7.89 (m, 1H), 9.9 (s, 1H), 10.8 (s, 1H). ¹³C NMR (CDCl₃) d: 52.5, 112.8, 114.9, 117.2, 125.6, 130.8, 137.0, 139.7, 143.7, 152.1, 161.8, 170.0, 182.8. [M + H]⁺: 263.8. M.p.: 123–25 °C. R_f AcOEt/Pet 1/2: 0.5

4.1.13. (7c) 3-(5-formylfuran-2-yl)-4-hydroxybenzoate methyl ester

Colorless solid, Yield: 72%. ¹H NMR (CDCl₃) d 4.00 (s, 3H), 6.75 (d, 1H, J = 3.6), 7.06 (d, 1H, J = 8.8), 7.31 (d, 1H, J = 3.6), 7.88 (m, 1H), 8.32 (d, 1H, J = 2.4), 9.6 (s, 1H), 11.0 (s, 1H). ¹³C NMR (CDCl₃) d: 52.6, 106.7, 112.8, 118.5, 120.7, 127.1, 132.5, 151.8, 158.6, 162.6, 170.1, 176.9. [M + H]⁺: 247.3. M.p.: 130–2 °C. R_f AcOEt/Pet 1/2: 0.2.

4.1.14. (7d) 4-(5-formylfuran-2-yl)benzoate methyl ester

Colorless solid, Yield: 83%. ¹H NMR (CDCl₃) d: 3–96 (s, 3H), 6.97 (d, 1H, J = 3.6), 7.35 (d, 1H, J = 3.6), 7.89 (m, 1H), 8.12 (m, 1H), 9.70 (s, 1H). ¹³C NMR (CDCl₃) d: 52.4, 109.4, 123.1, 125.1, 130.3, 130.8, 132.9, 152.6, 158.0, 166.5, 177.6. [M + H]⁺: 231.3. M.p.: 143–5 °C. R_f AcOEt/Pet 1/2: 0.4.

4.1.15. (7e) 5-(3-hydroxyphenyl)furan-2-carboxaldehyde

Colorless solid, Yield: 90%. ¹H NMR (CDCl₃) d: 6.82 (d, 1H, J = 3.6), 6.92 (m, 1H), 7.26–7.38 (m, 4H), 9.61 (s, 1H). ¹³C NMR (CDCl₃) d: 108.1, 112.1, 117.1, 117.8, 130.2, 130.3, 151.8, 156.4, 159.5, 177.4. [M + H]⁺: 189.2. M.p.: 128–30 °C. R_f AcOEt/Pet 1/2: 0.3.

4.1.16. (8a) 4-(5-formylfuran-2-yl)-2-hydroxybenzoic acid

Solid, Yield: 95%. ¹H NMR (DMSO) d 7.39–7.45 (m, 3H), 7.65 (d, 1H, J = 3.6), 7.86–7.89 (m, 1H), 9.63 (s, 1H). ¹³C NMR (DMSO) d: 111.6, 112.9, 114.2, 116.1, 124.9, 131.0, 135.1, 152.7, 157.0, 162.0, 171.4, 178.8. [M + H]⁺: 243.2. M.p.: 230 °C (Dec.). R_f CH₂Cl₂/MeOH 4/1: 0.3.

4.1.17. (8b) 4-(5-formylthiophen-2-yl)-2-hydroxybenzoic acid

Solid, Yield: 89%. ¹H NMR (DMSO) d: 7.04–7.07 (m, 2H), 7.71 (d, 1H, J = 4), 7.77 (d, 1H, J = 8), 8.02 (d, 1H, J = 4), 9.89 (s, 1H), 11.5 (br. s., 1H). ¹³C NMR (DMSO) d: 113.4, 114.0, 117, 127, 131.3, 138.7, 138.8, 143.0, 150.3, 161.3, 171.2, 184.2. [M + H]⁺: 259.7. M.p.: 203–5 °C (Dec.). R_f CH₂Cl₂/MeOH 3/1: 0.35.

4.1.18. (8c) 3-(5-formylfuran-2-yl)-4-hydroxybenzoic acid

Solid, Yield: 91%. ¹H NMR (DMSO) d: 6.94 (d, 1H, J = 12), 7.12 (d, 1H, J = 4), 7.55–7.60 (m, 2H), 7.86 (m, 1H), 8.20 (d, 1H, J = 2.4), 9.5 (s, 1H). ¹³C NMR (DMSO) d: 107.3, 116.7, 118.4, 119.1, 127.3, 131.5, 151.6, 159.0, 164.0, 171.4, 177.6, 206.9. [M + H]⁺: 243.5. M.p.: 213–15 °C. R_f CH₂Cl₂/MeOH 4/1: 0.3.

4.1.19. (8d) 4-(5-formylfuran-2-yl)benzoic acid

Solid, Yield: 96%. ¹H NMR (CDCl₃) d 7.43 (d, 1H, J = 3.6), 7.67 (d, 1H, J = 3.6), 7.66–8.04 (m, 4H), 9.64 (s, 1H), 13.18 (br s, 1H). ¹³C NMR (CDCl₃) d: 111.0, 125.4, 130.6, 131.7, 132.8, 152.6, 157.3, 167.1, 178.7, 206.9. [M + H]⁺: 217.8. M.p.: 130–2 °C. R_f CH₂Cl₂/MeOH 4/1: 0.4.

4.1.20. (9a) 2-Hydroxy-4-{5-[4-oxo-3-phenethyl-2-thioxothiazolidin-5-ylidenemethyl]furan-2-yl}benzoic acid

Orange solid, Yield 78%. ¹H NMR (CDCl₃) d 2.95–2.99 (m, 2H), 4.11–4.14 (m, 2H), 7.17–7.38 (m, 9H), 7.61 (s, 1H), 7.82 (d, 1H, J = 8.2). ¹³C NMR (CDCl₃) d: 32.6, 45.7, 111.7, 112.1, 113.8, 118.7, 119.1, 123.5, 127.1, 129.0, 129.1, 131.5, 132.6, 138.1, 149.8, 158.1, 163.2, 166.7, 171.8, 194.1. [M + H]⁺: 452.4. M.p.: 118–20 °C. R_f CH₂Cl₂/

MeOH 8/1: 0.33

4.1.21. (9b) 2-Hydroxy-4-{5-[4-oxo-3-phenylpropyl-2-thioxothiazolidin-5-ylidenemethyl]furan-2-yl}benzoic acid

Orange solid, Yield 81%. ¹H NMR (DMSO) d 1.94–1.98 (m, 2H), 2.65 (t, 2H, J = 7.6), 4.05 (t, 2H, J = 7.6), 6.90 (d, 1H, J = 8.4), 7.14–7.36 (m, 7H), 7.65 (s, 1H), 7.83 (d, 1H, J = 8.2), 8.21 (d, 1H, J = 8.4). ¹³C NMR (DMSO) d: 27.7, 32.2, 43.9, 106.7, 110.6, 111.4, 112.5, 118.1, 118.5, 122.9, 125.8, 128.1, 128.2, 130.8, 131.3, 140.7, 149.1, 158.0, 163.2, 166.5, 171.0, 193.8. [M + H]⁺: 466.6. M.p.: 188–190 °C. R_f CH₂Cl₂/MeOH 10/1: 0.3.

4.1.22. (9c) 2-Hydroxy-4-{5-[4-oxo-3-(4-methylphenylmethyl)-2-thioxothiazolidin-5-ylidenemethyl]furan-2-yl}benzoic acid

Orange solid, Yield 82%. ¹H NMR (DMSO) d 2.24, (s, 3H), 5.18 (s, 2H), 7.12 (d, 2H, J = 8), 7.19–7.23 (m, 4H), 7.36 (s, 2H), 7.69 (s, 1H), 7.85 (d, 1H, J = 8). ¹³C NMR (DMSO) d: 20.6, 46.7, 111.4, 111.6, 113.4, 118.5, 123.2, 127.6, 129.0, 131.0, 131.9, 136.8, 149.4, 157.6, 162.5, 166.5, 171.2, 193.7. [M + H]⁺: 452.3. M.p.: 267 °C (Dec.). R_f CH₂Cl₂/MeOH 8/1: 0.28.

4.1.23. (9d) 2-Hydroxy-4-{5-[4-oxo-3-(3',4'-dimethoxyphenyl)methyl]-2-thioxothiazolidin-5-ylidenemethyl]furan-2-yl}benzoic acid

Orange solid, Yield 75%. ¹H NMR (DMSO) d 3.00 (s, 3H), 3.69 (s, 3H), 4.10–4.12 (m, 2H), 5.16 (s, 1H), 6.70 (d, 1H, J = 7.6), 6.84–6.87 (m, 1H), 7.10–7.13 (m, 1H), 7.28–7.34 (m, 1H), 7.66–7.68 (m, 2H), 7.78 (d, 1H, J = 8), 8.12 (d, 1H, J = 6.8). ¹³C NMR (DMSO) d: 55.8, 67.8, 107.2, 111.2, 112.1, 112.4, 112.9, 119.1, 120.6, 123.8, 129.1, 132.0, 132.1, 146.0, 148.8, 149.0, 167.4, 171.3, 194.4. [M + H]⁺: 498.0. M.p.: 226–28 °C. R_f CH₂Cl₂/MeOH/Tol 17/2/1: 0.22.

4.1.24. (9e) (R)-2-Hydroxy-4-{5-[4-oxo-3-(2-phenylpropyl)methyl]-2-thioxothiazolidin-5-ylidenemethyl]furan-2-yl}benzoic acid

Orange solid, Yield 91%. ¹H NMR (DMSO) d 1.23 (d, 1H, J = 7.2), 3.40–3.45 (m, 1H), 4.14 (d, 2H, J = 7.6), 7.13–7.31 (m, 9H), 7.58 (s, 1H), 7.82 (d, 1H, J = 8.4). ¹³C NMR (DMSO) d: 18.7, 37.0, 51.0, 111.3, 112.0, 113.2, 118.6, 118.8, 121.0, 123.6, 127.2, 127.6, 128.9, 131.4, 131.9, 143.2, 149.6, 158.6, 163.7, 167.0, 171.7, 194.5. [M + H]⁺: 466.8. M.p.: 227–30 °C. R_f CH₂Cl₂/MeOH 6/1: 0.25.

4.1.25. (9f) (S)-2-Hydroxy-4-{5-[4-oxo-3-(2-phenylpropyl)methyl]-2-thioxothiazolidin-5-ylidenemethyl]furan-2-yl}benzoic acid

Orange solid, Yield 88%. ¹H NMR (DMSO) d 1.23 (d, 1H, J = 7.2), 3.40–3.45 (m, 1H), 4.14 (d, 2H, J = 7.6), 7.13–7.31 (m, 9H), 7.58 (s, 1H), 7.82 (d, 1H, J = 8.4). ¹³C NMR (DMSO) d: 18.7, 37.0, 51.0, 111.3, 112.0, 113.2, 118.6, 118.8, 121.0, 123.6, 127.2, 127.6, 128.9, 131.4, 131.9, 143.2, 149.6, 158.6, 163.7, 167.0, 171.7, 194.5. [M + H]⁺: 466.8. M.p.: 227–30 °C. R_f CH₂Cl₂/MeOH 6/1: 0.25.

4.1.26. (10a) 2-Hydroxy-4-{5-[4-oxo-3-phenethyl-2-thioxothiazolidin-5-ylidenemethyl]thiophen-2-yl}benzoic acid

Orange solid, Yield 65%. ¹H NMR (DMSO) d 2.92–2.96 (m, 2H), 4.19–4.23 (m, 2H), 7.04–7.08 (m, 2H), 7.20–7.31 (m, 5H), 7.71–7.75 (m, 3H), 8.03 (s, 1H). ¹³C NMR (DMSO) d: 32.6, 46.0, 11.4, 113.8, 119.8, 126.6, 127.1, 129.0, 129.1, 131.4, 136.0, 137.0, 138.3, 138.1, 152.3, 163.8, 166.8, 171.4, 192.4. [M + H]⁺: 468.7. M.p.: 190–192 °C (dec.). R_f CH₂Cl₂/MeOH 4/1: 0.32.

4.1.27. (10b) 2-Hydroxy-5-{5-[4-oxo-3-phenethyl-2-thioxothiazolidin-5-ylidenemethyl]furan-2-yl}benzoic acid

Orange solid, Yield 79%. ¹H NMR (DMSO) d 3.93–3.97 (m, 2H), 4.02–4.24 (m, 2H), 6.81 (d, 1H, J = 8.4), 7.05 (d, 1H, J = 4), 7.58 (s, 1H), 7.67–7.70 (m, 1H), 8.18–8.20 (m, 1H). ¹³C NMR (DMSO) d: 32.0, 45.1, 106.8, 107.3, 115.6, 116.0, 117.5, 118.4, 120.1, 124.4, 126.5, 126.7, 128.4, 128.6, 137.6, 140.0, 147.8, 156.5, 160.1, 166.2, 170.3, 193.4. [M + H]⁺: 452.2. M.p.: 230–2 (dec.) °C. R_f CH₂Cl₂/MeOH 8/1:

0.2.

4.1.28. (10c) 4-{5-[4-oxo-3-phenethyl-2-thioxothiazolidin-5-ylidene]methyl}furan-2-yl}benzoic acid

Yellow-orange solid, Yield 65%. ¹H NMR (DMSO) δ 2.94–2.98 (m, 2H), 4.21–4.25 (m, 2H), 7.64 (s, 1H), 7.23–7.46 (m, 7H), 7.92–7.94 (m, 2H), 8.07–8.09 (m, 2H), 13.19 (br s, 1H). ¹³C NMR (DMSO) δ: 32.0, 45.1, 112.0, 118.0, 119.2, 122.9, 124.2, 126.5, 128.4, 128.6, 130.2, 131.9, 137.5, 149.9, 159.7, 166.1, 166.7, 193.5. [M + H]⁺: 436.5. M.p.: 270 °C (dec.). R_f CH₂Cl₂/MeOH 2/1: 0.7.

4.1.29. (10d) 5-[[5-(4-hydroxyphenyl)-2-furanyl]methylene]-2-thioxo-3-phenethyl-4-thiazolidinone

Orange solid, Yield 66%. ¹H NMR (DMSO) δ 3.00–3.04 (m, 2H), 4.33–4.37 (m, 2H), 5.20 (br s, 1H), 6.84 (d, 1H, J = 3.6), 6.85–6.92 (m, 1H), 6.93 (d, 1H, J = 3.6), 7.26–7.36 (m, 8H), 7.44 (s, 1H). ¹³C NMR (DMSO) δ: 33.0, 45.7, 109.3, 111.3, 116.5, 117.4, 117.9, 119.8, 121.4, 126.7, 128.6, 129.0, 130.3, 130.5, 137.6, 149.4, 156.1, 158.5, 167.3, 194.2. [M + H]⁺: 408.4. M.p.: 194–6 °C. AcOEt/Pet 1/3: 0.2.

4.2. Biological evaluation

4.2.1. Cell culture and treatment

The human T cell line J-Jhan and Sup-T1 were cultured in RPMI-1640 (Gibco BRL, Invitrogen Corporation, Carlsbad, CA, USA) with 10% FCS supplemented with 100 U/ml each of penicillin and streptomycin and maintained at 37 °C in humidified atmosphere of 5% CO₂. J-Jhan and Sup-T1 have been selected since are known to represent cell lines of choice which allow HHV-6A and HHV-6B replication, respectively. Both cell lines were seeded into 24-well plate at the cell density of 0.5 × 10⁶ /ml and treated with synthesized HHV-6 inhibitors at concentration of 1, 10 and 100 μM, for 24 h.

4.2.2. Cell viability analysis by MTT assay

Cell viability was determined by MTT test (3-(4,5-dimethylthiazol-2-yl)-2,5-diphenyl tetrazolium bromide) colorimetric assay (Roche Diagnostics Corporation, Indianapolis, IN, USA) following the manufacturer's instructions as previously described [39]. Cell viability was determined by treating human lymphocyte cell lines with different concentration of HHV-6 inhibitors, 10-fold serially diluted from 0 to 100 μM, for 24 h. Afterwards, MTT assay was performed, and absorbance was read at 570 nm.

4.2.3. HHV-6 infection

J-Jhan cells were infected with a HHV-6A (U1102 strain) cell-free inoculum and Sup T1 cells were infected with a HHV-6B (Z29 strain) cell-free inoculum as previously described [24] at a 100:1 multiplicity of infection (MOI, virus genomes:cell ratio). Virus adsorption was carried out in a 1% FBS medium for 3 h, then the excess virus was eliminated by centrifugation and washing in PBS, and cells were finally seeded at 0.5 × 10⁶ cells/ml in complete medium with high FBS concentration. Control cells were treated with the same procedure but uninfected. At 1, 2, 3, and 7 days post-infection (d.p.i.) cell samples were collected by centrifugation at 1000 × g for 5 min at 4 °C. Cell pellets were then washed in PBS, and analyzed for viral DNA presence by Real Time PCR.

4.2.4. Analysis of HHV-6 replication inhibition

The inhibitory effect on HHV-6 replication was determined by analyzing viral DNA from J-Jhan HHV-6A infected cells and Sup T1 HHV-6B infected cells. Total DNA was extracted from cell pellets collected from both infected or uninfected cell lines by a commercial kit (Exgene Cell SV kit, GeneAll, Seoul, Korea), and quantified by spectrophotometric reading at 260 and 280 nm. 100 ng of total extracted DNA was analyzed by specific qPCR targeting U42 gene of HHV-6 in duplicate, as previously described [40]. Briefly, a standard curve ranging from 10⁷ to 10 copies of U42 gene was used to quantify the infection by

interpolation and normalized to the human RNaseP housekeeping gene (TaqMan™ Copy Number Reference Assay, human, RNase P, ThermoFisher Scientific, USA) used as a control.

4.2.5. Statistical analysis

Results obtained ad mean ± SD from 3 independent experiments were evaluated for statistical significance by Student T test using GraphPad Prism9 software.

Declaration of Competing Interest

The authors declare that they have no known competing financial interests or personal relationships that could have appeared to influence the work reported in this paper.

Acknowledgement

We thank Dr. Erika Marzola for HPLC analysis, Dr. Alberto Casolari for the acquisition of proton and carbon NMR spectra and Dr Ercolina Bianchini for the elemental analysis. We thank Iva Pivanti and Dr Mercedes Fernandez for technical support and Alessandro Sofia for statistical analysis. This study was supported by HHV-6 foundation grant and FISM – Fondazione Italiana Sclerosi Multipla – cod. 2019/R-Single/004 and financed or co-financed with the '5 per mille' public funding.

Appendix A. Supplementary material

Supplementary data to this article can be found online at <https://doi.org/10.1016/j.bioorg.2021.105518>.

References

- [1] E. De Clercq, A. Brancale, A.V. Hodge, H.J. Field, Antiviral chemistry and chemotherapy's current antiviral agents Fact File 2006 (1st edition), *Antivir. Chem. Chemother.* 17 (2006) 113–166, <https://doi.org/10.1177/095632020601700302>.
- [2] E. De Clercq, Three decades of antiviral drugs, *Nat. Rev. Drug Discov.* 6 (2007) 941, <https://doi.org/10.1038/nrd2485>.
- [3] D. Pillay, The priorities for antiviral drug resistance surveillance and research, *J. Antimicrob. Chemother.* 60 (Suppl 1) (2007) i57–i58, <https://doi.org/10.1093/jac/dkm159>.
- [4] G.P. Pattanaik, H. Chakraborty, Entry Inhibitors: Efficient Means to Block Viral Infection, *J. Membr. Biol.* 253 (5) (2020) 425–444, <https://doi.org/10.1007/s00232-020-00136-z>.
- [5] F. Vigant, N.C. Santos, B. Lee, Broad-spectrum antivirals against viral fusion, *Nat. Rev. Microbiol.* 13 (7) (2015) 426–437, <https://doi.org/10.1038/nrmicro3475>.
- [6] T.J. Henrich, D.R. Kuritzkes, HIV-1 entry inhibitors: recent development and clinical use, *Curr. Opin. Virol.* 3 (1) (2013) 51–57, <https://doi.org/10.1016/j.coviro.2012.12.002>.
- [7] S. Pollock, N.B. Nichita, A. Böhmer, C. Radulescu, R.A. Dwek, N. Zitzmann, Polyunsaturated liposomes are antiviral against hepatitis B and C viruses and HIV by decreasing cholesterol levels in infected cells, *PNAS* 107 (40) (2010) 17176–17181, <https://doi.org/10.1073/pnas.1009445107>.
- [8] F. Vigant, A. Hollmann, J. Lee, N.C. Santos, M.E. Jung, B. Lee, The rigid amphipathic fusion inhibitor dUY11 acts through photosensitization of viruses, *J. Virol.* 88 (3) (2014) 1849–1853, <https://doi.org/10.1128/JVI.02907-13>.
- [9] H. Badani, R.F. Garry, W.C. Wimley, Peptide entry inhibitors of enveloped viruses: the importance of interfacial hydrophobicity, *BBA* 1838 (9) (2014) 2180–2197, <https://doi.org/10.1016/j.bbame.2014.04.015>.
- [10] H. Jansen, P. Hamill, R.E.W. Hancock, Peptide antimicrobial agents, *Clin. Microbiol. Rev.* 19 (3) (2006) 491–511, <https://doi.org/10.1128/CMR.00056-05>.
- [11] G. Cheng, A. Montero, P. Gastaminza, C. Whitten-Bauer, S.F. Wieland, M. Isogawa, B. Fredericksen, S. Selvarajah, P.A. Gallay, M.R. Ghadiri, F.V. Chisari, A virocidal amphipathic α-helical peptide that inhibits hepatitis C virus infection in vitro, *PNAS* 105 (2008) 3088–3093, <https://doi.org/10.1073/pnas.0712380105>.
- [12] C.J. Sample, K.E. Hudak, B.E. Barefoot, M.D. Koci, M.S. Wanyonyi, S. Abraham, H. F. Staats, E.A. Ramsburg, A mastoparan-derived peptide has broad-spectrum antiviral activity against enveloped viruses, *Peptides* 48 (2013) 96–105, <https://doi.org/10.1016/j.peptides.2013.07.014>.
- [13] S.M. Mousavi, M. Zarei, S.A. Hashemi, A. Babapoor, A.M. Amani, A conceptual review of rhodanine: current applications of antiviral drugs, anticancer and antimicrobial activities, *Artif. Cells Nanomed. Biotechnol.* 47 (1) (2019) 1132–1148, <https://doi.org/10.1080/21691401.2019.1573824>.
- [14] N.A. Meanwell, Hepatitis C virus entry: an intriguing challenge for drug discovery, *Curr. Opin. Invest. Drugs* 7 (2006) 727–732.

- [15] J.P. Yang, D. Zhou, F. Wong-Staal, Screening of small-molecule compounds as inhibitors of HCV entry, *Methods Mol. Biol.* 510 (2009) 295–304, https://doi.org/10.1007/978-1-59745-394-3_22.
- [16] M.J. Brooks, J.J. Sasadeusz, G.A. Tannock, Antiviral chemotherapeutic agents against respiratory viruses: where are we now and what's in the pipeline? *Curr. Opin. Pulm. Med.* 10 (3) (2004) 197–203, <https://doi.org/10.1097/00063198-200405000-00009>.
- [17] Y.S. Boriskin, I.A. Leneva, E.I. Pecheur, S.J. Polyak, Arbidol: a broad-spectrum antiviral compound that blocks viral fusion, *Curr. Med. Chem.* 15 (2008) 997–1005, <https://doi.org/10.2174/092986708784049658>.
- [18] C.C. Colpitts, A.V. Ustinov, R.F. Epan, R.M. Epan, V.A. Korshun, L.M. Schang, 5-(Perylen-3-yl)ethynyl-arabino-uridine (aUY11), an arabino-based rigid amphipathic fusion inhibitor, targets virion envelope lipids to inhibit fusion of influenza virus, hepatitis C virus, and other enveloped viruses, *J. Virol.* 87 (7) (2013) 3640–3654, <https://doi.org/10.1128/JVI.02882-12>. Epub 2013 Jan 2.
- [19] Y.S. Boriskin, E.-I. Pécheur, S.J. Polyak, Arbidol: a broad-spectrum antiviral that inhibits acute and chronic HCV infection, *Virology* 378 (1) (2006), <https://doi.org/10.1186/1743-422X-3-56>.
- [20] R. Rizzo, D. Di Luca, Human herpesvirus 6A and 6B and NK cells, *Acta Microbiol. Immunol. Hung.* 65 (2) (2018) 119–125, <https://doi.org/10.1556/030.65.2018.010>. Epub 2018 Mar 7.
- [21] E. Caselli, M. D'Accolti, F. Caccuri, I. Soffritti, V. Gentili, D. Bortolotti, A. Rotola, E. Cassai, S. Fiorentini, A. Zani, A. Caruso, R. Rizzo, D. Di Luca, The U94 Gene of Human Herpesvirus 6: A Narrative Review of Its Role and Potential Functions, *Cells* 9 (12) (2020) 2608, <https://doi.org/10.3390/cells9122608>.
- [22] R. Rizzo, V. Gentili, I. Casetta, E. Caselli, R. De Gennaro, E. Granieri, E. Cassai, D. Di Luca, A. Rotola, Altered natural killer cells' response to herpes virus infection in multiple sclerosis involves KIR2DL2 expression, *J. Neuroimmunol.* 251 (1–2) (2012) 55–64, <https://doi.org/10.1016/j.jneuroim.2012.07.004>. Epub 2012 Aug 5.
- [23] R. Rizzo, D. Bortolotti, V. Gentili, A. Rotola, S. Bolzani, E. Caselli, M.R. Tola, D. Di Luca, T. Fülöp, KIR2DS2/KIR2DL2/HLA-C1 Haplotype Is Associated with Alzheimer's Disease: Implication for the Role of Herpesvirus Infections, *J. Alzheimers Dis.* 67 (4) (2019) 1379–1389, <https://doi.org/10.3233/JAD-180777>.
- [24] D. Bortolotti, V. Gentili, A. Rotola, E. Caselli, R. Rizzo, HHV-6A infection induces amyloid-beta expression and activation of microglial cells, *Alzheimers Res. Ther.* 11 (1) (2019), <https://doi.org/10.1186/s13195-019-0552-6>.
- [25] R. Marci, V. Gentili, D. Bortolotti, G. Lo Monte, E. Caselli, S. Bolzani, A. Rotola, D. Di Luca, R. Rizzo, Presence of HHV-6A in Endometrial Epithelial Cells from Women with Primary Unexplained Infertility, *PLoS One* 11 (7) (2016) e0158304, <https://doi.org/10.1371/journal.pone.0158304>, eCollection 2016.
- [26] D. Bortolotti, V. Gentili, A. Rotola, R. Cultrera, R. Marci, D. Di Luca, R. Rizzo, HHV-6A infection of endometrial epithelial cells affects immune profile and trophoblast invasion, *Am. J. Reprod. Immunol.* 82 (4) (2019) e13174, <https://doi.org/10.1111/aji.13174>. Epub 2019 Aug 17.
- [27] S.H. James, N.B. Price, C.B. Hartline, E.R. Lanier, M.N. Prichard, Selection and recombinant phenotyping of a novel CMX001 and cidofovir resistance mutation in human cytomegalovirus, *Antimicrob. Agents Chemother.* 57 (7) (2013) 3321–3325, <https://doi.org/10.1128/AAC.00062-13>. Epub 2013 May 6.
- [28] E. De Clercq, L. Naesens, In search of effective anti-HHV-6 agents, *Rev. J. Clin. Virol.* 37 (Suppl 1) (2006) S82–S86, [https://doi.org/10.1016/S1386-6532\(06\)70017-8](https://doi.org/10.1016/S1386-6532(06)70017-8).
- [29] P. Bonnafous, L. Naesens, S. Petrella, A. Gautheret-Dejean, D. Boutolleau, W. Sougakoff, H. Agut, Different mutations in the HHV-6 DNA polymerase gene accounting for resistance to foscarnet, *Antivir. Ther.* 12 (6) (2007) 877–888.
- [30] Y. Isegawa, C. Matsumoto, K. Nishinaka, K. Nakano, T. Tanaka, N. Sugimoto, A. Ohshima, PCR with quenching probes enables the rapid detection and identification of ganciclovir-resistance-causing U69 gene mutations in human herpesvirus 6, *Mol. Cell. Probes* 24 (4) (2010) 167–177, <https://doi.org/10.1016/j.mcp.2010.01.002>. Epub 2010 Jan 18.
- [31] N. Maeda, A. Furukawa, K. Kakita, M. Anada, S. Hashimoto, S. Matsunaga, K. Kuroki, T. Ose, A. Kato, J. Arii, Y. Kawaguchi, H. Arase, K. Maenaka, Rapid Screening by Cell-Based Fusion Assay for Identifying Novel Antivirals of Glycoprotein B-Mediated Herpes Simplex Virus Type 1 Infection, *Biol. Pharm. Bull.* 39 (11) (2016) 1897–1902, <https://doi.org/10.1248/bpb.16-00533>.
- [32] G.A. Wudiri, S.M. Schneider, A.V. Nicola, Herpes Simplex Virus 1 Envelope Cholesterol Facilitates Membrane Fusion, *Front. Microbiol.* 8 (2017) 2383, <https://doi.org/10.3389/fmicb.2017.02383>.
- [33] H. Tang, A. Kawabata, M. Takemoto, K. Yamanishi, Y. Mori, Human herpesvirus-6 infection induces the reorganization of membrane microdomains in target cells, which are required for virus entry, *Virology* 378 (2) (2008) 265–271, <https://doi.org/10.1016/j.virol.2008.05.028>.
- [34] V. Cagno, C. Tintori, A. Cibra, R. Cavalli, M. Tiberi, L. Botta, A. Brai, G. Poli, C. Tapparel, D. Lembo, M. Botta, Novel broad spectrum virucidal molecules against enveloped viruses, *PLoS One* 13 (12) (2018) e0208333, <https://doi.org/10.1371/journal.pone.0208333>, eCollection 2018.
- [35] R. Borenstein, B.A. Hanson, R.M. Markosyan, E.S. Gallo, S.D. Narasipura, M. Bhutta, O. Shechter, N.S. Lurain, F.S. Cohen, L. Al-Harhi, D.A. Nicholson, Ginkgolic acid inhibits fusion of enveloped viruses, *Sci. Rep.* 10 (1) (2020) 4746, <https://doi.org/10.1038/s41598-020-61700-0>.
- [36] S. Speerstra, A.A. Chistov, G.V. Proskurin, A.V. Aralov, E.A. Ulashchik, P. P. Streshnev, V.V. Shmanai, V.A. Korshun, L.M. Schang, Antivirals acting on viral envelopes via biophysical mechanism of actions, *Antiviral Res.* 149 (2018) 164–173, <https://doi.org/10.1016/j.antiviral.2017.11.018>.
- [37] D. Kaminsky, D. Khylyuk, O. Vasylenko, R. Lesyk, An efficient method for the transformation of 5-ylideneRhodanines into 2,3,5-trisubstituted-4-thiazolidinones, *Tetrahedron Lett.* 53 (5) (2012) 557–559, <https://doi.org/10.1016/j.tetlet.2011.11.095>.
- [38] A.R. Katritzky, S.R. Tala, H. Lu, A.V. Vakulenko, Q.-Y. Chen, J. Sivapakiam, K. Pandya, S. Jiang, A.K. Debnath, Design, Synthesis, and Structure–Activity Relationship of a Novel Series of 2-Aryl 5-(4-Oxo-3-phenethyl-2-thioxothiazolidinylidene)methyl)furans as HIV-1 Entry Inhibitors, *J. Med. Chem.* 52 (23) (2009) 7631–7639, <https://doi.org/10.1021/jm900450n>.
- [39] D. Bortolotti, J. LeMaout, C. Trapella, D. Di Luca, E.D. Carosella, R. Rizzo, Pseudomonas aeruginosa Quorum Sensing Molecule N-(3-Oxododecanoyl)-l-Homoserine-Lactone Induces HLA-G Expression in Human Immune Cells, *Infect. Immun.* 83 (2015) 3918–3925, <https://doi.org/10.1128/IAI.00803-15>.
- [40] R. Rizzo, I. Soffritti, M. D'Accolti, D. Bortolotti, D. Di Luca, E. Caselli, HHV-6A/6B infection of NK cells modulates the expression of miRNAs and transcription factors potentially associated to impaired NK activity, *Front. Microbiol.* 8 (2017) 2143, <https://doi.org/10.3389/fmicb.2017.02143>.



Inhibitory KIR2DL2 receptor and HHV-8 in classic or endemic Kaposi sarcoma

Daria Bortolotti¹ · Monica Corazza² · Antonella Rotola¹ · Dario Bencivelli² · Giovanna Schiuma¹ · Elisabetta Danese² · Sabrina Rizzo¹ · Silvia Beltrami¹ · Roberta Rizzo¹ · Alessandro Borghi²

Received: 23 December 2021 / Accepted: 21 January 2022 / Published online: 15 February 2022
© The Author(s) 2022

Abstract

KIR2DL2, an inhibitory Killer cell Immunoglobulin-like Receptor (KIR), has been shown to predispose to the development of several herpesvirus-associated diseases by inhibiting the efficiency of Natural Killer (NK) cells against virus-infected cells. The aim of this observational study was to assess the prevalence of KIR2DL2 and Human Herpes Virus 8 (HHV8) in patients affected with classical and endemic Kaposi sarcoma (KS), as well as in controls. Blood samples collected from 17 Caucasian, HIV-negative, immunocompetent patients affected with classical KS (c-KS), 12 African, HIV-negative patients with endemic KS (e-KS), 83 healthy subjects and 26 psoriatic patients were processed for genotyping by PCR for two KIR alleles, such as KIR2DL2 and KIR2DL3 and analyzed for HHV-8 presence. The totality of both c-KS and e-KS patients presented HHV-8 infection, whereas HHV8 was found in 26.9% of psoriatic subjects and 19.3% of healthy subjects. KIR2DL2 was found in the 76.5% of c-KS subjects, while the receptor was found in 41.7% of the e-KS group, 34.6% of psoriatic patients and 43.4% of healthy controls ($p < 0.0001$). A significantly higher prevalence of KIR2DL2 in c-KS patients than in all the other subjects was also confirmed comparing age-matched groups. Based on these results, the inhibitory KIR2DL2 genotype appears to be a possible cofactor which increases the risk of developing c-KS in HHV8-positive, immunocompetent subjects, while it seems less relevant in e-KS pathogenesis.

Keywords Kaposi's Sarcoma · KIR2DL2 · HHV-8 · Natural Killer (NK) cells

Introduction

Human Herpes Virus 8 (HHV8) was originally isolated in 1994 [13]. The infection is generally acquired during childhood mainly through saliva exchange, while blood, breast milk and semen are considered rarer sources of infection [1, 20]. Compared to the other members of the Herpes virus family, which are found almost universally in the adult

population, HHV8 seroprevalence is lower and with different geographical distribution ranges. According to its prevalence, three geographical areas may be distinguished, namely (1) high endemic areas, with > 25% seroprevalence, which include many regions in Africa, (2) mid-endemic areas, with 10–25% seroprevalence (e.g., in the Mediterranean Basin) and (3) non-endemic areas, where seroprevalence is lower than 10% [35].

HHV8 infection has been associated with several malignancies, mainly of hematologic origin, including Multicentric Castleman's Disease (MCD) and Primary Effusion Lymphomas (PEL), and post-transplant and germinotropic LPDs (GLPDs) rare lympho-proliferative disorders occurring prevalently in immunosuppressed subjects [13]. Moreover, a possible involvement of HHV8 in eruptive cherry angiomas (CAs) has recently been suggested [3].

The role of HHV-8 is crucial in Kaposi sarcoma (KS) development [23]. Among the KS lesions, HHV8 is predominantly found in the so-called tumor spindle cells, due to their elongated shape, which are probably endothelial

Daria Bortolotti and Monica Corazza These authors contributed equally to this study and share first authorship.

Roberta Rizzo, Alessandro Borghi These authors contributed equally to this study and share co-senior authorship.

✉ Dario Bencivelli
dario.bencivelli@unife.it

¹ Department of Chemical, Pharmaceutical and Agricultural Sciences, University of Ferrara, Ferrara, Italy

² Section of Dermatology and Infectious Diseases, Department of Medical Sciences, University of Ferrara, Ferrara, Italy

cells transformed by the virus [14]. HHV8 infection reprograms, in a very polymorphic and not yet fully known way, the host's blood endothelial cells leading to both spindle morphology acquisition and induction of a strong neo-angiogenic activity, which give rise to the typical KS lesions [3].

Nevertheless, HHV8 infection is not sufficient to provoke such progression, since only a small rate of HHV8-infected individuals develops KS [3]. Additional cofactors are necessary for the development of KS and the other HHV8-associated diseases.

HHV8 infection has a biphasic cycle comprising latent and lytic phases [36]. Latency is characterized by a state of quiescence in which the viral genome persists as a circular episome attached to the host chromatin, with limited expression of viral transcripts and down-regulated surface markers. On the contrary, the lytic phase of HHV-8 infection involves the expression of numerous genes and the production of viral particles [6, 28]. Like other herpes-viruses, in most cases HHV8 infection is controlled throughout life by immune surveillance. In this case, the virus remains latent within cells and clinically silent. On the other hand, since it has developed a variety of mechanisms to evade the host immune system [15, 30], HHV8 may lead to the proliferation of infected cells, up to cancer development [19]. The kinetics of virus-associated disease progression depends on the balance of power between host immune defenses and the virus [26]. HHV8 is considered an oncogenic virus mainly in a favorable context, such as immunosuppression. In keeping with this, the risk for KS is greatly increased with concomitant human immunodeficiency virus (HIV) infection and also substantially increased in the case of chronic use of corticosteroids and immunosuppressive treatments [21].

However, it is not currently understood in detail which components of the human immune response are essential for this pathophysiological process [2, 19].

Natural Killer (NK) cells are cytotoxic leucocytes involved both in innate immune defense against viral infections and tumor cells and in the regulation of adaptive immune responses [7, 8, 12]. NK cells are key effectors of the immune system due to their human leukocyte antigen (HLA)-restricted cytotoxic activity [7]. Killer cell immunoglobulin-like receptors (KIR), which are highly polymorphic members of the immunoglobulin superfamily, regulate human NK cell development and functions. A number of KIRs located in different haplotypes have been identified, with either inhibitory or activating functions on NK cells. Thus, KIR gene diversity concurs in determining NK cells' efficiency against transformed or virus-infected cells and, accordingly, the susceptibility of subjects to symptomatic herpesvirus infection [18, 25]. Specific inhibitory KIRs present on NK cells have been shown to impair the anti-herpetic immune response, predisposing to susceptibility to herpesvirus infection. In particular, subjects expressing

KIR2DL2 on NK cells fail to control herpes simplex virus 1 (HSV-1), Epstein-Barr virus (EBV), Human Herpes Virus-6 (HHV-6) and HHV8 infections [9, 10, 31, 33]. This specific KIR allotype appears to predispose to the development of herpesvirus-associated diseases as well, such as type 2 diabetes, Alzheimer disease, Multiple Sclerosis and eruptive cherry angiomas [4, 9, 10, 31, 33].

On the base of these data, a potential role of KIR genotype in KS pathogenesis as well might be supposed, even though the actual scenario is not clearly defined. Indeed, the combination of the activating haplotype KIR3DS1 and HLA-B Bw4-80I has been found to increase the risk of classic KS in a cohort of HHV8-positive and HIV-negative patients, [21] but not in HIV-positive subject [29]. In a cohort of Italian classic KS patients, the KIR2DS1 with its HLA-C2 ligand as well as the activating haplotypes KIR3DS1 and KIR2DS1 were statistically more frequent among classic KS cases than controls [22].

These previous findings support the hypothesis that KIR gene polymorphisms can, to some extent, account for the complex interactions between genetic background, HHV8 infection and the immune system, as cofactors in KS development.

Starting from this assumption, the main aims of the present study were to assess the prevalence of the inhibitory KIR2DL2 receptor in HIV-negative patients affected with classical KS and to compare it to that of African patients with endemic KS, psoriatic patients and healthy controls. This assessment could provide some insights into inhibitory KIR genotype involvement in the physiopathological process of KS.

Materials and methods

Study populations

In the present mono-centric, observational study we included all adult (≥ 18 yrs.), Caucasian, HIV-negative subjects affected with histologically proven classic KS consecutively referring to our outpatient Dermatology clinics over a 6-month period. Patients were excluded in the presence of the following: (1) lack of histological confirmation, (2) presence of ethnic, clinical, laboratory or history criteria suggesting varieties of KS other than the classical one, (3) chronic immunosuppressive treatments for any health condition, (4) refusal to undergo blood sampling or inclusion in the study.

The following three different control populations were recruited: (1) healthy donor subjects, (2) psoriatic patients and (3) HIV-negative African patients affected with endemic KS. Both healthy donors and psoriatic patients, whose blood samples were stored in the archive of the laboratory of the

University of Ferrara, were contacted for their agreement to use part of their blood samples for the specific purposes of this study. We established a priori the inclusion of healthy controls and psoriatic patients in order to have a gender distribution comparable to that of the enrolled KS patients. No age-based selections were made. Only the blood samples belonging to subjects who gave their consent were used. Healthy controls and psoriatic patients did not have concurrent documented infectious diseases. No further exclusion criteria were applied. Endemic KS skin lesions from Ugandan patients, stored in the archive of the laboratory of the University of Ferrara since their use in a previous study [24], were the biological source for this control population.

This was a spontaneous survey, with no funding from external sources. The principles outlined in the Helsinki Declaration of 1975, as revised in 1983, have been followed for all the patients included. The study was approved by the University-Hospital of Ferrara institutional review board (project identification code 162/2020/Oss/AOUFe). Both patients and controls, with the sole exception of patients with endemic KS, provided their written informed consent.

KIR2DL2 genotypization and HHV-8 search

Blood samples collected from the four study populations were processed for genomic DNA extraction using the QIAamp DNA blood Mini Kit (QIAGEN, Hilden, Germany) following the manufacturer’s protocol [32].

KIR alleles (KIR2DL2 and KIR2DL3) were genotyped by PCR by specific primers pairs [17] reported in Table 1 and visualized on 1% agarose gel, as previously reported [34].

HHV-8 genome was detected by PCR, specific for ORF50 gene, followed by nested PCR (Table 1), as previously described [10].

Statistical analysis

Results were evaluated for statistical significance by Graph-Pad Prism v.9 software. Frequency difference was analyzed by χ^2 -test, while difference between mean values was determined by Student-t test. *P*-values <0.01 were considered statistically significant.

Results

Study populations

All the 17 eligible patients affected with classical KS screened for entry into the study were included. Based on the inclusion and exclusion criteria, biological samples from 83 healthy subjects, 26 psoriatic patients and 12 African patients affected with endemic KS were included. Demographic characteristics of the four study populations are shown in Table 2.

HHV8 seroprevalence

HIV-negative, Caucasian classic KS (c-KS) and African endemic KS (e-KS) patients were characterized for the

Table 1 KIR2DL2/KIR2DL3 and HHV-8 ORF50 specific primer sets and amplified fragments length

Gene	Primers	Sequence	Fragment length (bp)
KIR2DL2	K2DL2f	CCA TGA TGG GGT CTC CAA A	1800 bp
	K2DL2r	GCC CTG CAG AGA ACC TAC A	
KIR2DL3	K2DL3f	CCT TCA TCG CTG GTG CTG	798 bp
	K2DL3r	CAG GAG ACA ACT TTG GAT CA	
ORF50	8–50-1	TTG GTG CGC TAT GTG GTC TG	420 bp
	8–50-2	GGA AGG TAG ACC GGT TGG AA	
ORF50 nested	8–50-3	TAT TCG GAT CCT CAC GGA GA	227 bp
	8–50-4	CGG TAT CGT ACG TGT TGT AG	

Table 2 Demographic characteristics of the study populations

Demographic features	c-KS (n = 17)	e-KS (n = 12)	Psoriatic patients (n = 26)	Healthy controls (n = 83)
Sex, n. (%)				
Males	16 (94.1%)	10 (83%)	24 (92.3%)	78 (93.9%)
Females	1 (5.9%)	2 (17%)	6 (7.7%)	5 (6.1%)
Age, mean ± SD [range]	77.3 ± 11 [47–95]	32 ± 9.8 [22–48]	53.7 ± 7.4 [28–81]	55.1 ± 10.6 [26–96]

c-KS, HIV-negative classic Kaposi Sarcoma patients; e-KS, HIV-negative endemic Kaposi Sarcoma patients; SD, standard deviation

presence of HHV-8 infection and compared to psoriatic and healthy groups. As shown in Fig. 1a, we found that the total of both c-KS and e-KS patients presented HHV-8 infection. On the contrary HHV8 was found in 5 (26.9%) and in 16 (19.3%) of the psoriatic and healthy subjects, respectively ($p < 0.0001$, χ^2 -test).

KIR2DL2 presence was associated with HHV-8 infection in classic KS, but not in endemic KS patients

The same groups were also compared considering KIR2DL2 frequency (Fig. 1b). We considered as KIR2DL2-positive subjects (KIR2+) those who presented either KIR2DL2 homozygous or KIR2DL2/KIR2DL3 heterozygous genotypes. KIR2DL3 homozygous subjects were considered as KIR2DL2-negative (KIR2-). We found the highest KIR2DL2 frequency in the c-KS group (13/17, 76.5%), while the presence of this receptor was significantly lower among the other three groups analyzed (5 out of 12 e-KS patients, i.e., 41.7, 9/26, 34.6%, psoriatic patients, and 36/83, 43.4%, healthy controls; $p < 0.0001$, χ^2 -test; these rates were all comparable to each other).

Given the significant difference between c-KS and e-KS groups' mean age (77.3 vs 32 years, respectively; $p < 0.0001$, Student-t test), in order to verify the reliability of these results regardless of age, we analyzed KIR2DL2 frequency dividing both the psoriatic and healthy groups accordingly with the mean ages of c-KS and e-KS patients (Table 3). As

shown in Fig. 2, the age-matched comparison confirmed the previous results, reporting a significantly higher frequency of KIR2DL2 in the c-KS group (Fig. 2a, $p < 0.0001$, χ^2 -test), but not in the e-KS group (Fig. 2b), compared to controls.

Discussion

In the present study we assessed the prevalence of a specific inhibitory KIR receptor, namely KIR2DL2, among KS patients in order to evaluate its possible role on HHV8 seroprevalence and KS development. In particular, we were interested in assessing its potential involvement in two varieties of KS, i.e., classic and endemic KS, in comparison with controls. We chose to investigate KIR2DL2, among others, since this receptor has been found, even by us, to facilitate herpes-virus infections, including those from HHV-8 [4, 9, 10, 31, 33]. The presence of KIR2DL2 appears to predispose to development of herpesvirus associated diseases as well. It has been supposed that its inhibitory function on NK cells may create favorable immunological conditions for HHV8 to carry out its functions, including angioproliferative and oncogenic activity, in infected individuals. Based on these observations, the present study aimed at analyzing the possible interplay among KIR2DL2, HHV8 infection and classic and endemic KS. In this exploratory phase of the study, we did not include patients affected with epidemic KS, since, in our opinion, in this specific subset the immunodeficiency induced by HIV could diminish, or overwhelm or hide, the

Fig. 1 Assessment of HHV-8 **a** and KIR2DL2 **b** frequencies in HIV-negative classic KS c-KS, endemic KS e-KS, psoriatic and control (cntr) groups. *** $p < 0.0001$

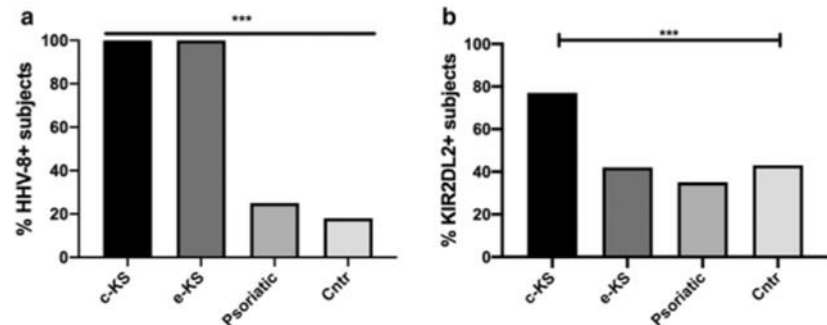
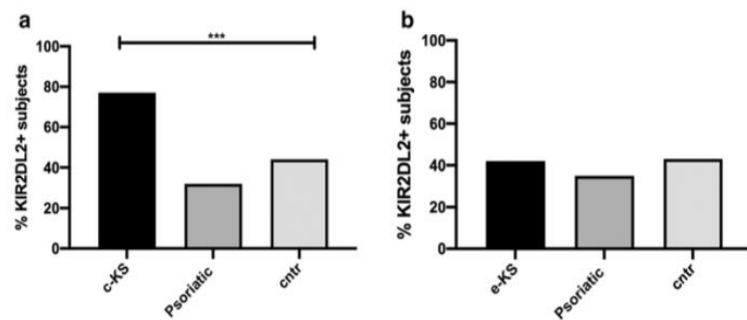


Table 3 Demographical characteristics of classic (c-KS) and endemic Kaposi sarcoma (e-KS) age-matched psoriatic and control groups

Demographic features	c-KS age-matched		e-KS age-matched	
	Psoriatic patients (n = 16)	Healthy controls (n = 50)	Psoriatic patients (n = 10)	Healthy controls (n = 33)
Sex, n. (%)				
males	15 (93.8%)	48 (96%)	9 (90%)	30 (91%)
females	1 (6.2%)	2 (4%)	1 (10%)	3 (9%)
Age, mean \pm SD [range]	69.6 \pm 8.4 [54–81]	73.6 \pm 10.6 [54–96]	37.8 \pm 6.4 [28–48]	36.5 \pm 10.5 [26–49]

c-KS, HIV-negative classic Kaposi Sarcoma patients; e-KS, HIV-negative endemic Kaposi Sarcoma patients; SD, standard deviation

Fig. 2 Evaluation of KIR2DL2 frequencies in HIV-negative classic KS (c-KS) **a**, endemic KS (e-KS) **b** compared with aged-matched psoriatic and control (cntr) groups. *** $p < 0.0001$



relevance of KIR arrangement in the physiopathological cascade of KS.

Our first finding was that the totality of subjects were positive for HHV8 in both c-KS and e-KS cohort, as expected. This confirms the well-recognized etiologic role of HHV8 in KS. On the other hand, HHV8 seroprevalence among psoriatic and healthy subjects was fully in line with its prevalence in the general population resident in a mid-endemic area, like the province of Ferrara, northern Italy [15, 33].

With reference to the main aim of this study, we found that KIR2DL2 prevalence was significantly higher in c-KS patients than in all the other study groups, including e-KS patients (Fig. 1). A higher prevalence of KIR2DL2 in c-KS patients was confirmed also comparing age-matched groups (Fig. 2). This finding suggests that KIR2DL2 is more relevant for the development of KS in Mediterranean subjects than for HHV8 infection in general. In fact, e-KS patients did not show a different prevalence of this KIR genotype when compared with controls, despite a significantly higher HHV8 seroprevalence. This is in line with previous results, which showed that in KS patients HHV8 seroprevalence had no significant association with any individual KIR gene or HLA allele [21, 22]. On the other hand, more than 76% of the c-KS patients were positive for KIR2DL2. Thus it can be supposed that in Caucasian, HIV-negative, nonimmunocompromised, HHV8-positive subjects, this KIR genotype may be a determinant for the risk of developing KS. In the aforesaid subjects, without further known predisposing factors, the following setting can be hypothesized. A particular KIR genotype, such as KIR2DL2, by binding HLA class I molecules, inhibits NK cell-mediated destruction of virus-infected and transformed tumor cells. This probably leads to an uncontrolled HHV8 activity, which may predispose to malignant transformation of infected cells and tumor progression, which underlie KS. On the other hand, in e-KS subjects, further cofactors seem to have a major relevance in KS pathogenesis than KIR2DL2. However, possible cofactors determining the high prevalence of e-KS in endemic African areas remain unknown [16].

Our results may appear in contrast with previous findings [21, 22]. In fact, two previous studies found a prevalent presence of activating KIR/HLA receptor/ligand combinations in c-KS. The authors of those studies hypothesized that the inflammation triggered by activated NK cells could be a key component of the oncogenesis, contributing to the proliferation and survival of tumor cells. It cannot be excluded that the different geographical origin of the c-KS patients included in these studies may, at least in part, account for this difference.

The study results should be viewed in light of some limitations. First of all, the small sample size of the study might have reduced the statistical power of these findings. Larger studies including a higher number of patients are needed to confirm our results. Furthermore, the HLA counterpart of the KIR2DL2 receptor was not typed. As some of us have shown in previous studies conducted under different clinical settings, this point would be important in order to know the proportion of patients with a possible activation of KIR-HLA complex [9]. The c-KS patients belong to a mid-endemic area for HHV8 seroprevalence. Thus, they may not be fully representative for patients from different geographical sites and a possible selection bias cannot be excluded. The e-KS skin samples originated from a historical population of HIV-negative Ugandan subjects of whom some relevant information had not been collected at the time, such as co-morbidities or further co-infections.

In conclusion, our study assessed for the first time the prevalence of the inhibitory KIR allotype KIR2DL2 in HIV-negative patients affected with classical KS, in comparison with African subjects affected with e-KS and controls. Based on our results, KIR2DL2 did not seem to influence the HHV8 seroprevalence in KS subjects, while it was significantly more present in c-KS patients than in the other groups. A likely impairment of NK-mediated immunity, due to the inhibitory KIR2DL2 genotype, may be a cofactor that increases the risk of developing c-KS in HHV8-positive subjects. This specific genotype may be one of the predisposing factors that concur on the development of KS in a part of subjects positive for HHV8, in the absence of further

recognized risk factors. Our results also highlighted the different relevance of KIR2DL2 on the outcome of HHV8 infection in HIV-negative Caucasian and African endemic KS populations.

Author contributions Study concept and design: AB, DB, MC, RR. Acquisition of data: DB, DB, AR, ED, GS, SR, SB. Analysis and interpretation of data: RR, DB, MC, AB, AR. Drafting of the manuscript: AB, DB, DB, RR, MC. Critical revision of the manuscript for important intellectual content: MC, RR, DB, AB, AR. Statistical analysis: DB, RR.

Funding None.

Declarations

Conflict of interest None of the authors have any declaration of interest to report.

Ethical approval The principles outlined in the Helsinki Declaration of 1975, as revised in 1983, have been followed for all the patients included. The study was approved by the University-Hospital of Ferrara institutional review board (project identification code 162/2020/Oss/AOUFe).

Consent to participate Both patients and controls, with the sole exception of patients with endemic KS, provided their written informed consent.

Open Access This article is licensed under a Creative Commons Attribution 4.0 International License, which permits use, sharing, adaptation, distribution and reproduction in any medium or format, as long as you give appropriate credit to the original author(s) and the source, provide a link to the Creative Commons licence, and indicate if changes were made. The images or other third party material in this article are included in the article's Creative Commons licence, unless indicated otherwise in a credit line to the material. If material is not included in the article's Creative Commons licence and your intended use is not permitted by statutory regulation or exceeds the permitted use, you will need to obtain permission directly from the copyright holder. To view a copy of this licence, visit <http://creativecommons.org/licenses/by/4.0/>.

References

- Becerril S, Corchado-Cobos R, García-Sancha N, et al. Viruses and skin cancer. *Int J Mol Sci*. 2021;22(10):5399. <https://doi.org/10.3390/ijms22105399>.
- Blumenthal MJ, Cornejo Castro EM, Whitby D, et al. Evidence for altered host genetic factors in KSHV infection and KSHV-related disease development. *Rev Med Virol*. 2021;31(2): e2160. <https://doi.org/10.1002/rmv.2160>.
- Borghì A, Benedetti S, Corazza M, et al. Detection of human herpesvirus 8 sequences in cutaneous cherry angiomas. *Arch Dermatol Res*. 2013;305(7):659–64. <https://doi.org/10.1007/s00403-013-1346-5>.
- Borghì A, D'Accolti M, Rizzo R, et al. High prevalence of specific KIR types in patients with HHV-8 positive cutaneous vascular lesions: a possible predisposing factor? *Arch Dermatol Res*. 2016;308(5):373–7. <https://doi.org/10.1007/s00403-016-1643-x>.
- Broussard G, Damania B. KSHV: immune modulation and immunotherapy. *Front Immunol*. 2020;10:3084. <https://doi.org/10.3389/fimmu.2019.03084>.
- Cai Q, Verma SC, Lu J, Robertson ES. Molecular biology of Kaposi's sarcoma-associated herpesvirus and related oncogenesis. In: Maramorosch K, Shatkin A, Murphy F, editors. *Advances in virus research*. Amsterdam: Elsevier; 2010. p. 87–142.
- Caligiuri MA. Human natural killer cells. *Blood*. 2008;112(3):461–9. <https://doi.org/10.1182/blood-2007-09-077438>.
- Carroll MC, Prodeus AP. Linkages of innate and adaptive immunity. *Curr Opin Immunol*. 1998;10(1):36–40. [https://doi.org/10.1016/S0952-7915\(98\)80028-9](https://doi.org/10.1016/S0952-7915(98)80028-9).
- Caselli E, Rizzo R, Ingianni A, et al. High prevalence of HHV8 infection and specific killer cell immunoglobulin-like receptors allotypes in Sardinian patients with type 2 diabetes mellitus: HHV8 and KIR prevalence in Type 2 diabetes. *J Med Virol*. 2014;86(10):1745–51. <https://doi.org/10.1002/jmv.23771>.
- Caselli E, Soffritti I, D'Accolti M, et al. HHV-6A infection and systemic sclerosis: clues of a possible association. *Microorganisms*. 2019;8(1):39. <https://doi.org/10.3390/microorganisms8010039>.
- Cattani P, Cerimele F, Porta D, et al. Age-specific seroprevalence of Human Herpesvirus 8 in Mediterranean regions. *Clin Microbiol Infect*. 2003;9(4):274–9. <https://doi.org/10.1046/j.1469-0691.2003.00490.x>.
- Cerwenka A, Lanier LL. Natural killer cells, viruses and cancer. *Nat Rev Immunol*. 2001;1(1):41–9. <https://doi.org/10.1038/35095564>.
- Chang Y, Cesarman E, Pessin M, et al. Identification of herpesvirus-like DNA sequences in AIDS-associated Kaposi's sarcoma. *Science*. 1994;266(5192):1865–9. <https://doi.org/10.1126/science.7997879>.
- Cousins E, Nicholas J. Molecular biology of human herpesvirus 8: novel functions and virus-host interactions implicated in viral pathogenesis and replication. In: Jeang K, Chang MH, editors. *Viruses and human cancer*. Berlin: Springer; 2014. p. 227–68. https://doi.org/10.1007/978-3-642-38965-8_13.
- Dal Maso L, Polesel J, Ascoli V, et al. Classic Kaposi's sarcoma in Italy, 1985–1998. *Br J Cancer*. 2005;92(1):188–9. <https://doi.org/10.1038/sj.bjc.6602265>.
- Dediccoat M, Newton R. Review of the distribution of Kaposi's sarcoma-associated herpesvirus (KSHV) in Africa in relation to the incidence of Kaposi's sarcoma. *Br J Cancer*. 2003;88(1):1–3. <https://doi.org/10.1038/sj.bjc.6600745>.
- Du Z, Gjertson DW, Reed EF, et al. Receptor-ligand analyses define minimal killer cell Ig-like receptor (KIR) in humans. *Immunogenetics*. 2006;59(1):1–15. <https://doi.org/10.1007/s00251-006-0168-4>.
- Estefanía E, Gómez-Lozano N, Portero F, et al. Influence of KIR gene diversity on the course of HSV-1 infection: resistance to the disease is associated with the absence of KIR2DL2 and KIR2DS2. *Tissue Antigens*. 2007;70(1):34–41. <https://doi.org/10.1111/j.1399-0039.2007.00844.x>.
- Fang Q, Liu Z, Zhang T. Human leukocyte antigen polymorphisms and Kaposi's sarcoma-associated herpesvirus infection outcomes: a call for deeper exploration. *J Med Virol*. 2019;91(4):541–8. <https://doi.org/10.1002/jmv.25342>.
- Ganem D. KSHV and the pathogenesis of Kaposi sarcoma: listening to human biology and medicine. *J Clin Invest*. 2010;120(4):939–49. <https://doi.org/10.1172/JCI40567>.
- Goedert JJ, Martin MP, Vitale F, et al. Risk of classic Kaposi sarcoma with combinations of killer immunoglobulin-like receptor and human leukocyte antigen loci: a population-based

- case-control study. *J Infect Dis.* 2016;213(3):432–8. <https://doi.org/10.1093/infdis/jiv413>.
22. Guerini FR, Mancuso R, Agostini S, et al. Activating KIR/HLA complexes in classic Kaposi's Sarcoma. *Infect Agent Cancer.* 2012;7(1):9. <https://doi.org/10.1186/1750-9378-7-9>.
 23. Karen M, Chang Y. Kaposi's Sarcoma. *N Engl J Med.* 2000;342(14):1027.
 24. Monini P, Rotola A, de Lellis L, et al. Latent BK virus infection and Kaposi's sarcoma pathogenesis. *Human Cancer.* 1996;66(6):717–22. [https://doi.org/10.1002/\(SICI\)1097-0215\(199606\)66:6%3c717::AID-IJC1%3e3.0.CO;2-2](https://doi.org/10.1002/(SICI)1097-0215(199606)66:6%3c717::AID-IJC1%3e3.0.CO;2-2).
 25. Moraru M, Cisneros E, Gómez-Lozano N, et al. Host genetic factors in susceptibility to herpes simplex type 1 virus infection: contribution of polymorphic genes at the interface of innate and adaptive immunity. *J Immunol.* 2012;188(9):4412–20. <https://doi.org/10.4049/jimmunol.1103434>.
 26. Münz C. Probing reconstituted human immune systems in mice with oncogenic γ -Herpesvirus infections. *Front Immunol.* 2020;11: 581419. <https://doi.org/10.3389/fimmu.2020.581419>.
 27. Oksenhendler E, Boutboul D, Galicier L. Kaposi's Sarcoma-associated Herpesvirus/Human Herpesvirus 8 associated lymphoproliferative disorders. *Blood.* 2019;133(11):1186–90. <https://doi.org/10.1182/blood-2018-11-852442>.
 28. Pardamean CI, Wu T-T. Inhibition of host gene expression by KSHV: sabotaging mRNA stability and nuclear export. *Front Cell Infect Microbiol.* 2021;11: 648055. <https://doi.org/10.3389/fcimb.2021.648055>.
 29. Qi Y, Martin MP, Gao X, et al. KIR/HLA pleiotropism: protection against both HIV and opportunistic infections. *PLoS Pathog.* 2006;2(8): e79. <https://doi.org/10.1371/journal.ppat.0020079>.
 30. Radu O, Pantanowitz L. Kaposi Sarcoma. *Arch Pathol Lab Med.* 2013;137(2):289–94. <https://doi.org/10.5858/arpa.2012-0101-RS>.
 31. Rizzo R, Bortolotti D, Fainardi E, et al. KIR2DL2 inhibitory pathway enhances Th17 cytokine secretion by NK cells in response to herpesvirus infection in multiple sclerosis patients. *J Neuroimmunol.* 2016;294:1–5. <https://doi.org/10.1016/j.jneuroim.2016.03.007>.
 32. Rizzo R, Bortolotti D, Gentili V, et al. KIR2DS2/KIR2DL2/HLA-C1 haplotype is associated with Alzheimer's disease: implication for the role of herpesvirus infections. *J Alzheimers Dis.* 2019;67(4):1379–89. <https://doi.org/10.3233/JAD-180777>.
 33. Rizzo R, Gentili V, Casetta I, et al. Altered natural killer cells response to herpes virus infection in multiple sclerosis involves KIR2DL2 expression. *J Neuroimmunol.* 2012;254(1–2):187. <https://doi.org/10.1016/j.jneuroim.2012.07.004>.
 34. Rizzo R, Gentili V, Rotola A, et al. Implication of HLA-C and KIR alleles in human papillomavirus infection and associated cervical lesions. *Viral Immunol.* 2014;27(9):468–70. <https://doi.org/10.1089/vim.2014.0017>.
 35. Tornesello ML, Biryahwaho B, Downing R, et al. Human herpesvirus type 8 variants circulating in Europe, Africa and North America in classic, endemic and epidemic Kaposi's sarcoma lesions during pre-AIDS and AIDS era. *Virology.* 2010;398(2):280–9. <https://doi.org/10.1016/j.virol.2009.12.005>.
 36. Ye F, Lei X, Gao S-J. Mechanisms of Kaposi's sarcoma-associated herpesvirus latency and reactivation. *Adv Virol.* 2011. <https://doi.org/10.1155/2011/193860>.

Publisher's Note Springer Nature remains neutral with regard to jurisdictional claims in published maps and institutional affiliations.

In addition, I focused during my PhD course on bacteria and correlated diseases. The topic of study are both Gram-positive (*S. aureus*, *Streptococcus spp.*) and Gram-negative (*P. aeruginosa*, *E. coli*, *Klebsiella*) species to identify new antimicrobial treatments, due to the emergent bacterial resistance to common antibiotics typical of biofilm formation [400]. Among these, we give peculiar attention in ophthalmology field highlighting the negative impact of ocular infections [401]. Given the necessity of alternative ophthalmic antiseptics, we evaluated the effectiveness of ozonated oil in liposome eyedrops in the reduction of bacteria activities, and we observed significant anti-microbicidal and anti-biofilm activity in human corneal cells (*Paper 6*, paper attached).



Communication

Ozonated Oil in Liposome Eyedrops Reduces the Formation of Biofilm, Selection of Antibiotic-Resistant Bacteria, and Adhesion of Bacteria to Human Corneal Cells

Valentina Gentili ^{1,†}, Giovanni Strazzabosco ^{1,†}, Nicolò Salgari ², Alessandra Mancini ³, Sabrina Rizzo ¹, Silvia Beltrami ¹, Giovanna Schiuma ¹, Fabio Casciano ^{2,4}, Andrea Alogna ¹, Daniela Passarella ⁵, Sergio Davinelli ⁵, Giovanni Scapagnini ⁵, Alessandro Medoro ^{5,*} and Roberta Rizzo ^{1,4}

- ¹ Department of Chemical, Pharmaceutical and Agricultural Science, University of Ferrara, 44121 Ferrara, Italy; valentina.gentili@unife.it (V.G.); giovanni.strazzabosco@unife.it (G.S.); sabrina.rizzo@unife.it (S.R.); silvia.beltrami@unife.it (S.B.); giovanna.schiuma@unife.it (G.S.); andrea.alogna@unife.it (A.A.); roberta.rizzo@unife.it (R.R.)
- ² Department of Translational Medicine, University of Ferrara, 44121 Ferrara, Italy; slgncl@unife.it (N.S.); fabio.casciano@unife.it (F.C.)
- ³ Department of Ophthalmology, University of “Magna Graecia”, 88100 Catanzaro, Italy; alessandra.mancini@unicz.it
- ⁴ Laboratory for Advanced Therapeutic Technologies (LTTA), University of Ferrara, 44121 Ferrara, Italy
- ⁵ Department of Medicine and Health Sciences “V. Tiberio”, University of Molise, 86100 Campobasso, Italy; daniela.passarella@unimol.it (D.P.); sergio.davinelli@unimol.it (S.D.); giovanni.scapagnini@unimol.it (G.S.)
- * Correspondence: alessandro.medoro@unimol.it
- † These authors contributed equally to this work.



Citation: Gentili, V.; Strazzabosco, G.; Salgari, N.; Mancini, A.; Rizzo, S.; Beltrami, S.; Schiuma, G.; Casciano, F.; Alogna, A.; Passarella, D.; et al. Ozonated Oil in Liposome Eyedrops Reduces the Formation of Biofilm, Selection of Antibiotic-Resistant Bacteria, and Adhesion of Bacteria to Human Corneal Cells. *Int. J. Mol. Sci.* **2023**, *24*, 14078. <https://doi.org/10.3390/ijms241814078>

Academic Editor: Lamberto Re

Received: 1 August 2023

Revised: 9 September 2023

Accepted: 12 September 2023

Published: 14 September 2023



Copyright: © 2023 by the authors. Licensee MDPI, Basel, Switzerland. This article is an open access article distributed under the terms and conditions of the Creative Commons Attribution (CC BY) license (<https://creativecommons.org/licenses/by/4.0/>).

Abstract: The recent attention to the risk of potential permanent eye damage triggered by ocular infections has been leading to a deeper investigation of the current antimicrobials. An antimicrobial agent used in ophthalmology should possess the following characteristics: a broad antimicrobial spectrum, prompt action even in the presence of organic matter, and nontoxicity. The objective of this study is to compare the antimicrobial efficacy of widely used ophthalmic antiseptics containing povidone-iodine, chlorhexidine, and liposomes containing ozonated sunflower oil. We determined the minimum inhibitory concentration (MIC) on various microbial strains: *Staphylococcus aureus* (ATCC 6538), methicillin-resistant *Staphylococcus aureus* (ATCC 33591), *Staphylococcus epidermidis* (ATCC 12228), *Pseudomonas aeruginosa* (ATCC 9027), and *Escherichia coli* (ATCC 873). Furthermore, we assessed its efficacy in controlling antibiotic resistance, biofilm formation, and bacterial adhesion. All three antiseptic ophthalmic preparations showed significant anti-microbicidal and anti-biofilm activity, with the liposomes containing ozonated sunflower oil with the highest ability to control antibiotic resistance and bacteria adhesion to human corneal cells.

Keywords: antiseptic; ophthalmology; antimicrobial agents; multidrug-resistant organisms; povidone-iodine; chlorhexidine; liposomal ozonated oil; toxicity; biofilm

1. Introduction

Intraocular procedures carry the risk of severe ocular complications including infectious endophthalmitis, which can have devastating consequences. This condition can primarily arise from bacterial infections. However, few observations have been made regarding ocular pathogens' epidemiology and susceptibility patterns, even though antimicrobial resistance (AMR) has been recognized as a significant healthcare threat worldwide [1]. Multidrug-resistant organisms (MDRO), or microorganisms that are resistant to several different drug classes, are on the rise [2]. MDRO, like *Staphylococcus aureus* and *Pseudomonas aeruginosa*, are growing in importance in the field of ophthalmology [3]. Also, methicillin-resistant *S. aureus* (MRSA) ocular infections are increasing, according to several

surveillance studies [4]. To provide coverage for the more prevalent Gram-positive (*S. aureus*, *Streptococcus* spp.) and Gram-negative (*P. aeruginosa*, *E. coli*, *Klebsiella*) species, empiric antibiotics are frequently recommended for these conditions prior to culture findings [5,6]. Also frequently prescribed are broad-spectrum antibiotics such as fluoroquinolones, gentamicin, tobramycin, polymixin B, and trimethoprim [7]. It is alarming to see that these antibiotics are becoming less effective against *S. aureus* and *P. aeruginosa* [8], suggesting alternative strategies.

For these reasons, the importance of using antiseptics in the perioperative phases has become increasingly crucial. Due to their proven efficacy, povidone-iodine (PVP-I) and chlorhexidine are widely used antiseptic agents in ophthalmic surgery [9,10]. Specifically, PVP-I is an iodophor, which is a water-soluble complex of iodine and a solubilizing polymer carrier called polyvinylpyrrolidone. Iodine quickly enters microorganisms and oxidizes essential macromolecules (proteins, nucleotides, and fatty acids), ultimately causing microbial death. Additionally, PVP-I exhibits a wide range of antibacterial action against fungi, protozoa, and Gram-positive and Gram-negative bacteria, including strains that are resistant to antibiotics and antiseptics [11,12]. It has also shown antimicrobial effects on enveloped and nonenveloped viruses, as well as certain bacterial spores when exposed for an extended period of time [11,13,14]. Furthermore, PVP-I has demonstrated effectiveness against in vitro and ex vivo mature bacterial and fungal biofilms [15,16]. On the other hand, chlorhexidine, a synthetic biguanide with cationic surfactant properties, exhibits a wide-ranging antibacterial effect as well as partial antifungal properties. By interfering with microbial cell membranes and inducing coagulation of cytoplasmic proteins, chlorhexidine maintains residual activity for several hours [17].

Although there is strong evidence for their efficacy and acceptable tolerability and safety in clinical practice, some adverse reactions associated with their use have been reported even at low concentrations, such as corneal epithelial toxicity, postoperative eye pain, persistent corneal epithelial defects, and an increased risk of keratitis [18–20]. Naor et al. demonstrated significant endothelial damage in bovine eyes when PVP-I concentrations exceeded 0.05% [21]. Moreover, although iodine allergies are rare, direct toxicity can occur, especially with repeated exposures, resulting in a high incidence of endophthalmitis [9,10]. Conversely, several other antiseptics (e.g., alcohol-containing disinfectants) are unsuitable for ophthalmic use due to their toxic effects on the corneal epithelium [16].

Given the increasing number of intravitreal injections performed each year and the importance of ocular antisepsis in intraocular procedures, alternative approaches and the development of new formulations are necessary. An ideal disinfectant should have a wide antimicrobial spectrum, rapid action even in the presence of organic matter, and be non-toxic [22]. In this context, liposomal ozonated oil represents a possible novel ocular formulation for preventing and treating ocular infections. Ozonated oils are obtained by a chemical process of ozonation of unsaturated fatty acids in vegetable oils, producing ozonated derivatives, the ozonides, which are more stable with fatty acids than ozone itself, with a relatively long lifetime [23,24]. These derivatives are highly reactive oxidants with documented bactericidal, antiviral, and antifungal activities, together with anti-inflammatory and tissue-repair properties, which can be applied to several pathologies such as skin diseases, pathologies of the vaginal mucosa, oral ulcers, periodontics, and eye infections [23,25–29]. Mechanistically, liposomes adhere to the surface of the pathogen, inducing its breaking through ozonolysis and releasing ozonides. These ozonides infiltrate the pathogen and undergo hydrolysis, generating oxygenated compounds like lipid peroxides and reactive oxygen species (ROS). These oxygenated compounds target proteins and lipids, as well as other macromolecules such as enzymes and DNA/RNA, inducing modifications in the pathogen's structure and destroying it. Consequently, liposomal ozonated oil exhibits dual antibacterial actions: direct oxidation of the pathogen's surface and alteration of structure and functions of pathogen macromolecules [23,25].

To further preserve the properties of ozonides and improve their tolerance by the ocular surface, a formulation based on liposomal sunflower ozonated oil and other ingre-

dients has recently been designed for ophthalmic applications [30]. Indeed, sunflower oil embedded in liposomes may favor the stabilization of the lipid phase of the tear film reducing the evaporation of the aqueous phase and guaranteeing immediate relief [25]. Moreover, the ozonated oil liposomes are often included in a solution of hypromellose methylcellulose (HPMC), which is extremely biocompatible with the delicate ocular surface tissue [31,32].

To this end, this study evaluated the antimicrobial activity and the ability to reduce the selection of antibiotic-resistant bacteria and biofilm formation of a liposomal ozonated oil preparation (Ozodrop, FB Vision, San Benedetto del Tronto, Italy) confronting it with widely used ophthalmic antiseptic preparations containing PVP-I (Iodim, Medivis, Tremestieri Etneo, Italy) and chlorhexidine (Dropsept, Sooft, Montegiorgio, Italy) as active principles.

2. Results

2.1. Antimicrobial Activity

The antimicrobial activity of Ozodrop (FB Vision, San Benedetto del Tronto, Italy), an eye drop preparation containing ozonated sunflower oil liposomes, was evaluated. Ozodrop also contains HPMC, boric acid, sodium tetraborate (which has mild antiseptic and astringent characteristics), disodium edetate sodium (used to remove calcium deposits from eyes), polihexanide (PHMB), and deionized water. The efficacy of this preparation was compared with two gold standard actives: PVP-I with hyaluronic acid, and chlorhexidine with tocopherol polyethylene glycol 1000 succinate, both in eye drop preparations.

The minimal inhibitory concentration (MIC) was determined using the EUCAST microdilution method [33], with a two-fold dilution ranging from 50 to 0.3%. After 24 h of treatment, absorbance was measured and compared to untreated bacteria. Table 1 shows the MIC values obtained for each ophthalmic antiseptic preparation on corresponding bacterial strains. The three preparations were effective on Gram-positive bacteria, in a range from 12.5 to 50%. Only the ozonated sunflower oil liposome preparation showed a quantifiable MIC against Gram-negative bacteria. PVP-I and chlorhexidine preparations had the highest MIC concentration used (100%) against Gram-negative bacteria.

Table 1. MIC values (% v/v) of the ophthalmic antiseptic preparations on the different microbial strains after 24 h of incubation.

Bacterial Strain	Ozonated Oil Ophthalmic Solution	PVP-I Ophthalmic Solution	Chlorhexidine Ophthalmic Solution
<i>E. coli</i> (ATCC 8739)	25%	100%	100%
<i>P. aeruginosa</i> (ATCC 9027)	50%	100%	100%
<i>S. aureus</i> (ATCC 6538)	12.5%	50%	12.5%
MRSA (ATCC 33591)	25%	50%	25%
<i>S. epidermidis</i> (ATCC 12228)	12.5%	50%	12.5%

2.2. Antibiofilm Activity

Since both *P. aeruginosa* (ATCC 9027) and *S. aureus* (ATCC 6538) can produce biofilm, the ability of the three ophthalmic preparations to prevent the formation and destruction of the preexisting biofilm was evaluated. Biofilm production is a complex, multi-step process that is often associated with various bacterial species [34]. Adhesion to surfaces is a critical step in biofilm development, leading to several metabolic changes in cells such as the expression of extracellular polymeric substances (EPS) and different microbial surface components that recognize adhesive matrix molecules, including fibronectin and fibrinogen [35]. Once formed, biofilms become resistant to immune system responses and antibiotic treatment, making them nearly impossible to remove [35].

This study examined the impact of three different ophthalmic solutions on eradicating pre-formed biofilm and inhibiting biofilm formation. The percentage of biomass removal was assessed using the ophthalmic solutions at their MIC values. The results showed that

the ophthalmic solutions varied in their effectiveness for biofilm eradication, ranging from acceptable to excellent (Figure 1). Notably, the ophthalmic solution containing ozonated sunflower oil demonstrated superior biofilm eradication compared to the other two ophthalmic solutions in all three bacteria tested ($p < 0.0001$; Fisher's exact test) (Figure 1a–c). Furthermore, all three ophthalmic solutions proved effective in reducing biofilm formation, with the ozonated sunflower oil solution showing the highest percentage of reduction ($p < 0.0001$; Fisher's exact test) (Figure 1d–f).

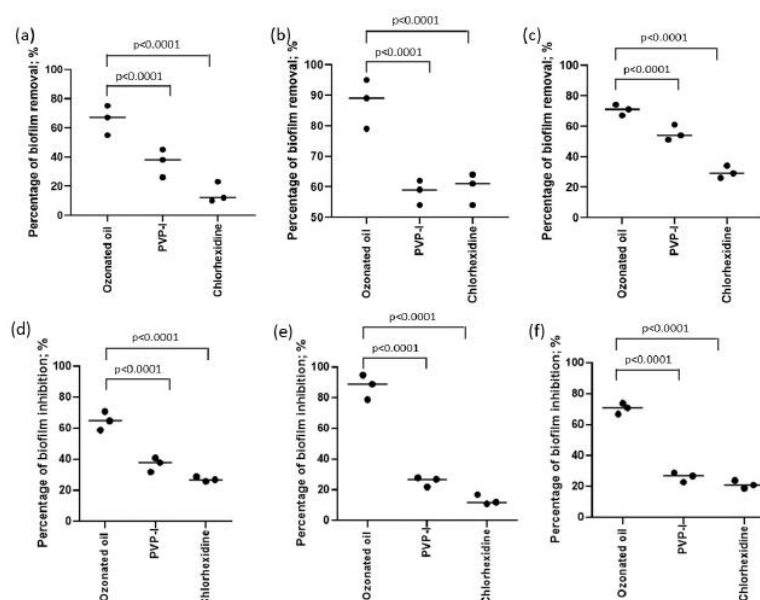


Figure 1. Percentage of biofilm removal in pre-formed (a) *P. aeruginosa* (ATCC 9027), (b) *S. aureus* (ATCC 6538), (c) MRSA (ATCC 33591) biofilm, and in forming (d) *P. aeruginosa* (ATCC 9027), (e) *S. aureus* (ATCC 6538), (f) MRSA (ATCC 33591) biofilm. Values are represented as the median of three experiments. p values were obtained by Fisher's exact test.

2.3. Antibiotic Resistance Evaluation

P. aeruginosa (ATCC 9027), *S. aureus* (ATCC 6538), and MRSA (ATCC 33591) were also tested for antibiotic resistance. We selected FDA-approved antibiotics used for curing ophthalmic infectious diseases [36], including aminoglycosides (gentamicin, tobramycin, and neomycin), chloramphenicol, macrolides (azithromycin and erythromycin), quinolones (ciprofloxacin, moxifloxacin, besifloxacin, gatifloxacin, levofloxacin, and ofloxacin), and tetracyclines. The percentage of resistance levels for each bacterium to the tested antibiotic families is reported in Table 2.

Table 2. Percentage (%) resistance levels of the detected genera to the tested antibiotic families.

Antibiotics	<i>P. aeruginosa</i> (ATCC 9027)	<i>S. aureus</i> (ATCC 6538)	MRSA (ATCC 33591)
Aminoglycosides (gentamicin, tobramycin, neomycin)	5.5%	6.2%	100.0%
Chloramphenicol	45.5%	5.0%	41.7%
Macrolides (azithromycin, erythromycin)	63.6%	30.8%	100.0%
Quinolones (ciprofloxacin, moxifloxacin, besifloxacin, gatifloxacin, levofloxacin, ofloxacin)	19.2%	5.0%	76.0%
Tetracyclines	54.5%	6.4%	25.0%

The resistance was determined by following EUCAST breakpoint values for zone diameter. We observed that *P. aeruginosa* (ATCC 9027) had a high susceptibility to amino-

glycosides and quinolones (94.5% and 80.8%, respectively), and *S. aureus* (ATCC 6538) had a high susceptibility to aminoglycosides, chloramphenicol, quinolones, and tetracyclines (93.8%, 95.0%, 95.0%, and 93.6%, respectively). However, MRSA (ATCC 33591) showed low susceptibility to all the treatments. Next, we pre-treated the bacteria with the ophthalmic solutions for 24 h before the addition of antibiotics. Treatment with the ophthalmic solution containing ozonated sunflower oil increased the susceptibility of *P. aeruginosa* (ATCC 9027) to chloramphenicol, macrolides, and tetracyclines (73.0%, 88.0%, and 67%, respectively) ($p = 0.012$; $p = 1.6 \times 10^{-14}$; and $p = 0.02$, respectively; Fisher's exact test) (Figure 2a). It also increased the susceptibility of *S. aureus* (ATCC 6538) to macrolides (94.2%) ($p = 0.00001$; Fisher's exact test) (Figure 2b). Furthermore, it increased the MRSA (ATCC 33591) susceptibility to aminoglycosides, chloramphenicol, macrolides, quinolones, and tetracyclines (65.7%, 87.7%, 70.3%, 87.4%, and 97.7%, respectively) ($p = 8.2 \times 10^{-11}$; $p = 1.0 \times 10^{-23}$; $p = 0.000007$; $p = 4.3 \times 10^{-20}$; and $p = 1.6 \times 10^{-27}$, respectively; Fisher's exact test) (Figure 2c). The ophthalmic solution containing PVP-I increased the susceptibility of *P. aeruginosa* (ATCC 9027) to chloramphenicol (65.2%), although not significantly, but increased the resistance to quinolones (56.8%) ($p = 1.0 \times 10^{-8}$; Fisher's exact test) (Figure 2a). It also increased the susceptibility of *S. aureus* (ATCC 6538) to macrolides (78.8%), although not significant (Figure 2b). The ophthalmic solution containing chlorhexidine increased the susceptibility of *P. aeruginosa* (ATCC 9027) to chloramphenicol (59.8%) ($p = 0.05$; Fisher's exact test) and the resistance to quinolones (57.3%) ($p = 1.0 \times 10^{-8}$; Fisher's exact test) (Figure 2a). It also increased the resistance of MRSA (ATCC 33591) to tetracyclines (34.6%), although this increase was not statistically significant (Figure 2c).

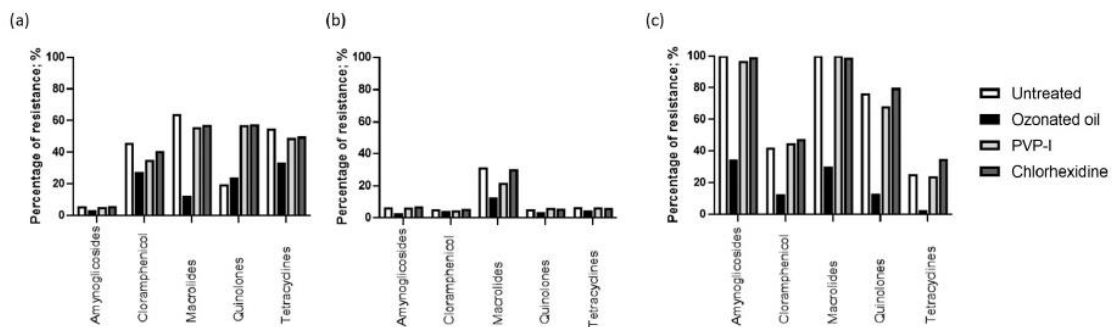


Figure 2. Percentage of resistant (a) *P. aeruginosa*, (b) *S. aureus*, and (c) MRSA to antibiotic classes, in co-treatment with the ophthalmic solutions. Values represent the mean of three experiments.

2.4. Bacteria Adhesion Test

Bacteria need to colonize their host in order to infect [37]. We evaluated the effect of bacteria with or without pre-treatment with the three ophthalmic solutions on cell adhesion in vitro. We used *P. aeruginosa* (ATCC 9027) as representative of Gram-negative, and *S. aureus* (ATCC 6538) and MRSA (ATCC 33591) as representative of Gram-positive bacteria. Firstly, we assessed the cytotoxicity of the three ophthalmic solutions at MIC concentrations. The viability of corneal epithelial HCE-2 cells was evaluated after 4 h of exposure to serial dilutions of the ophthalmic solutions. Figure 3a,b shows the results of the MTT and neutral red uptake (NRU) assays.

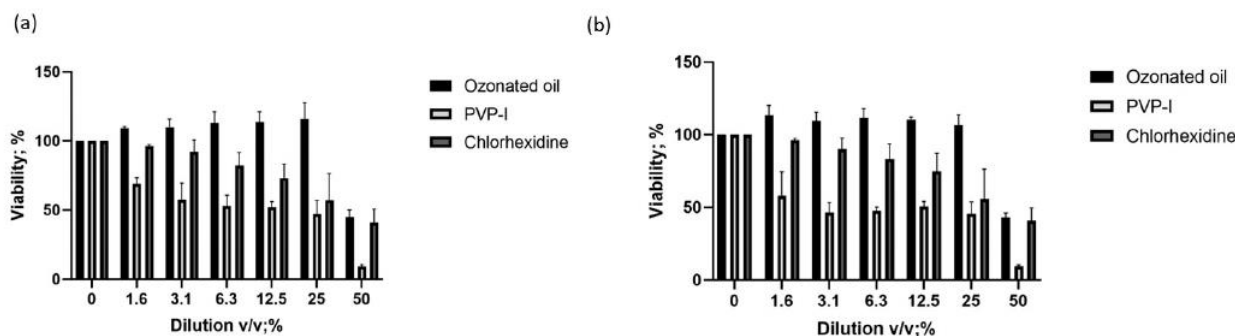


Figure 3. The viability of HCE-2 cells was evaluated by (a) MTT and (b) neutral red uptake after 4 h of exposure with serial dilution ranging from 50 to 1.5625% *v/v* of the ophthalmic antiseptic preparations. Values represent the mean ± standard deviation of three experiments.

The viability assay revealed that the ophthalmic solution containing ozonated sunflower oil had an IC_{50} of 50% *v/v*, while the IC_{50} for PVP-I was 1.56%, and for chlorhexidine was 6.25% *v/v*. We used IC_{50} concentrations to evaluate the ability to interfere with adhesion. The basal adhesion of *P. aeruginosa* (ATCC 9027) was 5.2×10^5 CFU, *S. aureus* (ATCC 6538) was 5.4×10^5 CFU, and MRSA (ATCC 33591) was 5.7×10^5 CFU. Co-treatment with the ophthalmic solutions reduced the bacteria adhesion. Both PVP-I and chlorhexidine preparations reduced the CFU of adherent bacteria by 1Log₁₀ ($p < 0.001$; Mann–Whitney U test). However, the ophthalmic solution containing ozonated sunflower oil was able to reduce adhesion by up to 2Log₁₀ ($p < 0.0001$ Mann–Whitney U test) (Table 3).

Table 3. CFU of adhered bacteria on HCE-2 cells after 4 h of exposure to IC_{50} concentration of the tested ophthalmic solutions.

Ophthalmic Solution	<i>P. aeruginosa</i> (ATCC 9027) (CFU)	<i>S. aureus</i> (ATCC 6538) (CFU)	MRSA (ATCC 33591) (CFU)
Ozonated sunflower oil	1.7×10^3	2.1×10^3	1.9×10^3
PVP-I	5.5×10^4	4.6×10^4	5.1×10^4
Chlorhexidine	3.2×10^4	2.2×10^4	5.2×10^4

2.5. Ophthalmologic Solution Resistance Evaluation

P. aeruginosa (ATCC 9027), *S. aureus* (ATCC 6538), and MRSA (ATCC 33591) were also tested for ophthalmic solution resistance. *P. aeruginosa* (ATCC 9027), *S. aureus* (ATCC 6538), and MRSA (ATCC 33591). These three bacterial strains were exposed to the MIC of the three ophthalmologic solutions for 7 days. After 24 h of microbial incubation, the MIC values were recorded. Table 4 shows that we obtained the same MIC values for all three ophthalmic solutions of those reported in Table 1.

Table 4. MIC values (% *v/v*) of the ophthalmic antiseptic preparations on the different microbial strains after 24 h of incubation. The bacterial strains were previously treated with ophthalmic solutions for a duration of 7 days.

Bacterial Strain	Ozonated Oil Ophthalmic Solution	PVP-I Ophthalmic Solution	Chlorhexidine Ophthalmic Solution
<i>E. coli</i> (ATCC 8739)	25%	100%	100%
<i>P. aeruginosa</i> (ATCC 9027)	50%	100%	100%
<i>S. aureus</i> (ATCC 6538)	12.5%	50%	12.5%
MRSA (ATCC 33591)	25%	50%	25%
<i>S. epidermidis</i> (ATCC 12228)	12.5%	50%	12.5%

3. Discussion

In this study, we evaluated the efficacy of liposomal ozonated oil for the first time in preventing biofilm formation, eliminating pre-existed biofilm, as well as maintaining antibiotic susceptibility of different bacterial strains. We compared it with widely used antiseptic agents such as PVP-I and chlorhexidine.

Our experiments demonstrated and confirmed that all three ophthalmic antiseptic preparations exhibited microbicidal activity at different concentrations. They were effective on Gram-positive bacteria, ranging from 12.5 to 50%. Only ozonated sunflower oil embedded in liposome preparation showed a MIC against Gram-negative bacteria. The MIC for Gram-negative bacteria with PVP-I and chlorhexidine preparations was above the highest concentration used (50%). The differences in these results compared to previously published analyses may be due to different microbial strains and experimental conditions [38]. The novelty of this research lies in evaluating the effect of the three ophthalmic solutions on biofilm formation, antibiotic susceptibility of bacteria, and cell adhesion. The ability to remove pre-formed biofilm ranged from fair to excellent, with the ophthalmic solution containing ozonated sunflower oil with the highest effect compared to the other two ophthalmic solutions. This may be attributed to the liposomal component, which can counteract biofilm surfaces that can absorb antimicrobial substances, reducing their bioavailability [39].

Treatment with the ophthalmic solutions increased susceptibility to the evaluated antibiotics, with the ophthalmic solution containing ozonated sunflower oil showing a wider range of action, particularly against macrolides and chloramphenicol, for the three bacteria tested. The efficacy of the ophthalmic solution containing ozonated sunflower oil might be ascribed to the presence of liposomes, which may facilitate the delivery not only of the ozone inside the bacteria but also of the antibiotics, creating a gap in the membrane where they interact. Similarly, liposomes can interfere with bacteria adhesion to cells, as demonstrated by the 2Log_{10} reduction in adherent bacteria, when the infection is treated with the ophthalmic solution containing ozonated sunflower oil. Interestingly, we observed that a 7-day treatment with the three ophthalmic solutions did not affect the MIC concentration for all the tested bacteria, suggesting their stable efficacy after prolonged use in common clinical practice. It is important to note that this study has limitations, including the absence of clinical isolates and in vivo models, but it represents an important starting point to further investigate the potential of liposomal ozonated oils in ophthalmic applications.

Overall, these results suggest that the three ophthalmic solutions can control bacteria replication and biofilm formation. The ophthalmic solution containing ozonated sunflower oil showed a higher ability to control antibiotic resistance, bacteria adhesion, and biofilm formation, supporting the validity of its use as an antiseptic. Additionally, when applied to the ocular surface, this solution has documented regenerative and anti-inflammatory properties [23,31,40–42]. This implies a possible use as an adjuvant in various ophthalmic diseases characterized by inflammation, infection, and tissue damage.

4. Materials and Methods

4.1. Antimicrobial Activity

The antimicrobial activity was assessed against *S. aureus* (ATCC 6538), MRSA (ATCC 33591), *S. epidermidis* (ATCC 12228), *P. aeruginosa* (ATCC 9027), and *E. coli* (ATCC 8739). Bacterial strains were cultured at 37 °C in Mueller–Hinton broth (Liofilchem, Roseto degli Abruzzi, Italy).

For each strain, the following ophthalmic antiseptic preparations were used: Ozodrop (self-preserved ozonated sunflower oil, hydroxypropyl methylcellulose, liposomes, boric acid, sodium tetraborate, disodium edetate sodium, PHMB, deionized water—concentration not specified; FB Vision, San Benedetto del Tronto, Italy), Iodim (PVP-I 0.6%, hyaluronic acid vehicle; Medivis, Tremestieri Etneo, Italy), Dropsept (chlorhexidine 0.02%, 0.5% tocopherol polyethylene glycol 1000 succinate (TPGS1000); Sooft, Montegiorgio, Italy). Ozonated

sunflower oil has been produced in accordance with patent IT201600078872A1, ensuring stability that meets the registration requirements outlined in the technical file submitted to the notification body. The product has been assessed and found to be compliant with all necessary requirements for market placement. The MIC was determined by performing the EUCAST broth microdilution method in 96-well U-bottom microplates defining it as the lowest concentration of drug that inhibits the visible growth of the organism after overnight incubation [33]. All ophthalmic antiseptic preparations were serially diluted in 1 × PBS by using a 2-fold dilution ranging from 100 to 0.3% and incubated with 5 × 10⁶ CFU/mL of each microorganism.

4.2. Antibiofilm Effect of Using Crystal Violet (CV) Assay

4.2.1. Effect on Biofilm Formation Ability

The ability of ozonated oils to prevent cell adhesion at the MIC value was tested. Briefly, 200 µL of bacterial suspension (OD 600 nm of 0.04 ± 0.02) was added to 96-well polystyrene microtiter plates and incubated at 37 °C for two hours without shaking to allow bacteria to adhere to the plate's surface [43]. After incubation, the contents of the plates were removed, and the plates were rinsed three times in 0.9% (*w/v*) saline solution to remove non-adherent cells. Then, 180 µL of fresh medium and 20 µL of the ophthalmic solution at MIC value were added to adherent cells. After 24 h of incubation at 37 °C, the contents of the plates were removed, and the wells were cleaned with saline solution, and dried overnight by air.

4.2.2. Effect on Established Biofilms

In a 96-well plate, each well received 200 µL of bacterial solution (OD 600 nm of 0.04 ± 0.02) and was incubated for 24 h at 37 °C with 150 rpm shaking. After the incubation period, the contents of each well were removed and cleaned with 0.9% (*w/v*) saline solution. Then, 20 µL of ophthalmic solution and 180 µL of new Mueller–Hinton medium were added to the 24-h-old biofilms. Control wells contained untreated Mueller–Hinton medium. The plates were once more incubated for 24 h at 37 °C and 150 rpm. After incubation, the contents of each well were removed, thoroughly cleaned with saline solution three times, and left to air dry overnight.

4.2.3. Assessment of Biofilm Biomass

The adhering bacteria were fixed with 200 µL of 96% (*v/v*) ethanol for 15 min to measure the biofilm mass. After that, 200 µL of 0.1% crystal violet (Sigma-Aldrich, St. Louis, MO, USA) was added to each plate well, and the plate was left to stain for 10 min at room temperature. The plates were then air-dried, the excess crystal violet rinsed off and gently washed in saline solution. The crystal violet was then dissolved in 200 µL of 33% (*v/v*) glacial acetic acid, and the biomass was determined by measuring the OD at 570 nm using a microplate reader BioTek ELx808U (BioTek, Winooski, VT, USA).

The percentage of biomass reduction (%BR) in comparison to biofilms not exposed to ophthalmic solution was calculated as follows:

$$\%BR = \frac{OD_{CTR} - OD_{OS}}{OD_{CTR}} \times 100$$

where OD_{CTR} is the OD_{570nm} value of control wells and OD_{OS} is the OD_{570nm} value for the ophthalmic solution-treated wells.

4.3. Antibiotic Susceptibility Test

Using the traditional disk diffusion method, the Kirby–Bauer test, and commercially available antibacterial disks, selected strains were evaluated for their susceptibility or resistance to various antibiotics. Bacteria were cultured on Tryptic soy agar (Liofilchem, Roseto degli Abruzzi, Italy) for 24 h at 37 °C for the disk diffusion experiment. Harvested soy agar was then suspended in sterile water to a turbidity of 0.5 McFarland, equivalent

to 1.5×10^8 CFU/mL. A cotton swab was used to inoculate the samples in triplicate onto plates of Mueller–Hinton agar. After 24 h at 37 °C, the diameter of inhibitory zones was precisely determined by a precision caliper (Mitutoyo, Andover, UK). The percentage of resistance was calculated as $100 - [(Control\ diameter\ of\ the\ inhibitory\ zone - (Sample\ diameter\ of\ inhibitory\ zone / Control\ diameter\ of\ the\ inhibitory\ zone))] \times 100$.

4.4. Cytotoxicity Assay

The human corneal epithelial cell line (HCE-2) (ATCC, Manassas, VA, USA; number CRL-11135) was cultured in keratinocyte serum-free medium (Gibco, Waltham, MA, USA; Number: 17005-042) supplemented with 0.05 mg/mL bovine pituitary extract (Gibco, USA), 5 ng/mL epidermal growth factor, 500 ng/mL hydrocortisone, and 0.005 mg/mL insulin (Gibco, USA) at 37 °C and 5% CO₂. Cell viability of HCE-2 was evaluated by performing the colorimetric MTT (3-[4,5-dimethylthiazole-2-yl]-2,5-diphenyltetrazolium bromide, Roche, Basilea, Switzerland) assay according to the manufacturer protocol. Briefly, HCE-2 cells were seeded in 96-well plates at a density of 5×10^3 cells per well and cultured overnight. The day after, HCE-2 cells were treated with the ophthalmic solutions at different 2-fold serial dilutions (ranging from 50 to 1.5625% *v/v*) for 4 h. After incubation time, MTT was performed and the absorbance was measured at 450 nm by using a microplate reader (Multiskan FC, Thermo Fisher, Waltham, MA, USA). Cytotoxicity was calculated as IC₅₀, the concentration of a given agent resulting in lethal to 50% of the cells.

4.5. Neutral Red Uptake (NRU) Assay

The HCE-2 cells were seeded in 96-well tissue culture plates and treated for the appropriate period. The plates were then incubated for 2 h with a medium containing neutral red (Abcam, Cambridge, UK). The cells were subsequently washed, the dye extracted in each well, and the absorbance read using a spectrophotometer (BioRad, Milan, Italy). Cytotoxicity was calculated as IC₅₀, the concentration of a given agent that is lethal to 50% of the cells.

4.6. Bacteria Adhesion Test

The HCE-2 cells were resuspended in fresh medium supplemented with 10% serum without antibiotics at a concentration of 2×10^5 cells/mL [44], as evaluated by a hemocytometer. One milliliter of cell suspension was seeded in three sets of duplicate wells (one for each strain) in the center of a 24-well plate and incubated overnight in a cell culture incubator. One isolated colony of each bacterial strain was inoculated in 5 mL of LB broth (1% tryptone, 0.5% sodium chloride, 0.5% yeast extract) and grown overnight at 37 °C with vigorous shaking (180 rpm).

The HCE-2 cells were washed with warm $1 \times$ DPBS and then added with 1 mL of fresh medium supplemented with 10% serum without antibiotics. Fresh medium without cells was used to determine the total number of bacteria in the inoculum for each strain. An aliquot (10^6 CFU) of each bacterial culture was added to one set of duplicate wells containing HCE-2 cells (multiplicity of infection of 5:1 bacteria:cells) and to one well not containing cells. The cells were incubated for 3 h at 37 °C with 5% CO₂. The medium was removed from the infected cells, which were washed 3 times with warm $1 \times$ DPBS. The adhered bacteria were detached with 100 μ L of 1% Triton X-100 for 10 min at room temperature and then added with 900 μ L of LB medium. After gentle homogenization, serial 10-fold dilutions of the suspensions of adhered bacteria were inoculated in LB broth and 100 μ L from 3 dilutions was plated on LB agar and incubated overnight at 37 °C. The colonies were counted as CFU of adhered bacteria. Only plates with 10–300 colonies were counted. To ensure that 1% Triton X-100 treatment did not affect bacteria viability, we performed a control experiment, maintaining the bacteria with and without 1% Triton X-100 for 10 min and evaluated CFU, as previously reported. We did not find evidence of any difference in CFU count (Table 5).

Table 5. CFU count with and without 1% Triton X-100.

Solutions	<i>P. aeruginosa</i> (ATCC 9027)	<i>S. aureus</i> (ATCC 6538)
LB	5.7×10^4	5.5×10^4
LB + 1% Triton X-100	5.8×10^4	5.6×10^4

4.7. Statistical Analysis

Statistical analyses were performed using GraphPad Prism software (v.8, San Diego, CA, USA). Data were statistically compared using the Mann–Whitney U test, as all the data did not display a normal distribution based on the Kolmogorov–Smirnov and D’Agostino–Pearson normality tests. Percentages were compared by Fisher’s exact test. *p* values < 0.05 were considered significant.

Author Contributions: Conceptualization, V.G., G.S. (Giovanni Scapagnini) and R.R.; methodology, G.S. (Giovanni Strazzabosco), S.R., S.B., G.S. (Giovanna Schiuma), F.C. and A.A.; formal analysis, G.S. (Giovanni Strazzabosco), S.R., S.B., G.S. (Giovanna Schiuma), F.C. and A.A.; data curation, N.S., A.M. (Alessandra Mancini), D.P., S.D. and A.M. (Alessandro Medoro); writing—original draft preparation, V.G., A.M. (Alessandra Mancini), A.M. (Alessandro Medoro) and R.R.; writing—review and editing, N.S., D.P., S.D. and A.M. (Alessandro Medoro); supervision, V.G., G.S. (Giovanni Scapagnini) and R.R.; funding acquisition, R.R. All authors have read and agreed to the published version of the manuscript.

Funding: This research was funded by the University of Ferrara FAR 2021. The funders had no role in study design, data collection, and analysis, decision to publish, or manuscript preparation.

Institutional Review Board Statement: Not applicable.

Informed Consent Statement: Not applicable.

Data Availability Statement: The data presented in this study are available on request from the corresponding author.

Acknowledgments: We thank Iva Pivanti and Mercedes Fernandez for the technical support.

Conflicts of Interest: The authors declare no conflict of interest.

References

- Lee, A.E.; Niruttan, K.; Rawson, T.M.; Moore, L.S.P. Antibacterial Resistance in Ophthalmic Infections: A Multi-Centre Analysis Across UK Care Settings. *BMC Infect. Dis.* **2019**, *19*, 768. [\[CrossRef\]](#)
- Marston, H.D.; Dixon, D.M.; Knisely, J.M.; Palmore, T.N.; Fauci, A.S. Antimicrobial Resistance. *JAMA* **2016**, *316*, 1193–1204. [\[CrossRef\]](#) [\[PubMed\]](#)
- Haas, W.; Pillar, C.M.; Torres, M.; Morris, T.W.; Sahm, D.F. Monitoring Antibiotic Resistance in Ocular Microorganisms: Results From the Antibiotic Resistance Monitoring in Ocular Microorganisms (ARMOR) 2009 Surveillance Study. *Am. J. Ophthalmol.* **2011**, *152*, 567–574.e3. [\[CrossRef\]](#) [\[PubMed\]](#)
- Asbell, P.A.; Sahm, D.F.; Shaw, M.; Draghi, D.C.; Brown, N.P. Increasing Prevalence of Methicillin Resistance in Serious Ocular Infections Caused by Staphylococcus Aureus in the United States: 2000 to 2005. *J. Cataract Refract. Surg.* **2008**, *34*, 814–818. [\[CrossRef\]](#) [\[PubMed\]](#)
- Getahun, E.; Gelaw, B.; Assefa, A.; Assefa, Y.; Amsalu, A. Bacterial Pathogens Associated with External Ocular Infections Alongside Eminent Proportion of Multidrug Resistant Isolates at the University of Gondar Hospital, Northwest Ethiopia. *BMC Ophthalmol.* **2017**, *17*, 151. [\[CrossRef\]](#)
- Asbell, P.A.; Sanfilippo, C.M.; Pillar, C.M.; DeCory, H.H.; Sahm, D.F.; Morris, T.W. Antibiotic Resistance Among Ocular Pathogens in the United States: Five-Year Results From the Antibiotic Resistance Monitoring in Ocular Microorganisms (ARMOR) Surveillance Study. *JAMA Ophthalmol.* **2015**, *133*, 1445–1454. [\[CrossRef\]](#) [\[PubMed\]](#)
- Kowalski, R.P.; Dhaliwal, D.K. Ocular Bacterial Infections: Current and Future Treatment Options. *Expert Rev. Anti Infect. Ther.* **2014**, *3*, 131–139. [\[CrossRef\]](#)
- Marangon, F.B.; Miller, D.; Muallem, M.S.; Romano, A.C.; Alfonso, E.C. Ciprofloxacin and Levofloxacin Resistance Among Methicillin-sensitive Staphylococcus Aureus Isolates From Keratitis and Conjunctivitis. *Am. J. Ophthalmol.* **2004**, *137*, 453–458. [\[CrossRef\]](#) [\[PubMed\]](#)
- Grzybowski, A.; Kanclerz, P.; Myers, W.G. The Use of Povidone-iodine in Ophthalmology. *Curr. Opin. Ophthalmol.* **2018**, *29*, 19–32. [\[CrossRef\]](#)

10. Merani, R.; McPherson, Z.E.; Luckie, A.P.; Gilhotra, J.S.; Runciman, J.; Durkin, S.; Muecke, J.; Donaldson, M.; Aralar, A.; Rao, A.; et al. Aqueous Chlorhexidine for Intravitreal Injection Antisepsis: A Case Series and Review of the Literature. *Ophthalmology* 2016, 123, 2588–2594. [CrossRef] [PubMed]
11. Lachapelle, J.-M.; Castel, O.; Casado, A.F.; Leroy, B.; Micali, G.; Tennstedt, D.; Lambert, J. Therapeutic Perspective Antiseptics in the Era of Bacterial Resistance: A Focus on Povidone Iodine. *Clin. Pract.* 2013, 10, 579–592. [CrossRef]
12. Kunisada, T.; Yamada, K.; Oda, S.; Hara, O. Investigation on the Efficacy of Povidone-iodine Against Antiseptic-resistant Species. *Dermatology* 1997, 195 (Suppl. S2), 14–18. [CrossRef]
13. Kawana, R.; Kitamura, T.; Nakagomi, O.; Matsumoto, I.; Arita, M.; Yoshihara, N.; Yanagi, K.; Yamada, A.; Morita, O.; Yoshida, Y.; et al. Inactivation of Human Viruses by Povidone-iodine in Comparison with Other Antiseptics. *Dermatology* 1997, 195 (Suppl. S2), 29–35. [CrossRef]
14. Wutzler, P.; Sauerbrei, A.; Klöcking, R.; Brögmann, B.; Reimer, K. Virucidal Activity and Cytotoxicity of The Liposomal Formulation of Povidone-Iodine. *Antiviral Res.* 2002, 54, 89–97. [CrossRef]
15. Hoekstra, M.J.; Westgate, S.J.; Mueller, S. Povidone-iodine Ointment Demonstrates In Vitro Efficacy Against Biofilm Formation. *Int. Wound J.* 2017, 14, 172–179. [CrossRef]
16. Capriotti, K.; Pelletier, J.; Barone, S.; Capriotti, J. Efficacy of Dilute Povidone-Iodine against Multi- Drug Resistant Bacterial Biofilms, Fungal Biofilms and Fungal Spores. *J. Clin. Res. Dermatol.* 2018, 5, 1–5. [CrossRef]
17. Lim, K.S.; Kam, P.C.A. Chlorhexidine—Pharmacology and Clinical Applications. *Anaesth. Intensive Care* 2008, 36, 502–512. [CrossRef] [PubMed]
18. Burstein, N.L. Preservative Cytotoxic Threshold for Benzalkonium Chloride and Chlorhexidine Digluconate in Cat and Rabbit Corneas. *Investig. Ophthalmol. Vis. Sci.* 1980, 19, 308–313.
19. Oakley, C.; Allen, P.; Hooshmand, J.; Vote, B.J.T. Pain and Antisepsis After Ocular Administration of Povidone-iodine versus Chlorhexidine. *Retina* 2018, 38, 2064–2066. [CrossRef] [PubMed]
20. Oh, J.Y.; Yu, J.M.; Ko, J.H. Analysis of Ethanol Effects on Corneal Epithelium. *Investig. Ophthalmol. Vis. Sci.* 2013, 54, 3852–3856. [CrossRef] [PubMed]
21. Naor, J.; Savion, N.; Blumenthal, M.; Assia, E.I. Corneal Endothelial Cytotoxicity of Diluted Povidone--iodine. *J. Cataract Refract. Surg.* 2001, 27, 941–947. [CrossRef]
22. Artasensi, A.; Mazzotta, S.; Fumagalli, L. Back to Basics: Choosing the Appropriate Surface Disinfectant. *Antibiotics* 2021, 10, 613. [CrossRef] [PubMed]
23. Celenza, G.; Iorio, R.; Cracchiolo, S.; Petricca, S.; Costagliola, C.; Cinque, B.; Segatore, B.; Amicosante, G.; Bellio, P. Antimycotic Activity of Ozonized Oil in Liposome Eye Drops against *Candida* spp. *Transl. Vis. Sci. Technol.* 2020, 9, 4. [CrossRef]
24. Kalinowski, J.; Heinonen, P.; Kilpeläinen, I.; Räsänen, M.; Gerber, R.B. Stability of criegee intermediates formed by ozonolysis of different double bonds. *J. Phys. Chem. A* 2015, 119, 2318–2325. [CrossRef] [PubMed]
25. Ugazio, E.; Tullio, V.; Binello, A.; Tagliapietra, S.; Dosio, F. Ozonated Oils as Antimicrobial Systems in Topical Applications. Their Characterization, Current Applications, and Advances in Improved Delivery Techniques. *Molecules* 2020, 25, 334. [CrossRef]
26. Zeng, J.; Lu, J. Mechanisms of Action Involved in Ozone-Therapy in Skin Diseases. *Int. Immunopharmacol.* 2018, 56, 235–241. [CrossRef]
27. Menéndez, S.; Falcón, L.; Maqueira, Y. Therapeutic Efficacy of Topical OLEOZON® in Patients Suffering from Onychomycosis. *Mycoses* 2011, 54, e272–e277. [CrossRef] [PubMed]
28. Menéndez, S.; Falcón, L.; Simón, D.R.; Landa, N. Efficacy of Ozonized Sunflower Oil in The Treatment of Tinea Pedis. *Mycoses* 2002, 45, 329–332. [CrossRef]
29. Guerra-Blanco, P.; Poznyak, T.; Pérez, A.; Gómez y Gómez, Y.M.; Bautista-Ramírez, M.E.; Chairez, I. Ozonation Degree of Vegetable Oils as the Factor of Their Anti-Inflammatory and Wound-Healing Effectiveness. *Ozone Sci. Eng.* 2017, 39, 374–384. [CrossRef]
30. Zerillo, L.; Polvere, I.; Varricchio, R.; Madera, J.R.; D’Andrea, S.; Voccola, S.; Franchini, I.; Stilo, R.; Vito, P.; Zotti, T. Antibiofilm and repair activity of ozonated oil in liposome. *Microb. Biotechnol.* 2022, 15, 1422–1433. [CrossRef]
31. Cutarelli, A.; Carlini, G.; Sarno, F.; Nebbioso, A.; Garofalo, F.; Altucci, L.; Corrado, F.; Cutarelli, A.; Carlini, G.; Sarno, F.; et al. The Role of Ozone Carried by Liposomes in the Therapy of Infectious and Skin-Regenerating Ocular Surface. *J. Biomed. Sci. Eng.* 2019, 12, 347–353. [CrossRef]
32. Pérez-Santonja, J.J.; Güell, J.L.; Gris, O.; Dorrego, X.M.V.; Pellicer, E.; Benitez-Del-castillo, J.M. Liposomal Ozonated Oil in Ocular Infections: A Review of Preclinical and Clinical Studies, Focusing on Its Antiseptic and Regenerative Properties. *Clin. Ophthalmol.* 2022, 16, 1953–1962. [CrossRef] [PubMed]
33. EUCAST. MIC Determination of Non-fastidious and Fastidious Organisms. Available online: https://www.eucast.org/ast_of_bacteria/mic_determination (accessed on 22 July 2023).
34. Khatoon, Z.; McTiernan, C.D.; Suuronen, E.J.; Mah, T.F.; Alarcon, E.I. Bacterial biofilm formation on implantable devices and approaches to its treatment and prevention. *Heliyon* 2018, 4, e01067. [CrossRef] [PubMed]
35. Perez, A.P.; Perez, N.; Lozano, C.M.S.; Altube, M.J.; de Farias, M.A.; Portugal, R.V.; Buzzola, F.; Morilla, M.J.; Romero, E.L. The anti MRSA biofilm activity of Thymus vulgaris essential oil in nanovesicles. *Phytomedicine* 2019, 57, 339–351. [CrossRef]
36. Bispo, P.J.M.; Sahm, D.F.; Asbell, P.A. A Systematic Review of Multi-decade Antibiotic Resistance Data for Ocular Bacterial Pathogens in the United States. *Ophthalmol. Ther.* 2022, 11, 503. [CrossRef]

37. Kline, K.A.; Falker, S.; Dahlberg, S.; Normark, S.; Henriques-Normark, B. Bacterial Adhesins in Host-Microbe Interactions. *Cell Host Microbe* **2009**, *5*, 580–592. [[CrossRef](#)]
38. Tognetto, D.; Pastore, M.R.; Guerin, G.M.; Decorti, G.; Franzin, M.; Lagatolla, C.; Cirigliano, G. Bactericidal Activity of Three Different Antiseptic Ophthalmic Preparations as Surgical Prophylaxis. *Graefes Arch. Clin. Exp. Ophthalmol.* **2022**, *260*, 289–293. [[CrossRef](#)]
39. Wang, Y. Liposome as a delivery system for the treatment of biofilm-mediated infections. *J. Appl. Microbiol.* **2021**, *131*, 2626–2639. [[CrossRef](#)]
40. Marchegiani, A.; Magagnini, M.; Cerquetella, M.; Troiano, P.; Franchini, I.; Franchini, A.; Scapagnini, G.; Spaterna, A. Preoperative topical liposomal ozone dispersion to reduce bacterial colonization in conjunctival sac and periocular skin: Preliminary study in dogs. *Exp. Eye Res.* **2019**, *189*, 107848. [[CrossRef](#)] [[PubMed](#)]
41. Spadea, L.; Tonti, E.; Spaterna, A.; Marchegiani, A. Use of Ozone-Based Eye Drops: A Series of Cases in Veterinary and Human Spontaneous Ocular Pathologies. *Case Rep. Ophthalmol.* **2018**, *9*, 287–298. [[CrossRef](#)]
42. Díaz, M.F.; Hernández, R.; Martínez, G.; Vidal, G.; Gómez, M.; Fernández, H.; Garcés, R. Comparative study of ozonized olive oil and ozonized sunflower oil. *J. Braz. Chem. Soc.* **2006**, *17*, 403–407. [[CrossRef](#)]
43. Silva, V.; Peirone, C.; Amaral, J.S.; Capita, R.; Alonso-Calleja, C.; Marques-Magallanes, J.A.; Martins, Â.; Carvalho, Â.; Maltez, L.; Pereira, J.E.; et al. High Efficacy of Ozonated Oils on the Removal of Biofilms Produced by Methicillin-Resistant *Staphylococcus aureus* (MRSA) from Infected Diabetic Foot Ulcers. *Molecules* **2020**, *25*, 3601. [[CrossRef](#)] [[PubMed](#)]
44. Letourneau, J.; Levesque, C.; Berthiaume, F.; Jacques, M.; Mourez, M. In Vitro Assay of Bacterial Adhesion onto Mammalian Epithelial Cells. *J. Vis. Exp.* **2011**, *51*, e2783. [[CrossRef](#)]

Disclaimer/Publisher's Note: The statements, opinions and data contained in all publications are solely those of the individual author(s) and contributor(s) and not of MDPI and/or the editor(s). MDPI and/or the editor(s) disclaim responsibility for any injury to people or property resulting from any ideas, methods, instructions or products referred to in the content.

10. References

1. Singh, D. and S.V. Yi, *On the origin and evolution of SARS-CoV-2*. Exp Mol Med, 2021. **53**(4): p. 537-547.
2. Zhu, N., et al., *A Novel Coronavirus from Patients with Pneumonia in China, 2019*. N Engl J Med, 2020. **382**(8): p. 727-733.
3. Li, Q., et al., *Early Transmission Dynamics in Wuhan, China, of Novel Coronavirus-Infected Pneumonia*. N Engl J Med, 2020. **382**(13): p. 1199-1207.
4. Estola, T., *Coronaviruses, a New Group of Animal RNA Viruses*. Avian Diseases, 1970. **14**(2).
5. Rabaan, A.A., et al., *SARS-CoV-2, SARS-CoV, and MERS-COV: A comparative overview*. Infez Med, 2020. **28**(2): p. 174-184.
6. Malik, Y.A., *Properties of Coronavirus and SARS-CoV-2*. Malays J Pathol, 2020. **42**(1): p. 3-11.
7. Woo, P.C., et al., *Discovery of seven novel Mammalian and avian coronaviruses in the genus deltacoronavirus supports bat coronaviruses as the gene source of alphacoronavirus and betacoronavirus and avian coronaviruses as the gene source of gammacoronavirus and deltacoronavirus*. J Virol, 2012. **86**(7): p. 3995-4008.
8. Wertheim, J.O., et al., *A case for the ancient origin of coronaviruses*. J Virol, 2013. **87**(12): p. 7039-45.
9. Chan, J.F., et al., *Middle East respiratory syndrome coronavirus: another zoonotic betacoronavirus causing SARS-like disease*. Clin Microbiol Rev, 2015. **28**(2): p. 465-522.
10. King, A.M.Q., et al., *Changes to taxonomy and the International Code of Virus Classification and Nomenclature ratified by the International Committee on Taxonomy of Viruses (2018)*. Arch Virol, 2018. **163**(9): p. 2601-2631.
11. Jo, W.K., et al., *Potential zoonotic sources of SARS-CoV-2 infections*. Transbound Emerg Dis, 2021. **68**(4): p. 1824-1834.
12. Zhang, Y.Z. and E.C. Holmes, *A Genomic Perspective on the Origin and Emergence of SARS-CoV-2*. Cell, 2020. **181**(2): p. 223-227.
13. Guan, Y., et al., *Isolation and characterization of viruses related to the SARS coronavirus from animals in southern China*. Science, 2003. **302**(5643): p. 276-8.
14. Freuling, C.M., et al., *Susceptibility of Raccoon Dogs for Experimental SARS-CoV-2 Infection*. Emerg Infect Dis, 2020. **26**(12): p. 2982-2985.
15. Xiao, X., et al., *Animal sales from Wuhan wet markets immediately prior to the COVID-19 pandemic*. Sci Rep, 2021. **11**(1): p. 11898.
16. Latinne, A., et al., *Origin and cross-species transmission of bat coronaviruses in China*. Nat Commun, 2020. **11**(1): p. 4235.
17. Ge, X.Y., et al., *Isolation and characterization of a bat SARS-like coronavirus that uses the ACE2 receptor*. Nature, 2013. **503**(7477): p. 535-8.

18. Ebihara, T., et al., *Detection of human coronavirus NL63 in young children with bronchiolitis*. J Med Virol, 2005. **75**(3): p. 463-5.
19. Bai, C., Q. Zhong, and G.F. Gao, *Overview of SARS-CoV-2 genome-encoded proteins*. Sci China Life Sci, 2022. **65**(2): p. 280-294.
20. Shereen, M.A., et al., *COVID-19 infection: Origin, transmission, and characteristics of human coronaviruses*. J Adv Res, 2020. **24**: p. 91-98.
21. Wu, A., et al., *Genome Composition and Divergence of the Novel Coronavirus (2019-nCoV) Originating in China*. Cell Host Microbe, 2020. **27**(3): p. 325-328.
22. Jackson, C.B., et al., *Mechanisms of SARS-CoV-2 entry into cells*. Nat Rev Mol Cell Biol, 2022. **23**(1): p. 3-20.
23. Arya, R., et al., *Structural insights into SARS-CoV-2 proteins*. J Mol Biol, 2021. **433**(2): p. 166725.
24. Zhang, J., et al., *Structure of SARS-CoV-2 spike protein*. Curr Opin Virol, 2021. **50**: p. 173-182.
25. Kadam, S.B., et al., *SARS-CoV-2, the pandemic coronavirus: Molecular and structural insights*. J Basic Microbiol, 2021. **61**(3): p. 180-202.
26. Wong, N.A. and M.H. Saier, Jr., *The SARS-Coronavirus Infection Cycle: A Survey of Viral Membrane Proteins, Their Functional Interactions and Pathogenesis*. Int J Mol Sci, 2021. **22**(3).
27. Mahtarin, R., et al., *Structure and dynamics of membrane protein in SARS-CoV-2*. Journal of Biomolecular Structure and Dynamics, 2020. **40**(10): p. 4725-4738.
28. Narayanan, K., et al., *Nucleocapsid-independent specific viral RNA packaging via viral envelope protein and viral RNA signal*. J Virol, 2003. **77**(5): p. 2922-7.
29. Zheng, Y., et al., *Severe acute respiratory syndrome coronavirus 2 (SARS-CoV-2) membrane (M) protein inhibits type I and III interferon production by targeting RIG-I/MDA-5 signaling*. Signal Transduct Target Ther, 2020. **5**(1): p. 299.
30. Fu, Y.Z., et al., *SARS-CoV-2 membrane glycoprotein M antagonizes the MAVS-mediated innate antiviral response*. Cell Mol Immunol, 2021. **18**(3): p. 613-620.
31. Ruch, T.R. and C.E. Machamer, *The coronavirus E protein: assembly and beyond*. Viruses, 2012. **4**(3): p. 363-82.
32. Cao, Y., et al., *Characterization of the SARS-CoV-2 E Protein: Sequence, Structure, Viroporin, and Inhibitors*. Protein Sci, 2021. **30**(6): p. 1114-1130.
33. Mandala, V.S., et al., *Structure and Drug Binding of the SARS-CoV-2 Envelope Protein in Phospholipid Bilayers*. Res Sq, 2020.
34. Wang, K., S. Xie, and B. Sun, *Viral proteins function as ion channels*. Biochim Biophys Acta, 2011. **1808**(2): p. 510-5.
35. Chai, J., et al., *Structural basis for SARS-CoV-2 envelope protein recognition of human cell junction protein PALS1*. Nat Commun, 2021. **12**(1): p. 3433.

36. Zhou, P., et al., *A pneumonia outbreak associated with a new coronavirus of probable bat origin*. Nature, 2020. **579**(7798): p. 270-273.
37. Schubert, K., et al., *SARS-CoV-2 Nsp1 binds the ribosomal mRNA channel to inhibit translation*. Nat Struct Mol Biol, 2020. **27**(10): p. 959-966.
38. Thoms, M., et al., *Structural basis for translational shutdown and immune evasion by the Nsp1 protein of SARS-CoV-2*. Science, 2020. **369**(6508): p. 1249-1255.
39. Cornillez-Ty, C.T., et al., *Severe acute respiratory syndrome coronavirus nonstructural protein 2 interacts with a host protein complex involved in mitochondrial biogenesis and intracellular signaling*. J Virol, 2009. **83**(19): p. 10314-8.
40. Angeletti, S., et al., *COVID-2019: The role of the nsp2 and nsp3 in its pathogenesis*. J Med Virol, 2020. **92**(6): p. 584-588.
41. Dong, S., et al., *A guideline for homology modeling of the proteins from newly discovered betacoronavirus, 2019 novel coronavirus (2019-nCoV)*. J Med Virol, 2020. **92**(9): p. 1542-1548.
42. Claverie, J.M., *A Putative Role of de-Mono-ADP-Ribosylation of STAT1 by the SARS-CoV-2 Nsp3 Protein in the Cytokine Storm Syndrome of COVID-19*. Viruses, 2020. **12**(6).
43. Yan, S. and G. Wu, *Spatial and temporal roles of SARS-CoV PL(pro) - A snapshot*. FASEB J, 2021. **35**(1): p. e21197.
44. Lv, Z., et al., *Targeting SARS-CoV-2 Proteases for COVID-19 Antiviral Development*. Front Chem, 2021. **9**: p. 819165.
45. Zhang, L., et al., *Crystal structure of SARS-CoV-2 main protease provides a basis for design of improved alpha-ketoamide inhibitors*. Science, 2020. **368**(6489): p. 409-412.
46. Mercorelli, B., et al., *Discovery of novel SARS-CoV-2 inhibitors targeting the main protease M(pro) by virtual screenings and hit optimization*. Antiviral Res, 2022. **204**: p. 105350.
47. Wang, Q., et al., *Structural Basis for RNA Replication by the SARS-CoV-2 Polymerase*. Cell, 2020. **182**(2): p. 417-428 e13.
48. Gao, Y., et al., *Structure of the RNA-dependent RNA polymerase from COVID-19 virus*. Science, 2020. **368**(6492): p. 779-782.
49. Zandi, M., et al., *The role of SARS-CoV-2 accessory proteins in immune evasion*. Biomed Pharmacother, 2022. **156**: p. 113889.
50. Araujo, F.C., et al., *Similarities and differences of X and Y chromosome homologous genes, SRY and SOX3, in regulating the renin-angiotensin system promoters*. Physiol Genomics, 2015. **47**(5): p. 177-86.
51. Lu, R., et al., *Genomic characterisation and epidemiology of 2019 novel coronavirus: implications for virus origins and receptor binding*. Lancet, 2020. **395**(10224): p. 565-574.

52. Boni, M.F., et al., *Evolutionary origins of the SARS-CoV-2 sarbecovirus lineage responsible for the COVID-19 pandemic*. Nat Microbiol, 2020. **5**(11): p. 1408-1417.
53. Shahhosseini, N., et al., *Mutation Signatures and In Silico Docking of Novel SARS-CoV-2 Variants of Concern*. Microorganisms, 2021. **9**(5).
54. Tao, K., et al., *The biological and clinical significance of emerging SARS-CoV-2 variants*. Nat Rev Genet, 2021. **22**(12): p. 757-773.
55. Araf, Y., et al., *Omicron variant of SARS-CoV-2: Genomics, transmissibility, and responses to current COVID-19 vaccines*. J Med Virol, 2022. **94**(5): p. 1825-1832.
56. Mlcochova, P., et al., *SARS-CoV-2 B.1.617.2 Delta variant replication and immune evasion*. Nature, 2021. **599**(7883): p. 114-119.
57. Torjesen, I., *Covid-19: Omicron may be more transmissible than other variants and partly resistant to existing vaccines, scientists fear*. BMJ, 2021. **375**: p. n2943.
58. Watanabe, Y., et al., *Site-specific glycan analysis of the SARS-CoV-2 spike*. Science, 2020. **369**(6501): p. 330-333.
59. Wang, M.Y., et al., *SARS-CoV-2: Structure, Biology, and Structure-Based Therapeutics Development*. Front Cell Infect Microbiol, 2020. **10**: p. 587269.
60. Walls, A.C., et al., *Structure, Function, and Antigenicity of the SARS-CoV-2 Spike Glycoprotein*. Cell, 2020. **183**(6): p. 1735.
61. Wrapp, D., et al., *Cryo-EM structure of the 2019-nCoV spike in the prefusion conformation*. Science, 2020. **367**(6483): p. 1260-1263.
62. Takeda, M., *Proteolytic activation of SARS-CoV-2 spike protein*. Microbiol Immunol, 2022. **66**(1): p. 15-23.
63. Matsuyama, S., et al., *Enhanced isolation of SARS-CoV-2 by TMPRSS2-expressing cells*. Proc Natl Acad Sci U S A, 2020. **117**(13): p. 7001-7003.
64. Benton, D.J., et al., *Receptor binding and priming of the spike protein of SARS-CoV-2 for membrane fusion*. Nature, 2020. **588**(7837): p. 327-330.
65. Essalmani, R., et al., *Distinctive Roles of Furin and TMPRSS2 in SARS-CoV-2 Infectivity*. J Virol, 2022. **96**(8): p. e0012822.
66. Shang, J., et al., *Structural basis of receptor recognition by SARS-CoV-2*. Nature, 2020. **581**(7807): p. 221-224.
67. Amoutzias, G.D., et al., *The Remarkable Evolutionary Plasticity of Coronaviruses by Mutation and Recombination: Insights for the COVID-19 Pandemic and the Future Evolutionary Paths of SARS-CoV-2*. Viruses, 2022. **14**(1).
68. Feng, W., et al., *Nucleocapsid protein of SARS-CoV-2 is a potential target for developing new generation of vaccine*. J Clin Lab Anal, 2022. **36**(6): p. e24479.
69. Kang, S., et al., *Crystal structure of SARS-CoV-2 nucleocapsid protein RNA binding domain reveals potential unique drug targeting sites*. Acta Pharm Sin B, 2020. **10**(7): p. 1228-1238.

70. Alenina, N. and M. Bader, *ACE2 in Brain Physiology and Pathophysiology: Evidence from Transgenic Animal Models*. *Neurochem Res*, 2019. **44**(6): p. 1323-1329.
71. Chang, C.K., et al., *The SARS coronavirus nucleocapsid protein--forms and functions*. *Antiviral Res*, 2014. **103**: p. 39-50.
72. Narayanan, K., K.H. Kim, and S. Makino, *Characterization of N protein self-association in coronavirus ribonucleoprotein complexes*. *Virus Res*, 2003. **98**(2): p. 131-40.
73. Sheikh, A., et al., *Analysis of preferred codon usage in the coronavirus N genes and their implications for genome evolution and vaccine design*. *J Virol Methods*, 2020. **277**: p. 113806.
74. McBride, R., M. van Zyl, and B.C. Fielding, *The coronavirus nucleocapsid is a multifunctional protein*. *Viruses*, 2014. **6**(8): p. 2991-3018.
75. Zhou, R., et al., *Structural characterization of the C-terminal domain of SARS-CoV-2 nucleocapsid protein*. *Mol Biomed*, 2020. **1**(1): p. 2.
76. Batlle, D., J. Wysocki, and K. Satchell, *Soluble angiotensin-converting enzyme 2: a potential approach for coronavirus infection therapy?* *Clin Sci (Lond)*, 2020. **134**(5): p. 543-545.
77. Donoghue, M., et al., *A novel angiotensin-converting enzyme-related carboxypeptidase (ACE2) converts angiotensin I to angiotensin 1-9*. *Circ Res*, 2000. **87**(5): p. E1-9.
78. Turner, A.J. and N.M. Hooper, *The angiotensin-converting enzyme gene family: genomics and pharmacology*. *Trends Pharmacol Sci*, 2002. **23**(4): p. 177-83.
79. Devaux, C.A., J.M. Rolain, and D. Raoult, *ACE2 receptor polymorphism: Susceptibility to SARS-CoV-2, hypertension, multi-organ failure, and COVID-19 disease outcome*. *J Microbiol Immunol Infect*, 2020. **53**(3): p. 425-435.
80. Scialo, F., et al., *ACE2: The Major Cell Entry Receptor for SARS-CoV-2*. *Lung*, 2020. **198**(6): p. 867-877.
81. Bourgonje, A.R., et al., *Angiotensin-converting enzyme 2 (ACE2), SARS-CoV-2 and the pathophysiology of coronavirus disease 2019 (COVID-19)*. *J Pathol*, 2020. **251**(3): p. 228-248.
82. Hamming, I., et al., *The emerging role of ACE2 in physiology and disease*. *J Pathol*, 2007. **212**(1): p. 1-11.
83. Tikellis, C. and M.C. Thomas, *Angiotensin-Converting Enzyme 2 (ACE2) Is a Key Modulator of the Renin Angiotensin System in Health and Disease*. *Int J Pept*, 2012. **2012**: p. 256294.
84. Sanchis-Gomar, F., et al., *Angiotensin-Converting Enzyme 2 and Antihypertensives (Angiotensin Receptor Blockers and Angiotensin-Converting Enzyme Inhibitors) in Coronavirus Disease 2019*. *Mayo Clin Proc*, 2020. **95**(6): p. 1222-1230.

85. Garg, M., S.G. Royce, and J.S. Lubel, *Letter: intestinal inflammation, COVID-19 and gastrointestinal ACE2-exploring RAS inhibitors*. *Aliment Pharmacol Ther*, 2020. **52**(3): p. 569-570.
86. Kashuba, E., et al., *The kinin-kallikrein system: physiological roles, pathophysiology and its relationship to cancer biomarkers*. *Biomarkers*, 2013. **18**(4): p. 279-96.
87. Su, J.B., *Different cross-talk sites between the renin-angiotensin and the kallikrein-kinin systems*. *J Renin Angiotensin Aldosterone Syst*, 2014. **15**(4): p. 319-28.
88. Rahman, A.M., et al., *Endothelium-derived hyperpolarizing factor mediates bradykinin-stimulated tissue plasminogen activator release in humans*. *J Vasc Res*, 2014. **51**(3): p. 200-8.
89. Glowacka, I., et al., *Differential downregulation of ACE2 by the spike proteins of severe acute respiratory syndrome coronavirus and human coronavirus NL63*. *J Virol*, 2010. **84**(2): p. 1198-205.
90. Imai, Y., et al., *Angiotensin-converting enzyme 2 protects from severe acute lung failure*. *Nature*, 2005. **436**(7047): p. 112-6.
91. Lee, J.S. and E.C. Shin, *The type I interferon response in COVID-19: implications for treatment*. *Nat Rev Immunol*, 2020. **20**(10): p. 585-586.
92. Welch, W.J., *Angiotensin II-dependent superoxide: effects on hypertension and vascular dysfunction*. *Hypertension*, 2008. **52**(1): p. 51-6.
93. Marchesi, C., P. Paradis, and E.L. Schiffrin, *Role of the renin-angiotensin system in vascular inflammation*. *Trends Pharmacol Sci*, 2008. **29**(7): p. 367-74.
94. van de Veerdonk, F.L., et al., *Kallikrein-kinin blockade in patients with COVID-19 to prevent acute respiratory distress syndrome*. *Elife*, 2020. **9**.
95. Hartard, C., et al., *Multiorgan and Vascular Tropism of SARS-CoV-2*. *Viruses*, 2022. **14**(3).
96. Wang, Y., et al., *A comprehensive investigation of the mRNA and protein level of ACE2, the putative receptor of SARS-CoV-2, in human tissues and blood cells*. *Int J Med Sci*, 2020. **17**(11): p. 1522-1531.
97. Hamming, I., et al., *Tissue distribution of ACE2 protein, the functional receptor for SARS coronavirus. A first step in understanding SARS pathogenesis*. *J Pathol*, 2004. **203**(2): p. 631-7.
98. Peiris, J.S., et al., *Clinical progression and viral load in a community outbreak of coronavirus-associated SARS pneumonia: a prospective study*. *Lancet*, 2003. **361**(9371): p. 1767-72.
99. Damiani, S., et al., *Pathological post-mortem findings in lungs infected with SARS-CoV-2*. *J Pathol*, 2021. **253**(1): p. 31-40.
100. Ahn, J.H., et al., *Nasal ciliated cells are primary targets for SARS-CoV-2 replication in the early stage of COVID-19*. *J Clin Invest*, 2021. **131**(13).

101. Jia, H.P., et al., *ACE2 receptor expression and severe acute respiratory syndrome coronavirus infection depend on differentiation of human airway epithelia*. J Virol, 2005. **79**(23): p. 14614-21.
102. Lamers, M.M. and B.L. Haagmans, *SARS-CoV-2 pathogenesis*. Nat Rev Microbiol, 2022. **20**(5): p. 270-284.
103. Hou, Y.J., et al., *SARS-CoV-2 Reverse Genetics Reveals a Variable Infection Gradient in the Respiratory Tract*. Cell, 2020. **182**(2): p. 429-446 e14.
104. Shulla, A., et al., *A transmembrane serine protease is linked to the severe acute respiratory syndrome coronavirus receptor and activates virus entry*. J Virol, 2011. **85**(2): p. 873-82.
105. Ziegler, C.G.K., et al., *SARS-CoV-2 Receptor ACE2 Is an Interferon-Stimulated Gene in Human Airway Epithelial Cells and Is Detected in Specific Cell Subsets across Tissues*. Cell, 2020. **181**(5): p. 1016-1035 e19.
106. Delgado-Gonzalez, P., et al., *Inflammatory effect on the gastrointestinal system associated with COVID-19*. World J Gastroenterol, 2021. **27**(26): p. 4160-4171.
107. Wang, M., et al., *Renal Injury by SARS-CoV-2 Infection: A Systematic Review*. Kidney Dis (Basel), 2021. **7**(2): p. 100-110.
108. Zhang, H., et al., *Digestive system is a potential route of COVID-19: an analysis of single-cell coexpression pattern of key proteins in viral entry process*. Gut, 2020. **69**(6): p. 1010-1018.
109. Hikmet, F., et al., *The protein expression profile of ACE2 in human tissues*. Mol Syst Biol, 2020. **16**(7): p. e9610.
110. Ghazanfar, H., et al., *Impact of COVID-19 on the Gastrointestinal Tract: A Clinical Review*. Cureus, 2022. **14**(3): p. e23333.
111. Xiao, F., et al., *Evidence for Gastrointestinal Infection of SARS-CoV-2*. Gastroenterology, 2020. **158**(6): p. 1831-1833 e3.
112. Guo, M., et al., *Potential intestinal infection and faecal-oral transmission of SARS-CoV-2*. Nat Rev Gastroenterol Hepatol, 2021. **18**(4): p. 269-283.
113. Al-Kuraishy, H.M. and A.I. Al-Gareeb, *Acute kidney injury and COVID-19*. Egypt J Intern Med, 2021. **33**(1): p. 34.
114. Pan, X.W., et al., *Identification of a potential mechanism of acute kidney injury during the COVID-19 outbreak: a study based on single-cell transcriptome analysis*. Intensive Care Med, 2020. **46**(6): p. 1114-1116.
115. Braun, F., et al., *SARS-CoV-2 renal tropism associates with acute kidney injury*. Lancet, 2020. **396**(10251): p. 597-598.
116. Puelles, V.G., et al., *Multiorgan and Renal Tropism of SARS-CoV-2*. N Engl J Med, 2020. **383**(6): p. 590-592.
117. Izzedine, H. and K.D. Jhaveri, *Acute kidney injury in patients with COVID-19: an update on the pathophysiology*. Nephrol Dial Transplant, 2021. **36**(2): p. 224-226.

118. Vaz-Silva, J., et al., *The vasoactive peptide angiotensin-(1-7), its receptor Mas and the angiotensin-converting enzyme type 2 are expressed in the human endometrium.* *Reprod Sci*, 2009. **16**(3): p. 247-56.
119. Hayashi, K.G., et al., *Involvement of angiotensin-ii system in bovine follicular development and atresia: messenger RNA expression in theca interna and effect on steroid secretion.* *Biol Reprod*, 2003. **69**(6): p. 2078-84.
120. Ferreira, R., et al., *Angiotensin II signaling promotes follicle growth and dominance in cattle.* *Endocrinology*, 2011. **152**(12): p. 4957-65.
121. Stefanello, J.R., et al., *Effect of angiotensin II with follicle cells and insulin-like growth factor-I or insulin on bovine oocyte maturation and embryo development.* *Theriogenology*, 2006. **66**(9): p. 2068-76.
122. Vaz-Silva, J., et al., *Tissue specific localization of angiotensin-(1-7) and its receptor Mas in the uterus of ovariectomized rats.* *J Mol Histol*, 2012. **43**(5): p. 597-602.
123. Cui, P., et al., *Clinical features and sexual transmission potential of SARS-CoV-2 infected female patients: a descriptive study in Wuhan, China.*
124. Pringle, K.G., et al., *The expression and localization of the human placental prorenin/renin-angiotensin system throughout pregnancy: roles in trophoblast invasion and angiogenesis?* *Placenta*, 2011. **32**(12): p. 956-62.
125. Jing, Y., et al., *Potential influence of COVID-19/ACE2 on the female reproductive system.* *Mol Hum Reprod*, 2020. **26**(6): p. 367-373.
126. Zeng, L., et al., *Neonatal Early-Onset Infection With SARS-CoV-2 in 33 Neonates Born to Mothers With COVID-19 in Wuhan, China.* *JAMA Pediatr*, 2020. **174**(7): p. 722-725.
127. Dong, L., et al., *Possible Vertical Transmission of SARS-CoV-2 From an Infected Mother to Her Newborn.* *JAMA*, 2020. **323**(18): p. 1846-1848.
128. Savasi, V.M., et al., *Clinical Findings and Disease Severity in Hospitalized Pregnant Women With Coronavirus Disease 2019 (COVID-19).* *Obstet Gynecol*, 2020. **136**(2): p. 252-258.
129. Liu, Y., et al., *Withdrawn: Clinical manifestations and outcome of SARS-CoV-2 infection during pregnancy.* *J Infect*, 2020.
130. Aditi Shastri, J.W., Satchee Agrawal, Nirjhar Chatterjee, Kith Pradhan, Mendel Goldfinger, Noah Kornblum, Ulrich Steidl, Amit Verma, Jayanthi Shastri, *Delayed clearance of SARS-CoV2 in male compared to female patients: High ACE2 expression in testes suggests possible existence of gender-specific viral reservoirs.*
131. Verma, S., S. Saksena, and H. Sadri-Ardekani, *ACE2 receptor expression in testes: implications in coronavirus disease 2019 pathogenesis* *Biomed Res Int*, 2020. **103**(3): p. 449-451.

132. Zou, X., et al., *Single-cell RNA-seq data analysis on the receptor ACE2 expression reveals the potential risk of different human organs vulnerable to 2019-nCoV infection*. *Front Med*, 2020. **14**(2): p. 185-192.
133. Sharun, K., R. Tiwari, and K. Dhama, *SARS-CoV-2 in semen: Potential for sexual transmission in COVID-19*. *Int J Surg*, 2020. **84**: p. 156-158.
134. Omolaoye, T.S., et al., *SARS-COV-2 (Covid-19) and male fertility: Where are we?* *Reprod Toxicol*, 2021. **99**: p. 65-70.
135. Shen, Q., et al., *The ACE2 expression in Sertoli cells and germ cells may cause male reproductive disorder after SARS-CoV-2 infection*. *J Cell Mol Med*, 2020. **24**(16): p. 9472-9477.
136. Dutta, S. and P. Sengupta, *SARS-CoV-2 and Male Infertility: Possible Multifaceted Pathology*. *Reprod Sci*, 2021. **28**(1): p. 23-26.
137. Zulli, A., et al., *ACE2 and AT4R are present in diseased human blood vessels*. *Eur J Histochem*, 2008. **52**(1): p. 39-44.
138. Kumar, A., et al., *SARS-CoV-2 cell entry receptor ACE2 mediated endothelial dysfunction leads to vascular thrombosis in COVID-19 patients*. *Med Hypotheses*, 2020. **145**: p. 110320.
139. Xu, J., et al., *Clinical Relevance and Role of Neuronal AT(1) Receptors in ADAM17-Mediated ACE2 Shedding in Neurogenic Hypertension*. *Circ Res*, 2017. **121**(1): p. 43-55.
140. Xu, J. and E. Lazartigues, *Expression of ACE2 in Human Neurons Supports the Neuro-Invasive Potential of COVID-19 Virus*. *Cell Mol Neurobiol*, 2022. **42**(1): p. 305-309.
141. Miyauchi, T., et al., *Basigin, a new, broadly distributed member of the immunoglobulin superfamily, has strong homology with both the immunoglobulin V domain and the beta-chain of major histocompatibility complex class II antigen*. *J Biochem*, 1990. **107**(2): p. 316-23.
142. Li, Y., et al., *HAb18G (CD147), a cancer-associated biomarker and its role in cancer detection*. *Histopathology*, 2009. **54**(6): p. 677-87.
143. Belton, R.J., Jr., et al., *Basigin-2 is a cell surface receptor for soluble basigin ligand*. *J Biol Chem*, 2008. **283**(26): p. 17805-14.
144. Liao, C.G., et al., *Characterization of basigin isoforms and the inhibitory function of basigin-3 in human hepatocellular carcinoma proliferation and invasion*. *Mol Cell Biol*, 2011. **31**(13): p. 2591-604.
145. Laopajon, W., et al., *Antibody biosensors for the measurement and characterization of soluble CD147 molecules*. *Asian Pac J Allergy Immunol*, 2018. **36**(3): p. 191-200.
146. Yurchenko, V., et al., *Regulation of CD147 cell surface expression: involvement of the proline residue in the CD147 transmembrane domain*. *J Biol Chem*, 2005. **280**(17): p. 17013-9.
147. Yan, L., S. Zucker, and B.P. Toole, *Roles of the multifunctional glycoprotein, emmprin (basigin; CD147), in tumour progression*. *Thromb Haemost*, 2005. **93**(2): p. 199-204.

148. Muramatsu, T. and T. Miyauchi, *Basigin (CD147): a multifunctional transmembrane protein involved in reproduction, neural function, inflammation and tumor invasion*. *Histol Histopathol*, 2003. **18**(3): p. 981-7.
149. Redzic, J.S., et al., *Extracellular vesicles secreted from cancer cell lines stimulate secretion of MMP-9, IL-6, TGF-beta1 and EMMPRIN*. *PLoS One*, 2013. **8**(8): p. e71225.
150. De Caluwe, L., et al., *The CD147 Protein Complex Is Involved in Entry of Chikungunya Virus and Related Alphaviruses in Human Cells*. *Front Microbiol*, 2021. **12**: p. 615165.
151. Vanarsdall, A.L., et al., *CD147 Promotes Entry of Pentamer-Expressing Human Cytomegalovirus into Epithelial and Endothelial Cells*. *mBio*, 2018. **9**(3).
152. Landras, A., et al., *CD147 Is a Promising Target of Tumor Progression and a Prognostic Biomarker*. *Cancers (Basel)*, 2019. **11**(11).
153. Kumar, D., et al., *Structural insights on druggable hotspots in CD147: A bull's eye view*. *Life Sci*, 2019. **224**: p. 76-87.
154. Grass, G.D. and B.P. Toole, *How, with whom and when: an overview of CD147-mediated regulatory networks influencing matrix metalloproteinase activity*. *Biosci Rep*, 2015. **36**(1): p. e00283.
155. Xin, X., et al., *CD147/EMMPRIN overexpression and prognosis in cancer: A systematic review and meta-analysis*. *Sci Rep*, 2016. **6**: p. 32804.
156. Tang, Y., et al., *Regulation of vascular endothelial growth factor expression by EMMPRIN via the PI3K-Akt signaling pathway*. *Mol Cancer Res*, 2006. **4**(6): p. 371-7.
157. Li, Y., et al., *Extracellular membrane-proximal domain of HAb18G/CD147 binds to metal ion-dependent adhesion site (MIDAS) motif of integrin beta1 to modulate malignant properties of hepatoma cells*. *J Biol Chem*, 2012. **287**(7): p. 4759-72.
158. Han, J.M. and H.J. Jung, *Cyclophilin A/CD147 Interaction: A Promising Target for Anticancer Therapy*. *Int J Mol Sci*, 2022. **23**(16).
159. Xiong, L., C.K. Edwards, 3rd, and L. Zhou, *The biological function and clinical utilization of CD147 in human diseases: a review of the current scientific literature*. *Int J Mol Sci*, 2014. **15**(10): p. 17411-41.
160. Kaushik, D.K., J.N. Hahn, and V.W. Yong, *EMMPRIN, an upstream regulator of MMPs, in CNS biology*. *Matrix Biol*, 2015. **44-46**: p. 138-46.
161. von Ungern-Sternberg, S.N.I., A. Zerneck, and P. Seizer, *Extracellular Matrix Metalloproteinase Inducer EMMPRIN (CD147) in Cardiovascular Disease*. *Int J Mol Sci*, 2018. **19**(2).
162. Fenizia, C., et al., *SARS-CoV-2 Entry: At the Crossroads of CD147 and ACE2*. *Cells*, 2021. **10**(6).

163. Kosugi, T., et al., *CD147 (EMMPRIN/Basigin) in kidney diseases: from an inflammation and immune system viewpoint*. *Nephrol Dial Transplant*, 2015. **30**(7): p. 1097-103.
164. Satoh, K., et al., *Basigin mediates pulmonary hypertension by promoting inflammation and vascular smooth muscle cell proliferation*. *Circ Res*, 2014. **115**(8): p. 738-50.
165. Hahn, J.N., D.K. Kaushik, and V.W. Yong, *The role of EMMPRIN in T cell biology and immunological diseases*. *J Leukoc Biol*, 2015. **98**(1): p. 33-48.
166. Yurchenko, V., et al., *Cyclophilin-CD147 interactions: a new target for anti-inflammatory therapeutics*. *Clin Exp Immunol*, 2010. **160**(3): p. 305-17.
167. Wang, K., et al., *CD147-spike protein is a novel route for SARS-CoV-2 infection to host cells*. *Signal Transduct Target Ther*, 2020. **5**(1): p. 283.
168. V'Kovski, P., et al., *Coronavirus biology and replication: implications for SARS-CoV-2*. *Nat Rev Microbiol*, 2021. **19**(3): p. 155-170.
169. Zhou, T., et al., *Cryo-EM Structures of SARS-CoV-2 Spike without and with ACE2 Reveal a pH-Dependent Switch to Mediate Endosomal Positioning of Receptor-Binding Domains*. *Cell Host Microbe*, 2020. **28**(6): p. 867-879 e5.
170. Walls, A.C., et al., *Tectonic conformational changes of a coronavirus spike glycoprotein promote membrane fusion*. *Proc Natl Acad Sci U S A*, 2017. **114**(42): p. 11157-11162.
171. Hasan, A., et al., *A review on the cleavage priming of the spike protein on coronavirus by angiotensin-converting enzyme-2 and furin*. *J Biomol Struct Dyn*, 2021. **39**(8): p. 3025-3033.
172. Belouzard, S., V.C. Chu, and G.R. Whittaker, *Activation of the SARS coronavirus spike protein via sequential proteolytic cleavage at two distinct sites*. *Proc Natl Acad Sci U S A*, 2009. **106**(14): p. 5871-6.
173. Hoffmann, M., H. Kleine-Weber, and S. Pohlmann, *A Multibasic Cleavage Site in the Spike Protein of SARS-CoV-2 Is Essential for Infection of Human Lung Cells*. *Mol Cell*, 2020. **78**(4): p. 779-784 e5.
174. Huang, I.C., et al., *SARS coronavirus, but not human coronavirus NL63, utilizes cathepsin L to infect ACE2-expressing cells*. *J Biol Chem*, 2006. **281**(6): p. 3198-203.
175. Bayati, A., et al., *SARS-CoV-2 infects cells after viral entry via clathrin-mediated endocytosis*. *J Biol Chem*, 2021. **296**: p. 100306.
176. Murgolo, N., et al., *SARS-CoV-2 tropism, entry, replication, and propagation: Considerations for drug discovery and development*. *PLoS Pathog*, 2021. **17**(2): p. e1009225.
177. Hoffmann M, H.-W.H., Pohlmann S., *Activation of Viruses by Host Proteases*. . Bo'ttcher-Friebertsha'user E, Garten W, Klenk HD, editors. Springer: p. 71-98.

178. Ou, X., et al., *Characterization of spike glycoprotein of SARS-CoV-2 on virus entry and its immune cross-reactivity with SARS-CoV*. Nat Commun, 2020. **11**(1): p. 1620.
179. Wang, D., et al., *The SARS-CoV-2 subgenome landscape and its novel regulatory features*. Mol Cell, 2021. **81**(10): p. 2135-2147 e5.
180. Kim, D., et al., *The Architecture of SARS-CoV-2 Transcriptome*. Cell, 2020. **181**(4): p. 914-921 e10.
181. Wu, F., et al., *A new coronavirus associated with human respiratory disease in China*. Nature, 2020. **579**(7798): p. 265-269.
182. Malone, B., et al., *Structures and functions of coronavirus replication-transcription complexes and their relevance for SARS-CoV-2 drug design*. Nat Rev Mol Cell Biol, 2022. **23**(1): p. 21-39.
183. Oranger, A., et al., *Accurate detection and quantification of SARS-CoV-2 genomic and subgenomic mRNAs by ddPCR and meta-transcriptomics analysis*. Commun Biol, 2021. **4**(1): p. 1215.
184. de Wilde, A.H., et al., *A Kinome-Wide Small Interfering RNA Screen Identifies Proviral and Antiviral Host Factors in Severe Acute Respiratory Syndrome Coronavirus Replication, Including Double-Stranded RNA-Activated Protein Kinase and Early Secretory Pathway Proteins*. J Virol, 2015. **89**(16): p. 8318-33.
185. Bojkova, D., et al., *Proteomics of SARS-CoV-2-infected host cells reveals therapy targets*. Nature, 2020. **583**(7816): p. 469-472.
186. Chen, J., et al., *Structural Basis for Helicase-Polymerase Coupling in the SARS-CoV-2 Replication-Transcription Complex*. Cell, 2020. **182**(6): p. 1560-1573 e13.
187. van Doremalen, N., et al., *Aerosol and Surface Stability of SARS-CoV-2 as Compared with SARS-CoV-1*. N Engl J Med, 2020. **382**(16): p. 1564-1567.
188. Harrison, A.G., T. Lin, and P. Wang, *Mechanisms of SARS-CoV-2 Transmission and Pathogenesis*. Trends Immunol, 2020. **41**(12): p. 1100-1115.
189. Ong, S.W.X., et al., *Air, Surface Environmental, and Personal Protective Equipment Contamination by Severe Acute Respiratory Syndrome Coronavirus 2 (SARS-CoV-2) From a Symptomatic Patient*. JAMA, 2020. **323**(16): p. 1610-1612.
190. Nouri-Vaskeh, M. and L. Alizadeh, *Fecal transmission in COVID-19: A potential shedding route*. J Med Virol, 2020. **92**(10): p. 1731-1732.
191. Mukhra, R., K. Krishan, and T. Kanchan, *Possible modes of transmission of Novel coronavirus SARS-CoV-2: a review*. Acta Biomed, 2020. **91**(3): p. e2020036.
192. Wang, Z. and X. Xu, *scRNA-seq Profiling of Human Testes Reveals the Presence of the ACE2 Receptor, A Target for SARS-CoV-2 Infection in Spermatogonia, Leydig and Sertoli Cells*. Cells, 2020. **9**(4).
193. Vivanti, A.J., et al., *Transplacental transmission of SARS-CoV-2 infection*. Nat Commun, 2020. **11**(1): p. 3572.

194. Wiersinga, W.J., et al., *Pathophysiology, Transmission, Diagnosis, and Treatment of Coronavirus Disease 2019 (COVID-19): A Review*. JAMA, 2020. **324**(8): p. 782-793.
195. Wu, Z. and J.M. McGoogan, *Characteristics of and Important Lessons From the Coronavirus Disease 2019 (COVID-19) Outbreak in China: Summary of a Report of 72 314 Cases From the Chinese Center for Disease Control and Prevention*. JAMA, 2020. **323**(13): p. 1239-1242.
196. Huang, C., et al., *Clinical features of patients infected with 2019 novel coronavirus in Wuhan, China*. Lancet, 2020. **395**(10223): p. 497-506.
197. Arons, M.M., et al., *Presymptomatic SARS-CoV-2 Infections and Transmission in a Skilled Nursing Facility*. N Engl J Med, 2020. **382**(22): p. 2081-2090.
198. Zou, L., et al., *SARS-CoV-2 Viral Load in Upper Respiratory Specimens of Infected Patients*. N Engl J Med, 2020. **382**(12): p. 1177-1179.
199. Chua, A.J., et al., *Acute Olfactory Loss Is Specific for COVID-19 at the Emergency Department*. Ann Emerg Med, 2020. **76**(4): p. 550-551.
200. Kornitzer, J., et al., *A Systematic Review of Characteristics Associated with COVID-19 in Children with Typical Presentation and with Multisystem Inflammatory Syndrome*. Int J Environ Res Public Health, 2021. **18**(16).
201. Meinhardt, J., et al., *Olfactory transmucosal SARS-CoV-2 invasion as a port of central nervous system entry in individuals with COVID-19*. Nat Neurosci, 2021. **24**(2): p. 168-175.
202. Khan, M., et al., *Visualizing in deceased COVID-19 patients how SARS-CoV-2 attacks the respiratory and olfactory mucosae but spares the olfactory bulb*. Cell, 2021. **184**(24): p. 5932-5949 e15.
203. Sungnak, W., et al., *SARS-CoV-2 entry factors are highly expressed in nasal epithelial cells together with innate immune genes*. Nat Med, 2020. **26**(5): p. 681-687.
204. Zhou, F., et al., *Clinical course and risk factors for mortality of adult inpatients with COVID-19 in Wuhan, China: a retrospective cohort study*. Lancet, 2020. **395**(10229): p. 1054-1062.
205. Tripathy, A.S., et al., *Pro-inflammatory CXCL-10, TNF-alpha, IL-1beta, and IL-6: biomarkers of SARS-CoV-2 infection*. Arch Virol, 2021. **166**(12): p. 3301-3310.
206. Hu, B., et al., *Characteristics of SARS-CoV-2 and COVID-19*. Nat Rev Microbiol, 2021. **19**(3): p. 141-154.
207. Yang, X., et al., *Clinical course and outcomes of critically ill patients with SARS-CoV-2 pneumonia in Wuhan, China: a single-centered, retrospective, observational study*. Lancet Respir Med, 2020. **8**(5): p. 475-481.
208. Fathi, N. and N. Rezaei, *Lymphopenia in COVID-19: Therapeutic opportunities*. Cell Biol Int, 2020. **44**(9): p. 1792-1797.

209. Diao, B., et al., *Reduction and Functional Exhaustion of T Cells in Patients With Coronavirus Disease 2019 (COVID-19)*. *Front Immunol*, 2020. **11**: p. 827.
210. Del Valle, D.M., et al., *An inflammatory cytokine signature predicts COVID-19 severity and survival*. *Nat Med*, 2020. **26**(10): p. 1636-1643.
211. Struyf, T., et al., *Signs and symptoms to determine if a patient presenting in primary care or hospital outpatient settings has COVID-19 disease*. *Cochrane Database Syst Rev*, 2020. **7**(7): p. CD013665.
212. Carsana, L., et al., *Pulmonary post-mortem findings in a series of COVID-19 cases from northern Italy: a two-centre descriptive study*. *Lancet Infect Dis*, 2020. **20**(10): p. 1135-1140.
213. Menter, T., et al., *Postmortem examination of COVID-19 patients reveals diffuse alveolar damage with severe capillary congestion and variegated findings in lungs and other organs suggesting vascular dysfunction*. *Histopathology*, 2020. **77**(2): p. 198-209.
214. Sudre, C.H., et al., *Symptom clusters in COVID-19: A potential clinical prediction tool from the COVID Symptom Study app*. *Sci Adv*, 2021. **7**(12).
215. Carfi, A., et al., *Persistent Symptoms in Patients After Acute COVID-19*. *JAMA*, 2020. **324**(6): p. 603-605.
216. Raveendran, A.V., R. Jayadevan, and S. Sashidharan, *Long COVID: An overview*. *Diabetes Metab Syndr*, 2021. **15**(3): p. 869-875.
217. Mandal, S., et al., *'Long-COVID': a cross-sectional study of persisting symptoms, biomarker and imaging abnormalities following hospitalisation for COVID-19*. *Thorax*, 2021. **76**(4): p. 396-398.
218. Greenhalgh, T., et al., *Management of post-acute covid-19 in primary care*. *BMJ*, 2020. **370**: p. m3026.
219. Louis, T.J., et al., *Extra-Pulmonary Complications in SARS-CoV-2 Infection: A Comprehensive Multi Organ-System Review*. *Microorganisms*, 2022. **10**(1).
220. Linehan, L., et al., *SARS-CoV-2 placentitis: An uncommon complication of maternal COVID-19*. *Placenta*, 2021. **104**: p. 261-266.
221. Beltrami, S., et al., *SARS-CoV-2 Systemic Effects: New Clues*. *Microorganisms*, 2023. **11**(5).
222. de Oliveira, G.L.V., et al., *Microbiota Modulation of the Gut-Lung Axis in COVID-19*. *Front Immunol*, 2021. **12**: p. 635471.
223. Kulkarni, A.V., et al., *Systematic review with meta-analysis: liver manifestations and outcomes in COVID-19*. *Aliment Pharmacol Ther*, 2020. **52**(4): p. 584-599.
224. Fan, Z., et al., *Clinical Features of COVID-19-Related Liver Functional Abnormality*. *Clin Gastroenterol Hepatol*, 2020. **18**(7): p. 1561-1566.
225. Jhaveri, K.D., et al., *Thrombotic microangiopathy in a patient with COVID-19*. *Kidney Int*, 2020. **98**(2): p. 509-512.

226. Sharma, P., et al., *COVID-19-Associated Kidney Injury: A Case Series of Kidney Biopsy Findings*. J Am Soc Nephrol, 2020. **31**(9): p. 1948-1958.
227. Madjid, M., et al., *Potential Effects of Coronaviruses on the Cardiovascular System: A Review*. JAMA Cardiol, 2020. **5**(7): p. 831-840.
228. Matthay, M.A., et al., *Acute respiratory distress syndrome*. Nat Rev Dis Primers, 2019. **5**(1): p. 18.
229. Bonaventura, A., et al., *Endothelial dysfunction and immunothrombosis as key pathogenic mechanisms in COVID-19*. Nat Rev Immunol, 2021. **21**(5): p. 319-329.
230. Zuo, Y., et al., *Plasma tissue plasminogen activator and plasminogen activator inhibitor-1 in hospitalized COVID-19 patients*. Sci Rep, 2021. **11**(1): p. 1580.
231. Caccuri, F., et al., *SARS-CoV-2 Infection Remodels the Phenotype and Promotes Angiogenesis of Primary Human Lung Endothelial Cells*. Microorganisms, 2021. **9**(7).
232. Shang, J., et al., *Cell entry mechanisms of SARS-CoV-2*. Proc Natl Acad Sci U S A, 2020. **117**(21): p. 11727-11734.
233. Klok, F.A., et al., *Incidence of thrombotic complications in critically ill ICU patients with COVID-19*. Thromb Res, 2020. **191**: p. 145-147.
234. Ouwendijk, W.J.D., et al., *High Levels of Neutrophil Extracellular Traps Persist in the Lower Respiratory Tract of Critically Ill Patients With Coronavirus Disease 2019*. J Infect Dis, 2021. **223**(9): p. 1512-1521.
235. Skendros, P., et al., *Complement and tissue factor-enriched neutrophil extracellular traps are key drivers in COVID-19 immunothrombosis*. J Clin Invest, 2020. **130**(11): p. 6151-6157.
236. Pique-Regi, R., et al., *Single cell transcriptional signatures of the human placenta in term and preterm parturition*. Elife, 2019. **8**.
237. Pique-Regi, R., et al., *Does the human placenta express the canonical cell entry mediators for SARS-CoV-2?* Elife, 2020. **9**.
238. Valdespino-Vazquez, M.Y., et al., *Fetal and placental infection with SARS-CoV-2 in early pregnancy*. J Med Virol, 2021. **93**(7): p. 4480-4487.
239. Agostinis, C., et al., *SARS-CoV-2 modulates virus receptor expression in placenta and can induce trophoblast fusion, inflammation and endothelial permeability*. Front Immunol, 2022. **13**: p. 957224.
240. Hadjadj, J., et al., *Impaired type I interferon activity and inflammatory responses in severe COVID-19 patients*. Science, 2020. **369**(6504): p. 718-724.
241. Murphy, S.P., et al., *Interferon gamma in successful pregnancies*. Biol Reprod, 2009. **80**(5): p. 848-59.
242. Cennamo, M., et al., *Low Interferon-gamma Levels in Cord and Peripheral Blood of Pregnant Women Infected with SARS-CoV-2*. Microorganisms, 2023. **11**(1).

243. Mao, L., et al., *Neurologic Manifestations of Hospitalized Patients With Coronavirus Disease 2019 in Wuhan, China*. JAMA Neurol, 2020. **77**(6): p. 683-690.
244. Bordi, L., et al., *Differential diagnosis of illness in patients under investigation for the novel coronavirus (SARS-CoV-2), Italy, February 2020*. Euro Surveill, 2020. **25**(8).
245. Zhang, W., et al., *Molecular and serological investigation of 2019-nCoV infected patients: implication of multiple shedding routes*. Emerg Microbes Infect, 2020. **9**(1): p. 386-389.
246. Lu, X., et al., *SARS-CoV-2 Infection in Children*. N Engl J Med, 2020. **382**(17): p. 1663-1665.
247. Chen, T., et al., *Clinical characteristics of 113 deceased patients with coronavirus disease 2019: retrospective study*. BMJ, 2020. **368**: p. m1091.
248. Cai, H., *Sex difference and smoking predisposition in patients with COVID-19*. Lancet Respir Med, 2020. **8**(4): p. e20.
249. Klein, S.L. and K.L. Flanagan, *Sex differences in immune responses*. Nat Rev Immunol, 2016. **16**(10): p. 626-38.
250. White, M.C., R. Fleeman, and A.C. Arnold, *Sex differences in the metabolic effects of the renin-angiotensin system*. Biol Sex Differ, 2019. **10**(1): p. 31.
251. Sama, I.E., et al., *Circulating plasma concentrations of angiotensin-converting enzyme 2 in men and women with heart failure and effects of renin-angiotensin-aldosterone inhibitors*. Eur Heart J, 2020. **41**(19): p. 1810-1817.
252. Ejaz, H., et al., *COVID-19 and comorbidities: Deleterious impact on infected patients*. J Infect Public Health, 2020. **13**(12): p. 1833-1839.
253. Cariou, B., et al., *Phenotypic characteristics and prognosis of inpatients with COVID-19 and diabetes: the CORONADO study*. Diabetologia, 2020. **63**(8): p. 1500-1515.
254. Shi, Q., et al., *Clinical Characteristics and Risk Factors for Mortality of COVID-19 Patients With Diabetes in Wuhan, China: A Two-Center, Retrospective Study*. Diabetes Care, 2020. **43**(7): p. 1382-1391.
255. Pinchera, B., et al., *Diabetes and COVID-19: The potential role of mTOR*. Diabetes Res Clin Pract, 2022. **186**: p. 109813.
256. Ryan, D.H., E. Ravussin, and S. Heymsfield, *COVID 19 and the Patient with Obesity - The Editors Speak Out*. Obesity (Silver Spring), 2020. **28**(5): p. 847.
257. Radzikowska, U., et al., *Distribution of ACE2, CD147, CD26, and other SARS-CoV-2 associated molecules in tissues and immune cells in health and in asthma, COPD, obesity, hypertension, and COVID-19 risk factors*. Allergy, 2020. **75**(11): p. 2829-2845.
258. Li, W., et al., *Receptor and viral determinants of SARS-coronavirus adaptation to human ACE2*. EMBO J, 2005. **24**(8): p. 1634-43.

259. Li, Q., Z. Cao, and P. Rahman, *Genetic variability of human angiotensin-converting enzyme 2 (hACE2) among various ethnic populations*. Mol Genet Genomic Med, 2020. **8**(8): p. e1344.
260. Guo, X., et al., *Investigation of the genetic variation in ACE2 on the structural recognition by the novel coronavirus (SARS-CoV-2)*. J Transl Med, 2020. **18**(1): p. 321.
261. Peters, M.C., et al., *COVID-19-related Genes in Sputum Cells in Asthma. Relationship to Demographic Features and Corticosteroids*. Am J Respir Crit Care Med, 2020. **202**(1): p. 83-90.
262. Sanyaolu, A., et al., *Comorbidity and its Impact on Patients with COVID-19*. SN Compr Clin Med, 2020. **2**(8): p. 1069-1076.
263. Asselta, R., et al., *ACE2 and TMPRSS2 variants and expression as candidates to sex and country differences in COVID-19 severity in Italy*. Aging (Albany NY), 2020. **12**(11): p. 10087-10098.
264. Singh, H., et al., *ACE2 and TMPRSS2 polymorphisms in various diseases with special reference to its impact on COVID-19 disease*. Microb Pathog, 2021. **150**: p. 104621.
265. Stasi, C., et al., *Treatment for COVID-19: An overview*. Eur J Pharmacol, 2020. **889**: p. 173644.
266. Mehra, M.R., et al., *RETRACTED: Hydroxychloroquine or chloroquine with or without a macrolide for treatment of COVID-19: a multinational registry analysis*. Lancet, 2020.
267. Yao, X., et al., *In Vitro Antiviral Activity and Projection of Optimized Dosing Design of Hydroxychloroquine for the Treatment of Severe Acute Respiratory Syndrome Coronavirus 2 (SARS-CoV-2)*. Clin Infect Dis, 2020. **71**(15): p. 732-739.
268. Hoffmann, M., et al., *SARS-CoV-2 Cell Entry Depends on ACE2 and TMPRSS2 and Is Blocked by a Clinically Proven Protease Inhibitor*. Cell, 2020. **181**(2): p. 271-280 e8.
269. Cvetkovic, R.S. and K.L. Goa, *Lopinavir/ritonavir: a review of its use in the management of HIV infection*. Drugs, 2003. **63**(8): p. 769-802.
270. Ali, M.J., et al., *Treatment Options for COVID-19: A Review*. Front Med (Lausanne), 2020. **7**: p. 480.
271. Chandwani, A. and J. Shuter, *Lopinavir/ritonavir in the treatment of HIV-1 infection: a review*. Ther Clin Risk Manag, 2008. **4**(5): p. 1023-33.
272. Chen, F., et al., *In vitro susceptibility of 10 clinical isolates of SARS coronavirus to selected antiviral compounds*. J Clin Virol, 2004. **31**(1): p. 69-75.
273. Tahir Ul Qamar, M., et al., *Structural basis of SARS-CoV-2 3CL(pro) and anti-COVID-19 drug discovery from medicinal plants*. J Pharm Anal, 2020. **10**(4): p. 313-319.
274. Gul, M.H., et al., *Potential specific therapies in COVID-19*. Ther Adv Respir Dis, 2020. **14**: p. 1753466620926853.

275. Maag, D., et al., *Hepatitis C virus RNA-dependent RNA polymerase (NS5B) as a mediator of the antiviral activity of ribavirin*. J Biol Chem, 2001. **276**(49): p. 46094-8.
276. Tong, S., et al., *Ribavirin therapy for severe COVID-19: a retrospective cohort study*. Int J Antimicrob Agents, 2020. **56**(3): p. 106114.
277. Paladugu, S. and A.A. Donato, *Remdesivir improved time to recovery in adults hospitalized with COVID-19 and lower respiratory tract involvement*. Ann Intern Med, 2020. **173**(2): p. JC4.
278. Carsetti, R., et al., *Different Innate and Adaptive Immune Responses to SARS-CoV-2 Infection of Asymptomatic, Mild, and Severe Cases*. Front Immunol, 2020. **11**: p. 610300.
279. Singh, A.K., et al., *Role of corticosteroid in the management of COVID-19: A systemic review and a Clinician's perspective*. Diabetes Metab Syndr, 2020. **14**(5): p. 971-978.
280. Aomar-Millan, I.F., et al., *Anakinra after treatment with corticosteroids alone or with tocilizumab in patients with severe COVID-19 pneumonia and moderate hyperinflammation. A retrospective cohort study*. Intern Emerg Med, 2021. **16**(4): p. 843-852.
281. Okuda, Y., *Review of tocilizumab in the treatment of rheumatoid arthritis*. Biologics, 2008. **2**(1): p. 75-82.
282. Guaraldi, G., et al., *Tocilizumab in patients with severe COVID-19: a retrospective cohort study*. Lancet Rheumatol, 2020. **2**(8): p. e474-e484.
283. Pang, X., Y. Cui, and Y. Zhu, *Recombinant human ACE2: potential therapeutics of SARS-CoV-2 infection and its complication*. Acta Pharmacol Sin, 2020. **41**(9): p. 1255-1257.
284. Chan, S.W., *Fusion assays for screening of fusion inhibitors targeting SARS-CoV-2 entry and syncytia formation*. Front Pharmacol, 2022. **13**: p. 1007527.
285. Franchini, M. and G.M. Liumbruno, *Convalescent Plasma for the Treatment of Severe COVID-19*. Biologics, 2021. **15**: p. 31-38.
286. Marcec, R., et al., *Intravenous immunoglobulin (IVIg) therapy in hospitalised adult COVID-19 patients: A systematic review and meta-analysis*. Rev Med Virol, 2022. **32**(6): p. e2397.
287. Shao, Z., et al., *Clinical efficacy of intravenous immunoglobulin therapy in critical ill patients with COVID-19: a multicenter retrospective cohort study*. Clin Transl Immunology, 2020. **9**(10): p. e1192.
288. Randolph, H.E. and L.B. Barreiro, *Herd Immunity: Understanding COVID-19*. Immunity, 2020. **52**(5): p. 737-741.
289. Premkumar, L., et al., *The receptor binding domain of the viral spike protein is an immunodominant and highly specific target of antibodies in SARS-CoV-2 patients*. Sci Immunol, 2020. **5**(48).
290. Fathizadeh, H., et al., *SARS-CoV-2 (Covid-19) vaccines structure, mechanisms and effectiveness: A review*. Int J Biol Macromol, 2021. **188**: p. 740-750.

291. Guo, X., et al., *Systemic and mucosal immunity in mice elicited by a single immunization with human adenovirus type 5 or 41 vector-based vaccines carrying the spike protein of Middle East respiratory syndrome coronavirus*. Immunology, 2015. **145**(4): p. 476-84.
292. Zhu, F.C., et al., *Immunogenicity and safety of a recombinant adenovirus type-5-vectored COVID-19 vaccine in healthy adults aged 18 years or older: a randomised, double-blind, placebo-controlled, phase 2 trial*. Lancet, 2020. **396**(10249): p. 479-488.
293. Dupuis, M., et al., *Distribution of DNA vaccines determines their immunogenicity after intramuscular injection in mice*. J Immunol, 2000. **165**(5): p. 2850-8.
294. Smith, T.R.F., et al., *Immunogenicity of a DNA vaccine candidate for COVID-19*. Nat Commun, 2020. **11**(1): p. 2601.
295. Zhang, C., et al., *Advances in mRNA Vaccines for Infectious Diseases*. Front Immunol, 2019. **10**: p. 594.
296. Bettini, E. and M. Locci, *SARS-CoV-2 mRNA Vaccines: Immunological Mechanism and Beyond*. Vaccines (Basel), 2021. **9**(2).
297. Fraussen, J., *IgM responses following SARS-CoV-2 vaccination: insights into protective and pre-existing immunity*. EBioMedicine, 2022. **77**: p. 103922.
298. Chin, A.W.H., et al., *Stability of SARS-CoV-2 in different environmental conditions*. Lancet Microbe, 2020. **1**(1): p. e10.
299. Fathizadeh, H., et al., *SARS-CoV-2 (Covid-19) vaccines structure, mechanisms and effectiveness: A review*. International Journal of Biological Macromolecules, 2021. **188**: p. 740-750.
300. Keech, C., et al., *Phase 1-2 Trial of a SARS-CoV-2 Recombinant Spike Protein Nanoparticle Vaccine*. N Engl J Med, 2020. **383**(24): p. 2320-2332.
301. Garcia, L.F., *Immune Response, Inflammation, and the Clinical Spectrum of COVID-19*. Front Immunol, 2020. **11**: p. 1441.
302. Diamond, M.S. and T.D. Kanneganti, *Innate immunity: the first line of defense against SARS-CoV-2*. Nat Immunol, 2022. **23**(2): p. 165-176.
303. Zheng, J., et al., *Severe Acute Respiratory Syndrome Coronavirus 2-Induced Immune Activation and Death of Monocyte-Derived Human Macrophages and Dendritic Cells*. J Infect Dis, 2021. **223**(5): p. 785-795.
304. Mogensen, T.H., *Pathogen recognition and inflammatory signaling in innate immune defenses*. Clin Microbiol Rev, 2009. **22**(2): p. 240-73, Table of Contents.
305. Wies, E., et al., *Dephosphorylation of the RNA sensors RIG-I and MDA5 by the phosphatase PPI is essential for innate immune signaling*. Immunity, 2013. **38**(3): p. 437-49.
306. Chan, Y.K. and M.U. Gack, *Viral evasion of intracellular DNA and RNA sensing*. Nat Rev Microbiol, 2016. **14**(6): p. 360-73.

307. Yin, X., et al., *MDA5 Governs the Innate Immune Response to SARS-CoV-2 in Lung Epithelial Cells*. Cell Rep, 2021. **34**(2): p. 108628.
308. Yang, D.M., et al., *Differential roles of RIG-I like receptors in SARS-CoV-2 infection*. Mil Med Res, 2021. **8**(1): p. 49.
309. Lee, B.L. and G.M. Barton, *Trafficking of endosomal Toll-like receptors*. Trends Cell Biol, 2014. **24**(6): p. 360-9.
310. Mogensen, T.H., *Pathogen Recognition and Inflammatory Signaling in Innate Immune Defenses*. Clinical Microbiology Reviews, 2009. **22**(2): p. 240-273.
311. Boehme, K.W. and T. Compton, *Innate sensing of viruses by toll-like receptors*. J Virol, 2004. **78**(15): p. 7867-73.
312. Conti, P., et al., *Induction of pro-inflammatory cytokines (IL-1 and IL-6) and lung inflammation by Coronavirus-19 (COVI-19 or SARS-CoV-2): anti-inflammatory strategies*. J Biol Regul Homeost Agents, 2020. **34**(2): p. 327-331.
313. Poulas, K., K. Farsalinos, and C. Zanidis, *Activation of TLR7 and Innate Immunity as an Efficient Method Against COVID-19 Pandemic: Imiquimod as a Potential Therapy*. Front Immunol, 2020. **11**: p. 1373.
314. Khanmohammadi, S. and N. Rezaei, *Role of Toll-like receptors in the pathogenesis of COVID-19*. J Med Virol, 2021. **93**(5): p. 2735-2739.
315. Bortolotti, D., et al., *TLR3 and TLR7 RNA Sensor Activation during SARS-CoV-2 Infection*. Microorganisms, 2021. **9**(9).
316. Yasmin, H., et al., *SARS-CoV-2: Pathogenic Mechanisms and Host Immune Response*. Adv Exp Med Biol, 2021. **1313**: p. 99-134.
317. Castro, A., et al., *In silico analysis suggests less effective MHC-II presentation of SARS-CoV-2 RBM peptides: Implication for neutralizing antibody responses*. PLoS One, 2021. **16**(2): p. e0246731.
318. Sidney, J., et al., *HLA class I supertypes: a revised and updated classification*. BMC Immunol, 2008. **9**: p. 1.
319. Wang, M. and M.H. Claesson, *Classification of human leukocyte antigen (HLA) supertypes*. Methods Mol Biol, 2014. **1184**: p. 309-17.
320. Halenius, A., C. Gerke, and H. Hengel, *Classical and non-classical MHC I molecule manipulation by human cytomegalovirus: so many targets-but how many arrows in the quiver?* Cell Mol Immunol, 2015. **12**(2): p. 139-53.
321. Spinetti, T., et al., *Reduced Monocytic Human Leukocyte Antigen-DR Expression Indicates Immunosuppression in Critically Ill COVID-19 Patients*. Anesth Analg, 2020. **131**(4): p. 993-999.
322. Agerer, B., et al., *SARS-CoV-2 mutations in MHC-I-restricted epitopes evade CD8(+) T cell responses*. Sci Immunol, 2021. **6**(57).
323. Beltrami, S., et al., *Non-classical HLA class I molecules and their potential role in viral infections*. Hum Immunol, 2023.
324. Yang, L., et al., *COVID-19: immunopathogenesis and Immunotherapeutics*. Signal Transduct Target Ther, 2020. **5**(1): p. 128.

325. Rizzo, R., et al., *HLA-G Molecules in Autoimmune Diseases and Infections*. Front Immunol, 2014. **5**: p. 592.
326. Larsen, M.H. and T.V. Hviid, *Human leukocyte antigen-G polymorphism in relation to expression, function, and disease*. Hum Immunol, 2009. **70**(12): p. 1026-34.
327. Rizzo, R., et al., *The Role of HLA-Class Ib Molecules in Immune-Related Diseases, Tumors, and Infections 2016*. J Immunol Res, 2017. **2017**: p. 2309574.
328. Seliger, B., et al., *Induction of pulmonary HLA-G expression by SARS-CoV-2 infection*. Cell Mol Life Sci, 2022. **79**(11): p. 582.
329. Morandi, F., et al., *Human Amnion Epithelial Cells Impair T Cell Proliferation: The Role of HLA-G and HLA-E Molecules*. Cells, 2020. **9**(9).
330. Lin, A. and W.H. Yan, *Perspective of HLA-G Induced Immunosuppression in SARS-CoV-2 Infection*. Front Immunol, 2021. **12**: p. 788769.
331. Bortolotti, D., et al., *Increased sHLA-G Is Associated with Improved COVID-19 Outcome and Reduced Neutrophil Adhesion*. Viruses, 2021. **13**(9).
332. Jin, Y., et al., *Endothelial activation and dysfunction in COVID-19: from basic mechanisms to potential therapeutic approaches*. Signal Transduct Target Ther, 2020. **5**(1): p. 293.
333. Zuo, Y., et al., *Neutrophil extracellular traps in COVID-19*. JCI Insight, 2020. **5**(11).
334. Middleton, E.A., et al., *Neutrophil extracellular traps contribute to immunothrombosis in COVID-19 acute respiratory distress syndrome*. Blood, 2020. **136**(10): p. 1169-1179.
335. Zheng, M., et al., *Functional exhaustion of antiviral lymphocytes in COVID-19 patients*. Cell Mol Immunol, 2020. **17**(5): p. 533-535.
336. Sun, J.C., J.N. Beilke, and L.L. Lanier, *Adaptive immune features of natural killer cells*. Nature, 2009. **457**(7229): p. 557-61.
337. de Mendonca Vieira, R., et al., *Human Term Pregnancy Decidual NK Cells Generate Distinct Cytotoxic Responses*. J Immunol, 2020. **204**(12): p. 3149-3159.
338. Cooper, M.A., T.A. Fehniger, and M.A. Caligiuri, *The biology of human natural killer-cell subsets*. Trends Immunol, 2001. **22**(11): p. 633-40.
339. Long, E.O., et al., *Controlling natural killer cell responses: integration of signals for activation and inhibition*. Annu Rev Immunol, 2013. **31**: p. 227-58.
340. Pegram, H.J., et al., *Activating and inhibitory receptors of natural killer cells*. Immunol Cell Biol, 2011. **89**(2): p. 216-24.
341. Farrell, H.E., M.A. Degli-Esposti, and N.J. Davis-Poynter, *Cytomegalovirus evasion of natural killer cell responses*. Immunol Rev, 1999. **168**: p. 187-97.

342. Nandakumar, S., et al., *Natural killer cells as novel helpers in anti-herpes simplex virus immune response*. J Virol, 2008. **82**(21): p. 10820-31.
343. Brunetta, E., K.L. Hudspeth, and D. Mavilio, *Pathologic natural killer cell subset redistribution in HIV-1 infection: new insights in pathophysiology and clinical outcomes*. J Leukoc Biol, 2010. **88**(6): p. 1119-30.
344. Malengier-Devlies, B., et al., *Severe COVID-19 patients display hyper-activated NK cells and NK cell-platelet aggregates*. Front Immunol, 2022. **13**: p. 861251.
345. Tan, L., et al., *Lymphopenia predicts disease severity of COVID-19: a descriptive and predictive study*. Signal Transduct Target Ther, 2020. **5**(1): p. 33.
346. Xiong, Y., et al., *Transcriptomic characteristics of bronchoalveolar lavage fluid and peripheral blood mononuclear cells in COVID-19 patients*. Emerg Microbes Infect, 2020. **9**(1): p. 761-770.
347. Rizzo, S., et al., *Role of KIR Receptor in NK Regulation during Viral Infections*. Immuno, 2021. **1**(3): p. 305-331.
348. Bortolotti, D., et al., *SARS-CoV-2 Spike 1 Protein Controls Natural Killer Cell Activation via the HLA-E/NKG2A Pathway*. Cells, 2020. **9**(9).
349. Miller, J.D., et al., *Analysis of HLA-E peptide-binding specificity and contact residues in bound peptide required for recognition by CD94/NKG2*. J Immunol, 2003. **171**(3): p. 1369-75.
350. Houchins, J.P., et al., *Natural killer cell cytolytic activity is inhibited by NKG2-A and activated by NKG2-C*. The Journal of Immunology, 1997. **158**(8): p. 3603-3609.
351. Aomar-Millan, I.F., J. Salvatierra, and J. Hernandez-Quero, *Anakinra after treatment with corticosteroids alone or with tocilizumab in patients with severe COVID-19 pneumonia and moderate hyperinflammation. A retrospective cohort study: reply*. Intern Emerg Med, 2021. **16**(4): p. 1105-1106.
352. Sette, A. and S. Crotty, *Adaptive immunity to SARS-CoV-2 and COVID-19*. Cell, 2021. **184**(4): p. 861-880.
353. Turner, J.S., et al., *SARS-CoV-2 mRNA vaccines induce persistent human germinal centre responses*. Nature, 2021. **596**(7870): p. 109-113.
354. Teijaro, J.R. and D.L. Farber, *COVID-19 vaccines: modes of immune activation and future challenges*. Nat Rev Immunol, 2021. **21**(4): p. 195-197.
355. Rizzo, R., et al., *Humoral and adaptive immune responses to the SARS-CoV-2 vaccine*. Int J Infect Dis, 2022. **122**: p. 412-414.
356. Geary, C.D. and J.C. Sun, *Memory responses of natural killer cells*. Semin Immunol, 2017. **31**: p. 11-19.
357. Lopez-Verges, S., et al., *CD57 defines a functionally distinct population of mature NK cells in the human CD56dimCD16+ NK-cell subset*. Blood, 2010. **116**(19): p. 3865-74.

358. Borrego, F., J. Pena, and R. Solana, *Regulation of CD69 expression on human natural killer cells: differential involvement of protein kinase C and protein tyrosine kinases*. Eur J Immunol, 1993. **23**(5): p. 1039-43.
359. Vosshenrich, C.A., et al., *A thymic pathway of mouse natural killer cell development characterized by expression of GATA-3 and CD127*. Nat Immunol, 2006. **7**(11): p. 1217-24.
360. Abel, A.M., et al., *Natural Killer Cells: Development, Maturation, and Clinical Utilization*. Front Immunol, 2018. **9**: p. 1869.
361. Polack, F.P., et al., *Safety and Efficacy of the BNT162b2 mRNA Covid-19 Vaccine*. N Engl J Med, 2020. **383**(27): p. 2603-2615.
362. Busa, R., et al., *Long-Term Effectiveness of BNT162b2 Pfizer-BioNTech mRNA-Based Vaccine on B Cell Compartment: Efficient Recall of SARS-CoV-2-Specific Memory B Cells*. Int J Mol Sci, 2022. **23**(23).
363. Gentili, V., et al., *Natural Killer Cells in SARS-CoV-2-Vaccinated Subjects with Increased Effector Cytotoxic CD56(dim) Cells and Memory-Like CD57(+)NKG2C(+)CD56(dim) Cells*. Front Biosci (Landmark Ed), 2023. **28**(7): p. 156.
364. Dockery, P., J. Bermingham, and D. Jenkins, *Structure-function relations in the human placenta*. Biochem Soc Trans, 2000. **28**(2): p. 202-8.
365. Zeldovich, V.B., et al., *Invasive extravillous trophoblasts restrict intracellular growth and spread of Listeria monocytogenes*. PLoS Pathog, 2011. **7**(3): p. e1002005.
366. Wallace, A.E., R. Fraser, and J.E. Cartwright, *Extravillous trophoblast and decidual natural killer cells: a remodelling partnership*. Hum Reprod Update, 2012. **18**(4): p. 458-71.
367. von Rango, U., *Fetal tolerance in human pregnancy--a crucial balance between acceptance and limitation of trophoblast invasion*. Immunol Lett, 2008. **115**(1): p. 21-32.
368. Steinborn, A., et al., *Early detection of decreased soluble HLA-G levels in the maternal circulation predicts the occurrence of preeclampsia and intrauterine growth retardation during further course of pregnancy*. Am J Reprod Immunol, 2007. **57**(4): p. 277-86.
369. Basak, S., et al., *Curcumin stimulates angiogenesis through VEGF and expression of HLA-G in first-trimester human placental trophoblasts*. Cell Biol Int, 2020. **44**(5): p. 1237-1251.
370. Rizzo, R., et al., *Allergic women have reduced sHLA-G plasma levels at delivery*. Am J Reprod Immunol, 2009. **61**(5): p. 368-76.
371. Cecati, M., et al., *HLA-G and pregnancy adverse outcomes*. Med Hypotheses, 2011. **76**(6): p. 782-4.
372. Beltrami, S., et al., *Gestational Viral Infections: Role of Host Immune System*. Microorganisms, 2023. **11**(7).
373. Caselli, E., et al., *Acute human herpesvirus-6A infection of human mesothelial cells modulates HLA molecules*. Arch Virol, 2015. **160**(9): p. 2141-9.

374. Rizzo, R., et al., *Human Herpesvirus 6A and 6B inhibit in vitro angiogenesis by induction of Human Leukocyte Antigen G*. *Sci Rep*, 2018. **8**(1): p. 17683.
375. Bortolotti, D., et al., *Late-onset intrauterine growth restriction and HHV-6 infection: A pilot study*. *J Med Virol*, 2021. **93**(11): p. 6317-6322.
376. da Silva, G.K., et al., *Influence of HLA-G polymorphisms in human immunodeficiency virus infection and hepatitis C virus co-infection in Brazilian and Italian individuals*. *Infect Genet Evol*, 2014. **21**: p. 418-23.
377. Li, C., et al., *Functional characterization of HLA-G(+) regulatory T cells in HIV-1 infection*. *PLoS Pathog*, 2013. **9**(1): p. e1003140.
378. Argueta, L.B., et al., *Inflammatory responses in the placenta upon SARS-CoV-2 infection late in pregnancy*. *iScience*, 2022. **25**(5): p. 104223.
379. Greco, S., et al., *Case report: Tissue positivity for SARS-CoV-2 in a preterm born infant death of thrombosis: possible intrauterine transmission*. *Front Med (Lausanne)*, 2023. **10**: p. 1127529.
380. Magro, C., et al., *Complement associated microvascular injury and thrombosis in the pathogenesis of severe COVID-19 infection: A report of five cases*. *Transl Res*, 2020. **220**: p. 1-13.
381. Baergen, R.N. and D.S. Heller, *Placental Pathology in Covid-19 Positive Mothers: Preliminary Findings*. *Pediatr Dev Pathol*, 2020. **23**(3): p. 177-180.
382. Cui, D., et al., *Single-cell RNA expression profiling of SARS-CoV-2-related ACE2 and TMPRSS2 in human trophectoderm and placenta*. *Ultrasound Obstet Gynecol*, 2021. **57**(2): p. 248-256.
383. Dong, L., et al., *Evaluation of vertical transmission of SARS-CoV-2 in utero: Nine pregnant women and their newborns*. *Placenta*, 2021. **111**: p. 91-96.
384. Forestieri, S., et al., *Relationship between pregnancy and coronavirus: what we know*. *J Matern Fetal Neonatal Med*, 2022. **35**(10): p. 1997-2008.
385. Minkoff, J.M. and B. tenOever, *Innate immune evasion strategies of SARS-CoV-2*. *Nat Rev Microbiol*, 2023. **21**(3): p. 178-194.
386. Schiuma, G., et al., *Effect of SARS-CoV-2 infection in pregnancy on CD147, ACE2 and HLA-G expression*. *Placenta*, 2023. **132**: p. 38-43.
387. Kalkeri, R., S. Goebel, and G.D. Sharma, *SARS-CoV-2 Shedding from Asymptomatic Patients: Contribution of Potential Extrapulmonary Tissue Reservoirs*. *Am J Trop Med Hyg*, 2020. **103**(1): p. 18-21.
388. Troisi, J., et al., *COVID-19 and the gastrointestinal tract: Source of infection or merely a target of the inflammatory process following SARS-CoV-2 infection?* *World J Gastroenterol*, 2021. **27**(14): p. 1406-1418.
389. Ueland, T., et al., *Distinct and early increase in circulating MMP-9 in COVID-19 patients with respiratory failure*. *J Infect*, 2020. **81**(3): p. e41-e43.

390. Bortolotti, D., et al., *Relevance of VEGF and CD147 in different SARS-CoV-2 positive digestive tracts characterized by thrombotic damage*. *FASEB J*, 2021. **35**(12): p. e21969.
391. Meini, S., T. Giani, and C. Tascini, *Intussusceptive angiogenesis in Covid-19: hypothesis on the significance and focus on the possible role of FGF2*. *Mol Biol Rep*, 2020. **47**(10): p. 8301-8304.
392. Vanzolini, T., et al., *Multitalented Synthetic Antimicrobial Peptides and Their Antibacterial, Antifungal and Antiviral Mechanisms*. *Int J Mol Sci*, 2022. **23**(1).
393. Siedenbiedel, F. and J.C. Tiller, *Antimicrobial Polymers in Solution and on Surfaces: Overview and Functional Principles*. *Polymers*, 2012. **4**(1): p. 46-71.
394. Monge, F.A., et al., *Highly Effective Inactivation of SARS-CoV-2 by Conjugated Polymers and Oligomers*. *ACS Appl Mater Interfaces*, 2020. **12**(50): p. 55688-55695.
395. Gentili, V., et al., *Transparent Polymeric Formulations Effective against SARS-CoV-2 Infection*. *ACS Appl Mater Interfaces*, 2021. **13**(46): p. 54648-54655.
396. Schiuma, G., et al., *Innate Immune Response in SARS-CoV-2 Infection*. *Microorganisms*, 2022. **10**(3).
397. Rizzo, R., *Controversial role of herpesviruses in Alzheimer's disease*. *PLoS Pathog*, 2020. **16**(6): p. e1008575.
398. Marci, R., et al., *Presence of HHV-6A in Endometrial Epithelial Cells from Women with Primary Unexplained Infertility*. *PLoS One*, 2016. **11**(7): p. e0158304.
399. Borghi, A., et al., *High prevalence of specific KIR types in patients with HHV-8 positive cutaneous vascular lesions: a possible predisposing factor?* *Arch Dermatol Res*, 2016. **308**(5): p. 373-7.
400. Marston, H.D., et al., *Antimicrobial Resistance*. *JAMA*, 2016. **316**(11): p. 1193-1204.
401. Kowalski, R.P. and D.K. Dhaliwal, *Ocular bacterial infections: current and future treatment options*. *Expert Review of Anti-infective Therapy*, 2014. **3**(1): p. 131-139.